NOTICE: When government or other drawings, specifications or other data are used for any purpose other than in connection with a definitely related government procurement operation, the U. S. Government thereby incurs no responsibility, nor any obligation whatsoever; and the fact that the Government may have formulated, furnished, or in any way supplied the said drawings, specifications, or other data is not to be regarded by implication or otherwise as in any manner licensing the holder or any other person or corporation, or conveying any rights or permission to manufacture, use or sell any patented invention that may in any way be related thereto.

SYMPOSIUM
on
GROUND EFFECT
PHENOMENA

Compilation of the Papers Presented
October 21, 22 - 23, 1959

PRINCETON UNIVERSITY
DEPARTMENT OF AERONAUTICAL ENGINEERING
in cooperation with
U. S. Army TRECOM
as part of the
ARMY
PROGRAM

SYMPOSIUM
on
GROUND EFFECT
PHENOMENA

A Compilation of the Papers Presented
October 21 - 22 - 23, 1959

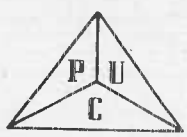

THE PRINCETON UNIVERSITY CONFERENCE
and
THE DEPARTMENT OF AERONAUTICAL ENGINEERING
in cooperation with
U. S. Army TRECOM
as part of the
ALART
PROGRAM

FOREWORD

This document contains reproductions of the technical papers presented by representatives of government and industry at the Symposium on Ground Effect Phenomena, sponsored by the Department of Aeronautical Engineering, Princeton University in cooperation with the United States Army Transportation Research and Engineering Command. The meetings were held at Woodrow Wilson Hall and Forrestal Research Center, Princeton University, on October 21, 22, and 23, 1959.

The purpose of this symposium was to provide a meeting place for the exchange of ideas and test data, in order to obtain a more thorough understanding of this recent development and to stimulate new approaches to the study of the fundamentals of ground effect phenomena. The papers include discussions of experimental progress at several locations, investigations into specific problems of ground effect, and the general performance characteristics of existing vehicles.

Courtland D. Perkins
Chairman, Department of
Aeronautical Engineering

LIST OF PARTICIPANTS

ALPER, William H.	National Research Associates, Inc.
AMANN, Charles A.	General Motors Research Laboratories
ANDERSON, Alfred G.	National Research Associates, Inc.
ASKEY, Charles M.	Hayes Aircraft Corporation
BALL, George A.	Chrysler Corporation
BARNETT, William F.	David Taylor Model Basin
BASTEDO, Walter, Jr.	Gyrodyne Company of America, Inc.
BAUMAN, Richard G.	B. F. Goodrich & Company Research Center
BEARDSLEY, Melville W.	National Research Associates, Inc.
BECK, Col. Vancel R.	U. S. Army TRECOM
BEEBE, John	U. S. Army, OCOFT TCACR-R
BELL, Flt. Lt. W. K.	Royal Canadian Air Force, Ottawa, Canada
BERTELSEN, J. W.	Bertelsen Manufacturing Company, Inc.
BERTELSEN, William R.	Bertelsen Manufacturing Company, Inc.
BLACK, Richard W.	U. S. Army TRECOM
BOEHLER, Gabriel D.	Aerophysics Company
BOHR, A. H.	Reaction Motors, Inc.
BOHRER, Lionel C.	Northwestern University
BOLLECH, T. V.	Fairchild Aircraft & Missiles Division
BOLLUM, Carl W., Sr.	Spacetronics, Inc.
BOTELER, Earl W.	Convair
BOWLBY, Lt. Col. Lawrence	U. S. Army, Fort Monroe
BOWMAN, Willis S.	North American Aviation, Inc.
BRABSON, Lt. Col. William H., Jr.	U. S. Army, Office of the Director of Defense Research and Engineering
BRADSHAW, Joseph G.	Princeton University
BRANDMAIER, Harold E.	Curtiss-Wright Corporation
BRUMER, Joseph A.	The Johns Hopkins University
BUSH, Lt. Col. Harry L.	Office Chief of R&D
BUTTERWORTH, Wesley T.	North American Aviation, Inc.
CAHILL, R. E.	Chrysler Corporation
CAMPBELL, George S.	Hughes Aircraft Corporation
CARNAHAN, Lt. Col. George D.	Office of the Chief of Ordnance
CARTER, Arthur W.	National Aeronautics & Space Administration
CASEY, Col. L. N.	U. S. Marine Corps.
CATHERS, Lt. Lincoln D.	U. S. Navy, Bureau of Ships
CHAMBERLAIN, Wing Comdr. A. H.	Royal Air Force
CHAPLIN, Harvey R., Jr.	David Taylor Model Basin
COCKERELL, C. S.	Hovercraft Development, Ltd.
COOLEY, James L.	United Aircraft Corporation
COOPER, Ralph D.	U. S. Navy, ONR
COSSAIRT, Keith R.	The Martin Company, Orlando, Florida
COWARD, Ken	Convair, San Diego, California
CRANE, C. L., Jr.	Society of Naval Architects & Marine Engineers
CRARY, R. W.	Standard Oil of California
CRUZ, E. S.	Lockheed Aircraft Corporation
CUMMING, Lt. Cdr. Donald W.	Royal Canadian Navy Headquarters
CURTISS, H. C., Jr.	Princeton University
DAVIDSON, William L.	Food Machinery & Chemical Corporation
DAVIES, Hubert	Princeton University
DEE, John B.	General Atomic Division of General Dynamics Corporation
DESMOND, Gerald L.	U. S. Navy Bureau of Aeronautics

DETORE, John A.	Bell Helicopter Corporation
DI RENDE, Joseph S.	U. S. Army TRECOM
DOBSON, Franklin A.	Aeronutronic, A Division, Ford Motor Company
DOUGLAS, L. L.	Vertol Aircraft Corporation
DOWNHILL, Maj. Jack E.	U. S. Air Force, Directorate of R&D
DOWNING, Col. Wayne E.	U. S. Army, Office Deputy Chief of Staff for Logistics
DUDDY, R. R.	British Joint Services Mission
EAGLE, Maj. J. N.	U. S. Marine Corps, Development Branch G-4
EARL, T. Desmond	Avro Aircraft Limited
ERKENEFF, Nicholas	U. S. Air Force, Directorate of Systems Management
ETKIN, Bernard	Institute of Aerophysics, University of Toronto
EVANS, Kenneth E.	The Martin Company, Orlando, Florida
FENG, T. Y.	Bell Aircraft Corporation
FRADENBURGH, Evan A.	Sikorsky Aircraft Division
FRESH, Norman J.	David Taylor Model Basin
FROST, J. C. M.	Avro Aircraft Limited
FUJITA, T.	Aerojet-General Corporation
GATES, M. F.	Hiller Aircraft Corporation
GEARAN, Capt. W. K.	U. S. Army Aviation Board, Fort Rucker
GOLAND, Leonard	Kellett Aircraft Corporation
GOLDMAN, Robert L.	The Martin Company, Baltimore, Maryland
GOLOVATO, Paul	David Taylor Model Basin
GRAHAM, Dunstan	Princeton University
GUMIENNY, Maj. Leo	U. S. Marine Corps Development Center
HAMPTOM, Peter	Princeton University
HARKLEROAD, Capt. Neil E.	David Taylor Model Basin
HARVEY, Jacque W.	McDonnell Aircraft Corporation
HAZEN, David C.	Princeton University
HENDERSON, Brig. Gen. F. P.	Advanced Military Systems, R. C. A., Princeton, New Jersey
HEWIN, Larry M.	U. S. Army TRECOM
HIGGINS, Harry C.	Boeing Airplane Company
HIRSCH, Arthur E.	David Taylor Model Basin
HOLLENBERG, Harold O.	U. S. Air Force Research Div., Bureau of Aeronautics
HOLLOWAY, Robert L.	American Machine & Foundry Co.
HORKEY, Edward J.	Horkey-Moore Associates
HORTON, C. F.	Office of Director of Defense, R&E
HUBBARD, Lt. Col. F. G.	U. S. Army Office of Chief of Transportation
JACK, Thomas N.	Boeing Airplane Company
JACKSON, Philip W., Jr.	National Research Associates, Inc.
JACOBSON, D. H.	Allison Division, General Motors
JAY, David J.	Ford Motor Company
JENNEY, David	United Aircraft Corporation
JOHNSON, Arthur E.	David Taylor Model Basin
JOHNSON, Harold S.	U. S. Army TRECOM
JOHNSTON, W. M.	Lockheed Aircraft Corporation
KAARIO, Toivo J.	Valmet Corporation, Linnavouri, Finland
KALIHER, Eugene C.	Douglas Aircraft Company, Inc.
KAPLAN, Paul	Stevens Institute of Technology
KAYTEN, Gerald G.	The Martin Company, Baltimore, Maryland

KELBER, Charles C.	Northrop Corporation
KELLY, Mark W.	National Aeronautics & Space Administration
KELSEY, Gen. Ben S.	Transportation Research Office, Gravelly Point, Virginia
KNECHT, Robert S.	Gyrodyne Company of America, Inc.
KNIGHT, Edward J., Jr.	National Research Associates, Inc.
KNOWLTON, Mark P.	Princeton University
KORBACHER, G. P.	University of Toronto
KRASE, William H.	The RAND Corporation
KRAUSE, Philip C.	Kellett Aircraft Corporation
KUHN, Richard E.	National Aeronautics & Space Administration
KURT, Franklin T.	Grumman Aircraft Engineering Corp.
LASTER, Col. C. A.	U. S. Marine Corps, Quantico
LAUB, J. H.	California Institute of Technology
LAZAREFF, Michel	Nord Aviation, Paris, France
LECOMTE, Lt. Col. Pierre E.	French Air Ministry, Paris
LEHNERT, Rudolph F.	Princeton University
LEJOHNHUD, Carl A	Atomic Energy Commission
LEVY, Sol J.	Monmouth Laboratories
LIBERATORE, E. K.	Bell Aircraft Corporation
LINDENBAUM, Bernard	Wright Air Development Center
LIPSON, Stanley	Fairchild Engine & Airplane Corporation
LONSDALE, James B.	Pratt & Whitney Aircraft Division
LOOS, James E.	Convair
LUCAS, V. E.	The Firestone Tire & Rubber Co.
LUCKETT, Edward H.	Princeton University
MACGOWAN, T. G.	The Firestone Tire & Rubber Co.
MACK, Lawrence R.	Iowa Institute of Hydraulic Research
MARKS, Marvin D.	McDonnell Aircraft Corporation
MARLIN, Don L.	Ryan Aeronautical Company
MARUCA, Anthony J.	Princeton University
MASSINGILL, E. C., Jr.	Allison Division, General Motors Corporation
MATTHEWS, George B.	Office of Naval Research
MAXEY, L. A.	Aerojet-General Corporation
McCALLUM, Bruce	Massachusetts Institute of Technology
McCARTER, W. B.	Defence Research Board, Ottawa, Canada
McLEAN, J. O.	Reynolds Metals Company
McMAHON, J. J.	American Machine & Foundry Company
MEYER, Brig. Gen. Richard D.	U. S. Army, Office Chief of Transportation
MILLER, J. L.	Firestone Tire & Rubber Company
MILLER, R. H.	Massachusetts Institute of Technology
MILLIKEN, William F., Jr.	Cornell Aeronautical Laboratory
MONTANARO, John O.	Kaman Aircraft Corporation
MYLLYMAKI, Bentti R.	U. S. Army Ordnance, Detroit Arsenal
NAGEY, Tibor F.	Allison Division, General Motors Corporation
NATHAN, Gerd	Atlantic Research Corporation
NAY, Harvey O.	Hughes Tool Company
NEWMAN, B. G.	McGill University
NICHOLL, C. I. H.	Laval University
NIKOLSKY, Alexander A.	Princeton University
NIXON, Barry	Princeton University
NOLLETT, Lt. Col. A. R.	U. S. Marine Corps, MCEB, Quantico
NORMAN, Leslie W.	Garrett Corporation
NOURSE, J. H.	Willys Motors, Inc.
O'DELL, Capt. V. L.	U. S. Army Aviation Board, Fort Rucker
PAPPAS, C. E.	Republic Aviation Corporation

PARKER, Col. David B.	Office Chief of Transportation
PARKER, Lt. Col. T. S.	Bureau of Ships
PAVANE, M.	United States Air Force, ARDC
PERKINS, Courtland D.	Princeton University
PETERSEN, T. K.	Douglas Aircraft Company, Inc.
PETROFF, Alex N.	Cessna Aircraft Company
PIASECKI, Frank N.	Piasecki Aircraft Corporation
PINNES, Robert W.	Bureau of Aeronautics
POCOCK, Philip J.	National Aeronautical Establishment, N. R. C., Ottawa, Canada
POISSON-QUINTON, Ph.	Office National Etudes et Recherches Aeronautiques, France
REMINGTON, Lt. David O.	U. S. Army TRECOM
RETHORST, Scott	Vehicle Research Corporation
RHOADES, Charles R.	Mason Shaver & Rhoades, Inc.
RHOADES, Lt. Col. James S.	U. S. Air Force
RICHARDSON, L. B., Jr.	Chance Vought Aircraft, Inc.
ROBERTSON, Maj. Lester C.	ONR, Washington, D. C.
ROCCATI, Arnold J.	National Research Associates, Inc.
RODGERS, Eric	Princeton University
ROSS, R. S.	Goodyear Aircraft Corporation
SACHS, Donald G.	Boeing Airplane Company
SCHADE, Robert O.	National Aeronautics & Space Administration
SCHEEL, Jerold W.	General Motors Corporation
SCHMIDT, Edward H.	E. I. Dupont de Nemours & Company
SCHOLES, K. N.	North American Aviation, Inc.
SCHWARTZBERG, M. A.	North American Aviation, Inc.
SEAGER, Donald B.	Lockheed Aircraft Corporation
SECKEL, Edward	Princeton University
SENTANCE, Alan P.	Army Development Establishment, Ottawa, Canada
SHARKOFF, Maj. Eugene G.	R & D Division, Office Chief of Ordnance
SHAW, R. A.	British Joint Services Mission
SHEPHERD, George R.	Garrett Corporation
SHERIDAN, P. F.	Vertol Aircraft Corporation
SILVERMAN, Stephan M.	North American Aviation
SILVERSTEIN, Bennett L.	Bureau of Ships
SISSINGH, G. J.	Hiller Aircraft Corporation
SMITH, A. M. O.	Douglas Aircraft Company, Inc.
SOO-HOO, Theodore L.	Office of Chief of Naval Operations
SOUTHCOTE, Murray F.	Aeronutronic Division, Ford Motor Company
SOUTHWICK, Rear Adm. E. P.	Spacetronics, Inc.
SPITZER, Lyman	Princeton University
SPOONER, Stanley H.	U. S. Army TRECOM
STANTON-JONES, R.	Saunders-Roe Limited
STEPNIEWSKI, W. Z.	Vertol Aircraft Corporation
STRAND, Torstein	Convair
STREETER, J. K.	Princeton University
STRONG, Edward	Gyrodyne Company of America, Inc.
SUGDEN, B. K.	The Firestone Tire & Rubber Co.
SUTTON, James F.	Lockheed Aircraft Corporation
SWEENEY, Thomas E.	Princeton University
THEODORSEN, T.	Republic Aviation Corporation
TIDMARSH, Lt. Col. Harold A.	U. S. Army TRECOM
TILGNER, Charles, Jr.	Grumman Aircraft Engineering Corporation
TILLINGHAST, N. W.	Ryan Aeronautical Company

TINAJERO, Anibal Alfredo	David Taylor Model Basin
TOWNSEND, Samuel J. C.	Chance Vought Aircraft
TOWNSEND, M. W., Jr.	U. S. Navy
TRAMMELL, Lt. Col. P. C.	U. S. Marine Corps, Quantico
TRAYBAR, Joseph J.	Princeton University
TUCKER, Jeffrey	Grumman Aircraft Engineering Corp.
TULIN, Marshall P.	Hydronautics, Inc.
TURNER, James J.	U. S. Navy Bureau of Ships
TWYFORD, Robert H.	Atlantic Research Corp.
VANIK, M. F.	Boeing Airplane Company
VAN TUYL, Lt. Cdr. Andrew J.	ONR, Washington, D. C.
VIDAL, Eugene	Army Research Office
VIVIAN, L. L.	Princeton University
WARNER, Douglas K.	Warner Research Laboratory
WATTSON, Robert K., Jr.	University of Wichita
WEILAND, Carl	Zurich, Switzerland
WELLINGER, David	Radio Corporation of America
WERNICKE, Kenneth G.	Bell Helicopter Corporation
WIEGEL, Robert L.	University of California
WILSON, Thomas L.	ONR, Washington, D. C.
WOSSER, Maj. J. L.	ONR, Washington, D. C.
YOUNG, Raymond A.	Douglas Aircraft Co., Inc.
YOUNG, Maj. William H.	Office Chief of Research and Development, Army

CONTENTS

CONTENTS (Continued)

TWO-DIMENSIONAL STUDIES OF A GROUND EFFECT PLATFORM

By Ph. Poisson-Quinton, Office National d'Etudes et
de Recherches Aéronautiques, Chatillon-sous-Bagneux (Seine), France

Translated by: D. C. Hazen, Department of Aeronautical
Engineering, Princeton University

SUMMARY

Experimental research at the Office National d'Etudes et de Recherches Aeronautiques has been limited to the study of the principles of a ground effect platform in the simple case of two dimensional flow.

The measurements of forces and pressures carried out in the wind tunnel at Cannes have been usefully complemented by visualization of the flow in the hydrodynamic tunnel at Chatillon.

After describing the conditions of the wind tunnel tests - in the presence of a movable ground plane, on a wing placed between end plates and equipped with two blowing ducts at the leading and trailing edges - the aerodynamic characteristics of the platform (lift, drag, longitudinal stability, pressure distribution) are examined:

1. Under static or zero forward flight conditions. Experiments show that the amplification of thrust in the immediate neighborhood of the ground grows essentially as the inverse of the altitude, but remains well below the value predicted by the simplified theory neglecting viscosity. The formation of parasitic vortices under the base of the platform results in a reduction of the desirable high pressures; this phenomenon accounts for the loss of amplification and explains its irregular variation at certain altitudes. Finally, experiments confirm the theory on the advantage of converging jets in the immediate neighborhood of the ground.

2. In translation. Experiments show that there are two regimes of operation, depending upon whether the jet at the leading edge escapes toward the front or back upon contact with the ground: in the first case, the configuration is essentially the same as that under static conditions; in the second case the platform behaves much like a classical jet wing, with a lifting efficiency that increases with speed for a given thrust. Experiments show that the amplification of thrust becomes practically independent of the altitude beyond a certain speed of translation. It is therefore possible to envision flying machines utilizing ground effect solely for taking-off and landing, propelled in cruising flight by means of a suitable orientation of the rear jet, the forward jet having been stopped. The possibility of this double regime of operation considerably increases the interest of the jet wing concept applied to high speed aircraft.

In the appendix, two preliminary French studies on the use of annular jets are summarized: one by ONERA, relating to a circular wing with a peripheral jet, and the other by the Société Bertin, dealing with the static test of a circular platform with a convergent peripheral jet.

INTRODUCTION

Considerable interest has been created recently by the possibility of utilizing the favorable ground effect on a platform sustained by an annular jet. Experimentation in

on this principle which has been conducted in England (the Hovercraft of Saunders-Roe), in Switzerland (K. Weiland), and in the United States (Navy-David Taylor Model Basin, Princeton University) has confirmed the feasibility of such machines, capable of performing over land or water, for specific military or civil applications.

Since the studies published so far (references 1, 2, 3 and 4) related to circular platforms, where the analysis of the base phenomena was already complex, it seemed interesting to orient the first researches of ONERA toward a simple two-dimensional study, which was a logical sequel to the preceding investigations of jet wings (references 5 and 6). This paper is strictly limited to a consideration of the principle of ground effect; the reader is referred to several recent publications (references 10, 11 and 12) for a realistic study of the performance of a platform.

The simultaneous use of the wind tunnel * for the quantitative study and of a hydrodynamic tunnel ** for the visualization of the phenomena has been particularly fruitful in leading to an understanding of the base phenomena.

TEST CONDITIONS

In wind tunnel. The measurements of forces and pressures were carried out in the ONERA wind tunnel at Cannes with a conventional model between end plates (Figure 1) and the compressed air installation previously used for blowing research (reference 7). The chord of the wing (ℓ = 0.3 m) was chosen small with respect to the width of the jet (D = 3 m) in order to minimize the wall effects. A movable floor or ground plane permitted study of the influence of the relative altitude H/ℓ of the platform above the ground.

The shape of the wing profile was established by the installation of two directionally adjustable cylindrical ducts distributing the blowing sheet at the leading and trailing edges (Figure 2a).

The utilization of the existing compressed air system of the wind tunnel necessitated the use of small flow quantities at high pressures, and thus thin jets of very high speeds (Figure 2b), hardly comparable to thosed used by the actual platforms. We shall see later that such jets considerably accentuate the viscous induction phenomena.

The jet momentum M_j was calculated from the measured mass flow and the velocity of the jet V_j, calculated on the supposition of an isentropic expansion from the pressure p_{ij} at the interior of the blowing duct to the reference static pressure p_o. This momentum M_j is over-estimated since the speed of the actual jet is certainly less than that calculated, owing to losses through the nozzles. For the translation tests, the classical blowing coefficient C_μ was used (Figure 2c). The three arrangements of blowing sheets through discrete holes or slots are shown in Figure 5.

In hydrodynamic tunnel. The flow visualization studies in the ONERA hydrodynamic tunnel at Chatillon (reference 8) were conducted on a model of 1/3 the scale of that used

---

* The research in the ONERA wind tunnel at Cannes was directed by A. Bevert.

** The visualization in the ONERA hydrodynamic tunnel at Chatillon was directed by H. Werle; a film on these visual studies was presented during the course of the Princeton Symposium.

in the wind tunnel. Figure 3 shows typical examples of flows obtained by photographing the trajectories of small bubbles of air suspended in the water*.

STATIC TESTS

The principle of the amplification of thrust as the ground is approached is well known (references 1 and 2) and a simple calculation, assuming a jet sheet of circular form (Figure 8) and the absence of any effects of viscosity, gives the relation connecting this amplification factor A to the relative height of the platform H/ℓ and the orientation Θ of the Jet**.

$$A = \frac{L_T}{q_m V_i} = \sin \Theta = \frac{\ell}{H} \sin^2 \frac{\Theta}{2}$$

The first objective of the experiments therefore was to experimentally check these theoretical predictions. As a matter of fact, the first tests showed that the values of amplification obtained were much less than those calculated; an analysis of the pressures furnished the explanation. Figure 4 gives an example of the pressure distribution over the undersurface of the wing and along the ground board, for a relative height $H/\ell = 0.5$ and a given intensity of the jets. Contrary to the theoretical hypothesis, a region of uniform high pressure does not exist under the platform and it is easy to locate the indications of a pair of contra-rotating vortices whose existence is caused by the viscous entrainment of the jets. This phenomenon is particularly intense in our case, owing to the high speed of the jets used here (reference 3). The immediate consequence of this parasitic vortex regime is a significant local pressure reduction, which is linked to the high velocities produced by this vortex, that is a loss of lift.

A second consequence of these high speed jets is that it is no longer possible to accept the initial hypothesis of a circular form of the jet sheet.

Influence of jet intensity and altitude on the amplification of thrust under static conditions. Figure 5a shows that the amplification factor, A, is practically independent of the blowing intensity Mj, although the jet velocity has large variations here (see Figure 2b).

The advantage of a continuous jet sheet (slot) over the multiple-hole arrangement is shown at every altitude. Furthermore the experiments illustrate the advantage of making the ejection area as nearly equal to that of the equivalent slot as possible, when one is led to utilize a multiple-hole configuration.

This same figure shows that the thrust measured in the absence of ground effect ($H/\ell = \infty$) is much less than the blowing momentum (a loss of thrust greater than 50 per cent, again accentuated for a discontinuous sheet), owing to the reduction in pressure produced under the platform by the jet.

Figure 5b gives the classical representation of the amplification factor as a function of altitude, for jets ejecting perpendicular to the plane of the platform ($\Theta = 90°$). Shown here, as indicated by their titles, are two curves that were calculated supposing (1) the absence of viscosity:

$$A = 1 + 0.5 \ell/H$$

---

* This emulsion is easily obtained by the introduction of a small quantity of detergent when refilling the tank.

** To be consistent with the notation relating to jet wings, the orientation Θ is measured with respect to the plane of the wing, and not with respect to the normal, as in the studies of references 1, 2, 3 and 4.

and (2) utilizing the scheme of viscous entrainment proposed by H. R. Chaplin (reference 3).* The last calculation comes closer to approaching the experimental curve.

In the neighborhood of the ground ($H/\ell < 0.3$ approximately) the measured amplification varied proportionately with ℓ/H. In the case of the slot, for example, this variation could be written:

$$A = 0.25 + 0.14\,\ell/H$$

For relative altitudes H/ℓ taken between .3 and about 1. the experimental curves present a characteristic waviness, which also appears in the majority of the published three-dimensional results. This behavior with the curvature displaying a maximum around $H/\ell = 0.6$ is again encountered when the development of the maximum pressures or of the loads on the ground is studied (Figure 6a). (Integration of the pressures is moreover in good accord with the direct measurement of the total lift, Figure 6b).

A physical explanation of this curvature was sought by more closely examining the flow visualizations obtained from the hydrodynamic tunnel (Figure 3a) and the ground pressure distributions, which permit the two vortices under the platforms to be located as a function of altitude. For example, Figure 7 shows that, for H/ℓ slightly greater than 0.5, the vortex tends to completely fill the space between the undersurface, the ground, the jet, and the plane symmetry.

The simple trigonometric relationship linking the altitude of the platform and the orientation of the jets leading to a centrally located vortex within the initial hypothesis of a circular jet sheet was therefore sought (Figure 8); this critical relative height diminishes for increasing values of Θ, that is, for convergent jets. Experimentation under static conditions for several orientations of the ducts (Θ = 75° - 90° - 100° - 110°, Figure 8) shows that the maximum points of the curvature qualitatively follow the prediction of the preceding scheme. This seems therefore to confirm that the waviness of these curves (A, H/ℓ) is linked to the existence of the vortex regime (particularly intense here for thin high speed jets) the local growth of the amplification in the vicinity of the critical altitude seems to arise from the momentary augmentation of the pressures at the center of the platform, which are linked to the optimum positioning of the two vortices under the base.

Influence of the orientation of the jets on the amplification factor under static conditions. Figure 9 shows that the amplification varies linearly with $\sin^2 \frac{\Theta}{2}$ for a given altitude of the platform, conforming with the theoretical prediction; this remains true for jets directed by means of small flaps activated by the rotation of the blowing duct. These flaps produce an improvement of the amplification factor for a given effective altitude above the ground, owing to the lower resultant velocity and a better continuity of the jets along the span (Figure 10, Θ = 90°). When the convergent jets (Θ = 135°) meet before striking the ground, an abrupt reduction of the amplification is noted (Figure 10a); the visualization of the flow around this configuration is shown in Figures 3d, 3e and 3f for decreasing altitude

* Figure 4 of reference 3 was utilized here to obtain the ratio of amplification calculated respectively with and without mixing phenomena, from the knowledge of the parameter $c/K_2 \cdot s$, introducing the rate of expansion ($K_2 \cong 6.25$ for $p_{ij}/p_o \cong 2$) and the rectangular size of the slot with respect to the distance c between the jets. (Here $s/c = 0.3280$); from which $c/K_2 \cdot s \cong 150$. The influence of viscosity appears to be appreciable in the neighborhood of the ground: for $H/c = 0.05$, for example A(mixing)/A (non-mixing) = 5/11.

The plot of the amplification factor as a function of ℓ/H (Figure 10b) clearly shows the linear domain of its variation to be in the immediate vicinity of the ground ($H/\ell < 0.3$ approximately), and clearly shows the gain contributed by the convergence of the jets as long as they do not join before striking the ground.

Longitudinal stability of the platform under static conditions. No systematic study of stability under static conditions was made in the wind tunnel; in the sole case studied ($H/\ell = 0.5$), with the jets at $\Theta = 90°$, the platform was slightly unstable: in fact, the center of pressure moved from 49 to 51 per cent of the chord when the angle of attack decreased from +6° to -6°.

This instability appears to be explained by the relative displacement of the two vortices at the leading and trailing edges, which produce lower local pressures on the side where the edge of the platform approaches the ground. A thorough study of methods designed to avoid this instability (fences or auxiliary jets under the platform) appears to be indispensable.

Comparison of two-dimensional and circular platforms under static conditions. It seemed interesting to compare the preceding two-dimensional results with those obtained on circular platforms.

The development of the amplification as a function of the relative altitude has been compared using, first, some unpublished NASA tests (Ames Laboratory; see references 2 and 10) on a circular platform having an annular jet ejecting normal to the plane of the wing ($\Theta = 90°$) and, second, the DTMB tests (reference 4) on a platform with converging jets ($\Theta = 135°$).

Figure 11a illustrates the comparison of the amplification A as a function of c/H or r_o/H.*

1. For jets issuing at $\Theta = 90°$, the NASA tests are compared to those from ONERA relating to the 1/1,000 slot. The behavior is similar in both cases: at proximity to the ground, the amplification varies linearly with the inverse of the altitude; the existence of the curvature related to the vortex regime is also noted for relative altitudes close to the critical; and finally, the amplifications obtained far from the ground are entirely comparable.

2. For the converging jets ($\Theta = 135°$) the DTMB tests are compared to those from ONERA obtained with small flaps guiding the jets issuing from the multi-hole ducts (Figures 9 and 10).

The similarity of the development of A as a function of altitude is even more striking, the absolute values being very close in this case.

TRANSLATION TESTS

The tests on the two-dimensional wing with a relative wind were carried out with the Cannes wind tunnel model described above (Figure 1). It is necessary to point out here that the technique of testing in the presence of a ground board does not truly represent the actual operating conditions of a translating platform. This is due to the existence of

---

* For the comparisons presented in Figures 11a and b, the distance c between the two-dimensional jets and the corresponding radius r_o for circular platforms have been adopted as the reference lengths, this correspondence having been demonstrated in references 1 and 2 the reference surface is that bounded by the jets.

a thick boundary layer on the ground, which certainly distorts the flow around the platform when the jets strike the ground.* Only quantitative tests on a moving carriage over a fixed ground will enable the importance of this parasitic interaction to be judged, which is particularly severe when the altitude of the platform is of the same order of size as the thickness of the boundary layer on the ground board.

The initial aim of the ONERA study was to seek a possible relationship between the double-jet platform and the classical rear-mounted jet flap; systematic tests were therefore conducted, with variable translation speeds, on these two configurations by utilizing the same model. The unfavorable effect of the presence of the ground on a jet wing as soon as the jet touches the ground is well known; the problem has been studied theoretically in the rheoelectric analogy tank at ONERA (reference 9). Blowing is schematized by a sheet of constant radius, which allows a limiting value of the blowing intensity, $C_{\mu lim}$, to be determined, when the jet touches the ground:

$$C_{\mu\ lim} = 2\frac{H}{\ell}\sin^2\frac{\theta}{2}$$

This calculated limiting C_μ has been shown on the experimental curves (C_{L_T}, $\sqrt{C_\mu}$) of Figure 12: the calculation gives a good prediction of the intensity of the blowing from which the lift ceases to vary linearly with $\sqrt{C_\mu}$, the well-known relationship for the jet wing out of ground effect ($H/\ell = \infty$). The pressure measurements on the ground plane and the flow visualizations show that this loss of lift is related to the blockage of the flow under the lower surface of the wing, resulting in a reduction of circulation.

In the case of the double-jet platform, Figure 12b shows that this variation of the total lift is essentially proportional to C_μ beyond a critical value of blowing that we will define later. Out of ground effect ($H/\ell = \infty$), the lift varies essentially as $\sqrt{C_\mu}$, but the efficiency is clearly less than that obtained with a wing employing only a downstream jet, the forward jet eventually not producing a circulation increase.** Flight out of ground effect should therefore be conducted with a properly oriented rear jet alone.

The next step was to look for the mechanism by which the flow changes from the jet wing regime to that of the platform; the analysis of the pressure distribution over the ground did not show this change of regime. Figures 13 and 14 illustrate two typical test cases. (1) at a constant altitude and variable C_μ and (2) at constant C_μ and variable altitude for which the effects of the jets and the vortices on the ground either appear or not. One notes no discontinuity in the development of the lift as a function of C_μ or of H/ℓ ; all these cases are therefore representative of the jet-wing type of flow.

However, the experiments did show that, in the operational range, the ground effect could produce a secondary modification of the flow in the neighborhood of the leading edge of the wing. Figure 15 gives a typical example of this (also shown in Figures 3b and 3c) for a given altitude ($H/\ell = 0.5$). The pressure distributions on the two faces of the wing for two values of C_μ corresponding successively to an upstream jet passing between the

---

* The flow visualizations of the hydrodynamic tunnel and the analysis of the ground pressures reveal moreover the presence of a significant separation upstream of the vortex being created ahead of the leading edge jet (see Figures 3b and 17).

** For a given total value of blowing intensity, $C_\mu = 3$, Figure 12 shows that the lift coefficients for $H/\ell = \infty$ are respectively $C_{L_T} = 6.3$ and 3.5 for the simple jet wing and the double-jet platform.

platform and the ground plane (Figure 15a) or, to the contrary, touching the ground (Figure 15b) have been measured. In the first case, the curvature at the leading edge is so accentuated that a separation bubble appears on the upper surface; in the second case a vortex forms upstream of the leading edge jet, which sufficiently reduces the inclination of the streamlines so that there is no longer a separation at the nose of the profile. The pressure measurements on the wing also indicate the vortex regime under the platform. Finally, the development of the lift is quite linear with $\sqrt{C_\mu}$ (the jet wing regime, quite insensitive to Reynolds number), but presents a characteristic discontinuity confirming the domain where the separation bubble on the upper surface appears. It should be recalled here that, under the existing experimental conditions, the presence of a boundary layer on the ground board can appreciably distort the flow upstream of the leading edge.

Amplification factor in translation. The profile of the platform being cambered, the lift in the absence of blowing is not negligible ($C_{L_o} = 0.26$, at $\alpha = 0°$ and for $H/\ell = \infty$). It is therefore necessary to subtract this value of C_{L_o} from the lift measured in translation in order to calculate the amplification factor.

$$A = \frac{C_{L_{c_\mu}} - C_{L_{(c_\mu = o)}}}{C_\mu}$$

Representing A as a function of $1/C_\mu$* permits the results of the static and translation tests to be shown at the same time: Figure 16a shows the good continuity of the curves between the static point and tests with increasing velocity. It can be seen from this figure that, in the immediate vicinity of the ground ($H/\ell = 0.05$ or 0.1), the amplification factor begins to diminish as the platform starts up, to grow again past a critical value of C_μ. Out of ground effect ($H/\ell = \infty$), on the other hand, only the jet wing flow regime appears.

The influence of the relative altitude in translation is shown in Figure 16b. The amplification factor A is shown here as a function of ℓ/H in order to be able to also represent the values obtained out of ground effect ($H/\ell = \infty$). The improvement of the amplification factor for increasing velocity (that is, decreasing values of C_μ, at a given specific thrust) clearly appears in this figure. In conclusion, the proximity of the ground no longer contributes a notable gain of amplification beyond a certain flight speed.

Search for the frontier between the platform and the jet wing regimes. The flow visualizations shown in Figure 17 examine the fundamental difference of the flows between the two regimes:

1. Figure 17a relates to static conditions and Figure 17b corresponds to a very low translation velocity; in the two cases, the flow under the wing is exactly the same. This identity of the platform regime is confirmed in Figure 19 by the coincidence of the pressure distribution measured on the ground.

2. Figure 17c relates to a large translation velocity, for which the diameter of the upstream vortex created by the jet passing over the platform is diminished.

3. Finally, beyond a critical velocity of translation, the upstream jet sheet abruptly passes under the platform. This is the jet wing regime shown in Figure 17d.

---

* $1/C_\mu$ for a given specific thrust M_j/S represents in coefficient form a value proportional to the dynamic pressure q_o.

These two types of flow clearly appear when the amplification A is presented as a function of $1/C_\mu$. Figure 18 presents a summary of experiments with the blowing accomplished by slot or multiple holes (the curves being shifted uniformly to show the similarity of the variation in the jet wing regime at all altitudes); the mimimum of each curve furnished the critical blowing intensity $C_{\mu_{cr}}$ separating these two regimes of operation. The experiments show then (Figure 18) that the critical blowing coefficient varies linearly with the relative height above the ground.

Next, the best method of graphically determining the value of the critical C_μ was sought. Figure 20 presents successively:

1. The augmentation of lift ΔC_L as a function of C_μ which shows the linear development of the curve in the platform regime.

2. The amplification A as a function of C_μ, which shows in a better manner than the preceding the discontinuity separating the two regimes.

3. The amplification A as a function of $1/C_\mu$. This representation seems the most judicious, as indicated by the use of a supplimentary value of A relating to static conditions, and because the quasi-linearity of the curves for each of the two regimes precisely defines $C_{\mu_{cr}}$

It must be noted here that the influence of the test Reynolds number appears negligible (U_o = 10 and 20 m/s).

The change of the regime of operation appears in the ground pressure distribution (Figure 21) by a much greater extension of the vortex upstream of the leading edge in the platform regime (case a), for which the upstream jet escapes over the leading edge.

Lifting advantage of the platform. The lifting advantage of the platform must finally be expressed in the form of ratio of the total lift L_T (knowing the lift of the wing without blowing L_o) to the ejected momentum M_j.

In Figure 22a, $L_T/M_j = C_{L_T}/C_\mu$ has been plotted as a function of the altitude H/ℓ, for constant values of C_μ ; these curves have also been graduated for values of flight speed U_o, by assuming a specific thrust M_j/S = 20 kg/m². This figure confirms that beyond a certain flight velocity the influence of the ground becomes negligible and the lift efficiencies then attain very high values.

Figure 22b demonstrates the same tendency in another form: here, as a function of velocity, the thrust necessary to develop a given total lift was sought. L_T = 10 kg, assuming a wing loading P/S = 100 kg; for flight velocities higher than 40 m/s, the proximity of the ground no longer produced a reduction of the thrust required. It must be remarked that, close to the ground (H/ℓ = .047, for example), the thrust required for lift is essentially constant from the static point to about 30 m/s, although the amplification factor A decreases slightly with speed in the platform regime (see Figure 20c), owing to the growth of the aerodynamic lift L_o related to the camber of the platform profile.

The influence of jet orientation in translation. The augmentation of lift to the convergence of the jets found during the static tests (see Figure 9) persists in translating. Figure 23 shows that, close to the ground (H/ℓ = 0.05), the curve of lifting efficiency C_{L_T}/C_μ as a function of $1/C_\mu$ for convergent flaps (Θ = 135°) remains essentially parallel

and appreciably above that for the flaps at $\Theta = 90°$. The same advantage of the small flap tangent to the blowing holes already pointed out during the static tests is again observed, at least as long as one remains in the proximity of the ground. On the other hand, these little orienting flaps are detrimental out of ground effect ($H/\ell = \infty$) and it is advisable to bend them back progressively during the transition.

Polars of a platform in translation. Figures 24 and 25 give two examples of the classical aerodynamic characteristics of the platform (polars, lift curves, and longitudinal stability) in the particular case of the multi-hole ducts ($d/\ell = 2.3/1,000$) oriented with $\Theta = 110°$:

1. For a rather large constant relative altitude ($H/\ell = 0.5$), Figure 24 shows that the platform presents the well-known characteristics of the jet wing: displacement of all the curves (C_L, α) with increasing C_μ, slight augmentation of the stability and growth of the nose-down pitching moment (note that the platform is practically neutrally stable about the 25 per cent chord point), and displacement of the polars towards negative C_D for increasinc C_μ.

2. For a given intensity of blowing ($C_\mu = 0.5$), Figure 25 indicates the existence of a change cf regime in the immediate proximity of the ground ($H/\ell = 0.1$): augmentation of the slope C_{L_α} but a premature stall starting at about 0° angle of attack, augmentation of the longitudinal stability but a dangerous pitch up, and a marked displacement of the polar toward the negative values of C_D.

In conclusion, these examples show that a thorough study of the ground effect as a function of angle of attack with the more controlled test conditions (suction of the boundary layer from the ground board, for example) will be necessary. It will also be necessary to study methods of balancing the pitching moments, either by working with the relative intensity of the up and down stream jets or by employing an empennage. Finally the problem of the stall of the platform at low angles of attack in the immediate neighborhood of the ground merits particular attention.

Propulsion or braking of the platform. A summary study of propulsion or braking has been carried out by working with the different orientations of the up and down stream jets Figure 26 gives an example of the variations of the total lift C_{L_T}, of the drag ΔC_D, and of the center of pressure x_{cp}/ℓ, as a function of the intensity of blowing for a configuration tested at a constant altitude ($H/\ell = 0.1$) and 0° angle of attack, with the jets initially oriented at $\Theta = 110°$.

One notes first of all that the premature stall of the platform spotted previously on the polars ($\Theta_A = \Theta_F = 110°$) also appears for the asymmetric configuration ($\Theta_A = 90°$, $\Theta_F = 110°$) relating to the braking of the platform. In the propulsive configuration ($\Theta_A = 110°$, $\Theta_F = 90°$), this separation does not appear, and the measured propulsive component conforms with the calculation.* The positions of the center of pressure are on either side of those obtained for the symmetrically convergent jets, the propulsive configuration evidently resulting in the most rearward motion of the c_p.

Transition between the platform and jet wing configurations. One can imagine the transition from hovering flight to forward flight out of ground effect in three steps which

---

*Remember that, when considering the drag of an actual platform, the momentum drag associated with the intake of the air must be added: $\Delta D = qm\ U_o$ is not represented in this test.

have been summarized in Figure 27 and illustrated in Figure 28a. Under static conditions the jets are symmetrical and convergent (here $\Theta_A = \Theta_F = 120°$); propulsion close to the ground is provided by a rotation of the jets toward the rear (here $\Theta_A = 120°$, $\Theta_F = 60°$); and finally, flight at altitude is provided by only the downstream propulsive jet. (Here the classical jet wing $\Theta_F = 60°$).

The curves of Figure 27 relating to tests out of ground effect ($H/\ell = \infty$) clearly show the advantage of this classical jet wing configuration.

Figure 28b illustrates a possible use of the ground effect for the take-off and landing of a high speed airplane. The peripheral blowing on the delta wing should provide the support of the airplane in the immediate neighborhood of the ground (doing away with the landing gear, making motion over unprepared terrain possible; in cruising flight only the downstream jet will be in use to provide part of the propulsion and the rolling control; and a blowing Canard surface provides longitudinal trim for all flight regimes.

Comparison of two-dimensional and circular platforms in translation. As for the static experiments, discussed earlier, it is interesting to compare the variation of the amplification A obtained for circular platforms with that just described for the two-dimensional case, as a function of the parameter $1/C_\mu$.

Figure 11b illustrates this comparison for two wind tunnel tests made at the NASA (jets at $\Theta = 90°$) and the DTMB (convergent jets $\Theta = 135°$. In three dimensions the two very distinct platform and jet wing regimes are found again for values in the neighborhood of the relative altitudes H/c or H/r_o.

CONCLUSION

The two-dimensional investigation of a ground effect platform permits a better understanding of the complex aerodynamic phenomena associated with such configurations both in hovering flight and translation.

1. Under static conditions. Amplification of the thrust with the approach of the ground grows as the inverse of the altitude, but experiments furnish values very much below those predicted by the calculation, neglecting the effect of viscosity. This divergence is reduced by introducing the mixing phenomena in the neighborhood of the jets into the theoretical estimation.

The formation, by the viscous effects of two counter-rotating vortices under the platform, explains not only the reduction of the base lift but also seems to cause the irregular behavior of the amplification curves as a function of altitude.

The amplification factor of the thrust increases with the convergence of the jets as predicted by theory; small flaps guiding the jets produce an improvement of the amplification in the particular case of discontinuous high speed jets.

2. In translation. The comparison of the lifting characteristics of a classical aft-mounted jet wing and a double-jet platform shows not only the advantage of this last solution in the neighborhood of the ground, but also the better efficiency of the jet wing out of ground effect.

The analysis of the variation of the amplification factor as a function of the intensity of blowing causes two distinct regimes of operation to appear, depending on whether or not the leading edge jet escapes upstream or under the platform: in the first case, one again finds essentially the characteristics of the flow observed under static conditions

(the platform regime). In the second case, the variation of the lift with the intensity of blowing is similar to that encountered with the classical jet wing, and the influence of altitude becomes secondary. The amplification of lift then increases linearly with the square of the flight velocity for a given thrust.

Representation of the factor of amplification as a function of the parameter of $1/C_\mu$ permits the study of the characteristics of the platform from static conditions to high speeds of translation and gives a precise value of the critical intensity of blowing, corresponding to the change of regime at each altitude. This critical C_μ varies linearly with the altitude of the platform.

The improvement of amplification for increasing velocity appears practically independent of altitude, which gives rise to the possibility of cruising flight of a platform out of ground effect; in this case, the leading edge jet must be stopped and the platform becomes a classic jet wing. The influence of Reynolds number appears negligible in these blowing tests.

The characteristics of the platform at variable angles of attack have only been approached in a summary manner here. A thorough study of the stability both under static and translation conditions seems indispensible; likewise the problems of separation and stall must be examined with care for translation in the vicinity of the ground.

3. In resumé. The actual two-dimensional study cannot pretend to provide the quantitative elements to the project engineer, the test conditions being too removed from reality. However, it has permitted a better understanding of the nature of the flow, thanks to the help of flow visualization in the hydrodynamic tunnel. Furthermore, the essential aerodynamic phenomena encountered here under static and translation conditions have been found to be qualitatively similar to those encountered in tests made on circular platforms. Finally, this study has shown the relationship between the platform and the classical jet wing, suggesting the use of ground effect for the take-off and landing of STOL aircraft.

APPENDIX 1

Peripheral blowing on circular wing. Within the mass of systematic researches on jet wings, in 1956 ONERA tried a circular wing on which the slot, directed normal to the plane of the wing ($\Theta = 90°$), affected a more or less extended portion of the pheriphery. Figure 29 shows a schematic drawing of this wing constructed of an ellipsoid of 12.5 per cent thickness and tested in the form of a half model up to transonic Mach numbers.*

No study of the ground effect was made at this time, but the static tests showed a very significant loss of thrust owing to the low pressures induced by the jets under the lower surface.

Figure 29 shows an example of the results obtained in translation at $M = 0.3$, for different extensions of the blowing slot and for the same intensity of blowing ($C_\mu = 0.13$). The best lifting efficiency and the maximum propulsive effect were obtained here for the slot extending slightly beyond the downstream quarter of the circle ($\Psi = 110°$). For a slight negative angle of attack ($\alpha = -5°$), it is possible to balance the drag ($C_D = 0$) while profiting from an appreciable lift ($C_L = 0.25$).

---

* The tests showed that, on this type of low aspect ratio wing ($\lambda = 1.27$), compressibility troubles do not appear until a high Mach number ($M = 0.92$) is reached in spite of the relatively large thickness.

It is therefore possible to envision a circular platform sustained under static conditions and at low velocity by a pheripheral jet, and then propelled at altitude by a properly oriented jet affecting only the downstream part of the periphery.

APPENDIX II

Study under static conditions of a convergent annular jet by the Societe Bertin. The remarkable properties of annular jets were demonstrated for the first time in France during an experimental study by the Societe Bertin in 1957* on a circular platform having a convergent peripheral blowing slot ($\Theta = 135°$).

Figure 30 shows a typical example of the amplification factor A, obtained as a function of the relative height above the ground H/D. Simultaneously the authors demonstrated by calculation that the amplification was inversely proportional to the ratio H/D and showed the advantage of convergent jets.

---

*Compare Technical Note 15-8, registered at the Institut de Propriété Industrielle 16/7/57: "Vérin fluid et calcul de la poussé recueillie en incompressible on a surface ciruclaire" by J. Bertin and B. Salmon.

REFERENCES

1. Chaplin, H. R., "Theory of the annular nozzle in proximity to the ground." DTMB Aero Rept. 923, July 1957.

2. Boehler, G. D., "Aerodynamic theory of the annular jet." IAS, 27th Annual Meeting, New York, January 1959; IAS paper 59-77.

3. Chaplin, H. R., "Effect of jet mixing on the annular jet." DTMB Aero Rept. 953, February 1959.

4. Tinajero, A. A., "Comparison of experimental and theoretical design parameters of a 6-inch annular jet model with a jet angle of -45°." DTMB Aero Rept. 954, May 1959.

5. Roy, M., "Principe d' étude de l'aile à jet." Recherche Aeronautique 52, 1956.

6. Malavard, L., Poisson-Quinton, Ph., and Jousserandot, P., "Recherches théoriques et experimentales sur le contrôle de circulation par soufflage appliqué aux ailes d'avions. ONERA Note Technique 37, 1956. (Princeton University, Dept. of Aeronaut. Eng., Rept. 358, July 1956. Translated by T. M. Berthoff and D. C. Hazen.)

7. Bevert, A., "Technique d'essais de soufflage dans la soufflerie de CANNES." Recherche Aeronautique 67, 1958.

8. Werle, H., "Apercu sur les possibilités expérimentales du tunnel hydrodynamique à visualizations de l'ONERA." ONERA Note Technique 48, 1958.

9. Duquenne, R., and Werle, H., "Effets de paroi sur une aile avec soufflage." AGAR Meeting, Wind Tunnel Panel, Bruxelles, March 1959.

10. Matthews, G. B., and Vosser, J. L., "Ground proximity: a critical review." IAS Paper 59-121, Los Angeles, June 1959.

11. Chaplin, H. R., "A preliminary design technique for annular - jet ground effect machines (GEM'S)." DTMB TED AD 3242, September 59.

12. Pinnes, R. W., "A power plant man's look at the ground effect machine." Navy Dept., BuAer, R. D. R. 1958, April 1959.

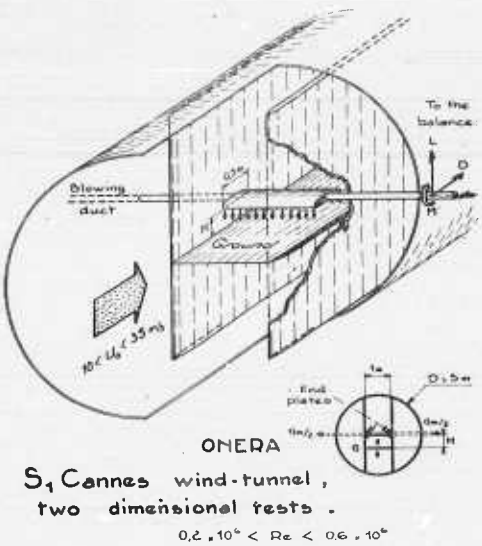

Figure 1

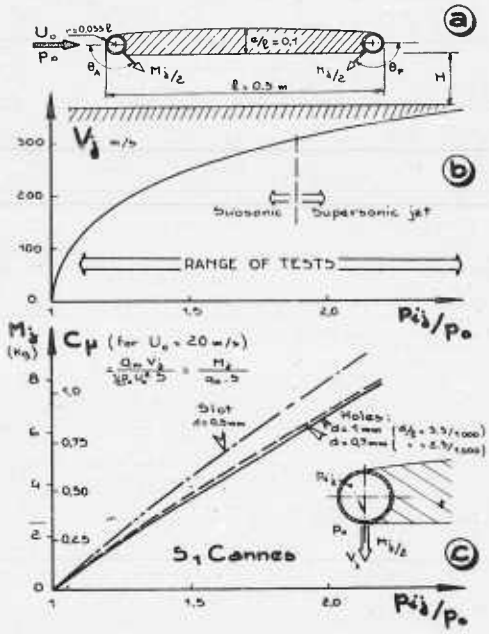

Figure 2.

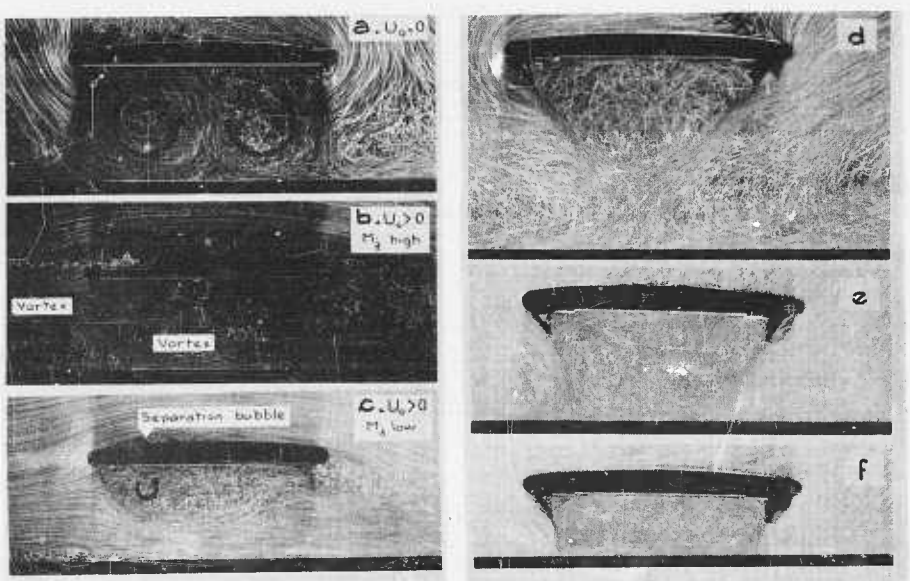

H/ℓ = ct , hovering and forward speed

Platform with flaps θ=135°, variable H/ℓ

Figure 3.

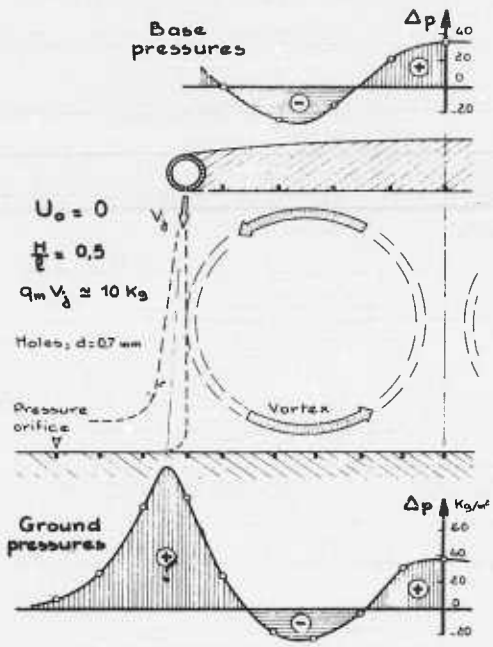

Figure 4.

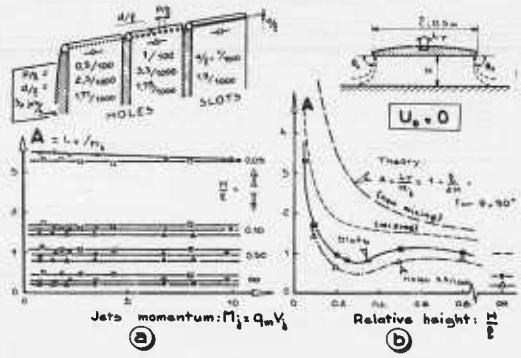

Figure 5

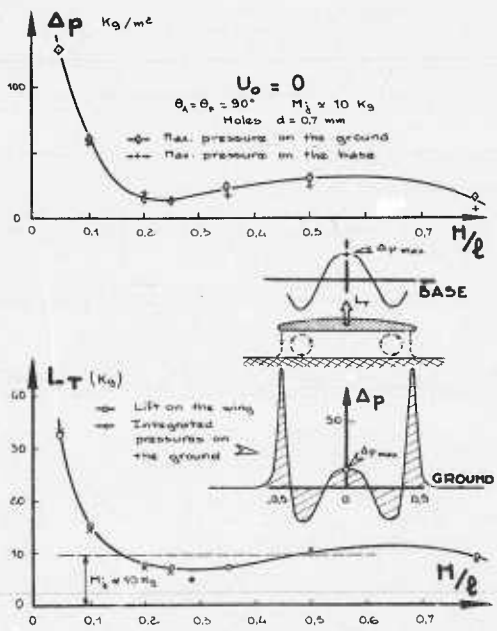

Figure 6.

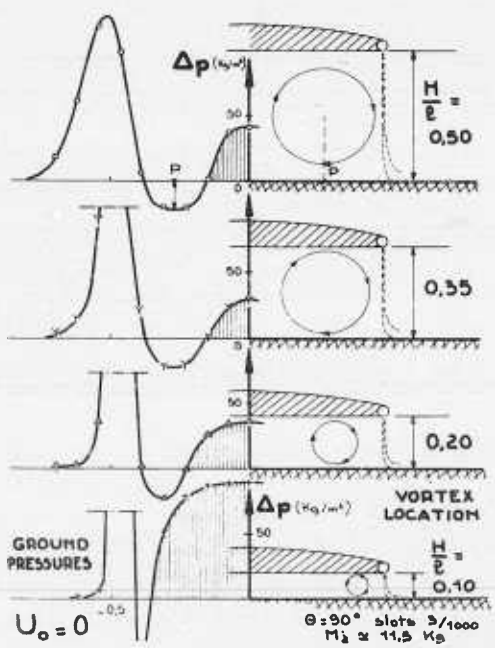

Figure 7.

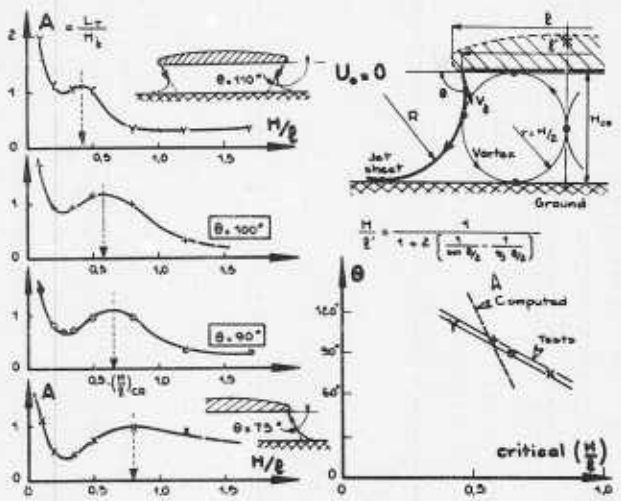

Figure 8.

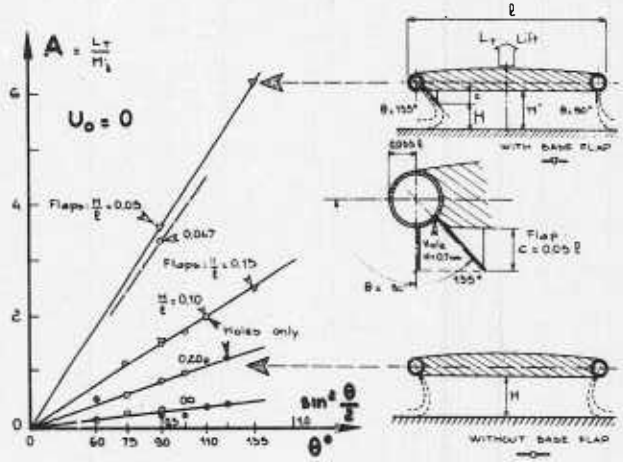

Figure 9.

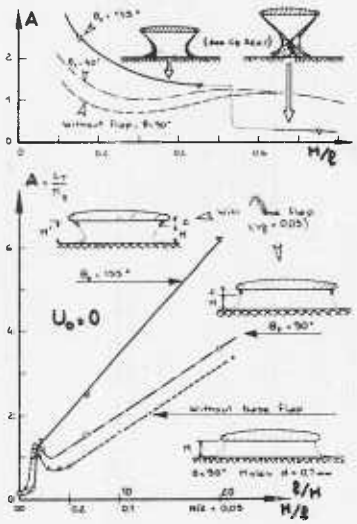

Figure 10.

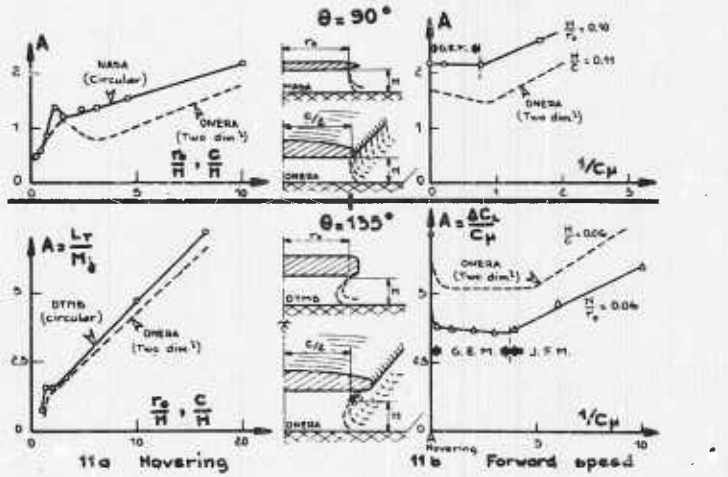

Figure 11.

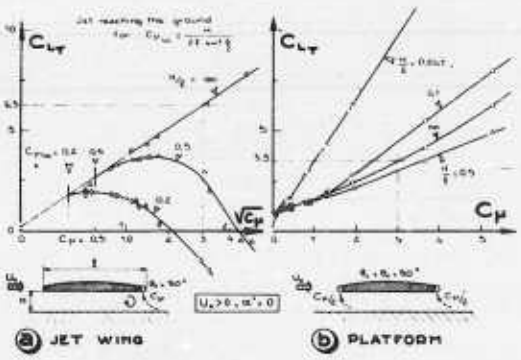

Figure 12.

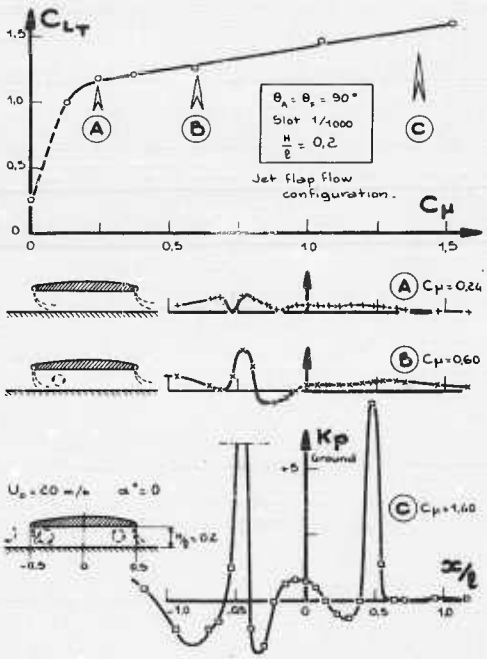

Figure 13.

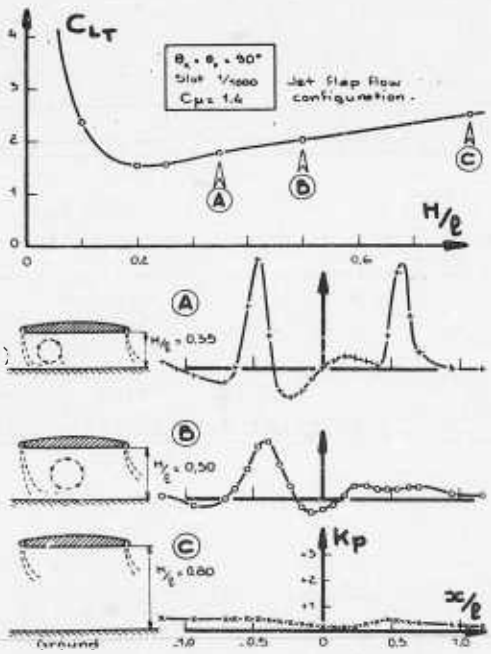

Figure 14.

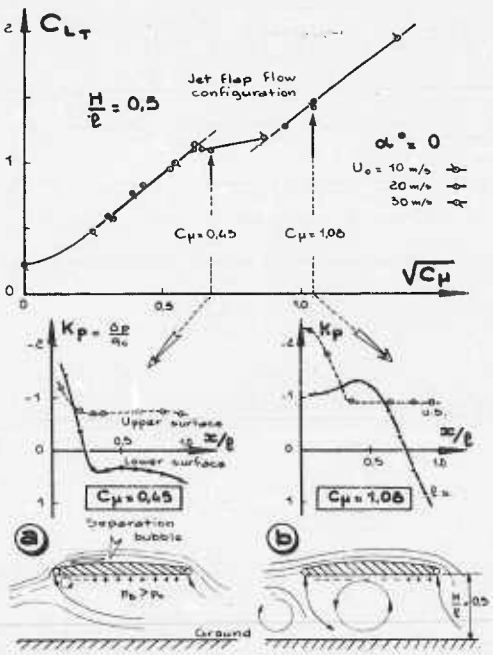

Figure 15.

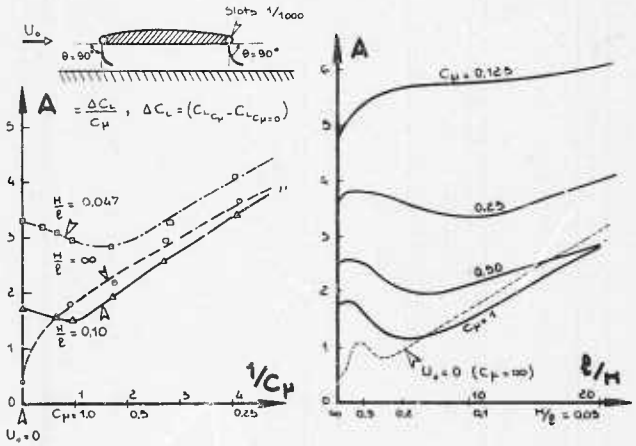

Figure 16.

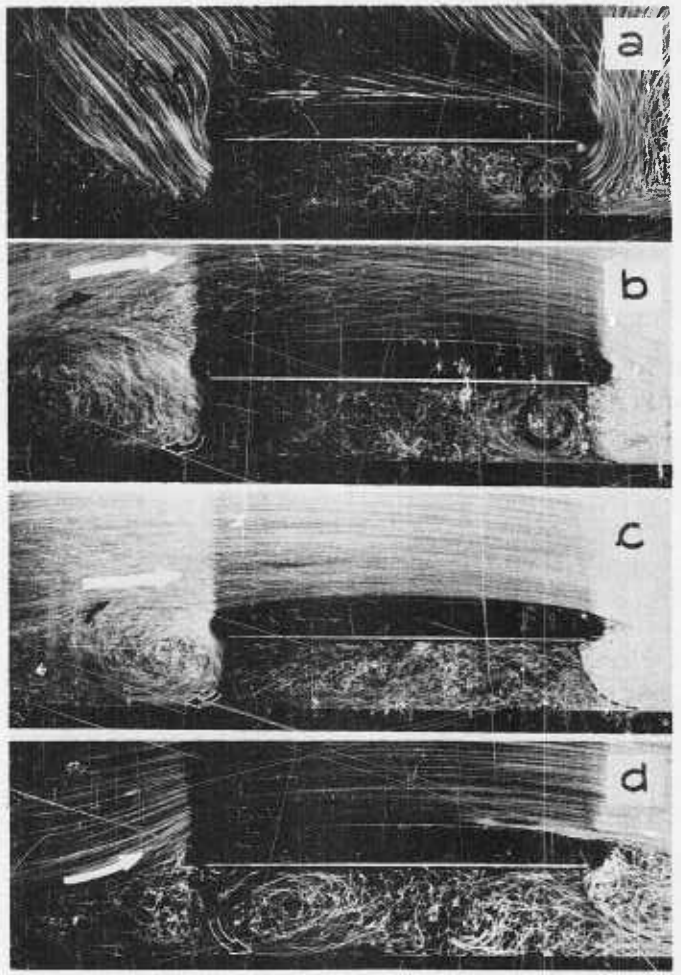

Figure 17.

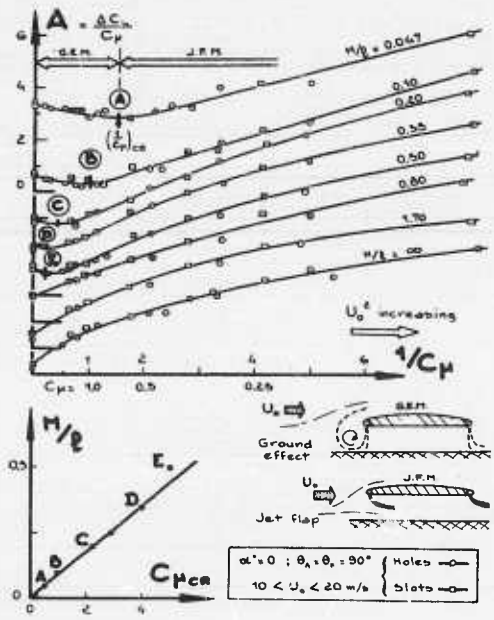

Figure 18.

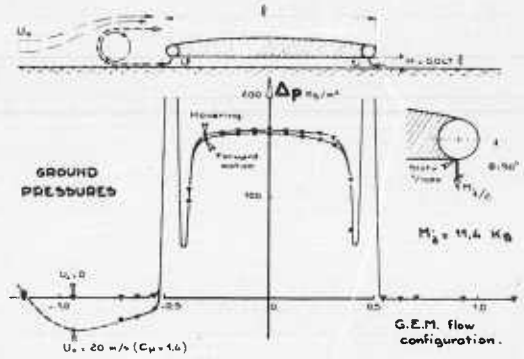

Figure 19.

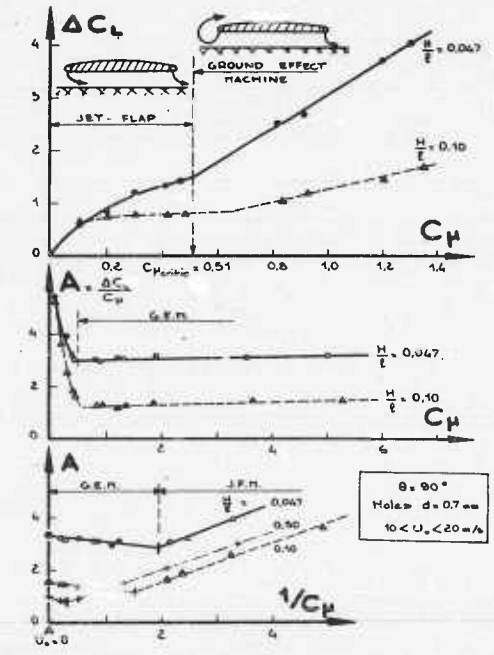

Figure 20.

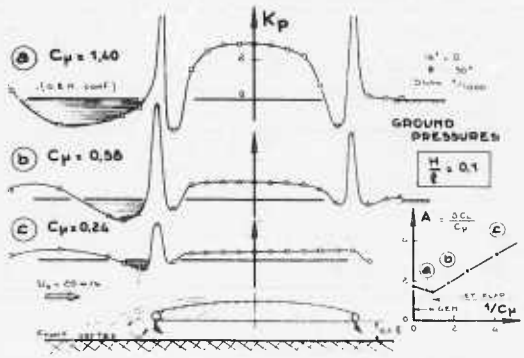

Figure 21.

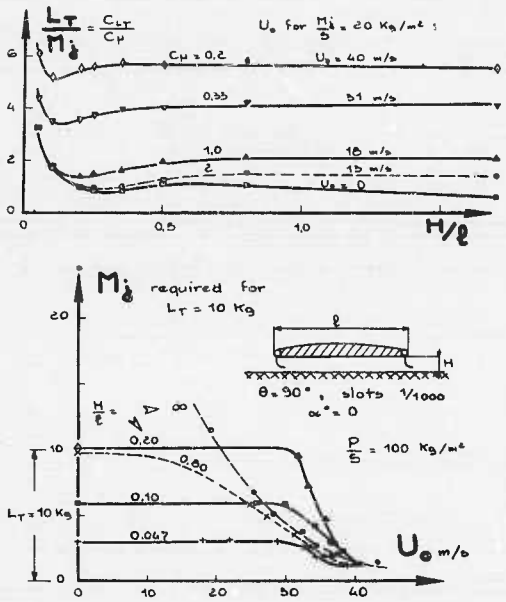

Figure 22.

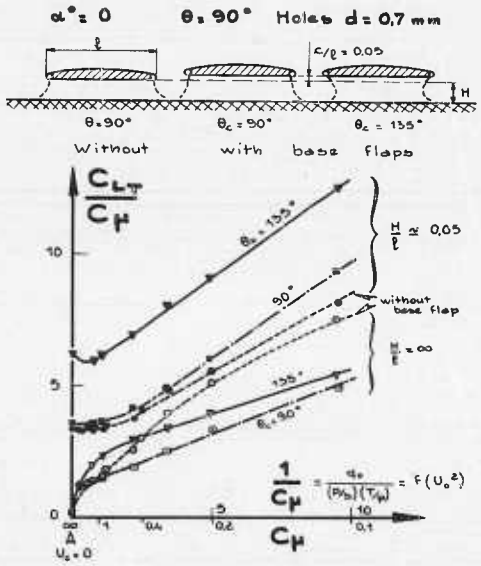

Figure 23.

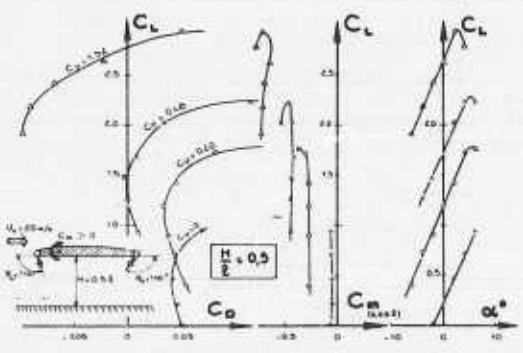

Figure 24.

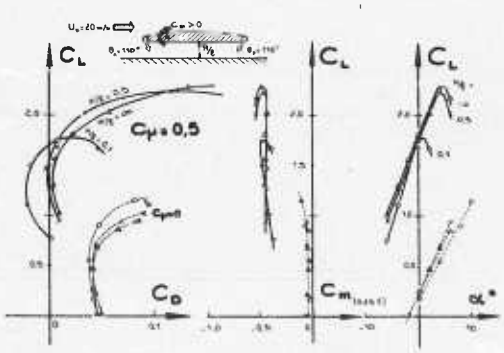

Figure 25.

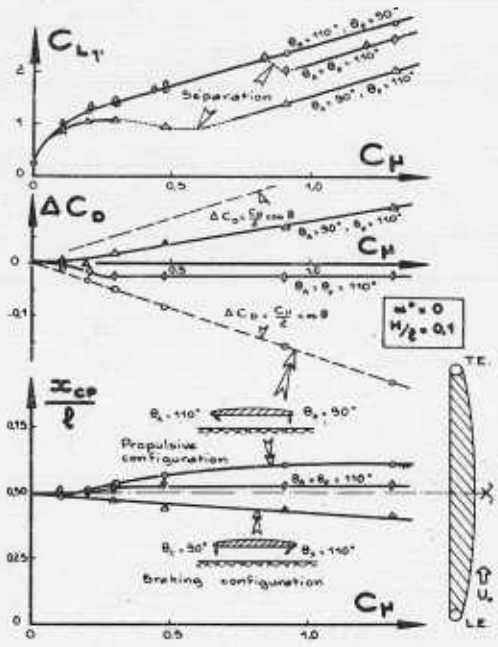

Figure 26.

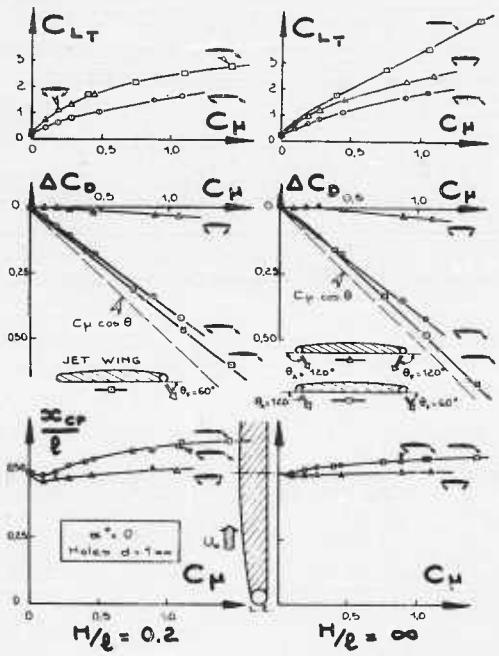

Figure 27.

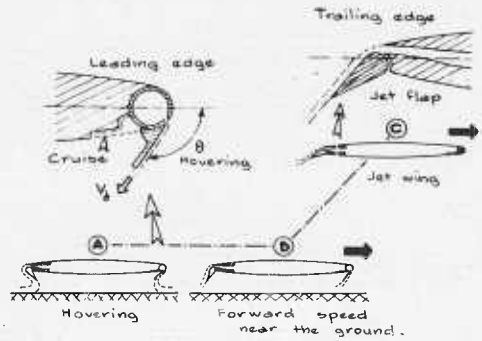

Figure 28a.

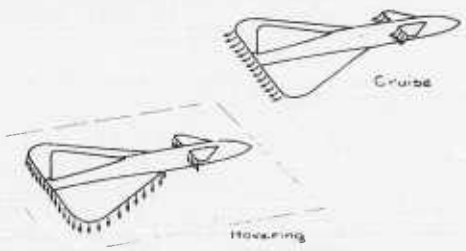

Figure 28b.

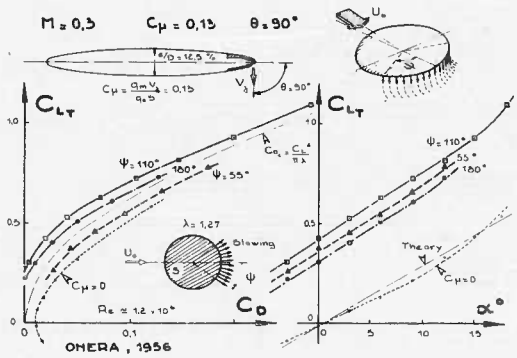

Figure 29.

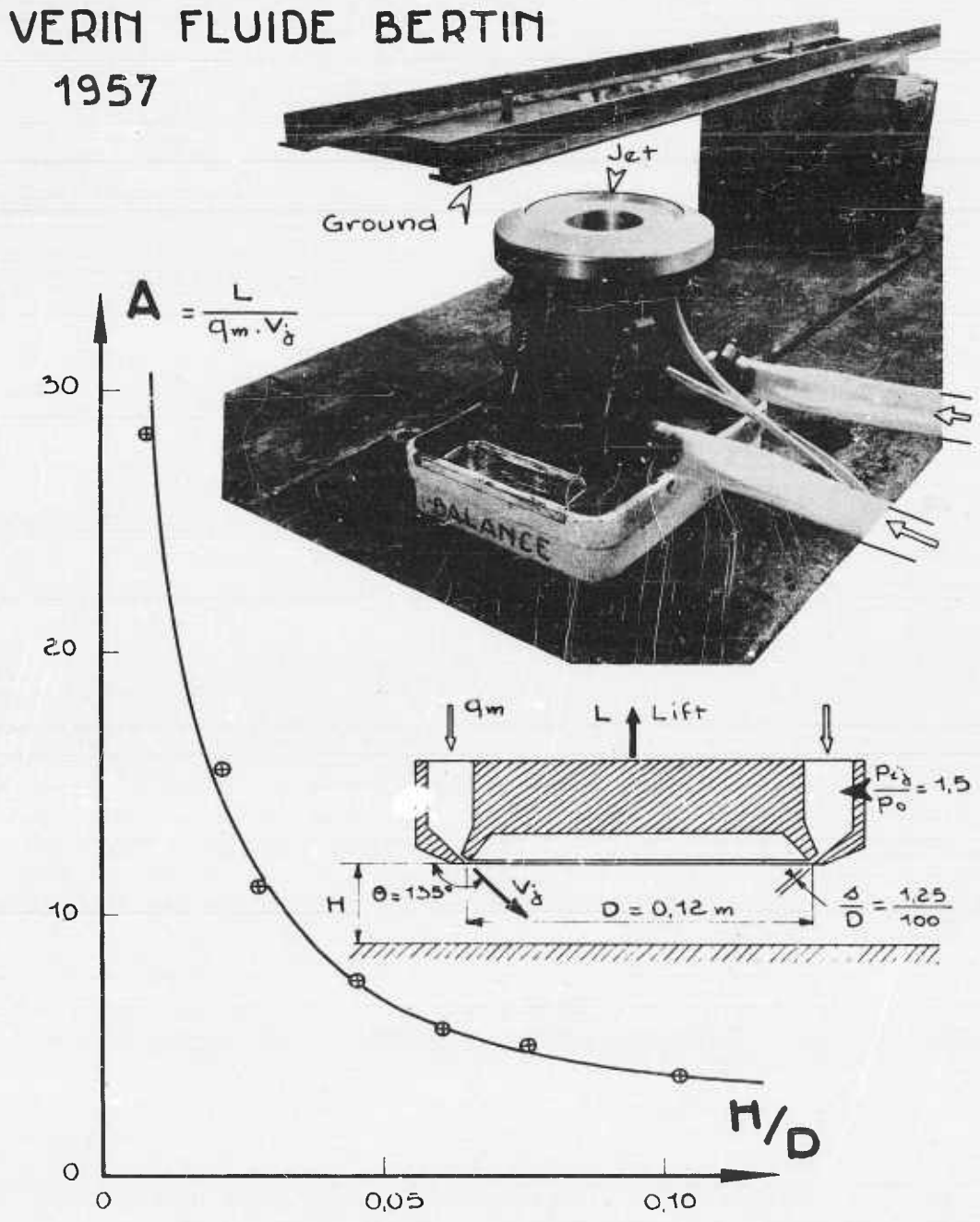
VERIN FLUIDE BERTIN
1957
Jet
Ground
BALANCE
A = L / qm . Vj
30
20
10
0
0
0,05
0,10
H/D
qm
L
Lift
Pj / Po = 1,5
H
θ = 135°
Vj
D = 0,12 m
δ/D = 1,25/100

Figure 30.

RESEARCH RELATED TO GROUND EFFECT MACHINES

By Richard E. Kuhn and Arthur W. Carter, NASA Langley

Research Center, Langley Field, Virginia

INTRODUCTION

NASA research related to ground effect machines has been directed primarily at obtaining basic data on the ground effect phenomena with a view to determining the potential scope and the limitations of its application. For the most part the investigations undertaken have been those for which the Langley Research Center has uniquely qualified personnel or facilities that may not be available to other researchers. For instance, the Hydrodynamic Towing Tank has been used for investigations of the effects of operating over water both statically and at forward speeds. Also, studies of the dynamic stability of ground effect machines have been made by the personnel of the Dynamic Stability Branch, who have had a vast amount of experience in studying the dynamic stability characteristics of aircraft by using dynamically scaled models. Work on the static hovering characteristics has been done both to support the work mentioned above and to investigate areas that had not been previously covered by others.

This paper reviews the results of this work and attempts to point out the more significant results.

SYMBOLS

L	measured lift, lb
D	measured drag, lb
D_e	effective total drag, lb
m	mass flow, slugs/sec
V_j	jet velocity, ft/sec
h	height above ground or free water surface, ft
V	forward velocity, ft/sec
h'	height above displaced water surface, ft
t	jet thickness at exit, ft
q_{max}	maximum dynamic pressure of air flow along ground, lb/ft^2
p_a	atmospheric pressure, lb/ft^2, gauge
p_T	total pressure, lb/ft^2, gauge
p_S	static pressure, lb/ft^2, gauge
p_b	base pressure, lb/ft^2, gauge

A_j jet area, $\frac{\pi}{4}\left(d^2 - d_b^2\right)$, ft^2

A_T total area, $\frac{\pi}{4} d^2$, ft^2

d outside diameter of annulus, ft

d_e equivalent diameter of oblong planform, ft

d_b base diameter, ft

di inlet diameter to plenum chamber, ft

P_a air horsepower at exit, $\frac{mV_j^2}{1100}$, hp

P_T total power $\frac{DV}{550} + \frac{mV_j^2}{1100}$, hp

M moment, ft/lb

$(L/D)_e$ effective lift-drag ratio

z depth of plenum chamber, ft

ϕ angle of bank, deg

α angle of attack, deg

ρ mass density of air, $slug/ft^3$

THRUST AUGMENTATION AND POWER REQUIREMENTS IN HOVERING

Effect of pressure ratio. The effects of pressure ratio and jet area to total area ratio on the thrust augmentation in hovering have been studied in an investigation employing small (4-inch and 8-inch diameter) nozzles and the laboratory air supply. A sample of the data obtained is presented in Figure 1. In these tests the mass flow was established out of the region of ground effect and held constant through the range of heights investigated. As a result, the pressure ratio did not remain constant but increased as the nozzle was brought closer to the ground (top of Figure 1). The augmentation ratio $\frac{L}{mV_j}$, however, was found to be independent of pressure ratio and mass flow within the range investigated. The data shown in Figure 1 are for a jet area of 40 per cent of the total area. Tests with other nozzles having ratios of jet area to total area ranging from 0.06 to 0.6 also indicated that the effect of pressure ratio was negligible or at least within the scatter of the data. A moderate increase in augmentation at intermediate heights was observed with increasing pressure ratio for the smallest jet area investigated $\left(\frac{A_j}{A_T} = 0.02\right)$.

Effect of jet area to total area ratio. Changing the ratio of jet area to total area, however, was found to have a significant effect on the augmentation factor, as shown in

Figure 2. Decreasing the jet area is seen to increase the augmentation factor, as would be expected, but only down to jet areas of 10 to 20 per cent of the total area. Below a jet area of 10 per cent the augmentation factor decreases rapidly. This decrease is due to the decay of these very thin jets which is caused by mixing with the outside air.

The data of Figure 2 are compared with the theory by Chaplin (references 1 and 2) in Figure 3. It is seen that in the present case the theory adequately predicts the trends but predicts augmentation factors somewhat higher than experiment, particularly at the lower height. The mixing theory also predicts the reduction in augmentation factor for thin jets at $h/d = 0.12$ and closely approximates the losses out of the ground effect region. In its present form, however, the mixing theory does not predict a loss in augmentation factor for thin jets at $h/d = 0.5$, whereas the experimental data definitely show the effects of mixing at this height.

Some observations concerning the effects of model size can also be made from the data presented in Figure 2. Most of the data were obtained with 4-inch- and 8-inch-diameter models. A few points obtained with a ducted-fan-powered 42-inch-diameter model are also included. Although perfect agreement is not obtained, Figure 2 indicates that there are no first order scale effects. The effect of scale can be expected to be only those associated with the change in Reynolds number of the flow.

The change in jet area was accomplished by changing the size of the internal plug (see insert on Figure 2). A jet area to total area ratio of 1.0 was obtained simply by removing the internal plug and thus leaving a simple nozzle. Note that significant augmentation is obtained with this simple nozzle and arises from the back pressure buildup as in a plenum chamber. This configuration is a plenum chamber in which the inlet diameter is equal to the skirt diameter. Further data on plenum chamber characteristics, including the effect of plenum chamber depth, and inlet diameter to skirt diameter ratio will be discussed later.

The data of Figure 2 indicate an optimum ratio of a jet area to total area of about 10 to 20 per cent as far as lift per lb of thrust is concerned. Lift per lb of thrust may not be the most important criteria, however. If minimum fuel consumption in hovering is desired, the maximum ratio of lift to power is the important criteria regardless of whether the machine is to be powered by a turbojet or an engine-driven fan. Note that for a given thrust the exhaust velocity, and therefore the power, will increase as the jet area is reduced. Thus the maximum ratio of lift to power would be expected to occur with a somewhat larger jet area than that for the maximum ratio of lift to thrust.

The data of Figure 2 have been converted to lift-power ratio in Figure 4. The data are presented for a loading of $\frac{L}{A_T} = 20\ \text{lb/ft}^2$. Changes in the loading will change the values of lift per horsepower obtained but will not change the shape of the curve. Note also that the power used is the air horsepower at the jet exit and does not include the efficiency of the pumping system or any losses in the ducting system.

As was expected, the maximum lift per horsepower occurs at jet areas much higher than those for maximum lift to thrust ratio. The data, of course, are strictly applicable to the type of configuration shown in the insert sketch, and if practical considerations limit the height of the vehicle they will force compromises which may make it impossible to achieve the results shown at the higher jet area to total area ratios.

Also, Figure 4 applies only to hovering characteristics. At forward speeds there are several additional power terms, one of which is the power to overcome the inlet momentum drag. The inlet momentum drag is the force required to accelerate the inlet mass flow

to the velocity of the vehicle, and the power required is the inlet momentum drag multiplied by the velocity of translation (power = mV^2). Thus, increasing the jet exit area (increasing mass flow m) results in increasing the power required at forward speeds. The designer is therefore faced with a compromise which can be resolved only on the basis of the intended mission of the vehicle.

Nevertheless, the data indicate that, all other things being equal, minimum power and therefore minimum fuel consumption in hovering requires the use of a relatively large ratio of jet area to total area.

Effect of discontinuities in annular jet curtain. Some data on the effects of leaving gaps in the curtain of an annular jet are shown in Figure 5. The data for the continuous curtain (100 per cent) were obtained with an 8-inch-diameter model. Those for the 40 to 80 per cent curtains were obtained with a 5-inch-diameter model made up of 12 discrete 1.05-inch by 0.06-inch jets (reference 3). The percentage of periphery covered was varied by cutting off the flow to symmetrically disposed jets. The jet width to diameter ratio was held constant at 0.0125.

Only small losses in augmentation factor result from leaving small gaps in the annular jet curtain. Large losses result, however, when only about 50 per cent of the periphery is covered by the jet curtain. Inasmuch as the conclusions concerning the effects of small gaps are based on a comparison of data from two different investigations and no data exist for curtains between 80 and 100 per cent coverage, further studies of the effects of gaps in this range would be desirable.

Comparison of annular jet and plenum chamber. When an annular jet is operating at a height which is less than the width of the annular jet exit, the critical flow area is transferred from jet exit area to the area between the outer lip and the ground, as in a plenum chamber. In this condition, the augmentation characteristics of an annular jet would be expected to approach those of a plenum chamber. In order to check this hypothesis, tests of a fan-powered 42-inch-diameter model were made, both as an annular jet with the base plate in and as a simple plenum chamber by removing the base plate. Also, with the base plate installed, surveys were made of the flow at the annular jet exit at heights both greater than, and less than, the jet thickness. The results are shown in Figures 6 to 8. For this model the jet area was 14 per cent of the total area and the jet width was 3.6 per cent of the diameter.

At very low heights the augmentation of the annular jet (Figure 6) falls well below the theory for the annular jet and closely approaches that for the plenum chamber. Even at heights considerably less than the jet exit width, however, the annular jet produces somewhat greater thrust augmentation than was measured on the simple plenum chamber. The differences are due to the differences in the flow developed.

The flow distribution at the exit of the annular jet at heights greater than jet thickness is shown in Figure 7. Under these conditions the static pressure varies linearly from the average pressure on the base plate at the inside edge to atmospheric pressure at the outside edge. The total pressure at the exit is distorted at all heights, because of the poor flow inside the model and the relatively small radius on the inside fairing.

At a height less than the jet exit width (Figure 8), the static pressure no longer varies linearly. Under these conditions the base pressure is approximately equal to the total pressure, and there is very little flow at the inside edge of the jet. The flow differs from that of a simple plenum chamber (to be discussed later), however, in that the flow is vertical at the exit and must curve outward as in an annular jet.

Simple plenum chamber theory. A simple expression for the thrust augmentation of a circular plenum chamber can be obtained from momentum considerations, if the plenum

chamber is assumed to be a pressure vellel from which air is leaking between the edge and the ground. Under this assumption the lift is given by

$$L = p_T \frac{\pi}{4} d^2$$

The momentum of the air escaping is equal to the thrust that would be obtained in a perfect nozzle at the same pressure

$$T = mV_j = \rho \pi dhKV_j^2$$

where K is the orifice coefficient of the gap between the edge of the plenum chamber and the ground.

The dynamic pressure of the air escaping will be equal to the internal pressure, and the exit velocity will then be given by

$$V_j = \sqrt{\frac{p_T}{\rho/2}}$$

Substituting in the expression for thrust

$$mV_j = 2p_T \pi dhK$$

if the orifice coefficient is assumed equal to 1.0 the augmentation factor is

$$\frac{L}{mV_j} = \frac{1}{8\frac{h}{d}}$$

Effect of plenum chamber geometry. In Figure 6 it can be noted that the measured augmentation for the plenum chamber falls somewhat below the theory given above and that the variation with height was somewhat steeper than that predicted by theory. These differences are due to the effects of the secondary flow induced within the plenum chamber (Figure 9), which are not considered in the simple theory. This flow is similar to that for a nozzle issuing through a flat plate near the ground as discussed in reference 4 and as depicted at the bottom of Figure 9. For either a simple plenum chamber or a flat plate (plenum chamber of zero depth) at some distance above the ground there is a secondary flow induced by the entrainment action of the primary flow of air outward along the ground, as shown in the bottom righthand corner of Figure 9. When the plate or plenum chamber is brought close enough to the ground so that the primary flow fills the gap between the ground and the edge of the plate or plenum chamber, the secondary flow changes to that of a trapped vortex between the plate and the ground. If the flat plate were brought closer to the ground than was possible in the present investigations, augmentation could be obtained at heights corresponding to air-bearing, or Levapad, operation. The orifice effect of the gap between the edge of the plenum chamber and the ground causes the development of an appreciable pressure in the plenum chamber to produce the augmentation shown. The effect of the trapped vortex is to reduce the augmentation considerably from that predicted by theory. The strength of this vortex and the augmentation obtained is strongly a function of the geometry as shown by the data of Figures 9 and 10. Increasing the inlet diameter to total diameter ratio d_i/d is a very effective means of increasing the augmentation factor, as can be seen in Figure 9. The simple nozzle, $\frac{d_i}{d} = 1.0$, is essentially an "ideal" plenum chamber in that the trapped vortex is eliminated. Note that the nozzle gives a thrust augmentation greater than that predicted by theory, indicating that the orifice coefficient of the edge is, as would be expected, less than 1.0.

The effect of changing plenum chamber depth is shown in Figure 10, and indicates that the maximum augmentation factor (for an inlet diameter to total diameter ratio of 0.15), will occur at depths of 5 to 10 per cent of the diameter unless the height is very low ($h/d < 0.01$). The reasons for this characteristic are not understood, but are probably associated with changes in the strength of the trapped vortex with depth.

The characteristics of plenum chambers can probably be improved appreciably if the flow from the inlet can be deflected so as to "fill" the plenum chamber and eliminate or reduce the strength of the trapped vortex. Further work is needed in this area as well as on the effect of depth at other inlet diameter to total diameter ratios.

Annular jet characteristics over water. The thrust augmentation characteristics of a 42-inch-diameter model were measured over water as well as over fixed ground (Figure 11). The results indicate a reduction in augmentation factor over water when the height is measured from the free water level. However, the water surface below the base plate is being displaced by the base pressure. When this displacement is calculated using the measured base pressure, and the thrust augmentation is presented with respect to the height from the displaced water level, an augmentation slightly greater than that obtained over fixed groundboard is obtained. This improvement in augmentation is probably due to the effect of the local distortion of the water surface under the annular jet causing a greater curvature of the jet curtain, similar to that obtained if the jet were inclined inward.

Spray. Photographs of the spray experienced with the 42-inch-diameter annular jet models are shown in Figure 12 for several conditions. These pictures were taken during the tests of thrust augmentation factor over water, and were run at constant fan rpm. As a result, the lift is not constant, but decreases rapidly with increasing height. The reduction of spray shown then is not primarily a function of height, but a combination of factors.

The primary factor determining the onset of spray with hovering aircraft has been found to be the dynamic pressure of the air flowing radially outward along the surface of the water. In reference 5 and from related observations in winds on the open ocean (reference 6), it was found that spray would not be formed if the maximum dynamic pressure of the outward flow of air did not exceed about 1.5 to 2.5 lb/ft^2.

The outward flow of air from the 42-inch-diameter annular jet along the groundboard was surveyed at several stations, and the maximum dynamic pressure measured is plotted in Figure 13 as a function of height. These data have been used to estimate the dynamic pressure over the water for the picture shown in Figure 12. In general, below a dynamic pressure of 2.2 to 2.4 lb/ft^2, spray was not observed.

The effects of the spray in hovering can be appreciably reduced by the addition of spray deflectors as shown by the photographs of Figure 14. These deflectors effectively intercept the spray and deflect it out laterally, away from the model. Care must be exercised in locating spray deflectors, however, that they are not placed too low or made too wide so that, when operating over ground, they create a download due to the induced secondary flows as shown for flat plates in Figure 9.

FORWARD SPEED CHARACTERISTICS

Effects of water on drag. To determine any differences that may exist between operating an annular jet over water and over a fixed surface, an investigation was made in the hydrodynamic towing tank using the 42-inch-diameter model. For this investigation, plywood groundboards were installed in part of the tank to simulate the fixed surface.

One effect of operating over water has already been discussed. In hovering, the water level is displaced below the model. There had been some concern that at forward speeds

there would be a large drag associated with this displacement of the water, similar to that experienced by a ship's hull. Such a displacement wave drag, if expected at all, would only be experienced under deep water conditions. For the depth of the tank used for these tests (12 ft), the critical speed is about 18 ft/sec. Above this speed the tank would correspond to shallow water and displacement wave drag would not be expected. Below this speed the tank corresponds to deep water and displacement wave drag would be experienced on a conventional hull. If a displacement drag were associated with the operation of an annular jet over water, it would only be experienced in the present tests at speeds below about 18 ft/sec.

As can be seen in Figure 15, there is no significant difference between the drag measured over water and over the groundboards. There are several factors involved in the fact that no difference in drag could be measured. First of all, an appreciable displacement of the water was observed only in hovering and at very low speeds. A ground effect machine displaces water through the action of the base pressure. At forward speeds this base pressure is felt by a particle of water under the machine only for a finite period of time: the time required for the length of the machine to pass over a given point. Thus the greater the speed the shorter the time that the base pressure has to act on a given particle of water and the smaller the displacement of the water. In the present tests an appreciable displacement of the water and the associated displacement wave train were observed only at speeds of less than about 5 ft/sec. At this speed the drag is so low that accuracy considerations preclude detecting any difference in the drag that may arise over water.

In the present tests also, the model was held at zero angle of attack. At zero angle of attack and with a flush bottom as used on this model there is no obvious way that the effects of displacing the water could be transmitted to the model, so that they would show up as a change in drag. If the model had been free to trim, however, the inherent stability at a height of 0.05d would have caused the model to attempt to align itself with the displaced water contour. This displaced water contour, which is displaced in accordance with the period of time the base pressure has to act, would assume a slope such as shown in Figure 15, with the greatest displacement at the rear of the model. Thus, the model would seek to trim in a nose-up attitude and the lift vector would be inclined rearward, producing a drag force as a component of the inclined lift vector. A ground effect vehicle over water, however, does not necessarily have to be allowed to trim nose up. If controls are made powerful enough, zero attitude could be maintained. However, there probably would be a power or weight penalty associated with these controls.

Effect of water on lift. Merely keeping the machine level, so as to minimize the effects of water on drag, however, does not make it possible to eliminate the effects of the water. As already mentioned in the discussion of the hovering thrust augmentation over water, the water is displaced by the base pressure and the machine will ride lower, with respect to the free water level, than over ground. This accounts for the difference in lift between the over-water and over-fixed groundboard curves at zero velocity in Figure 16. The lift that would be experienced at a height of 5 per cent of the diameter measured from the displaced water level at zero speed is shown by the flagged symbol. At forward speeds the exact displacement of the water is not known, except that at speeds above about 15 to 20 ft/sec no noticeable displacement of the water could be seen. Thus, the lift over water would probably follow a curve such as that shown by the dotted line, if height is measured from the displaced water level. The greater lift experienced over water (measured from the displaced water level) than over fixed ground is believed to be due to the local distortion of the water surface due to the impingement of the jet, which causes an increased curvature of the jet similar to that due to inclining the jet inward. This increased lift would not be expected if the jet were already inclined at the optimum angle.

Variation of lift with speed. In references 7 and 8 a large loss in lift at forward speed (as compared to hovering) was reported. A slight loss in lift is shown in Figure 16

for the 42-inch model as tested at a height of 0.05d over fixed groundboards, but this decrease in lift is much less than that reported in references 7 and 8. Figure 17 presents the thrust augmentation curve at several velocities, and again shows a negligible effect of velocity, except at heights of about 1 diameter and above, where lift increases with speed (also shown in Figure 16). In the present tests the power-off lift at forward speeds was zero for all heights.

There are many differences between the present model and testing environment, and that reported in reference 7. The model of reference 7 was tested in a wind tunnel with a fixed groundboard, with a boundary layer on the groundboard. The present tests in the tank avoided any interaction with such a boundary layer by moving the model with respect to the air and groundboard. In order to obtain some information which might help to determine whether this boundary layer was contributing to the losses in lift, the 42-inch model was also tested in the 17-ft test section of the Langley 300-MPH 7- by 10- ft tunnel. A comparison of the results obtained there and on the towing carriage of the tank over fixed groundboards (Figure 18) shows negligible differences, and indicates that, for the present model at least, the boundary layer was not a problem. This does not necessarily prove, however, that such a boundary layer can always be ignored.

Experience with jet flap models has shown that tests of such models in a wind tunnel with a boundary layer on the groundboard give much larger losses in lift than tests of the same model on a moving carriage over a ground without a boundary layer. In the case of the jet flap models, the jet sheet was very thin: of the same order thickness as the boundary layer, whereas, in the present tests of the 42-inch annular jet model, the jet thickness was of the order of 10 times as thick as the boundary layer. It should be noted that the model of reference 7 also used an extremely thin jet, and thus either the interaction with the boundary layer on the groundboard or simply the mixing and decay of the jet curtain itself could have contributed to the losses experienced.

Effect of speed on base pressures and exit velocity distribution. The pressures on the base of the 42-inch-diameter model along the plane of symmetry were measured at 5 stations as shown in Figure 19. Over water, the base pressure increased with increasing velocity, and the increase was predominantly on the rear part of the base. It should be remembered here that the distance from the displaced water level changed with speed.

The distribution of exit velocity of the jet and the effects of speed on this distribution are shown in Figure 20. No attempt was made to obtain good internal flow characteristics on this mode. The flow from the fan was simply dumped into the plenum chamber above the base plate and allowed to seek the path of least resistance to the exit. Six 1/2-inch-diameter base support members and the pressure tubes from the base pressure taps traversed this plenum chamber. As a result, the exit velocity distribution is not as uniform as might be desired.

The effects of forward speed on the distribution, however, were found to be small. The main effect of forward speed was a small increase in mass flow, due to some ram pressure recovery at the inlet, with the accompanying increase in exit velocity.

Drag and power breakdown. As discussed previously, tests over water showed no measurable difference in drag when compared with tests over ground. In both instances, however, considerable drag was present. The breakdown of drag, at a lift of 40 lbs, is shown in Figure 21. No attempt at streamlining was made on this model and as a result the parasite drag is high. The measured power-on drag, however, is considerably smaller than the sum of the inlet momentum drag and the parasite drag. This result is similar to that experienced with jet flap configurations in which induced thrust is obtained even with the jet sheet deflected 90° (vertical) at the exit (reference 9). The effect of the inlet flow in clearing up some of the flow on the upper surfaces of the model may also contribute to the differences shown.

The power breakdown is shown in Figure 22. This is the air horsepower required; that is, assuming a 100 per cent efficient thrust system and pumping system and zero duct losses. The jet power increases slightly for the model because of the increase in mass flow with forward speed. The propulsion power, of course, includes the rather high parasite power of the present model. In order to reduce the power required at forward speeds it is necessary to apply the conventional aerodynamic techniques of streamlining to reduce parasite drag and to decrease the mass flow. Note, however, that if the mass flow is decreased in hovering the power required in hovering will increase. It may be possible to decrease the mass flow required at forward speeds without decreasing it at hovering, if the vehicle can be properly shaped so that conventional aerodynamic lift can be obtained which thereby reduces the jet and base pressure lift required at forward speeds.

Effective lift-drag ratio. The total power required can be used to calculate an effective drag and effective lift-drag ratio as follows:

$$P_T = \frac{D_e V}{550}$$

then

$$\left(\frac{L}{D}\right)_e = \frac{LV}{550 P_T}$$

The effective lift-drag ratio for the 42-inch-diameter model, using the total power required from Figure 22 is presented in Figure 23. The lift-drag ratios obtained are quite small. Even if the parasite drag were reduced to zero, the lift-drag ratios are small when compared to those of a conventional airplane (12 to 15) or to a helicopter (5 to 7). Clearly, if a ground effect machine is to achieve appreciable range, considerable improvement in the lift-drag ratio will have to be obtained. Improved streamlining will help (but only to the extent shown for zero parasite drag in Figure 23). Perhaps some marriage of the ground effect machine with a conventional airplane can be achieved, such that the ground effect phenomena are only used in hovering and at low speeds.

Spray at forward speeds. In the discussion of spray in hovering, it was pointed out that spray is a function of the velocity of the air with respect to the water. At forward speeds, the effect of the forward velocity on the velocity of the air over the water must also be considered. At the rear of the model, the velocity of the air with respect to the water is reduced; at the front of the model, the extent of forward projection of the air sheet from the jet is reduced, and if sufficient forward speed is achieved, the jet does not flow forward along the water surface at all. Thus, as forward speed is increased, the spray at the front and rear of the model is decreased, and most of the spray is formed at the sides. Also, the spray that is formed is quickly left behind, so that there is an appearance of much less spray, as shown in Figure 24. However, as disk loading is increased (Figure 24 corresponds to a disk loading of 4 lb/ft^2), the spray formation ahead of the model will be maintained to correspondingly higher speeds than those shown in Figure 24.

ATTITUDE STABILITY AND CONTROL

Stability. The stability and control characteristics of ground effect machines have been studied by the personnel of the Dynamic Stability Branch. Some effects of base plate configuration on the lateral stability of an oblong configuration are presented in Figure 25. The moments are nondimensionalized by dividing by the lift times the diameter of a circle having the same planform area (d_e), so that the moment parameter M/Ld_e represents the ratio of the shift in the center of the lift force to the effective diameter. Thus, if

$M/Ld_e = 0.01$, the center of lift is 1 per cent of the diameter off of the moment reference point.

On the left side of Figure 25, the movement of the center of lift per degree of bank angle is shown as a function of height. The model with the slot and the 45° jet is stable up to a height of $0.1d_e$. Closing the slot or changing the jet to vertical causes a decrease in the limiting height for stability. Figure 26 shows the marked dependence of the stability on the shape by the very much greater longitudinal stability at low heights, as compared to the lateral stability for this oblong model. The stability shown is that obtained at small tilt angles. The shapes of the moment curves for the model with the slot and 45° jet are shown on the right of Figure 25 for 3 heights. At low heights the configuration is stable for small tilt angles, but unstable for large tilt angles. This, however, is not a general observation. Some configurations have been observed which show an increase in stability at the larger tilt angles, as was observed for the longitudinal stability shown in Figure 26.

Effect of speed on stability. The effect of speed on moment and stability is shown in Figure 27 for the 42-inch-diameter model. The data show a large forward shift of the center of lift with speed. This forward shift is believed to be due largely to the nose-up moment arising from the inlet momentum drag. The data of reference 7, on the other hand, show a diving moment at forward speeds. Air was supplied to the model (reference 7) through the model support from the laboratory air supply. The inlet momentum drag and its contribution to pitching moment was therefore excluded from the data of reference 7. The diving moment probably arises from the jet flap effect of the jet curtain, which causes an increase in pressure on the rear part of the base plate (Figure 19), and a decrease in pressure on the rear-part upper surface of the model. With the 42-inch-diameter ducted fan model (Figure 27), the nose-up moment contribution from the inlet momentum drag was apparently greater than the nose-down moment from the jet flap effect.

The model exhibits about the same level of stability in hovering as the lateral stability of the oblong model, but as speed is increased the stability decreases, as would be expected for a wing with the moment reference point at the center of area.

Control. One observation concerning the control effectiveness can be made from the data of Figure 28. In this test, a moment was created by blocking off part of the flow area on one side. The control effectiveness decreases markedly with decrease in height. This decrease is due to the decrease in momentum thrust available to manipulate for control. As the height is decreased, the augmentation factor increases and the momentum thrust required to hold a given lift decreases. Note also that in Figures 25 and 26 the stability increased with decrease in height. Thus, a given control deflection will produce a much smaller tilt angle at the lower heights.

CONCLUDING REMARKS

The results of NASA research on the lift augmentation of annular jets in proximity to the ground are in general agreement with other work, in that large lift augmentation can be obtained. However, the height involved is only a small percentage of the diameter. Large losses in lift augmentation are encountered with thin jets (jet thickness less than about 3 per cent of the diameter), as predicted by Chaplin's mixing theory due to the decay of these thin jets. Inherent attitude stability is a function of the base plate configuration, but, in general, it is limited to heights of 10 per cent of the diameter or less.

The lift augmentation obtained with a simple plenum chamber depends primarily on the ratio of inlet diameter to skirt diameter, and, to a limited extent, on the plenum chamber depth. Unless the inlet diameter is essentially equal to the overall diameter, the lift augmentation obtained falls well below that predicted by plenum chamber theory.

At forward speeds, tests of an annular jet model having a moderately thick jet did not show the large loss in lift experienced by previous investigations. The reasons for the difference in results are not presently known, but it may be associated with the effects of jet interaction with the boundary layer on the groundboard used in the previous wind tunnel tests and/or the effects of using very thin jets. Because of the large inlet momentum drag, the effective lift-drag ratio of an annular jet configuration is relatively low.

The effects of operating over water are primarily the generation of a large amount of spray and a reduction in hovering height for a given weight due to the displacement of the water by the base pressure. The spray problem, however, can be appreciably reduced by the addition of spray deflectors.

Because large lift augmentation can only be obtained at very low height-to-diameter ratios, any vehicle built to operate entirely on the basis of this ground effect phenomena will be restricted to operating over relatively smooth terrain or it will have to be very large. Also, the inlet momentum drag arising at forward speeds will probably have to be reduced by transferring some of the lift to something approaching airplane-type wings (to reduce the jet thrust and base lift required) if reasonably high speeds and long ranges are expected.

REFERENCES

1. Chaplin, H. and Stephenson, B., "Preliminary Study of the Hovering Performance of Annular Jet Vehicles in Proximity to the Ground." AERO REPT. 947, TED TMB AD-3242, August 1958.

2. Chaplin, H., "Effect of Jet Mixing on the Annular Jet." AERO REPT. 953, TED TMB AD-3242, February 1959.

3. Davenport, E. E., Kuhn, R. E., and Sherman, I. R., "Static Force Tests of Several Annular Jet Configurations in Proximity to Smooth and Irregular Ground." NASA TN D-168, 1959.

4. Spreemann, K. P. and Sherman, I. R., "Effects of Ground Proximity on the Thrust of a Simple Downward-Directed Jet Beneath a Flat Surface." NACA TN 4407, 1958.

5. Kuhn, R. E., "An Investigation to Determine Conditions under which Downwash from VTOL Aircraft Will Start Surface Erosion from Various Types of Terrain." NASA TN D-56, 1959.

6. Russell, R. C. H. and MacMillan, D. H., "Waves and Tides." Hutchinson's Scientific and Technical Publications, 1952.

7. Tinajero, A. A., "Comparison of Experimental and Theoretical Design Parameters of a 6-Inch-Diameter Annular Jet Model with a Jet Angle of -45° Hovering in Proximity to the Ground; and Experimental Results for Forward Flight at Zero Angle of Attack." AERO REPT. 954, TED TMB AD-3242, May 1959.

8. Matthews, G. B. and Wosser, J. L., "Ground Proximity: A Critical Review." IAS Paper 59-121. Presented at the IAS National Summer Meeting, Los Angeles, California, June 16-19, 1959.

9. Lowry, J. G., Riebe, J. M., and Campbell, John P., "The Jet-Augmented Flap." IAS Preprint 715. Presented at the 25th Annual Meeting, January 28-31, 1957.

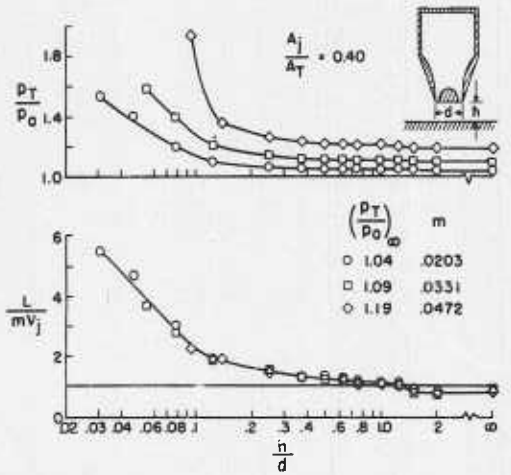

Figure 1. Effect of pressure ratio on the thrust augmentation of a 4-inch-diameter annular-jet model. (Mass flow constant)

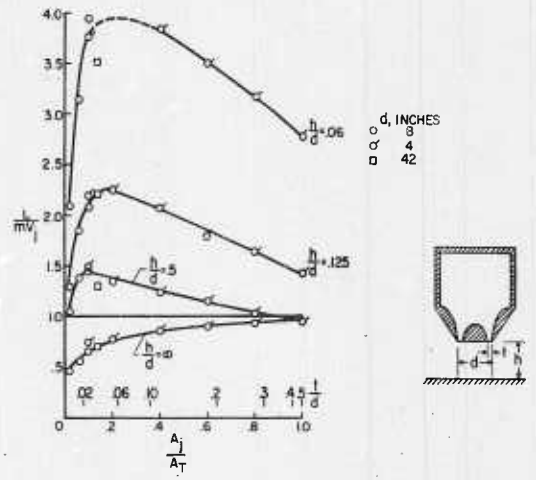

Figure 2. Effect of ratio of jet area to total area on thrust augmentation.

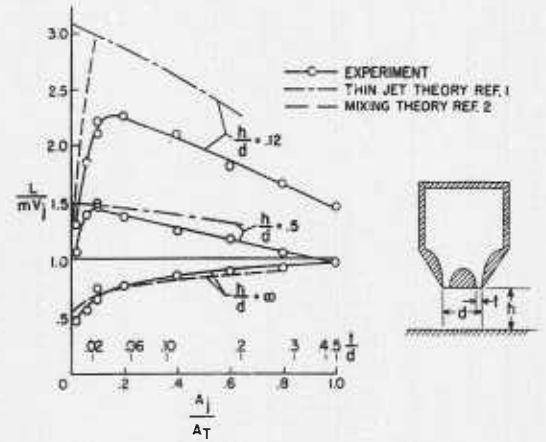

Figure 3. Comparison of theory and experiment.

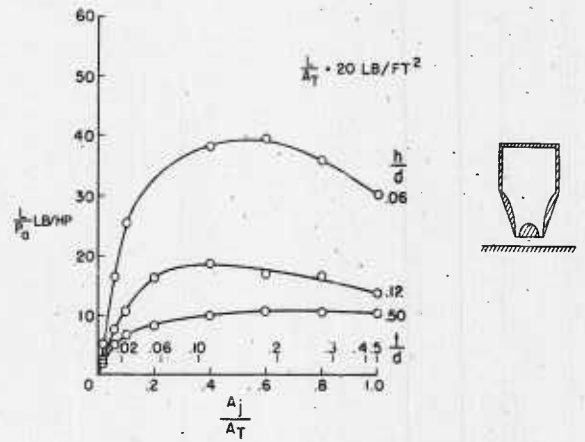

Figure 4. Effect of ratio of jet area to total area on lift per air horsepower at exit.

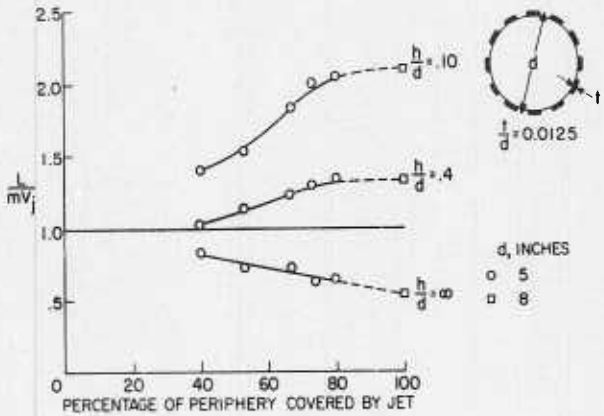

Figure 5. Effect of gaps in annular-jet curtain.

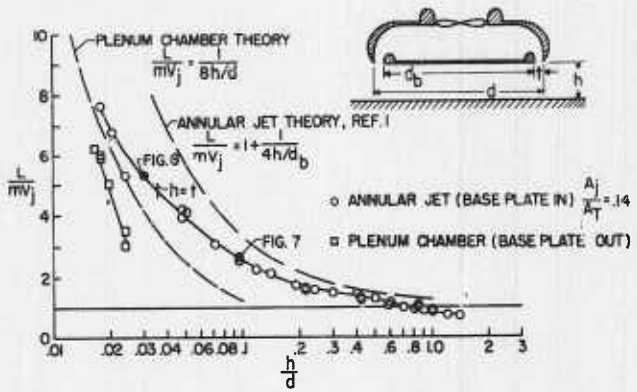

Figure 6. Comparison of annular jet and plenum chamber. (42-inch-diameter model)

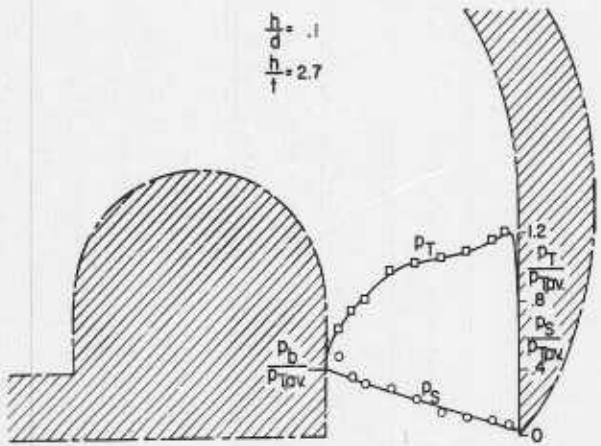

Figure 7. Flow distribution at exit of 42-inch-diameter annular-jet model at height greater than jet thickness.

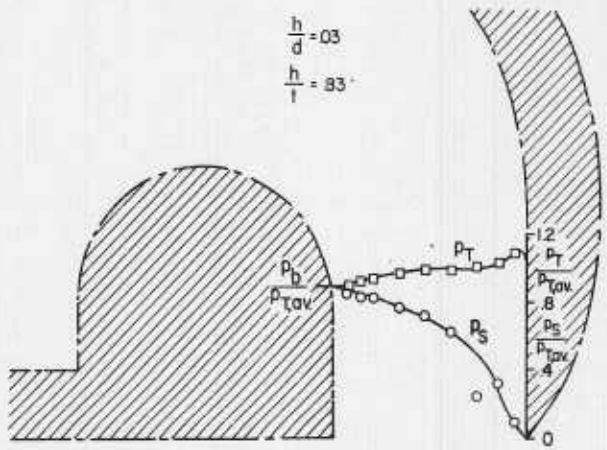

Figure 8. Flow distribution at exit of 42-inch-diameter annular-jet model at height less than jet thickness.

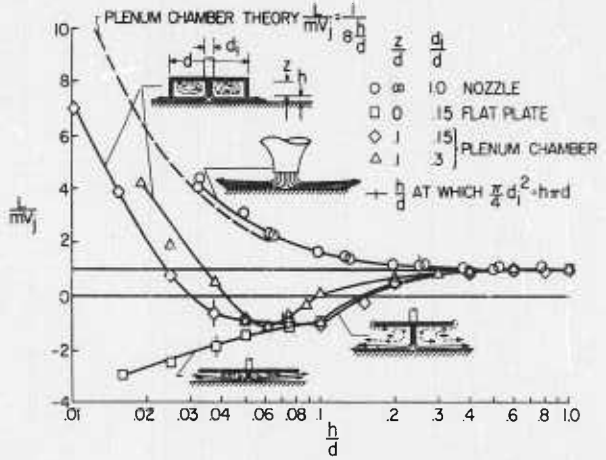

Figure 9. Comparison of characteristics of nozzle, plenum chamber, and flat plate, including effect of plenum-chamber inlet diameter

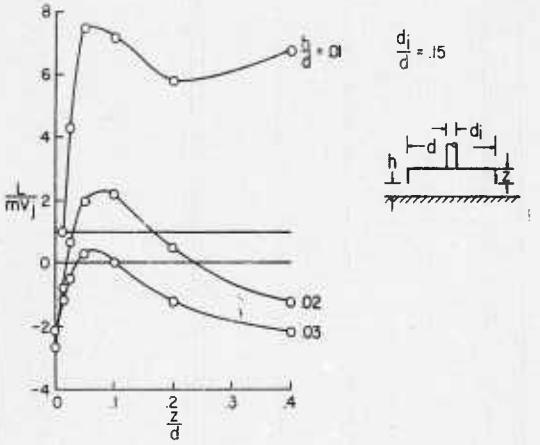

Figure 10. Effect of plenum-chamber depth on thrust augmentation.

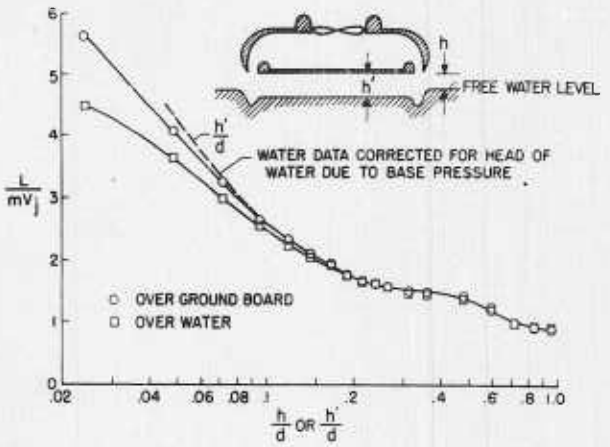

Figure 11. Comparison of thrust augmentation obtained over water and over fixed groundboard.

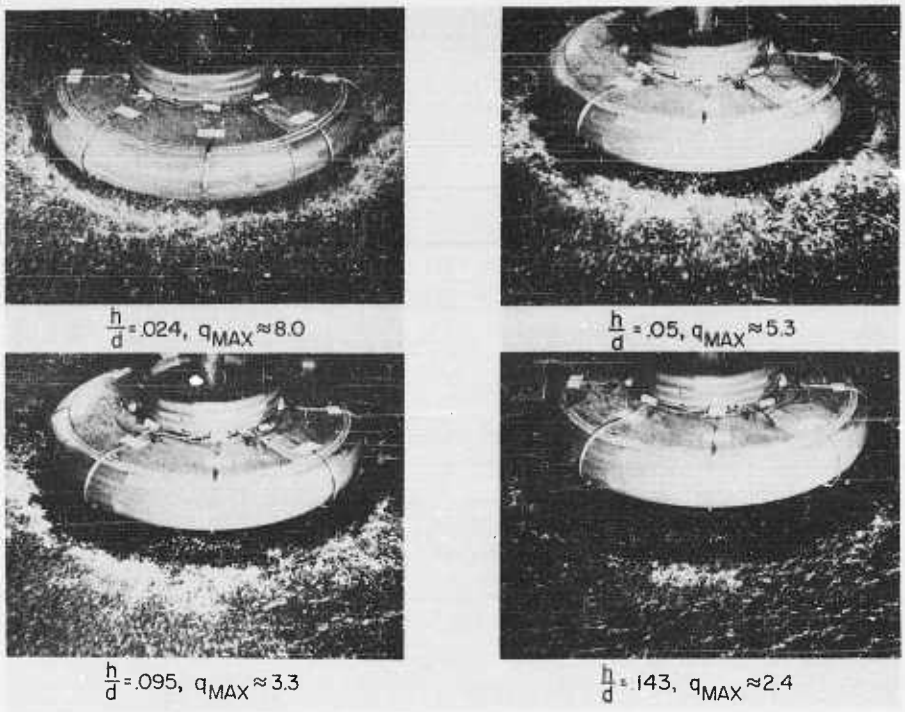

Figure 12. Spray experienced with 42-inch-diameter model in hovering.

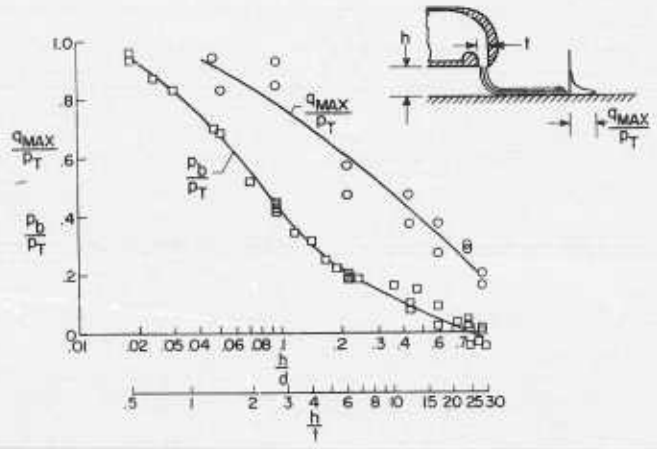

Figure 13. Variation of maximum dynamic pressure of flow parallel to ground and base pressure with height.

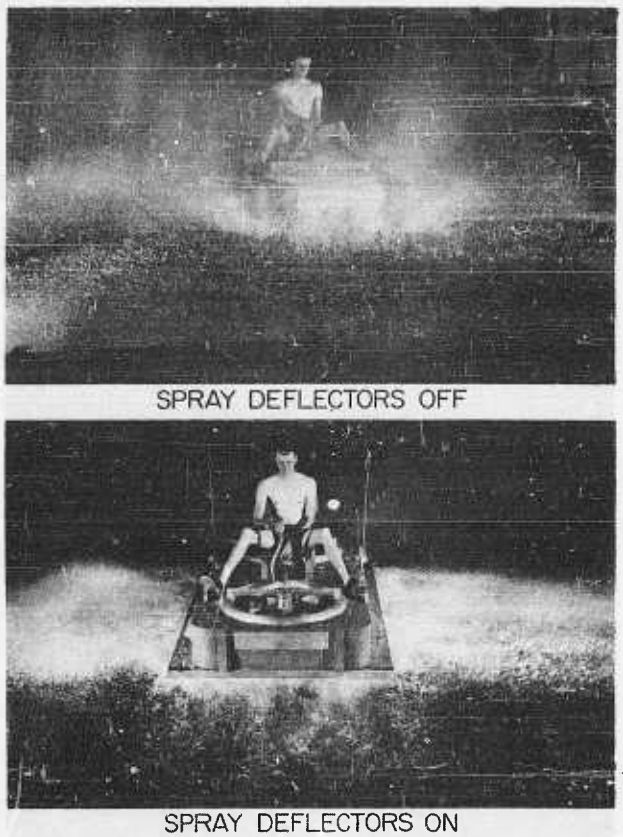

Figure 14. Effect of spray deflectors.

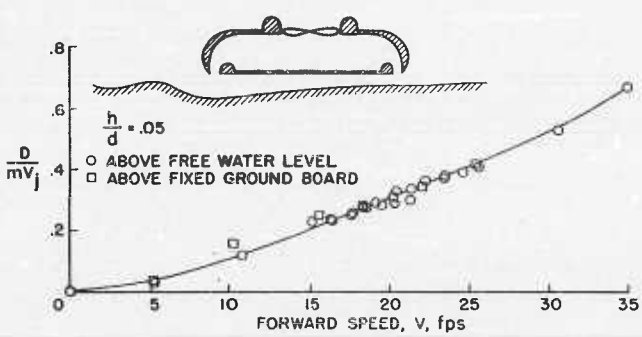

Figure 15. Comparison of drag of 42-inch-diameter model over water and over fixed groundboard. ($\alpha = 0$)

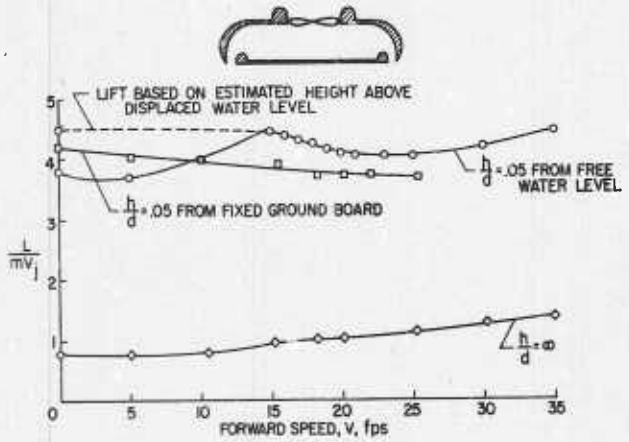

Figure 16. Comparison of lift of 42-inch-diameter model over water and over fixed groundboard. ($\alpha = 0$)

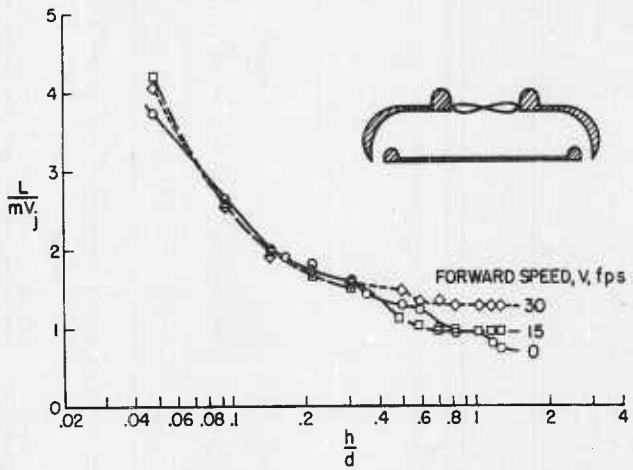

Figure 17. Effect of forward velocity on thrust augmentation. (42-inch-diameter model, $\alpha = 0$)

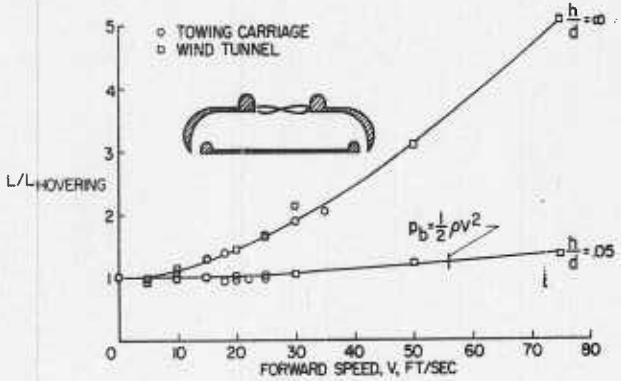

Figure 18. Comparison of testing techniques. ($\alpha = 0$)

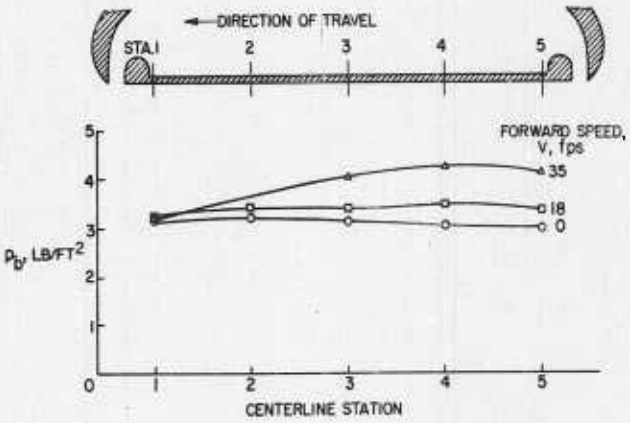

Figure 19. Effect of forward velocity on base pressure over water. (42-inch-diameter model, $\alpha = 0$, $h/d = 0.05$)

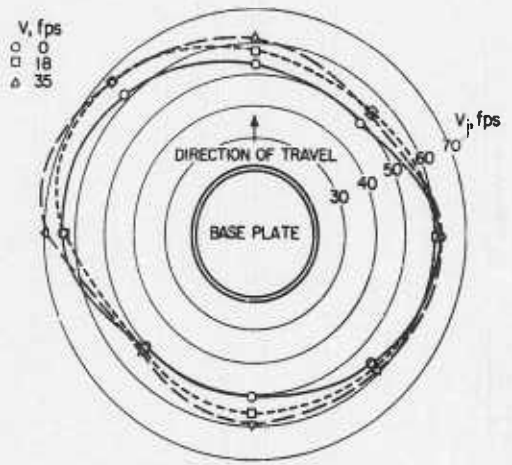

Figure 20. Effect of forward velocity on exit velocity distribution. (42-inch-diameter model, $\alpha = 0$, $h/d = 0.05$)

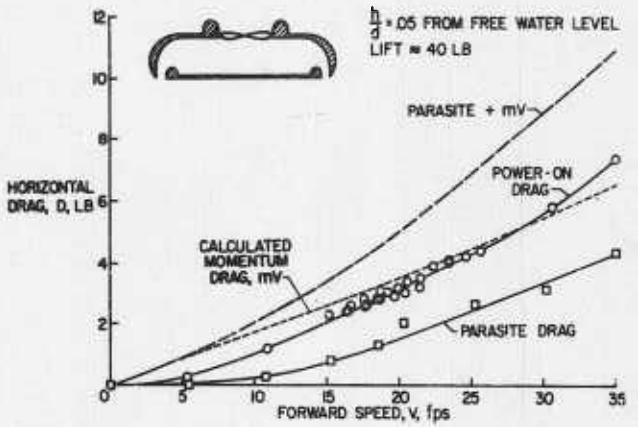

Figure 21. Drag breakdown for the 42-inch-diameter model. ($\alpha = 0$)

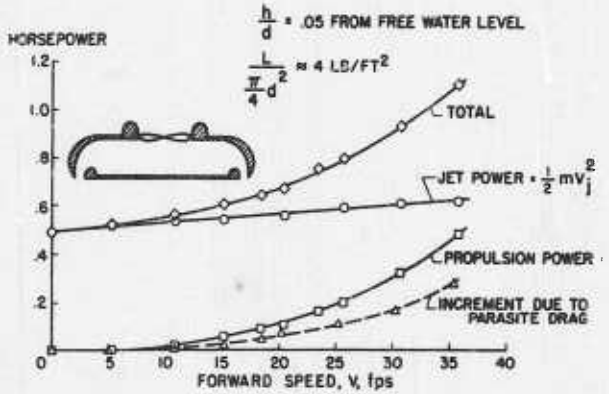

Figure 22. Power required by the 42-inch-diameter model. (Lift = 40 lb, $\alpha = 0$)

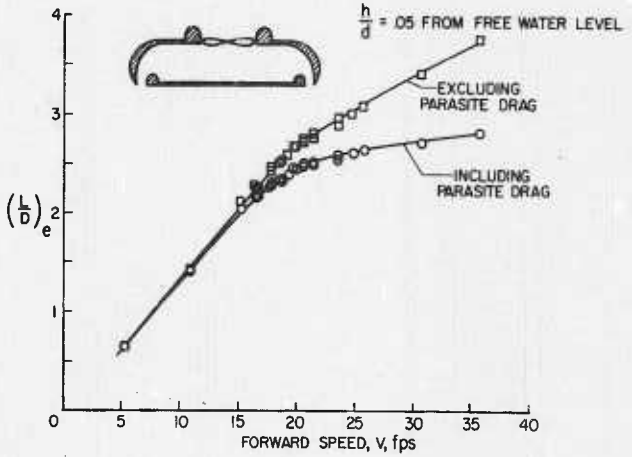

Figure 23. Effective lift-drag ratio of the 42-inch-diameter model. (Lift = 40 lb, $\alpha = 0$)

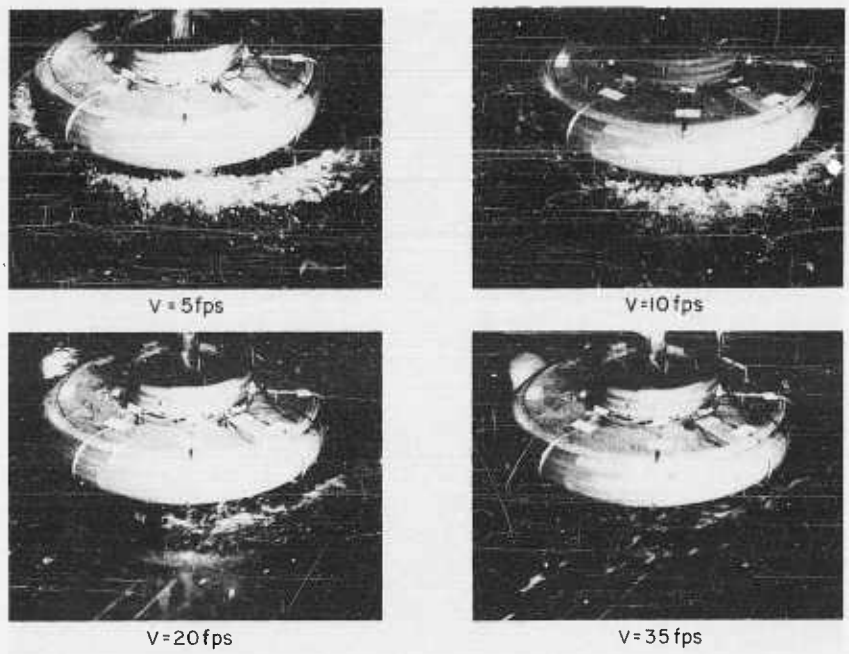

Figure 24. Effect of forward speed on spray from 42-inch-diameter model. (h/d = 0.05).

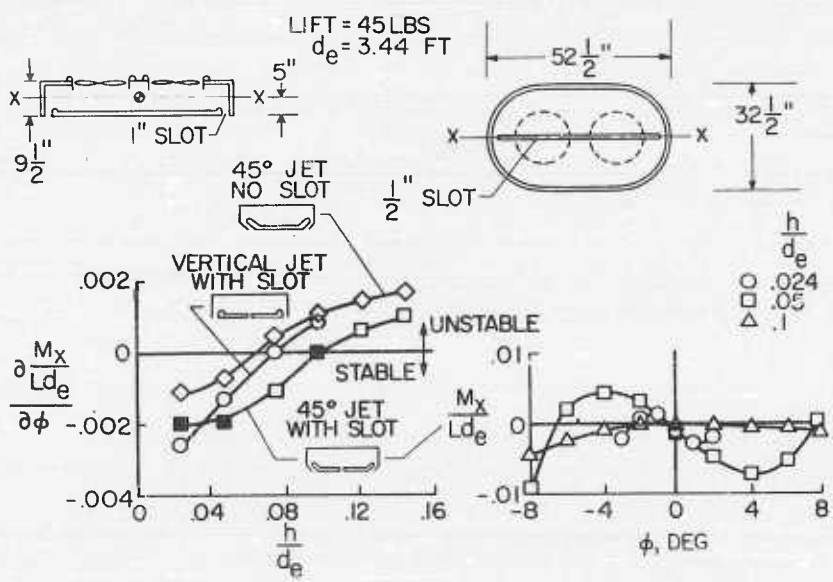

Figure 25. Effect of base configuration on lateral stability.

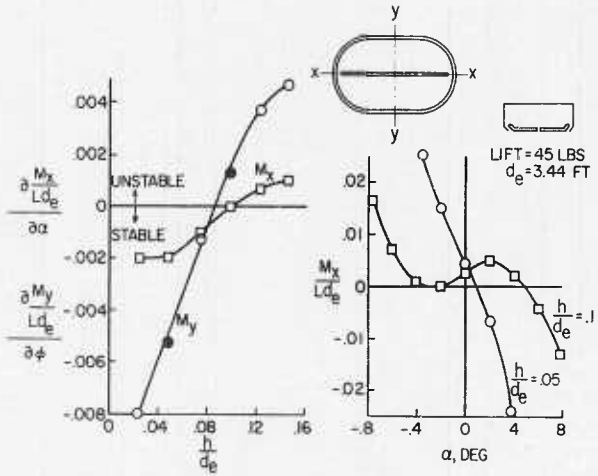

Figure 26. Comparison of longtidunal and lateral stability of an oblong configuration.

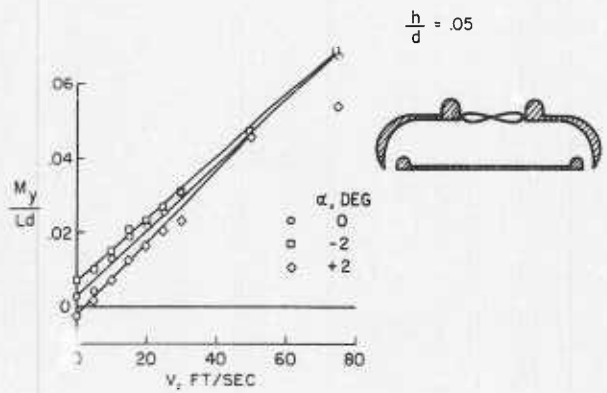

Figure 27. Effect of forward speed on pitching moment and stability of 42-inch-diameter model.

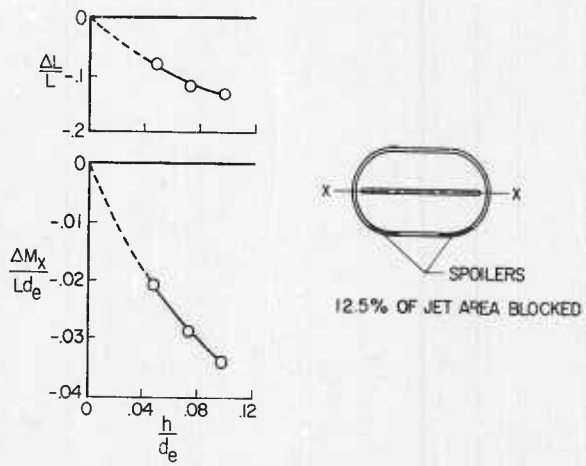

Figure 28. Effect of height on control effectiveness.

A REVIEW OF THE PRINCETON GROUND EFFECT PROGRAM

By W. B. Nixon and T. E. Sweeney, Department of Aeronautical Engineering, Princeton University, Princeton, New Jersey

ABSTRACT

Pressure distribution and smoke visualization studies have been conducted on a two-dimensional annular jet model in hovering flight. The behavior of the base cavity vortex with variations in height, initial jet angle, and inclination is plotted, and the effect upon static instability is discussed. Some observations are made on the unsteady flow pattern which develops at a critical height.

A set of three-dimensional models, geometrically similar, were tested to investigate the possibility of a scale effect. The results to date are inconclusive. The pressure distributions provide some understanding of the inflections in the augmentation curve and the nature of the unsteady flow pattern above a critical height. The same models tested as plenums illustrate the detrimental influence upon performance that may be encountered with certain configurations.

Present work with wind tunnel and forward flight models is mentioned, and there are a few remarks on the free flight vehicles that have been tested.

INTRODUCTION

The past effort of the Princeton research program in ground effect phenomena has been directed mainly toward experimental work which was exploratory in nature and which would provide a qualitative insight into some of the characteristics of these devices. There has been no attempt to systematically and thoroughly investigate a given set of parameters for the purpose of establishing design criteria, but a quantitative approach was chosen when it was considered necessary to the comprehension of fundamentals.

Three general phases are discussed in this paper. The first series of experiments dealt with a two-dimensional annular jet model in simulated hovering flight, and the text presented here is essentially that of a report by the authors, now being printed, which is entitled "Some Qualitative Characteristics of a Two-Dimensional Peripheral Jet." The second phase discusses the status of work with several three-dimensional models constructed for general scaling, aspect ratio, planform, plenum, and forward flight experiments. The final part consists of some observations on the behavior of several free flight models and man-carrying machines.

TWO-DIMENSIONAL EXPERIMENTS

Apparatus. The experimental apparatus used for this study is shown in the drawing of Figure 1. The blower provided pressure ratios as high as 1.1, although much of the experiment was performed at lower pressure ratios. This parameter was dictated by the capacity of the smoke generator, which, due to mixing of the jets with the more quiescent enclosed air, could provide visible smoke only at much lower jet velocities. The model was made of wood; however, the nozzle blocks were of machined aluminum, carefully spaced and aligned to assure symmetry with regard to slot width and angle of blowing ($\Theta_o = 0^o$).

Discussion. Since lift augmentation at constant mass flow was not of particular importance to these experiments, no attempt was made to maintain a constant slot velocity

for the altitude range under study. Rather, a constant blower power setting was established, which permitted $\triangle$ P and mass flow variations much as they would occur in a free flight machine with a given air horsepower capability.

Manometer readings were recorded for several values of h/b and angles of inclination (α). These results are presented in Figures 2 and 3. Figure 2 shows the typical variations in base pressure with altitude for zero angle of inclination in the static condition. The very gentle wave shape of the pressure distribution at high h/b is observed to develop into rather pronounced peaks, separated by a broad flat valley as h/b is reduced. Such pressure distribution characteristics suggested the presence of a vortex, which was deduced to appear as shown in Figure 2. Smoke studies confirmed the presence of the vortex and its behavior with altitude. It is interesting to note that the diameter of the vortex appears to be equal to the distance of the model from the ground plane.

As indicated by the pressure distributions and as observed during the smoke studies, the vortex tends to maintain a constant circulation, since at the higher values of h/b the vortex is large and slow, becoming faster as its size is reduced with decreasing altitude.

Figure 3 shows the base pressures for several values of α. It should be observed that the shape of these curves is such as to move the center of pressure toward the high end of the model, which, of course, indicates static instability. It should be noted that the two segments of a vortex, as shown in Figure 2, are tangent to the base of the level model. However, with increasing angle of inclination, the vortex segment on the high end separates from the base of the model, thus permitting the higher center base pressures to influence this region. The vortex segment on the low end of the model, however, is flattened slightly by tilting the model, causing the vortex to attach to the base to a greater extent than in the zero angle of inclination case. This lack of symmetry of the vortex segments relative to the base of the model seems to explain, at least in part, the characteristic pressure distributions for the tilted model. Another flow characteristic tending to produce the pressure distributions shown in Figure 3 is the spillage from the high end. This results in a portion of the air from the low slot passing beneath the base and ejecting from the high end. Thus, the two-dimensional model in proximity to the ground plane becomes an effective two-dimensional diffuser for this transverse flow.

The next phase of this work utilized model configurations b and c. These differed from the original configuration by the addition of curved metal vanes attached in such a manner as to turn the peripheral jet inward, in one case 45°, and in the other 80°, from the vertical. The pressure ratio for these studies was approximately 1.04, and the height of the model above the ground plane was measured from the bottom of the vanes.

Base pressure distributions were graphically integrated and an average base pressure was obtained, which, being a function of both lift and augmentation ratio, was plotted versus h/b in Figure 4. As shown in this figure, there is a general improvement in performance at low altitudes as the initial jet angle is increased in the negative direction, as predicted by theory. More significant, there is an obvious discontinuity in the lift curve. Smoke was injected into the cavity, and the observed characteristic flow patterns are presented in Figure 4. The first diagram for each configuration is a low altitude, balanced condition, while the second and third diagrams represent conditions just before and after the discontinuity. For initial jet angles of $\Theta_o = 0^\circ$ and $\Theta_o = -45^\circ$, the flow pattern degenerates into what appears to be an oscillating Karman vortex street, while for $\Theta_o = 80^\circ$ the jet sheet curves upward and attaches to the base of the model.

Considering now the relationship between initial jet angle and static instability, Figures 2 and 3 indicate that the vortex is the source of the unfavorable pressure distribution, while Figure 4 shows that turning the jet inward displaces the vortex toward the center of the base, thus tending to reduce its effect. To measure this effect, the model was

set at different inclinations (α), with h/b equal to 0.18, and the pressure distributions for the three initial jet angles were plotted. The location of the center of pressure was obtained and its displacement from mid-span was plotted versus inclination. The results are shown in Figure 5. It is seen that turning the jet inward appreciably decreases the static instability in the hovering case while definitely improving performance.

THREE-DIMENSIONAL EXPERIMENTS

Apparatus. The apparatus used for hovering tests of the three-dimensional models is shown in Figure 6. A one-horsepower blower supplied air through a calibrated pitot tube section to a tee which diverted the air equally through two flexible hoses and couplings to a tee on the model. The models were placed inverted on a three-point straingauge balance which measured lift and moment. Pressure taps in the base were connected to a multiple-manometer board, and the ground plane could be adjusted in height and inclination. The three geometrically similar models were circular in planform, with a vertical nozzle, and had a cross section approximately as shown in Figure 8. The nominal diameters were 4, 6, and 8 inches. They were made of machined aluminum with the important dimensions held to a tolerance of ± .001 inch. The aspect ratio was 122.5 and the maximum pressure ratio was about 1.03. Two extra bases have been made for the six-inch model in order to vary the aspect ratio, and a six-inch triangular model is representative of the variation in planform to be studied. The bases were readily removed for testing the same models as plenum chambers.

Discussion. Only the scale effect and plenum chamber experiments are discussed here. It was originally thought that with scaled models and proportional mass flows there should be no scale effect except for a very small Reynolds number effect. The first set of runs consisted of force measurements only. The augmentation curves based on remote lift for nearly proportional mass flows were plotted and found to be coincident within a few per cent. The average curve is shown in Figure 7, along with the non-mixing theory curve. This was the expected result, and the next step was to reduce the augmentation curves to their proper value by basing them on a calculated jet thrust. The thrust was assumed to be that of a known mass flow issuing from a solid circular nozzle of area equal to the annular jet. This procedure placed the curves in the appropriate region, but also developed a noticeable systematic spread. Checking the test set-up for leaks or balance malfunction produced no discrepancies, and it was thought necessary to pressure tap the base of the models in order to determine the correct ratio of momentum and pressure forces.

The resulting pressure distributions for the 4-inch model are shown in Figure 8. Smoke was injected into the cavity to aid in the visualization of the jet sheet and the ring vortex inside. The top curve represents the negative pressures found when the model is essentially remote from the ground plane. The flow is somewhat unsteady in that the vortex oscillates and the point of impingement on the ground plane moves randomly away from the centerline of the model. At a height of one diameter the presence of the ground begins to show. Just above an h/d of .6 the flow becomes very unsteady as the "tulip" is forced open, and the jet curtain oscillates from one side to another. At an h/d of .6 the flow becomes steady and a gentle hump in the augmentation curve is noted at this point. Passing through an h/d of .4, the pressure distributions mingle and cross, and these curves have been omitted in Figure 8 for clarity. However, the nature of this transition is such as to cause a second hump at this point. Below an h/d of .2 the influence of the vortex decreases rapidly.

The pressure distributions of Figure 8 were integrated numerically to obtain a base lift for each height. The total lift was read from the balance, and the difference of the two values was taken to be the actual jet thrust. These curves are shown in Figure 9. The variation in the jet lift values indicates that the pressure integration was not precise, but

even so, the average value was only 3 per cent greater than the calculated jet thrust and thus seems to validate the original method of data reduction. However, this same procedure will have to be followed with the other models before there can be any conclusions concerning a scale effect.

The augmentation curve for the particular run discussed above is shown in Figure 10. Out of ground effect there is a 30 per cent loss of lift due to negative base pressures; another loss occurs in the region about an h/d of .2. At an h/d of .45 the performance appears to exceed that predicted by theory. At this height the ring vortex tends to converge upon itself, and it may have a beneficial effect upon the jet curtain which more than offsets its detrimental effect upon the base.

There has been a continuing interest in the plenum-chamber type of ground cushion vehicle on the basis of its simplicity. One rather peculiar characteristic noticed with certain configurations was the existence of a strong "suction" effect when the model was raised above its equilibrium altitude. In order to determine the nature and magnitude of this effect, the bottoms were removed from the three scaled models. This provided a set of models which were proportional in the ratio of depth to diameter. But since the inlets were equal in area, the ratios of base area to inlet area were about 8, 18, and 32. The augmentation curves are shown in Figure 11. The thrust above an h/d of .5 is that of a solid circular jet, but below this altitude a ring vortex forms in the cavity and reduces the pressure on the base. This loss becomes very severe in the region of h/d equal to .1, below which the augmentation rises sharply to high positive values.

The effect of a smaller base to inlet area ratio is to diminish the magnitude of the negative pressures, and at the limit of a 1/1 ratio, a straight tube, there is no loss of lift. As the area ratio is increased there is apparently a limit to the strength of the vortex action, since the augmentation curve for the 8-inch model is observed to abruptly reverse direction as it approaches a minimum.

This is not meant to imply that negative lift is a serious problem; it can be effectively eliminated by increasing the depth ratio, by diffusing into the plenum, or by inserting proper baffling. But it is thought to be an interesting phenomenon of the low-profile, simple plenum-chamber type of device.

Forward flight data is being obtained from two sources. A 20-inch circular wind tunnel model has been constructed as a 1/12 scale model of the large, man-carrying machine. Preliminary data indicate an appreciable increase in lift at a moderate forward speed due to the jet flap effect of the annular jet. But it has not been ascertained if there is a loss of lift during the transition from hovering to low forward speed for this particular configuration.

Also constructed and now in the instrumentation stage is an 8-foot, scaled model of the large machine. Trial runs on the carriage of the Princeton Long Track Facility have been successful, and future results will be compared with those of the wind tunnel model and the full scale machine.

FREE FLIGHT MODELS

Eight-foot remote control model. The first free flight model, shown in Figure 12, was 8 ft in diameter with vertical blowing and with no stabilizing slots in the base. It was powered with a 2 horsepower D.C. motor, weighed 100 lbs, and hovered at an altitude of 3 inches. At this height the model was stable but was difficult to trim, since it was sensitive to the slightest unbalanced weight distribution. A hoisting sling was attached so as to pivot through the center of gravity. At an h/d of .05 the model became neutrally stable,

and above an h/d of .06 it became unstable. At a height of a half-diameter, there was evidence of an unsteady flow condition as the model "danced" in its sling.

As a first attempt at control, four butterfly vanes were installed in the nozzle at cardinal points. Each vane, when closed, throttled off 8 per cent of the periphery and caused the model to tilt and move in that direction. Vertical vanes were installed in the nozzle to provide yaw control. The vanes were powered by servo motors which were wired to a control stick and rudder pedals on a nearby chair. Control effectiveness was marginal, and the response seemed to be sluggish. Also, whenever the model yawed more than 90° from the heading of the control chair, the operator was subject to disorientation. This made it desirable for subsequent controlled models to be designed as man-carrying machines.

Kinesthetic air scooter. It was noted with the first model that at very low altitudes there was mild stability, but the trim attitude could be altered with a very small shift of the center of gravity. These conditions appeared favorable for the application of kinesthetic control, and the model built for this experiment is shown in Figure 13. It has an 8-ft diameter base, a 5 hp engine driving a 26-inch wooden propeller, and a single annular slot. It weighs 120 lbs without a rider. A flexible cloth skirt was attached to the perimeter in order to turn the jet inward and to allow greater inclination for control. When level, the skirt clears the ground by only 1 1/2 inches. Thus the model cannot climb a grade, and its forward speed is less than 10 knots. But it can be controlled easily and effectively by a subtle shift of the rider's weight. The results are so promising that further experiments involving increased performance are planned.

Twenty-foot diameter machine. A large manned vehicle was considered necessary for realistic control and handling qualities experiments. The problems of operation in strong cross winds and maneuverability in confined areas were thought to be best investigated with a full scale machine. It would provide full scale data which could be correlated with wind tunnel results. The transition to forward flight and the effect of wing lift could be readily explored. And finally, it could be a test bed for later dynamic experiments.

The recently completed vehicle is shown in Figure 14. It has a gross weight of about 1000 lbs. The single annular jet is 4 inches in width and provides an initial jet angle of -45°. There are provisions for four radial slots in the base. A 43 hp Nelson helicopter engine drives a 4-ft ducted propeller for lift, and a 5 hp swivelled engine in the tail provides thrust and yaw control. The major control is accomplished through tilting the machine by throttling portions of the peripheral jet. The controls are actuated by servos, and autopilot operation can be obtained with the addition of gyros, should it become desirable.

The first experiments are being conducted as this paper is written. In the final stages of construction, only the base covering was lacking and the vehicle was flown as a plenum chamber. It attained a height of three inches, approximately the result predicted on the basis of exit area equal to inlet area. The first flights as an annular jet have averaged a height of about 10 inches, but the engine tends to overspeed. A newly designed propeller is expected to increase the height to 15 inches. The machine is stable at 10 inches and control effectiveness is fair. Its forward speed is about ten knots at this altitude.

In conclusion, it is hoped that this review has not only described the nature and scope of the Princeton research program, but has presented some findings of interest which may aid in a further understanding of the ground effect phenomenon.

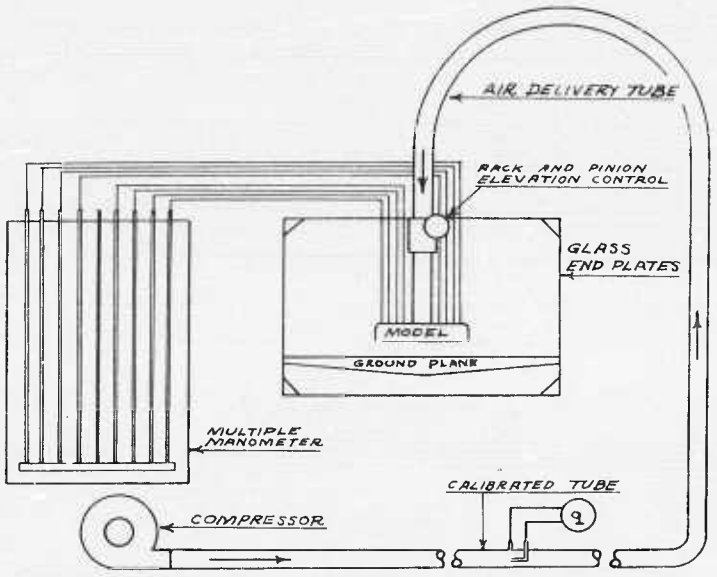

Figure 1. Schematic diagram of experimental set up

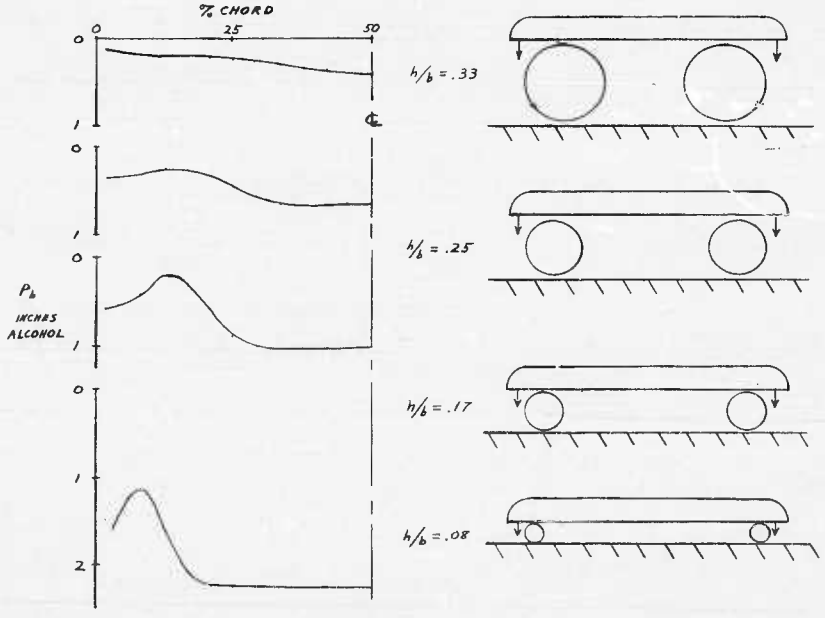

Figure 2. Two-dimensional pressure distributions

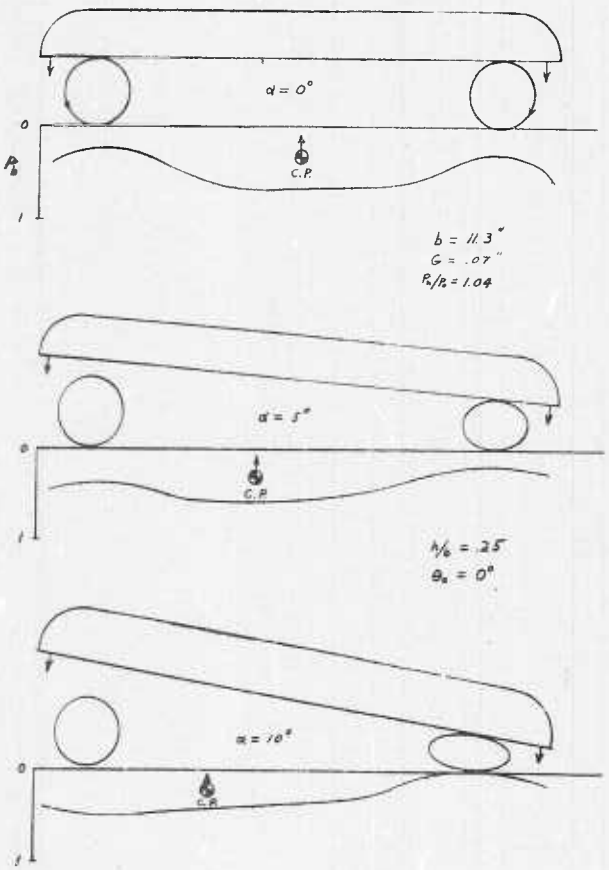

Figure 3. Two-dimensional pressure distributions

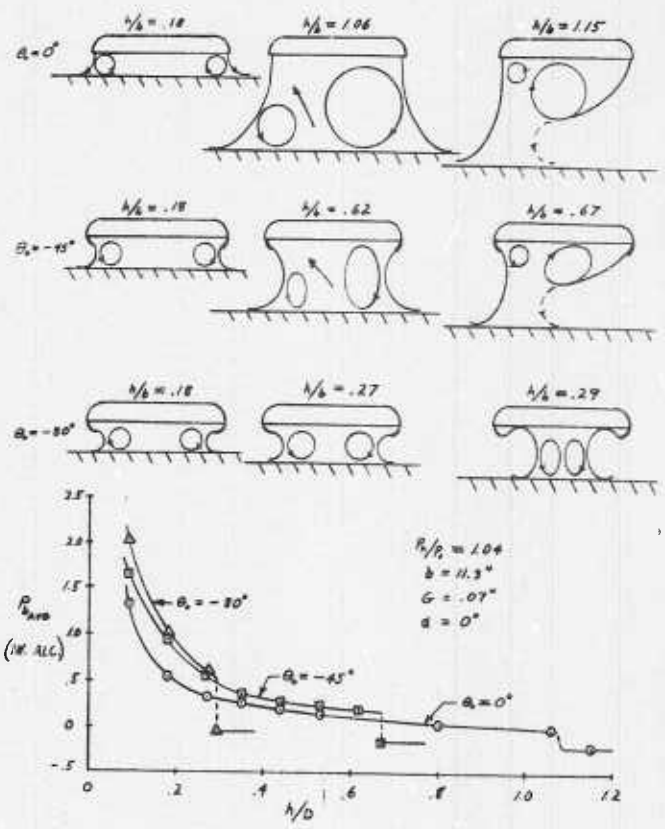

Figure 4. Two-dimensional flow patterns

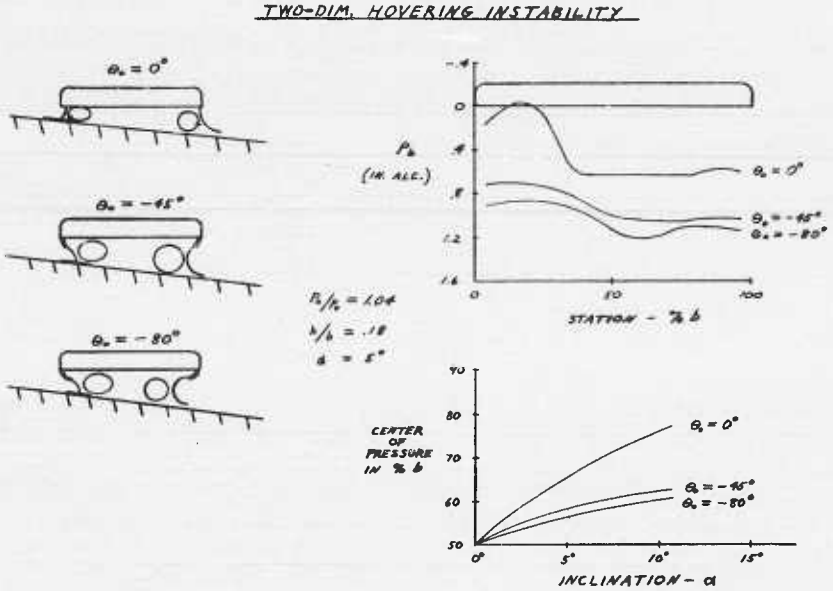

Figure 5.

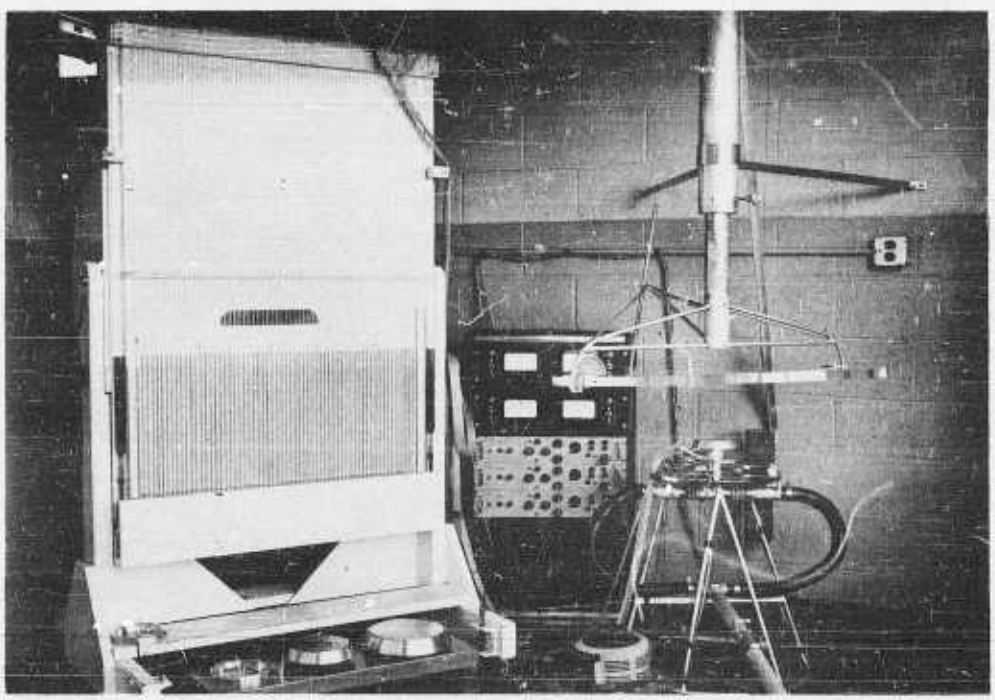

Figure 6.

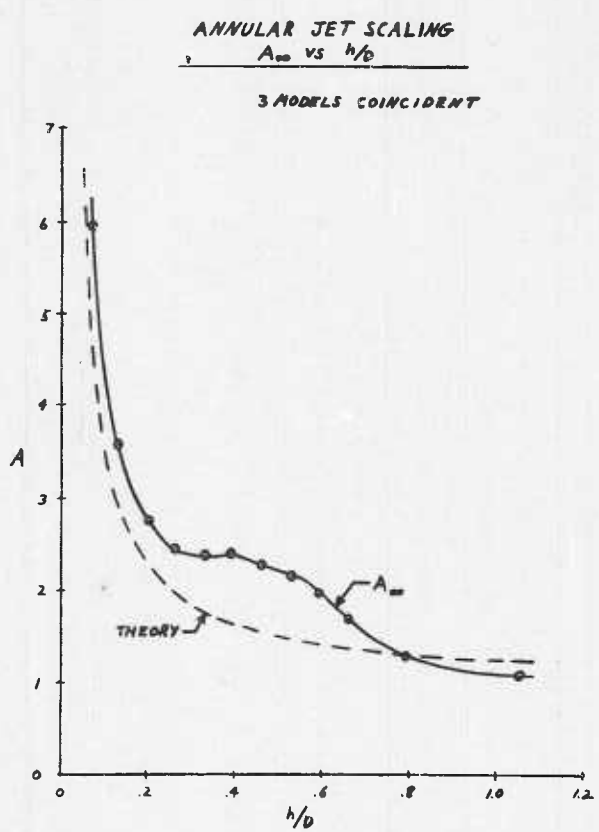

Figure 7.

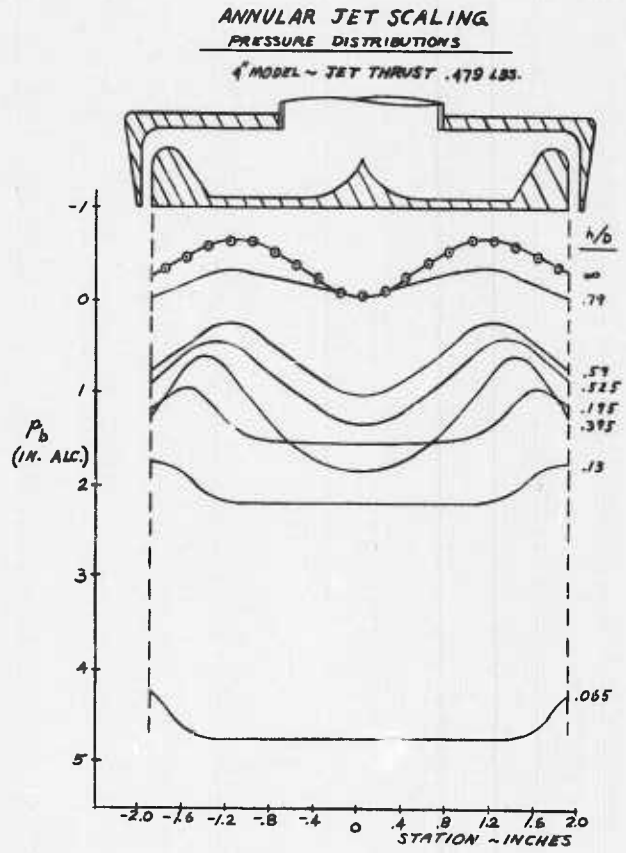

Figure 8.

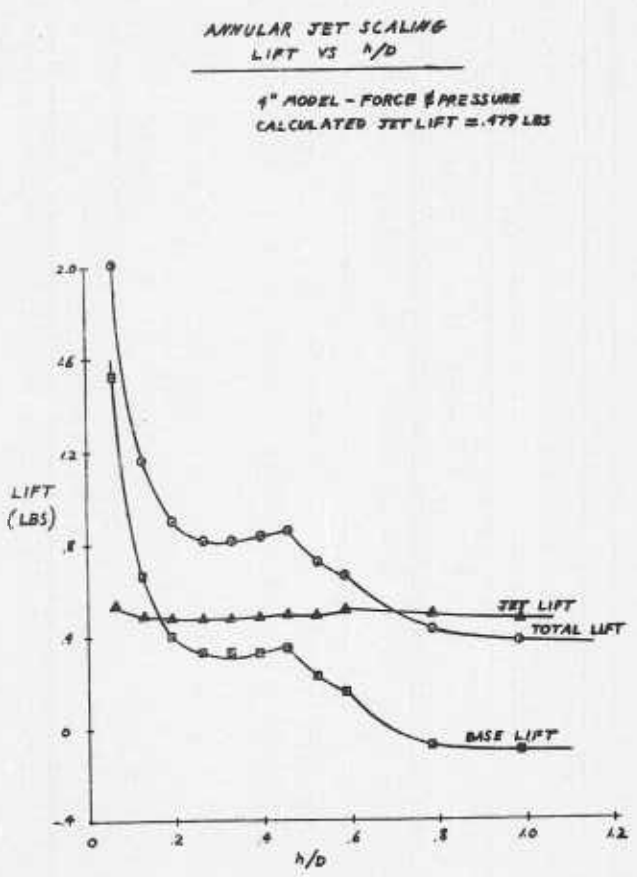

Figure 9.

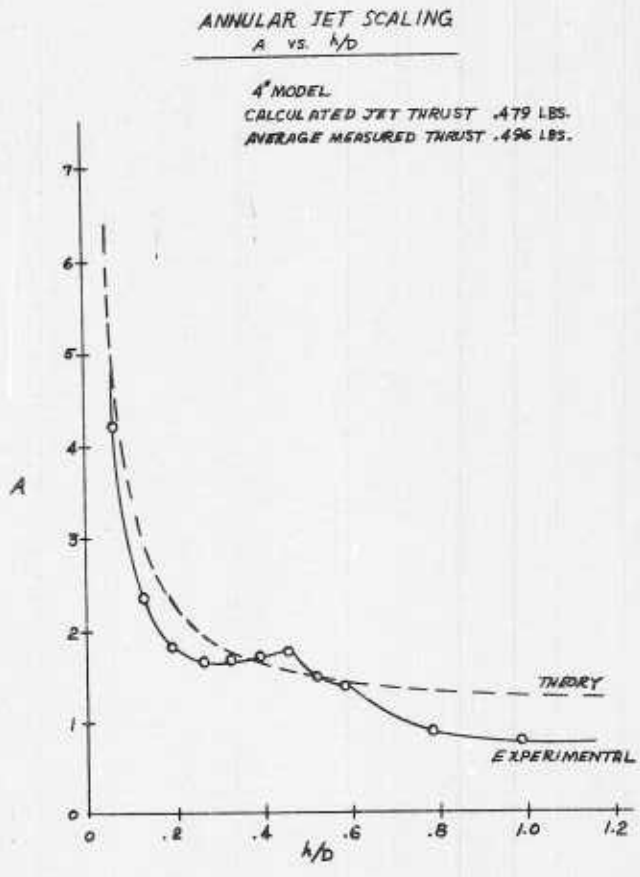

Figure 10.

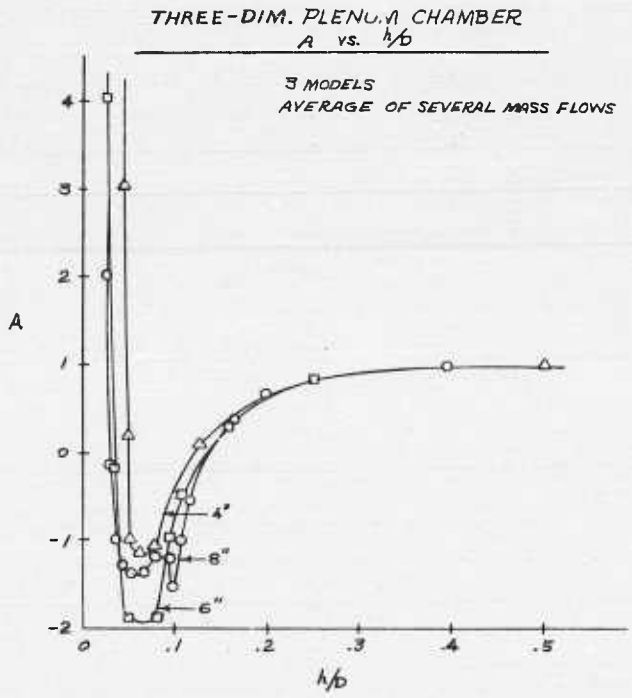

Figure 11.

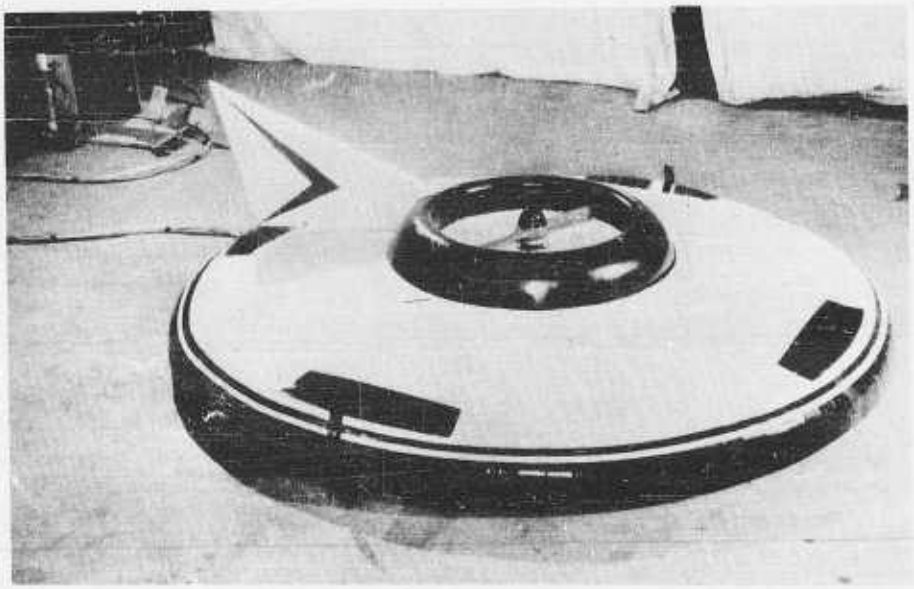

Figure 12.

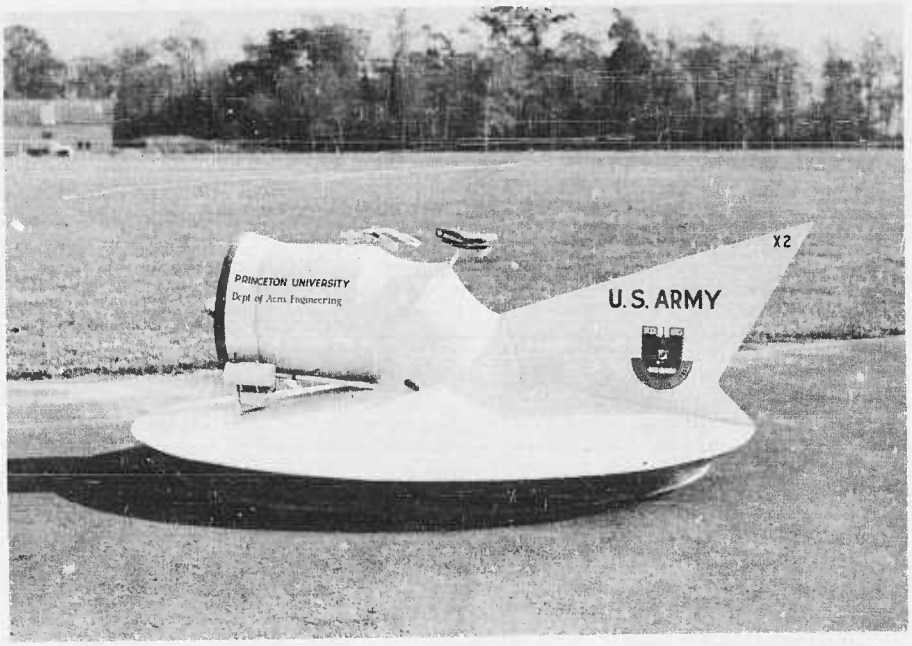

Figure 13.

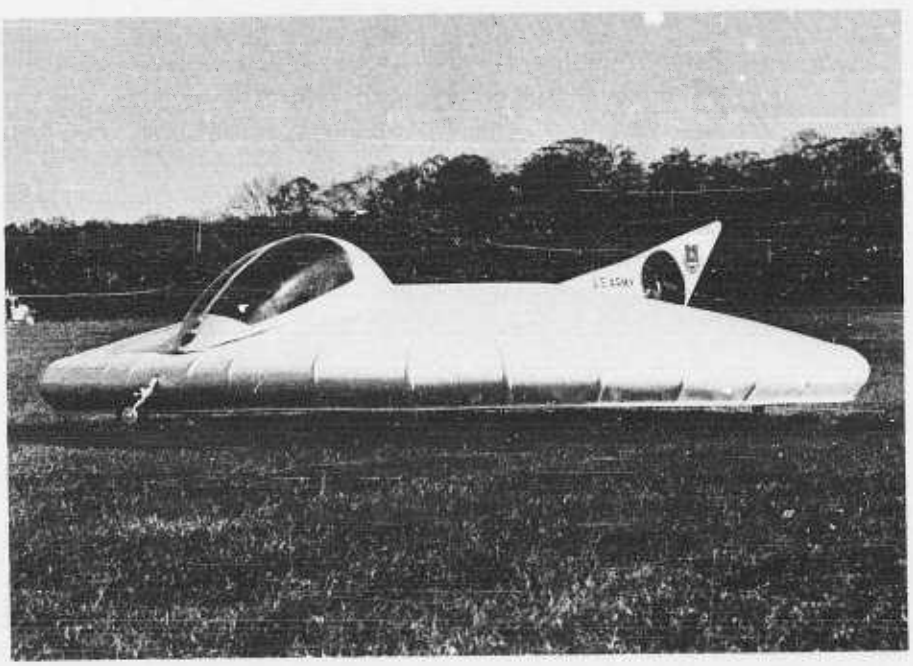

Figure 14.

GROUND CUSHION RESEARCH AT THE DAVID TAYLOR MODEL BASIN -- A BRIEF SUMMARY OF PROGRESS TO DATE*

By Harvey R. Chaplin, Aerodynamics Laboratory,
David Taylor Model Basin, Washington, D. C.

SUMMARY

The currently available research information pertinent to the design or evaluation of annular jet ground effect machines (GEM's) is briefly summarized. Fairly general and reliable information is available for treating hovering performance. Adequate treatment of cruising performance, stability, and control must await further progress of experimental research. A rational treatment of cruising performance for a special class of GEM (having slender planform and uniform conditions over the preponderant part of the periphery) is developed. The results suggest that only extremely large GEM's can better the cruise economy of current transport airplanes.

SYMBOLS

S	reference area in ft^2 (plan area enclosed by outer edge of nozzle exit)
h	altitude in ft measured from the surface to the lower edge of the nozzle exit
G	nozzle width in ft.
C	perimeter in ft measured at the nozzle center line in the nozzle exit (see Figure 1)
Θ	normal jet discharge angle in degrees measured from vertical at the nozzle exit; negative for an inward-inclined jet (see Figures 1 and 5)
β	tangential jet deflection angle in degrees (see Figure 5)
J	scalar total peripheral jet momentum flux in lbs
Δp	effective base pressure in lb/ft^2 gauge (total base pressure lift, accounting for the static pressure over the nozzle exit, divided by $\left(S - \frac{GC}{2}\right)$
p_{tj}	weighted-average jet total pressure in lb/ft^2, gauge, measured at the nozzle exit, the pressure at a point being weighted proportional to the normal velocity at that point
Δp_{prop}	weighted-average pressure rise through the peripheral jet compressor in lb/ft^2
p_i	effective induced static pressure at the outside surface of the peripheral jet in lb/ft^2 gauge
V_j	average jet velocity in ft/sec measured at the nozzle exit

*This paper was also presented at the UTIA Decennial Symposium on October 14, 1959.

V_o free stream velocity in ft/sec

ρ air density in slugs per ft^3

q_o free stream dynamic pressure in lb/ft^2 $\left(q_o = \frac{1}{2} \rho V_o^2 \right)$

σ relative air density $\left(\sigma = \frac{\rho}{\rho_o}, \text{ where } \rho_o = 0.002378 \text{ slugs per ft}^3 \right)$

γ_{H_2O} weight density of water in lb/ft^3

L total lift in lbs

D total drag in lbs

P_j shaft power delivered to the peripheral jet compressor in lb-ft/sec

P_p shaft power delivered to a separate propulsion device in lb-ft/sec

P total shaft power in lb-ft/sec

HP horsepower $\left(HP = \frac{P}{550} \right)$

M figure of merit $\left(M = \frac{1}{2\sqrt{\rho S}} \frac{L}{P}^{\frac{3}{2}} \right)$

η efficiency factor (see Table 1)

C_L total lift coefficient $\left(C_L = \frac{L}{q_o S} \right)$

C_D total drag coefficient $\left(C_D = \frac{D}{q_o S} \right)$

C_{Di} induced drag coefficient

C_{Df} friction drag coefficient $\left(D_{Df} = C_D - C_{Di} \right)$

C_P induced pressure coefficient $\left(C_P = \frac{P_i}{q_o} \right)$

ν normalized forward velocity parameter

$$\left(\nu = \frac{V_o}{\sqrt{\frac{L}{S}}} = \sqrt{\frac{2}{C_L}} \right)$$

ρ normalized power parameter

$$\rho = \frac{P}{L\sqrt{\frac{L}{\rho S}}} 2 \frac{S}{hC} \eta_A$$

ξ normalized cruise economy parameter

$$\xi = \frac{L\ V_o}{P} \div 2\ \frac{S}{hC}\ \eta_A = \frac{v}{\rho}$$

INTRODUCTION

The David Taylor Model Basin ground cushion research program was begun in May 1957. Its original purpose was to explore the fundamental principles underlying the annular jet ground cushion phenonenon, and to examine the feasibility of applying this phenomenon to a vehicle. Its purpose was recently expanded to include development of practical aerodynamic information pertinent to the design of annular jet ground effect machines (GEM's). From the outset, consideration has been confined to vehicles which remain at all times in close proximity to the ground.

During its existence (two and a half years), this program has involved more than half a dozen model test projects and a continuous theoretical analysis effort. The present paper attempts to summarize the state of understanding which has thus far evolved from this work. Detailed descriptions of the experiments and detailed mathematical derivations are largely omitted. This material can be found in the DTMB reports listed at the end of this paper, and in other reports to be published soon.

HOVERING PERFORMANCE

The early ground cushion experiments and theories dealt almost exclusively with stationary models and hovering flight. It is thus hardly surprising that the technique of predicting hovering performance has reached a relatively advanced state.

The hovering performance equations currently employed at DTMB are formulated by inserting into the simple momentum theory a sufficient number of empirical "efficiency" factors (Table 1) to render it exact. (Actually, of the factors listed in Table 1, the last three are not efficiencies in the strictest sense, but corrections for various influences ignored by the simple theory.) The objective was to define these efficiency factors so that they would (1.) be precisely measurable by conventional laboratory techniques and (2.) remain near unity for a properly designed GEM operating within its design range. With this formulation, the role of experimental research is reduced to the job of providing adequate correlations of the values of the efficiency factors -- a job on which a fair start has already been made.

Basic relations. The principal element of the ground cushion is the base pressure $\triangle p$ which acts upward on the GEM to support a considerable part of its weight (in extreme cases, all of the weight). Its magnitude is roughly determined by equating the change of horizontal jet momentum $J(1 - \sin \Theta)$ to the reaction of the base pressure against the imaginary cylindrical surface hC (Figure 1). Exactly,

$$J(1 - \sin \Theta)\ \eta_A = \triangle p\ h\ C\ \eta_J$$

The average static pressure (gauge) of the jet at nozzle exit is roughly half the base pressure, making the average dynamic pressure approximately $\left(p_{tj} = \frac{\triangle p}{2} \right)$, where p_{tj} is the average total pressure (gauge) of the jet. The jet momentum is twice the dynamic pressure times the nozzle area, or exactly

$$J = 2\left(p_{tj} - \frac{\triangle p}{2} \right) G\ C\ \eta_j$$

The average jet velocity is given approximately by equating the average dynamic pressure to $\frac{1}{2}\rho V_j^2$, or exactly

$$\frac{1}{2}\rho V_j^2 \eta_V^2 = p_{tj} - \frac{\Delta p}{2}$$

The hovering performance equation. A very useful form of hovering performance parameter is provided by the figure of merit,

$$M = \frac{1}{53.66}\frac{L}{HP}\sqrt{\frac{L}{\sigma S}}$$

The figure of merit provides a direct index to the important quantity, lift per horsepower, and also a convenient comparison with the performance of the helicopter or ducted fan, which ideally have figures of merit of $\sqrt{\frac{1}{2}}$ and 1.0, respectively.

Using the basic relations given in the previous section, the lift

$$L = J \cos \Theta + \Delta p \left(S - \frac{GC}{2} \right)$$

and power

$$HP = \frac{V_j\, GC\, p_{tj}}{550}\,\frac{1}{\eta_{int}\,\eta_V}$$

can be readily reduced to give

$$\frac{M}{\eta_{int}\,\eta_V} = \sqrt{\frac{\frac{G}{h}\eta_A}{\frac{S}{hC}\eta_A}}\,\frac{\left[\cos\Theta\,\eta_J + (1 - \sin\Theta)\left(\frac{S}{hC}\,\eta_A - \frac{1}{2}\,\frac{G}{h}\,\eta_A\right)\right]^{\frac{3}{2}}}{1 + (1 - \sin\Theta)\,\frac{G}{h}\,\eta_A}$$

Except at low values of the size parameter $\frac{S}{hC}\,\eta_A$, the jet momentum efficiency η_J has very little influence on the result, and can be safely assumed to be unity. The equation is then in the form

$$\frac{M}{\eta_{int}\,\eta_V} = f\left(\frac{S}{hC}\,\eta_A,\ \frac{G}{h}\,\eta_A,\ \Theta\right)$$

making it a simple matter to determine "optimum" configurations (combinations of $\frac{G}{h}\eta_A$ and Θ giving maximum $\frac{M}{\eta_{int}\,\eta_V}$) and figures of merit for given values of $\frac{S}{hC}\,\eta_A$. The results of such calculations are plotted in Figure 2, which also giver per cent power increase in $\eta_{int}\,\eta_V$ P) incurred by using a nonoptimum value of nozzle parameter $\frac{G}{h}\eta_A$ or jet dis-discharge angle.

Concerning the "optimum configurations" it should be noted that:

1. They are based on hovering performance only, and may not be the best possible from overall design considerations.

2. They are based on maximum values of $\frac{M}{\eta_{int}\,\eta_V}$, which correspond exactly to maximum values of M only if the product $\eta_{int}\,\eta_V$ is independent of $\frac{S}{hC}\,\eta_A$. (However, this discrepancy appears to be very slight in practice.)

The most important single determinant of GEM hovering performance is clearly the size/altitude parameter $\frac{S}{hC}$. From Figure 2, it is evident that the figure of merit for a near-optimum design can be estimated to a very good approximation from simply

$$M \doteq \frac{S}{hC}\,\eta_A\,\eta_{int}\,\eta_V$$

This parameter $\frac{S}{hC}$ depends on the area S, the altitude h, and the planform shape (since the perimeter C is determined by the area and the shape). The "best" planform for hovering is circular, since the circle has minimum perimeter for given area. Other considerations (some of which are brought out in the next section of this paper) suggest that the best overall performance might require a planform shape somewhat elongated in the direction of flight.

The relative effects of size and elongation on hovering performance, for a family of planform shapes at some typical conditions, are represented in Figure 3. The estimated hovering performance for one member of this family is compared, in Figure 4, with the hovering performance of other types of aircraft. Both Figures 3 and 4 are based on an altitude of 10 ft. They may be used approximately for other altitudes by correcting the values of figure of merit and lift per horsepower by the factor $\frac{10}{h}$.

CRUISING PERFORMANCE

The problem of predicting cruising performance is complicated by the lack of any comprehensive experimental data. This should soon be partly remedied by programs now underway and by two major physical influences:

1. In addition to producing a lift force equal to its wieght, the GEM must product a propulsive force equal to its drag. The lift and propulsive forces are interdependent, since a major part of the drag is "induced" drag associated with the air mass flow of the jet producing the lift.

2. The GEM in forward motion induces a nonuniform pressure field around itself. This means (a) the pressure difference across the jet is no longer identical to the base pressure Δp; (b) the conditions defining the jet behavior are different at different points around the perimeter.

3. These complications prevent, for the present, any general formulation for cruising performance comparable with that of the hovering performance equations. However, for one special class of vehicle (the "constant pressure GEM of slender planform") a relatively simple formulation of some practical significance can be made. This class of vehicle is characterized by:

1. An induced pressure distribution, along the outside surface of the jet curtain, which is the same at all stations around the periphery except in the immediate vicinity of the front and rear stagnation points.

2. A planform shape sufficiently elongated so that the preponderant part of the periphery lies approximately parallel (say within about twenty degs) to the direction of flight.

3. Uniform nozzle width, jet discharge angles, etc. along this preponderant part of the peripheral jet.

Within this constant-pressure, slender-planform class, we shall consider two basic types of GEM (Figure 5): (1) the "integrated-system" GEM, which produces its propulsive force by tangential deflection of its main peripheral jet, and (2) the "separate-system" GEM, which produces its propulsive force by means of a horizontally exhausted slipstream. (This includes horizontally disposed jets or propellers, no matter whether they are supplied with power from the same source as the peripheral jet or from a separate source.)

Simplified basic relations. A considerable simplification of the equations can be gained by setting

$$\Theta = -90°$$

$$\frac{G}{2h} << \frac{S}{hC}$$

The optimum performance calculated under this simplification will be very little different from that given by the more general equations, except at small values of $\frac{S}{hC}\eta_A$. (For example, applying this simplification to the hovering performance equations gives

$$\left.\begin{aligned} \frac{G}{h}\eta_A &= 0.5 \\ \frac{M}{\eta_{int}\eta_V} &\quad \frac{S}{hC}\eta_A \end{aligned}\right\} \text{(optimum hovering)}$$

which, comparing with Figure 2, is seen to be an excellent approximation over most of the range of interest.

In the discussion that follows, it will be assumed that $\eta_J = \eta_V = 1.0$.

The base pressure is roughly determined by equating the change of horizontal jet momentum 2 J cosβ to the net reaction of the base pressure and induced pressure against the imaginary cylindrical surface hC.

$$2\ J\ \cos\beta\ \eta_A = (\Delta p - p_i)\ hC$$

The average static pressure of the jet at nozzle exit is roughly the mean of the base pressure and induced pressure, $\frac{\Delta p + P_i}{2}$. With tangential jet deflection β, the effective nozzle exit area is reduced from its basic value GC in proportion to cosβ. The jet momentum is given by

$$J = 2\left(p_{tj} - \frac{\Delta p + p_i}{2}\right) GC \cos\beta$$

The jet velocity is determined from

$$\frac{1}{2}\rho V_j^2 = p_{tj} - \frac{\Delta p + p_i}{2}$$

Neglecting any aerodynamic lift induced by forward motion, the total lift is simply

$$L = \Delta p\ S$$

The power required to maintain the peripheral jet is

$$\eta_{int}\ P_j = V_j\ GC\ \cos\beta\ (p_{tj} - \eta_d\ q_o)$$

The drag is the sum of induced drag and friction drag

$$D = \rho\ V_j\ GC\ \cos\beta\ V_o + C_{Df}\ q_o\ S$$

The propulsive component of peripheral jet momentum is

$$T_j = J\ \sin\beta = \rho V_j^2\ GC\ \cos\beta\ \sin\beta$$

Cruising performance equations. The cruising performance is conveniently expressed by the normalized forward velocity parameter

$$\nu = \frac{V_o}{\sqrt{\frac{L}{\rho S}}} = \sqrt{\frac{2}{C_L}}$$

the normalized power parameter

$$\mathcal{P} = \frac{P}{L\sqrt{\frac{L}{\rho S}}}\ 2\ \frac{S}{hC}\ \eta_A$$

and the normalized economy parameter

$$\xi = \frac{L\ V_o}{P} \div 2\ \frac{S}{hC}\eta_A = \frac{\nu}{\mathcal{P}}$$

Physically, $\mathcal{P}$ is the ratio of power required to ideal hovering power, and $\xi \cdot 2\ \frac{S}{hC}\eta_A$ is proportional to the important quantity "gross ton-miles per horsepower-hour."

Integrated-system Gem. For the integrated-system GEM the tital power required is the power required for the peripheral jet

$$P = P_j$$

and the forward speed is determined by setting the drag equal to the propulsive component of jet momentum

$$D = T_j$$

Combining these conditions with the basic relations given in the previous section gives

$$\nu = \frac{\tan\beta}{\sqrt{2\,\frac{G}{h}\eta_A}} \qquad K_1 = \sqrt{\frac{2}{C_L}}$$

$$\eta_{int}\,\rho = \frac{1 + 2\,\frac{G}{h}\eta_A}{2\sqrt{2\,\frac{G}{h}\eta_A}} \left[1 + \tan^2\beta\, \frac{1 - \eta_d\, K_1^{\,2}}{1 + 2\,\frac{G}{h}\eta_A} - \frac{C_p}{C_L}\, \frac{1 - 2\,\frac{G}{h}\eta_A \cos^2\beta}{\left(1 + 2\,\frac{G}{h}\eta_A\right)\cos^2\beta} \right] \cdot \left(\sqrt{1 - \frac{C_p}{C_L}} \right)$$

where

$$K_1 = \frac{2}{1 + \sqrt{1 + \dfrac{2\,\frac{S}{hC}\eta_A\, C_{Df}}{\frac{G}{h}\eta_A}\tan^2\beta}} \sqrt{1 - \frac{C_p}{C_L}}$$

$$\frac{\xi}{\eta_{int}} = \frac{\nu}{\eta_{int}\rho}$$

The equations for ν and ρ can easily be combined to eliminate β, but the result is less convenient.

Separate-system gem. For the separate-system GEM, the total power required is the sum of the peripheral jet power plus the propulsive power.

$$P = P_j + P_p$$

where

$$P_p = \frac{1}{\eta_F}\, D\, V_o$$

Combining these conditions, and the further condition $\beta = 0$, with the basic relations given in the previous section gives

$$\nu = \frac{V_o}{V_j}\, \frac{\sqrt{1 - \frac{C_p}{C_L}}}{\sqrt{2\,\frac{G}{h}\eta_A}} = \sqrt{\frac{2}{C_L}}$$

$$\eta_{int}\,\rho = \frac{1 + 2\,\frac{G}{h}\eta_A + \frac{V_o^{\,2}}{V_j^{\,2}}}{2\sqrt{2\,\frac{G}{h}\eta_A}}\, K_2 \sqrt{1 - \frac{C_p}{C_L}}$$

where

$$K_2 = 1 + \frac{\left[\left(2\frac{\eta_{int}}{\eta_F} - \eta_d\right)\left(1 - \frac{C_p}{C_L}\right) - 1\right]\frac{V_o^2}{V_j^2} + \frac{C_{Df}\frac{S}{hC}\eta_A}{\frac{G}{h}\eta_A}\frac{V_o^3}{V_j^3}}{1 + 2\frac{G}{h}\eta_A + \frac{V_o^2}{V_j^2}} -$$

$$\frac{\frac{C_p}{C_L}\left(1 - 2\frac{G}{h}\eta_A\right)}{1 + 2\frac{G}{h}\eta_A + \frac{V_o^2}{V_j^2}}$$

$$\frac{\xi}{\eta_{int}} = \frac{\nu}{\eta_{int}\rho}$$

The equations for ν and ρ can easily be combined to eliminate $\frac{V_o}{V_j}$, but the result is less convenient.

Results of cruise performance calculations. The cruise performance equations contain a sizable number of independent parameters. Complete graphical representation of the effects of all of them requires a large number of plots. Fairly extensive plotting has been completed, and will be published shortly in a DTMB Aero Report. But, for present purposes, we will confine ourselves to a few typical plots.

In Figures 6 (for the integrated-system GEM) and 7 (for the separate-system GEM), $\frac{\xi}{\eta_{int}}$ and $\eta_{int}\rho$ are plotted against ν for three cases: (1) no duct losses, friction drag or speed-induced pressures, (2) with duct losses and friction drag, but no speed-induced pressures, and (3) with duct losses, friction drag, and speed-induced pressures.

In Figure 8, cross plots from a series of graphs like Figures 6 and 7 afford direct comparisons between the integrated and separate-system GEM's for some typical conditions.

A few useful generalizations might be tentatively drawn:

1. The integrated-system GEM gives the better cruise economy under all conditions considered. It also has a "hidden" advantage, in that its compressor operating condition changes relatively little with speed, as compared with that of the separate-system GEM. Peripheral jet power of the separate-system GEM decreases with increasing speed, even while its total required power is rapidly increasing. This might lead to either a complex power transmission system or to a disproportionately large amount of total installed power.

2. It would appear that a nozzle thickness ratio of $\frac{G}{h}\eta_A = 0.3$ might give reasonable performance under nearly all practical conditions.

3. Best cruise economy occurs at a progressively lower speed as the "losses"; i.e., $(1 - \eta_d)$, (C_{Df}), $(-C_p)$, or "size" $\frac{S}{hC}\eta_A$ are increased. However, the most economical cruise speed falls in the vicinity of $V = 1$ $(C_L = 2)$ for a very wide range of practical conditions. This is a speed of roughly 100 miles per hour for a vehicle with wing loading of 50 lb/ft^2.

4. If it is assumed that the GEM will have an internal efficienty η_{int} about equal to the propulsive efficiency of an airplane, then the parameter $\frac{LV_o}{\eta_{int}P}$ (plotted against size parameter for some typical conditions in Figure 8b) can be compared directly with the lift drag ratio of an airplane. Typical lift drag values for transport airplanes run between 10 and 20. From Figure 8b it is evident that only very large GEM's will be superior to airplanes by this comparison, which is equivalent to comparing "gross ton-miles per horsepower-hour." The more important comparison "ton-miles payload per horsepower-hour" cannot be made without more reliable structural weight studies (from which to predict gross-weight / empty-weight ratios for GEM's). It seems likely, however, that GEM's will compare more favorably on this latter basis.

Flight over water. Even though the likeliest applications for GEM's involve flight over water, present knowledge of the problems involved is rather sketchy. The basic problems are:

1. Depression of the water surface, resulting in a loss of useful altitude, or in "wave drag."

2. Asymmetric yielding of the water surface under a pitching or rolling GEM, resulting in a reduction of the stability derivatives.

3. Spray generation.

4. Dynamic response to waves.

Practical quantitative understanding of these problems must await further progress of the experimental programs.

The scanty information now available indicates that the hovering performance equations can be used practically unchanged for hovering over water if the altitude h is measured from a point $\frac{L/S}{\gamma_{H_2O}}$ ft below the free water surface. (This amounts to about 0.8 ft for a vehicle of 50 lb/ft^2 wing loading.)

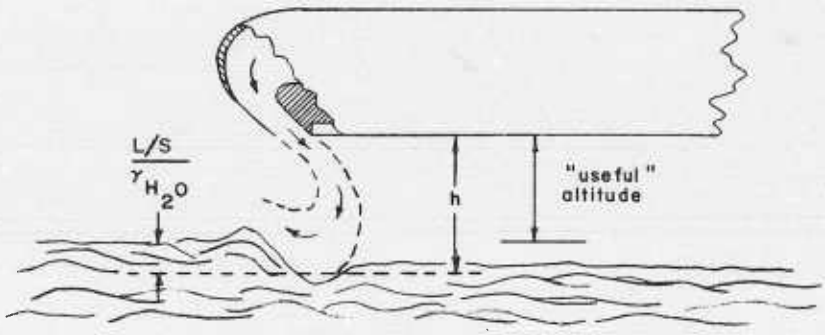

Hovering Over Water

Cruising flight will generally be at speeds above the "planing speed," and the depressed water surface beneath the vehicle will slope from front to rear. If the GEM is flown in a horizontal attitude, this depression will cause a loss of useful altitude, similar to (but probably of smaller magnitude than) that experienced in hovering. If the GEM is flown "parallel" to the depressed water surface, the lift vector will be tilted rearward to produce a "wave drag" component. Reliable estimates of the magnitude of these effects are not yet available. They are expected to be appreciable, but not prohibitive.

Stability and control. This extremely important area is only just now beginning to receive a fair share of research effort. There is no definitive experimental information available as yet.

At present, the likeliest means of providing attitude stability seems to be through the use of secondary jets exhausted through nozzles in the base of the vehicle, arranged so as to subdivide the base into a number of "cells," each of which is sensitive to altitude changes. The best method of attitude control seems to be differentially controlling the jet momentum of various sections of the peripheral jet.

It remains for future research efforts to provide means of estimating the degree of stability and controllability a given practical vehicle should have for safe flight, the degree of stability and controllability which a particular vehicle configuration can provide, the performance penalties associated with the necessary stability and control equipment itself, and the additional performance penalty in the form of an altitude margin which must be maintained to allow for imperfect stability and control.

REFERENCES

1. Chaplin, H. R., "Theory of the Annular Nozzle in Proximity to the Ground." David Taylor Model Basin Rept. 1373, Aero Rept. 923, Washington, D. C., July 1957.

2. Chaplin, H., and Stephenson, B., "Preliminary Study of the Hovering Performance of Annular Jet Vehicles in Proximity to the Ground." illus. David Taylor Model Basin. Rept. 1374, Aero Rept. Washington, D. C., September 1958.

3. Chaplin, H. R., "Effect of Jet Mixing on the Annular Jet." David Taylor Model Basin Rept. 1375, Aero Rept. 953, Washington, D. C., February 1959.

4. Tinajero, A. A., "Comparison of Experimental and Theoretical Design Parameters of a 6-Inch-Diameter Annular Jet Model with a Jet Angle of -45° Hovering in Proximity to the Ground; and Experimental Results for Forward Flight at Zero Angle of Attack." David Taylor Model Basin Rept. 1376, Aero Rept. 954, Washington, D. C., May 1959.

5. Chaplin, H. R., "A Preliminary Design Technique for Annular Jet Ground Effect Machines (GEM's)." David Taylor Model Basin Rept. 1371, Aero Rept. 966, Washington, D. C., September 1959.

6. Johnson, A. E., "Preliminary Hovering Tests of a Three-Foot-Diameter Powered Annular Jet Model." In preparation.

7. Tinajero, A. A., "Preliminary Investigation of Planform Effect on Augmentation Parameter for Peripheral Jet Ground Proximity Vehicles." In preparation.

8. Johnson, A. E., "Preliminary Wind-Tunnel Tests of a Three-Foot-Diameter Powered Annular Jet Model." In preparation.

	Hovering	Cruising	Typical Value*
Duct Efficiency	$\eta_d = \frac{P_{tj}}{\Delta p_{prop}}$	$\eta_d = \frac{P_{tj}}{\Delta p_{prop} + q_o}$	0.8 - 0.9
Compressor Efficiency	$\eta_p = \frac{\Delta p_{prop} V_j G C}{P_j}$	(same)	0.8 - 0.9
Internal Efficiency	$\eta_{int} = \eta_d \eta_p$	(same)	0.7 - 0.8
Propulsive Efficiency	---	$\eta_F = \frac{D V_o}{P_p}$	0.8 - 0.9
Augmentation "Efficiency"	$\eta_A = \frac{\Delta p}{(2 p_{tj} - \Delta p)(1 - \sin\theta)\frac{G}{h}}$	$\eta_A = \frac{\Delta p - p_i}{(2 p_{tj} - \Delta p - p_i)(1 - \sin\theta)\cos^2\beta \frac{G}{h}}$	0.8
Jet Velocity "Efficiency"	$\eta_V = \frac{1}{V_j}\sqrt{\frac{1}{\rho}(2 p_{tj} - \Delta p)}$	$\eta_V = \frac{1}{V_j}\sqrt{\frac{1}{\rho}(2 p_{tj} - \Delta p - p_i)}$	1.0
Jet Momentum "Efficiency"	$\eta_J = \frac{J}{(2 p_{tj} - \Delta p) G C}$	$\eta_J = \frac{J}{(2 p_{tj} - \Delta p - p_i) G C \cos\beta}$	1.0

*Based on good design practice, operation within the range:

$$0.1 < \frac{G}{h}\eta_A < 0.3$$

$$2 < \frac{S}{hC}\eta_A$$

Table 1. Efficency factors

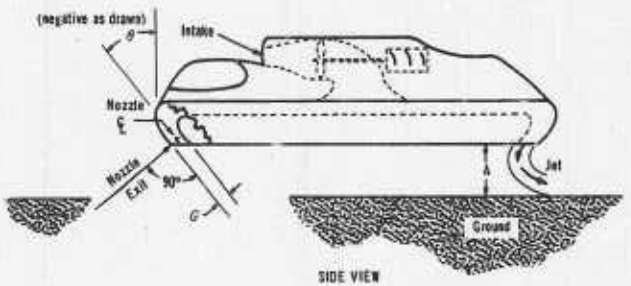

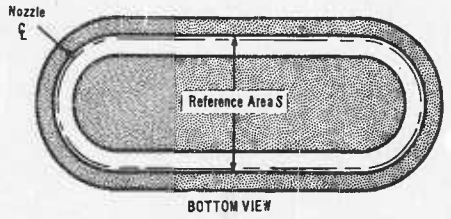

Sketch Showing Vehicle Geometry Notation

Figure 1.

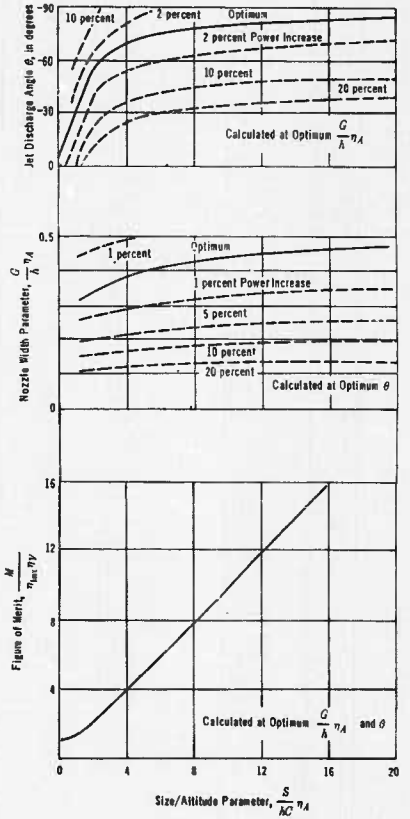

Optimum Nozzle Configuration and Figure of Merit versus $\frac{S}{hC}\eta_A$

Figure 2.

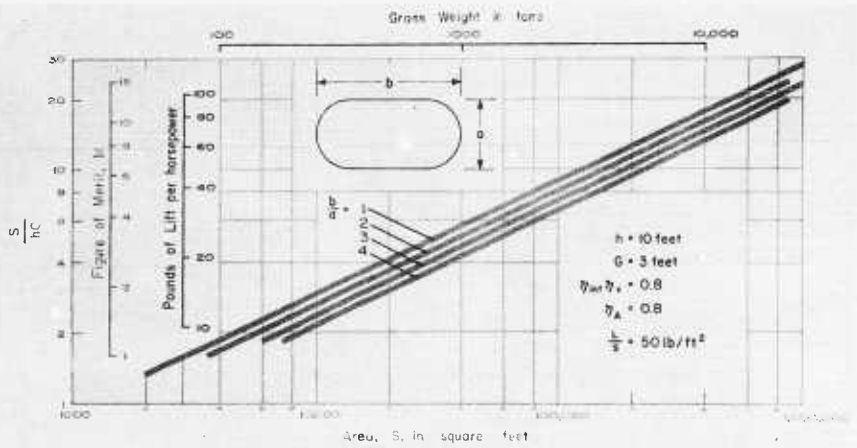

APPROXIMATE EFFECT OF SIZE AND ELONGATION ON THE HOVERING PERFORMANCE OF A FAMILY OF OVAL GEMS AT 10-FOOT ALTITUDE

Figure 3.

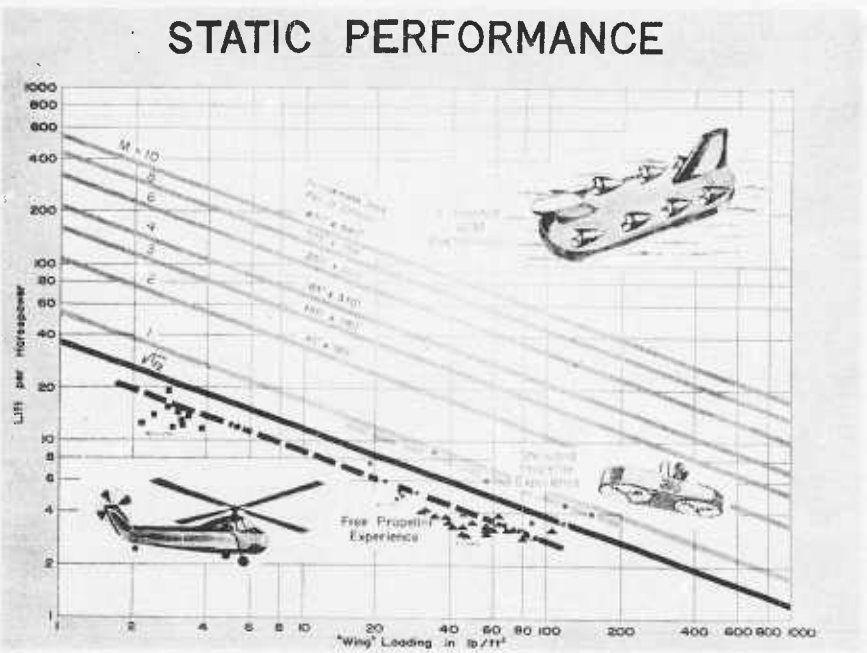

Figure 4.

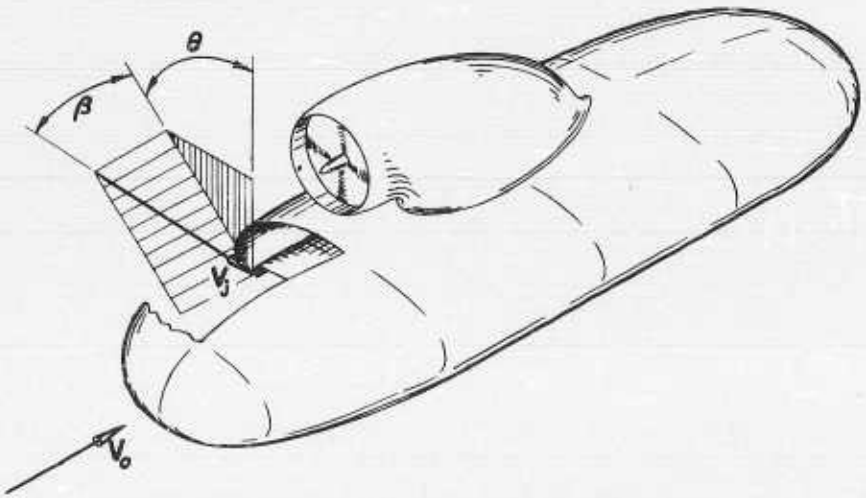

INTEGRATED-SYSTEM GEM

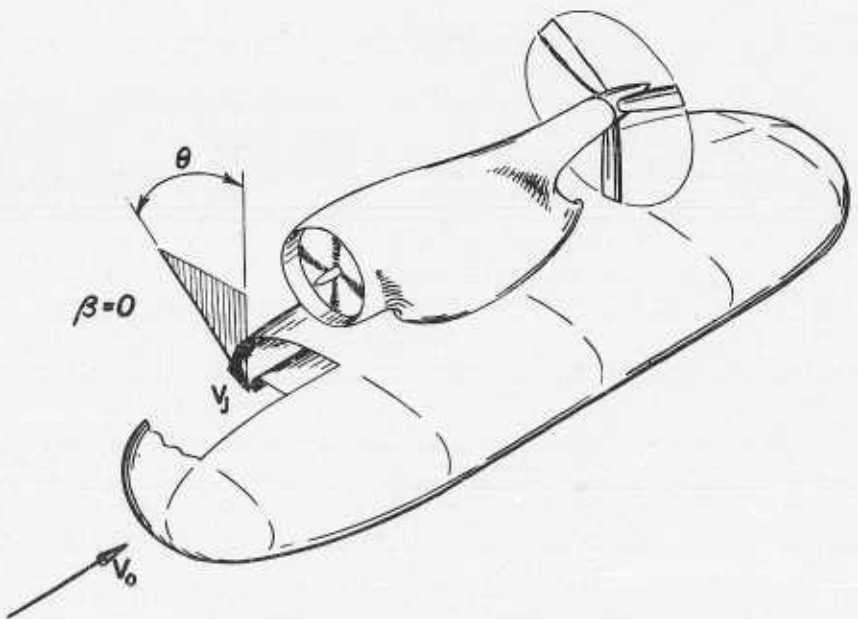

SEPARATE-SYSTEM GEM

SCHEMATIC REPRESENTATION OF TWO BASIC TYPES OF GEM

Figure 5.

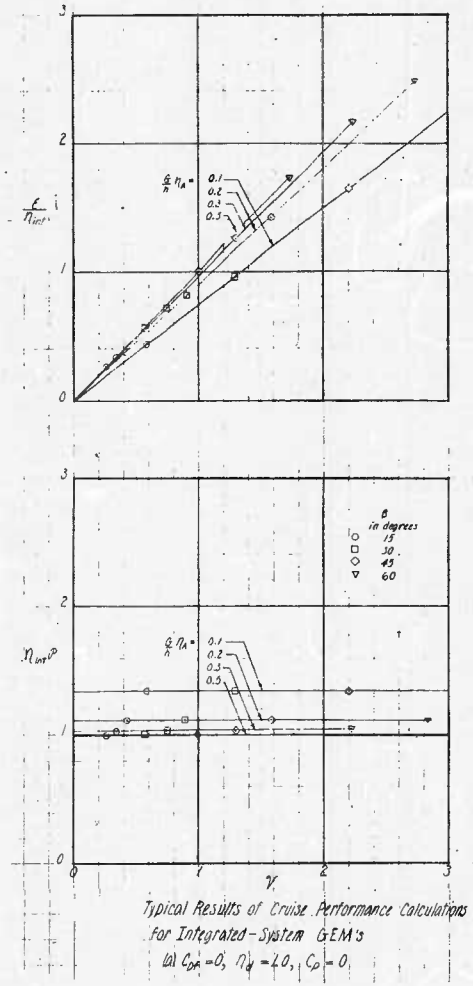

Typical Results of Cruise Performance Calculations for Integrated-System GEM's

(a) $C_{DF}=0$, $\eta_d=1.0$, $C_p=0$

Figure 6.

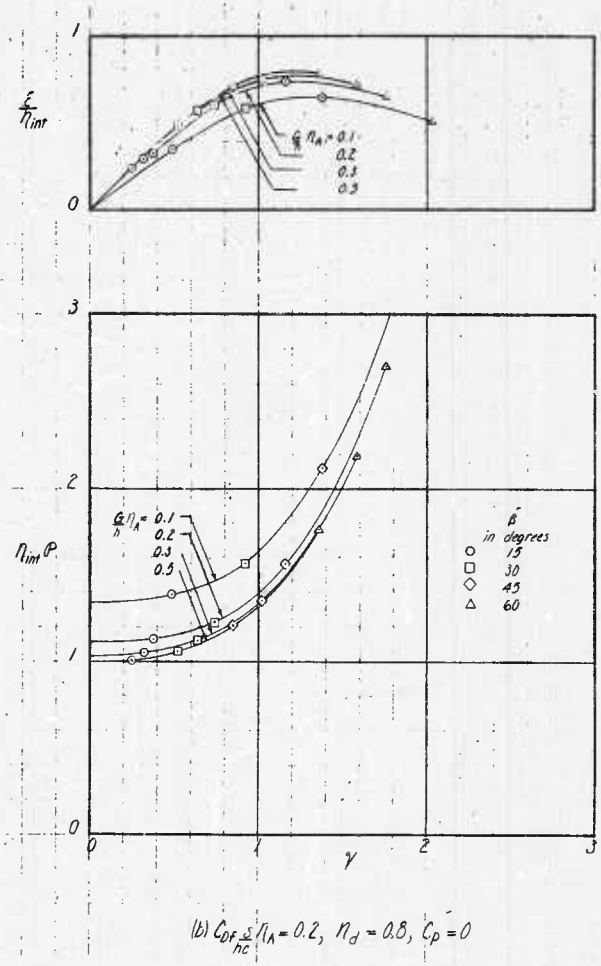

(b) $C_{DF}\frac{S}{hc}\eta_A=0.2$, $\eta_d=0.8$, $C_p=0$

Figure 6. (Continued)

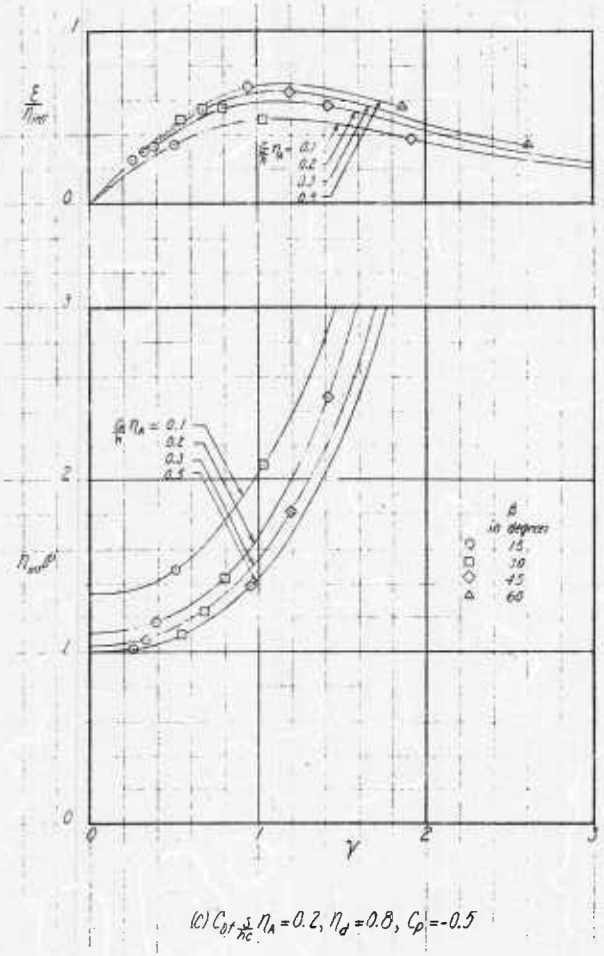

(c) $C_{Df}\frac{S}{hc}$, $\eta_A = 0.2$, $\eta_d = 0.8$, $C_p = -0.5$

Figure 6 (Concluded)

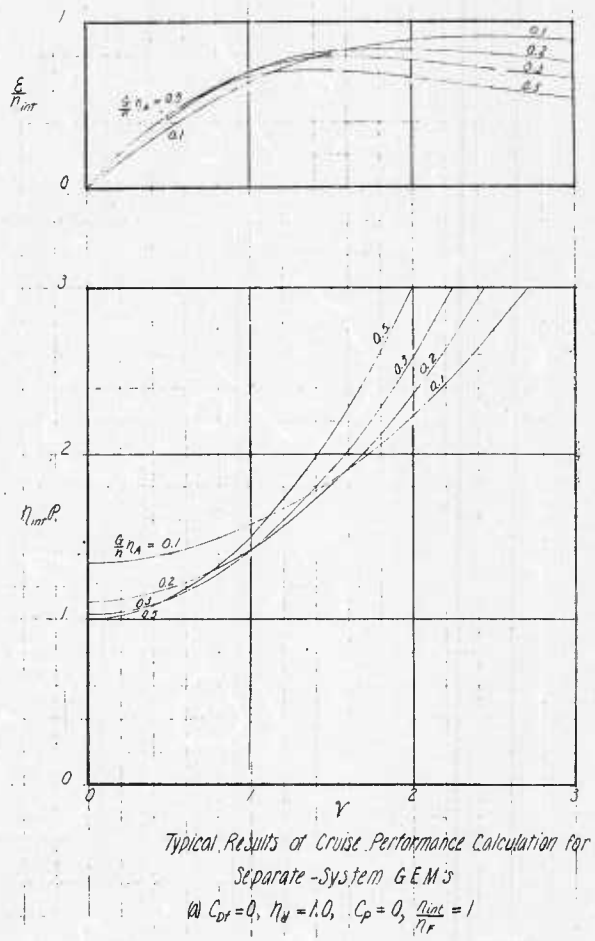

Typical Results of Cruise Performance Calculation for Separate-System GEM's

(a) $C_{Df} = 0$, $\eta_d = 1.0$, $C_p = 0$, $\frac{\eta_{int}}{\eta_r} = 1$

Figure 7.

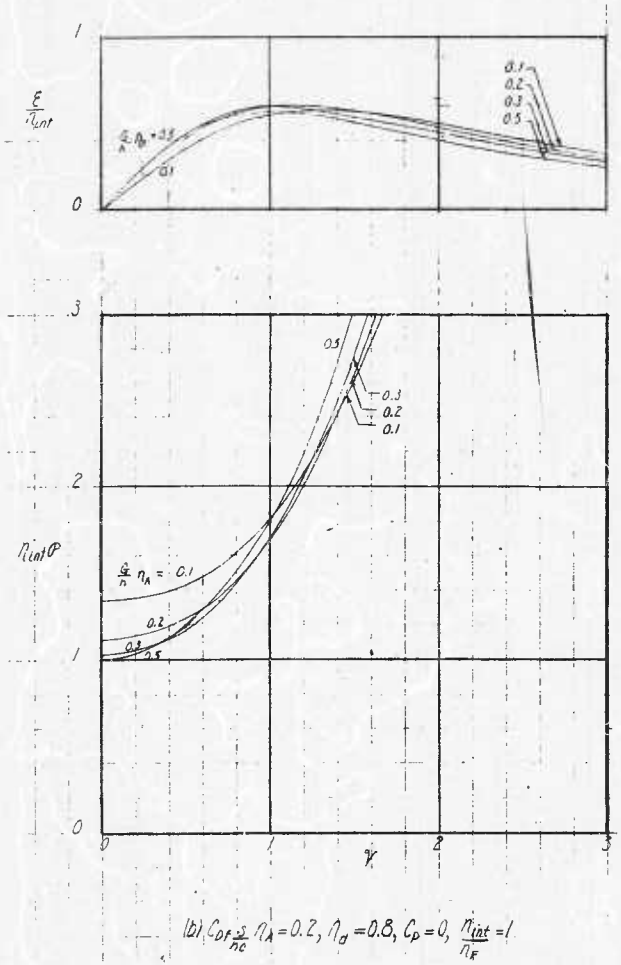

(b) $C_{DF}\frac{S}{nc}\eta_A = 0.2,\ \eta_d = 0.8,\ C_p = 0,\ \frac{\eta_{int}}{\eta_F} = 1$

Figure 7. (Continued)

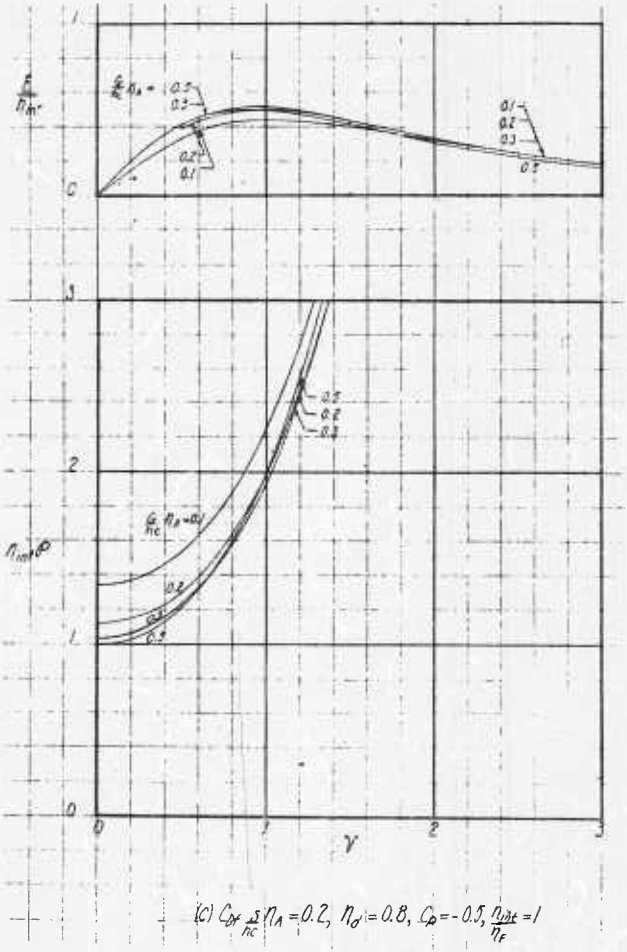

(c) $C_{DF}\frac{S}{nc}\eta_A = 0.2,\ \eta_d = 0.8,\ C_p = -0.5,\ \frac{\eta_{int}}{\eta_F} = 1$

Figure 7. (Concluded)

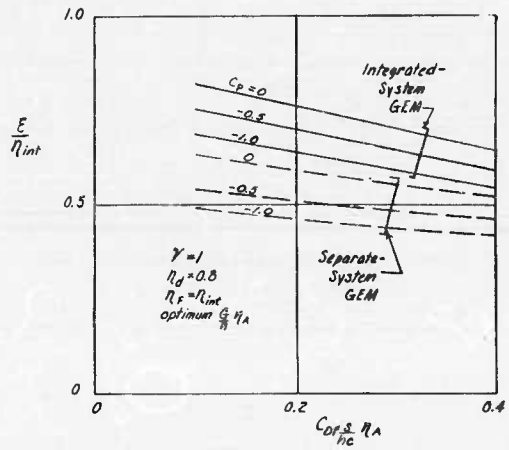

Cruise Economy; Comparison Between Integrated-System and Separate-System GEM's

(a) $\frac{E}{\eta_{int}}$ vs $C_{Df}\frac{S}{hc}\eta_A$

Figure 8.

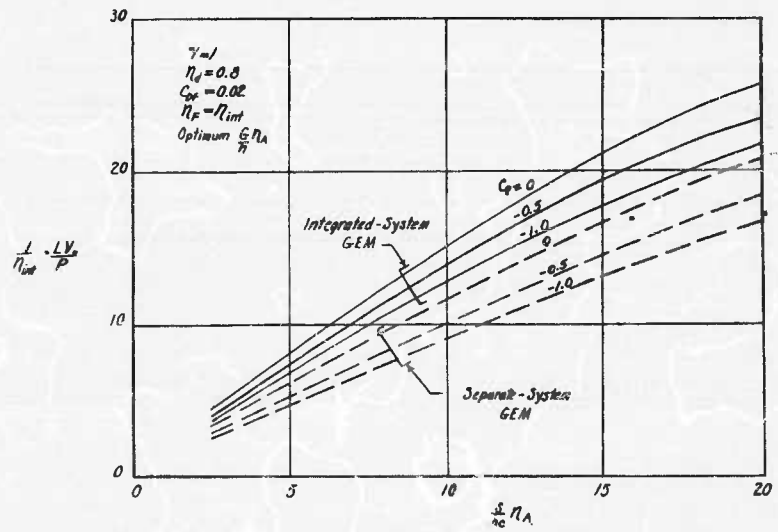

(b) $\frac{L}{\eta_{int}}\frac{LV_o}{P}$ vs $\frac{S}{hc}\eta_A$

Figure 8. (Concluded)

A PRELIMINARY DESIGN TECHNIQUE FOR ANNULAR JET GROUND EFFECT MACHINES (GEM'S)

By Harvey R. Chaplin, Aerodynamics Laboratory, David Taylor Model Basin, Washington, D. C.

TED No. TMB AD-3242, Report 1371 Aero Rept. 966, September 1959

NOTATION

S reference area in ft^2 (plan area enclosed by outer edge of nozzle exit)

h altitude in ft measured from the surface to the lower edge of the nozzle exit

G nozzle width in ft

C perimeter in ft measured at the nozzle centerline in the nozzle exit (the nozzle exit is taken normal to the jet discharge direction)

Θ jet discharge angle in degrees measured from vertical at the nozzle exit; negative for an inward-inclined jet

J scalar total jet momentum flux in lbs

Δp effective base pressure in lbs/ft^2 (gauge) (total base pressure lift, accounting for the static pressure over the nozzle exit, divided by $S - \left(\frac{GC}{2}\right)$

P_{tj} weighted-average jet total pressure in lbs/ft^2 (gauge)

V_j average jet velocity in ft/sec measured at the nozzle exit

ρ air density in $slugs/ft^3$

σ relative air density ($\sigma = \frac{\rho}{\rho_o}$, where ρ_o = 0.002378 slugs per ft^3)

L total lift in lbs

P shaft power delivered to the compressor in ft lb/sec

HP horsepower $\left(HP = \frac{P}{550}\right)$

M figure of merit $\left(M = \frac{1}{2\sqrt{\rho S}} \frac{L^{3/2}}{P}\right)$

η efficiency factor (see Table 1)

ABSTRACT

This paper provides mathematical formulas and curves sufficient to describe an annular jet ground cushion vehicle and its hovering performance. The mathematical approach consists of a "Mathematical Model" incorporating all of the significant descriptive

of the vehicle. In addition, several efficiency factors have been introduced to account for effects to be encountered in operation. Additional supporting equations are provided to fully describe the physical conditions of the vehicle in hovering. This performance description method also allows comparisons to be made of different vehicle designs.

INTRODUCTION

Early research on annular-jet ground-cushion vehicles concentrated largely on hovering performance. These efforts have produced a sound practical understanding in this single area, and hovering performance calculations can now be carried out with a fairly high level of confidence. Research into the other essential areas-cruising performance, stability, and control-has barely begun to produce results, and only qualitative understanding exists in these areas.

HOVERING PERFORMANCE

The hovering performance is conveniently expressed by the dimensionless parameter "figure of merit" M. The figure of merit as defined here is directly proportional to one of the most interesting dimensional quantities (the lift per horsepower) and further provides a convenient comparison to the performance of the helicopter and ducted fan, which ideally have values of $M = \sqrt{1/2}$ and $M = 1.0$, respectively. For the annular jet, M is a function of the annular jet "nozzle parameter" $\frac{G}{h}\eta_A$, the annular jet "size parameter $\frac{S}{hC}\eta_A$, the jet discharge angle Θ, and the efficiency factors.

$$M = \frac{1}{53.66}\frac{L}{HP}\sqrt{\frac{L}{\sigma s}} = f\left(\frac{G}{h}\eta_A,\ \frac{S}{hC}\eta_A,\ \Theta,\ \eta_V, \eta_j, \eta_{int}\right) \tag{1}$$

The mathematical model that has been developed for this relationship is

$$\frac{M}{\eta_{int}\eta_V} = \sqrt{\frac{\frac{G}{h}\eta_A}{\frac{S}{hC}\eta_A}}\left\{\frac{\left[\eta_j \cos\Theta + (1-\sin\Theta)\left(\frac{S}{hC} - \frac{G}{2h}\right)\eta_A\right]^{3/2}}{1 + (1-\sin\Theta)\frac{G}{h}\eta_A}\right\} \tag{2}$$

This expression is the basis used to determine the optimum performance of the proposed vehicle and to determine the power penalty for "off-optimum" design features during hovering conditions.

The parameters used have been selected to most fully describe the controlling physical features of the annular jet vehicle in its simplest form, a single continuous jet sheet around the periphery of the vehicle with a cross section as shown in Figure 1. The outline shape is not defined except by the S/C relationship. Comments on shape are made later.

The various efficiencies that are introduced into the mathematical model were selected to permit maximum practical usefulness of the model, account for some design peculiarities, account for minor simplifying assumptions, and yet remain reasonably constant and near unity over a practical design range. More detailed discussion of these factors is given later.

The mathematical model is displayed as solid curves in the plots of Figure 2 for the parameters shown in Figure 1. These plots also show by dashed curves the percentage deterioration of the figure of merit M (percentage of increase in power required) for

deviations from optimum $\frac{G}{h}\eta_A$ or Θ_o design conditions. An example is given for the use of equation (2) and Figure 2.

The theoretical and experimental work in annular jet hovering performance indicates, at this time, that practical designs will fall within the following limits:

$$0.1 < \frac{G}{h}\eta_A < 0.3$$

$$\frac{S}{hC}\eta_A > 2$$

$$-90° < \Theta < -30°$$

$$\frac{L}{S} < 200 \text{ lb/ft}^2$$

The mathematical model within these limits is considered adequate for normal engineering purposes.

Example: first design approximation. Initially, a general planform must be determined, and the desired operating altitude fixed. For the example, the following efficiencies will be used:

$$\eta_A = 0.8$$

$$\eta_V = 1.0$$

$$\eta_j = 1.0$$

Suppose S/hC = 10, giving $\frac{S}{hC}\eta_A = 8$ for the initial assumptions. From Figure 2,

$$\text{optimum } \Theta_o = -80°$$

$$\text{optimum } \frac{G}{h}\eta_A = 0.425$$

$$\frac{M}{\eta_{int}} = 7.70$$

If, for other reasons, the value desired for $\frac{G}{h}\eta_A$ is 0.18 instead of 0.425, a power increase of 10 per cent is required, which decreases M/η_{int} from 7.70 to 7.00 (see Figure 2).

If also a jet angle Θ of -45 deg is used, Figure 2 shows that a further power increase of 10 per cent is required, which decreases M/η_{int} from 7.00 to approximately 6.36. (Direct calculation of M should be made from equation (2) for more accurate values where

neither Θ nor $\frac{G}{h}\eta_A$ are optimum.) The "optimum" nozzle configuration of the mathematical model, equation (2) and its plot in Figure 2, are for hovering flight only. Vehicles stressing cruising performance are expected to have a slightly lower value of $\frac{G}{h}\eta_A$ (thinner nozzle) than would be used for the hovering optimum. Other design considerations may dictate a value of Θ different from the optimum for hovering.

PHYSICAL CONDITIONS AT HOVERING

The figure of merit is determined by the dimensionless size and nozzle parameters and jet discharge angle. The dimensional quantities (lift, size, power, altitude, pressure, etc.) are easily interrelated once these dimensionless parameters are established. Given the dimensionless parameters (and hence the figure of merit), as in the foregoing example, lift, power, and area are interdetermined from the definition.

$$M = \frac{1}{53.66}\,\frac{L}{HP}\sqrt{\frac{L}{\sigma S}}$$

This relationship is plotted in Figure 3, from which, given lift (gross weight) and area, the power may be determined; given power and area, the lift may be determined, etc. The other important design quantities may be obtained as explained below.

The mean total pressure (gauge) of the jet at nozzle exit is computed from

$$P_{tj} = \frac{L}{S}\left[\frac{\frac{S}{hC}\eta_A}{\frac{M}{\eta_{int}\eta_V}}\right]^{2/3}\sqrt[3]{\frac{1 + (1 - \sin\Theta)\frac{G}{h}\eta_A}{2\quad 2\left(\frac{G}{h}\eta_A\right)^2}} \tag{3}$$

The bracketed factor is readily computed from Figure 2. The cube root factor is plotted in Figure 4 for simplified calculation.

The effective base pressure (gauge), Xp, acting upon the base of the vehicle is computed from

$$\frac{\Delta P}{P_{tj}} = \frac{2\,(1-\sin\Theta)\,\frac{G}{h}\eta_A}{1 + (-\sin\Theta)\frac{G}{h}\eta_A} \tag{4}$$

This formula is also plotted in Figure 4.

The mean velocity of the jet at exit V_j is computed from

$$V_j = \frac{550\ HP\ \eta_{int}\ \eta_V}{P_{tj}\ G\ C} \tag{5}$$

If it is desired, the jet momentum J at the nozzle exit can be computed from:

$$J = \frac{L}{\cos\Theta + (1-\sin\Theta)\left(\frac{S}{hC}\eta_A - \frac{1}{2}\frac{G}{h}\eta_A\right)\frac{1}{\eta_J}} \tag{6}$$

This relationship is given as a plot of L/J in Figure 5.

DISCUSSION OF MATHEMATICAL MODEL

Equation (2), with its efficiencies set to unity, is an approximate theoretical result described in detail in a separate paper. The simple theory is approximate because it is based on:

1. Two-dimensional, incompressible jet curtain flow.
2. An average jet velocity at the nozzle exit.
3. A weighted average jet total pressure at the nozzle exit.
4. No effect of mixing of the jet with external air or with trapped base air.
5. Uniform conditions at all points of the jet curtain. (This ignores some secondary effects of planform shape, although the S/hC function accounts for the primary effects.)

The insertion of the efficiencies into Equation (2) accounts for these simplifications and renders Equation (2) exact. Its unique usefulness, however, is restricted to a range of conditions wherein the efficiencies are predictable and are not highly sensitive to design variations.

The efficiency factors account for the following variations from the exact:

1. The internal efficiency η_{int} is a common factor to any inlet, compressor, and duct air-flow situation. Considerable work exists on efficiencies of these components, and the prediction of a value sufficiently accurate for preliminary design should be possible. The internal efficiency depends to a large extent on the complexity of the internal flow of the design. A vehicle of any significant size will undoubtedly require several compressor fan units (nacelles) with their associated ducts and a form of integration into a peripheral nozzle. If for practical reasons a contorted duct flow is designed to keep the number of nacelles to a minimum, duct losses can be significant. A vehicle with multiple nacelles having a minimum internal duct travel to the nozzle and single-stage compressors with good inlets is expected to realize an internal efficiency of about 80 per cent; whereas, if a single compressor is ducted to power the entire nozzle, the η_{int} might not exceed about 70 per cent.

2. The jet velocity efficiency η_V and jet momentum efficiency η_J are simple corrections for the usual approximations of one-dimensional analysis. A nominal research effort should render these efficiencies accurately predictable. For the present an assumption of $\eta_V = \eta_J = 1.0$ is sufficient.

3. The augmentation efficiency η_A peculiar to the annular jet, is the most important factor to maintain the validity of the mathematical model. In addition to reflecting approximations employed in the simple theory, η_A could be influenced by a number of vehicle design features, among which are: (a) planform variation from circular, which includes the effect of planform aspect ratio, (b) nonuniformity in the jet curtain arising from internal losses or arrangements of planform and nacelles which result in "corners" in the nozzle and gaps in the jet curtain, and (c) the effect of jet mixing with the outside air and with the trapped air under the base (becomes serious when S/hC or G/h becomes very small).

It presently appears that η_A will be easily correlated between various experiments and not be too sensitive to design variables. Present experimental results show η_A varying between only 0.75 and 0.85 for planform variations up to 4:1 length to width ratios, jet angles from -30 deg to -60 deg, and nozzle ratios G/h from 0.05 to 0.30. Other work

has indicated that small gaps in the jet curtain are not too serious. Within the probable practical design range,

$$0.1 < \frac{G}{h}\eta_A < 0.3$$

$$\frac{S}{hC}\eta_A > 2$$

$$-90° < \Theta < -30°$$

an η_A of 0.8 appears to be reasonable for performance calculations not requiring great accuracy.

CRUISING PERFORMANCE

The research results to date on cruising performance, stability, and control have been of a very rudimentary form. Only a few qualitative and tentative observations can now be made.

The hovering performance theory and test work show that the circular planform affords the most efficient hovering; on the other hand, an elongated planform may give better overall performance for forward flight conditions. In forward flight, a pressure field is induced around the vehicle, which has a net adverse effect on the performance. The intensity of this pressure field is reduced if the vehicle is given a streamlined planform shape, elongated in the direction of flight. The size parameter $\frac{S}{hC}\eta_A$ provides for noncircular planforms.

There is a "ram drag" associated with the air drawn into the compressors equal to the mass flow rate of this air times the forward velocity of the vehicle. This drag is reduced if the nozzles are made thinner, reducing the mass flow for a given momentum, but at the expense of an increase in power required to hover. An educated guess at this time puts the best value of $\frac{G}{h}\eta_A$ in the neighborhood of 0.2 to 0.3 for speeds of the order of $V_o = 20\sqrt{\frac{L}{\sigma S}}$.

There is, theoretically, a very definite advantage in propelling the vehicle by exhausting the main peripheral jet in a rearward-inclined direction, rather than by the use of a separate propulsion device. It is not yet clear what the relative practical merits of these two methods will be.

STABILITY AND CONTROL

The only positive inherent stability which the simple annular jet possess is altitude stability. If prevented from pitching or rolling, the simple annular jet at a fixed power setting has a strong tendency to seek a fixed altitude, and to return to that altitude if disturbed. If three or more annular jets are properly fastened together by a rigid framework, the resulting combination is also stable in pitch and roll, since each jet will seek its own altitude, thus fixing the attitude of the combination. The same effect can be achieved on a single vehicle by dividing the base into compartments by means of downward-exhausting secondary air jets. Each compartment behaves like a weak annular jet superimposed upon the single strong annular jet. It is not yet clear what the best arrangement

of secondary nozzles is, nor how strong (and how power-consuming) the secondary jets have to be. Compartmentation is not the only possibility for achieving stability, but it appears to be the most promising means.

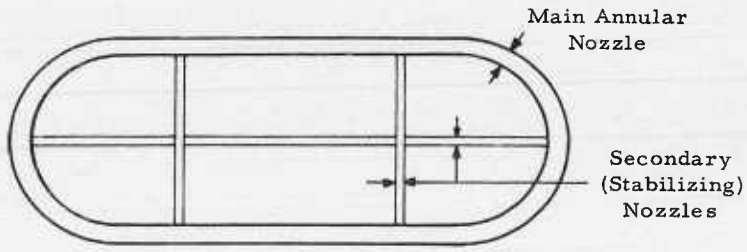

Nozzle arrangement on one of DTMB's research models. Bottom View.

Directional stability may be provided by means of stabilizing fins similar to those used on other aircraft.

Compartmentation also provides an effective means of attitude control, since the pressure lift of a single compartment can be controlled by controlling the momentum of the section of main annular jet adjacent to that compartment. This may be done by throttling the engine supplying that section of nozzle, diverting air from it to another section, changing its jet exhaust area, or "spoiling" the air flow through it.

The method of forward speed control depends on the method used to propel the vehicle. It is theoretically possible to control the speed by tilting the vehicle, but this is impractical for high augmentation vehicles (vehicles operating at a high value of S/hC). Directional control may be incorporated with the forward speed control, turning being accomplished by providing more propulsive thrust on one side of the vehicle than on the other.

Name	Definition	Probable Value in Design Range*
Internal Efficiency Factor	$\eta_{int} = \dfrac{V_j G C P_{tj}}{P}$	0.8†, 0.7††
Augmentation Efficiency Factor	$\eta_A = \dfrac{\Delta p}{(2P_{tj} - \Delta p)(1 - \sin\theta)\dfrac{G}{h}}$	0.8
Jet Velocity Efficiency Factor	$\eta_V = \dfrac{\sqrt{\dfrac{2}{\rho}\left(\dfrac{P_{tj}}{1 + (1-\sin\theta)\dfrac{C}{h}\eta_A}\right)}}{V_j}$	1.0
Jet Momentum Efficiency Factor	$\eta_J = \dfrac{J}{\dfrac{2P_{tj} G C}{1 + (1-\sin\theta)\dfrac{G}{h}\eta_A}}$	1.0

*Probable values based on good design practices and operation within the range:

$$0.1 < \frac{G}{h}\eta_A < 0.3, \qquad \frac{S}{hC}\eta_A > 2$$

$$-90^\circ < \theta < -30^\circ, \qquad \frac{L}{S} < 200 \text{ lb/ft}^2$$

†For vehicle with numerous short, regular ducts.

††For vehicle with one or a few long irregular ducts.

Table 1. Hovering efficiency factors

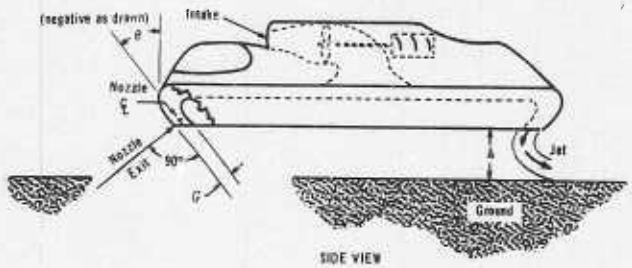

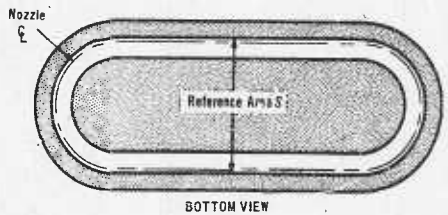

Figure 1. Sketch showing vehicle geometry notation

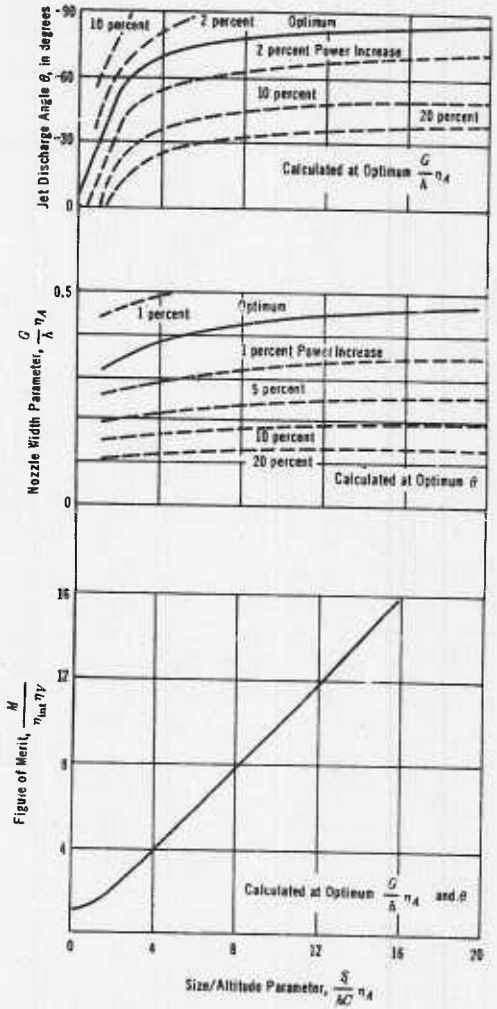

Figure 2. Optimum nozzle configuration and figure of merit versus $\frac{S}{hC}\ \eta\ A$

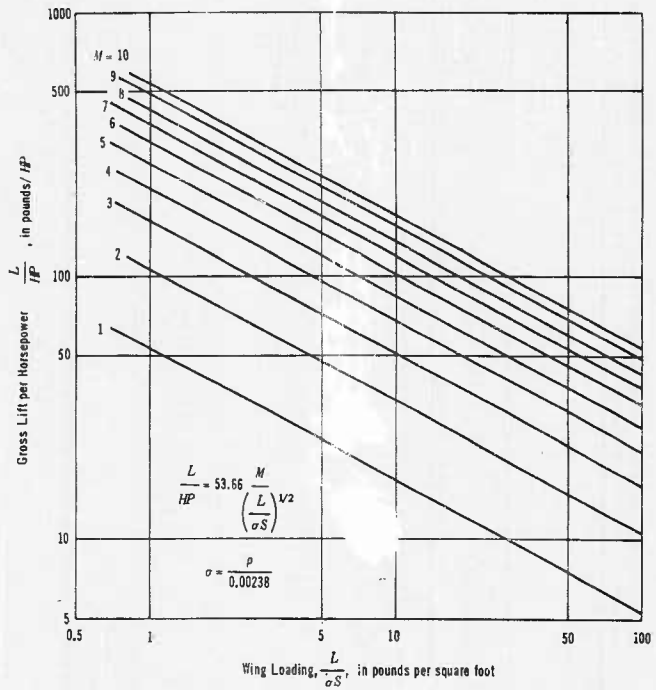

Figure 3. Lift per horsepower versus wing loading for several figures of merit

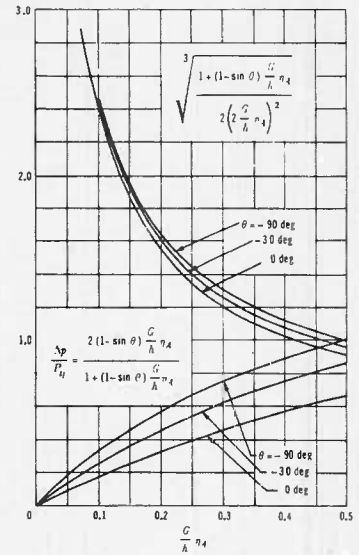

Figure 4. Chart for simplified evaluation of equations (3) and (4)

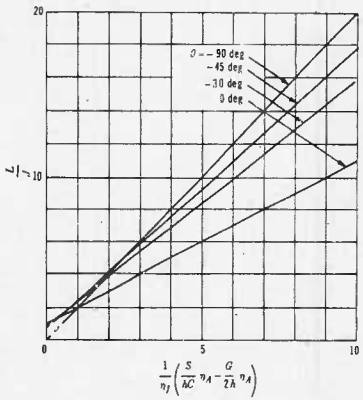

Figure 5. Ratio of total lift to total jet momentum

FLOW PHENOMENA OF THE FOCUSED ANNULAR JET

By J. C. M. Frost and T. D. Earl, Avro Aircraft, Limited

INTRODUCTION

The discovery in 1953 that a circular jet curtain would produce a powerful ground cushion was received by engineers at Avro with considerable enthusiasm. Not as a means for suspension of a new type of automobile, but as the undercarriage for a vertical take-off jet aircraft. Avro had considered the possibility of a purely ground cushion vehicle, but if the power requirements were not to exceed those of existing road vehicles, a lot of work would have to be done before such a device could be put to good use. The problems of maneuvering at speed and the comparatively flat surfaces necessary for the operation of a vehicle with a very low ground clearance would have to be considered.

The area into which we felt the ground cushion machine would most naturally fit, was that of a flying machine using its body as the wing, capable of either travel on the ground cushion or able to rise into free air to clear woods, hills, lakes, and the like. For such a vehicle to be successful, the main requirements are the following:

1. An effective ground cushion of two to three feet must be realized. This is thought to be a minimum for normal operation over unprepared terrain.

2. With forward speed the ground cushion must not disappear, but must be evenly replaced by the aerodynamic lift of the wing. The vehicle must be stable and maneuverable in free flight and in the ground cushion.

3. As the vehicle develops flying speed it must be possible to direct the jet from downwards to rearwards. The penalty for not directing the jet sufficiently rearwards is a heavy momentum drag and the loss of propulsive efficiency.

A circular planform wing was thought to be the best compromise in which the poor lift/drag ratio in forward flight, due to the low aspect ratio of the circle, was largely offset by the fact that the circle provided for the optimum duct system with minimum internal aerodynamic losses. The circle was also the best shape according to our tests for an annular ground cushion jet, and the optimum shape for structural simplicity and lightness.

Since, however, the center of lift in the ground cushion is in the center of the wing and moves forward to the quarter chord during forward flight, and because the center of gravity must be near the center of the wing, an artificial stabilizer will be required. This must be simple enough to withstand the rigors of everyday use, and must not require electronics or the services of a trained expert.

We are at present developing an annular jet aircraft called the Avrocar, in a program jointly sponsored by the U. S. Air Force and U. S. Army, which we hope will overcome these problems. This project is at present classified and it is not therefore possible to give details; however, some of the test results on the annular jet ground cushion have been released and are thought to be of interest at this time.

THE GROUND CUSHION

The annular jet as an adjunct to VTO. The annular jet ground cushion, regarded as the undercarriage for a vertical take-off jet aircraft, seems to possess, at first sight:

1. Excellent vertical take-off and landing characteristics and stability with respect to height.
2. The ability to take-off from rough and uneven ground from any reasonably open space with the weight of the aircraft greater than the basic thrust.

Using an annular jet wing, it should be possible to pick up speed in the cushion and exchange the lift/thrust ratio it provides for the conventional wing lift/drag ratio. Thus, besides having a stable characteristic for VTOL at whatever useful load should prove feasible, ground cushion take-off with a greater load will always be possible and thus range-payload capability beyond the reach of VTO can be got. This characteristic seems remarkably attractive since, in all probability, ground cushion take-off can be made over fences, ditches, across fields, rough ground, snow, water, etc. Indeed from almost anywhere except in forests or cities or over the edge of a cliff.

Annular jet static tests. Appreciating these advantages, the USAF, with Avro, started a program of model tests in 1954. The parameters considered likely to be important were jet aspect ratio (defined as mean circumference divided by width of jet); pressure ratio (since the jet-energy/jet-momentum relationship was thought essentially bound up with the lift augmentation); nozzle configuration (for example, discrete jets as opposed to an uninterrupted annulus, or the addition of a central jet or jets); and inclination of the jet to the vertical.

Broadly the results of these early tests showed that the ground cushion was an extremely stable phenomenon, that it was difficult to interfere with, and that almost any enclosing jet would produce a ground cushion of some sort. However, a great variety of lift augmentation curves are possible and a smooth curve of lift increase versus distances from the ground was the exception rather than the rule.

Tests were started on a simple annular jet curtain with the jet exhausting at 90° to the wing chord. The following major problems emerged:

1. About 40 per cent of the nozzle reactive thrust is lost in "free air," out of ground effect.
2. The wing is unstable at all heights within the ground influence, reaching a violently unstable condition at some critical height (about 1/2 a diameter) above the ground.
3. The wing is unstable with forward speed, tending to give a negative stick force gradient.
4. A hump in the curve of lift augmentation (lift/thrust ratio) versus height is produced, a characteristic which will motor a sustained vertical oscillation.

The static performance of this simple jet curtain is shown in Figures 1 and 2, the results being taken from a fairly large (3-ft diameter) 1/2 plane model of a circular wing with a peripheral jet. These results apply for a jet aspect ratio of about 200 and a pressure ratio of 1.5. The effects of these two parameters, determined in tests using small models (10 and 20 inch diameter) were not very large. Within the limits tested, these tests indicated that higher pressure ratio was better and so was lower nozzle aspect ratio (Figures 3 and 4). In practice, these effects tend to cancel since the higher pressure jet is usually smaller in relation to wing size.

Attempts were made to improve both the stability and free air thrust by varying the nozzle configuration. Two schemes gave favorable results: the addition of a moderately powerful central jet (up to 20 per cent of the peripheral thrust) for stability, and the introduction of gaps into the jet annulus for greater free air thrust.

The addition of the central jet was expected to improve the stability, since it is clear that the reason for the instability is the tendency of the whole annulus to escape from one

side in the manner sketched in Figure 5, when the aircraft is angled to the ground. Stability was in fact greatly improved. However, there was also a powerful effect on lift augmentation (Figure 6). This is a rather startling extension of the ground cushion "plateau," as one may call it, but it is doubtful if this plateau of augmentation is usable in view of cross-flow effects outlined later.

The jet curtain was broken or vented in a test series to determine how much venting was required to restore the free air thrust and whether a ground cushion would remain. The loss is clearly due to the turbulence under the wing and is analogous to the separation behind any bluff body in a flow; alternatively, it may be regarded as a reversal of the jet curvature required to maintain a positive pressure in the cushion (Figure 7). These tests showed that the free air thrust could be restored to about 90 per cent of the nozzle thrust by approximately 1/3 venting in three places but the cushion close to the ground was spoiled (Figure 8). A possible method of re-establishing free air thrust for VTO was thus to segment the annulus after initial take-off.

However, later tests showed a better compromise. The last important parameter investigated in the early tests was the jet angle; the results of a series in which the angle was varied are given in Figure 9. It is fairly clear that lift augmentation close to the ground is improved by inward angle as is predicted by theory, and it is obvious that the unacceptable hump can be eliminated. No noticeable improvement in free air thrust was found at an inward angle of up to 20°. However, it was realized that since this loss was essentially due to a separation it could possibly be saved if the peripheral jet was attached to the undersurface or 'focused' as we have called it, and that this configuration would also give a satisfactory cushion characteristic. This was found to be the case, although some loss is likely to remain because of the additional jet bending involved in focusing the jet. On the Avrocar we use a focused jet and measurements indicate that 80 to 90 per cent of the nozzle thrust is recovered.

An idealized family of lift augmentation curves drawn from various data is shown in Figure 10, from which it is seen that focusing largely overcomes two problems of the plain annular curtain jet, that is, the reflex in the curve of lift augmentation and free air thrust loss.

This method of jet deployment is also favorable from the point of view of static stability.

At the top of the cushion the focused jet forms a thick central jet core which is neutrally stable, as would be expected. As the aircraft closes with the ground and lift augmentation increases, the central core or tree-trunk tends to thicken, remaining approximately neutrally stable, until at some height, depending on how well the jet is focused, the flow will detach from underneath the wing becoming rather similar to the vertical curtain, although better, because of the inward angle. A somewhat unstable static moment now exists, but this can be made very positively stable by the retention of a central jet. Figure 11 summarizes our findings on the stability of these various jet configurations. Figure 12 summarizes the lift augmentation and shows the straight curtain, the inwardly angled curtain with central jet, and the focused case. Also shown is the well-known negative effect where the lift is reduced by the presence of the ground. Measurements of this case were made to determine the zero-lift height (10 per cent span) and the height of the ground influence (approximately 45 per cent span).

Dynamic considerations. To this point we have been preoccupied with static forces and moments. However, in considering the ground cushion as a means of leaving the ground in a VTO aircraft, dynamic considerations are of equal importance.

If the lift augmentation is a smooth curve, as in the case of the focused jet, it seems, at first sight, to be simply a nonlinear pneumatic spring. In the hovering case it is

practically true to say that aerodynamic forces are too low to produce any but the most feeble contribution to damping. Thus it might be expected that with this lift augmentation we have an undamped spring. If, for example, the cushion were entered in a vertical landing maneuver, a sustained bounce would result which the pilot would find very difficult to control. An electronic simulation study proved this to be the case. This behavior did not seem to correspond to that observed in free hovering experiments with a focused annular jet model. Therefore it was concluded that the ground cushion must itself provide substantial damping and tests were done to find out if this were so.

Again, two conditions of jet were studied: (1) the unfocused curtain, with and without central jet and (2) the focused case. In these tests a model (Figure 13) was suspended from a spring and dropped into the cushion from various heights above the ground. The time to damp to 1/2 amplitude was noted.

In the case of the curtain jet a sustained oscillation was found. This is believed to be due to the hump in the lift augmentation curve previously mentioned. Clearly, this type of curve (see Figure 10) is made up of two height-stable slopes, one near the ground and one in the top half of the cushion, with an unstable region between them. If the thrust is set to balance the weight in the unstable region, then the model will motor up and down between the stable heights.

In the case of the focused jet or with a central jet added to the curtain jet, behavior is quite satisfactory and considerable damping is provided by the ground cushion itself, becoming greater as the ground is approached. The result for the focused case is given in Figure 14 and indicated an acceptable characteristic on the simulator.

Further damping contributions in pitch, roll and yaw are provided by the jet flow itself. For example, a rate of yaw will produce a moment N of MR^2/g ft lb per rad/sec where M is the jet mass flow and R is the radius of the annular jet. This contribution is highly significant to the hovering behavior as determined by analogue simulation. This moment has to appear as an internal differential static pressure and may be likened to an internal fin effect.

Similar contributions in pitch and roll are evident.

Transition to forward flight. The initial stage of transition is visualized as analogous to helicopter flight. The nose is depressed to give a forward thrust component and the aircraft accelerates, the small loss of vertical thrust being balanced by the aircraft sinking, either in free air or a little way into the ground cushion. Within the cushion the first vital question is "What happens to the augmented lift?"

We have done some tests on a small model using both a curtain jet angled inwards, the same jet with a central jet added, and a focused jet. The results form an interesting comparison.

Figure 15 shows wing loading, at -5° angle of attack, plotted against dynamic head and Figure 16 shows center of pressure (zero is the center of the circular wing) also plotted against dynamic head. In the cushion at a height of 20 per cent where both flow regimes are similar, lift increases with speed (curves A of Figure 15) even at this negative angle, and little change of trim is found (curves A of Figure 16) almost an ideal state of affairs. At 82 per cent, out of lift effect but where the ground can still influence the stability of the curtain jet, the two cases are very different. The lost free air thrust of the curtain jet tends to be quickly restored by the air flow, whereas the focused jet lift stays more or less constant initially, starting to build up rapidly as speed is increased beyond a certain value (curve B of Figure 15). Statically, the curtain jet is extremely unstable; furthermore, the addition of cross flow immediately increases the nose-down

moment at -5° to a point where control is not practical. The focused jet on the other hand is neutrally stable statically (hence has no moment at zero speed) and develops a nose-up moment as speed is increased to a certain point, after which the moment tends to reduce (curve B of Figure 16). This speed is beyond that visualized for transition to forward flight and is not considered important. A mental picture of what the jet flow is doing will explain this behavior (Figure 17). The recovery of lift by the curtain jet is explained by the tendency of the cross flow to blow the forward sector of jet back into the cavity formed by the rest of the jet annulus and so reduce the separated area; and the nose-down moment comes from the front jet coalescing with the rear jet to form a "jet-flap" at the wing trailing edge. Eventually, a speed is reached when the focused jet gets "blown back" in a similar way. It should be noted that the air intake, not shown here, was operating to approximately 80 per cent of the jet flow in these tests and that this has a nose-up moment contribution. This moment is an important one for any fan-in-wing design.

Addition of a central jet to the curtain considerably improves the situation but the same characteristics are observed (curves A of Figures 18 and 19).

Curve C of Figure 15 indicates that the ground cushion "plateau" of the curtain jet may not be usable in practice, since we found that the augmented lift at a height well out on the knee of the augmentation curve for the curtain jet is "blown away." Indeed, as far as lift is concerned, there is little to choose between curves B and C (representing free air and 40 per cent span) above a speed corresponding to a dynamic head of 3 lb/ft. We conclude again that the front sector of jet is easily blown back much the same as in the free air case, although the moment is much less drastic (curve C of Figure 16). Addition of a central jet (curve C Figures 18 and 19) does quite a bit to improve this situation, particularly with regard to moment; however, it seems doubtful if the extended plateau which we found could be achieved with a central jet is really usable. We have not done tests to explore this area.

As far as lift and moment are concerned, we concl de that the focused configuration will be satisfactory in or out of the ground cushion in slow translational flight. The question of how drag builds up with forward speed now arises.

The drag may be considered as made up of friction drag, drag due to aerodynamic lift, and momentum drag of the propulsion jet-lift system. The friction drag is small in the transition speed range in relation to other thrust/drag forces present. Variations of these elements of drag for a low energy jet exhaust typical of the popular ducted fan are shown in Figure 20, where a series of lines for momentum drag corresponding to different thrusts and thus representing different heights in the ground cushion is shown. If we assume that no part of the jet-lift can be recovered as thrust, these curves indicate that with an augmentation factor of 2.0 (obtained at a height of about 20 per cent span) it would be better to support the aircraft weight with the wing at all speeds above 158 ft/sec (point A). This is rather an oversimplified picture for several reasons:

1. The assumption of zero thrust recovery (in the sense that the jet-flap as presented by Davidson should recover thrust from a jet exhausted in the lift direction) is not necessarily valid.

2. A forward component of thrust should certainly be expected if the nose of the aircraft is tilted downwards in the ground cushion. At heights above the ground where a reasonable angle is possible, this alone should allow a satisfactory ground speed. The angle required to equate momentum and friction drag with $-W \tan\alpha$ is given in Figure 21.

3. As previously outlined, lift increases with forward speed, even at negative angle of attack. (Figure 15.)

If a high energy jet were to be used, momentum drag would clearly be less important; however, the low speed fuel consumption would be increased, tending to defeat the object of ground cushion cruising. However, it is clear from the typical plot of Figure 20 that the aircraft will have to travel close to the ground to achieve a drag competitive with the minimum aerodynamic drag. Thus we foresee a transition phase where the pilot will "unstick" and the jet be deployed aft as in Figure 22 and we visualize transition flight paths in and out of ground cushion as depicted in Figure 23.

The impingement problem. Another advantage of the focused jet is derived from the jet stream which, before turning to strike the ground, becomes more and more diluted as the aircraft rises in the ground cushion. Problems of ground impingement are therefore vastly less serious by comparison with those arising from the use of a concentrated jet.

To determine the order of velocity magnitude at various points in the exhaust stream of a focused jet, a survey was conducted. The average velocity of the stream at the exhaust nozzle was found to be three times that in the "tree-trunk" at a point 0.4 spans below the model.

Use of the turbojet as a generator of high pressure gas for a focused jet thrust places the combination in an attractive light, since the entrainment of air will dissipate not only the impingement velocity but also heat. Purely from the jet VTOL point of view there seems, therefore, little against using a turbojet exhausting into an annular nozzle since, from our experience, the specific weight of fans when used as a means of power conversion is hardly better than that of turbojet engines. During the take-off operation, turbojet fuel consumption would be high, but for many missions take-off can be a small proportion of flight time.

THE CIRCULAR WING IN FORWARD FLIGHT

The annular jet, a simple structure, and a high volumetric efficiency lead to the choice of a circular planform wing for aircraft with ground cushion take-off and landing capability. There is not much data published on the aerodynamic characteristics of circular planform wings. Some of the earliest tests were done by C. Zimmerman (NACA TN 539) on a Clark Y Section. These showed a nonlinear lift curve (typical of the low aspect ratio) and an aerodynamic center varying with angle of attack from approximately 22 per cent to 35 per cent of the root chord. Tests that we have done on thin wings show this to be a characteristic of the planform when used in the conventional aerodynamic manner. However, the addition of a trailing edge jet sheet as on the Avrocar in forward flight, appears to stabilize the aerodynamic center close to 31 per cent for all angles.

Since the aspect ratio is $4/\pi$, the lift/drag ratio is obtained from the gratifying simple expression $(L/D)_m = \sqrt{e/C_{D_o}}$ (assuming these invariant with speed). e is the Oswald efficiency factor and C_{D_o} the zero-lift drag coefficient. Values of L/D max of up to 12.0 have been obtained from tests of thin wings.

Other than its low aspect ratio (1.27), there appears to be no salient aerodynamic disadvantage to the circular wing. To put it to use, it is necessary to accept an aft C of G position which probably cannot be brought ahead of the neutral point. Because of this, artificial stabilization over the complete speed range in forward flight will be necessary. We think acceptance of these conditions is feasible with jet control and a simple mechanical system.

CONCLUDING REMARKS

The Avrocar embodies the focused annular jet and is intended primarily to serve as a research vehicle to study the whole panorama of ground cushion operations. It is, for

instance, greatly overpowered for the ground cushion role alone. This is intentional since, as previously explained, we mean to study its operation when flying clear of the ground, arriving there either vertically or using the ground cushion as an undercarriage. It is intended to study its operation over water using very low power settings with and without a skirt, and with various control arrangements.

It represents a genuine attempt to design a low pressure duct for minimum losses, and has a novel type of power transmission system which is thought to be most suitable for this type of vehicle. Problems of noise, temperature distribution, and aerodynamic and thermodynamic efficiency are already being studied. At the time of writing, the Avrocar has just started intensive ground testing. It is sincerely hoped that within the next few months it will be able to make a genuine contribution towards furthering the knowledge of this subject for the benefit of all.

Acknowledgment. We wish to express our appreciation to various members of the staff of Avro Aircraft, especially Mr. B. Roden, who have been largely responsible for the preparation of this paper.

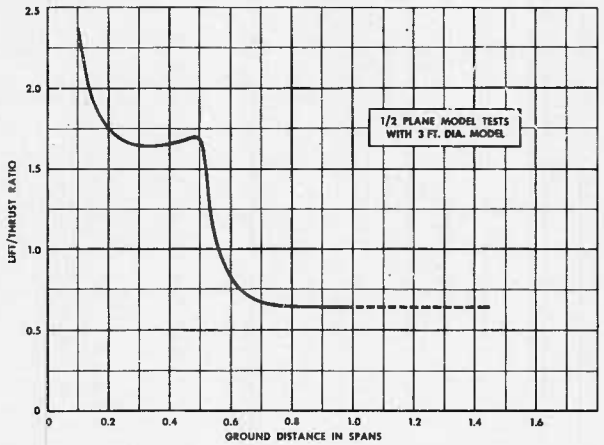

Figure 1. Effect of ground distance on lift/thrust ratio

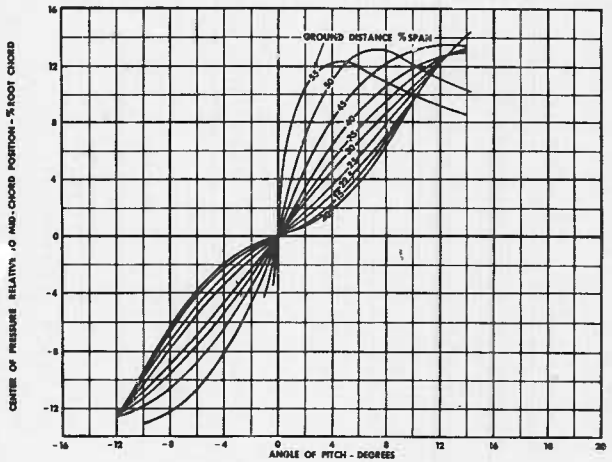

Figure 2. Effect of angle of pitch on center of pressure location

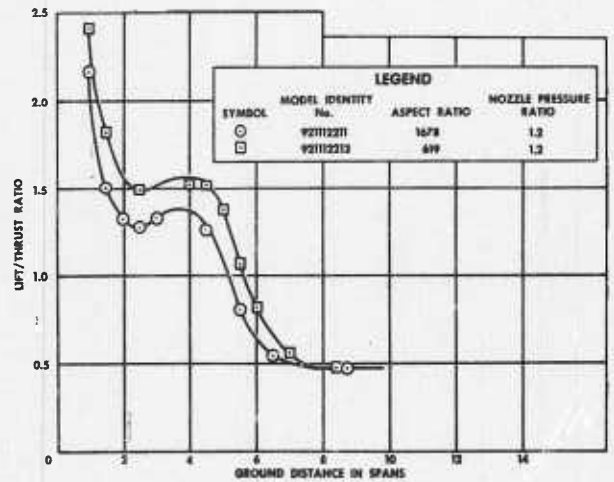

Figure 3. Effect of nozzle aspect ratio on lift/thrust ratio

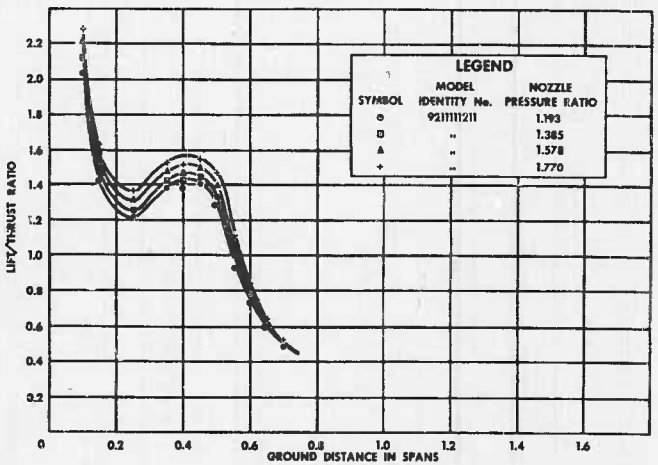

Figure 4. Effect of nozzle pressure ratio on lift/thrust ratio

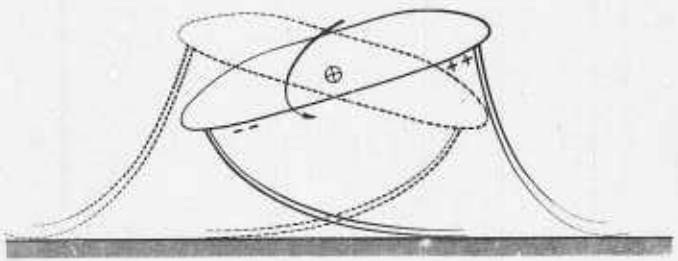

Figure 5. Static Instability with annular curtain type jet

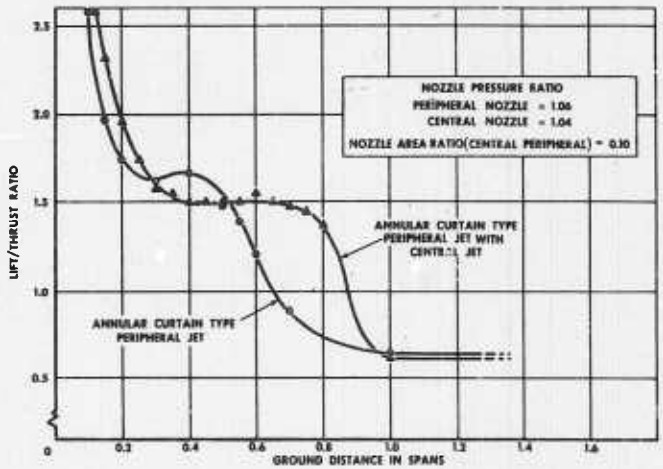

Figure 6. Effect of central jet on lift/thrust ratio

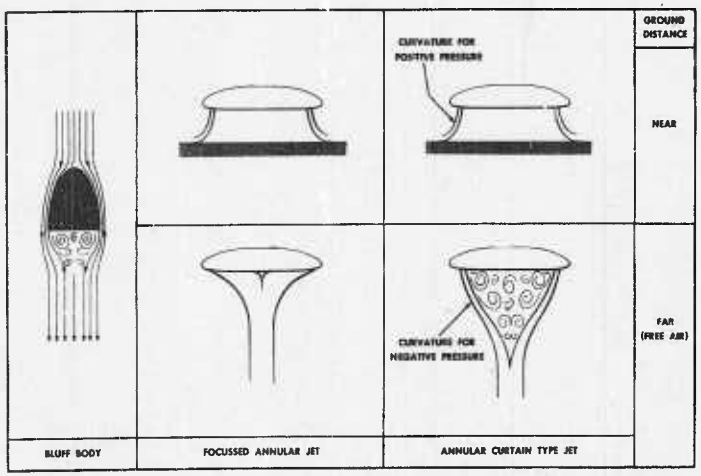

Figure 7. Bluff body analogy

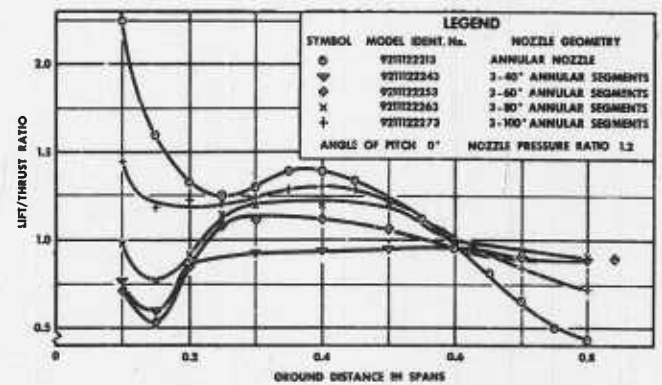

Figure 8. Effect of nozzle geometry on lift/thrust ratio

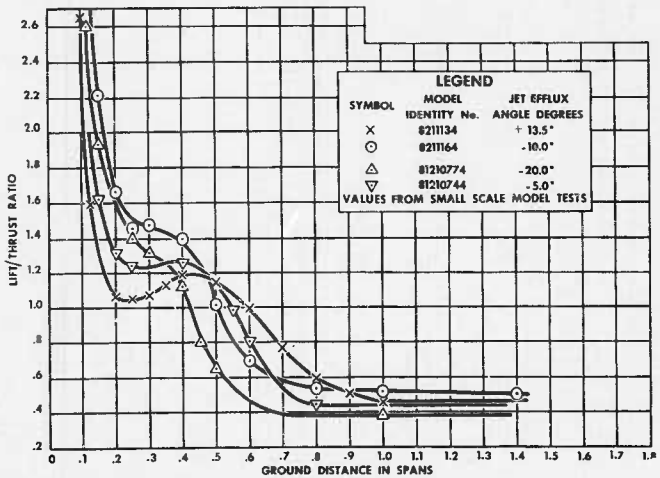

Figure 9. Effect of jet efflux angle on lift/thrust ratio

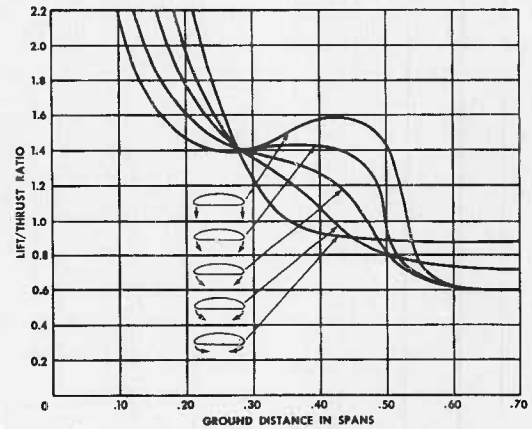

Figure 10. Idealized effect of jet efflux Angle on lift/thrust ratio

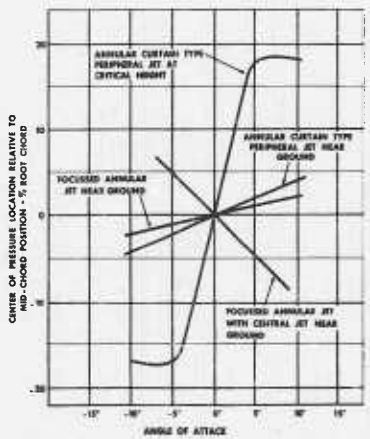

Figure 11. Static stability with annular curtain, central and focussed jets

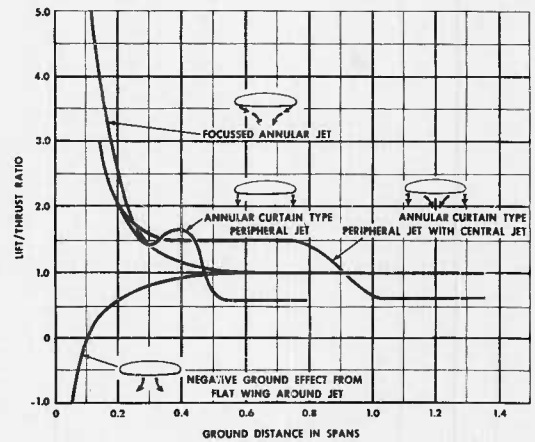

Figure 12. Ground cushion effects with annular curtain, central and focussed jets

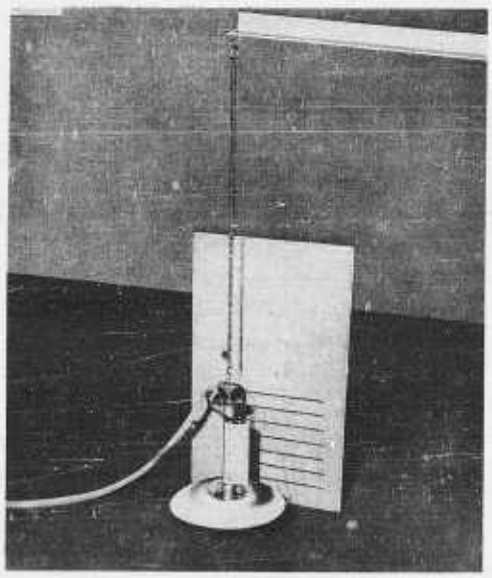

Figure 13. Ground damping test

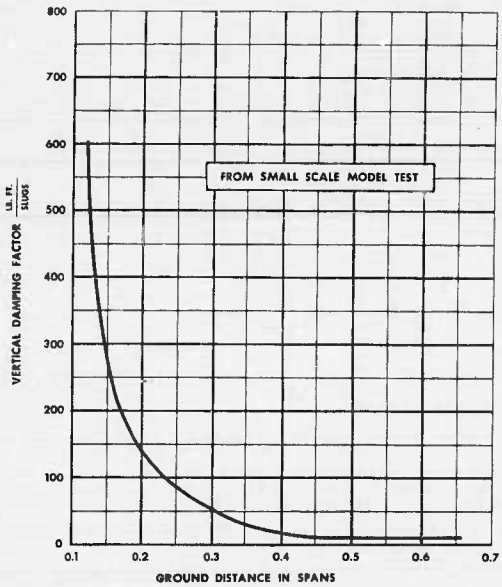

Figure 14. Vertical damping characteristic in ground cushion

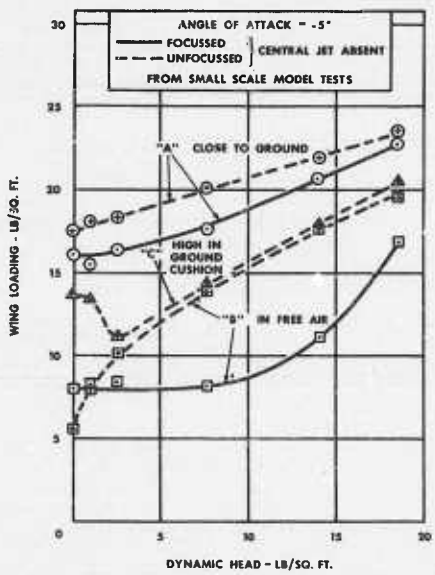

Figure 15. Effect of focussed annular jet on wing loading

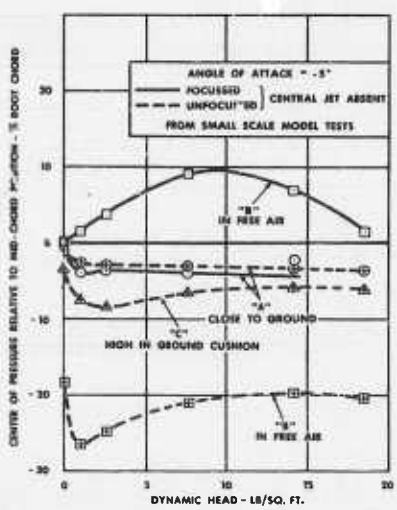

Figure 16. Effect of focussed annular jet on center of pressure location

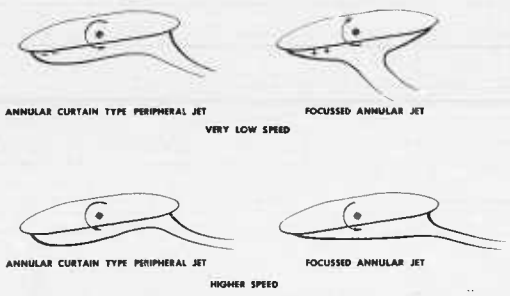

Figure 17. Effect of translation on jet flow

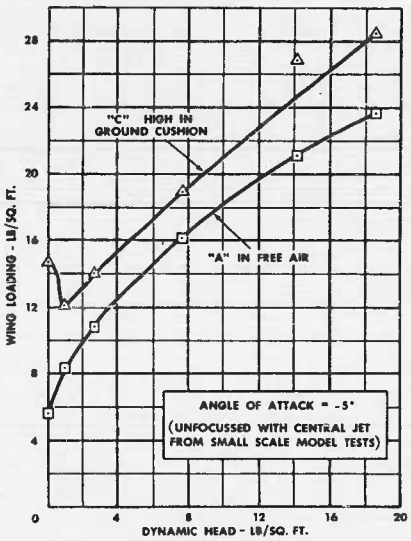

Figure 18. Effect of introducing central jet on wing loading

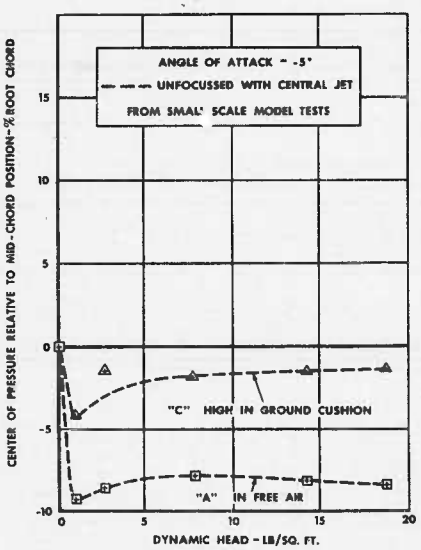

Figure 19. Effect of introducing central jet on center of pressure location

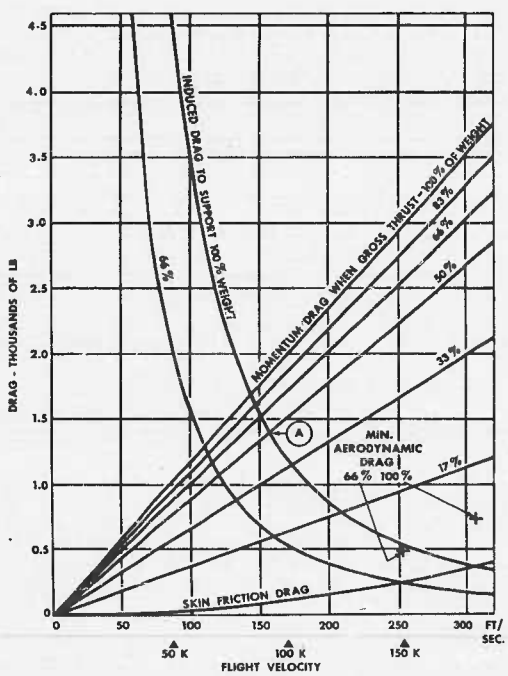

Figure 20. Low speed drag elements

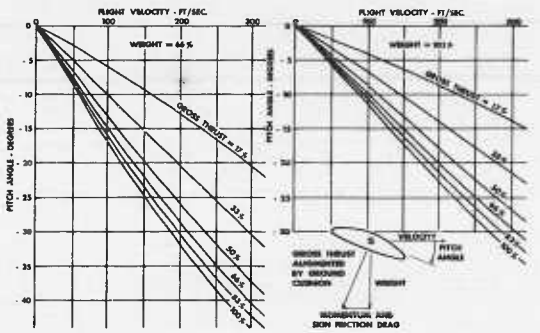

Figure 21. Effect of speed on equilibrium pitch angles

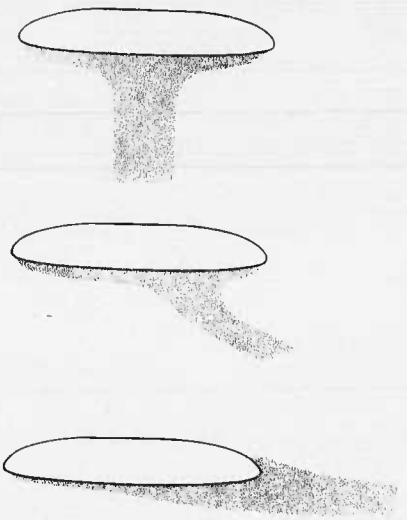

Figure 22. Envisaged flow in transition from hovering to forward flight

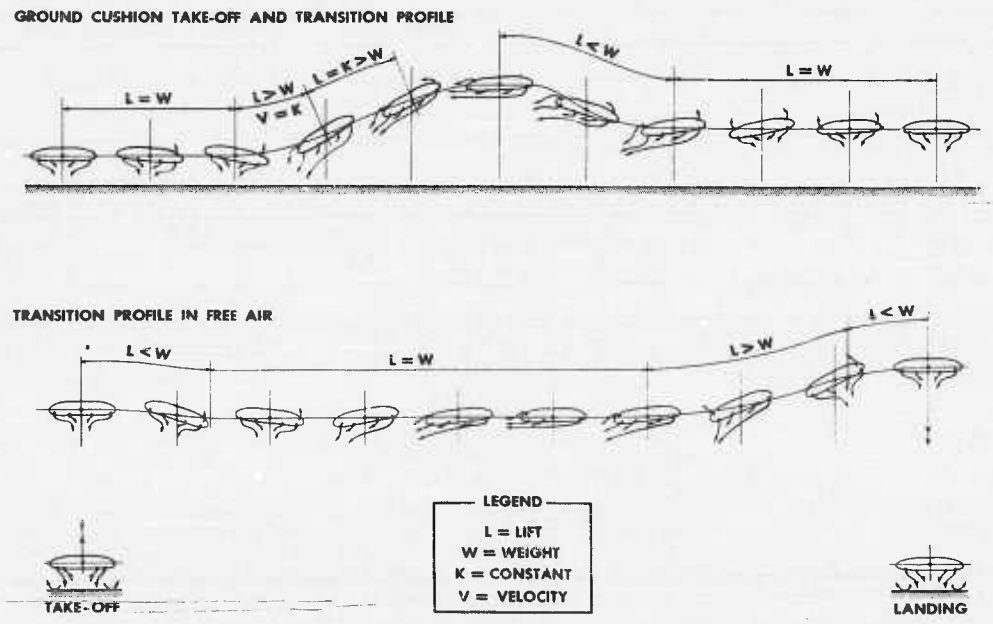

Figure 23. Transition flight paths

TWO-DIMENSIONAL STUDY OF A LOW PRESSURE ANNULAR GROUND EFFECT MACHINE AT FORWARD SPEED

By Jeffrey Tucker, Grumman Aircraft Engineering Corporation,
Bethpage, New York

SUMMARY

The results of several studies of low pressure annular jet ground effect machines are presented. A brief discussion of the qualitative results obtained from a small dynamic free flight model is presented along with comments on some of the problems associated with predicting the performance of ground effect machines at forward speed. Two-dimensional experimental investigations of the parameters governing hovering and forward flight are also discussed.

INTRODUCTION

The work done at Grumman on ground effect machines has been carried out on a modest budget entirely within the Research Department. The Research Department has tried to develop a performance theory so that the position of the ground effect machine in the field of military and commercial transportation could be determined. It was felt that the publicity given the ground effect concept was a little unrealistic when the only data available at Grumman consisted of Chaplin's basic theory of an inviscid two-dimensional jet of zero thickness (reference 1) and von Glahn's experimental data (reference 2).

In order to obtain qualitative information on the behavior of ground effect machines, a two-foot diameter free flight demonstration model was constructed. Based upon the observations made of the performance of the demonstration model over both land and water, a two-dimensional test rig was constructed to gather preliminary qualitative data on the effects of varying nozzle angle on the base pressure of a hovering GEM. Comparison of base pressures over both fixed and fluid surfaces and an attempt to determine the correlating parameters of a jet of finite thickness were also made. Other improved models added substantiation to the theory that had been developed for a finite thick jet by Lee Fuller of Grumman (reference 3) and also by Pinnes (reference 4). The most recently tested two-dimensional model simulated the effects of forward speed on the base pressure of a ground effect machine.

DISCUSSION

Free flight model. In an effort to obtain qualitative information on the inherent stability of annular jet ground effect machines (GEM) a 20-inch diameter demonstration model was constructed. Two concentric circular nozzles, pointed inward 45 degrees, were used for most of the testing. The inlet was 10 inches in diameter. The power was supplied by a 1 horsepower model airplane engine, which in this installation operated at considerably less than its rated rpm and power. The vertically mounted inlet discharged into a plenum chamber from which the air exhausted through the nozzles. The total exhaust area was half the inlet area. The maximum pressure ratio attainable with this engine propeller combination was approximately 1.01. The 14 lb model "flew" at a height of 1-1/2 inches over a fixed surface. The same configuration lifted a total of 44 lb to a height of 1/4 inch.

The most interesting part of the testing of the demonstration model was its instability when tested in water. The same configuration that exhibited stability over land was

violently unstable over water. The model was not above the free surface of the water and appeared to be sitting in the cavity produced by the jets. The spray pattern was considered excessive. To suppress the spray and recover some of the energy lost in producing it, a circular plate parallel to the base and extending outward 4 inches from the sides of the model was added. This modification not only suppressed the spray and increased the hovering height over the water to 1/4 inch, but it made the model stable. This configuration with the flat spray plate was then retested over land. The large overhang of the spray plate reduced the hovering height from the previous 1-1/2 inches to 1/4 inch. This was undoubtedly due to the negative pressure developed between the horizontal spray plate and the ground. In an effort to reduce this negative pressure a series of spray plates were fitted to the model, which made an angle above the horizontal of 5, 10, and 15 degrees. Increasing the angle increased the model's hovering height over land but progressively reduced the stability over water. The final configuration made use of a spray deflector which in section was a half circle concave downward. This configuration was stable over both land and water. The configurations are illustrated in Figures 1 and 2. Figure 1 shows the model with the 10-degree skirt in the water. The string is attached to the deck only to keep the model within camera range. The second figure shows the final configuration over land; the height is approximately 1-1/2 inches.

Several conclusions can be drawn from the qualitative testing of the free flight demonstration model. The instability of GEM over water can be a serious problem. The stability achieved with the model was accomplished by reaction with the spray, and is not inherent in the configuration. Flight above the free surface of the water was only obtained by recovering some of the energy lost in generating the spray by the use of a suitably shaped skirt.

Two-dimensional hovering tests. In an effort to understand the performance of the demonstration model, a two-dimensional test rig was constructed and tested in conjunction with the free flight model (reference 5). It was hoped that a preliminary quantitative evaluation would be obtained between base pressure, air horsepower and height above land and water. At the time this test was started, no theory accounting for jets of finite thickness was available. An experimental attempt at determining the correlating parameters was begun.

The model was simply a plenum chamber fed by a large vacuum cleaner which supplied approximately 6#/min air flow at a pressure of approximately 4 inches of water. The jet was a two-dimensional section 6 inches in length. The jet thickness could be varied from 1/8 to 3/8 of an inch. There was only one jet on this model, the other side of the base cavity being closed by a fixed vertical wall.

The first testing was done over water in an effort to explain the instability of the previously described free flight model and to investigate the effect of nozzle angle on base pressure. For a constant weight flow, jet velocity, and height there appeared to be a linear increase in base pressure with increasing jet angles (positive inward). In one example, where the nozzle was placed on the free surface of the water before the air was turned on, the base pressure increased linearly from approximately 2.5 psf with the jet directed vertically, to 12 psf with the jet pointed inward at 75°.

Studies of the cavity shape led to several interesting conclusions. These may be best illustrated with the aid of Figure 3. In this figure the jet inclined inward at 45°, the weight flow is 6#/min and the jet velocity 100 psf. The nozzle can be seen as an imprint in the gasket. The nozzle was 1 inch off the free surface of the water before the air was turned on. Several features of the ground effect phenomenon over water are apparent in this picture. One is the local depression under the jet. The difference in depth between this depression and the depth of the cavity produced by the base pressure was found to decrease as the jet angle was increased (positive inward). Another observation was the

standing vortex produced by the jet and its entrainment of the spray. The shape of the jet over water was also observed to turn nearly 180 degrees after leaving the nozzle, instead of the 90 degrees plus the jet angle as would be anticipated over a fixed surface. The amount of spray thrown by this particular configuration was impressive, and led to experimentation with various shaped skirts to control the spray and possibly recover some of the energy lost in generating the spray. The usefulness of "spray skirts" was borne out by subsequent tests on the free flight model. Since the jet shape over water is not closely approximated by any theory available to date, no correlation of the experimental data has been made. Attempts at empirical correlation were not found satisfactory.

The major conclusion reached from these preliminary tests indicated that theories derived for use over a fixed surface did not hold over a fluid surface. Therefore, performance estimates of water-borne vehicles should not be regarded too seriously intil the phenomenon of ground effect machines over fluid surfaces has been explored more carefully.

Since the testing over water did not yield the desired design information, the model was modified to include a ground board. A series of runs was made with varying nozzle angles to compare with the tests over water. A typical comparison of data is shown in Figure 4. The data shown are for a nozzle angle of 60° (inward) at constant thrust. The differences are readily apparent. For example, a machine with a base loading of 15 psf, hovering over land would sink below the free surface of the water to maintain the same base pressure. As the jet thickness to height ratio (t/h) and the base pressure decrease (toward the right on this figure) the difference between height over land and water to maintain the same base pressure also decreases. At a base pressure of approximately 5 psf, the height to maintain the same base pressure is equal over land and water. The full scale implications of this type of data are obvious. The deeper a vehicle must "sit" in the water the higher is going to be the drag associated with accelerating it to its cruising speed, where it is hoped that the wave drag will approach that of a planing hull rather than that of a displacement vehicle.

By the time the test program was completed, the theory accounting for jets of finite thickness, by Fuller (reference 3), had become available and the correlation of the experimental data with the parameters of this theory was made. Briefly, for a jet directed vertically downward ($\Theta = 0$) the theory can be written:

$$\triangle P = q_{j_o} \left[1 - (1 - t/h)^2 \right]$$

where $\triangle P$ = the base pressure, gauge

q_{j_o} = dynamic pressure of the jet, as expanded from the plenum total pressure to atmospheric pressure

t/h = jet thickness to height ratio

For correlation purposes it can be stated that $\triangle P/q_{j_o}$ should be a function of t/h only. The experimental data appeared to correlate with the parameters of the theory. However, the experimental points fell below the theoretical values of base pressure. Additional testing with various other models (reference 6) provided data that fell on a curve that was 75 per cent of the theoretical curve. This is illustrated in Figure 5. This apparently constant 25 per cent loss could be explained as a form of nozzle loss or as a loss resulting from the failure of the theory to account for the effects of jet mixing and jet curvatures other than circular. Since the data were obtained from both single and double-jet models with different nozzle configurations, it would seem that the effect of nozzle losses is small.

PERFORMANCE ESTIMATES

In an effort to understand the limitations of the available theories, some performance calculations (references 7) were made, based on Pinnes work (reference 4). Since the hydrofoil boat concept has been under consideration at Grumman for some time, and GEM has some problems in common with hydrofoil boats, a comparison between the two concepts was made.

While working with the theory it became evident that at low forward speeds the augmentation factor (A) is approximately equal to the lift to drag ratio (L/D) if the power required to hover is included in the drag term. Pinnes (equation 86, reference 4) describes the ability of a GEM to lift a load in lbs per horsepower, as the compressor-engine augmentation ratio.

Using this relationship, an idea of what is considered a practical operating range for GEM is shown in Figure 6. It can be seen from the figure that to obtain an L/D (A) above 10, an h/d less than .05 is required. To theoretically exceed lifting 30#/HP with an h/d of .05, a pressure ratio less than 1.08 must be used. On the basis of calculations of this type, it was concluded that a practical GEM would have to be designed with height to diameter ratios less than 0.1 and pressure ratios below 1.05 to be competitive with other forms of transportation.

Initial calculations using Pinnes paper (reference 4) showed that low pressure ratios of the order of 1.01 to 1.02 appeared to be the most efficient. The theory made what were considered unrealistically thin jets ($t/h \leq .1$) appear increasingly efficient. For this reason, additional calculations were made assuming constant t/h.

An example of the calculations will be described, not because the results are considered significant, but to outline the number of assumptions that must be made before performance can be calculated. The following assumptions were chosen:

structural weight	- 1/3 gross weight
propulsive efficiency	- 50 per cent
propulsive weight	- a function of pressure ratio (Figure 16, reference 4)
specific fuel consumption (SFC)	- .5
t/h, assumed constant	- .28
diameter of machine	- 100 ft
jets directed vertically ($\Theta = 0$)	

In order to make an estimate of the forward speed, range, and endurance, some "guess" as to the power required to move the GEM must be made. Since the theory of reference 8 shows that the gravity wave drag approaches zero with proper design, the only drag associated with forward speed is assumed to be that due to skin friction. Pinnes' theory for vertically directed jets was used, since it was felt that these theoretical values of base pressure could be realized by tilting the jets inward. The GEM was assumed to be limited in forward speed when the dynamic pressure due to forward speed was equal to the base pressure. There is no justification for this assumption.

The hydrofoil boat used for comparison had the following characteristics (reference 9):

weight - 100 tons
cruise speed - 80 kts
height above water - 10 ft
installed horsepower - 9500

The boat was equipped with supercavitating hydrofoils and utilized air propellers for forward propulsion.

The results of one of the calculations is shown as Figure 7. It can be seen from the figure that the GEM can only compete with the hydrofoil boat if it operates at a height of 3 ft. Three-foot wave heights correspond to a sea state of 2, while the hydrofoil boat could operate in sea state 5.

The GEM curves shown here represent a family of machines, since, with the previously mentioned assumptions, the limiting forward speed, range, and endurance were proportional to the base loading. As an example, one machine that would be represented by the h = 3 ft curve had the following characteristics:

base loading	- 21 psf
gross weight	- 82 tons
installed horsepower	- 7800
power plant weight	- 11000#
maximum jet velocity	- 188 fps
assumed top speed	- 80 kts

The results of these calculations are in no way meant to be complete or conclusive, but are presented to illustrate the number of assumptions that must be made to obtain performance estimates of GEM. Since the theory is limited, the performance can be heavily influenced by the choice of assumptions. Practical investigations of the structural design, propulsion efficiencies, and the relationship of base pressure to forward speed would have to be made before the GEM can be successfully evaluated.

Two-dimensional tests at forward speed. Preliminary attempts at estimating the performance led to interest in the effects of forward speed on the jets of an annular jet ground effect machine. The preliminary calculations showed range directly dependent upon the maximum attainable speed. To explore this problem experimentally, a two-dimensional model was constructed. It was reasoned, largely through intuitive processes, that there should be a relationship between the $\triangle P/q_{j_o}$ ratio that had correlated the two-dimensional hovering data and the total pressure due to forward speed.

The model is shown schematically in Figure 8. The two-dimensional section is 3 inches wide. The two jets are approximately 10 inches apart. The nozzle blocks were made of circular arcs to reduce any nozzle losses that may have been associated with the earlier test models. The nozzle gap was adjustable from 1/4 inch to 1 inch. The air simulating the forward speed was the exhaust from a 4-inch pipe. Only pressure data were taken, since it was expected that pressure or velocity ratio would adequately correlate the data. For the tests made to date, a constant height was maintained. The nozzle gap was varied to provide a variation in t/h.

It should be pointed out that this two-dimensional model represents the stagnation point of a three-dimensional model and therefore is probably more affected by forward speed.

The results of the testing to date with this model are shown in Figure 9. The previously established parameter $\triangle P/q_{j_o}$ is plotted against $P_{T_o}/\triangle P$, which is the ratio of the total pressure due to forward speed divided by the base pressure. It was originally conjectured that as $P_{T_o}/\triangle P$ approached one, the jet would be blown inward and unfavorable moments would limit the maximum forward speed. As can be seen by the data, the base pressure

first decreased slightly and then increased, with increasing $P_{T_o}/\Delta P$. No significant variation in the base pressures was observed that would indicate a large moment change. The same data has been replotted in Figure 10 to show the percentage change in $\Delta P/q_{j_o}$ due to forward speed. The scatter is believed to be within the accuracy to which the data could be read. It can be seen in Figure 10 that the base pressure for a given plenum pressure decreases less than 5 per cent with increasing forward speed until $P_{T_o}/\Delta P$ reaches approximately 1.2. Above that value the base pressure increased rapidly, reaching a value 30 per cent greater than the hovering value at $P_{T_o}/\Delta P = 2.0$.

Instead of continuing the testing with the two-dimensional model, a three-dimensional model, 2 ft in diameter, will be used. The model has already been constructed and will be tested in the Grumman low speed wind tunnel as soon as testing time becomes available. The model will have a 1/4-inch nozzle gap. The air supply will be a centrifugal compressor capable of delivering 1000 cfm at a total head of 16 inches of water. It is hoped that this three-dimensional model will provide more useful data with greater accuracy than the two-dimensional model.

CONCLUSIONS

Based upon the preliminary work done at Grumman the following conclusions are advanced:

1. Two-dimensional tests at forward speed indicate that the base pressure increases with forward speed after the forward jet is blown inward.
2. No significant changes in moment were detected under forward speed that would indicate instability of a GEM.
3. Two-dimensional experimental tests established the validity of the parameters of the theory of hovering annular jet GEM (reference 3). The experimental values of base pressure are approximately 75 per cent of the theoretical values.
4. Stability over water and reduction of excessive spray can be obtained by the use of suitably shaped skirts.
5. Pressure ratios below 1.05 and height to diameter ratios below 0.05 appear to be the most promising in obtaining competitive lifting power (#/hp).
6. Current methods of predicting the performance of ground effect machines are inadequate to determine the feasibility of the concept.

It appears that the ground effect concept is still in the research stage. Not only is research in aerodynamics needed but a combined effort including hydrodynamics, propulsion, and structural design is required. A great deal of basic experimental and theoretical research remains to be done before the ground effect machine can confidently be moved from the area of research into the realm of development and, finally, production.

REFERENCES

1. Chaplin, H. R., "Theory of the Annular Nozzle in Proximity to the Ground." DTMB Aero Rept. 923, July 1957.

2. von Glahn, U. H., "Exploratory Study of Ground Proximity Effects on Thrust of Annular and Circular Nozzles." NACA TN 3982, April 1957.

3. Fuller, F. L., "An Approximate Theory for the Ground Effect Vehicle Employing a Thin Sheet Jet." GAEC Research Note RN-109, March 1959.

4. Pinnes, R. W., "A Power Plant Man's Look at the Ground Effect Machine." NAVAER Research Division, Rept. DR-1958, April 1959.

5. Tucker, J., "Preliminary Two-Dimensional Tests of the Annular Jet Ground Effect Principle." GAEC Research Mem. RM-158, May 1959.

6. Tucker, J., "Experimental Verification of the Theory for Two-Dimensional Hovering Annular Jet Ground Effect Machines." GAEC Research Note RN-120, October 1959.

7. Tucker, J., "Comments on the Performance Prediction of Annular Jet Ground Effect Machines." GAEC Research Note RN-116, August 1959.

8. Fuller, F. L., "Gravity Wave Drag Theory for Water-Borne Ground Effect Vehicle." GAEC Research Note RN-111, June 1959.

9. "Study of Hydrofoil Seacraft." U. S. Dept. of Commerce, Maritime Administration, Contract MA-1730, Rept. executed by GAEC, October 1958.

Figure 1. GEM model over water with 10° spray skirt

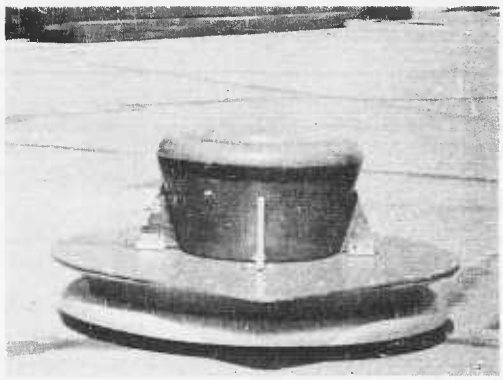

Figure 2. GEM model over land with half circle spray skirt

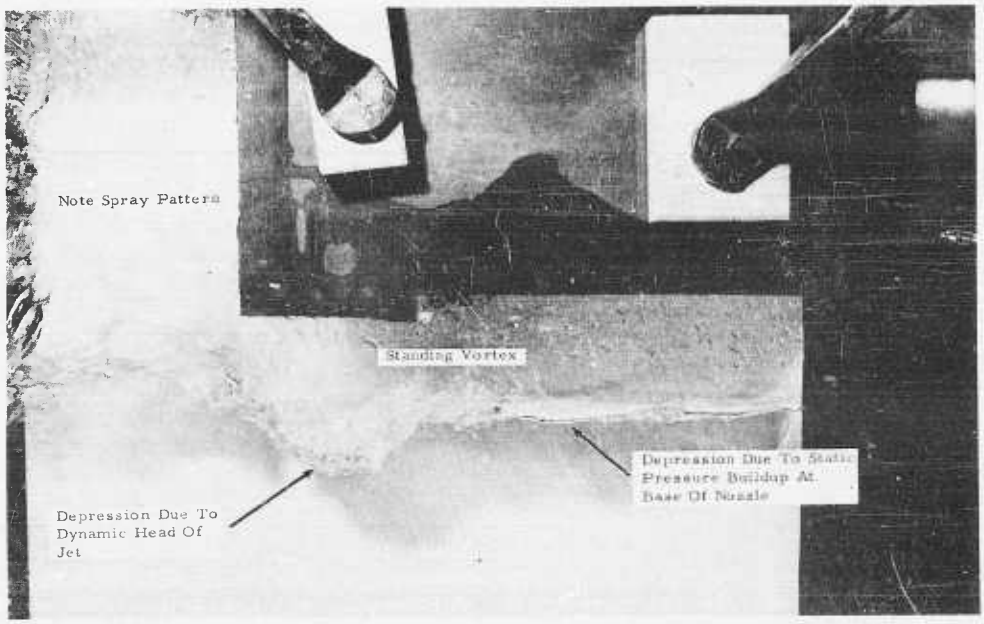

Figure 3. Two-dimensional annular jet test rig with 45° jet

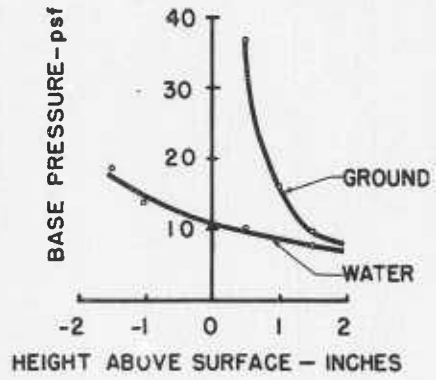

Figure 4.

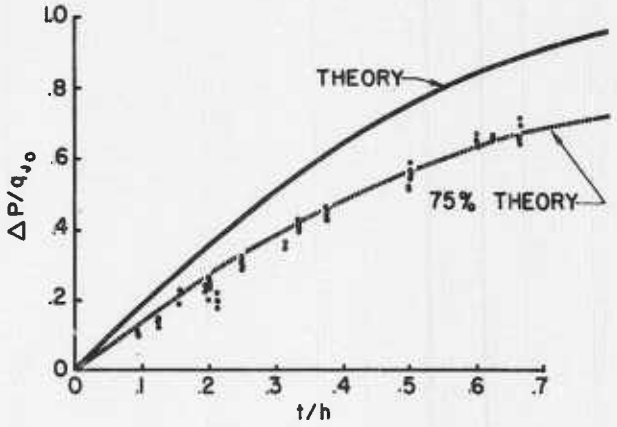

Figure 5.

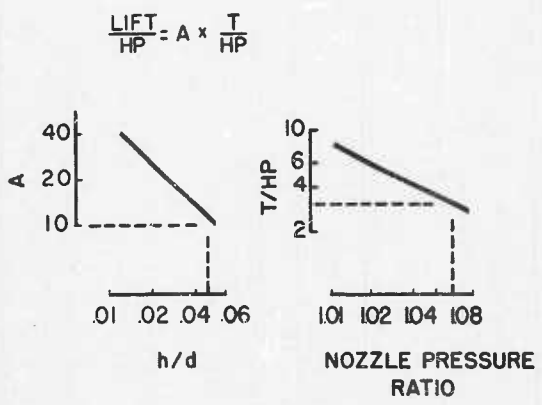

Figure 6.

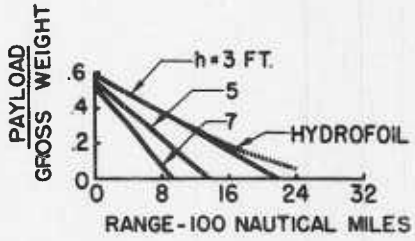

SAMPLE MACHINES

PRESSURE RATIO	BASE PRESSURE	WEIGHT (TONS)	CRUISE SPEED
1.01	10.5 psf	41	55kts
1.02	21.0	82	80
1.05	52.5	205	125

Figure 7.

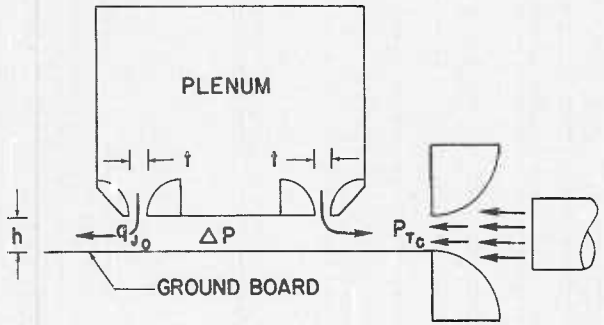

Figure 8.

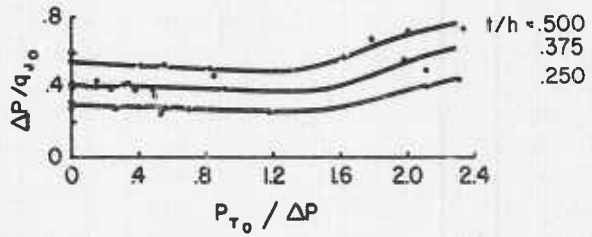

Figure 9.

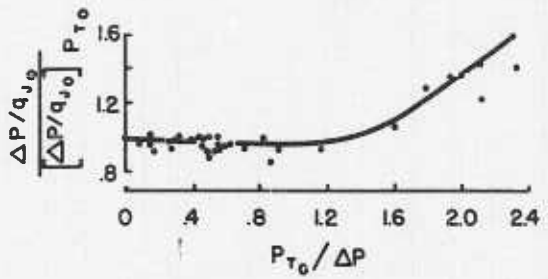

Figure 10.

LABYRINTH SEALS

Federal Aircraft Works, Emmen, Switzerland

By C. Weiland, Zurich, Switzerland

When the first spell of heavenly ecstasy is over, it is natural that the bridegroom should begin to wonder whether the bride knows anything about cooking. It is much the same with these ground effect machines. You know they function well enough in theory, and even in practice, as far as it has been possible to try them out; but the time has come when it is necessary to get down to brass tacks, to the practical aspects of keeping house and launching the bride on the waters of married life. In other words, we now come to the second phase of air-cushioned married life, when we need proof that the bride is a commercial proposition and not merely an extravagant "floosey."

This brings us to the vital question of air consumption. It is on this factor that speed and payload, and also radius of operation depend.

A useful means of reducing air consumption is the application of the labyrinth sealing system. The effect of the labyrinth is to lower the pressure underneath the craft in a number of stages and to let it escape into the atmosphere with a minimum of loss.

Labyrinths are in common use on steam and gas turbines, and also on turbo-compressors. Without metallic contact, they seal the shafts internally, that is to say, against external influences. Admittedly, the gaps they have to seal are extremely small, amounting as a rule to no more than a thousandth of an inch. Simple labyrinths of this kind are, unfortunately, not applicable in the case of GEM, because the gaps to be blocked are ten thousand to a hundred thousand times bigger than that. That is why we have to take a different approach.

This leads us to Figure 1, which illustrates a labyrinth system of a type practicable for our purpose. Its special feature is the method of air circulation. As it is novel in conception, I have taken out the necessary patents for its protection.

The picture shows a section of the periphery of a GEM. You see the bottom of the machine on the right, beneath which the air pressure is highest. Then you see two chambers running along the entire circumference of the machine. Inside these chambers, fans are mounted. The arrows indicate the directions in which the air is impelled. This system functions as follows: The air underneath the bottom of the machine tends to escape to the left into the atmosphere outside. When the stream of air enters the first labyrinth chamber it divides in two. One part flows along the bottom of the machine, and the other is sucked in by the fan and blown through a slit against the flow direction of the primary air stream. This reduces the velocity of both streams, which mingle and create eddies when they meet. The amount of air escaping through this cross section, therefore, is obviously smaller than if the chamber and the fan were not there. From this first chamber the air now flows into a second, where again its pressure and velocity are reduced. And from here, finally, it escapes from the system. Its exit, however, is greatly checked and retarded, and its quantity is substantially smaller than if it had not passed through the labyrinth system I have just described.

We have tested the effect of the labyrinth in a whole series of experiments, in the research laboratory of the Federal Aircraft Works, Emmen, Switzerland, since we were anxious to establish the difference between it and the conventional, straightforward

gap-sealing design. You can see the laboratory test model in Figure 2 and the entire test set-up in Figure 3.

The two-dimensional canal was so laid out that it could be adapted to requirements, so that in addition to the set-up shown in Figure 1 a variant shown in Figure 4 could be tested. Here the fans have been omitted.

Furthermore, a series of tests was carried out with the model altered as shown in Figure 5. The chambers here are designed very simply, without air-reversal slits. And, finally, the model shown in Figure 6 was another version. This adaptation corresponds to the well-known design, which has only one slit on the circumference of the machine and is inclined inwards slightly to fill the air cushion and maintain pressure.

It would take me too long to report on the whole test set-up, the objectives aimed at, and the results obtained. I can, however, state that these tests were very carefully prepared and carried out.

Figure 7 shows a photograph depicting pressure distribution in the labyrinth system. On top you see the outlines of the model with the air slits fed from the fans. At the bottom the pressures are illustrated. You can see quite distinctly the stagewise reduction of pressure and, just as clearly, the sealing action at the slits.

I have included Figure 8 to afford an insight into the quantities involved. It shows input in horsepower per ton as a function of lift for two different pressures. It is an efficiency comparison between the conventional air slits of Figure 6 which shows the upper curve marked E, and the labyrinth system shown in Figure 1, indicated by the curve A. It proves that the input for GEM with a labyrinth system is fundamentally lower, regardless of the operational pressures. In the system depicted, the input saving is as much as 25 per cent, and this economy increases in proportion to the number of chambers incorporated in the system. With three chambers and a slightly adapted air-feed arrangement, the input saving works out at over 40 per cent.

Figure 9 again shows the actual test model; Figure 10 shows the conventional arrangement of the air ducts; and Figure 11 shows the model incorporating the labyrinth system.

In terms of aerodynamics, therefore, the labyrinth seal is a means for creating maximum flow resistance. As a rule the technical problem to be solved is just the reverse, namely, how to produce minimum flow resistance. But here we have a case in which the worst possible flow conditions have to be attained. In fact, though it might sound paradoxical, in our case we are anxious to lose as much energy as possible, our purpose being to let a minimum amount of air escape from the air cushion.

The more turbulent the air jet is, the easier it is to get rid of energy, to allow a minimum of energy to enter the succeeding chambers. This increases the pressure drop and lowers air flow velocities accordingly.

The labyrinth seal can incidentally also be compared to a fish ladder of the kind often built beside river barrages to enable the fish to ascend to the upper reaches. The flow velocity over the single steps of the ladder is considerably lower than if the water were allowed to plunge down unchecked over the entire head of fall.

Generally speaking, the labyrinth can in fact be compared to a ladder, or rather to a flight of stairs. It is a pressure stairway. The difference is about the same as if, instead of walking downstairs, we were to jump to the floor below. The impact on landing is then of course far more impressive.

All the same, the labyrinth system does obviously raise a complication. It would be easy just to make an ordinary slit. But fans are cheap to produce and need practically no maintenance, so that there is little trouble in incorporating them. We find a parallel development, by the way, in jet power units. The new jets are mostly designed as twin-flow machines. Here, too, there is a departure from the simple way of doing it, but this is a matter of economy which becomes an important factor outside the power unit in terms of radius of operation and payload.

The great advantage of the labyrinth system, however, does not lie in power-saving alone, which is important in respect to operational economy and action radius; it also enables floor load to be substantially increased without additional power. I would like to explain this with a practical example: We have set out to build a small craft measuring 16 by 32 ft. The output available is 215 horsepower. With the method used hitherto, which only comprises a simple slit all around the circumference and thus allows the air flow to escape into the atmosphere in a single stage or step, it is possible with the output mentioned to lift a craft having a total weight of 8,800 lbs. In this case the payload is about 25 per cent, or 2,200 lbs.

Exactly the same craft, however, but now fitted with a labyrinth, again measuring 16 by 32 ft and powered by a 215 hp engine, can weigh as much as 13,700 lbs. The payload in this case is 4,900 lbs, as against 2,200 lbs in the first case. And so for exactly the same size of craft, developing the same speed and consuming the same amount of fuel, the payload has risen by 220 per cent. In other words, it definitely pays to use labyrinths! It is the same in shipbuilding, where the requirement is also to attain maximum floor loading, for this facilitates the building of strong hulls. In shipbuilding quarters the main arguments against GEM are that the lightweight structure is inadequate. We will not probe this objection to find out how much of it is based on habit and tradition. But nevertheless the fact remains that the more solidly the hull is built, the more at ease one feels on board a ship. At least this is my personal view, for although I am a Swiss and my country is many miles away from the sea - and will remain so unless we decide to conquer half of Europe - I have weathered many a storm myself and I realize that seawater is not quite like cotton wool.

Thus two fundamentally different requirements stand opposed. On the one hand, it is desirable to have a low-pressure air cushion so as to keep down losses and lift and propel the craft with a minimum of power output. This means low floor load and thus lightweight hulls. A lightly built hull is of course more expensive to build than the conventional structure.

On the other hand, however, high floor load is desirable, primarily in the case of land vehicles for full space exploitation and also to make the hull relatively sturdy. The labyrinth system bridges these two opposing requirements. Practically speaking, it superimposes several layers of air on top of one another, just like plywood in which the single layers may be thin and weak but which form a tough board when glued together.

The labyrinth is not only an energy saver but also an air consumption economizer. The saving quickly rises to from 30 to 50 per cent. But now you will say, this Swiss fellow is even meaner than a Scotsman - now he is trying to save air, as if there weren't plenty of it about. That's all very well, but air that has to be driven through fans and channeled through ducts is no longer just thin air, for the fans and ducts entail expense, weight, and - what is even more important - they occupy space or volume. But volume, particularly for the coming high speed GEM, is synonymous with air resistance. Air resistance in turn means greater propulsion engines, which again mean expense, weight, and fuel consumption, and of course lower payload, smaller radius, and lower economy in operation. All of these factors are interrelated and influence each other reciprocally. It

is therefore advisable to take care of economy everywhere, and I always say that what my wife saves I need not save myself.

There is a widespread opinion that in the case of military craft and vehicles economy does not matter so much. I beg leave to doubt this, for I cannot see why one should spend more than is absolutely necessary in order to attain a definite object; and furthermore I see no advantage in having to build up an over-dimensioned rearward supply system. War is to a great extent a problem of transportation, to be resolved in the most efficient manner.

In this connection I would also raise the question of radius of operation. We have an excellent criterion for this, namely the Atlantic ocean, which measures about 3200 nautical miles across. We intend to cross the Atlantic in the near future with GEMs at a speed which will give us the useful travel time of 25 to 30 hours - slow enough to spend a jolly night on board and fast enough to fit the journey into our brief but busy lives.

In order to do this, our craft must have a sufficiently good lift over drag ratio and be able to carry sufficient fuel in proportion to its total weight. There is a simple method for establishing at once whether a vessel can get across the ocean. You need only multiply the lift over drag ratio by the percentage of fuel weight relative to the total weight. If the product is 750 or over, a transoceanic crossing is possible. Let us take a practical example. An ocean liner has an L/D ratio of about 100, that is, 100 lbs weight create a drag of one pound. If she carries 7.5 per cent of her weight at departure in the form of fuel, her figure is 7.5 times 100 = 750, and she will be able to complete the passage.

An automobile, on the other hand, has an L/D ratio of only 20. It can only carry about 4 per cent of its overall weight in fuel, at least with a standard fuel tank. Thus the product of the L/D and fuel ratios is 20 times 4 = 80. So it would not be able to get across the ocean without refueling. Indeed, it would have to be refueled ten times on the way.

An aircraft has an L/D ratio of about 18. To fly across the ocean it must therefore carry fuel amounting to 750 divided by 18, in other words around 40 per cent of its take-off weight.

The GEM is governed by the same laws: the L/D ratio must be at least 20 for an ocean crossing, and even then more than a third of the fuel weight at departure must be carried on board. How much better it would be if this could be converted into payload!

There is one fundamental means of improving the L/D ratio and that is to increase speed. Since the air-cushion fans are being paid by the hour, as it were, the longer the distance we can travel per hour, the better. This improves the L/D ratio. But our endeavor to increase speed is hampered by the air resistance of the hull. And now we have arrived back at the point we started from, at which I pointed out the desirability of building hulls as compactly as possible because these naturally have a lower air resistance. However, this in turn necessitates higher floor loading.

The GEMs of the future will consume about the same power in overcoming air resistance as in maintaining the air cushion. For big ocean liners, floor loads of about 200 lbs per ft^2 will be necessary. To allow air to escape from the cushion in a single stage at such high pressure is about as sensible as jumping off a skyscraper to get down to the street.

In conclusion I would like to discuss an air-cushion craft built in Switzerland. (See Figure 12) This vessel sank 4 1/2 hours after a violent storm - the actual cause of the mishap has never been discovered. There had been storms and gales on several occasions during the previous weeks, but the ship, riding easily at her moorings, had weathered them

without the slightest trouble. During the salvage operation she was badly damaged owing to clumsy handling, but she is being reconstructed and will be afloat again, or rather airborne, next month.

This craft is built primarily for speed. In fact, the basic idea of GEM is to increase speed. The air intake apertures are mounted in the square bow, the reason being that, in the first place, air flow ought to be as far as possible in the streamline direction and without major deflection; and in the second place, the apertures serve to reduce the air resistance of the bow to a minimum. There are six fans, or propellers, driven by two Oldsmobile engines. The sides of the craft are straight so as to give her a good hold when turning. These sides merge aft into two big tail-fin rudders, similar to those on aircraft which suffice to control the vessel when she has enough steerage way. Reverse travel is effected by three air jets on either side of the bow, which can be opened in any combination when required. There are also jets in the stern of the ship which can be opened groupwise to assist manoeuvering at low speeds. The cockpit, which is arranged to accommodate 12 persons, is situated amidships. This craft will possibly be on view in Washington early next year, and I hope you will take a ride in it.

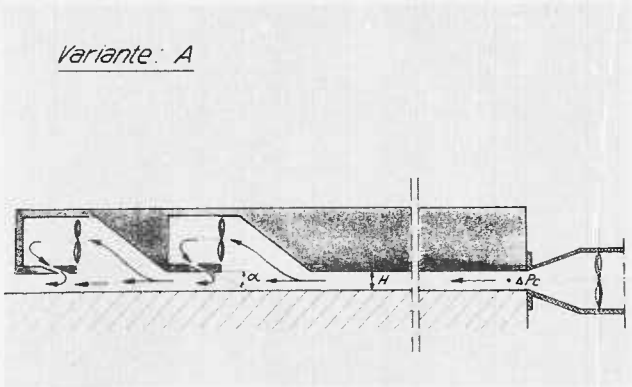

Figure 1.

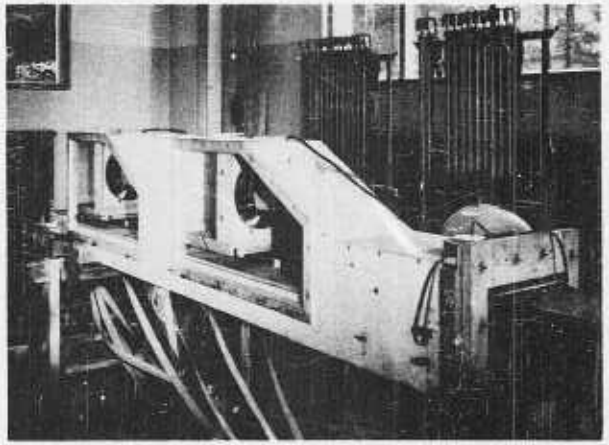

Figure 2.

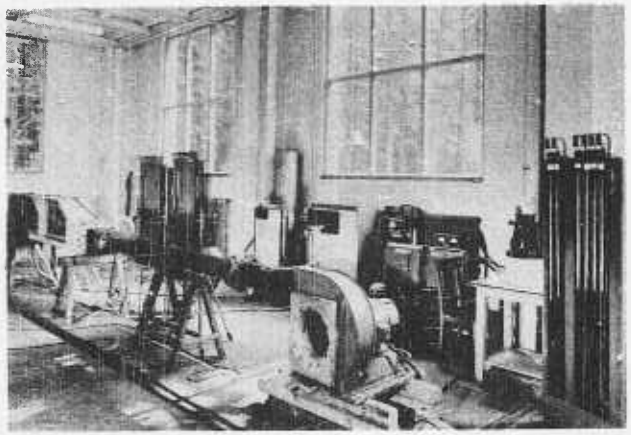

Figure 3.

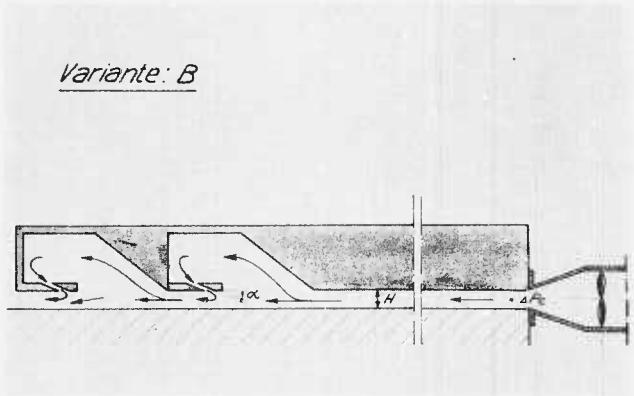

Figure 4.

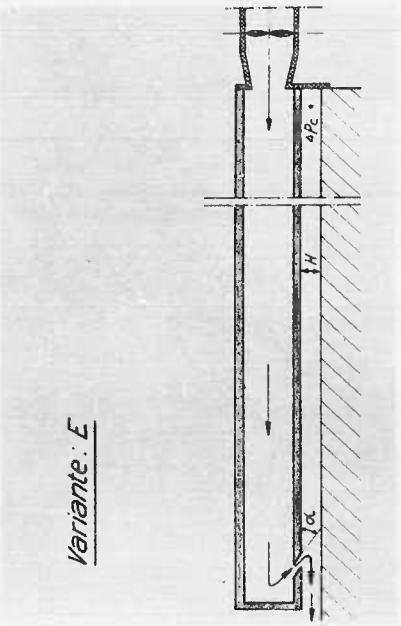

Figure 6.

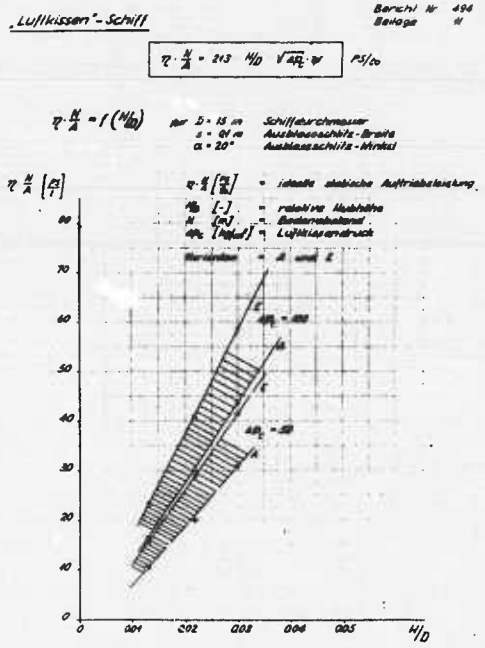

Figure 8.

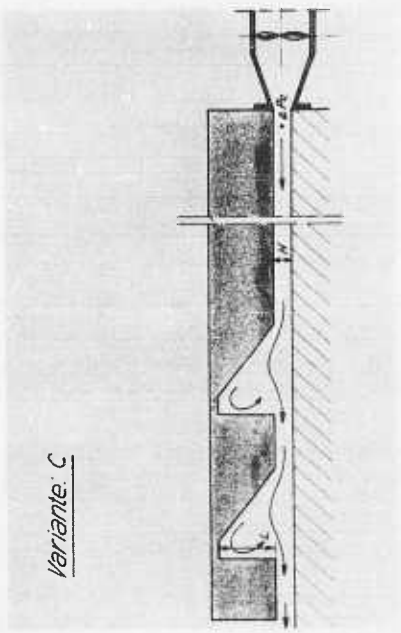

Figure 5.

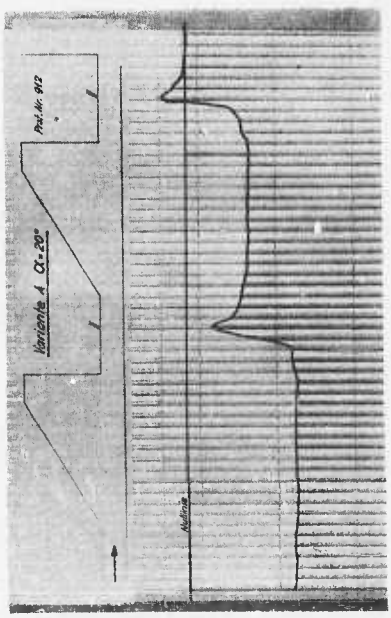

Figure 7.

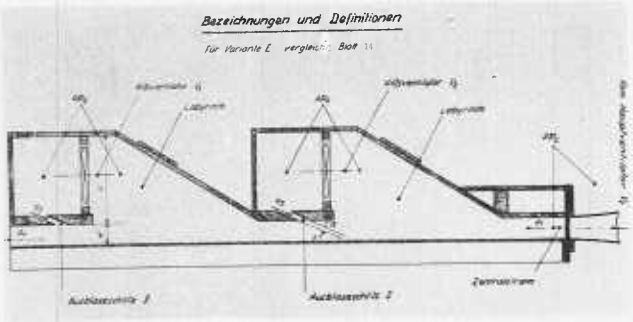

Figure 9.

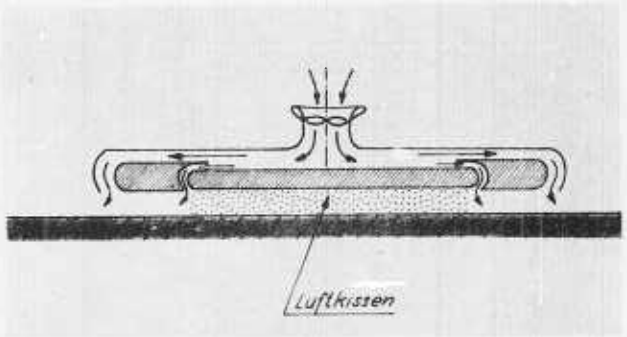

Figure 10.

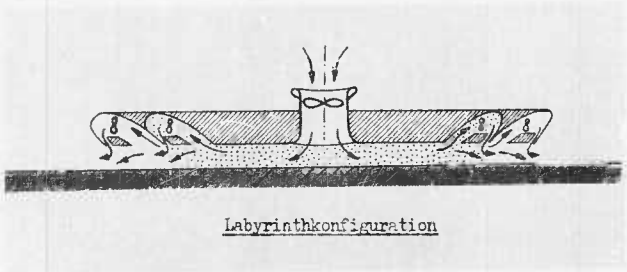

Figure 11.

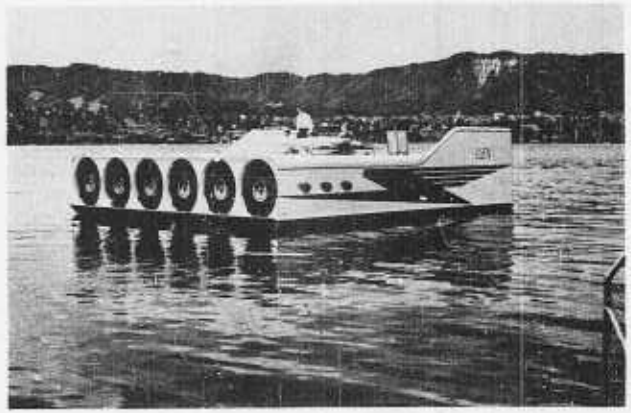

Figure 12.

ON THE VERTICAL MOTIONS OF EDGE JET VEHICLES

By Marshall P. Tulin, Hydronautics, Incorporated

ABSTRACT

The vertical motions of edge jet vehicles have been studied with particular reference to their travel over undulating surfaces. Such motions are of special concern in connection with the possible use of edge jet vehicles for naval purposes. The important assumptions underlying the present analysis are: The vehicle is two-dimensional and has identical jets at its right and left edges; the motions are purely verticle; the mass flow delivered to the jets does not vary while the vehicle is in verticle motion; the jets are incompressible.

During dynamic motions the jets of an edge jet vehicle generally operate in an unbalanced condition. The behavior of the jets is quantitatively hypothesized for "underfed" and "overfed" operation and the relation between these separate types of operation and the position of the vehicle relative to equilibrium is discussed. The possibility of self-excited vertical motions is raised, and it is shown how the occurrence of such motions depends on the magnitude of the loading of the vehicle and the configuration of its underbottom. Vehicles for which the bottom is level with the jet exits are incapable of self-excited motions -- at least according to this incompressible jet analysis. Possibilities of self-excitation only occur for vehicles with indented bottoms (or under-pockets) and for very heavy loadings.

The motion of a vehicle over an undulating surface is shown to depend on an inhomogeneous third order equation with the resultant implication that the vehicle has two resonance frequencies or frequencies of peak response. The frequency of encounter of the vehicle with waves or other surface undulations is thus of paramount importance with regard to the vehicle's response, and a band of dangerous frequencies is defined. At the center of this band is the lowest of the two resonance frequencies:

$$\omega_{n_1} \text{ (cycles/sec.)} = 1/2\pi \sqrt{g/H_e}$$

It is pointed out that this just happens to be the frequency of a pendulum of length equal to the equilibrium altitude.

The amplitude of vertical motions near the frequencies of peak response are shown to depend upon two parameters. For frequencies of encounter relatively small in comparison to the lowest of the two resonance frequencies, the vehicle follows the surface undulations very well, but as the first resonant frequency is approached, increasing vertical response is obtained with the possibility of catastrophically large motions not remote. For frequencies several times the first resonant frequency the vehicle motions stiffen and as frequency increases the vehicle becomes increasingly unable to respond at all to the surface beneath it and tends to maintain itself in level flight. As stated before, this high frequency behavior obviously limits the ability of a vehicle experiencing such encounter frequencies to negotiate waves or bumps, although it implies a smooth ride so long as contact with the ground or sea can be avoided.

NOTATION

a rate at equilibrium altitude at which an unbalanced jet flow changes with vehicle altitude, $- \partial (p_u \, v_u \, t_u \, / \, \partial_H \, \Big|_{\text{at equil.}}$

a_o coefficient in the equation of vertical motion, $a_o = \frac{aC^2}{M H_o}$

a_1 coefficient in the equation of vertical motion, $a_1 = \frac{\rho_u C^2 W}{M H_o}$

a_2 coefficient in the equation of vertical motion, $a_2 = \frac{bC^2}{W H_o}$

b rate at equilibrium altitude at which an unbalanced jet flow changes with the pressure under the vehicle, $- \partial (p_u v_u t_u) / \partial p_u$ at equil.

C speed of sound in the space under the vehicle

g acceleration of gravity

h_o local altitude of a wave or other undulating surface relative to the mean level (see Figure 8)

$\bar{h}_o$ half-amplitude of h_o for sinusoidal oscillations

H altitude of an edge jet vehicle measured from the local ground level to the jet exits

H_o altitude of an edge jet vehicle measured from the local ground level to the undersurface or bottom of the vehicle

H_e equilibrium vehicle altitude - which results when the jets are in balanced operation.

H' distance from the bottom of the horizontally turned jet to the jet exit in underfed operation

δH difference between actual altitude and the equilibrium altitude, $H - H_e$

$\delta \bar{H}$ half-amplitude of the equilibrium-disturbed motions that occur during travel over a sinusoidally undulating surface

M mass of the edge jet vehicle

p_o total pressure in the chamber feeding the jets

p_a atmospheric pressure

p_u pressure under the vehicle

δp_u difference between the actual pressure under the vehicle at any time, and the pressure there when the vehicle is not in vertical motion

t time

t_a thickness of a jet which has exited to the atmosphere from the jet exit

t_u thickness of the jet which exits under the vehicle in overfed operation, or which blows out from under the vehicle in underfed operation (see Figures 2 and 3)

U_s translational speed of an edge jet vehicle

U_w translational speed of a water wave

v_a velocity of a jet which has exited to the atmosphere from the jet exit

v_u velocity of the jet which exits under the vehicle in overfed operation, or which blows out from under the vehicle in underfed operation (see Figures 2 and 3)

V volume of the space under the vehicle. In the present case, $V = WH_o$

W length of a two-dimensional edge jet vehicle

β important non-dimensional parameter determining the vertical motions,

$$\beta = \frac{H_o}{H_e} \frac{\gamma p_u}{p_u - p_a}$$

γ ratio of specific heats of air, $\gamma = 1.4$

δ important non-dimensional parameter determining the vertical motion (see equation 24)

Θ inclination of a jet to the vertical, positive inwards

λ length of waves or other surface undulations

ρ density of air in the edge jet, assumed here not to vary

ρ_u density of air in the space under the vehicle

ϕ phase angle between sinusoidal surface undulations and the sinusoidal response of the edge jet vehicle

ω frequency of the vehicle's vertical oscillations, in rad./sec. unless otherwise stated

ω_{n_1} one of two resonance frequencies for an edge jet vehicle, $\omega_{n_1} = \sqrt{g/H_e}$

ω_{n_2} the other resonance frequency, $\omega_{n_2} = \sqrt{\beta g/H_e}$

DISCUSSION

Considerable recent attention has been given to ground effect vehicles utilizing the so-called annular or edge jet principle. Various configurations have been proposed, for use over both land and water, and a few prototypes have actually been constructed. A limited number of experimental and theoretical studies of the performance of edge jet configurations have been carried out (see for example references 1, 2, and 3). These, however, seem to be concerned only with the equilibrium or static behavior of such vehicles, whereas the present paper considers their vertical motions. Particularly studied are,

first, the question of what happens when an edge jet vehicle is vertically disturbed from its equilibrium position, and particularly whether self-excited vertical oscillations are possible -- and second, the question of how such vehicle respond to rough terrain or to seaways. The latter question is of especial concern in connection with the possible use of edge jet vehicles for naval purposes.

Balanced edge jets. An edge jet may be used all around the periphery of a platform in order to seal the sustaining pressure beneath it, or it may be used only around part of the periphery, the other part being sealed otherwise. The edge jet, which is usually aimed downwards and inwards is, in normal or balanced operation, finally pushed outwards by the high pressure region underneath the platform just enough to cause the edge jet to meet and flow smoothly outwards along the ground. The pressure difference across a given edge jet in balanced operation depends on the height of the jet at exit from the nozzle, on the thickness and velocity in the jet after it becomes parallel to the ground, and on the angle of the jet as it leaves the nozzle. In Figure 1, a vertically exiting two-dimensional edge jet is shown.

For incompressible two-dimensional jets, it may be shown that to a good approximation, even for jets not very thin in comparison to their altitude H, the following relation holds when the jet is in balanced operation:

$$p_u - p_a = \frac{t_a}{H_e} \rho v_a^2 \tag{1}$$

If the jet is inclined not vertically at exit but at an angle Θ to the vertical (Θ positive denotes a jet inclined inwards), then the condition for balanced operation becomes

$$p_u - p_a = \frac{t_a}{H_e} \rho v_a^2 \left[1 + \sin \Theta \right] \tag{2}$$

Unbalanced edge jets. Under certain conditions and particularly when an edge jet vehicle is tilted in order to obtain thrust, or when it is undergoing unsteady motions as discussed here, the jet will not be in balanced operation as depicted in Figure 1. If the pressure, p_u, is too high for a given edge jet, the jet will not entirely seal the space under the platform, but may allow the pressurized air there to escape along the ground to the atmosphere. In Figure 2, such an underfed jet is shown in operation.

Note that the flow escaping the high pressure region flows out with a velocity v_u somewhat less than the final velocity of th edge jet, v_a.

$$\frac{v_u}{v_a} = \sqrt{\frac{p_u - p_a}{p_o - p_a}} \tag{3}$$

The thickness t_a of the escaping jet is H-H', where H' is the altitude at which the edge jet would be balanced, or

$$p_u - p_a = \frac{t_a \rho v_a^2}{H'} \tag{4}$$

It is clear, of course, that this analysis has assumed that the flows involved occur without mixing or other complicating viscous effects that may actually occur in practice, but it is felt that meaningful general results are nevertheless obtained.

If the sealed pressure under a platform is less than necessary for the balanced operation of a given edge jet, then part of the jet will be sucked into the space under the platform, as shown in Figure 3.

An overfed or split jet satisfies the following relation:

$$p_u - p_a = \frac{t_a}{H} \rho v_a^2 - \frac{t_u}{H} \rho v_u^2 \tag{5}$$

where the incoming jet velocity is less than the outgoing jet velocity:

$$\frac{v_u}{v_a} = \sqrt{\frac{p_o - p_u}{p_o - p_a}} \tag{6}$$

The edge jet vehicle disturbed. In all that follows, a two-dimensional vehicle which has a horizontal platform and which has identical jets at its right and left edges is being dealt with. Later considered are vehicles which are in motion to the right over undulating terrain and even than it is assumed that the front (right) and rear (left) jets behave similarly, as would be the case if the speed of the vehicle were substantially less than the speed of the flow in the jets. It is further assumed that the mass flow delivered to the jets is constant for a given vehicle and operating altitude, not varying with the vertical or forward motion of the vehicle, and that the vehicle does not tilt. For the purposes of this initial study of the dynamics of edge jet vehicles, it is believed that these simplifying assumptions are not only justified but even sensible. The simple vehicle whose verticle motions are to be studied is shown in Figure 4 in balanced operation.

If this vehicle is disturbed so as to decrease its altitude H, caused say by a sudden increase in its mass M, then two important effects occur: (1) the volume ($V = w H_o$) of the sealed space under the platform decreases, thus increasing the density ρ_u and hence pressure p_u of the sealed gas (the change in density is assumed to occur so rapidly that an adiabatic compression occurs), and (2) since both the pressure p_u and altitude H are changed, the jet may no longer be able to operate in a balanced condition. It is not easy to say offhand how the jet behaves in this circumstance, for two opposing tendencies are involved: The tendency of a reduction in altitude without a change in under-pressure p_u is to cause the jet to split and to operate in overfed condition, while the increase in pressure p_u due to compression of the sealed air tends to alleviate this effect and, if great enough, even to cause the jet to be underfed and for air to thus escape. It is even conceivable that a balance could occur between the compression and loss of altitude such that the jet even in its disturbed state would operate in balanced condition. This condition occurs when

$$\left.\frac{\partial p_u}{\partial H}\right|_{\text{due to compression}} = \left.-\frac{\partial p_u}{\partial H}\right|_{\text{for a balanced jet}} \tag{7}$$

or, as is easily shown, when

$$-\frac{p_u C^2}{H_o} = -\frac{t_a \rho v_a^2}{H^2}\left[1 + \sin\Theta\right] \tag{8}$$

where C is the speed of sound in the gas trapped under the vehicle and ρ is atmospheric density.

An edge jet will thus maintain itself in balanced operation for both small up and down disturbances from equilibrium when $\beta = 1$, where

$$\beta = \frac{H_e}{H_o}\frac{\rho_u}{\rho}\frac{C^2}{v_a^2}\frac{H_e}{t_a\left[1+\sin\Theta\right]} = \frac{H_e}{H_o}\frac{\gamma p_u}{p_u - p_a} \qquad (9)$$

When β is greater than one, the pressure drop due to expansion of the air under the vehicle for vehicle positions above equilibrium is more than enough to cause the jet to be overfed, and conversely when the vehicle is in a position below equilibrium the jet becomes underfed, as shown in Figure 5.

If $\beta < 1$ then, as may be seen from inspection of Figure 6, the jet becomes overfed when the vehicle is depressed below equilibrium, and underfed when the vehicle rises above equilibrium. This behavior is of course a consequence of the relatively smaller changes in the pressure of the air in the space below the vehicle.

Self-excited vertical motions. When $\beta = 1$, the pressure changes under the vehicle are due only to compression, the jet being always balanced. Of course these pressure changes cause vertical accelerations of the vehicle. The equation of motion of a vehicle not acted upon by other outside forces becomes in this case:

$$\frac{d^2H}{dt^2} + \left(\frac{Wp_uC^2}{H_oM}\right)H = O \qquad (10)$$

Thus, a vehicle with $\beta = 1$ is capable of performing undamped harmonic motions about equilibrium and with a frequency,

$$\omega = \sqrt{\frac{Wp_uC^2}{H_oM}} = \sqrt{\frac{g}{H_e}}$$

It is interesting that this frequency is precisely that of a pendulum of length equal to the vehicle's flying altitude.

Consider the effect on these neutral oscillations of changes in β. If $\beta < 1$, then the pressure build-up due to jet behavior for altitudes below equilibrium and the pressure diminution for altitudes above equilibrium act in the same direction as the already exiting accelerations, resulting in increasing amplitudes of motion. Conversely, if $\beta > 1$, the jet behavior produces pressures opposing the already existing accelerations. The important conclusion is therefore reached that:

For $\beta < 1$ an edge effect vehicle <u>is</u> capable of self-excited oscillations.

For $\beta > 1$ an edge effect vehicle is <u>not</u> capable of self-excited oscillations.

Inspection of equation 9 shows that β cannot possibly be less than one unless $H_o/H_e > 1$, i. e. if the underside of the vehicle is indented so as to be further above the ground than the edge jet exit itself. Even when such a "pocket" exists under the vehicle, very substantial loadings must also be used in order to obtain an unstable configuration. Thus, except for very heavily loaded configurations with substantial underpockets, the existence of self-excited vertical oscillations in edge jet vehicles is not to be expected.

The existence of self-excited oscillations in systems somewhat resembling edge jet vehicles has been pointed out previously elsewhere. The stability of pressurized gas bearings is particularly discussed in references 4 to 7, and it is interesting to note that,

unlike edge effect vehicles, pressurized gas bearings in their usual very heavily loaded configurations are notoriously susceptible to self-excited oscillations.

Edge jet vehicles traversing rough terrain or a seaway. When a vehicle is in forward motion over an unlevel surface, then the changes in altitude and volume of sealed air will cause changes in the pressures under the vehicle and force its motion. The fashion in which the vehicle responds to the unlevel surface if of the greatest importance and is the subject of the analysis that follows.

For small surface undulations, the motion of the vehicle obeys a linear equation with constant coefficients and it is thus possible to deal separately with each harmonic component in the elecation of the terrain or seaway. In Figure 7, a vehicle is shown traveling to the right with speed U_s over a sinusoidally undulating surface. It is assumed that the wave length λ of these undulations is long compared with the length W of the vehicle. A closer view is shown in Figure 8.

The acceleration of the vehicle is $\ddot{h}_o + \ddot{H} = \ddot{h}_o + \delta\ddot{H}$
The pressure p_u under the vehicle both sustains and accelerates it upward:

$$M(\ddot{h}_o + \delta\ddot{H}) = W\ \delta p_u \tag{11}$$

The mass flow into or out of the space under the platform is balanced by changes in the volume of the space and of the density (and pressure) of the gas trapped there, as follows:

$$\frac{\partial p_u v_u t_u}{\partial H}\ \delta H + \frac{\partial p_u v_u t_u}{\partial p_u}\ \delta p_u = \frac{d}{dt}(\rho_u V) \tag{12}$$

or

$$-a\ .\ \delta H - b\ .\ \delta p_u = \frac{V}{C^2}\ \delta p_u + \rho_u W\ \delta H \tag{13}$$

where

$$a = \frac{-(\rho_u v_u t_u)}{\partial H}\Bigg|_{\text{at equil.}} \quad \text{and } b = \frac{-\partial(p_u v_u t_u)}{\partial p_u}\Bigg|_{\text{at equil.}} \tag{14}$$

When (11) and (13) are combined, there results a third order equation of motion:

$$\left[\delta\dddot{H} + a_1\ \delta\dot{H}\right] + \left[a_2\ \delta\ddot{H} + a_o\ \delta H\right] = -\left[\ddot{h}_o + a_2\ \dot{h}_o\right] \tag{15}$$

where

$$a_o = \frac{aC^2}{M H_o};\quad a_1 = \frac{\rho_u C^2 W}{M H_o};\quad a_2 = \frac{bC^2}{W H_o} \tag{16}$$

and all of these coefficients are positive.

The two separate groups of terms on the left are 90° out of phase with each other. Each group considered separately has a natural or resonance frequency, that of the lower

order group being $\omega_{n_1} = \sqrt{a_o/a_2}$ and that of the higher order group being $\omega_{n_2} = \sqrt{a_1}$.

It can further be shown that $\beta = \frac{a_1 a_2}{a_o}$, so that

$$\omega_{n_1} = \sqrt{a_o/a_2}; \quad \omega_{n_2} = \sqrt{a_1} = \sqrt{\beta \omega_{n_1}} \tag{17}$$

and for a stable vehicle therefore,

$$\omega_{n_1} < \omega_{n_2}$$

Because of the occurrence of these two "resonance frequencies," it may be expected that the response of the system will be particularly strong when it is forced at each of these frequencies, and, as a result, the amplification curve will have two separate peaks whose separation increases with $\beta^{1/2}$. It might also be expected that the vehicle motion will tend to lag the wave oscillations, and it develops that at a frequency somewhere between the resonance frequencies given in equation (17), the lag becomes 90° and increases to 180° as the forcing frequency is further increased. Of course, the ability of the vehicle to respond to the wave motions decreases as the frequency becomes increasingly greater than the second resonance frequency.

Before quantitatively studying the forced motions of an edge jet vehicle, some further comments must be made about the linear equation of motion, (15), which defines the small amplitude vertical motions of such a vehicle about its equilibrium position. The coefficients a_o and a_2 depend upon a and b, and these in turn upon the detailed behavior of the edge jet in unbalanced operation. It has earlier been shown that the unbalanced jet is somewhat different in its behavior for the two separate conditions that exist, one on each side of equilibrium. It might thus be anticipated that these coefficients a and b might have different values on either side of equilibrium, and such is actually the case. The values of a, b, a_o, and a_2 may be determined through the use of equations (3), (4), (5), (6), (14), and (16). They are given below for the two separate cases of overfed and underfed jets.

	Overfed	Underfed
a	$\sqrt{\frac{\rho}{2}} \frac{p_u - p_a}{\sqrt{p_o - p_u}}$	$\sqrt{2\rho} \sqrt{p_u - p_a}$
b	$\frac{\sqrt{\rho/2}\, H_e}{\sqrt{p_o - p_u}}$	$\frac{\sqrt{2\rho}\, H_e}{\sqrt{p_u - p_a}}$
a_o	$\frac{c^2 g \sqrt{\rho/2}}{W H_o \sqrt{p_o - p_u}}$	$\frac{c^2 g \sqrt{2\rho}}{W H_o \sqrt{p_u - p_a}}$
a_2	$\frac{c^2 H_e \sqrt{\rho/2}}{W H_o \sqrt{p_o - p_u}}$	$\frac{c^2 H_e \sqrt{2\rho}}{W H_o \sqrt{p_u - p_a}}$

Table I. Relations for a, b, a_o, and a_2.

Fortunately, the ratio a_o/a_2 is the same on both sides of equilibrium, and, of course, so is a_1. There thus exists no apparent ambiguity with regard to the specification of the frequencies at which maximum amplification may be expected. However, the precise motions of a system in which some of the coefficients change their values as the system passes through equilbrium are not simple to specify. For the purposes of this initial study, the existence of this change in the value of the coefficients will be ignored, and the system will be assumed to behave as if the coefficients of equation (15) are constant. The motions are now quantitatively studied.

Let the non-equilbrium and time-varying component of the vehicle's motion be taken as

$$\delta H = \delta \bar{H} \sin wt \tag{18}$$

and the motion of the ground relative to an observer moving rectilinearly with the velocity of the vehicle as

$$h_o = \bar{h}_o \sin (wt + d) \tag{19}$$

The frequency ω is, as inspection of Figure 7 shows

$$\omega = \frac{U_s \text{ (vehicle)} - U_w \text{ (wave)}}{\lambda} \tag{20}$$

Upon substitution of (18) and (19) in the equation of the motion of the vehicle, (15), the following relations for the vehicle's motion are obtained:

$$\left(\frac{\delta \bar{H}}{\bar{h}_o}\right) = \frac{\omega^2}{\sqrt{1 + \tan^2 \phi}} \left[\frac{(\omega + a_2) + (a_2 - \omega) \tan \phi}{(a_1\omega - \omega^3) + (a_o - a_2\omega^2)}\right] \tag{21}$$

and

$$\tan \phi = \frac{a_o \omega (\beta - 1)}{\left[a_o a_2 + \omega^2 (a_1 - a_2^2) - \omega^4\right]} \tag{22}$$

The amplitudes and phase angles at the two critical frequencies ω_{n_1}, and ω_{n_2}, are of particular interest. They are:

$$\text{at } \omega = \omega_{n_1} = \sqrt{g/H_e}:$$

$$\left(\frac{\phi \bar{H}}{\bar{h}_o}\right) = \frac{1 + \beta/\phi^2}{1 + \sqrt{\beta/\phi}} \tag{23}$$

$$\tan \phi = \sqrt{\beta/\phi}$$

$$\text{at } \omega_{n_2} = \sqrt{\beta}\ \sqrt{g/H_e}:$$

$$\left(\frac{\delta \bar{H}}{\bar{h}_o}\right) = \frac{\beta \sqrt{1 + \delta^2}}{(1 - \beta)} \tag{24}$$

$$\tan \phi = - \delta$$

where

$$\beta = \frac{a_1 a_2}{a_o} \text{ as stated earlier, and } \delta = \frac{\sqrt{a_1}}{a_2} .$$

A schematic amplification $\left(\frac{\delta \bar{H}}{\bar{h}_o} \right)$ curve is presented as Figure 9.

The general shape of the amplification is seen to depend only on the three parameters: ω_{n_1}, β, and δ. The relation between these parameters and the physical and operating characteristics of an edge jet vehicle is summarized below:

$$\omega_{n_1} = \sqrt{g/H_e}$$

$$\beta = \left(\frac{H_e}{H_o} \right) \frac{\gamma p_u}{p_u - p_a}$$

$$\delta = \begin{cases} \dfrac{\sqrt{g H_o}}{C} \dfrac{W}{H_e} \dfrac{1}{\sqrt{2}} & \text{(underfed)} \\ \dfrac{\sqrt{g H_o}}{C} \dfrac{W}{H_e} \sqrt{2} \dfrac{\sqrt{p_o - p_u}}{\sqrt{p_u - p_a}} & \text{(overfed)} \end{cases} \qquad (25)$$

Because of the particular dependence of δ on $\frac{\sqrt{g H_o}}{c} \cdot \frac{W}{H_e}$, it seems likely that values of considerably less than unity will be typical. Thus the response to forcing frequencies approximately equal to and greater than $\sqrt{\frac{\rho g}{H_e}}$ will typically depend primarily on β. However, for forcing frequencies approximately equal to $\sqrt{g/H_e}$, the value of δ is of considerable importance in determining the motion. In general, too, small values of δ will result in most severe motions near the first resonance frequency, $\omega_{n_1} = \sqrt{g/H_e}$. It is thus the forcing frequencies in the band $\frac{1}{2} \sqrt{g/H_e} < \omega < 2 \sqrt{g/H_e}$ which are most to be avoided and which if encountered could conceivably result in catastrophic

vertical motions of an edge jet vehicle. Some numbers defining the band of dangerous frequencies are given in Table II below:

$1/4\pi \sqrt{g/H_e}$	H_e	$1/\pi \sqrt{g/H_e}$
Cycles/sec.	Ft.	Cycles/sec.
1.45	.1	5.80
.63	.5	2.52
.45	1	1.80
.20	5	.80
.09	25	.36

← Dangerous frequency band →

Table II

For slowly moving water waves or for ground undulations, the frequency of encounter in cycles/sec. is U_s/λ . Generally, waves of length about 3/2 the vehicle's length are most difficult to negotiate, so that when $1/2\pi\sqrt{g/H_e} \approx \frac{2U_s}{3W}$, unhappy motions of an edge jet vehicle of the type studied might result, i.e. when

$$\frac{\sqrt{g\,W}}{U_s}\sqrt{\frac{W}{H_e}} \approx \frac{4}{3}\pi \tag{26}$$

As an example, a 100-foot edge jet ship traveling at 40 knots with a four-foot altitude might be expected to encounter serious jet-excited motions.

The appearance of a Froude number $\frac{\sqrt{g\,W}}{U_s}\sqrt{\frac{W}{H_e}}$ in equation (26) indicate that Froude scaling is necessary in order to simulate frequencies properly on the model scale. It is to be noted though that the vehicle speed does not appear in the parameters β and δ which determine amplifications - although the vehicle scale does appear. The difficulty of properly scaling motion amplitudes in model studies would thus seem apparent.

It should perhaps be again pointed out that as the frequency of encounter of an edge jet vehicle traveling over an undulating surface exceeds something like twice the first resonant frequency, $\sqrt{g/H_e}$, the ability of the vehicle to respond becomes limited and 180° out of phase, until for very high encounter frequencies the vehicle will maintain essentially horizontal flight regardless of the surface undulations going on underneath it. This high frequency behavior obviously limits the ability of a vehicle experiencing such encounter frequencies to negotiate waves or bumps, although it certainly implies a smooth ride so long as contact with the ground or sea can be avoided.

This initial theoretical study of the dynamics of an edge jet vehicle in vertical motion has been made with the aid of a number of simplifying assumptions; it is nevertheless believed that some important and fundamental aspects of the dynamics of edge jet vehicles have thus been revealed and that quantitatively interesting information has been produced for the designer's use.

SUMMARY AND CONCLUSIONS.

The vertical motions of edge jet vehicles have been studied with particular reference to their travel over undulating surfaces. Such motions are of special concern in connection with the possible use of edge jet vehicles for naval purposes. The important assumptions underlying the present analysis are: The vehicle is two-dimensional and has identical jets at its right and left edges; the motions are purely vertical; the mass flow delivered to the jets does not vary while the vehicle is in vertical motion; the jets are incompressible. A schematic illustration of the kind of vehicle considered is shown Figure 4.

During dynamic motions the jets of an edge jet vehicle generally operate in an unbalanced condition. The behavior of the jets is quantitatively hypothesized for "underfed" and "overfed" operation and the relation between these separate types of operation and the position of the vehicle relative to equilibrium is discussed. The possibility of self-excited vertical motions is raised, and it is shown how the occurrence of such motions depends on the value of a parameter (see equation 9) which depends on the magnitude of the loading of the vehicle and the configuration of its underbottom. Vehicles for which the bottom is level with the jet exits are incapable of self-excited motions - at least according to this incompressible jet analysis. Possibilities of self-excitation only occur for vehicles with indented bottoms (or under-pockets) and for very heavy loadings.

The motion of a vehicle over an undulating surface is shown to depend on an inhomogeneous third order equation with the resultant implication that the vehicle has two resonance frequencies or frequencies of peak response. The frequency of encounter of the vehicle with waves or other surface undulations is thus of paramount importance with regard to the vehicle's response, and it is estimated that the "dangerous" band of wave encounter frequencies is approximately

$$1/4\pi\sqrt{g/H_e} < \omega(\text{cycles/sec.}) < 1/\pi\sqrt{g/H_e}$$

where H_e is the equilibrium altitude of the vehicle in feet, measured from the ground to jet exits. At the center of this band is the lowest of the two resonance frequencies:

$$\omega_{n_1}\ (\text{cycles/sec.}) = 1/2\pi\sqrt{g/H_e}$$

It is pointed out that this just happens to be the frequency of a pendulum of length equal to the equilibrium altitude.

The amplitude of vertical motions near the frequencies of peak response are shown to depend upon two parameters β and δ (see Figure 9 and equations 23 and 24). For frequencies of encounter relatively small in comparison to the lowest of the two resonance frequencies the vehicle follows the surface undulations very well, but as the first resonant frequency is approached, increasing vertical response is obtained with the possibility of catastrophically large motions not remote. For frequencies several times the first resonant frequency the vehicle motions stiffen, and as frequency increases the vehicle becomes increasingly unable to respond at all to the surface beneath it and tends to maintain itself in level flight. As stated before, this high frequency behavior obviously limits the ability of a vehicle experiencing such encounter frequencies to negotiate waves or bumps, although it implies a smooth ride so long as contact with the ground or sea can be avoided.

REFERENCES

1. von Glahn, U. H., "Exploratory Study of Ground Proximity Effects on Thrust of Annular and Circular Nozzles". NACA TN 3982, Washington, D. C., April 1957.

2. Chaplin, H. R., "Theory of the Annular Nozzle in Proximity to the Ground." DTMB Aero Rept. 923, Navy Dept., Washington, D. C., July 1957.

3. Chaplin, H., and Stephenson, B., "Preliminary Study of the Hovering Performance of Annular Jet Vehicles in Proximity to the Ground." DTMB Aero Rept. 947, Navy Dept., Washington, D. C., August 1958.

4. Richardson, H. H., "A Dynamic Analysis of Externally Pressurized Air Bearings." M. I. T. Dept. of Mechanical Engineering, MS Thesis, Cambridge, Mass., 1955.

5. Roudebush, W. H., "An Analysis of the Effect of Several Parameters on the Stability of an Air-Lubricated Hydrostatic Thrust Bearing." NACA TN 4095, Washington, D. C., October 1957.

6. Licht, L., Fuller, D. D., and Sternlicht, B., "Self-Excited Vibrations of an Air-Lubricated Thrust Bearing." Trans. ASME, Vol. 80, No. 2, February 1958.

7. Richardson, H. H., "Static and Dynamic Characteristics of Compensated Gas Bearings." Trans. ASME, Vol. 80, No. 7, October 1958.

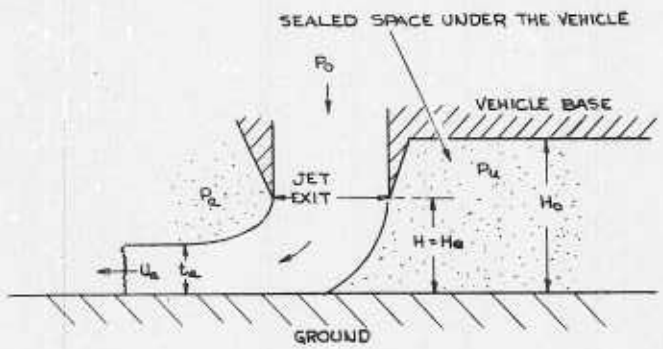

Figure 1. Edge jet in balanced operation

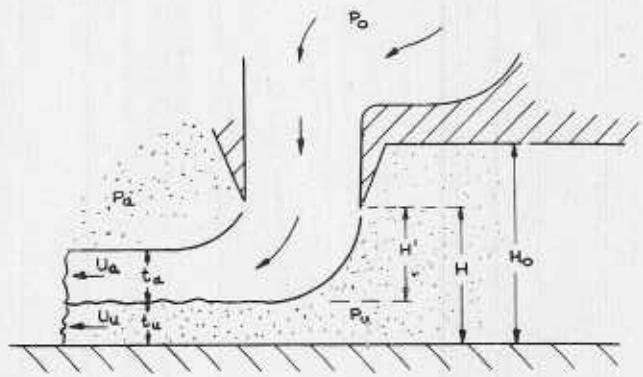

Figure 2. Edge jet in underfed condition

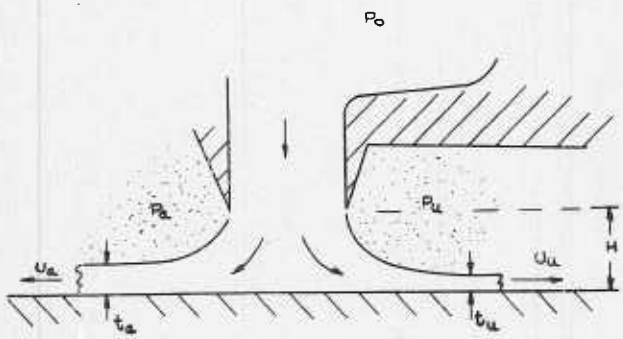

Figure 3. Edge jet in overfed condition

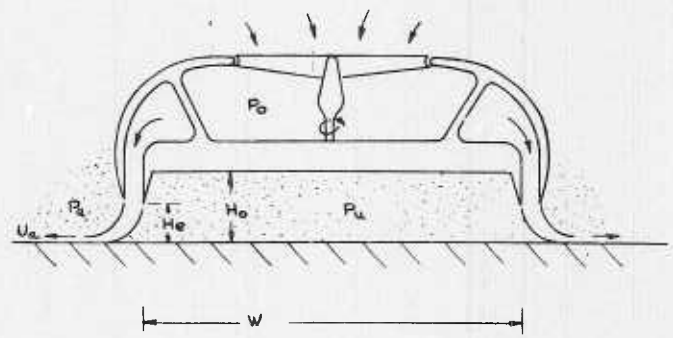

Figure 4. Edge jet vehicle

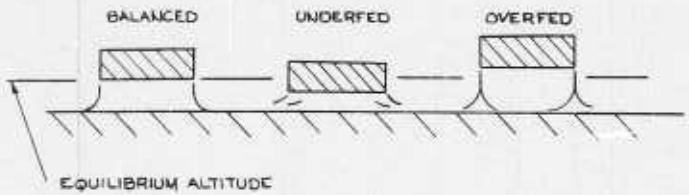

Figure 5. Jet behavior $\beta > 1$

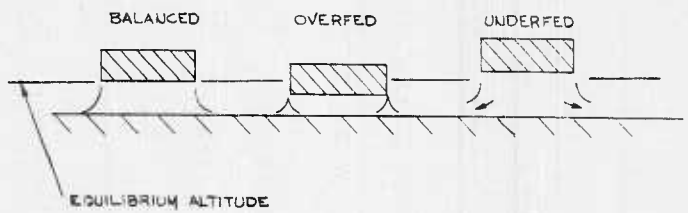

Figure 6. Jet behavior $\beta > 1$

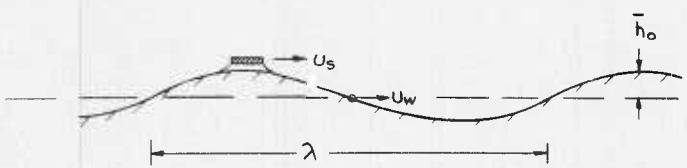

Figure 7. Vehicle traversing a wave

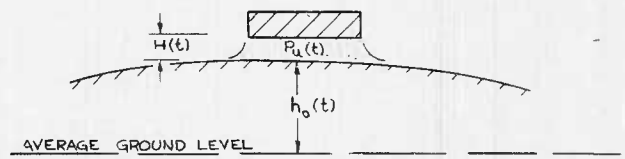

Figure 8. Vehicle over a wave

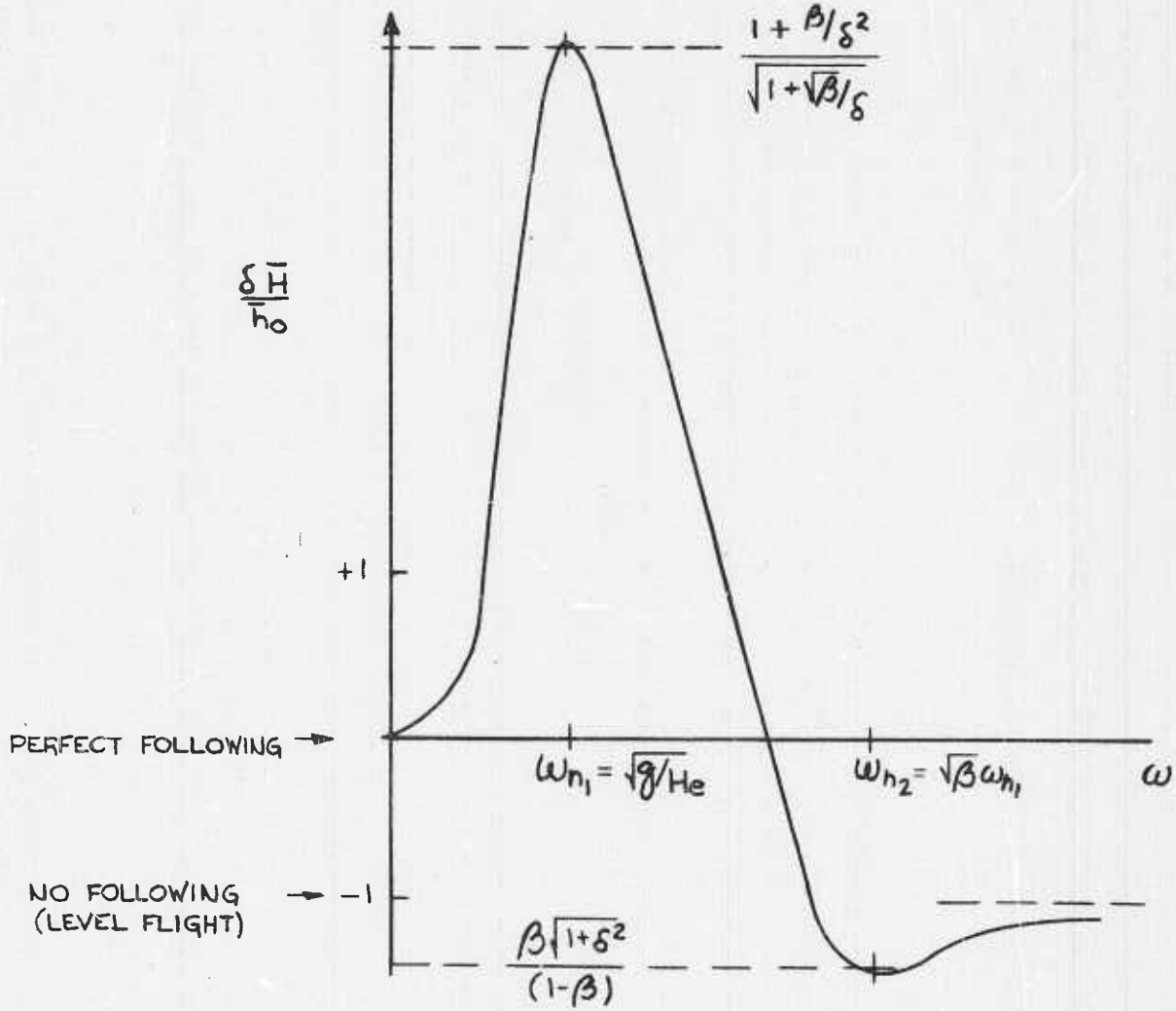

Figure 9. Schematic amplification curve

DEVELOPMENT OF A UNIQUE GEM CONCEPT WITH POTENTIAL FOR ACHIEVING EFFICIENT FORWARD FLIGHT

By M. F. Gates and E. R. Sargent, Hiller Aircraft Corporation,
Palo Alto, California

SYMBOLS*

A_1	diffuser inlet area, ft^2
A_2	diffuser outlet area, ft^2
A_3	jet outlet area = $A_g - A_1$, ft^2
A_4	contracted jet outlet area = $C_c A_3$, ft^2
A_B	inner base area of annular nozzle = $A_P - A_J$, ft^2
A_D	diffuser planform area, ft^2
A_g	total peripheral gap area, ft^2
A_J	jet nozzle area (assumed equal to A_1 here for simplicity) ft^2
A_P	planform area (effective) ft^2
C_c	contraction coefficient
F_H	horizontal propulsive thrust, lb
F_J	jet force, lb
F_{J_e}	equivalent jet force of circular nozzle with same mass flow expanded to ambient pressure from a pressure of XP_f above ambient, lbs
h	ground clearance, ft
hp	air horsepower, hp
K	general loss coefficient, $\frac{\text{pressure loss}}{q}$
K_1	nozzle-gap spanning loss
K_2	ground friction loss
K_3	diffuser loss
K_4	duct loss

*See appendix for pictorial definition.

K_5	residual velocity loss = $\left(\frac{A_J}{A_2}\right)^2$
K_D	$K_1 + K_2 + K_3$
K_L	$K_1 + K_2 + K_3 + K_4 + K_5$
L	total lift, lb
P_J	static pressure at jet outlet, lb/ft^2
P_o	ambient pressure, lb/ft^2
P_1	static pressure at diffuser inlet, lb/ft^2
P_2	static pressure at diffuser outlet, lb/ft^2
$\triangle P_f$	total pressure rise across fan or compressor, lb/ft^2
q_J	dynamic pressure at fan or compressor = P_f, lb/ft^2
q_2	dynamic pressure at diffuser outlet, lb/ft^2
V_J	jet velocity, ft/sec
$\dot{w}$	weight flow rate, lb/sec
$\frac{L}{A_P}$	plate loading, lb/ft^2
ρ	density, $slugs/ft^3$
Θ	jet inclination, negative inwards, degrees

DISCUSSION

Our interest at Hiller in both the beneficial and detrimental ground effects resulting from the operation of jet-supported aircraft in ground proximity began in 1955. At that time, a study of jet lift was made and published in a proprietary report entitled "Proposal for Direct Lift Propulsion Research," reference 1. Later, in January 1958, test work was published as an appendix to a proposal presented for a high speed combined body-jet lift aircraft. This test work was conducted primarily to determine if harmful ground effect existed with the proposed aircraft configuration. Much to our pleasure, it was found that the particular arrangement proposed had no detrimental ground effect; rather, with slight modification, a ground cushion was obtained. Our interest again became active in late 1958 with a company-backed program which provides the basis for this paper.

The intent of this paper is to describe the evolution of the Hiller diffuser concept and its variations as applied to the Ground Effect Machine. Figure 1 illustrates this concept in two variations: the diffuser-recirculation, and diffuser-plenum chamber concepts. These concepts will be considered here with specific emphasis on their static, or hovering performance. The forward flight capability will be discussed briefly. These studies are now being expanded with ONR support.

For purposes of comparison, the concept cycles currently being investigated by others are illustrated in Figure 2: the annular jet, plenum chamber, air bearing, and the labyrinth seal.

The diffuser-recirculation concept was conceived as the result of a desire to eliminate the energy loss inherent in the existing systems, which utilize the reaction of an escaping jet to effect a pressure seal, or which utilize a modified labyrinth seal wherein the seal air is recirculated to conserve power (Wieland's concept). The pictorial presentations of Wieland's concept by Aviation Week (reference 2 and by Boehler reference 3 indicate that the conversion of the dynamic pressure to static pressure is accomplished without the aid of a diffuser. There is also an apparent lack of mechanism for turning the jet. Consequently losses associated with an abrupt expansion and turning may occur. As mentioned previously, it is the intent of the Hiller diffuser-recirculation concept to eliminate this loss.

The mathematical expressions which are summarized in Figure 3 were derived for this diffuser-recirculation concept, and also the diffuser-plenum concept and the conventional plenum-chamber concept. The derivations are given in the appendix. These expressions describe the required fan pressure rise and mass flux parameter for hovering flight in terms of the planform loading (L/Ap) the associated loss coefficients, and other pertinent variables where required. It will be noted that the mass flux parameter is in actuality the quantity of flow per unit of sealed gap area. The air horsepower parameter, which properly compares the systems, is the product of the fan pressure rise and mass flux parameter.

In the Hiller diffuser-recirculation concept analysis, the entire gap or diffuser inlet is assumed to be exactly filled by the horizontal jet. The jet is then diffused between the ground surface and lower surface of the GEM to convert its kinetic energy (or dynamic pressure) to potential energy (or static pressure). This static pressure is applied over a large surface to produce the lift force. This air from the pressurized zone is then recirculated by giving it a small pressure boost with the fan to overcome the frictional losses and the slight residual velocity head loss due to the finite expansion ratio of the diffuser. (The assumption that residual velocity is a complete loss may be overly conservative.) It will be recognized that this cycle is analogous to an open throat wind tunnel.

It was seen from this analysis that the concept did approach the ultimate in lift effectiveness in the ideal case (no pressure rise required, once circulation is established) by virtue of the fact that the jet energy is conserved. It is also seen that the mass flux required equals that of the conventional plenum chamber configuration in the ideal case. (In general, the ideal case is defined as that case in which there are no frictional losses, the escaping-jet-outlet-gap is flowing full (C_c = 1), and an infinite diffuser expansion ratio exists.)

In this analysis, it was assumed for simplicity that continuity is maintained throughout the system - that is to say, there is no efflux or influx to the system. In a practical application of this concept, it is likely that make-up air will be required. This air could be supplied by an auxiliary fan installed so as to introduce air directly into the pressurized zone from the ambient. Another variation, which overcomes this problem with an ejector pump, is discussed later.

A variation of the diffuser concept which has excellent potential, particularly for forward flight, is the diffuser-plenum concept. The features which give it this potential are: (1) a forward propulsive thrust (F_H) which is a free by-product of the lift system and, (2) a reduced mass flux parameter for a given planform loading, both of which are achieved by virtue of the fact that part of the peripheral gap is sealed by the incoming jet at the diffuser inlet, while the remainder is sealed by the escaping jet. This concept also

utilize the diffuser to achieve efficient energy conversion from dynamic to static pressure. However, rather than recirculate the pressurized, and possibly contaminated air, as in the previous concept, it is discharged through the gap at the rear of the vehicle in a manner identical to the plenum chamber configuration.

Examination of the expressions derived for this diffuser-plenum concept reveals that the mass flux parameter is one-half that required for the conventional plenum concept when the peripheral gap is flowing full (contraction coefficient equals 1). The required fan pressure rise has been increased approximately by the factor of one minus the sum of the loss coefficients ($1 - K_L$) or to the same value as the conventional plenum concept. If, in both concepts, means are employed to reduce the outlet gap contraction coefficient to 0.5, the mass flux parameter of the diffuser-plenum concept is 1/3, and the conventional plenum chamber 1/2 of that which results from the peripheral gap of the conventional plenum concept flowing full. (It might be mentioned here that reduction of the contraction coefficient below 0.6, which results from a sharp edge, to 0.5 by use of a reentrant-type orifice such as a "Borda" outlet tends to have a destabilizing effect in regard to changes in ground clearance. A sharp edge can be seen to be neutrally stable in this regard while a typical rounded outlet has a stabilizing effect.)

In addition to the advantage of a reduced mass flux, a horizontal propulsive thrust is obtained as was mentioned earlier by virtue of the portion of the escaping jet which is opposed to the diffuser inlet. This thrust is a free by-product of the lift-producing system. In the ideal case (with the contraction coefficient = 1) it is equal to twice the planform loading times the unbalanced area which is the projected inlet area. As may be seen by examination of the expression in Figure 3, the effect of the contraction coefficient is to decrease the horizontal thrust while the loss coefficient effect is nil. The reduction in mass flux, the production of free forward thrust, and the utilization of the high velocity air directly from the fan without prior diffusion and contraction gives this concept the potential for improved performance over existing systems.

Another variation of the Hiller diffuser concept utilizes an ejector pump to provide the required pressure rise for recirculation. The primary flow of the ejector which is obtained from the ambient would provide the pressure for initial "lift-off" of the diffuser-recirculation concept as well as provide the make-up air required by the system due to changes in the inlet gap, which are brought about by irregularities of the surfaces over which the GEM is operating. The primary flow in excess over that required for make-up could be used for forward thrust through means of a nozzle that could be directed as required to supply both forward propulsion and control forces. An ejector pump's insensitivity to dust, debris, and water-laden air, when compared to a fan, may serve well in a recirculation concept in spite of its basic poor pumping efficiency. The internal flow intricacies of such a system are intriguing. However, we have not as yet thoroughly investigated this system.

The analysis of the annular nozzle concept and its expressions are complicated by the addition of the jet reaction to the lift system and also by the dependence of the base pressure on the radius of curvature of the exhausting jet. The analysis of this concept has been well covered by others (Chaplin, Boehler, Pinnes) and will not be repeated here. Most existing analyses, after the required simplifying assumptions are made, result in expressions for the ratio of fan pressure rise to the pressure existing over the annular nozzle center body which indicate values smaller than one. An exception to this general statement is the analysis of Pinnes of the thick jet (reference 4) which properly describes the limits. This analysis shows that, while it is not possible to achieve a base pressure greater than the fan pressure, it is possible to achieve a planform loading equal to twice the fan pressure rise. Such is the case when the annular nozzle geometry converts to a plenum chamber (or ducted propeller) out of ground effect. However, it can be shown by a simplified analysis that the required air horsepower at a constant planform loading

for a plenum concept in ground effect (altitude ratio h/d of 0.05) is approximately 0.57 times that of the circular nozzle out of ground effect. While it is realized that this does not represent optimum configurations or rigorous analysis, it does serve to indicate that the required altitude ratio to realize these high values of the fan pressure rise to planform loading ratio puts these high ratios out of the area of interest. Consequently, it has been reasoned that the conventional plenum chamber concept, which is a circular nozzle in ground effect, is a practical limit to the capabilities of the annular nozzle from the standpoint of hovering performance.

Figure 4 gives a pictorial presentation of these results which reflect static considerations only. The upper plot shows the required fan pressure rise, the middle plot gives the mass flux parameter, and the lower one the air horsepower per unit sealed gap area. These parameters are plotted versus the planform loading. The solid lines represent the ideal values of the plotted parameters (i.e., zero losses and contraction coefficient = 1) while the labeled arrows at the side indicate the effect of frictional losses and of contraction coefficient. The pressure loss coefficients play an important part in the concept analyses. For the purposes of the analyses the loss coefficients were broken down into (1) a combined nozzle and gap spanning loss, (2) a ground friction loss, (3) a diffuser loss, (4) ducting loss when appropriate, and (5) a small residual velocity head loss at the diffuser outlet. The value of the sum of the first three losses itemized above was found to be 0.285 by tests that are discussed later. Efficiency of the annular nozzle configuration was obtained from the DTMB work. No data is known for the plenum concept. Consequently, the losses were assumed equal to 15 per cent of the fan dynamic pressure. A contraction coefficient of 0.5 was used universally where applicable. Such a value is possible with a "Borda" outlet.

The curved arrows represent the regime of the annular nozzle configuration described previously. It is shown for the annular nozzle configuration that the fan pressure rise in the ideal case for a given planform loading decreases to the value of the conventional plenum concept as the ratio of the jet area to planform area increases to 1. The dashed line indicates a plenum concept (ducted propeller) out of ground effect. The effect of this ratio on the mass flux parameter at a given plate loading is the reverse, i.e., the mass flux increases. The effect of inward jet inclination (Θ) is to increase the ground clearance while decreasing the allowable planform loading for the same fan pressure rise. (Jet inclination has no effect on the base pressure, which is a function of jet turning radius only, but it does reduce the jet's direct contribution to the lift by the cosine of the of the angle, reference 4.) The actual performance of an annular nozzle GEM was calculated from the data of reference 5. This performance is plotted in Figure 4 for comparison.

The net effect of the considered variables on system performance is shown by the lower plot of Figure 4 which gives the air horsepower required per unit gap area. It is seen that the minimum power requirement is given by the diffuser-plenum concept.

The specific identified points indicate performance values based on the coefficient values discussed earlier. The data supporting the conventional plenum concept is meager, as is the data supporting the single annular nozzle configuration, the geometry of which is not necessarily ideal. (We expect to have more data for comparison after this symposium.) However, we believe that the potential of these Hiller concepts is still real. It should be re-emphasized that Figure 4 is for the hover (static) case only.

Our test program, which dealt with the hover case only, utilized what we call the "component technique." This amounts to evaluating a two-dimensional slice of a concept cycle. Such a test setup is shown in the photograph of Figure 5. It will be noted that the component model is upside down. Shown in Figure 6 is a cross section of the test model which indicates the axial location of the pressure-measuring stations. This cross

section, differing slightly from one shown in Figure 5, depicts the geometry of the one used in the tests reported here. The model surfaces in the jet nozzle and diffuser areas were made of standard mill finish aluminum; those in the plenum area were unfinished plywood, with the exception of the surface forming the outlet gap. This surface was aluminum, so that a sharp edge could be maintained at the outlet gap. The side plates were of low friction material; the far one is Formica, the near one of plexiglass to permit flow visualization. The ground surface was simulated by unfinished plywood. The width (or depth) of this model was approximately 18 inches while the jet thickness was 0.88 inch. This resulted in an aspect ratio of approximately 20. It is believed that this substantially eliminates side plate effects from consideration, particularly when pressure measurements are made as they were, halfway between the side plates. The tests were made at a constant jet thickness, while the gap area was adjusted to give values both greater and less than the jet area. The discharge area was varied for each gap area to give the different operating modes. For instance, the discharge area was adjusted to give continuity through system, then reduced to give reverse flow at the diffuser inlet, and finally increased to where the mass flow through system exceeded the primary mass flow i.e., where ejector pumping occurred. An attempt was made to maintain identical reverse and pumping flow fractions for each value of sealed gap. In the reverse flow case, through-flow was approximately 80 per cent of the primary, while in the pumping case through-flow was approximately 108 per cent of the primary.

Figure 6 also shows a typical pressure distribution obtained from these component tests. Such pressure distributions were obtained over a range of gap values. This data provides the basis for the pressure loss coefficient shown in Figure 7 and, also, for stability studies. This coefficient covers the losses between the nozzle inlet and the diffuser outlet and is applicable to both the diffuser-plenum and diffuser-recirculation concepts. The pressure loss coefficient of .285 for continuity flow when the gap equalled the jet was taken as the design point. It is interesting to note that the pressure loss factor provides a measure of vertical stability by counteracting forces which tend to increase altitude, because the loss coefficient increases with altitude. This occurs at altitudes exceeding the initial jet thickness. It is also recognized that if a constant-head fan characteristic is assumed, the loss coefficient (which increases for values of gap below that of jet thickness) will not act to counteract disturbances which tend to reduce the gap. However, a fan head characteristic could be matched to this loss curve to overcome this deficiency. Also of interest are the apparent decreased losses in the reverse flow mode. The exact explanation of this is not known at this time, but it is believed that the improved performance is due to eliminating the turbulent, de-energized free jet boundary from the flow system. This increased performance in the reverse flow mode may indicate that the best operating condition is not one of continuity flow, as assumed in our analysis thus far. The increased losses in the pumping mode can be attributed to a total head loss due to turbulent mixing between the primary jet and ambient air.

Tests are continuing to further substantiate the data and, also, to obtain a more detailed map of "off-design" operation. This, in turn, will obviously permit more rigorous analysis of the system and subsequently lead to accurate performance, stability, and control predictions.

We believe that the diffuser concepts are ideal for forward flight. Some researchers have expressed concern for the magnitude of momentum drag of the conventional GEM concepts (annular jet and plenum chamber) in forward flight. If momentum drag is a problem, the Hiller diffuser concepts will materially reduce it. It should be emphasized that the ram pressure rise associated with momentum drag can be utilized to unload the lift-producing system. Earlier work at Hiller, covered by reference 1 indicated that a ducted propeller operating out of ground effect and with the duct inlet aligned with the free stream could operate subsonically with a decreasing power requirement as flight speed was increased. Figure 8 shows this concept. It will be noted that

the propeller wake is directed downward at such an angle that the resultant of the gross thrust vector and the momentum drag vector provide the required lift. This assumes that no lift is provided by the external flow, i.e., all the lift is derived from the internal flow. This analysis has not been extended to the ground effect regime, but in its present form supports our contention that the ram pressure rise that is associated with the inlet momentum drag can be used to advantage if handled correctly.

The momentum drag characteristics of the diffuser concepts can be best discussed by again referring to Figure 4, in particular to the mass flux parameter. Assuming that this parameter is not affected by forward flight, it can be seen that the mass flux requirements and consequently the momentum drag of the diffuser-plenum concept is only two thirds that of the conventional plenum concept on the basis of these static considerations. The effect of forward flight on these static requirements has not been analyzed quantitatively, but it is not expected to seriously alter the picture. Inspection of the diffuser-recirculation concept will indicate that it has the lowest possible momentum drag, since the lift-producing flow is entirely internal. Its momentum drag is similar to that of a conventional aircraft where the momentum drag is only that associated with producing the horizontal propulsive force. This is again based on static mass flux considerations. Make-up air requirements are also excluded. In regard to the momentum drag associated with forward propulsion, it should again be pointed out that the diffuser-plenum concept incorporates a "free" horizontal propulsive thrust.

In conclusion we would like tc emphasize that the ideal GEM lift-propulsion cycle and its potential, which will vary with application, can only be determined by careful, detailed evaluation of all facets of the various possible cycles. To do otherwise is dangerous conjecture. While this is an obvious truth, our enthusiasm for our pet concepts may tend to blind us to the concepts of others. We have endeavored in this paper to present the comparison as fairly as possible.

In this vein it is believed that the diffuser concepts possess good potential for effective Ground Effect Machines, particularly when both hovering and forward flight are considered.

APPENDIX: DERIVATION OF FAN PRESSURE RISE, MASS FLUX, AND AIR HORSEPOWER PARAMETERS

Diffuser-recirculation concept. Assumptions: $P_1 = P_J = P_o$; two-dimensional flow.

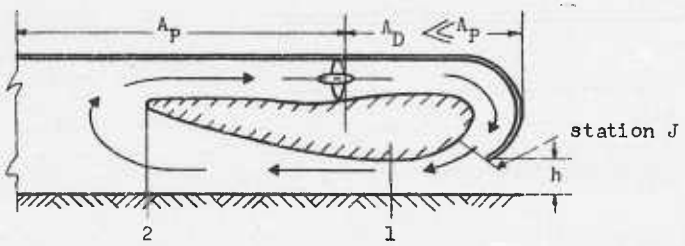

Fan pressure rise

$$\triangle P_f = K_L \, q_J \tag{1}$$

by definition

$$L = P_2 \, A_P \tag{2}$$

by inspection

$$P_2 = q_J - q_2 - (K_1 + K_2 + K_3)\, q_J \tag{3}$$

by continuity

$$q_2 = \left(\frac{A_J}{A_2}\right)^2 q_J \tag{4}$$

Combining (2), (3), and (4) gives .

$$\frac{L}{A_P} = P_2 = q_J \left[1 - K_D - \left(\frac{A_J}{A_2}\right)^2\right] \qquad \text{where } K_D = K_1 + K_2 + K_3 \tag{5}$$

and rearranging (5)

$$q_J = \frac{L}{A_P}\left[\frac{1}{1 - K_D - \left(\frac{A_J}{A_2}\right)^2}\right] \tag{5a}$$

Substituting (5a) into (1) gives

$$\Delta P_f = \frac{K_L\, L/A_P}{1 - K_D - \left(\frac{A_J}{A_2}\right)^2} \tag{6}$$

The mass flux parameter

$$\frac{\dot{w}}{g\rho}\frac{1}{A_g} = \frac{A_J\, V_J}{A_g} \tag{7}$$

Since $P_J = P_o$ by assumption

$$V_J = \sqrt{\frac{2}{\rho}\, q_J} \tag{8}$$

substituting (5a) into (8) gives

$$V_J = \sqrt{\frac{2}{\rho}}\sqrt{\frac{L}{A\rho}}\sqrt{\frac{1}{1 - K_D - \left(\frac{A_J}{A_2}\right)^2}} \tag{9}$$

Substituting (9) into (7) gives

$$\frac{\dot{w}}{g\rho}\frac{1}{A_g} = \frac{A_J}{A_1}\sqrt{\frac{2}{\rho}}\sqrt{\frac{L}{A_P}}\sqrt{\frac{1}{1 - K_D - \left(\frac{A_J}{A_2}\right)^2}} \tag{10}$$

where $A_1 = A_g$

Assuming $A_1 = A_J$ for simplicity, the air horsepower parameter

$$\frac{hp_{air}}{Ag} = \frac{\triangle P_f}{550} \cdot \frac{\dot{w}}{g\rho} \frac{1}{Ag}$$

$$= \frac{K_L}{550} \sqrt{\frac{2}{\rho}} \left\{ \frac{L/A_P}{1-K_D-\left(\frac{A_J}{A_2}\right)^2} \right\}^{3/2} \tag{11}$$

Diffuser-plenum concept. Assumption: $P_1 = P_J = P_o$; $q_4 = P_2 + q_2$; two-dimensional flow.

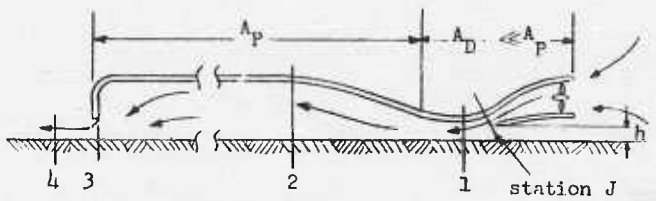

Fan pressure rise

$$\triangle P_f = q_J \tag{12}$$

The diffuser outlet pressure is the same as in the case of the diffuser-recirculation concept:

$$\frac{L}{hp} = P_2 = q_J \left[1-K_D-\left(\frac{A_J}{A_2}\right)^2 \right] \tag{5}$$

Substituting (5a) into (12) gives

$$\triangle P_f = \frac{L}{A_P} \left[\frac{1}{1-K_D-\left(\frac{A_J}{A_2}\right)^2} \right] \tag{13}$$

Mass flux parameter

$$\frac{\dot{w}}{g\rho} \frac{1}{A_g} = \frac{A_J}{A_g} V_J \tag{7}$$

by inspection

$$A_g = A_1 + A_3 \tag{14}$$

by definition

$$A_3 = \frac{A_4}{C_c} \tag{15}$$

from continuity

$$\frac{A_4}{A_J} = \frac{V_J}{V_4} = \sqrt{q_J/q_4} \tag{16}$$

by assumption and equation (3)

$$q_4 = P_2 + q_2 = q_J\,(1-K_D) \tag{17}$$

substituting (17) into (16) and rearranging gives

$$A_4 = A_J \frac{1}{\sqrt{1-K_D}} \tag{18}$$

substituting (15) and (18) into (14) gives

$$A_g = A_1 + \frac{A_J}{C_c} \frac{1}{\sqrt{1-K_D}} \tag{19}$$

rearranging

$$\frac{A_J}{A_g} = \frac{1}{\frac{A_1}{A_J} + \frac{1}{C_c\sqrt{1-K_D}}} \tag{19a}$$

substituting (8), (12), (13), and (19a) into (7) gives

$$\frac{\dot{w}}{g\rho}\frac{1}{A_g} = \frac{\sqrt{\frac{Z}{\rho}}\sqrt{\frac{L}{A_P}}\sqrt{\frac{1}{1-K_D-\left(\frac{A_J}{A_2}\right)^2}}}{\frac{A_1}{A_J} + \frac{1}{C_c\sqrt{1-K_D}}} \tag{20}$$

Air horsepower parameter, assuming $A_1 = A_J$,

$$\frac{hp_{air}}{A_g} = \frac{\Delta P_f}{550}\frac{\dot{w}}{gp}\frac{1}{A_g} = \frac{1}{550}\sqrt{\frac{Z}{P}}\left[\frac{\frac{L}{A_P}}{1-K_D-\left(\frac{A_1}{A_2}\right)^2}\right]^{3/2}\frac{1}{1+\frac{1}{C_c\sqrt{1-K_D}}} \tag{21}$$

Conventional Plenum Concept. Assumption: $P_4 = P_o$; $q_4 = P_2 + q_2$; $A_4 << A_2$.

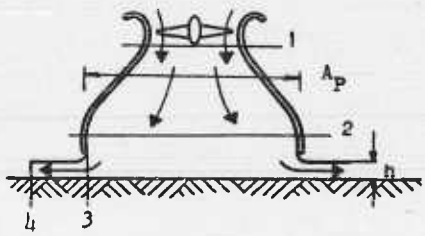

Fan pressure rise by momentum

$$L = A_2 P_2 + \frac{\dot{w}}{g} V_2 = A_2 P_2 + \rho A_2 V_2^2 \tag{22}$$

by energy

$$\Delta P_f = P_2 + q_2 + (K_3 + K_4)\, q, \tag{23}$$

where

$$q_2 = \frac{1}{2} \rho V_2^2 \tag{24}$$

by continuity

$$q_1 = q_4 \left(\frac{A_4}{A_1} \right)^2 \tag{25}$$

$$q_2 = q_4 \left(\frac{A_4}{A_2} \right)^2 \tag{26}$$

Substituting (24) into (22) and rearranging

$$\frac{L}{A_P} = P_2 + {}^2 q_2 \quad \text{where } A_P = A_2 \tag{27}$$

Substituting (25) and the assumption

$$q_4 = P_2 + q_2 \tag{28}$$

into (23) and rearranging gives

$$\Delta P_f = q_4 \left[1 + (K_3 + K_4) \left(\frac{A_4}{A_1} \right)^2 \right] \tag{29}$$

Substituting (28) into (27) gives

$$\frac{L}{A_P} = q_1 + q_2 \tag{30}$$

Substituting (26) into (30) and rearranging gives

$$q_4 = \frac{\dfrac{L}{A_P}}{\left[1 + \left(\dfrac{A_4}{A_2}\right)^2\right]} \tag{31}$$

Substituting (31) into (29) gives

$$\Delta P_f = \frac{\dfrac{L}{A_P}}{\left[1 + \left(\dfrac{C_c A_g}{A_2}\right)^2\right]} \left[1 + (K_3 + K_4)\left(\frac{C_c A_g}{A_1}\right)^2\right] \tag{32}$$

$$\text{where } A_g = \frac{A_4}{C_c}$$

We are interested in $\frac{h}{r}$ 0.05

$$\text{o}^{\text{o}}\text{o} \quad \left(\frac{A_g}{A_2}\right)^2 < .01$$

Therefore at height ratios of interest,

$$\Delta P_f = \frac{L}{A_P}\left[1 + (K_3 + K_4)\left(\frac{C_c A_g}{A_1}\right)^2\right] \tag{33}$$

Mass flux parameter

$$\frac{\dot{w}}{g\rho} \cdot \frac{1}{A_g} = \frac{A_4}{A_g} V_4 \tag{34}$$

$$V_4 = \sqrt{\frac{2}{\rho}}\ \sqrt{q_4} \quad \text{Since } P_4 = P_o \tag{35}$$

by combining the reasoning applied to the ratio of $\left(\frac{A_4}{A_2}\right)$ in arriving at (33) with the statement of (24) and subsequently applying it to (27), it can be reasoned that q_2 will be insignificant when compared with q_4. Consequently we may say

$$q_4 \approx P_2 \approx \frac{L}{A_P} \tag{36}$$

Subsittuting (35) and (36) into (34) gives

$$\frac{\dot{w}}{gp} \cdot \frac{1}{A_g} = C_c \sqrt{\frac{2}{P}} \sqrt{\frac{L}{AP}} \quad \text{where } \frac{A_4}{A_g} = C_c \tag{37}$$

air horsepower parameter

$$\frac{hp_{air}}{A_g} = \frac{\Delta P_f}{550} \cdot \frac{\dot{w}}{g\rho} \cdot \frac{1}{A_g}$$

$$= \frac{1}{550} \sqrt{\frac{2}{\rho}} \left(\frac{L}{A_P}\right)^{3/2} C_c \left[1 + C_c^{\,2} (K_3 + K_4) \left(\frac{A_g}{A_1}\right)^2\right] \tag{38}$$

REFERENCES

1. Sargent, E. R., and Lockwood, R. M., "Proposal for Direct-Lift Propulsion Research." Hiller Aircraft Corporation Engineering Rept. 533.3, November 5, 1953.

2. Butz, J. S., Jr., "Designers Study Air Cushion Principles for Vehicles." Aviation Week, January 12, 1959.

3. Boehler, G. D., "Remarks on the Ground Effect Machine." Paper presented at the Fifth Annual Western Forum of the American Helicopter Society, September 25-26, 1958.

4. Pinnes, R. W., "A Power Plant Man's Look at the Ground Effect Machine." Bureau of Aeronautics Research Division Rept. DR-1958, April 1959.

5. Tinajero, A. A., "Comparison of Experimental and Theoretical Design Parameters of a 6-inch-diameter Annular Jet Model with a Jet Angle of -45° Hovering in Proximity to the Ground: and Experimental Results for Forward Flight at Zero Angle of Attack." David Taylor Model Basin Aero Rept. 954, May 1959.

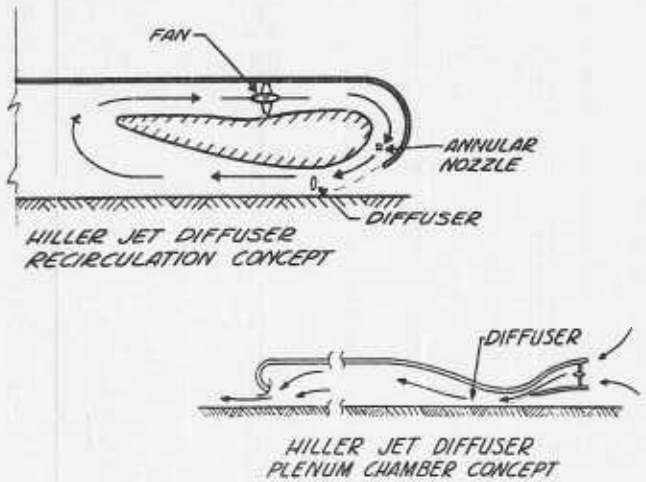

Figure 1. Hiller diffuser concepts

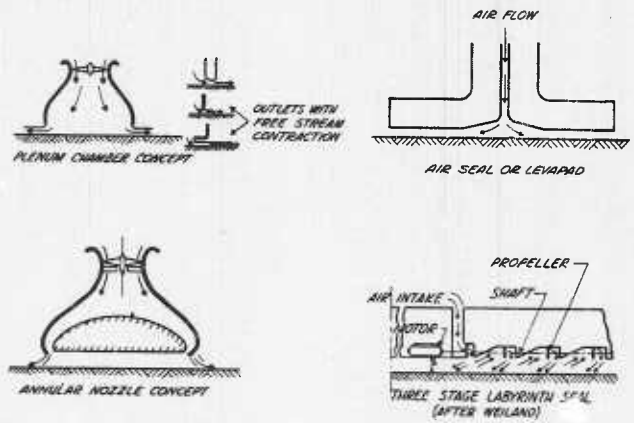

Figure 2. Current GEM concepts

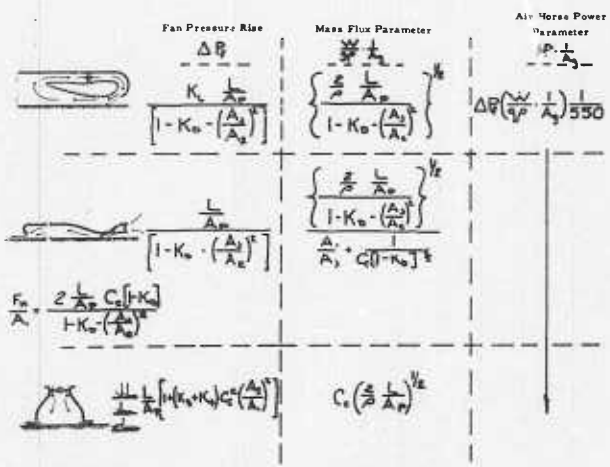

Figure 3. Summary tabulation of performance expressions

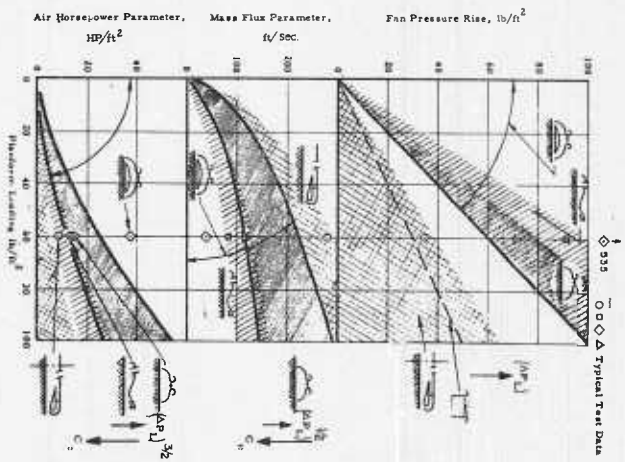

Figure 4. GEM hover performance

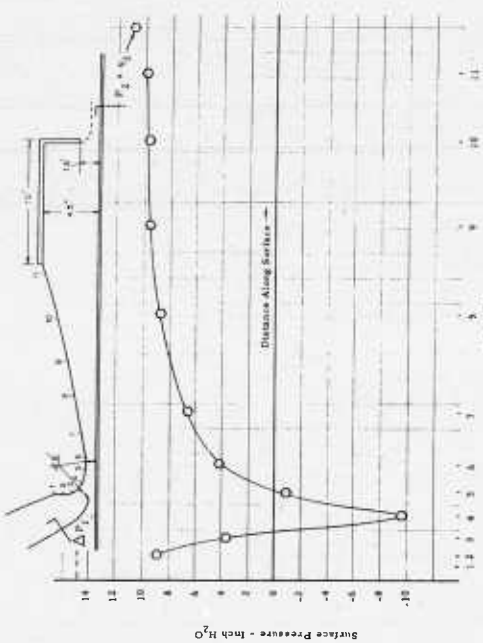

Figure 6. Typical pressure distribution - diffuser concept

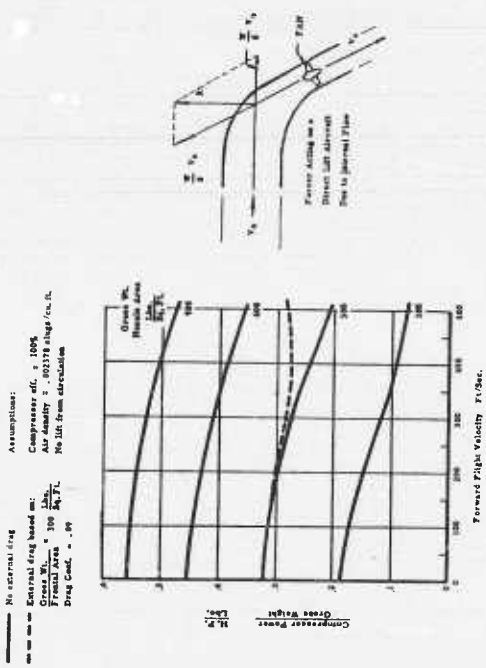

Figure 8. Forward flight power required for direct lift aircraft

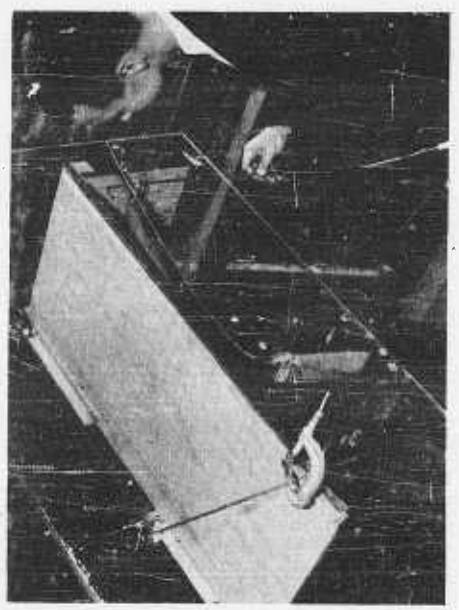

Figure 5. GEM component test

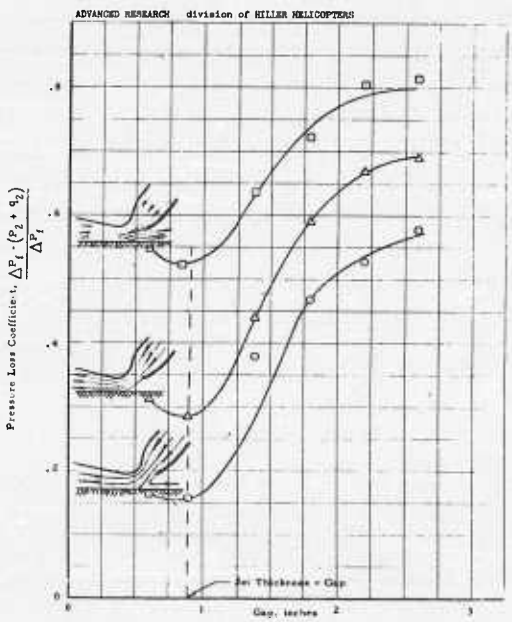

Figure 7. Pressure loss coefficients - diffuser concept

TEST RESULTS OF AN ANNULAR-JET GROUND-EFFECT VEHICLE

By Stephen Silverman, North American Aviation,
Incorporated, Columbus, Ohio

INTRODUCTION

Approximately one and a half years ago, after examining the preliminary work that had been accomplished in the field of ground effect vehicles, by such organizations as the NACA and the David Taylor Model Basin, it was decided by NAA Columbus that the basic concept was well worthy of pursuit by our own research and development staff. This viewpoint was naturally spurred on by the many promising applications that could readily be visualized.

Our first question was whether or not we could duplicate the results, which had previously been obtained with a compressed air supply whose mass flow and pressure are constantly under control, with a propeller system. As is well known, a propeller is a temperamental device which under high back pressure will surge or stall. The significance of this question has since been well emphasized by Pinnes at BuAer. With these thoughts in mind we began our studies with a small annular jet model (Figure 1).

The results of this preliminary test were very encouraging (Figure 2) and showed that good ground effects could be experienced with a propeller-driven air supply.

The next step in our experimental program, then, was to build a more versatile model. The primary objective of the test was to evaluate the following items:

1. The effect on lift of the following area variations: the ratio of total base area to propeller area and the ratio of total base area to solid base area.
2. The effect of these area ratios on the thrust to power ratio.
3. The effect of adding a skirt to the model. This would essentially raise the base height of the model while keeping the model at a constant altitude.
4. The use of exit guide vanes in order to cancel out the vehicle torque.
5. The effect of base area ratio on the inherently neutral stability characteristics of this type of ground effect vehicle.

MODEL DESCRIPTION

The power plant for the model was a variable frequency water-cooled electric motor which drove an available four-bladed 12-inch diameter propeller. This propeller was originally designed for 0.8 Mach number operation and consequently was not optimum for static operation. The model was fully instrumented to allow determination of lift, torque, pitching moment, rpm, and power. Figure 3 shows one of the configurations on the test stand and Figure 4 shows the miscellaneous model parts which were subsequently tested. Figure 5 shows a schematic of the model.

Values of 1.0, 2.25, and 4.0 were arbitrarily selected for A_T/A_p. It was now necessary to obtain corresponding values of A_B/A_T which would provide the maximum lift. The

following method was used. The ratio of the thrust of a shrouded propeller to the thrust of an unshrouded propeller can be described as

$$\frac{T_{shrouded}}{T_{unshrouded}} = \left\{ \frac{2A_E}{A_p} \right\}^{1/3} = \left\{ 2 \left[\frac{A_T - A_B}{A_p} \right] \right\}^{1/3}$$

Using thin jet theory, the thrust in the vicinity of the ground can be expressed as follows:

$$\frac{T_{augmented}}{T_{basic}} = 1 + \frac{\text{Base radius}}{2 \times \text{Alt.}}$$

It can be seen by examining the two above equations that when the total base area (solid base plus annular exit) is fixed, increasing the solid base radius increases the augmentation, while decreasing the shrouded propeller thrust out of the vicinity of the ground. Therefore, there should exist a ratio of solid base radius to total base radius which gives a maximum augmented thrust.

The two above equations are now combined to give

$$\frac{T_{augmented}}{T_{unshrouded}} = \left[\frac{2\pi}{A_p} \right]^{1/3} \left[r_T^2 - r_B^2 \right]^{1/3} \left[1 + \frac{r_B}{2h} \right]$$

We differentiate this equation with respect to r_S, holding r_T constant, and set the derivative equal to zero to obtain the maximum thrust.

$$\frac{\partial \frac{T_{augmented}}{T_{unshrouded}}}{\partial r_B} = \left[\frac{2\pi}{A_p} \right]^{1/3} \left\{ \left[r_T^2 - r_B^2 \right]^{-2/3} \left[-\frac{2}{3} r_B \right] \left[1 + \frac{r_B}{2h} \right] + \left[r_T^2 - r_B^2 \right]^{1/3} \left[\frac{1}{2h} \right] \right\}$$

Solving we find

$$\frac{r_B}{r_T} = \frac{\left[16 \left(h/r_T \right)^2 + 60 \right]^{1/2} - 4 h/r_T}{10}$$

where the geometry which gives the maximum thrust is a function of the altitude.

For the purposes of our test a value was picked for h/r_B to size r_B/r_T, in order to design all the basic configurations for the same physical height above the ground.

It was realized that the configuration resulting from the above analysis would have thick jets, whereas the analysis was for thin jets. Since this fact may invalidate the above theoretical results, additional configurations were tested with other area ratios. The eight configurations tested aresummarized below:

Configuration number	A_T/A_p	A_B/A_T
1	1.0	.487
2	2.25	.521
3	4.0	.544
4	2.25	.968
5	4.0	.122
6	4.0	.763
7	4.0	.294
8	4.0	-0-

DISCUSSION OF RESULTS

One of the primary differences between the present test and those reported elsewhere to date is the fact that the air source for this test was a shrouded propeller rather than a compressed air supply, whose pressure and mass flow are constantly under control. The precise operating characteristics of this particular propeller under the effect of high back pressure are not known. However, it is felt that this type of experimental setup more realistically simulates the conditions likely to be encountered in an actual vehicle.

If we first consider the five configurations for which the outer casing diameter was maintained constant, while the inner base diameter was varied, and compare the test results in the manner suggested by the thin jet theory, i.e., lift/thrust = $1 + 1/4\ (h/D_B)$, we obtain Figure 6. Note that the absolute values thus obtained are not in themselves directly comparable with the exact theoretical values, since the experimental thrust values are those measured at a height of 26 inches. Nevertheless we can see that the general trend of the data for the configurations with the thinnest jets is to follow the theoretical line until the capability of the propeller to maintain the requisite increasing pressure is exceeded. We also note that the smaller the inner base (i.e., the thicker the jet) the steeper is the slope of the experimental curve and this we attribute to the configuration performing as a plenum chamber rather than an annular jet vehicle. This is evident in Figure 7 where the configuration with no inner base at all can also be included. The results for it and the two configurations with the smallest inner bases follow the same trend as the curve:

$$\frac{L}{T} = \frac{1}{4\left(\frac{h}{D_T}\right)}$$

which typifies the plenum chamber arrangement. We also note that the configuration with the thinnest jet ($A_B/A_E = 3.22$) Provides the greatest augmentation within the height range of interest. This is in accordance with the indications of the thick jet theory of Pinnes (see NAVAER Research Development Report DR-1958). For all of the configurations a limiting augmentation of the order of four was reached, presumably because of the propeller characteristics.

As a further comparison of interest we can consider those configurations for which both the overall base diameter and the inner base diameter were different, but where the ratio of base area to jet area was maintained essentially constant. This is shown in Figure 8. Again we can note the trend to follow the thin jet theoretical line as far as the propeller will permit. The smaller configurations, of course, cannot achieve the augmentation of the largest one since the maximum output pressure acts only over their smaller bases. The results obtained with the smallest configuration are of questionable value because of the constriction of the annular exit area to about one-half of the propeller disk area.

As a further check on the basic thrust levels, it was found for several of the configurations that the life measured at a height of 26 inches was approximately 15 per cent greater than that at 41 inches. This emphasizes the fact that our absolute values of augmentation are not to be taken at face value but only considered as indications of trends.

As a matter if interest and analytical value, the annular exit of one of the configurations was instrumented with a small rake of total and static pressure tubes in the plane of the base at one point on its circumference. The measurements obtained through the height range at one propeller speed are shown in Figure 9. A considerable variation of total pressure is seen to exist across the annulus, and this is relatively unchanged by proximity to the ground until a height that is less than the jet thickness is reached. The static pressure across the annulus increases considerably with decreasing height and the entire pressure picture points up the existence of a strong force tending to direct the exiting flow outward as the ground is approached.

Although computations concerned with determination of the net power supplied to the propeller have as yet not been completed, we can still examine in an indirect way some of the power effects. Figure 10 shows that the higher the rpm or power level, the lower the augmentation. Although this plot was for a particular configuration, the same trend holds for all the configurations tested. The pressure measurements were an aid in explaining this phenomenen. It was found that the higher the rpm, the greater the positive pressure change as the vehicle is moved toward the ground. Thus for high rpm, as the ground is approached, the stall limit of the propeller would be approached more rapidly than for low rpm. This then would give a lower augmentation.

It was found that installing the skirt on the model, which has the effect of raising the base while keeping the vehicle at constant altitude, increased the thrust at all ground levels. This can be seen in Figure 11.

Since some of the small ground effect vehicles may be using only one propeller, a torque problem could easily exist. It was decided to test exit guide vanes as anti-torque devices. These vanes were 12 per cent thick symmetrical airfoils whose angle relative to the propeller axis could be varied. It was found that with the vanes set at 15° to 20° from the vertical that minimum torque resulted. The vanes canceled about 80 per cent of the initial torque. In this test four vanes were used. It is felt that either additional vanes or a modification of the existing vanes with either leading edge camber or a trailing edge flap, in order to increase the lift on the vanes, would essentially cancel all the torque.

The effect of torque cancellation on the resulting lift was also determined. It was found that canceling 80 per cent of the torque resulted in about a 5 per cent loss in lift. These results are applicable either in or out of ground effect. Results of torque testing are found in Figures 12 and 13.

Although the inherent instability of GEV was recognized prior to testing, it was decided to measure pitching moments to test the effect of any of the wide variation of area ratios on stability. Pitching moment data were obtained with the vehicle at several altitudes, with the ground plans at various angles. In general, the resulting pitching moment was zero, except for random cases where a small destabilizing moment was found. These results apply for all the configurations tested.

CONCLUSIONS

Based on the results of the investigation to date, it has been found that

1. For a ground effect vehicle with a shrouded propeller and a relatively thin annular jet. the augmentation due to ground proximity tends to follow the thin jet theory up

to some point where back pressure affects the fan performance. This point to a large extent will be dependent upon propeller characteristics and the ratio of exit area to propeller area.

2. For the same vehicle with a thick annular jet, the augmentation is similar to that expected for a plenum chamber configuration with the same back pressure limitation on the fan.

3. The maximum attainable augmentation for a given overall vehicle diameter is determined by the fan capabilities and is independent of the inner base size.

4. Anti-torque vanes provide a relatively simple means of controlling the torque without excessive losses in lift.

5. Installation of a skirt on the model, which increased the height of the base above the ground while maintaining the vehicle at the same altitude, increased the lift.

6. Variation of the ratio of total base area to propeller area and of the ratio of solid base area to total base area did not affect the neutral stability characteristic of the vehicle.

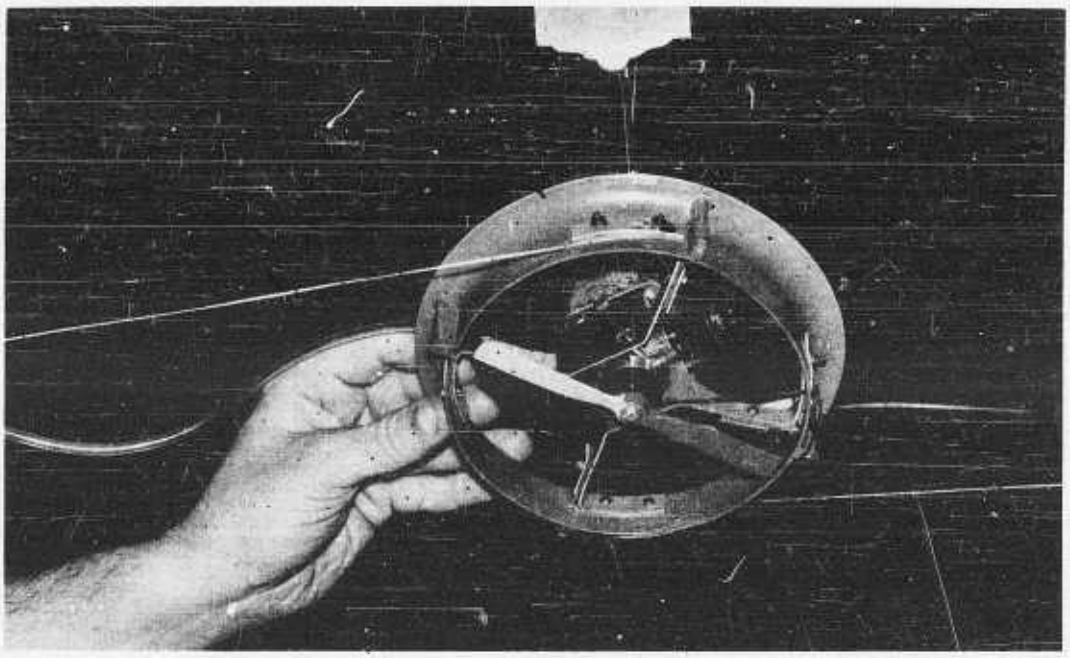

Figure 1.

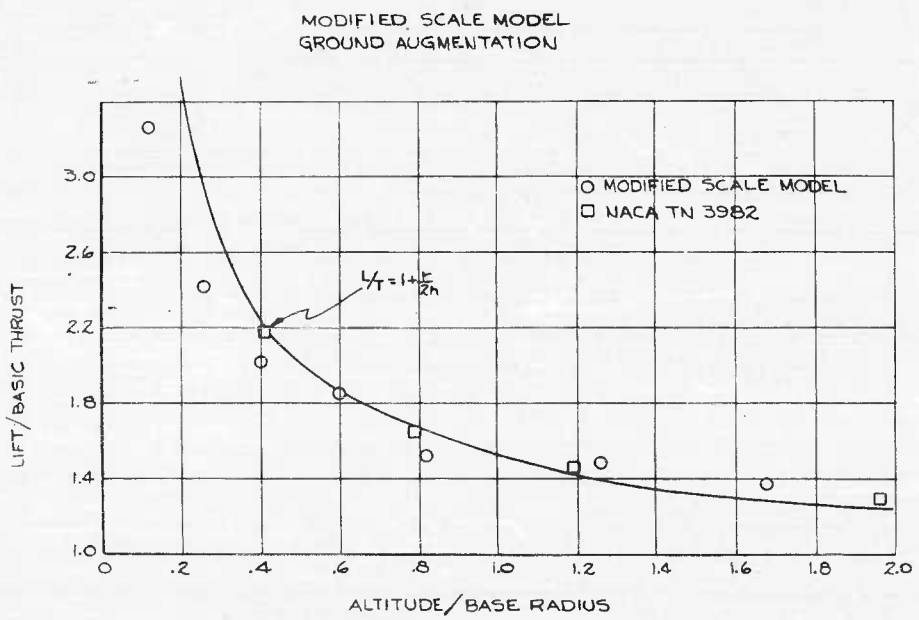

Figure 2.

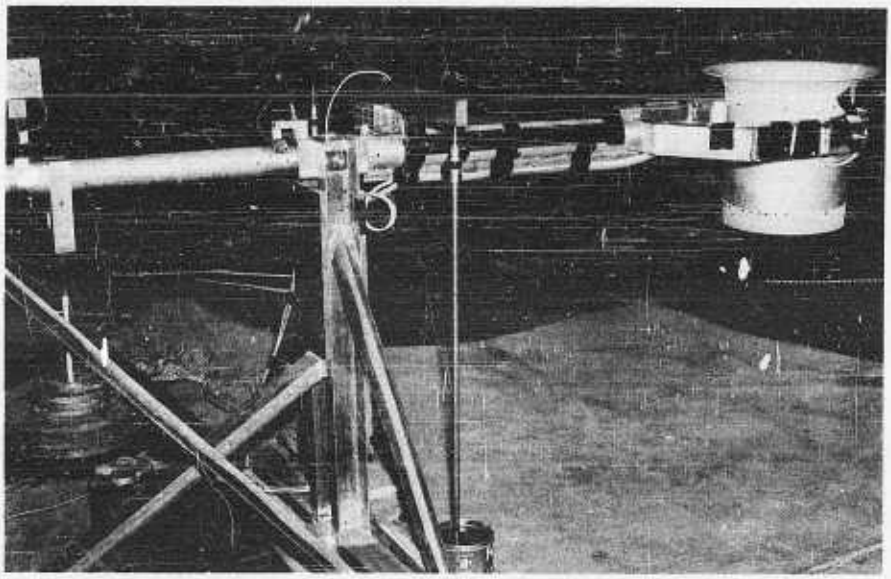

Figure 3.

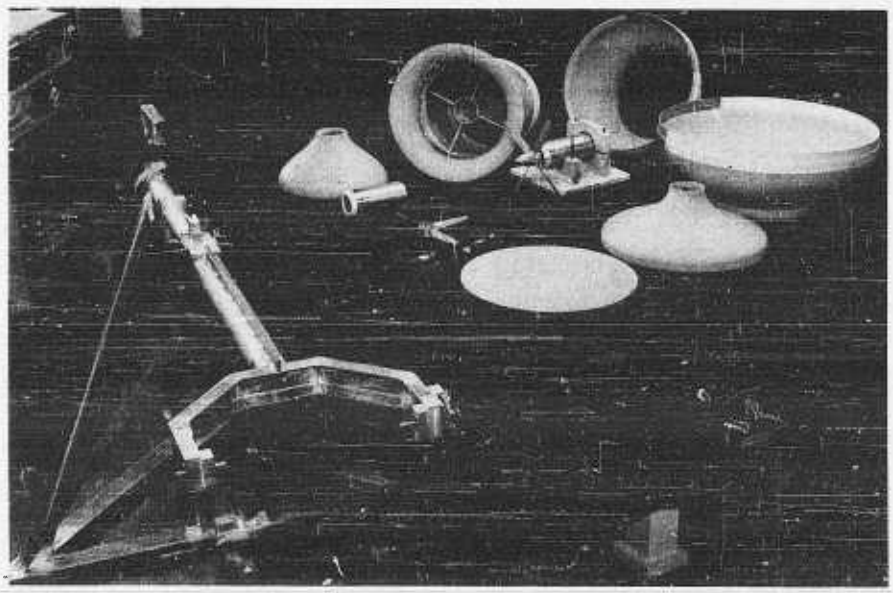

Figure 4.

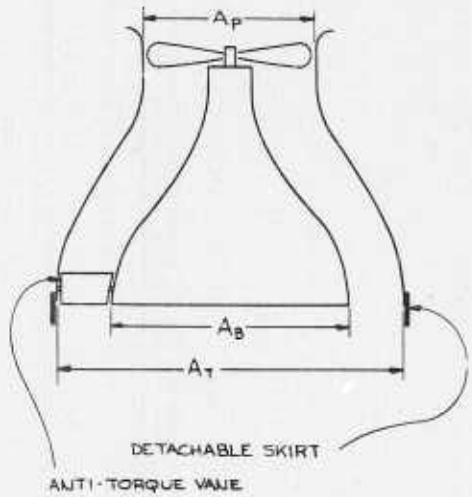

Figure 5.

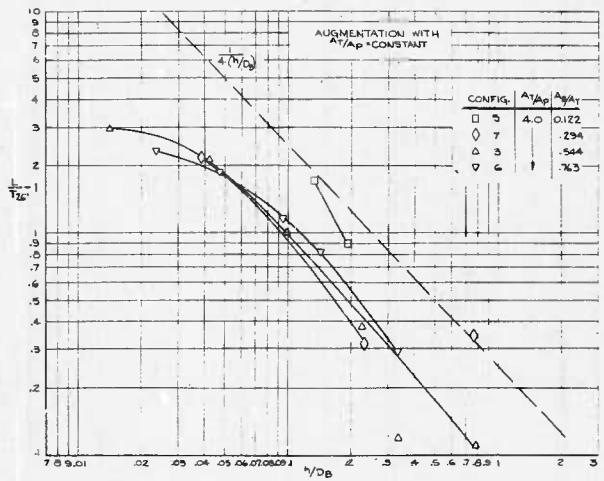

Figure 6.

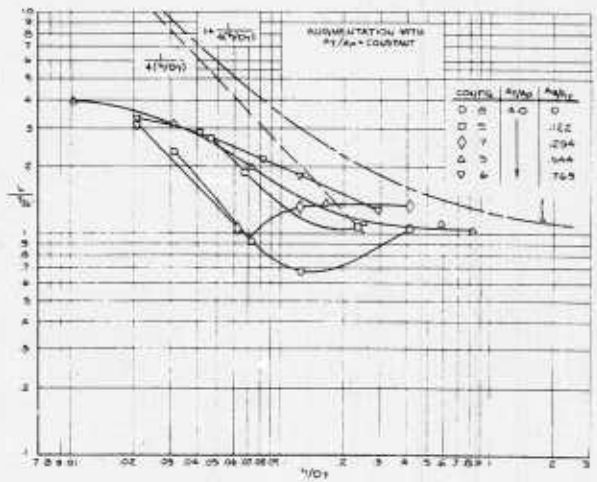

Figure 7.

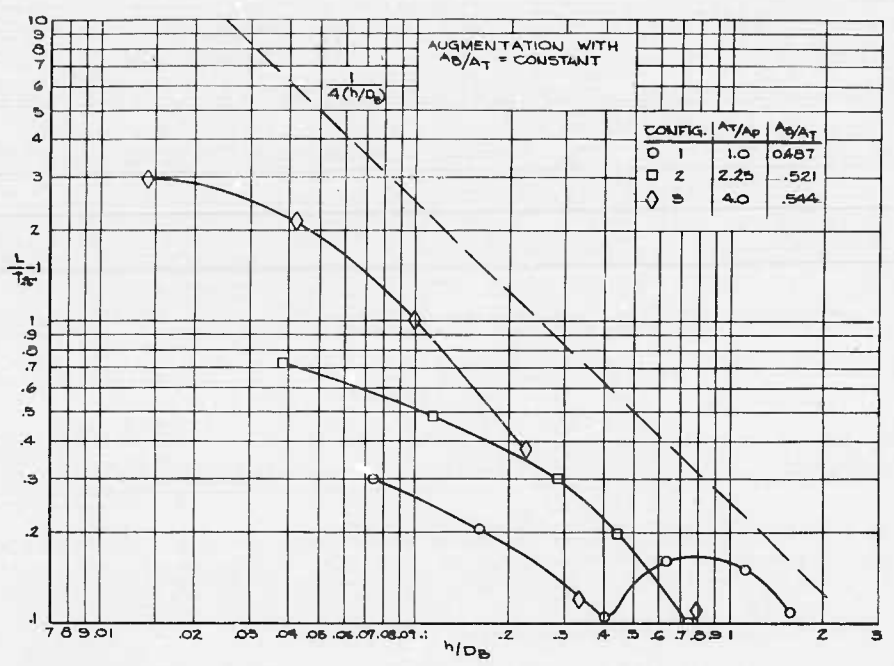

Figure 8.

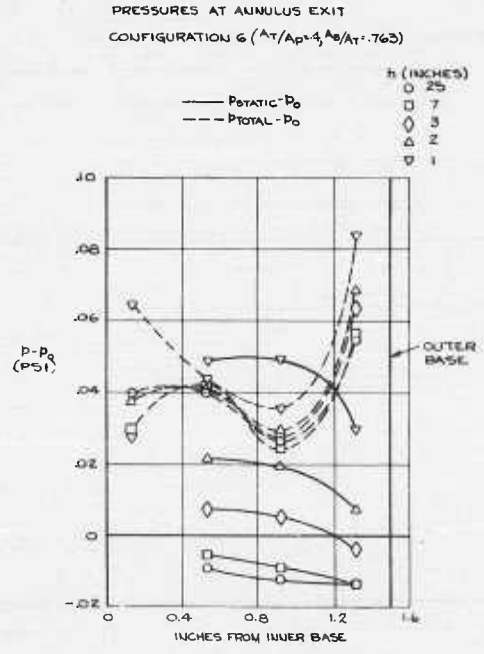

Figure 9.

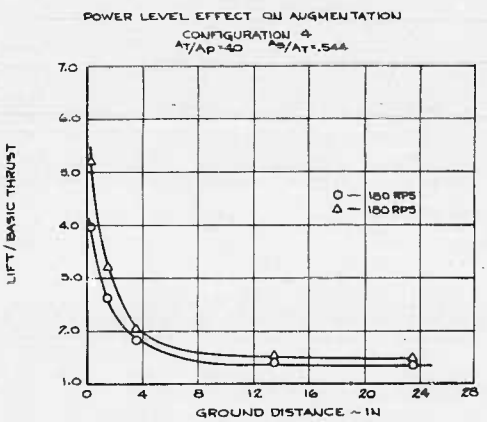

Figure 10.

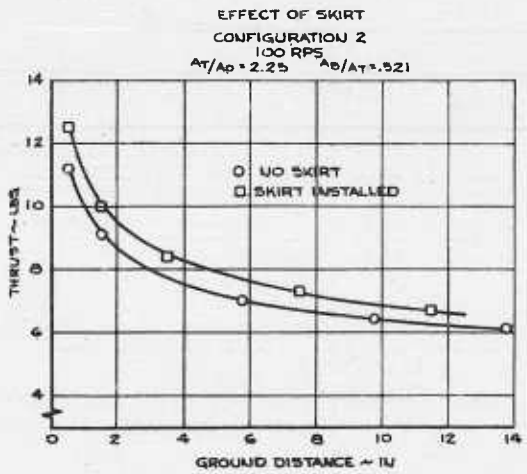

Figure 11.

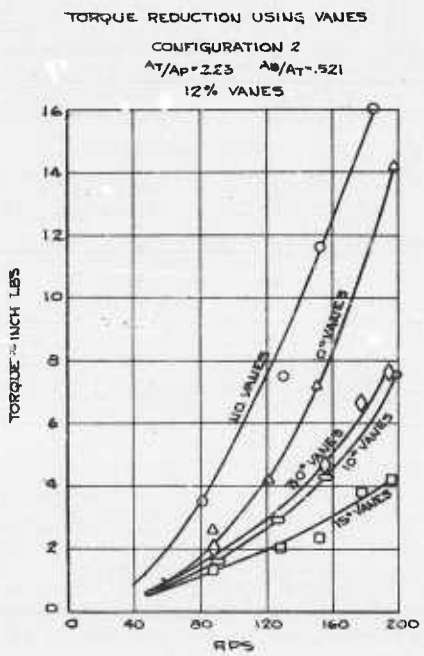

Figure 12.

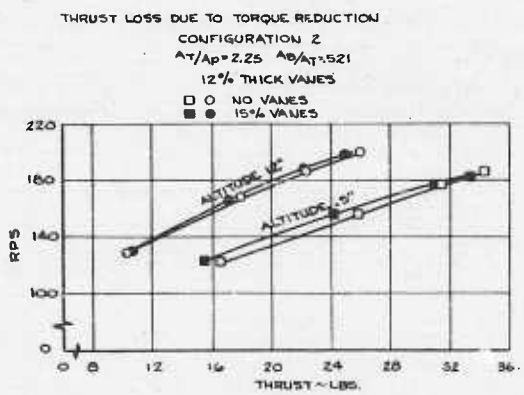

Figure 13.

FORWARD FLIGHT CHARACTERISTICS OF ANNULAR JETS

By Gabriel D. Boehler, Aerophysics Company,
Washington, D. C.

INTRODUCTION

One can distinguish two phases in the early development of ground effect machines. The nature of these two phases can be understood by relating it to attempts to find answers to the following two questions:

1. Will GEM's work?
2. Will GEM's work well, i.e., will they be capable of performing useful missions?

The first phase can be considered to have officially ended on July 15, 1959, following the successful crossing of the English Channel by the Saunders-Roe Hovercraft SR-N1 machine. As a result thereof, it is safe to state that the first question has been answered in the affirmative and that the full-scale aerodynamic, structural, and evironmental feasibility of GEM's in and near hovering has been conclusively demonstrated.

In October 1959, we are only at the beginning of the second phase and it is too early to tell if it will have the same successful ending as the first one. Missions are presently being proposed for GEM's and machines designed to fulfil them. A fairly constant requirement of these missions, which was completely absent in the earlier period, is that of a fairly high minimum forward speed: 50 to 60 knots is an immediate objective for large nautical machines, 100 to 150 knots is a desirable one in the foreseeable future. The attention is therefore being displaced away from the hovering problems, which are pretty well under control anyway, to the forward flight problems, about which very little is known, but an understanding of which will be decisive in answering the second question.

The purpose of this paper is to offer a contribution to the second phase of the GEM work in the form of some comments concerning the forward flight aerodynamic characteristics of annular jets in close proximity to the ground, based on theoretical considerations as well as on the limited experimental results available to date. It is also to propose an explanation for the features displayed by these experimental results. These comments are a small part of an analysis performed by the Aerophysics Company for the Office of Naval Research under Contracts Nonr-2398(00) and Nonr-2747(00).

SYMBOLS

C_L	lift coefficient, $L/q\,S$
ΔC_L	increment in C_L due to C_μ, $C_{L_{(C_\mu)}} - C_{L_{(C_\mu=0)}}$
C_μ	jet momentum coefficient, $m_j\ V_j/q\,S$
A	augmentation factor in hovering, $T/(m_j\ V_{ji})$
A*	augmentation factor at a velocity V, $\Delta C_L/C_u$
A R	Aspect ratio, c/t

c	average circumferential length of annulus
d	base diameter, measured to outer edge of outermost jet
h	altitude (measured to wing lower surface)
m_j	mass rate of flow in annular jet, measured
p	pressure
p_o	static pressure
p_{t_j}	total pressure at nozzle exit
$\triangle p$	pressure difference across jet
q	free stream dynamic pressure, $\frac{1}{2} \rho V^2$
r	base radius, d/2
R	local radius of curvature of curved jet
S	wing surface area
t	jet thickness
T	total thrust
T_j	jet momentum, $m_j V_j$
V	forward velocity, parallel to the ground
V_j	jet velocity at the nozzle
V_{j_i}	jet velocity (calculated assuming isentropic expansion from p_{t_j} to p_o)
ρ	free stream density

PRELIMINARY CONSIDERATIONS

The first question that one may ask is how quickly the air cushion under the base of a GEM is "blown away" if the machine is moved in a direction parallel to the ground. A very simple qualitative answer can be found by comparing the value of the pressure within the cushion to that of the dynamic pressure corresponding to the forward speed V of the machine (see reference 1). Consider point A on Figure 1 which is, for reasons of symmetry, the stagnation point of the "leading edge" of the machine. The pressure on the left of A is the dynamic pressure $q = \frac{1}{2} \rho V^2$; the pressure to the right of A is the cushion pressure:

$$\triangle p = \frac{\rho V_j^2 t}{h}$$

given by the momentum theory.

As long as Δp is larger than q, the base of the machine will behave essentially like an obstacle and the free stream V will spill around it. It is therefore logical to suspect that the "strength" of the cushion will depend upon the ratio $\Delta p/q$:

$$\frac{\Delta p}{q} = \frac{2t}{h}\left(\frac{V_j}{V}\right)^2$$

The ability of the cushion to be maintained in forward flight can be expressed using the ratio A*/A, where A* is the augmentation factor for the machine at a forward velocity V and A is the augmentation factor for V =) (augmentation factors are defined in the list of symbols).

From the above, one can therefore expect A*/A to be proportional to t/h, the ratio of slot thickness to height above the ground and $(V_j/V)^2$, the square of the ratio of jet velocity to forward velocity. These results intuitively make sense, since low h and high V_j do mean a better conservation of the cushion. Naturally, this analysis is incomplete, since it only tries to represent things around point A and does not account for the effect on the cushion pressure Δp of the pressure distribution die to the free stream V around the periphery of the cylindrical surface formed by the annular jet. Therefore, the formula

$$\Delta p = \frac{\rho V_j^2 t}{h}$$

is not valid in forward flight.

EXPERIMENTAL RESULTS

Wind tunnel tests of annular jets at Catholic University, 1958-1959. Early in 1958, an experimental program was conducted at the Catholic University of America, in the Department of Aeronautical Engineering, to determine the effect of a speed parallel to the ground on the cushion under the base of an annular nozzle in close proximity to the ground (reference 2).

The purpose of this program was to extend to forward flight the results obtained by von Glahn in hovering (reference 3). It was decided to go ahead with it after a letter, dated November 22, 1957, was received by the Aerophysics Company from von Glahn stating that the Lewis Laboratory of the NACA did not intend to extend the tests of reference 3 to forward flight, and after efforts to interest the Langley Laboratory of the NACA in this problem had proved unsuccessful.

The objectives of the test program were very modest, due to budget limitations; they were limited to a study of the variation of the cushion pressures as a function of tunnel speeds. A general idea of the test set-up can be obtained from Figures 2 to 5. Air for the annular nozzle was provided by a 10 hp General Electric two-stage axial flow fan (Figure 2 The air was ducted from the fan to the nozzle as shown in Figure 3. The fan could provide jet speeds up to about 200 ft/sec. The annular nozzle was mounted vertically in the 6 X 6-foot subsonic wind tunnel, as shown in Figure 4. Tunnel speeds were approximately 50 and 60 ft/sec. The nozzle resembled very closely the one used by von Glahn in reference 3; it is shown schematically in Figure 5. The pressure distribution over the base of the model was measured with twenty-five pressure taps, and the base thrust was obtained by integration of the pressures. The stand shown in Figure 4 was used to support the nozzle. The ground plate could be raised or lowered by raising or lowering the legs of the small table; it also could be tilted.

The ratio of cushion total lift at a forward speed V to the cushion total lift in hovering was plotted against h/d for given forward speeds V, or against V for various h/d. It was found that, for small values of V, the cushion pressure remained nearly constant, decreasing gradually.

In the spring of 1959, the Aerophysics Company made a design study covering a small GEM (reference 4). During the course of this study, it was found that no reliable force data were available for annular jets in forward flight. It was then decided to rerun the 1958 set-up more carefully and systematically than the first time. Results of the second series of tests are reported in reference 5. It was found that the results of reference 5 checked exactly with those of reference 2. Additional runs were made, in particular at lower h/d than previously.

Results were now plotted in terms of the augmentation ratio A*/A. An attempt was made to plot all the data on a universal curve in the form of a variation of A*/A as a function of $(V/V_j)^n (h/t)^{n'}$, where n and n' are constants to be determined. This attempt was successful, using n = 2, n' = 0.5. The universal augmentation curve is shown in Figure 6.

This indicates, therefore, in agreement with the elementary considerations discussed above, that the augmentation ratio is a function of the square of the ratio of forward velocity to jet velocity. As to the functional relationship between A*/A and $(h/t)^{1/2}$, it should be accepted with caution, since t was kept constant during all tests, and V, V_j, and h were not varied within a wide enough range of values to insure that one would really have here a universal law.

The results of Figure 6 can be useful to give a "ball park" figure of the loss in cushion pressure in forward flight. However, they must be used with caution since:

1. They were obtained at low jet velocities, for a low aspect nozzle.

2. The wind tunnel model, a cylinder extending vertically to infinity, was far from representing a practical GEM configuration. This means a different induced pressure field around the annular jet, and no possibility of a generation of an aerodynamic circulation lift which would compensate the loss in cushion lift at high forward speeds.

In fact, though the Catholic University results were first used in the design study of reference 4, they were later discarded and replaced by the Ames results discussed in a subsequent section.

Two-dimensional ONERA work, 1959. This work is reported and discussed elsewhere in these Proceedings (reference 6) and only a passing reference should be made to it here. Suffice to say that both the ONERA flow visualization in a water tunnel and wind tunnel tests of a two-dimensional platform in close proximity to the ground represent vital contributions to an understanding of the flow mechanics of annular nozzles in forward flight. It may be of interest to note that the ONERA wind tunnel tests were started at the suggestion of the Aerophysics Company, because ONERA had unique two-dimensional test facilities not readily available in the U. S. This work was followed closely, while in progress, by the Aerophysics Company as the result of a working agreement with ONERA concerning the exchange of unclassified information in the field of ground effect phenomena.

As shown clearly in Figures 17 to 20 of reference 6, a two-dimensional platform can behave in two different ways, depending upon whether its forward velocity is small or large. If it is small, the ground cushion is hardly affected at first, if the machine is very close to the ground, and the empirical rules established by the Catholic University

tests, i.e., that the lift ΔC_L is proportional to C_μ (C_μ being proportional to $1/V^2$, this means: inversely proportional to V^2) and inversely proportional to h, do hold. This corresponds to the operation as a ground effect machine; the free stream and the forward jet cannot flow under the machine and the cushion can still be regarded as a fence.

On the other hand, if the forward velocity is large enough, the fence develops a leakage; the free stream and the forward jet can flow between the platform and the ground and the cushion is blown away. However, a strong aerodynamic circulation does establish, with the effect that the total lift on the platform for a given momentum flux of the annular slot becomes larger than in hovering. This corresponds to the operation of the platform as a jet flap wing. The lift ΔC_L is then proportional to $\sqrt{C_\mu}$, rather than to C_μ.

The transition between GEM operation and jet flap operation can be spotted by a break in the curves of variation of ΔC_L against C_μ, or of $\Delta C_L/C_\mu$ against C_μ, or of $\Delta C_L/C_\mu$ against $1/C_\mu$ (Figure 20 of reference 6).

The following limitations of the ONERA tests must be recognized:

1. The tests were made, for reasons of expediency in order to use available air supplies, with high velocity, low mass flow, thin air jets. Therefore, the viscous effects (resulting in large flow entrainment) are very pronounced. Results of the tests would be dangerous to extrapolate for low velocity, larger mass flow jets.

2. The two- and three-dimensional behavior of annular platforms close to the ground are not exactly the same. In the three-dimensional case, the free stream can "spill" on the side as well as on the top; two-dimensional free streams can only spill on the top. The spillage on the side of the three-dimensional platform results in a suction which can weaken the cushion; this suction cannot exist in two dimensions.

   The great advantage of two-dimensional testing over three-dimensional testing is that the flow is much simpler and can therefore be more easily understood and more easily compared to theory.

Three-dimensional Ames data, 1958. Preliminary data were obtained in 1958 in the Ames 7 X 10-foot wind-tunnel on a circular wing combined with an annular nozzle (reference 7). These data are presently unpublished, but have been referenced before (reference 8 of reference 8).

The model tested at Ames is shown in Figure 7.

The data were plotted by the original investigators as shown in Figure 8, i.e., as a plot of $\Delta C_L/C_\mu$ against h/d for constant values of the momentum coefficient C_μ.

The choice of the parameter $\Delta C_L/C_\mu$ in ordinate is a logical one (also adopted by Poisson-Quinton in reference 6 and by previous jet flap investigators) since it reduces to the hovering augmentation factor when V = O. In the form of Figure 8, the results are hard to understand. Commenting ontthem, the authors of reference 8 state that "the extreme scatter...is indicative of the complexity of interactions between external and internal flows".

Using the two-dimensional results of reference 6 as a guide, one can plot, for various h/d, ΔC_L against C_μ (Figure 9), $\Delta C_L/C_\mu$ against C_μ (Figure 10) and $\Delta C_L/C_\mu$ against $1/C_\mu$ (Figure 11). In Figure 9, consider first the curve labeled "pure jet flap" which

corresponds to h/d = 2.65, in which case the circular wing is practically outside the influence of the ground. Therefore, this curve shows the lift increase against momentum coefficient for a modified jet flap configuration. In a true jet flap configuration, one would certainly not blow over the whole periphery in a direction normal to the plane of the wing.

The "pure jet flap" curve of Figure 9 is replotted in Figure 12 on logarithmic paper and its equation is found to be:

$$C_L = 0.82\ C_\mu^{2/3}$$

This compares with the conventional true jet flap effect (reference 9), which is well known to give:

$$C_L = K\ \sqrt{C_\mu}$$

where K can have values between 3 and 6 depending upon the configuration.

One can therefore, looking back at Figure 8, draw the important conclusion that, while in hovering the augmentation factor is independent of the momentum flux of the nular jet, in forward flight the augmentation factor depends strongly upon it, and this can be understood as a jet flap effect.

Note that the annular wing does behave like a rather ineffective jet flap, since the lift increase is only a fraction of what would be obtained with a conventional jet flap. Comparing now Figures 9, 10, and 11 with the corresponding plots for the two-dimensional tests of reference 6, one can recognize, but less clearly that in two-dimensions, the two regimes of operation of the platform: at low speeds (high C_μ), as a GEM; at high speed (low C_μ), as a jet flap.

In Figure 11, the abscissa $1/C_\mu$ is proportional to V^2 and, in particular, $1/C_\mu = 0$ corresponds to the hovering condition. It is interesting to note that, initially, when V increases, $\Delta C_L/C_\mu$ increases, i.e., the cushion is being strengthened rather than weakened. A possible explanation for this phenomenon will be presented later on.

Three-dimensional David Taylor Model Basin data, 1959. The David Taylor Model Basin tested in 1958 and 1959 a 6-inch-diameter annular jet model in a subsonic wind tunnel (reference 10). The main difference between this model and the Ames model, except for size, was that the DTMB model had a jet angle inclined 45 degrees from the vertical towards the base.

Using these data, $\Delta C_L/C_\mu$ can be plotted against $1/C_\mu$ as was done with the Ames data. Again, the two regimes, as a ground effect machine at low forward speeds and as a jet flap machine at high forward speeds (Figure 13) can be plotted. This plot was first made by Poisson-Quinton.

THEORETICAL APPROACH

The experimental results reported above have done a great deal to help clarify the mechanism of operation of annular jets in forward flight. The next job is to try to use them as a background for the formulation of analytical methods which will represent the performance of annular jets in forward flight. The initial goal is an inviscid theory based on momentum considerations which would extend the hovering theory by introducing the

velocity V in a simple form. The possibility of extending the momentum theory to forward flight is presently under investigation both at the David Taylor Model Basin (reference 11) and at the Aerophysics Company. The following discussion is only intended to indicate a possible method of approach to the problem.

Consider the two-dimensional platform shown in Figure 14 and divide arbitrarily the cushion space into two equal halves; assume that the left half is at a constant static pressure p_1, which is mostly influenced by the forward jet, and the right half is at a static pressure p_2, which is mostly determined by the behavior of the aft jet. Assume further that, though p_1 may be different from p_2, there is no flow from p_1 to p_2. In hovering, the theory postulates that $p_1 = p_2$, which has a constant value within the whole cavity; as a result the jet trajectories are circles, and the flow is symmetrical about the plane of symmetry of the platform.

If one adds a forward velocity V assumed not too large, the following happens: at the upstream end of the platform, forward of the jet sheet, a vortex is formed (see conclusive evidence on Figure 17c of reference 6) and the mass flow originating from the forward slot is turned around 270° and spilled over the top of the platform. As far as the free stream is concerned, it is deflected upwards since the region between platform and ground behaves like an obstacle. In very first approximation, the pressure on the left of the forward jet is not p_o, but $p_o + q$ (where $q = 1/2\rho V^2$). Hence, one can reason as follows: the total difference of pressure across the jet is a function of the momentum flux of the jet and of its curvature only. If in hovering

$$p_1 = p_o + \Delta p_1$$

then, in forward flight, since the outside pressure is assumed to be $p_o + q$,

$$p_1^* = p_o + q + \Delta p_1^*$$

Δp_1^* is larger than or equal to Δp_1 since the momentum flux is the same and the curvature, if anything, is increased. Let us assume $\Delta p_1^* = \Delta p_1$, which is then conservative.

Hence

$$p_1^* = p_o + q + \Delta p_1$$

$$= p_o + q + \frac{\rho V_j^2 t}{R}$$

At the downstream end, the flow of the aft jet is entrained by the free stream flow, the amount of entrainment depending upon the relative velocities V_j and V. This tends to weaken the jet and to reduce the pressure p_2 within the cavity. If the velocity V is low, one can assume that p_2 is the same as in hovering.

The total cushion lift under the conditions of Figure 14 is then:

$$T_b = \frac{(p_1 - p_o) + (p_2 - p_o)}{2} \ell = \frac{q\ell}{2} + \frac{\rho V_j^2 t}{R}$$

where ℓ is the chord of the platform

$$T = T_j + T_b$$

$$= 2 \rho V_j^2 t + \frac{q\ell}{2} + \frac{\rho V_j^2 t}{R} \ell$$

Hence

$$A^* = \frac{T}{T_j} = 1 + \frac{1}{2h/\ell} + \frac{q\ell}{4\rho V_j^2 t}$$

Finally,

$$A^* = 1 + \frac{1}{2h/\ell} + \frac{\ell}{8t} \left(\frac{V}{V_j} \right)^2$$

The augmentation factor is the same as in hovering, plus an additional term including the forward velocity V, which can increase the cushion pressure on the forward side of the machine by ram effect. Now, in practice, the forward cushion p_1 being reinforced, the aft cushion p_2 is weakened and anything can happen. When viscous effects are not pronounced, one would expect an increase of cushion lift at small V; when they are important, such as in the ONERA tests of reference 6, one would expect the cushion lift to be decreased. What is of interest here is that, at least in principle, the cushion lift can be increased by a forward motion.

In three dimensions, the situation is similar. Near the forward stagnation point, there is a tendency to increase the cushion pressure. On the sides, there may be outside the jet sheet a negative pressure field which will destroy the cushion more than the other effect builds it up. Here the situation depends mostly upon the planform of the machine. It also depends naturally upon the aspect ratio of the annulus and the height from the ground.

For a circular planform, the following approach can be used. Assume that the volume between the base of the machine and the ground behaves like a cylindrical obstacle. The free stream flow around this obstacle is a potential flow and the pressure p_i is given, in terms of an azimuth angle Θ as:

$$p_i = \frac{1}{2} \rho V^2 (1 - 4 \sin^2 \Theta)$$

$$= q (1 - 4 \sin^2 \Theta)$$

What is important is that p_i is independent of the radius of the cylinder. Therefore, the reasoning used in two dimensions can be repeated, except that the base of the machine must be divided in sectors with respective base pressures p_1, p_2, $p_3 \cdots$, p_k and that for each sector the equilibrium of the curved jet between the base pressures p_k and the

outside pressures $p_i + p_o$ must be expressed. Varying Θ between O and 2η and integrating the pressures, one can finally find an expression for the total cushion lift.

RECOMMENDATIONS FOR FUTURE TESTING

The task of understanding annular jets in forward flight will be made much easier if one is to be provided with the proper experimental data. Therefore, a brief discussion of what one would like to have is made here.

Assuming that the tests are to be made in a wind tunnel, it is not sufficient to measure total lift and total drag on a balance. One wishes to know separately:

(a) the cushion lift

(b) the jet reaction lift

(c) the circulation lift

Referring to Figure 15, the cushion lift can be found by measuring the pressure distribution under the base of the model; jet reaction lift can be calculated by measuring velocity and mass flow at the nozzle; circulation lift can be found by subtracting cushion and reaction lift from the total lift read on the balance (C_{L_o} of the airfoil can be measured separately and subtracted also). Hence the need for a rather extensively instrumented model.

In connection with an understanding of the lift picture, it is not enough to have the above information; it is necessary to find out, by using different models, the effect of planform on cushion lift (possible suction on the sides) and that of airfoil thickness on circulation lift. Obviously, the benefits of the jet flap operation, which will come in handy to alleviate the loss in cushion lift at high forward speeds, can only be derived if the inboard profile of the machine looks something like an airfoil, not a "box."

Concerning drag, one wishes to be able to know separately:

(a) the friction drag on the machine

(b) the friction drag on the ground due to the cushion

(c) the momentum drag

To get this drag breakdown, one disposes of only one drag equation. Therefore, one will have to find one more equation; for example, obtain drag by integration of pressure surveys in the wake of the machine. Or, as shown in Figure 15, one can test, for the same jet flow conditions, two model configurations; one (Figure 15 A) with an outside air supply, the other (Figure 15 B) with the air taken directly in the tunnel.

One may note finally that the Ames data (reference 7) indicate that a certain amount of momentum drag is recovered as a thrust; it is important to determine precisely in future tests how much this amount can be.

CONCLUSION

Rapid progress has been made in the past six months towards an understanding of the forward flight characteristics of annular jets in close proximity to the ground. Considerable experience has been gained in the analysis of hovering jets, and this leads to the optimistic prediction that in the not too distant future one will be able to predict analytically the behavior of GEMs in forward flight with good accuracy (this statement holds for

performance problems only; stability problems fall outside the scope of this paper). In the meantime, the designers must be warned not to design future machines on the basis of hovering criterions alone any more.

The annular jet situation is a rather unique one today in the lowspeed aerodynamic field, inasmuch as, contrary to most other cases, theoretical developments seem to be slightly ahead of experimental ones. This is a healthy situation, but it will only be a rewarding one if one is willing to let that theoretical knowledge be used in the planning of future experiments.

REFERENCES

1. Boehler, G. D., "Remarks on the Ground Effect Machine." Paper presented at the Fifth Annual Western Forum of the American Helicopter Society, Los Angeles, September 25-26, 1959.

2. Andyshak, R. J., and Ronn, B., "Experimental Study of Forward Velocity Effects on Thrust of Annular Nozzle in Close Proximity to the Ground." Thesis, Department of Aeronautical Engineering, the Catholic University of America, June 1958.

3. Von Glahn, U. H., "Exploratory Study of Ground Proximity Effects on Thrust of Annular and Circular Nozzles." NACA TN 3982, April 1957.

4. Whitehurst, J. W., "Design Study of a Small Rectangular Annular Jet Ground Effect Machine." Aerophysics Company Rept. AR-591, May 1959, revised October 1959.

5. Burns, R. S., and Tracy, R. J., "An Experimental Study of the Change in Thrust Augmentation of an Annular Jet with Varying Forward Velocity and Changing Ground Proximity." Thesis, Department of Aeronautical Engineering, the Catholic University of America, June 1959.

6. Poisson-Quinton, P., "Two-Dimensional Study of a Ground Effect Machine." Proceedings of the Symposium on Ground Effect Phenomena, Princeton University, October 21-23, 1959.

7. Unpublished Research. "Preliminary Data from 7 X 10-ft. Wind-Tunnel Tests of a Circular Wing with an Annular Nozzle Exhausting from the Lower Surface." NASA Ames Research Center, Moffett Field, California, April 1959.

8. Matthews, G. B., and Wosser, J. L., "Ground Proximity: A Critical Review." I. A. S. Paper 59-121. Presented at the I. A. S. National Summer Meeting, Los Angeles, California, June 16-19, 1959.

9. Malavard, L., Poisson-Quinton, P., and Jousserandot, P., "Theoretical and Experimental Investigations of Circulation Control." ONERA Note Technique 37, June 1956. Translated by Princeton University as Aeronautical Engineering Laboratory Rept. 358, July 1956.

10. Tinajero, A. A., "Comparison of Experimental and Theoretical Design Parameters of a 6-inch-diameter Annular Jet Model with a Jet Angle of -45° Hovering in Proximity to the Ground; and Experimental Results for Forward Flight at Zero Angle of Attack." DTMB Aero Rept. 954, May 1959.

11. Chaplin, H. R., "Ground Cushion Research at the David Taylor Model Basin - A Brief Summary of Progress To-date." Paper presented at the University of Toronto, Institute of Aerophysics Decennial Symposium, October 1959.

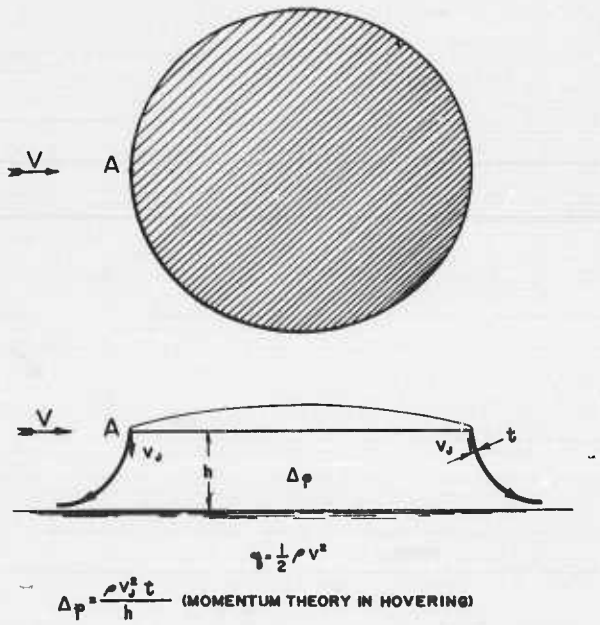

Figure 1. Schematic of annular jet in forward flight (elementary)

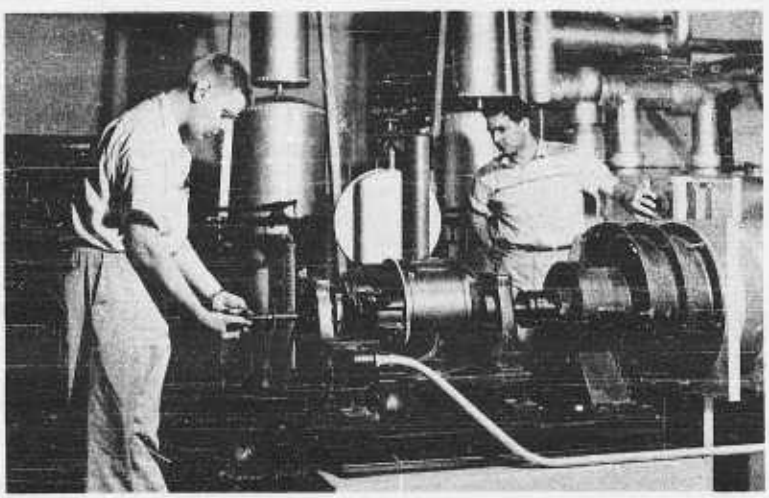

Figure 2. Axial flow fan Catholic Univ. tests 1958-1959

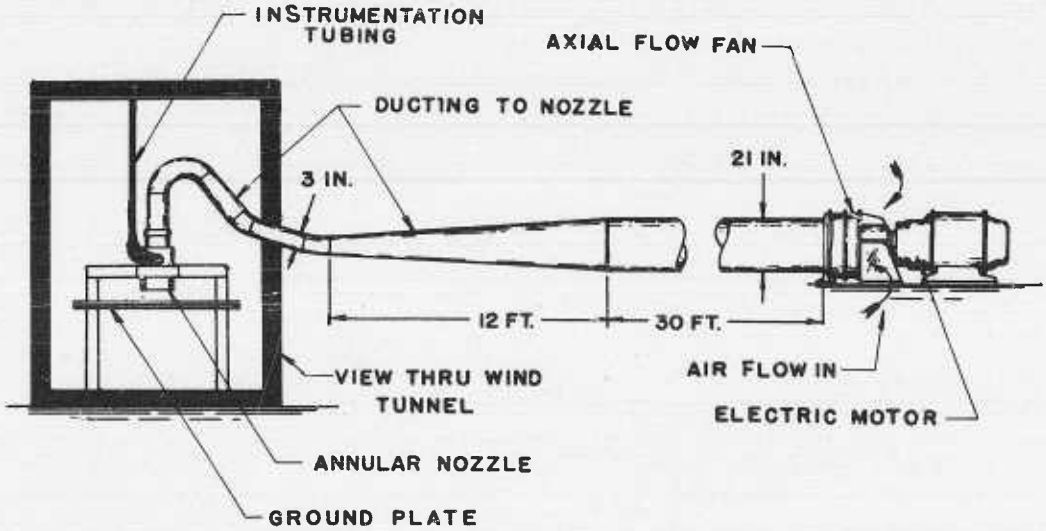

Figure 3. Layout of Catholic Univ. test set-up
1958-1959

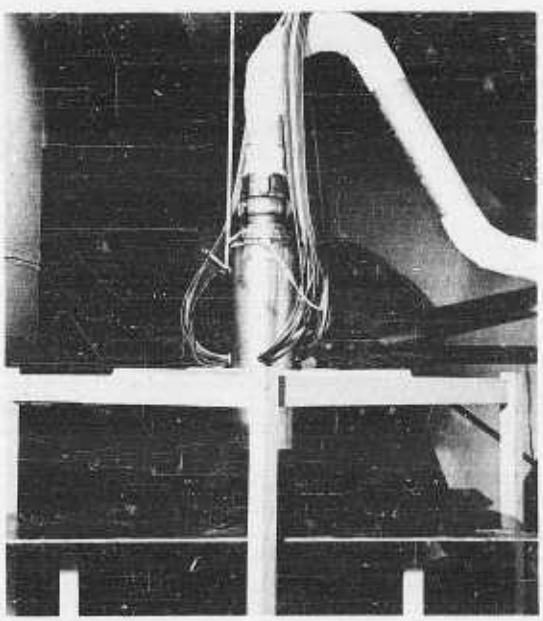

Figure 4. Annular nozzle Catholic Univ. tests
1958-1959

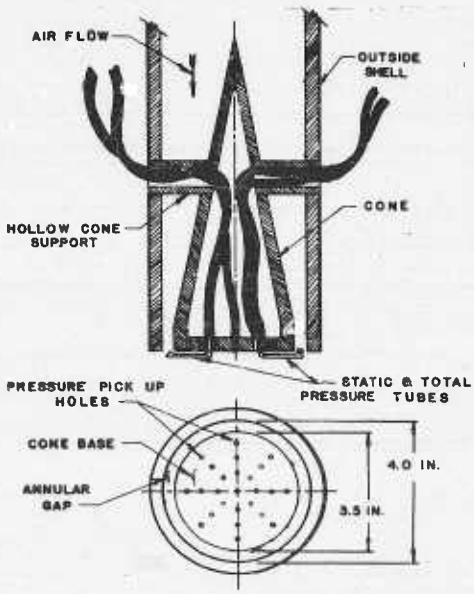

Figure 5. Annular nozzle Catholic Univ. tests
1958-1959

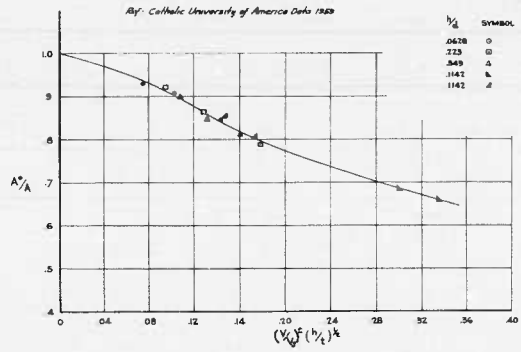

Figure 6.

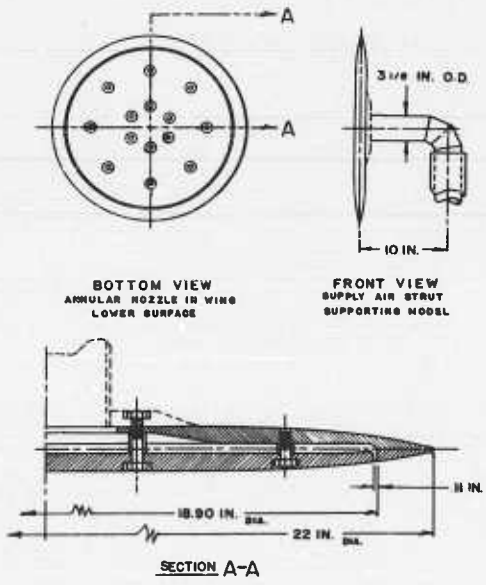

Figure 7. Annular nozzle NASA Ames tests 1958

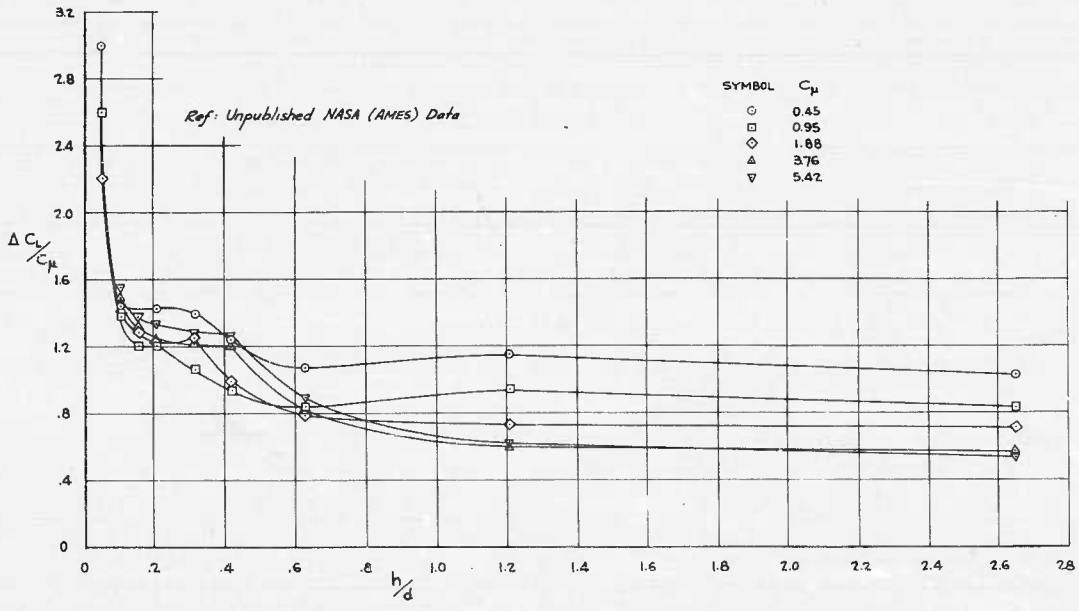

Figure 8.

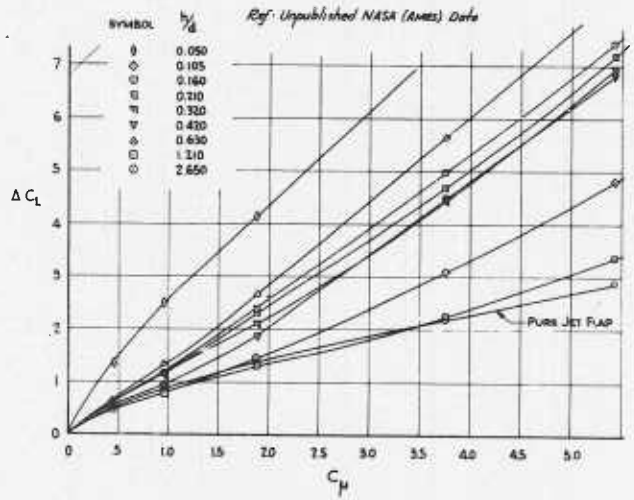

Figure 9.

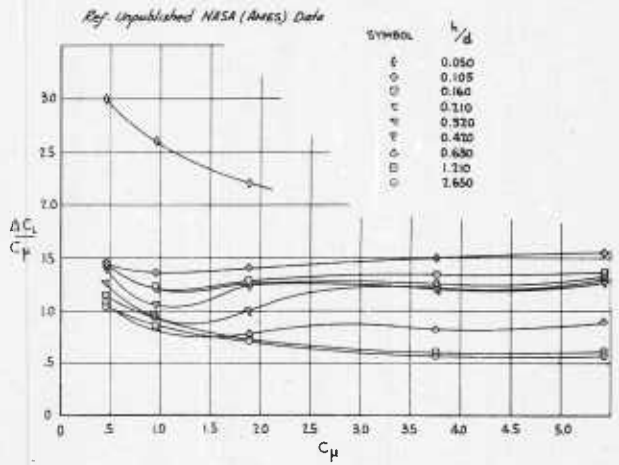

Figure 10.

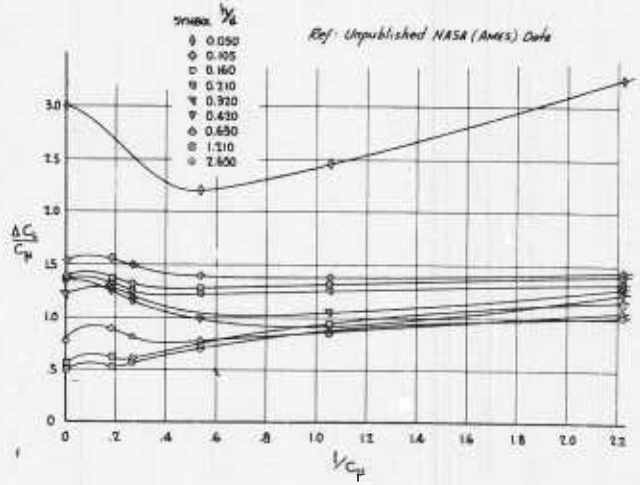

Figure 11.

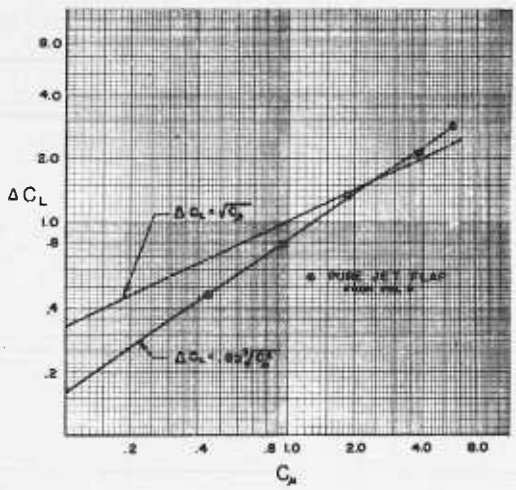

Figure 12.

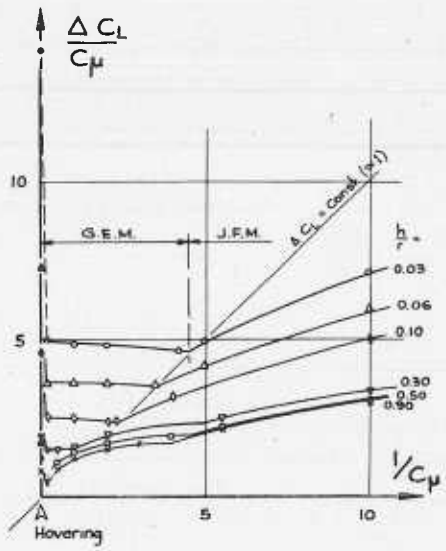

Figure 13.

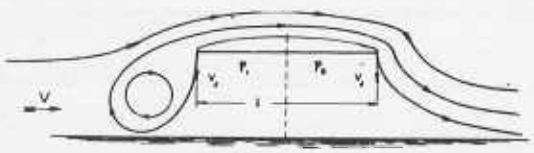

Figure 14. Schematic of annular jet in forward flight (more complex than Figure 1)

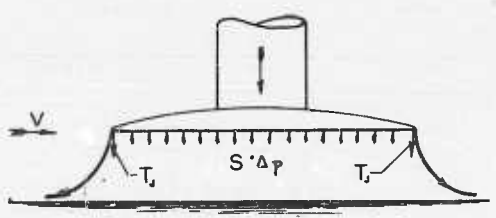

(A) NO MOMENTUM DRAG – OUTSIDE AIR SUPPLY

(B) MOMENTUM DRAG $\dot{m}_j V$

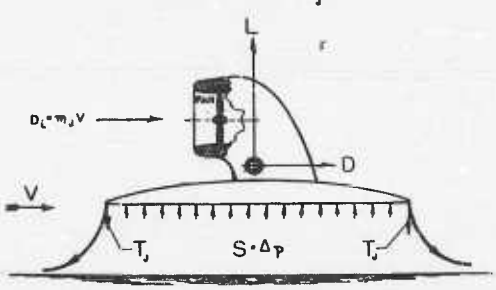

Figure 15. Wind-tunnel model of an annular jet

EXPERIENCE WITH SEVERAL MAN-CARRYING GROUND EFFECT MACHINES

By William R. Bertelsen, M. D., Bertelsen Manufacturing Company, Inc., Neponset, Illinois

Medicine is indeed a broad field: medical instruments include any device that aids in the care of the patient. This includes the ambulance, the evacuation helicopter, the physician's car, etc. The ground effect machine promises to provide a new and better means of transporting both patients and those giving them care. The author entered the ground effect field through the urgent need to improve transportation to and from rural patients. The status quo of all-weather transportation is still very poor in this age of space: there are many weeks each year when certain roads in the northern United States are impassable. There are usually several days when a given farm is isolated because of deep snow, and even the doctor's car may be helpless in the driveway at those times.

The helicopter or some other VTOL is the logical device for anyone who must "get through" despite weather conditions. However, in addition to its aerodynamic shortcomings, the helicopter is an economic failure. No doctor, veterinarian, or other individual can economically purchase, maintain, and operate a helicopter. Charges of $75 to $100 per hour for traveling to see patients is obviously out of the question.

As to the "other VTOL," there is none available.

FROM FAN UNIT TO MAN-CARRYING MACHINE

There was no concept of a ground effect machine available when my search for a good and economical air vehicle began. Initial effort was centered on the design of a stable, piston-powered, inexpensive VTOL. After considering the merits of the various choices of obtaining vertical thrust at zero speed which could be converted to efficient, fast, forward flight, the deflected slip stream system using Fowler flaps and a unique spanwise arc-shaped wing was developed (Figure 1). An advantage is seen in this craft as a VTOL: it has good efficiency in turning the slip stream, because of the circular wing fitting the circular slip stream and the inherent boundary layer acceleration of the Fowler flap design. Another advantage is its simple canard control system which is slip stream bathed under all conditions and is completely adequate to control the craft without tail rotors, fans, nozzles, etc. It is compact and has a small wetted surface with the Fowler flaps retracted for high speed forward flight. This machine is called the ARCOPTER because of its arc-shaped wing. It will be further developed as a VTOL with a very excellent ground effect.

Then began the investigation of specific ground effect machines. The ARCOPTER became a plenum-chamber-type ground effect machine in the glow plug configuration that was first tried. It became a crude peripheral jet machine with a stubby fuselage inserted within the rounding wing. A great deal more weight could be lifted near the ground than at altitude. It became obvious that, if no need existed for high flight, a very efficient realm of flight existed in the air-supported groung vehicle.

A series of models was then built to explore low-flight starting with a vacuum cleaner motor fan unit. The machine progressed through the 2 1/2 hp four-ft-square plenum chamber model, first with two blades, then with four (Figures 2 and 3) to the four-ft-square peripheral jet machine of first 2 1/2 hp and then 35 hp (Figure 4) to make it a

man-carrying machine (Figures 5 and 6). It became abundantly clear that the peripheral jet configuration offered a great deal more than the plenum chamber design.

ADVANTAGES OF THE PERIPHERAL JET OVER THE PLENUM CHAMBER

1. The jet gives higher altitude and greater weight lifting for given power, since it both builds and confines the pressure under the center body.
2. Controliability is inherent in the peripheral jet machine by varying the local thrust of the jet.
3. Propulsion is inherent in the peripheral jet machine without additional power source or propulsion equipment by tilting through the control of the local thrust of the jet.
4. Stability is greatest in the peripheral jet since all reaction thrust produced is at the perimeter at the widest possible base. There is considerable allowable center of gravity travel in the peripheral jet machine which can be trimmed by flap deflection. There is little or no allowable center of gravity travel in the single-plenum-chamber types of machine except as trimmed by ballast shift.
5. The peripheral jet machine can be designed lower in silhouette, lighter in weight, and more compact, since it needs only one fan, one engine, a ducting system, and flaps with remote control.

EXPERIMENTAL RESULTS

Exhaustive tests of this 35 hp four-ft-square machine were made to find the ideal configuration for the base and to attempt to produce lift, propulsion, and control from a single power source. This process involved many modifications of the base testing total jet area change, local jet area change, jet angle deflection changes both local and total, maximum altitude tests, etc. (See Figure 7.)

Some of the results of this experimentation were:

1. Large moments in pitch and roll are obtainable by deflection of the peripheral jet locally.
2. Powerful propulsive force can be obtained by pitch and roll motions in which the horizontal component of the main lift vector in tilt becomes large in proportion to the degree of tilt. The machine moves spiritedly in the direction of tilt.
3. Inward deflection of one flap locally decreases its thrust and produces the strongest tilting force.
4. Widening or flaring a jet locally has only limited ability to increase the thrust locally.
5. Little gain in altitude was experienced by directing all jets inward. Great deterioration in stability and a decrease in controllability using the flaps resulted since all flaps were already at negative angles.
6. A single flap outside the jet was as effective as a double row of flaps both inside and outside the jet.
7. No other use of the air from the fan will produce as powerful a propulsive force as tilting the machine. Direct thrust by bleeding air out through a nozzle was inferior in horizontal force production and caused the total altitude of the machine to drop.
8. Total jet width has little critical effect on the altitude performance, but stability of the machine decreases as the jet widens.

9. Altitude increase can only be accomplished by increasing the power and/or efficiency of the fan and the internal flow, or by lightening the vehicle. Changes in the base configuration have very little effect on altitude.

With the data accumulated in the tests of the 35 hp four-ft-square model, a second man-carrying machine was designed and built for the same power system (Figure 8). This one was 101 inches long and 71 inches wide, and had a fixed jet width of 2 inches with aluminum flaps around the external edge of the jet which were controllable by a central "stick." This machine performed exceedingly well in trim and control. Its propulsion, hill-climbing, and resistance to cross winds was poor becuase of its low power and altitude. This machine was then converted to 72 hp with an 8-blade maple wood fan. The performance was markedly improved. Later an 8-blade aluminum adjustable pitch fan was fitted (Figure 9).

DESIGN PLANS FOR THE FUTURE

The prospects for designing a really efficient vehicle using these principles are good. The shortcomings of the existing machine are clearly limited to its modest horsepower and internal efficiency. It will need more power to achieve greater altitude to allow clearance over rougher terrain, a greater degree of tilt for improved acceleration, braking, and hill-climbing. We know that if the machine can out-tilt a hill it will climb it. In the design stage now is a really good vehicle of 300 to 450 hp (Figure 10) with which I expect to go everywhere in Illinois, over land or water, under all weather conditions, any time of the year.

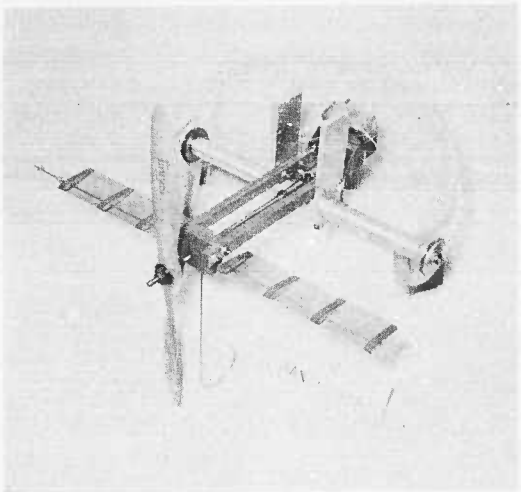

Figure 1.

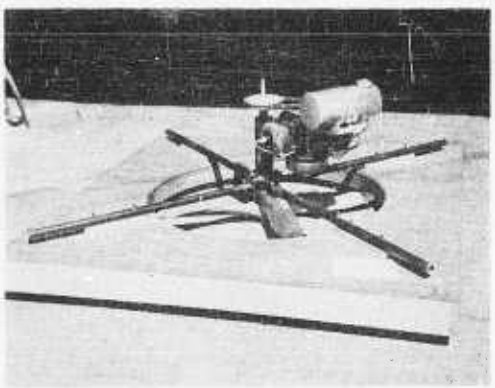

Figure 2.

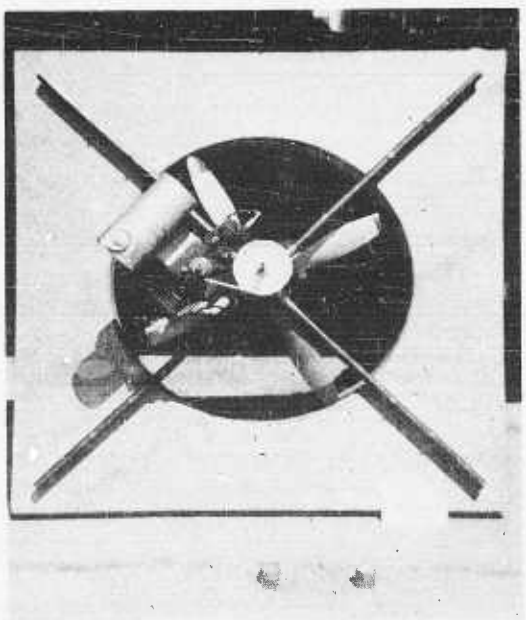

Figure 3.

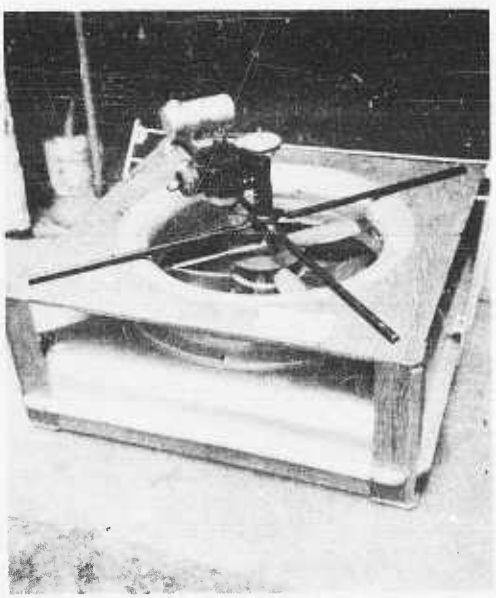

Figure 4.

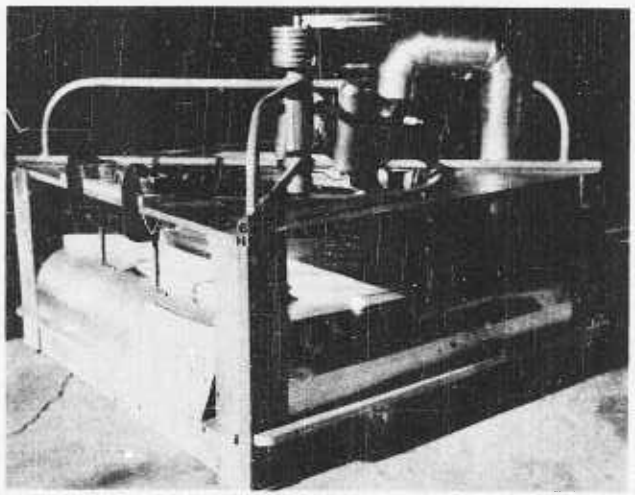

Figure 5.

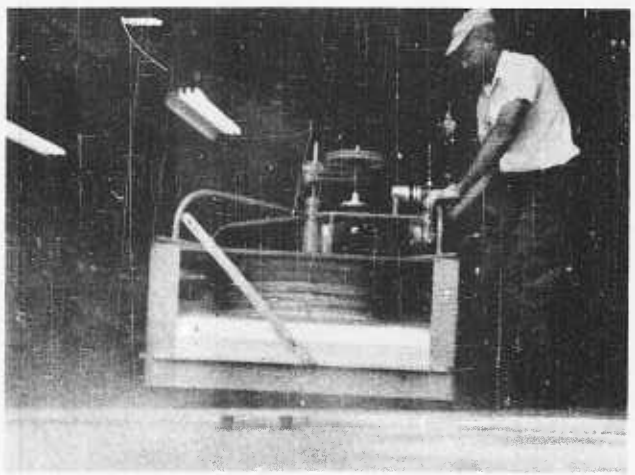

Figure 6.

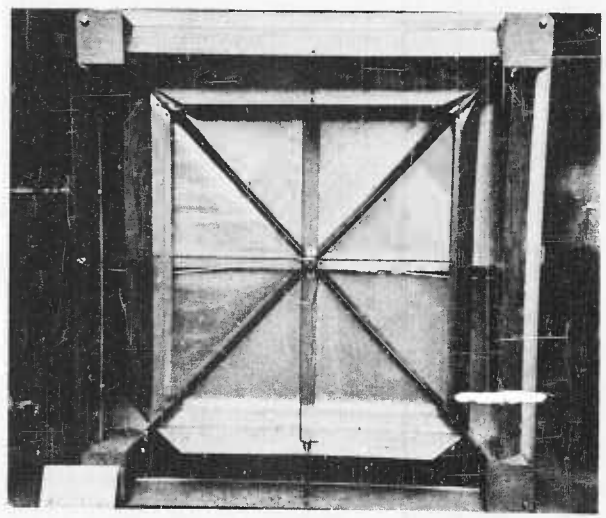

Figure 7.

Figure 8.

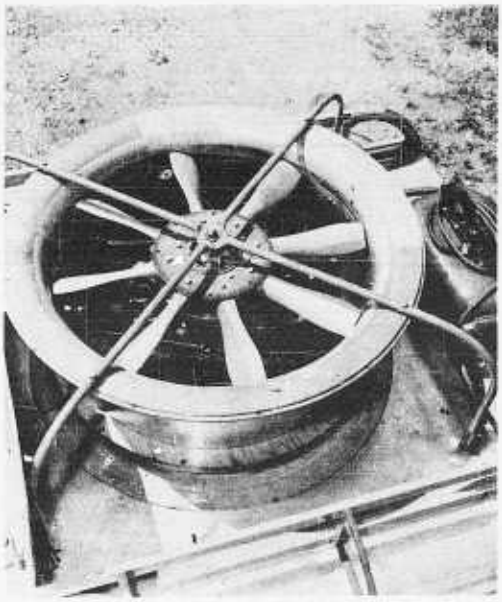

Figure 9.

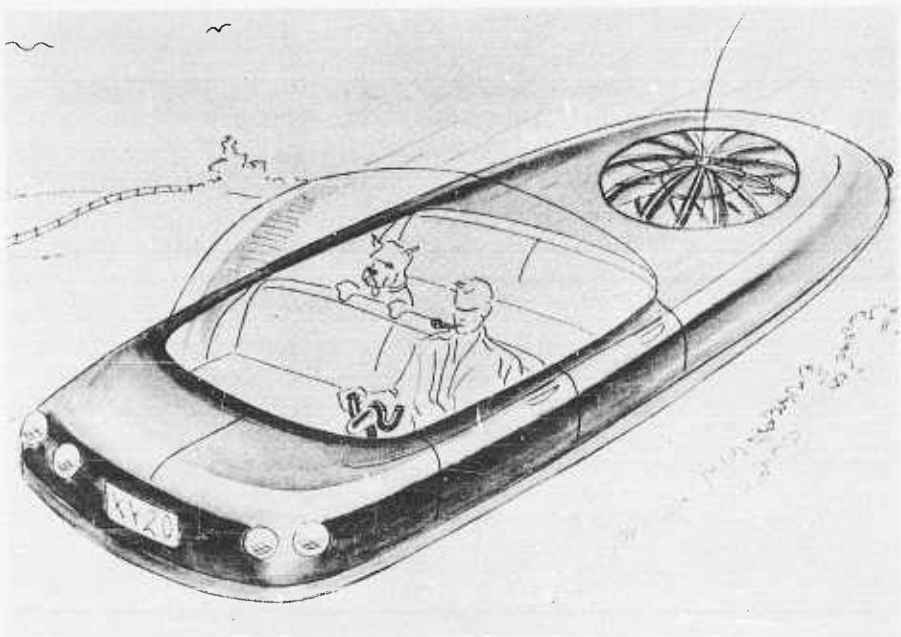

Figure 10.

THE DEVELOPMENT OF THE SAUNDERS-ROE HOVERCRAFT SR-N1

By R. Stanton Jones, Saunders-Roe Limited

DISCUSSION

The SR-N1 started life about the middle of 1958, but in those days it looked rather different from the machine which finally emerged.

It was in September of 1958 that Saunders-Roe put up its first firm proposal to the National Research Development Corporation for the design of a manned model. This machine, which is shown in Figure 1, had an area of about 245 ft^2 and weighed 4,000 lb. It was anticipated that it would have a hover height of between 1 and 2 ft and a still air speed of approximately 30 knots. The design was basically a plenum chamber arrangement with a 450 hp Alvis Leonides driving a horizontally mounted fan through a gearbox. The machine was elliptical in shape and had a single annular jet which was approximately three inches wide pointing inwards at an angle of 45° to the horizontal. The propulsion was obtained by bleeding off from the plenum chamber through two large ducts at the sides of the machine.

Detailed design work began in October 1958 when NRDC gave Saunders-Roe the contract to proceed with the manned model. However, it soon became clear that our first thoughts would need considerable modification. The plenum chamber, which contained a great deal of internal bracing, was clearly not going to be particularly efficient, and where the exit from the fan suddenly expanded into the plenum chamber, we could expect very severe losses. Consequently, we decided to design a more conventional ducting arrangement between the fan and the peripheral jet. A good deal of the early model test work was aimed at the design of this ducting. Furthermore, the elliptical planform shape required rather an unnecessary amount of tooling to form the nozzles, so the shape was changed to semi-circular ends with a short straight piece in the middle.

ABSTRACT

This paper describes the development of the Saunders-Roe hovercraft from its initial conception as a plenum chamber machine with a single peripheral jet to its final configuration as a twin peripheral jet system. In the course of the paper the reasons for the various design steps in terms of stability, performance, and stressing requirements are dealt with in a broad way. Complete aerodynamic design details are given together with the final actual trial information on the stability, performance, and general operational "now-how" that has been gained.

The gearbox proved expensive, so we chose a helicopter version of the Leonides engine and mounted it on its back, although this led to servicing problems, because the engine was now buried in the middle of the machine.

About a month after the start of the design, the SR-N1 looked like the diagram in Figure 2. Detailed drawings and the manufacture of some of the hardware were then begun in earnest.

At this stage of the development there was one very big unknown factor and one rather awkard design difficulty that stood in the way of further progress. The difficulty was how to provide a suitable propulsion system, and the unknown factor was whether a single jet system would be stable. The propulsion problem was eventually decided by financial

considerations. The best solution would have been to use a separate propulsion engine on the back of the craft with a reversible pitch propeller in order to obtain reverse thrust. However, the cost of this was prohibitive and so the propulsion system was obtained by bleeding off a portion of the air from the main intake.

The problem of stability was not quite so easily solved. A great deal of work was done on single-jet arrangements, measuring the pressure distribution both on the bottom of the model and on the ground beneath the model in an attempt to understand the mechanism of stability. Literally dozens of results, of the type shown in Figure 3, were obtained with various single jet arrangements. When these results were analyzed, some of the models showed a certain degree of stability, but others did not. However, in general, at a height approximately equal to twice the jet width, which, on these models, was equivalent to roughly 3 per cent of the diameter, the degree of stability was such that it would only allow the C. G. position to be about half-an-inch off center on the full scale craft. Furthermore, the stability only applied to small angles of pitch, and as the rim of the craft approached the ground it became violently unstable. The main reason for this instability was due to the inward pointing jets and it is possible, by shaping the undersurface of the craft and by arranging the jets so that they point nearly vertically, to obtain a stable single-jet craft up to heights of 5 to 6 per cent of the diameter. (See Figure 4.) Naturally this leads to a reduction in the cushion pressure and performance.

The results of our single-jet experiments led us to believe that the stability would be inadequate, so we decided to compartment the cushion. We did not particularly like the idea of using transverse jets along the centerlines of the machine and, in any case, the main structural platform or buoyancy tank was now practically built. Therefore we decided to extend the area of the craft and put an extra peripheral jet all the way around the outside.

A relatively simple theory for a twin-jet system shows that the stability will become small when the distance between the jets is equal to the hover height. Since we were hoping for a hover height of 1 1/2 feet, it was decided to make the distance between the jets about twice this value in order to ensure an adequate margin of stability. (See Figure 5.)

In order to check on the stability of double-jet systems we made a two-dimensional model which was one-third full scale and which was representative of a cross section through the SR-N1. This model was pivoted and placed above a water tank so that we could investigate its stability at various heights over both ground and water. The results are shown in Figure 6 where it will be seen that, although a fair degree of stability was obtained for small angles of pitch, the model again became unstable as its outer rim approached the ground or water. This particular model had a perspex side so that we were able to watch the behavior of the jets as the incidence was increased.

At first the outer jet behaves in a normal fashion, turning through nearly 180°. As it approaches closer and closer to the ground or water the cushion pressure between the two jets increases, causing a strong stable restoring moment. The inner jet splits into two portions and as the incidence increases the greater proportion of the jet goes inwards underneath the model. However, at a certain point the pressure between the jets becomes too great, the inner jet coandas on to the bottom surface of the model, and the outer jet also passes straight through underneath the model, causing a loss of lift and a strong destabilizing moment which tends to suck the edge of the model closer to the ground. The simple way of curing this is to add a wedge at the inside of the inner jet and to make this of such a depth so as to ensure that the wedge touches the ground or water surface before the outer jet touches. This ensures that the outer jet can never shoot underneath the model and make it unstable. The size of the wedge needed to do this job would have been six inches and it was quite impractical to fit this to the SR-N1. However, the same effect can be achieved by inclining the bottom surface between the two jets at a shallow angle of about

6°. This not only completely eliminates the instability but in fact makes the machine very much more stable at larger angles of pitch or roll.

By the time we had discovered the solution to this stability problem, the outer segments of the SR-N1 were actually being built and it was necessary to quickly modify them in order to provide the necessary angle of 6° between the inner and outer jets. SR-N1 then looked like the diagram shown in Figure 7 and it had changed considerably from its original conception. It was no longer a single-jet machine but was a twin-jet system with a total cushion area of 535 ft^2 and its estimated weight had increased from 4,000 lb to about 6,600 lb.

When the design was started, there was very little information upon which to base the design stressing conditions. However, since the machine was primarily intended for operation over water, we assumed that the engine failure case would provide a suitably severe design criterion. The assumptions made were that there would be a sudden engine failure when the machine was operating over waves of critical length and 2 ft high from trough to crest. This led to two main conditions which are shown in Figure 8.

The first is the condition where the machine has been rotated by striking a wave with its stern in such a way that the maximum slamming load comes on to the bow. This leads to about 8g acceleration on the pilot which is equivalent to a load approximately equal to 1.25 of the weight of the machine acting right on its bow. Furthermore, we assumed that this could apply to angles of yaw up to 45°. This virtually stresses the attachment point of the outer rims, the engine mounting, and determines such things as the fan clearance.

The other case is the condition where the machine just dives over one wave and plows into the next, so that we get a maximum longitudinal deceleration of about 1 1/2g.

However, there is a worse case than this, which is a crash case. If the craft hit a log of wood so that the front structure crumples, then this gives us the maximum deceleration of about 4g, which the engine should be capable of withstanding. The other design criterion is the pressure on the bottom plating which is a maximum of about 10 lb/$in.^2$ Tests were made on an inert model which was catapulted into a ditching tank; this confirmed the orders of the accelerations that could be expected, but this model had no cushion and when the engine failed the cushion took a finite time to decay so that the vertical rate of descent of the model much less than that of an inert model.

When allowance was made for the cushion, the maximum acceleration on the bow was only of the order of 1/2g instead of 8g. We believe that our design conditions are probably more appropriate to speeds of 90 knots than to speeds of 30-40 knots. The maximum g that we recorded during the trials was 0.6g, when we inadvertently ran into the wake of the "America" as she was steaming down the Solent.

There were two other important design criteria which were used on the SR-N1. The first was whether it could be stood on without buckling and the second was whether the material was available in the stores. This philosophy led to a fairly considerable increase in weight and the N1 ended up at a weight of 8,500 lbs, instead of the original estimate of 6,600 lb.

Some of the details of the design of the SR-N1 are shown in Figures 9 and 10. These diagrams show the guide veins and control arrangements in the main lifting ducts and indicate the quantities and variations of the total head at different points in the ducts. For pitch and roll control, butterfly valves were fitted in the main lifting ducts. These shut off a portion of the air to the peripheral jets and caused the machine to roll or pitch a small amount. To help this rolling and pitching control, elevons were placed on the exits of the propulsion ducts, but the stability of the machine about its trim position was such

that these had only a relatively small effect and so they were removed during the course of the trials.

From Figure 9 you will see that the air, which is taken off to the propulsion ducts, is extracted through ports on either side of the main chimney. This has the effect of creating a virtual barrier between the air to the front half and to the rear half of the machine. This effect, coupled with the fact that the air suffers an enormous expansion between leaving the fan and entering the peripheral nozzles, makes it easy for flow break-away to occur in the lifting ducts. One of the most serious problems that we have had on the N1' has been the instability which has been caused by these effects and which is shown in Figure 11. This characteristic only occurs in pitch and causes the machine to trim itself either nose down or tail down at an angle of about 1 1/2°. We eventually found that the solution to this problem was to block off portions to the inner jet. This increases the back pressure on the fan and avoids the tendency to flow break-away within the ducts, but it reduces the margin of stability by about 20 to 30 per cent. Figure 11 shows how the present pitching moment curve compares with the original curve which was violently unstable over the zero pitch region.

In the design of the SR-N1 we did not make a very special effort to design low loss ducting, and in fact the total head loss in the lifting ducts is as high as 25 per cent while in the propulsion ducts it is as high as 50 per cent. Although the propulsion system on the craft takes one third of the engine power, it only develops 25 hp at its top speed. With careful design, even on a machine with the same layout as the SR-N1, we believe that these efficiency figures could be considerably improved.

The drag curve of the N1 is shown in Figure 12 where it will be seen that the major contribution of the drag is caused by the change of momentum of the air being drawn into the funnel. The second largest contribution, which occurs when operating over water, is the wavedrag. Whe wave drag characteristic is very similar to an ordinary planing craft. This wave drag is transmitted to the craft in the form of a change of incidence. This incidence, or trim, reaches a maximum at the hump speed, which is the function only of the length of the craft and occurs at about 12 to 14 knots on the SR-N1. The present indications are that this wave drag is less than the theoretical value at the hump speed, but is more than the theoretical value at speeds above the hump. Furthermore, we have found that the depth of the water in which the N1 is operating plays an important part, and Figure 13 shows a picture of the N1 operating in about 3 ft of water, bringing in an enormous bow wave that completely blocks up its front jets.

During the early trials of the craft we ran into the usual crop of development problems. The engine cooling was not right; the control valves fluttered; but, worst of all, our original design for the propulsion duct control was almost completely unmanageable. This system had to be completely revised and four large gate valves were installed in the propulsion ducts in place of the simple flap valve that we had originally designed.

The main lessons that have been learned during the past three months of trials and demonstrations are that over land the dust created with this type of ground effect machine would be very serious indeed, while on the sea the spray is an equally serious problem, although it is alleviated to a certain extent as the speed of the machine increases and is only likely to be a problem at low forward speeds. However, the cushion loading on the N1 is very low and theoretical studies indicate that cushion loadings of the order of 50 to 100 lb/ft^2 instead of 17 lb ft^2 are more likely economical values for practical hovercraft. At these conditions the dust and spray would be three or four times as bas as on the N1. For example, during a two-hour operation over the sea, we got as much as a quarter-of-an-inch of salt on the cylinders of our engine and after each operation we had to completely wash down the whole machine with fresh water. This is acceptable on a research vehicle,

but it would clearly be quite impractical and uneconomical on any sort of operational machine.

We believe that we now understand fairly well the theory of the momentum curtain system and, as Figure 14 shows, the comparison between the achieved and calculated hovering performances are fairly reasonable. We still have a long way to go in developing operating techniques and improving the control of the machine, particularly over land.

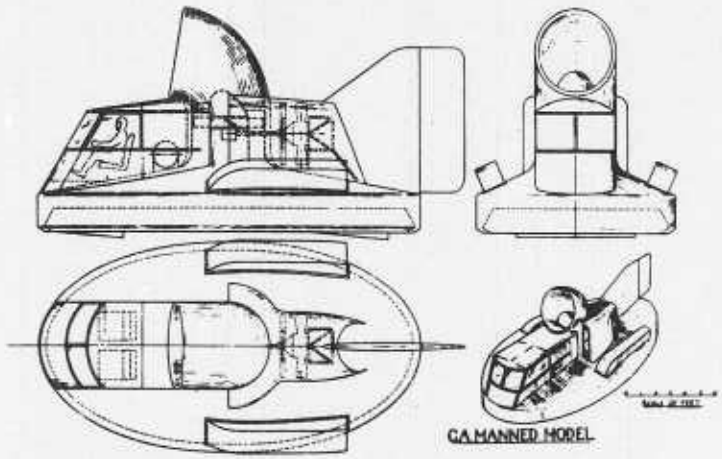

ORIGINAL PROPOSAL FOR THE MANNED MODEL

Figure 1.

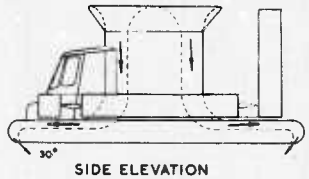

SIDE ELEVATION

INTERIM SINGLE JET VERSION OF SRN1

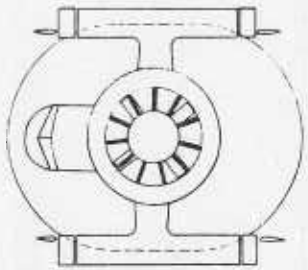

PLAN VIEW

Figure 2.

TYPICAL PRESSURE DISTRIBUTION BENEATH S.R. N1. MODEL AT INCIDENCE

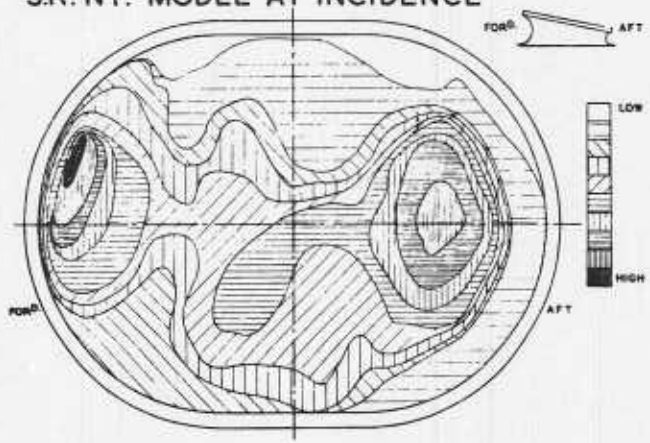

Figure 3.

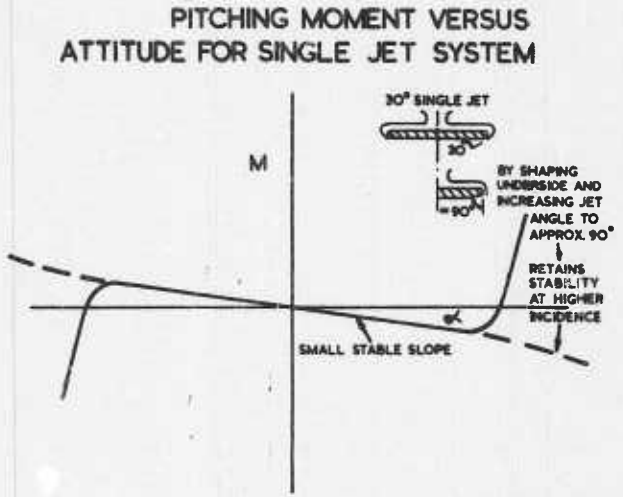

Figure 4.

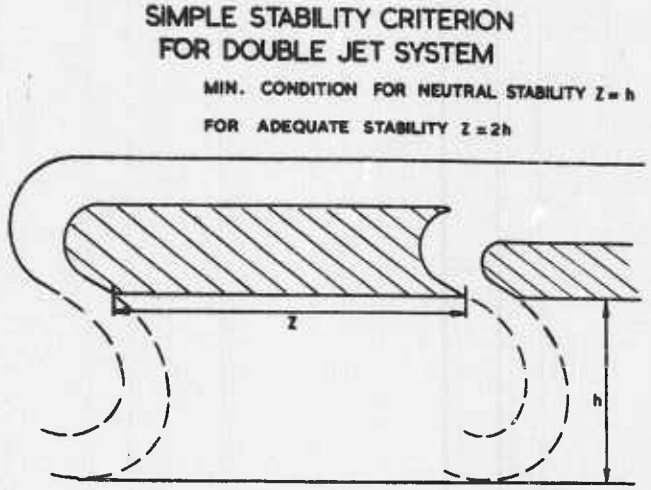

Figure 5.

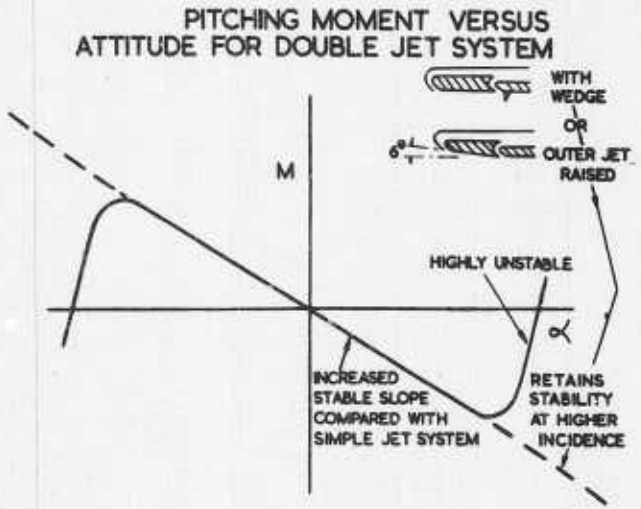

Figure 6.

S.R.N.I. EXPERIMENTAL CRAFT

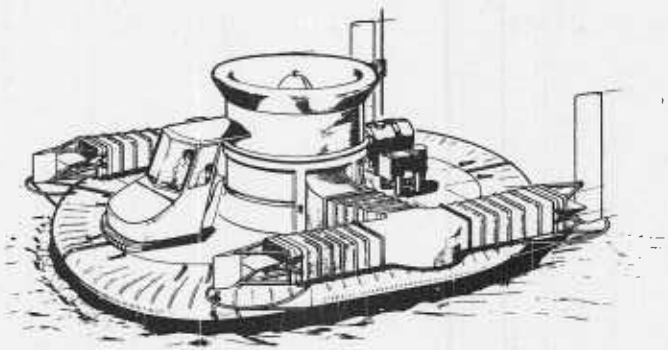

Figure 7.

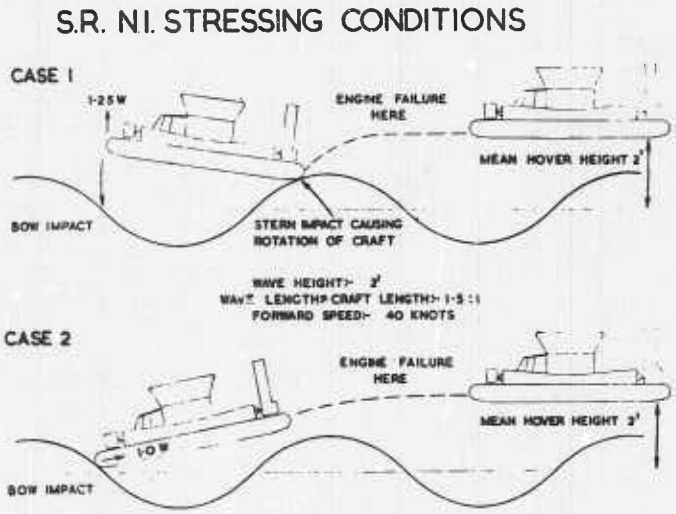

Figure 8.

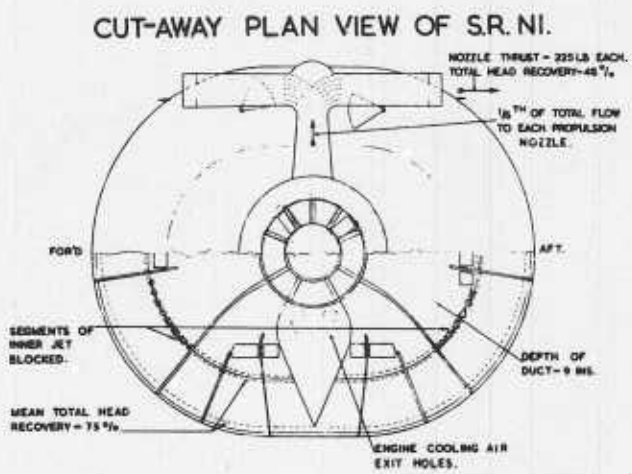

Figure 9.

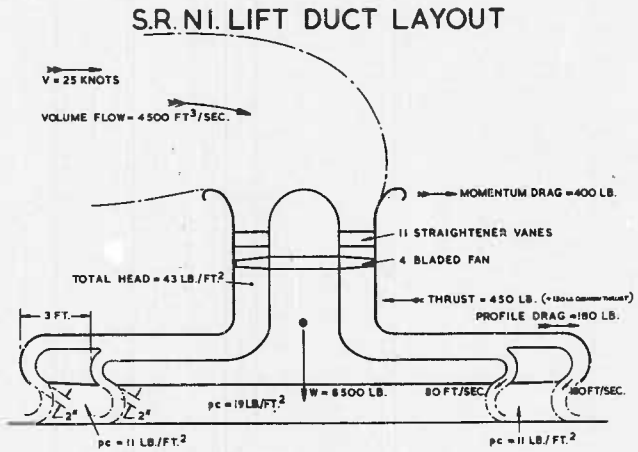

Figure 10.

S.R. N1. MODEL PITCHING MOMENT VARIATION WITH INCIDENCE.

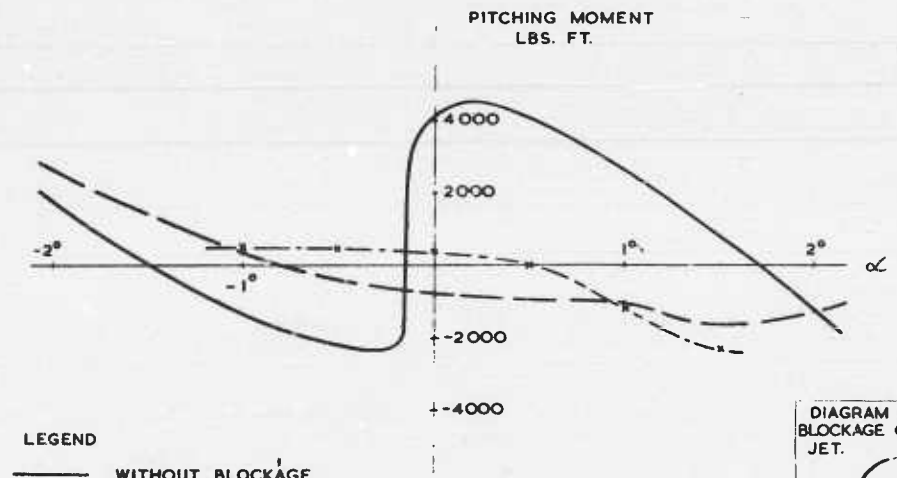

Figure 11.

DRAG CURVE OF S.R.N1.

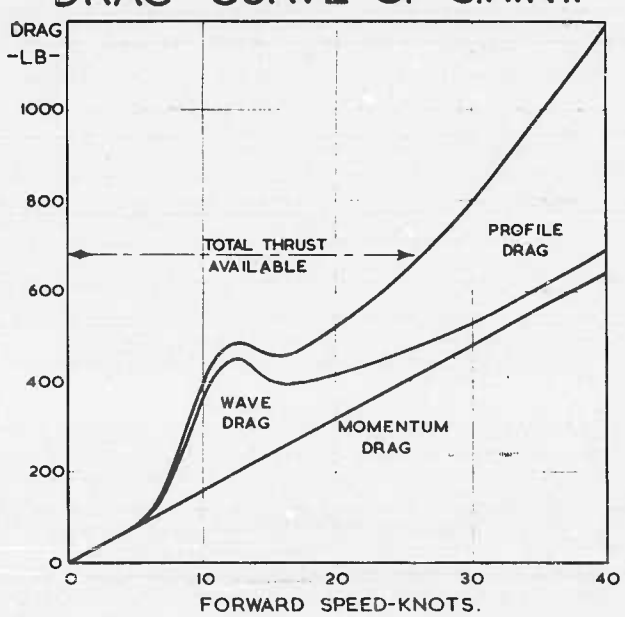

Figure 12.

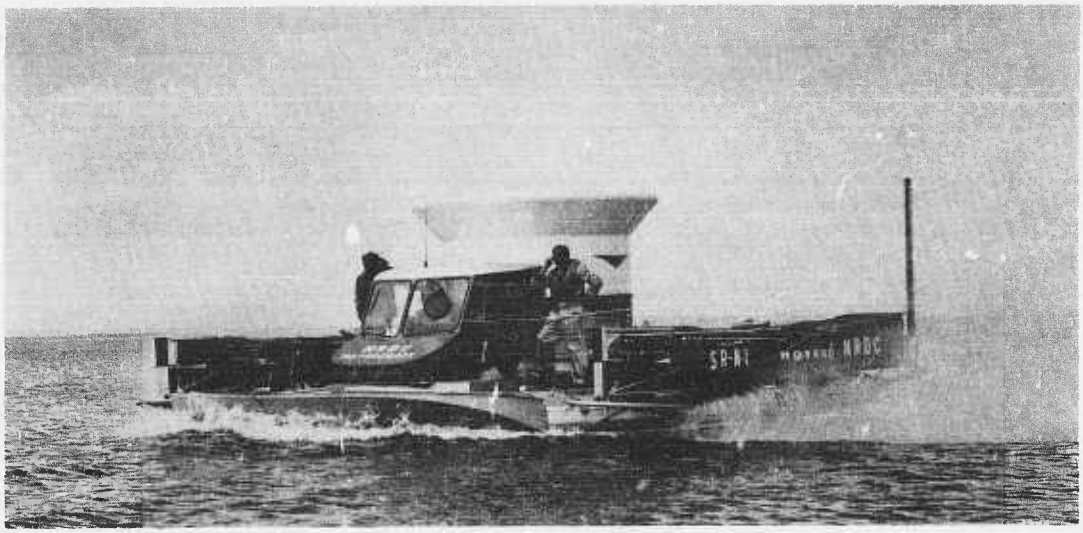

Figure 13.

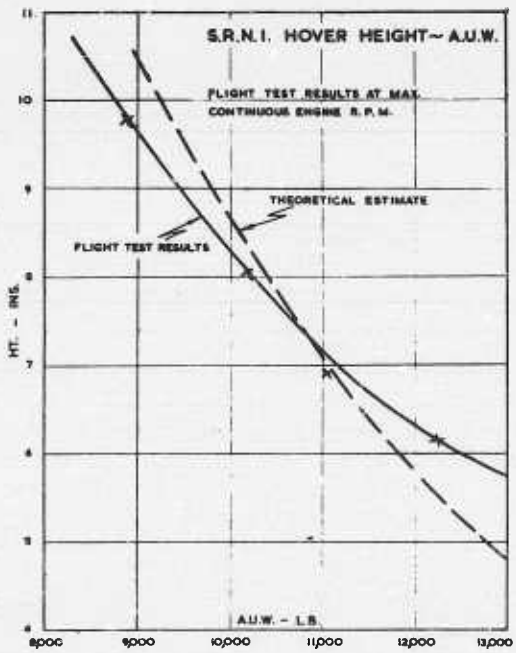

Figure 14.

SOME REMARKS ON THE ENGLISH CHANNEL CROSSING OF THE HOVERCRAFT ON JULY 25, 1959

By C. S. Cockerell, Hovercraft Development Limited
Appendices by R. Stanton Jones, Lt. Cdr. P. Lamb, and the author.

We were lucky to get away with it. The experimental SR-N1 was not designed for this sort of thing. The top air speed of about 22 knots means a ground speed of less than 12 knots against a 10-knot wind.

When the crossing was first suggested to the Directors of Hovercraft Development Limited, there was dead silence. After a few weeks the idea sank in. Saunders-Roe was not enthusiastic at first. It might mean failure and a setback. After the initial shock they set about all the necessary preparations with a will. If you chance your arm, you may not succeed. If you do not chance your arm you are certain not to succeed. Conditions and circumstances are never just as one would have them, but if one waits - the time has gone by.

We planned to go from Dover to Calais, to pay our respects to the French, and to commemorate the epic flight of Monsieur Bleriot on July 25th, 1909. On the morning of Bleriot's crossing, his rival, an Englishman, put his head out of the window at 5 in the morning, decided conditions were not right and went back to bed. Meanwhile Bleriot set off and some 25 minutes later - and in mid-Channel - his engine began to overheat. 25 minutes was as long as he had ever managed to keep it running. A heavy rain storm started, cooled his 25 hp engine, and it regained its power. He landed in a little field on Dover Cliffs. The first journalist to interview him was Lt. Cdr. Peter Lamb's uncle.

I said "to commemorate Bleriot's flight" not to compete with it. There was no danger for us, only the danger of feeling very small should we fail.

Our plan was to go from Dover to Calais; but the weather forecast was east or north-east winds for some days - head winds - so, after thinking things over, we decided that it would be more complimentary to the French if we reversed our plan and tackled the crossing from Calais to Dover.

The Navy turned on a flattie to transport the SR-N1 from the Isle of Wight to Calais. The Customs turned up - had we an export license? No, we hadn't. Much ink!

The flattie set off and we flew by aeroplane to Dover and next morning set off in an RAF launch for Calais. Quite a chop, too much sea, too much wind. We arrived in Calais Harbor and there was the flattie with the SR-N1 on top, and a Naval tug in attendance. We set off to find some lunch and found some beer and I think a sandwich or two.

What to do? Too much wind and sea to attempt the crossing, so we went out in the Naval tug and wallowed about in mid-Channel and observed the sea, and rather ran out of conversation and felt depressed.

We returned about 4 p. m. and found rather large crowds all expecting us to do something, so we decided to give a demonstration. Meanwhile the French Ministry of Aviation turned up. They had not been notified. Was it an aeroplane or was it a ship? There do not seem to be any Hovercraft forms yet. Long, extremely polite arguments - maybe it was a ship. Exit polite official.

The SR-N1 was cast off, and Peter Lamb scooted her about the Harbor, then went out of the Harbor and turned for the flat sandy beach. It was swarming with people. We came in slowly, and the people divided in front of us and closed up behind us, but the craft seemed to want to go one way and we found it was making for a very pretty girl in a Bikini. However, she fled, and Peter Lamb managed to turn the craft round. We went out to sea again and then back in over the sands again and of course there was the girl in the Bikini. So it looks as if Hovercraft are not Shee-like ships, but it could of course have been Pilot trouble.

We were given bunks for the night in the Tug's Sick Bay, with a porthole looking onto the quay - nobody else seemed to want to go to bed that night, so little sleep; up at 3:30, no breakfast, off at 4 a.m. in the RAF launch to look at conditions outside the harbor, with Peter Lamb and Dick Stanton-Jones, Saunders-Roe's Chief Designer.

And then we set off in the SR-N1, clearing the Harbor at 4:55 a.m. on Saturday the 25th. With Peter Lamb as driver, and Chaplin and I as crew and movable ballast.

It was just light, with no wind, a little mist, and a gentle swell. We scotted along nicely, peering into sea and more sea. Chaplin and I were on the fore-deck to counter-balance the extra petrol.

Soon it was daylight and the mist was gone and there was a light wind from the North-East, but still only sea to be seen. Mostly the swell was on our aft quarter, but occasionally one was with us, and it was exhilarating to skim down the face of it and rush up the next. The fine salt spray kicked up by the jets got into everything and made one's eyes stream. So, for a time I didn't look and then when I did, there, faintly, were the Cliffs of Dover. How many people in all history must have been gladdened by that sight!

There was more swell now and a popple on top of it, and rather more wind. Sometimes we hit the wave tops and fell below hump speed and sometimes we scooted nicely but its a very kindly motion, much more gentle than a boat's. I was sopping wet and rather cold. Those cliffs seemed to be shrinking and little aircraft began to appear, full of pressmen skimming past at nought feet, practically hitting our flower-pot. I wondered whether we would have to do some air-sea rescues.

The cliffs really were larger now and soon we were stopped to pour some of our reserve petrol into the fuel tanks, with the cliffs about 2 miles off. Then away again at a very good clip, with the movable ballast sitting aft.

Soon we were under the cliffs, shielded from the wind, with a flat sea. I observed the wash. At hump speed the SR-N1 trails about 18-inch waves but at this speed, about 25 or 30 knots, there is absolutely no wave formation to be seen, just water stroked by a shaving brush.

Into the Harbor and across it and there was the beach, a very steep shingle beach. Up we went and came to rest - and I fell off aft, due to the angle, along with a couple of empty petrol cans. It was 6:58 a.m. and it was over. Breakfast, that is what I wanted most.

APPENDIX A.

REPORT ON THE CHANNEL CROSSING AS OBSERVED FROM THE ACCOMPANYING RAF AIR/SEA RESCUE LAUNCH

By R. Stanton Jones, Saunders-Roe Limited

At 3:30 a. m. on Saturday morning, the 25th of July, there was a flat calm in Calais Harbor. Since weather forecasts indicated that the winds would continue from the north to northeast direction, it was clear that we should take immediate advantage of the zero wind condition. Commander Lamb went out in the RAF launch at 4 a. m. to check conditions outside the harbor while the ground crew unloaded the SR-N1 from the lighter.

The numbers of the following paragraphs relate to the points on the accompanying diagram.

1. At 4:50, in flat calm and zero wind, the N1 made its run down the harbor from the lighter. It appeared to be well over the hump with plenty of clearance at the front and going very smoothly. The speed of the launch outside of the harbor was 16 knots and the N1 was gradually overtaking. Probable speed in these conditions was 18 to 22 knots.

2. Cleared harbor entrance at 4:55 a. m. About 1 mile outside the harbor there was a slight swell about 60 to 80 ft long and a mean of 1 ft from trough to crest with a slight chop of 6 inches at the most. The wind was 5 knots from the northeast. At this point the N1 veered off slightly to the north. We considered this was a good move in view of the wind direction, bearing in mind that this was likely to increase in strength during the journey. It was decided to maintain the launch on the true Calais-Dover heading, but a 2-knot northerly current was sweeping us in the same direction as the N1. The launch throttled back to 10 knots. The N1 appeared to be below hump and making only 8 to 10 knots for quite long periods. It was noticeable that when the N1 turned slightly off wind it would accelerate away over the hump and move easily over the slight swell, but it would fall quickly below the hump when it turned back onto a more northerly course into the wind.

3. When the N1 was about 3 miles north of the launch, I requested the Captain to alter course since it was now clear from the heading of the N1 that Commander Lamb was having no difficulty with navigation. When we were in a position about half-a-mile from the N1 we turned back onto a course parallel to the Calais-Dover track. The Captain of the launch checked our position, which was 9 nautical miles from Calais, 50 minutes after leaving the harbor entrance, and about 3 miles north of the Calais-Dover track. The N1's mean speed to this point was 11 knots.

At this point the launch was able to keep station for quite a long time and the average speed of the N1 was 14 knots in a 5 knot wind from north to northeast. Hence its true air speed was approximately 18 knots. On several occasions when the N1 turned slightly south it would accelerate to approximately 20 knots, going at a true air speed of 22 to 23 knots. In this mid-Channel region, the swell had increased to between 80 and 100 ft long and about 2 ft from trough to crest, with a superimposed chop of about 9 inches. It was noticeable from the launch that on the downwind runs the engine was throttle back.

4. About 9 miles from Dover the RAF launch lost one engine but was able to keep station at a speed of 14 knots. During this period a near collision was observed between

the N1 and a small boat. The N1 turned sideways during the maneuver to avoid the boat, which was probably misled by the fact that the N1's heading was approximately 20° to its track.

Fuel estimates made at this time indicated that the N1 was most unlikely to make Dover Harbor without refueling.

5. The N1 encountered large swells from the ship which were estimated at about 4 ft from trough to crest and approximately 60 ft long. It was averaging 15 to 18 knots at the time and appeared to take the first swells quite comfortably, but at one point it appeared to dig its nose right in and was seen to ship green water. The height of these larger swells was confirmed by J. W. Lloyd, who was using a long range telescope at the Dover Signal Station. He noted that the N1 disappeared into the troughs so that only the portion of the craft above the top of the propulsion ducts was visible.

The N1 stopped to refuel 8 gallons when approximately 2 miles from Dover Harbor, 1 hour and 50 minutes after starting the engine.

The remainder of the trip was uneventful but it was noted that speed downwind through the harbor was greatly increased. The fuel left after beaching was only 2 gallons.

Approximimate analysis of trip.

True distance covered from Calais Harbor to Dover Harbor entrances	...	25 nautical miles approx.
Running time (allowing 3 minutes for refueling)	...	1.81 hours
Mean speed	...	13.8 knots
Maximum observed speed	...	20 knots
Maximum calculated air speed	...	23 knots
Total fuel carried:		
Usable fuel in tanks	...	73 gallons
Fuel in cans on deck	...	16 gallons
Total fuel consumed in crossing	...	79 gallons
Approximate starting weight	...	9,300 lb
Weight at end of trip	...	8,700 lb approx.

At these weights the calculated maximum air speed at 2,900 rpm = 22.5 knots; at 2,700 rpm = 22 knots.

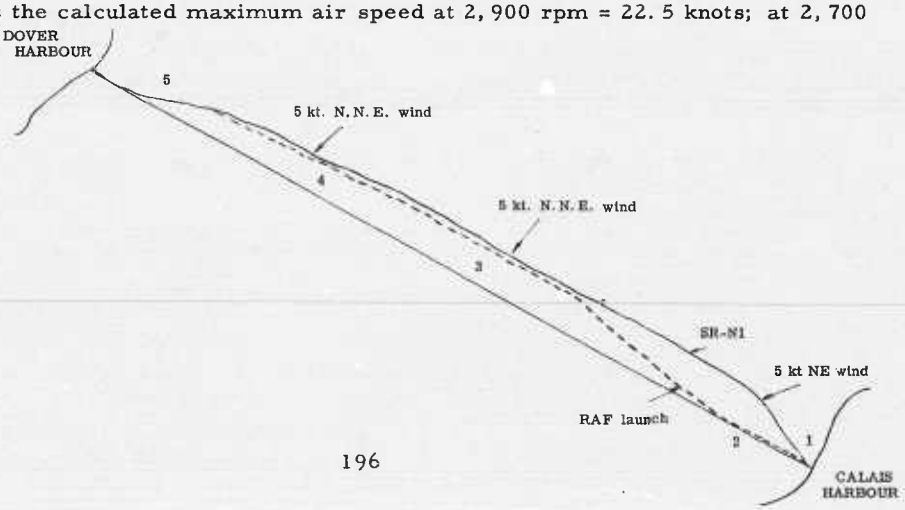

APPENDIX B.

PILOT'S HANDLING ASSESSMENT OF THE SR-N1 DURING CHANNEL CROSSING FROM CALAIS TO DOVER

By Lt. Cdr. P. M. Lamb, Chief Test Pilot, Saunders-Roe Limited,

In view of the Chief Designer's detailed report of the 28th of July, 1959, and the fact that the Chief Test Pilot proceeded on summer vacation immediately following the Channel crossing of the Hovercraft, this report has been condensed into a few details of general interest. The Chief Test Pilot is in entire agreement with the Chief Designer's report previously mentioned.

On Friday, the 24th of July, the first day selected for the cross-Channel attempt, conditions were far from ideal. The wind was north easterly force 3 - 4 backing north north easterly during the afternoon. There was a moderate swell with an estimated height of 4 feet between trough and crest with white caps everywhere. At approximately 5 p. m. on Friday, after sitting in mid Channel aboard the H. M. S. Warden, for the whole of the afternoon observing the wind, sea, and swell conditions, the Chief Test Pilot decided to abandon the attempt until the following day.

Upon arriving back in Calais it was agreed after discussion between the representatives of Hovercraft Development Limited and Saunders-Roe to put on a demonstration for the local residents. This demonstration took place at 7:30 in the evening when the harbor was clear of shipping. In view of the fact there was so little time in which to spread the word, it was remarkable to see the very large number of people who gathered. The starting of the Hovercraft engine was rather like the tune of the Pied Piper. Children appeared from everywhere to throng the harbor wall. After the initial demonstration in the calm waters of the harbor to show the maneuverability, acceleration, and turning performance of the SR-N1, the craft proceeded outside the breakwater to the sandy beach area westward of the entrance. The crowd moved faster than the Hovercraft. By the time the Hovercraft approached the sands, a large number of excited children and equally interested adults were running hither and thither over the beach to obtain a good view at close quarters. An odd suicidal enthusiast decided to lie down in the approaching path of the SR-N1 to ascertain that there were no wheels underneath. This colorful, but somewhat over enthusiastic, welcome by an excited crowd necessitated a restricted performance, especially as regards speed over the beach.

The craft returned to the harbor and tied up alongside the lighter after a 35-minute demonstration. Slight damage was caused to the starboard rudder as the craft maneuvered alongside the lighter. This was partially due to the fact that the rudder guards had been removed to save as much weight as possible on the cross-Channel attempt. This whole demonstration was considered to be of extremely good value, which was shown by the somewhat disbelieving, high spirited, and jocular mood with which it was received.

The following morning at 3:30 a. m. there was a flat calm, and after a brief look at the sea outside the harbor the Chief Test Pilot decided to make an attempt with as little delay as possible. The ground crew, with recommendable anticipation had hoisted the craft off the lighter, warmed up the engine, and topped-up the internal tanks. As a safety precaution, in view of the lack of following wind, the pilot decided to take aboard 16 additional gallons in cans on the deck of the SR-N1. With C. S. Cockerell and J. Chaplin aboard, the craft cleared the harbor entrance at 4:55 a. m. just ahead of the RAF. Rescue Launch. The wind, such as it was, outside the harbor was about 5 knots from

the north east. With the craft above hump speed the pilot decided to make as much northing as possible, for the true track was 294°. Any increase of wind, which was to be expected with sunrise, could then be used as a quarter to tail wind in the latter stages. When the craft was well clear of the Whistle Buoy, marking the approach entrance to Calais, the pilot decreased rpm to 2, 700 with the craft still above hump speed (estimated 18 - 20 knots). At this time the loom of the South Foreland light was just visible but fast disappearing with the approach of daylight.

For the next 5 miles, navigation was made by dead reckoning, with the RAF Rescue Launch, which had previously agreed to maintain the true track from Calais to Dover, well away on the port side. At approximately 5:30 a. m., the white cliffs of Dover, tinged red in the morning sunrise, were first visible. Up to this time the SR-N1 appeared to have made extremely good progress at a constant setting of 2, 700 rpm. However, a slight swell was now apparent which retarded the progress of the craft and on several occasions dropped her back below the hump speed. When this happened the pilot was forced to accelerate by increasing rpm and altering to a westerly heading to rise above the hump, before resuming the true course with minimum cruise engine power.

In mid-Channel the wind appeared to increase. This was especially noticeable by the drift of the craft when well above the hump. This factor, coupled with the larger swell which appeared to be traveling in the same direction as the wind, produced at times the disconcerting fact of nosing-in with the port propulsion duct. Generally the pilot could anticipate when this was going to happen and could either reduce the SR-N1's speed by half settling on the water or preferably turn onto a westerly heading and combat the swell head-on. It was at this point that a small boat, over which the SR-N1 had the right of way appeared on a constant bearing. When it was obvious that a collision would be imminent if both craft pursued their courses, the pilot was forced to alter heading into wind to starboard. At the same time the small boat, which either had not been keeping a good lookout, or had been completely misled by the drift of the SR-N1, altered course to port. With muttered oaths to mariners, the pilot was forced to put the SR-N1 statically on the water and allow this small boat to maneuver out of the awkward situation in which it found itself. After this incident, the SR-N1 took an appreciable time to get above the hump speed, in all probability due to the variable wind and moderate swell. Both Chaplin and Cockerell tried moving their positions with little success. After proceeding for 2 miles below hump speed, the craft crossed the swell of a large ship proceeding north through the Straits of Dover. An appreciable amount of water was shipped on the port side from this swell and both observers moved to starboard to compensate the trim of the craft and to avoid getting washed overboard.

Some 2 miles outside Dover Harbor, when the internal fuel had fallen to 2 gallons, the pilot decided to refuel from the additional amount carried aboard. Eight gallons were poured into the tank while the craft idled on the water. This operation took 3 minutes. After refueling, the craft was clear of the swell in the lee of St. Margaret's Bay, and it proceeded at the best speed it had obtained throughout the whole passage up to and through the entrance to Dover Harbor. It was estimated that the craft probably achieved 30 knots in the last mad dash. The craft proceeded throughout the length of the harbor and beached adjacent to the Clock Tower, some 2 hours and 3 minutes after getting underway at Calais. The first personnel to board the craft were the Customs Officials with the request "Anything to declare?" The obvious reply "that it was good to be in England" appeared to satisfy one and all.

APPENDIC C.

SHORT HISTORY OF BRITISH PROJECT

By C. S. COCKERELL

It was in 1953 that I first started thinking and working on the problems of how to make a ship go faster. It soon became obvious that if there was a solution, it must lie in the bringing-about of a reduction in the skin friction, and this led to the idea of air lubrication.

A 16-ft rectangular flat-bottomed boat was constructed with the sides extended below the bottom, forming the side keels, and air was pumped out of a slot across the bottom of the craft right forward. The drag with and without the air was measured, and the results were compared with the calculated drag. The drag with the air film present was considerably less than without air, but, since some jet propulsion was present, the conclusions were not dependable.

Then a large centrifugal blower was installed in a 20-ft, 20-knot launch, and the air supply was taken over the bow and fed out at the rear of a hollow step. This work was also somewhat inconclusive, but nevertheless most instructive. There must be a thick layer of air. The next scheme was for a craft with deep side walls, hinged trailing doors fore and aft, with the center pumped up with a blower.

Next it was thought that the hinged doors at the ends could be replaced by thin water curtains, pumped down from the craft. The power required to sustain the water curtains was difficult to assess, and so calculations were made substituting an inward-facing air curtain for the water curtain idea, calculating the force required to deflect an element of the curtain through so many degrees at such and such a radius. These calculations looked hopeful and so a three-dimensional annular jet was constructed out of a couple of tins and tested on some kitchen scales. This was followed by a two-dimensional test gear, which gave results within 20 per cent of those calculated. It was then the middle of 1955. Efforts were made to interest other people without success. Progress was very slow, and as I was all this time on my own, trying to build up a boat business, my resources were stretched to the limited.

In 1956, a friend constructed a model that performed well over land, and later well over water. Meanwhile I pursued my business and did some more work with the two-dimensional test gear, modifying it so that in the autumn of 1956 I could test closed vortex systems, wherein the same air is recirculated continuously. The tests showed that such a system could build up and contain a pressure.

Then, in October 1956, I brought the project to the notice of the Ministries and it was classified; a small contract being given to Saunders-Roe in August 1957 to verify and extend my results. Much help was forthcoming from R. A. Shaw, Assistant Director, Aircraft Research, of the Ministry of Supply; but in spite of all his efforts the project languished.

I continued to do work on deflectors, toroidal vortices, and other power-saving devices, not forgetting flexible hovercraft.

It was not until September 1958 that the project was declassified, thus freeing me to take it to the National Research Development Corporation.

Mr. Hennessey of NRDC took over the project and pursued it with a will, with the result that, in October, Saunders-Roe had a new contract for research and the construction of an experimental craft.

There was real enthusiasm within the firm, and great credit was due to the people in it, for the 4-ton experimental craft was complete and became cushion-borne just eight months later in June 1959. All sorts of tests were carried out, culminating in the crossing of the Channel from Calais to Dover on the 25th of July.

ANNULAR JETS WITH DEFLECTORS

By C. S. COCKERELL

SUMMARY

This paper briefly discusses the case for deflectors, which are a means of providing safe operation of ground effect machines with annular jets in severe wave conditions. The results of experimental tests made on a two-dimensional static model are given.

INTRODUCTION

One of the main problems in designing an annular jet ground effect machine to operate over water is to make the craft operationally safe in all wave conditions that might be encountered and at the same time to maintain good overall efficiency. Statistics show that, in open water, severe wave conditions occur only for a very small proportion of the time, yet the craft must be capable of operating in these conditions, perhaps at reduced speed. Critical waves for ground effect machines are not necessarily those of maximum height but are rather of the shorter breaking type.

This paper briefly deals with the deflector, which is a means of providing safe operation in initial wave conditions without loss of performance in normal operating conditions.

THEORY OF DEFLECTOR

The theory of the deflector is illustrated in Figure 1, which gives a diagrammatic flow pattern. The deflector, which is situated between the undersurface of the craft and the water surface, receives air that is flowing away from the cushion and gives it a momentum change toward the cushion. When a deflector is employed, the result is that the radius of curvature of the jet stream, instead of being of the order of one-half the operating height as for the case of simple annular jets, is of the order of one-quarter of the operating height. Since the pressure differential across a jet stream is inversely proportional to its radius of curvature, the deflector can double the cushion pressure for given values of jet thrust and height of craft undersurface above the water.

Alternatively, by using deflectors the height of the main body of the craft can be doubled. This is of great importance when considering operation over a wide range of wave conditions. Of course, there is a price to pay for this in the form of the structure weight of the deflectors. Further, in this more severe wave conditions, the deflectors hit the tips of the waves; this results in appreciable hydrodynamic drag with corresponding reductions in speed. In order to reduce the hydrodynamic loads on the deflectors, fairings are used at the front and perhaps at the rear.

RESULTS OF EXPERIMENTAL TESTS

Some of the results obtained from two-dimensional static experimental tests made on an annular jet with deflectors are given in Figure 2. These results confirm that a single deflector can about double the craft height at a given cushion pressure. In this particular example, for a cushion pressure of 68 per cent jet stagnation pressure, the height of craft undersurface is increased from 2.5 to 4.9 times the jet width by using a single deflector. By adjusting the height of the deflector, the operating height could be about doubled for any cushion pressure.

The results also show that using a second deflector can increase the operating height further. For example, at a cushion pressure of 64 per cent jet stagnation pressure, the height of craft undersurface is increased from 2.9 to 7.0 times the jet width. This is an increase of over 140 per cent, which again could be obtained at any value of cushion pressure.

STABILITY IN HEAVE

An interesting result shown in Figure 2 is that, when deflectors are used over the central part of the curve, there is but a very small change in cushion pressure for a large variation in height. This means that over this height range the stability margin in heave is very small indeed.

The property of negligible heave stability is a useful tool in designing hovercraft to have small vertical accelerations when traversing waves. It is pointed out that adequate stability is available at the extreme heights.

The heave stability margin may be increased by arranging the vanes of the deflector to have a graduated change of incidence from front to rear. This arrangement is shown in Figure 3. It is seen that, when height is reduced, the symmetrical deflector gives a smaller jet stream curvature radius below the deflector to that above it. The balance of cushion pressure then reduces the curvature radius above the deflector and the jet stream splits. In the case of the deflector with vanes of graduated incidence, the curvature radii above and below the deflector remain equal as the craft height changes, which means that the cushion pressure changes with craft height.

APPLICATION OF DEFLECTOR

It is considered that deflectors should be used at the front and rear of a craft rather than around its whole periphery. A suitable configuration, in which deflectors are applied, is that illustrated in Figure 4. The planform is rectangular and the fore and aft deflectors are attached to side walls. The latter are of good hydrodynamic shape and the side jet stream nozzles are located on their undersurface. The use of side walls is consistent with the philosophy of deflectors in that both contact severe waves only, resulting in safe operation at reduced speed.

In conclusion, it should be added that, while the application of deflectors may be somewhat limited, it is felt that they have a place in the development of ground effect machines with annular jets.

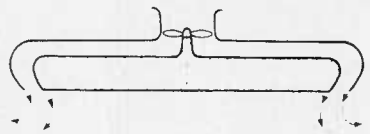

SIMPLE ANNULAR JET

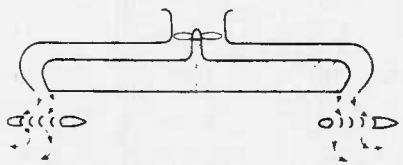

ANNULAR JET WITH DEFLECTOR

Figure 1.

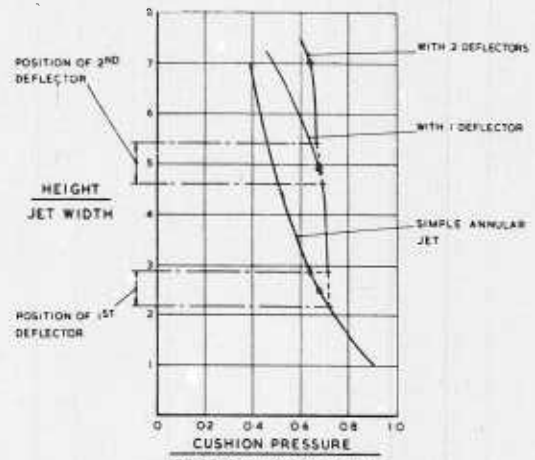

EXPERIMENTAL HEIGHT – LIFT LAW

Figure 2.

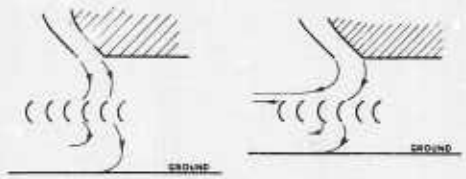

SYMMETRICAL DEFLECTOR

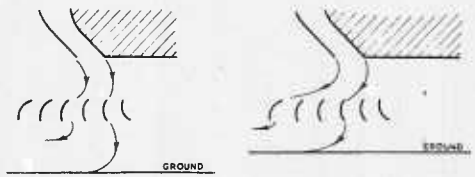

DEFLECTOR WITH VANES OF GRADUATED INCIDENCE

STABILITY IN HEAVE

Figure 3.

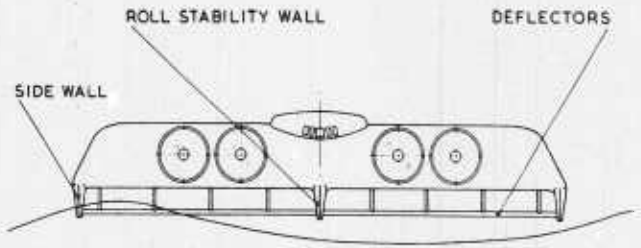

CRAFT WITH SIDEWALLS AND DEFLECTORS

Figure 4.

THE HELICOPTER AS A GROUND EFFECT MACHINE

By Evan A. Fradenburgh, Sikorsky Aircraft Division, United Aircraft Corporation, Stratford, Connecticut

SUMMARY

The ground effect of the helicopter is described in terms of performance effects and hovering flow mechanics. Benefits to payload or power levels required in hovering can be substantial. Furthermore, experimental data indicates that a helicopter in ground effect requires only a minor, increase in power if any, during transition to forward flight, and that only minor losses of ground effect occur when hovering over a sloped surface. It is also shown that surface area suitably located in the field of flow near the ground can increase the lift increment due to ground proximity because of favorable pressures, although this device was not intended to represent a practical scheme for augmenting lift.

A comparison of the lifting efficiencies of the helicopter and peripheral jet ground effect machines is presented, with the conclusion that the helicopter is the superior type for the many missions which it now performs, and that the utility of the ground effect machine will be restricted to very specialized missions or extremely large machines.

INTRODUCTION

The current interest in machines utilizing the "ground cushion" phenomenon to help support themselves in the air is directed at a wide variety of configurations and a correspondingly wide variety of missions. In some cases the ground effect machine appears to be directly competitive with the helicopter, and the question arises as to the relative merits of the two types. It is well known that the helicopter experiences an increase in its lifting capability within ground effect, but since the "augmentation ratio" for a helicopter near the ground is lower than that for an annular jet at the same height-diameter ratio, it might be concluded that the annular jet represents a more efficient hovering machine. This conclusion is not necessarily correct, of course. since many factors other than the augmentation ratio are involved.

It is the purpose of this paper to describe the ground effect of the helicopter, including some of the flow mechanics as well as performance effects, and to make a comparison of the helicopter's performance with the peripheral jet vehicle.

SYMBOLS

A	augmentation ratio, total lift/jet momentum
A_j	jet exit area
b	number of blades
c	blade chord
C_Q	rotor torque coefficient, torque/$\pi R^2 \rho \lvert \Omega R \rvert^2 R$
C_T	rotor thrust coefficient, thrust/$\pi R^2 \rho \lvert \Omega R \rvert^2$
D_o	annular jet machine outer diameter

D. L.	disk loading, thrust/πR^2
P	static pressure relative to ambient pressure
R	rotor radius
R_o	annular jet machine outer radius
T	rotor thrust in ground effect
T_∞	rotor thrust out of ground effect at constant power
t	jet thickness
v	local wake velocity
v_j	jet velocity
v_o	mean induced velocity in plane of rotor, $\Omega R \sqrt{C_T/2}$
ρ	atmospheric density
σ	rotor solidity, $bC/\pi R$
Ω	rotor angular velocity

EFFECT OF GROUND ON HELICOPTER PERFORMANCE

A hovering helicopter rotor derives its lift from the downward vertical momentum it imparts to the air flowing through the disk. At the surface of the ground, however, the vertical velocity of the slipstream is reduced to zero, assuming the ground to be horizontal, since no flow through the ground can occur. The flow pattern of a rotor near the ground can theoretically be duplicated without the presence of a ground surface; a second rotor which is a mirror image of the first, located below the first rotor and lifting in the opposite direction, will ideally induce the same flow pattern as the ground because of the plane of symmetry halfway between the two rotors. This scheme for representing a ground plane, shown in Figure 1, is useful for theoretical treatments of the subject as well as for developing some appreciation of the nature of the flow. Most mathematical analyses, such as the ones used in references 1 and 2, assume that the trailing vortex system, which determines the characteristics of the induced flow field, may be replaced with a system of cylindrical vortex sheets and a corresponding image system, which permits calculation of induced velocities at any point in the flow field. As only a qualitative understanding of the phenomenon is necessary for the present analysis, it is sufficient to imagine that the upper rotor is effectively "descending" in the slipstream of the image rotor, and, as would be the case for descent in free air, requires less power to produce a given lift, or produces more lift for a given power expended.

Quantitative effects of the ground on hovering performance is shown in Figure 2, which presents test data obtained with a 2-bladed, 2-ft diameter model rotor having untwisted, untapered blades of 2-inch chord, and operating at a tip speed of approximately 600 ft/sec. This test equipment is the same used in the flow field investigation reported in reference 3. Curves of thrust coefficient versus torque coefficient are presented for this rotor out of ground effect and for height-radius ratios from 0.1 to 2.0. It is apparent from this figure that the presence of the ground can produce substantial performance effects.

These results are shown in another form in Figure 3, in which the ratio of thrust within ground effect to thrust out of ground effect at constant power, T/T_∞, is plotted against height-radius ratio. According to some theoretical analyses, such as that of reference 1, the ratio T/T_∞ should be variable with different thrust or torque coefficient levels; these test results, however, show no such variation below stall within the limits of experimental accuracy, and may thus be presented as a single curve.

Values of T/T_∞ up to 2.2 were recorded for the model rotor, at a height-radius ratio of 0.10. Conventional helicopters, of course, cannot be operated this close to the ground because of the fuselage and landing gear; with the landing gear on the ground, the rotor height-radius ratio is normally on the order of 0.5. At this height, the measured thrust for a given power was about 30 per cent higher than when out of ground effect. It should also be pointed out that any given combination of rotor geometry and tip speed will have some limiting value of attainable rotor thrust, corresponding to the maximum attainable lift coefficient on the blades. Operation near the ground will not significantly increase this limiting value, so that the high values of T/T_∞ noted are obtained only when the rotor out of ground effect is well below the stall point.

Also shown in Figure 3 for comparison is the augmentation-ratio for a thin vertical jet ground effect machine, based on the analysis of reference 4 for low height-radius ratios. The augmentation ratio for a given height-radius ratio is considerably higher than for the helicopter rotor, as is well known. This does not mean that the ground effect machine automatically has superior performance; a discussion of the relative merits of the two types is presented in a later section.

The significance of ground effect in terms of the payload of an existing helicopter is shown in Figure 4, in which the model test data has been applied to the Sikorsky S-60 flying crane prototype, having a rotor diameter of 72 ft. This machine has a payload of about 8,000 pounds for a typical mission of 100 nautical miles range; with this payload it can hover out-of-ground effect. By full utilization of the ground effect, however, the payload can be approximately doubled. Even with the wheels 20 feet off the ground, the hovering payload may be increased by nearly 50 per cent. The advantage of large size helicopters is apparent in this respect, since any given "working" height off the ground represents a smaller fraction of the rotor radius than for a smaller machine. A large helicopter will also tend to have its rotor relatively closer to the ground to begin with.

The ability to hover with increased payload is not necessarily useful, however, unless the helicopter can fly away with this payload. A helicopter out-of-ground effect normally requires more power to hover than to fly forward at moderate speeds, because of the reduction with speed of induced power required to produce a given lift. The speed for minimum power is usually on the order of 40 to 60 knots for a machine the size of the S-60. However, if the beneficial effect that the ground produces in hover disappears at a very low speed, 10 to 20 knots for example, then the power required might initially increase with speed, and a machine utilizing maximum available horsepower to get off the ground could not easily fly away except by the use of a ground roll.

The effect of low forward speeds (or wind) on rotor performance in ground effect was checked by testing the model in a wind tunnel. Results of these tests for a typical rotor thrust are shown in Figure 5. These results include approximate corrections for tunnel-wall interference effects. Data for the out-of-ground-effect case could not be obtained because of the relative sizes of the model and the wind tunnel; however, the Z/R-2.0 condition is nearly out of ground effect. The data in Figure 5 show that the reduction due to ground effect of rotor power required is much less at forward speed than in hovering. However, the benefits of forward speed on induced power tend to compensate for this loss of ground effect, so there is not a sharp rise in power required in translating from hovering in ground effect to forward flight. At the lowest height tested, $Z/R = 0.5$, corresponding

roughly to the wheels-on-ground condition, a slight rise in power was noted up to about 10 knots; this effect is similar to results obtained in reference 5. At lower heights above the ground, the relative rise in rotor power would presumably be somewhat more severe.

The effects of forward speed on the performance of an annular jet ground effect model was reported in reference 6. It was shown that for this model a severe drop in augmentation ratio, and therefore an increase in power required for a given height, occurred at low forward speeds. If this result is typical for the ground effect machine, the helicopter will have a substantial relative advantage in forward flight.

It is apparent, then, that most of the benefits noted for the helicopter hovering in ground effect can be utilized if desired. It must be remembered, however, that a highly overloaded condition has some undesirable aspects, besides the inability to hover away from the ground, including a lack of proper acceleration capability, reduced top speed, and relatively poor landing characteristics. These practical considerations will often outweigh the benefits of increased payload, so that the theoretical maximum gross weight allowed by ground effect will not usually be utilized. At gross weights allowing hovering away from the ground, ground effect may still be utilized to good advantage by allowing take-off or hovering near the ground at reduced engine power levels, with beneficial effects on fuel consumption and life of component parts. A common application of ground effect is to use the thrust increment available to provide very rapid acceleration to the optimum climb speed to clear obstacles in a steep climb-out gradient. In this connection it is worth noting that a tilted helicopter rotor can provide a horizontal accelerating force of 50 per cent of the aircraft gross weight for a thrust increase of only 12 per cent of the gross weight; this illustrates one of the advantages of the integrated lifting-propulsion system inherent in the helicopter. Ground effect is also frequently used to permit hovering take-offs at high altitudes where hovering out-of-ground-effect is not possible.

Another aspect of ground effect requiring consideration is the sensitivity of the results to ground slope. Figure 6 presents thrust ratios obtained with the model rotor for ground angles up to 40 degrees. The results indicate that only a slight loss of ground effect occurs, and that a helicopter hovering on a typical hillside receives nearly as much benefit as it would over flat ground. This also implies that ground effect is not suddenly lost by tilting the rotor disk forward to accelerate away from a hovering condition.

For comparison, the effect of ground angle on the augmentation ratio of an annular jet is also shown in Figure 6. This data was reported in reference 4, and was derived from the experimental studies of reference 7. In general, this data seems to indicate that the annular jet is much more sensitive to ground slope than the helicopter rotor.

FLOW FIELD UNDER A HOVERING ROTOR

Velocity and pressure fields. A photograph of the flow field under the model rotor hovering one radius above the ground is shown in Figure 7. Figures 7 through 10 were first presented in reference 3.) The flow streamlines are revealed by smoke filaments introduced above the disk. A prominent feature of the photograph is the pattern made by the vortices from the blade tips, which spiral downward and then outward along the ground surface. These tip vortices are strong because of the large gradient of lift per unit span, from a maximum value near the tip to zero at the tip. Not so evident is the vortex sheet shed by the rest of each blade having circulation in the opposite sense. This sheet extends inboard of the point of maximum strength of the blade "bound vortex," which is related to the lift distribution of the rotor. The maximum strength of the bound vortex occurs in this case very close to the tip so that the inboard vortex sheet is spread out over a relatively large area. For this reason, it is not readily visible, and does not roll up rapidly into a concentrated vortex, but it has the same total strength as the tip vortex.

In the center of the flow field there is a large region of relatively low-velocity air extending from the ground to a point somewhat above the rotor disk. This "dead air" region, which exists only when the rotor is within ground effect, forces the main downwash stream outward from the center of rotation.

A survey of the flow velocities in this region for the same height-radius ratio is presented in Figure 8 in the form of contours of constant wake velocity ratios, v/v_o, where v is the mean local velocity and v_o is the out-of-ground-effect value of the mean induced velocity in the plane of the disk. The dashed lines in the figure represent various positions of the flow survey equipment used in the investigation. The maximum velocities below the rotor occur in a fairly narrow band near the tip; the helicopter may, if desired, be classified as an annular jet machine. Blade twist will alter this picture somewhat in that the "optimum twist will theoretically produce a uniform downwash over the entire disk, at least when away from the ground. Practical rotors, however, nearly invariably have a downwash distribution qualitively, if not quantitatively, like the one shown. The central "dead air" region is actually a region of relatively low velocity upwash, as indicated by the negative values of the velocity ratio near the center.

Note that the annular "jet" of high velocity flow curves outward in roughly a circular arc; there is evidently a nearly constant pressure differential across the "jet" to cause this curvature. This pressure differential may be seen in Figure 9, which presents measured pressures in dimensionless form as contours of the ratio of local time-average static pressure to rotor disk loading. In the center of the rotor there is a large region of more or less constant static pressure, which has a positive valueequal to about half of the disk loading. This picture is presumably similar to the pressure field beneath a true annular jet ground effect machine. Under the rotor, however, the pressures near the outside edge of the annular "jet" are negative, because of the vortex cores which traverse this path. There is a flow stagnation point on the ground at about 80 per cent of the rotor radius, evidenced by the static pressure peak which occurs there. This stagnation point divides the flow into two parts; the main downwash stream which flows outboard along the ground, and the inner recirculatory flow which flows inward along the ground and upward toward the rotor. This inner flow along the ground does not reach high velocities at this ground height because the static pressure potential difference between the stagnation point and the axis of rotation is less than 20 per cent of the disk loading.

This static pressure drop along the ground is not always as low as this, however. Figure 10 presents pressures measured along the ground for several rotor height-radius ratios. As the rotor height above the ground is decreased, the maximum ground pressure is increased, as might be expected. At a height of one-half radius or less, however, a severe drop in ground static pressure was noted at the center. This pressure drop is believed to be associated with a rather strong vortex on the vertical centerline, which results from a slight rotation imparted to the downwash and the conservation of angular momentum as the air flows inward along the ground.

Root end vortex system. A somewhat more detailed description of the pheonomenon noted above is proposed in Figure 11. As stated previously, the vorticity produced inboard of the tip region is actually a distributed sheet, but for simplicity it is represented in the figure by a single line vortex. Both the tip and "root end" vortex filaments of one blade are shown in the top half of Figure 11, spiraling down from the blade to the ground as the blade rotates. The presence of the low-velocity upwash region is assumed, and the "root end" vortex must of necessity be located outside of this region. Proper placement of this vortex system is necessary to ensure reliable representation of the induced flow field. Reference 2 discusses a method of successive approximations that ideally allows an accurate calculation of this field; however, a qualitative analysis is all that is desired here.

The arrows drawn on the vortex filament in Figure 11 do not represent flow directions; rather, they indicate the direction of circulation around the vortices according to the "right hand rule."

In the lower half of Figure 11, the details of the inner part of the flow system are expanded. The root end vortex system, consisting of a spiral filament (actually vortex sheet) from each blade is replaced by an equivalent system of coaxial rings and vertical elements which represent the horizontal and vertical components, respectively, of the spirals. The arrows again indicate the direction of circulation around the vortex elements. Note that the rings help the tip vortices (not shown) induce the main downwash flow outside of the rings, and also induce upwash in the center region. The vertical components have a circulation that induces rotation of the main downwash flow in the same direction as the blade rotation whereas inside the upwash region the flow rotation must be in the opposite direction.

At the ground, the elements of this vortex system will, for the most part, continue radially outward along the ground. A portion of the vorticity, however, will be inboard of the stagnation point on the ground and will flow radially inward instead. The viscous shearing and turbulent mixing actions undoubtedly play an important part in this aspect of the flow, but will be nearly impossible to predict. That part of the vorticity that is directed inward will converge at the axis of rotation and will then flow vertically upward. Because of the convergence, a strong concentrated vortex can thus appear at the center of rotation; this is evidently the origin of the negative pressures noted in Figure 10. At the top of the upwash region, this vortex could either diverge in an axially symmetric pattern to recirculate in approximately the original path, or under some circumstances could conceivably remain concentrated as shown and be carried away in some nonsymmetrical manner by the main downwash stream. It is believed that the long-period flow instability reported in reference 8 for a rotor near the ground may be such a manifestation. This periodic instability consisted of a large vortex apparently originating near the center of rotation which then passed downwash and outward through the main downwash flow. This instability was found to exist only when the rotor was very close to the ground, just as the negative ground pressures measured on the axis of rotation were found only when the rotor was close to the ground.

This central vortex which has been shown to exist under a rotor under some conditions could have a counterpart in an annular jet ground effect machine. Because of jet mixing, there will be a circulatory flow beneath the machine as described in reference 9. This flow is qualitatively similar to the flow beneath a rotor in ground effect, and if any rotation is imparted to this flow, a vortex system is likely to develop. Since the annular jet can only sustain a given pressure differential for a given height, a vortex extending from the ground to the bottom of the machine, with the associated severe drop in local pressure, will necessarily reduce the lift augmentation ratio. In reference 6, as mentioned previously, it was reported that a rather severe drop in augmentation ratio occurred for an annular jet model at low forward speeds. It is probable that the external distribution caused by the forward speed distorts the inner recirculatory flow into a non-axially-symmetric pattern, and it is possible that vortices, most likely in pairs, may be responsible for this loss.

EFFECT OF SURFACE AREA BELOW THE ROTOR

As part of a general study of the ground effect of rotors, tests were conducted with the model rotor previously described to determine the vertical drag characteristics of various simple body shapes located in the downwash stream. Since any downward force exerted by the slipstream on the helicopter body will detract from the payload capability an understanding of the basic nature of this phenomenon is of considerable importance. Test results for two of these models, flat disks with diameters of 40 and 60 per cent

of the rotor diameter, are presented in Figure 12 in the form of vertical drag versus height-radius ratio. The disks in this case were located one-third rotor radius below the rotor. Note that there are two curves for each disk model. The upper curve represents the actual downward force measured on the model in per cent of the rotor thrust measured simultaneously. This is not the significant result in terms of performance, however, since the disk induces a favorable "ground effect" on the rotor, so that rotor thrust is increased for a given power. The lower curve presents the net or "effective" vertical drag, that is, the net reduction in lifting ability for a given power expressed in per cent of rotor thrust measured without the disk. The effective vertical drag may be seen to be substantially lower than the vertical force on the disk for most test conditions, particularly when far from the ground. This result was also found to be true for most of the other models tested.

This "built-in" ground effect cannot, of course, be used to improve the hovering performance of a helicopter away from the ground, since the lift is produced solely by imparting downward momentum to the air, and anything which impedes the slipstream is certain to have an adverse effect. This conclusion, however, does not hold true for the helicopter in ground effect; at a rotor height of one-half radius from the ground, both the 40 and 60 per cent disk models had negative vertical drags on the order of 5 per cent of the rotor thrust, due to actual uploads on the disks. This favorable effect increases the benefit that the rotor already receives from ground proximity.

Surface pressures were measured on the 60 per cent disk model and are presented in Figure 13 in the form of local pressure divided by rotor disk loading. As the height above the ground is reduced, pressures on the top surface remain more or less constant, but the lower surface pressures increase from negative values out of ground effect to positive values approaching the rotor disk loading at a height-radius ratio of 0.5, and it is this increase in lower surface pressure that accounts for the upward vertical force on the disk. Integration of the pressure differential between the two surfaces of the disk give results which are in good agreement with the measured vertical force. At a height-radius ratio of 0.5, the pressure distribution on the upper surface suggests that a center vortex, as described in a previous section, has formed above the disk. There is no clear indication that a similar vortex exists below the disk; however, measurements at the center of the lower surface were not possible because of the mounting details of the model, and a lower center vortex might very well form under some circumstances.

COMPARISON OF THE HELICOPTER WITH THE GROUND EFFECT MACHINE (GEM)

Consideration of "ground effect" machines has been restricted to the peripheral jet configuration in this analysis, since this type promises greater lifting efficiency for given height above the ground than any other type of "airborne" ground effect vehicle receiving current attention. Because of its relative ability to rise above in its path, this configuration appears to be the most competitive with the helicopter.

Relative augmentation ratios of the helicopter and the peripheral jet GEM have been discussed briefly in a preceding section, and there is no question that the latter type of machine can develop substantially higher values of this parameter. Augmentation ratio, however, is but one of many factors to be considered. Lift produced per unit power is much closer to being a reasonable criterion of merit than augmentation ratio, and is the factor most frequently cited in favor of the ground effect machine, but this also has little meaning by itself, since a large lift per unit power is useless if the machine weight still exceeds total lift. A proper theoretical performance comparison must also include consideration of lift per unit area and an estimate of the likely relative values for the two types of machine.

Calculation of the theoretical hovering performance of annular jet ground effect machines was based on the equations developed in reference 10. A vertical jet was assumed, partly for simplicity, although it is realized that a higher theoretical performance is attainable by the use of inward-directed jets. However, the error resulting from the use of this assumption will tend to compensate for the duct losses involved in the real case and the fact that practical ground effect machines will most likely have non-circular shapes and will therefore have lower hovering efficiencies than the ideal values for circular planforms. At best, the comparisons between the helicopter and the peripheral jet machine will be qualitative in nature because of many current unknowns with regard to the latter. The hovering performance of the two types are compared on a theoretical basis without regard to such power consuming items as torque compensation on the helicopter, or forward propulsion and control requirements on the ground effect machine.

The following equations summarize the basic relations involved in the calculation of disk loading and power loading, and are based on simple momentum considerations:

Ground Effect Machine (ducted jet)

$$\frac{W}{\pi R_o^2} = \rho v_j^2 \left(\frac{A_j}{\pi R_o^2} \right) A, \quad \frac{W}{HP} = \frac{1100}{v_j} A$$

Helicopter (unducted rotor)

$$\frac{W}{\pi R^2} = 2 \rho v_o^2 \left(\frac{T}{T_\infty} \right), \quad \frac{W}{HP} = \frac{550}{v_o} \left(\frac{T}{T_\infty} \right)$$

The theoretical hovering performance of the GEM is presented in Figure 14 for height radius ratios of 0.25, 0.10, and 0.05. Power loading in pounds per horsepower is plotted against "disk loading" which is meant to represent gross weight divided by total planform area. Other variables considered are the jet velocity and the thickness of the jet. Several important characteristics may be noted by an examination of these charts. First, the thinnest jets (small t/R) have the highest augmentation ratios and, for any given jet velocity, the highest lift per unit power. It is readily apparent from the charts, however, that this provides about the worst overall performance. For a given disk loading, improved performance is obtained by increasing the jet thickness and reducing the jet velocity, or, for a given velocity, increasing the jet thickness will increase the disk loading from an impractically low value to a usable one. In either case, the same optimum geometry will result, giving the maximum power loading for the disk loading involved. The optimum jet thickness appears to be somewhere between one-quarter and one-half of the height off the ground for the three heights considered.

One of the most important aspects revealed by the charts is the fundamental effect of disk loading, which applies to the ground effect machine in exactly the same manner as it does to the helicopter. For any given geometry, the power loading is inversely proportional to the square root of the disk loading, so that these constant geometry lines all have a slope of minus one-half on the logarithmic plot.

Also shown on Figure 14 is the ideal theoretical performance of the hovering rotor for operation out of ground effect, and also for operation in approximate maximum practical ground effect (height-radius ratio 0.5, $T/T_\infty = 1.3$). In Figure 14(a), for an annular jet machine height-diameter ratio of 0.25, comparison of the two types of machines shows that the helicopter in ground effect has superior theoretical performance for a given disk

loading, while the helicopter out of ground effect has inferior performance to the optimum GEM. A most important point to consider, however, is that the two types of machines unquestionably will not have the same disk loading for the same gross weight. The helicopter rotor disk is mostly air, and therefore very light for its diameter, whereas the GEM must utilize a solid surface to obtain its pressure lift. Forward speed considerations will also tend to dictate low frontal area for minimum propulsion power, with a resultant tendency toward high area loadings. In general, it is believed that the GEM will have on the order of four times the disk loading of a helicopter for the same gross weight. As an example, the Sikorsky S-55 helicopter has a normal gross weight of 7200 pounds and a disk loading at that weight of 3.25 lbs/ft^2. At the same gross weight the Saunders Roe SR-N1 Hovercraft discussed by its inventor in reference 11 has an average area loading of about 12 lbs/ft^2, nearly four times as high.

When this difference of disk loadings is taken into account, the helicopter immediately becomes more attractive relative to the GEM. To illustrate this effect, circles have been placed on the charts at a representative helicopter disk loading, 5 lbs/ft^2, for the helicopter in and out of ground effect, and at a disk loading of 20 lbs/ft^2 for the optimum GEM. For the GEM height-diameter ratio of 0.25 (Figure 14), the helicopter has superior hovering performance in or out of ground effect. At a GEM height of 0.1 diameter (Figure 14), the GEM has superior performance to the helicopter out of ground effect, but still inferior to the helicopter making full use of its ground effect (it must be remembered that the helicopter thus overloaded can still fly out of ground effect at forward speed). At a GEM height-diameter ratio of 0.05 (Figure 14), the optimum GEM has theoretical hovering performance superior to the helicopter in or out of ground effect, although the power loading is only about one-third higher than the helicopter in ground effect.

If 5 ft is considered a useful minimum height for clearing fences, hedges, or other obstacles, a height-diameter ratio of .05 requires a 100 ft diameter machine, and the use of such a machine over land would be restricted to very flat areas where trees, telephone poles, houses, or other tall obstacles are no closer to each other than 100 ft. For diameters of 50 ft or less, the helicopter in ground effect will have better performance than the GEM, and does not have the restriction of staying close to the ground. A GEM with a diameter of 20 ft operating at a height of 5 ft sounds like a compact and desirable utility-reconnaissance vehicle, but the helicopter will out-perform it in every respect, having better hovering performance, high speed due to lower parasite drag and higher propulsive efficiency, better maneuverability (a lateral acceleration of 1 g. in forward flight in accomplished by the simple expedient of a 45-degree bank, whereas a GEM would require auxiliary thrust equal to the gross weight), and precise control in all regimes of flight. The overwhelming advantage of the helicopter, of course, is that it can free itself completely of the ground and thus serve an unlimited variety of purposes.

For very large machines operating very close to the surface, probably water in most practical cases, the ground effect machine may very well be able to perform missions for which the the helicopter is not competitive. References 11 and 12 concur that the GEM may be practical only in very large sizes. Even in large sizes, however, the GEM designer may be faced with difficulty obtaining satsifactorily low area loading, because of the "square-cube" tendency for area loading to increase directly with weight, and the large machines may be too heavy to "fly" economically.

CONCLUDING REMARKS

It has been shown that the helicopter can derive substantial benefit from ground effect, including an increased payload when the other performance penalties are not objectionable. The benefits of ground effect will apply particularly to large size machines. The helicopter, moreover, retains in all cases the capability of operating out of ground

effect in forward flight, an advantage not shared with the peripheral jet ground effect machine. Moreover, a performance comparison of the two types of machine indicates that the ground effect vehicle cannot compete with the helicopter in the missions that the latter performs routinely, and that use of the ground effect vehicle will probably be confined to very specialized applications where the inferior capability is a secondary consideration, or to extremely large machines over water.

REFERENCES

1. Knight, M., and Hefner, R. A., "Analysis of Ground Effect on the Lifting Airscrews." NACA TN 835, December, 1941.

2. Heyson, H. H., "An Evaluation of Linearized Vortex Theory as Applied to Single and Multiple Rotors Hovering In and Out of Ground Effect." NASA TN D-43, September, 1959.

3. Fradenburgh, E. A., "Flow Field Measurements for a Hovering Rotor Near the Ground." Paper presented before the American Helicopter Society Fifth Annual Western Forum, Los Angeles, California, September 25-26, 1958.

4. Chaplin, H. R., "Theory of the Annular Nozzle in Proximity to the Ground." David Taylor Model Basin Aero Rept. 932, July, 1957.

5. Cheeseman, I. C., and Bennett, N. E., "The Effect of the Ground on a Helicopter Rotor in Forward Flight." Aeroplane and Armanent Experimental Establishment Rept. AAEE/RES/288, July, 1955.

6. Tinajero, A. A., "Comparison of Experimental and Theoretical Design Parameters of a 6-Inch-Diameter Annular Jet Model with a Jet Angle of -45° Hovering in Proximity to the Ground; and Experimental Results for Forward Flight at Zero Angle of Attack." David Taylor Model Basin Aero Rept. 954, May, 1959.

7. Von Glahn, V. H., "Exploratory Study of Ground Proximity Effects on Thrust of Annular and Circular Nozzles." NACA TN 3982, April, 1957.

8. Taylor, M. K., "A Balsa-Dust Technique for Air-Flow Visualization and Its Application to Flow Through Model Helicopter Rotors in Static Thrust." NACA TN 2220, November, 1950.

9. Chaplin, H. R., "Effect of Jet Mixing on the Annular Jet." David Taylor Model Basin Aero Rept. 953, February, 1959.

10. Pinnes, R. W., "A Power Plant Man's Look at the Ground Effect Machine." Journal American Helicopter Society, Vol. 4 (3), July, 1959.

11. Cockerell, C. S., "The Hovercraft." Flight Magazine, September 11, 1959.

12. Chaplin, H., and Stephenson, B., "Preliminary Study of the Hovering Performance of Annular Jet Vehicles in Proximity to the Ground." David Taylor Model Basin Aero Rept. 947, August, 1958.

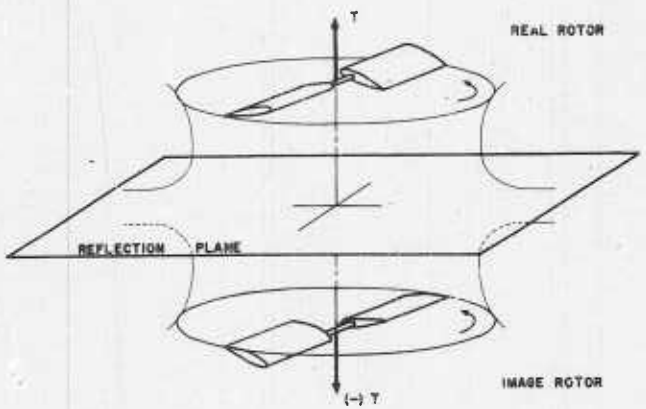

Figure 1. Image system representation of ground

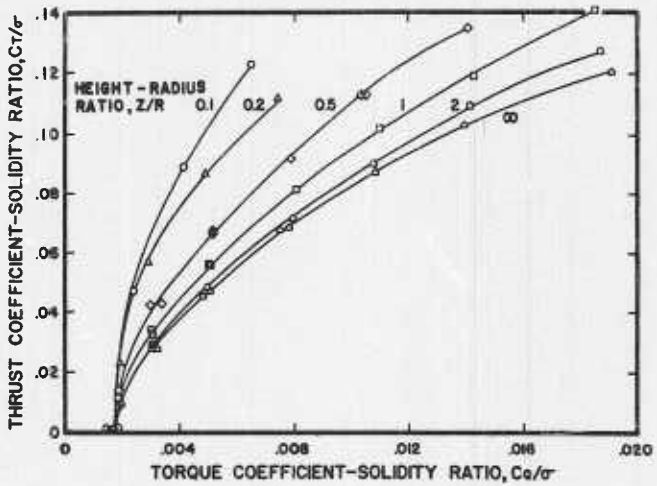

Figure 2. Hovering performance in ground effect-model test results

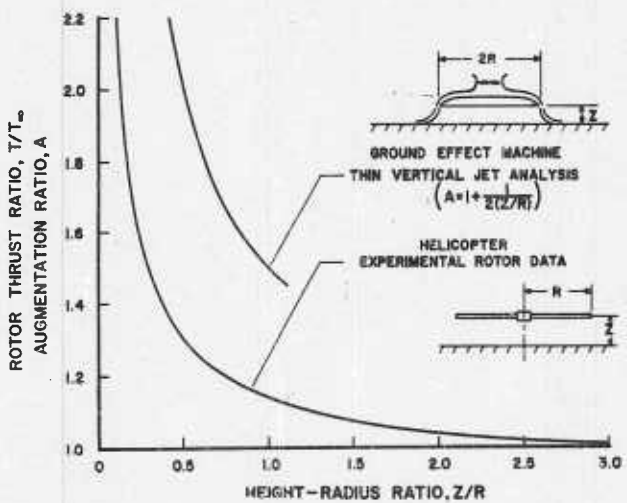

Figure 3. Effect of height on rotor thrust ratio and ground effect machine augmentation ratio

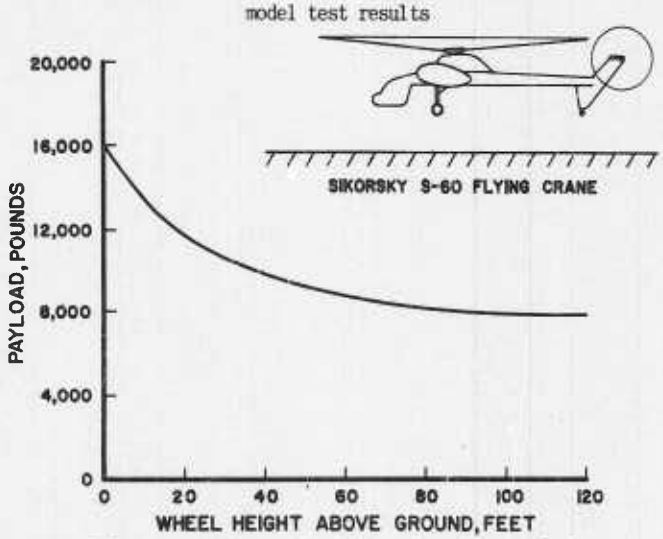

Figure 4. Effect of height on hovering payload of S-60 helicopter

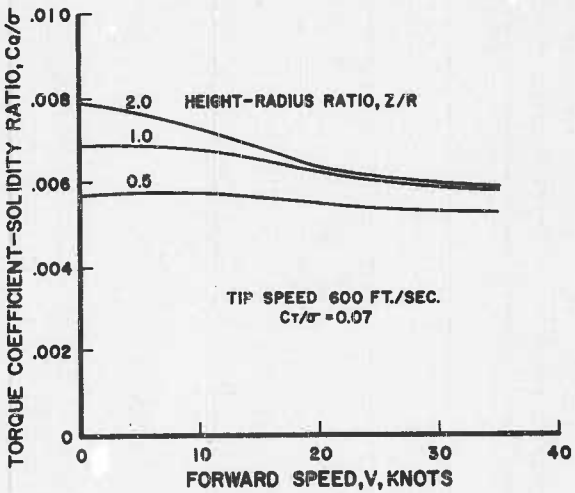

Figure 5. Effect of forward speed on rotor power-model test results

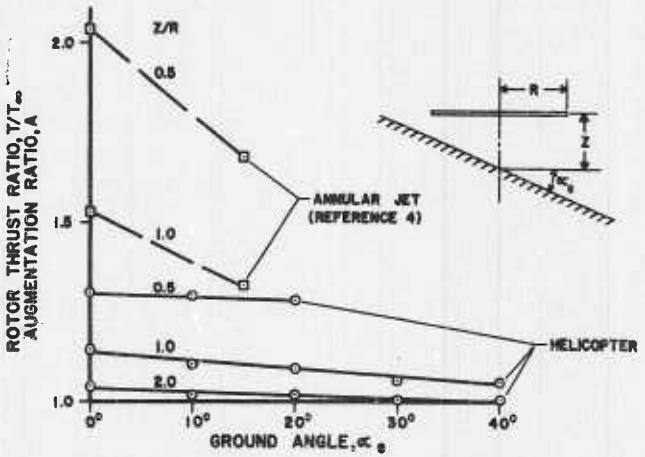

Figure 6. Influence of ground angle on hovering performance

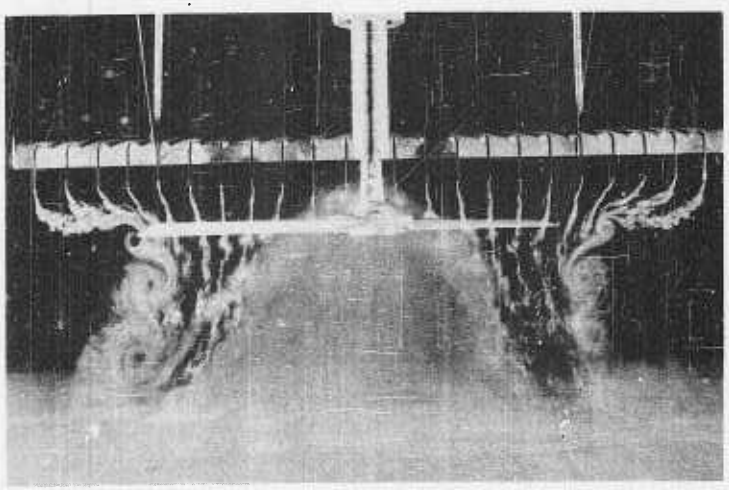

Figure 7.

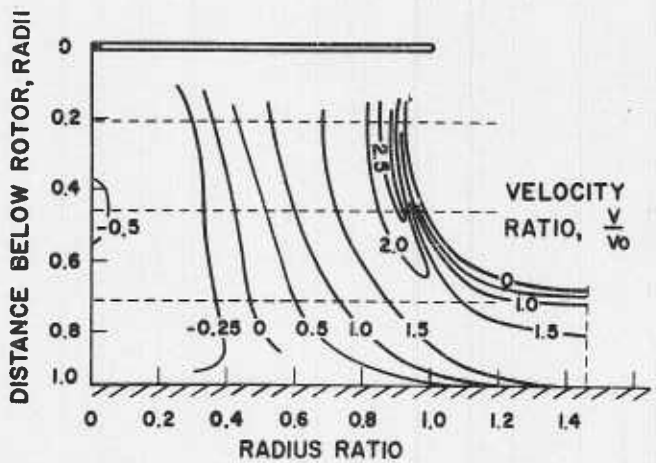

Figure 8. Velocity contour map for model rotor 1.0 radius above ground

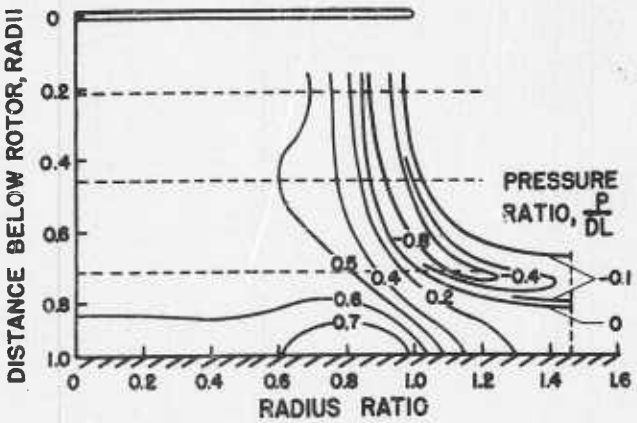

Figure 9. Static pressure contour map for model rotor 1.0 radius above ground

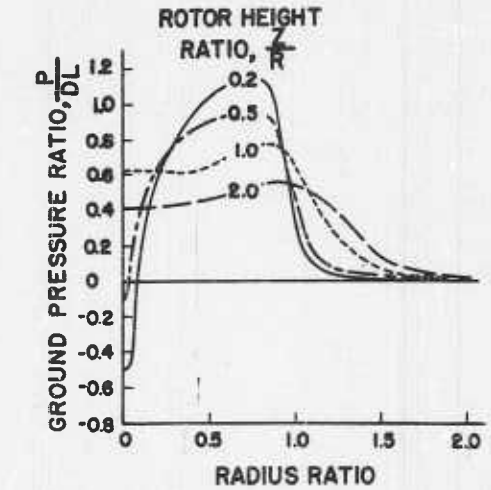

Figure 10. Ground static pressures

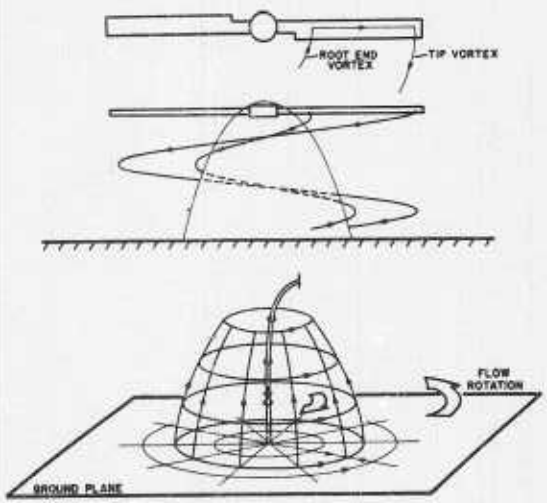

Figure 11. Inboard vortex system

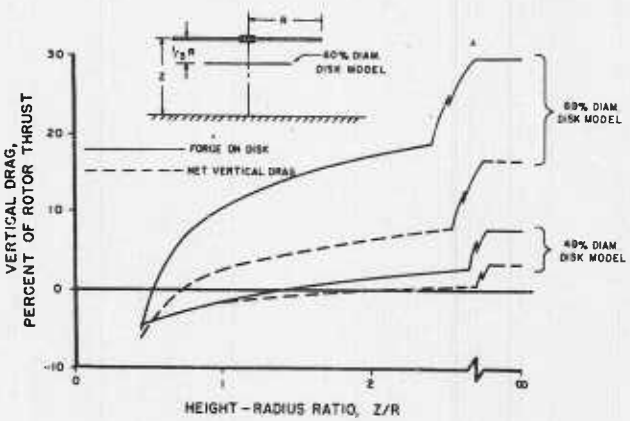

Figure 12. Effect of height on vertical drag of two disk models

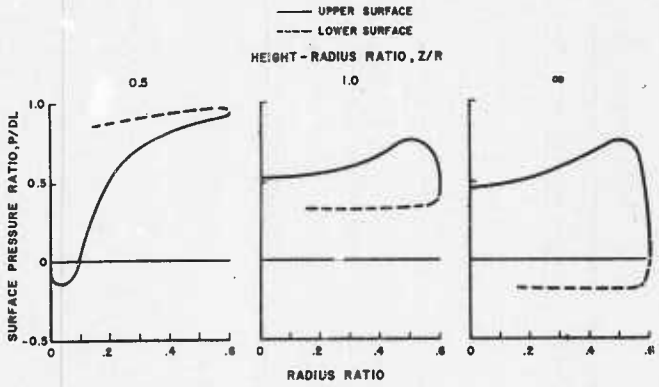

Figure 13. Measured surface pressures on 60 per cent diameter disk model

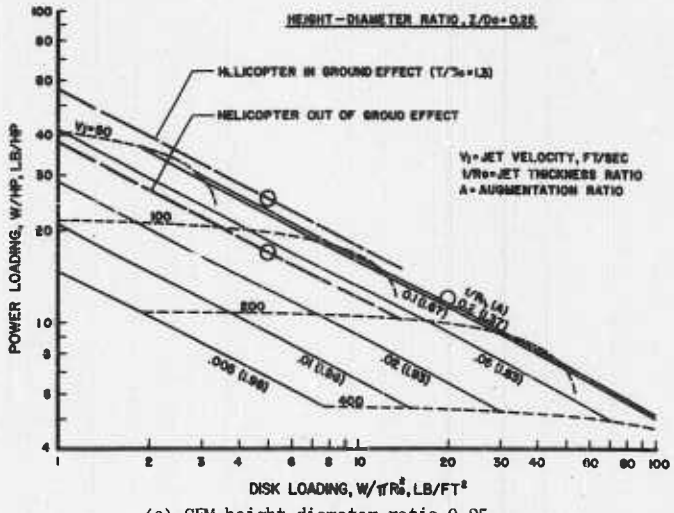

(a) GEM height-diameter ratio 0.25

Figure 14. Ideal hovering performance chart for vertical annular jet ground effect machines at sea level and comparison with the helicopter

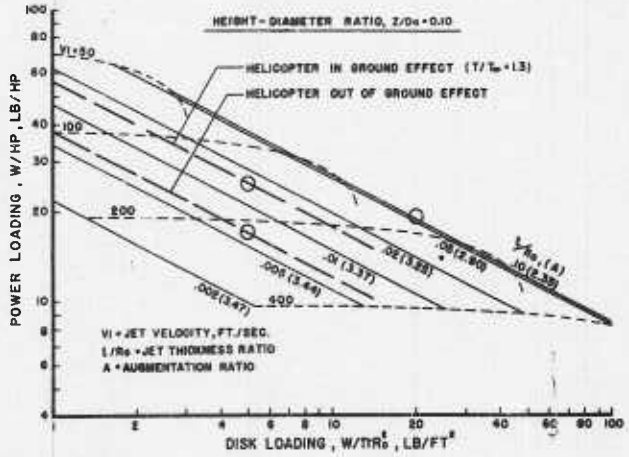

Figure 14. (continued). (b) GEM height-diameter ratio 0.10

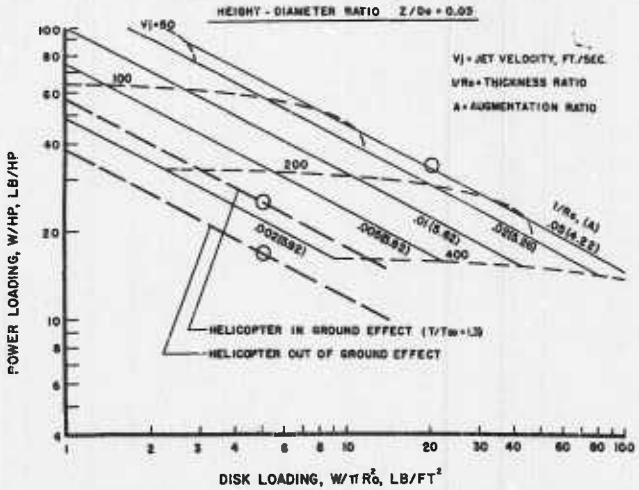

Figure 14. (concluded). (c) GEM height diameter ratio 0.05

SOME TESTS OF A 7-FOOT GEM DYNAMIC MODEL OVER UNEVEN SURFACES

By J. Norman Fresh, Aerodynamics Laboratory,
David Taylor Model Basin, Washington, D. C.

SUMMARY

Tests are being made over uneven surfaces using a 7-ft dynamic GEM model. The surface is represented by sine-wave contours of various wave lengths. Preliminary date, presented in nondimensional form, indicate that a "critical speed" may be encountered which will result in collision with the surface. Depending on the size and speed of the vehicle, however, this may not be a dangerous problem.

INTRODUCTION

Shortly after the early theoretical and experimental work on ground effect machines (GEM) was done at the aerodynamics Laboratory, many questions arose on the practical aspects of such a vehicle.

1. How well will it fly?
2. What kind of stability does it have?
3. What is the best way to control it?
4. What sort of terrain or waves can it traverse?
5. What will its resulting motion be?

The answers to some of these questions can be determined by static models, while the others can be learned more quickly by dynamic models or prototype machines. Consequently, any laboratory test information that would shed light on dynamic behavior was desired. A simplified machine, powered by an induction air system, was designed and constructed to obtain dynamic information over various types of terrain. It is expected that the tests will be completed early in November 1959 and a report will be published, presenting all of the data obtained.

MODEL

Procurement of the power plant and fan normally require considerable lead time, so an alternative powering arrangement was suggested using the available compressed air from the house line. The model, shown in Figure 1, was thus designed using this source of powering. The available compressed air supply consisted of a maximum flow of two lbs/sec at a pressure of 120 lbs/in.^{2}. To most effectively use this quantity of air it was decided to build an induction system. The air was fed into a manifold and then distributed to a bank of four injector nozzles on either side of the vehicle. The nozzles discharged into individual ducts, as shown in Figure 1, inducing an additional 18 lbs of air per second for a total of 20 lbs/sec. The racy rake of the duct system was more functional than esthetic. It was desired to keep the center of gravity as low as possible. Slanting the ducts gave the required mixing length while reducing the height. The curved portion at the bottom of the ducts provided some diffusion before the air entered the plenum chamber. The plenum chamber fed both the peripheral primary jet and the stabilizing secondary jets. The primary peripheral jet had a slot width of about 1 1/4 inches and the secondary or stabilizing jets were about 1/2 inch wide. Control vanes were located in the jet along the

straight sides. They permitted forward or backward flight by simultaneous deflection and turning by differential deflection.

It was recognized that this was not a very efficient method of powering. However, it did permit design and construction of an operating model in about three weeks.

Control of the air supply was achieved through a quick-opening valve. A small booster nozzle was added to produce direct thrust for acceleration in unfavorable winds. Fore and aft adjustments for center-of-gravity shift were made by sliding a weight. The total weight of the vehicle equipped for manned flight was about 180 lbs.

TEST APPARATUS

A test track 46 ft in outside diameter and 34 ft inside diameter was built (see Figure 2). A level concrete track was laid covering 270° of the circle. The remaining 90° segment was used for simulating various waves or step functions. Compressed air was brought up through a vertical pipe, which also served as a pylon about which the machine rotated. Flexible plastic tubing carried the air into the manifold on the model. It may be noted that two tubes were used. This was merely a convenience, since a larger line was not easily available and two were required to handle the mass flow.

Data were recorded by a motion picture camera, which was mounted over the center of rotation. The main support member was a light aluminum tube, Figure 3, attached to the pylon through a self-aligning ball bearing and to the model by a wishbone arrangement. Roll from centrifugal forces was prevented by two small aluminum tubes at the top. The system permitted freedom to pitch with little torsional restraint.

Two targets were mounted on the centerline of the machine for measuring the motions. A background reference grid was established for determining model measurements. The grid extended around nearly one-third of the track overlapping the 90° test portion at both start and finish. This permitted the recording of beginning and ending conditions. A single horizontal reference line was used for reading displacements, as shown by the targets. The vertical lines were projected back from the target plane to represent 1-ft intervals. With the timing marks on the film, it was thus easy to determine both distance and velocity.

The lower part of the grid supports was later covered with a burlap screen to prevent unfavorable winds from influencing the action of the model.

Construction of the test portion of the track was rather unique. The surface had to be relatively smooth, hard enough to support the air pressure without eroding, inexpensive, and capable of easy change. Templates representing the test surface were made for the inner and outer arcs using radially located stations. Wet sand was then lightly tamped and screeded to follow the contours, Figure 3. After this was completed, cement was sifted over the sand and the moisture from the wet sand was drawn up sufficiently to set the cement, forming a thin crust. The crust was strong enough for the purpose but could not stand concentrated loads or sharp blows. Puncturing and raking was an easy task to remove the crust for the next contour.

TEST RESULTS

Sine-wave forms were used to simulate uneven surfaces. The length of the wave was computed to give full waves within the 90° test portion of the track.

Tests have already been completed for 2, 4, and 8 waves with amplitudes of ±1 and ±2 inches. A range of air pressures and forward velocities were included for each

surface configuration. Step functions both up and down in 1-inch increments are planned. The test results have not all been reduced, but they are sufficient to indicate trends. Typical data and cross plots are given in Figures 4 and 5.

SPRING-SUSPENSION ANALOGY

A GEM flying over an uneven surface is considered analogous to a spring-mass system with displacement excitation. This same analogy is sometimes applied to spring-suspended wheeled vehicles. For the GEM, the "spring constant" (i. e., the resilience of the ground cushion) is nonlinear. For small disturbances, the local gradient of the lift versus height, and curves may be used for a linearized spring constant.

Natural frequencies. Pure heave mode:

$$L = W \frac{h_o}{h} \qquad \text{where } h_o \text{ is equilibrium altitude}$$

$$\Delta L = L - W = W \left(\frac{h_o}{h_o + \Delta h} - 1 \right)$$

$$= W \frac{\Delta h}{h_o}$$

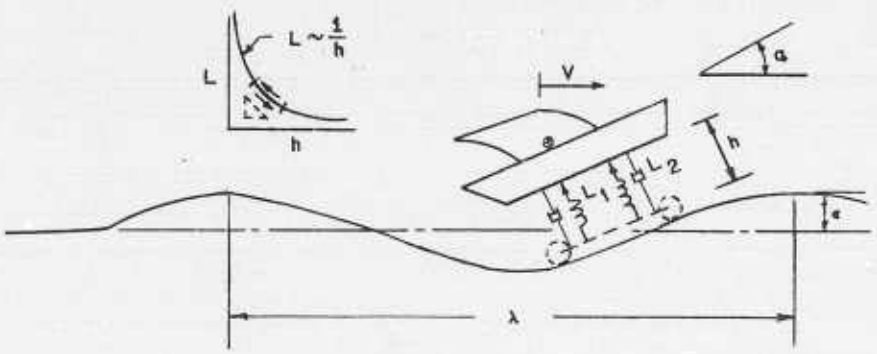

Spring-suspension analogy.

Heave "spring constant"

$$k_h = \frac{\Delta L}{\Delta h} = \frac{W}{h_o}$$

Natural frequency of heave

$$\omega_{n_h} = \sqrt{\frac{k_n}{m}} = \sqrt{\frac{W/h_o}{W/g}} = \sqrt{\frac{g}{h_o}}$$

Pure pitch mode: For GEM's with compartmenting secondary nozzles, experiments have shown the pitch "spring constant" is approximately of the form

$$k_a = \frac{B}{h_o}$$

(where the quantity B depends on planform and arrangement of secondary slots)

$$\omega_{n_a} = \sqrt{\frac{k_a}{I}} = \sqrt{\frac{B/h_o}{\frac{W}{g}\bar{r}^2}} = C\sqrt{\frac{g}{h_o}}$$

where $C = \sqrt{\frac{B}{W\bar{r}^2}}$ = constant

Disturbance frequency.

$$\omega = \frac{2\pi}{\lambda}V$$

The theoretical natural frequency for heave is exactly $\sqrt{g/h_o}$; the natural frequency for pitch is proportional to $\sqrt{g/h_o}$. If we plot (amplitude of response) ÷ (amplitude of disturbance) versus (frequency of disturbance) ÷ $\sqrt{g/h_o}$, we may hope to get a systematic family of curves, independent of model scale, just as we do in the case of a spring-mass system.

DISCUSSION

Prior to controlled testing, the 7-ft GEM was flown and demonstrated a number of times in the manned configuration shown in Figure 6. Although flight was limited by the restraining cable during this period, control and maneuvering was easily learned.

The GEM stability problem is twofold:

1. How does one design stability into a vehicle? (or how does one predict the stability derivatives of a particular configuration?)

2. How stable does a vehicle have to be in order to fly safely under practical conditions?

The latter question can only be answered by dynamic model tests under carefully scaled conditions. Such tests are expensive and time-consuming. Before we get into such a program, we would want to have a good idea of what kind of vehicle we should try to simulate.

Meanwhile, the 7-ft GEM is giving us some preliminary data. We might call these tests "quasi-dynamic tests." The inertial effects and the static stability characteristics of the ground cushion are properly scaled; that is, properly scaled to a prototype of the same design. We don't know how to scale to a prototype of practical design until we know what a practical design is. All external aerodynamic effects (and, possibly, the damping

characteristics of the ground cushion) are out of scale. Even so, we expect that the model behavior is similar to the behavior that a scaled-up prototype would have at high gross lift coefficients (say $C_L > 2$), flying over the same (scaled-up) terrain.

For a linear system, the frequency ratio completely determines the steady state motion of a particular physical arrangement. Our nonlinear GEM can be expected to exhibit some additional effects of:

1. Amplitude - since the nonlinearity is more important with large amplitude motion.
2. Wave length - when the wave length is very long, the GEM "sees" the surface as a flat surface of gradually changing slope and height. When the wave length is very short, the GEM "sees" a "wiggly" surface, which it cannot follow exactly regardless of the frequency ratio.

Figure 4 shows typical data for an eight-wave surface configuration with an amplitude of ±2 inches. All test conditions were the same for both sets of data except for forward velocity. The low speed data show how the vehicle tries to follow the wave pattern. Its amplitude of oscillation is diverging and would, if continued, result in collision with the surface. The forward velocity is near the "critical speed." The high speed data show a much reduced height change and small oscillations which do not follow the surface. In fact, movies which were made of these test conditions very clearly showed the model reactions. At the higher forward speeds the model hardly knows the waves exist and there is little perceptible motion as it skims across them.

Cross-plotted data of amplitude ratio versus frequency ratio are given in Figure 5. The peaks of the curves are not well defined becuase of actual collision with the surface. However, there is a definite trend that indicates, on the basis of these preliminary data, that there is a "critical speed" which may be encountered. The critical speed is defined as the speed at which the pitching amplitude of the vehicle increases until collision with the surface results. The situation is not entirely gloomy, since some vehicles with low forward velocities may never reach the critical speed. For example, consider a vehicle 30 ft long flying 2 ft high at a velocity of about 20 ft/sec over a sea state of 2. This condition has waves about 2 to 3 ft high and 50 ft long. The ratio of vehicle length to wave length, b/λ, would be 0.6 and the frequency ratio would be about 0.6, thus placing it in the critical speed region. Assuming that the machine was power limited, reducing the speed or height or both would permit operation in a safe area.

For large machines, where the ratio of b/λ becomes large, the effect of the waves is reduced, as shown by the lower curve. If the vehicle has sufficient acceleration, it may pass through the critical region with no danger.

No data have been reduced for the step input tests so it is not known whether other critical conditions may develop. A report will be issued soon giving the complete results of the tests with a more complete analysis of the data.

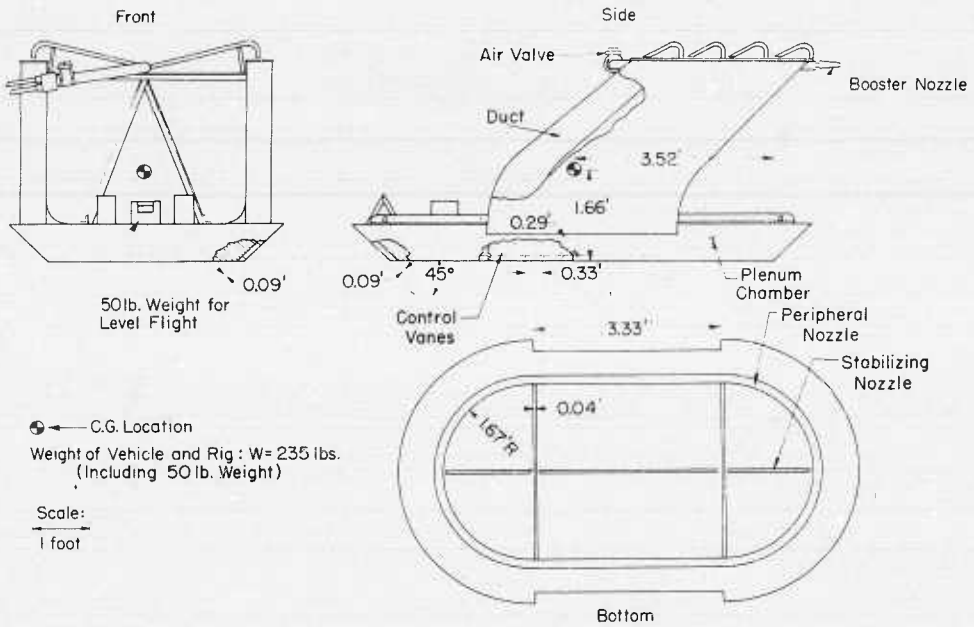

Figure 1. Sketch of a GEM quasi-dynamic model

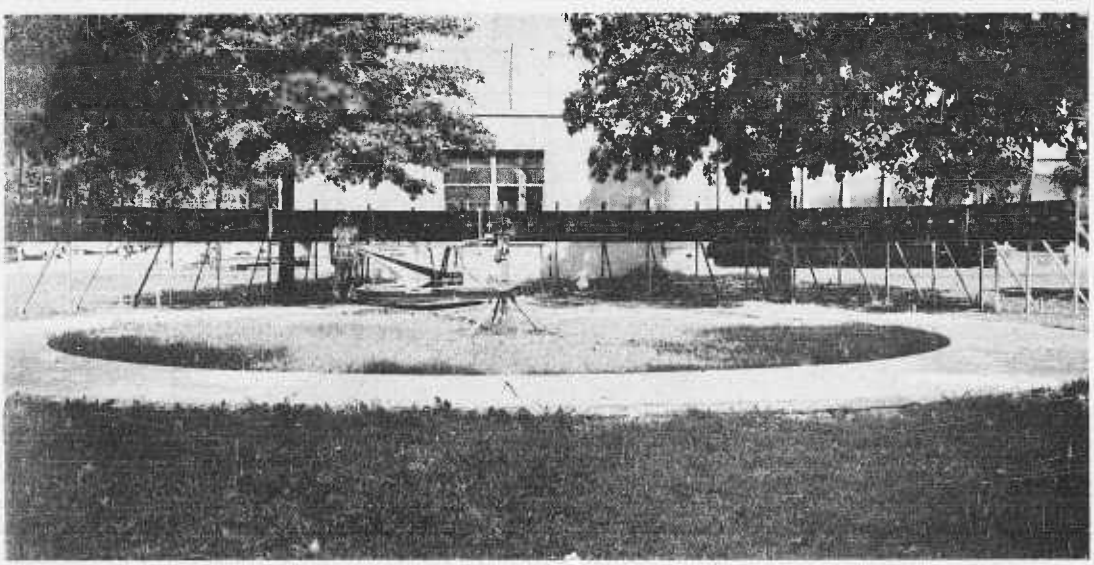

Figure 2. Test track and model setup for 7-foot dynamic GEM tests

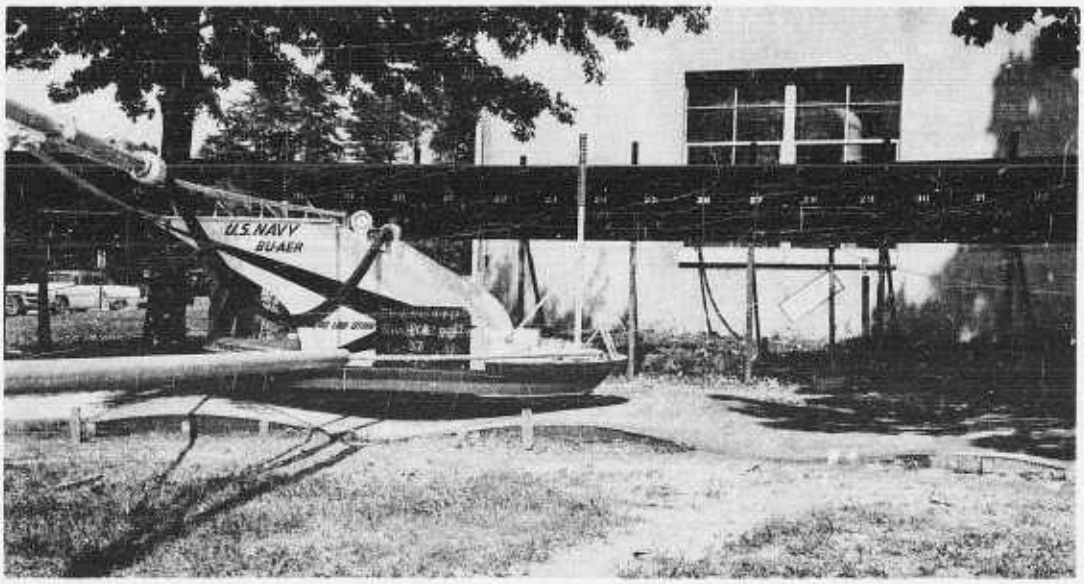

Figure 3. 7-foot dynamic GEM model hovering over test track (Reference targets and grid are shown.)

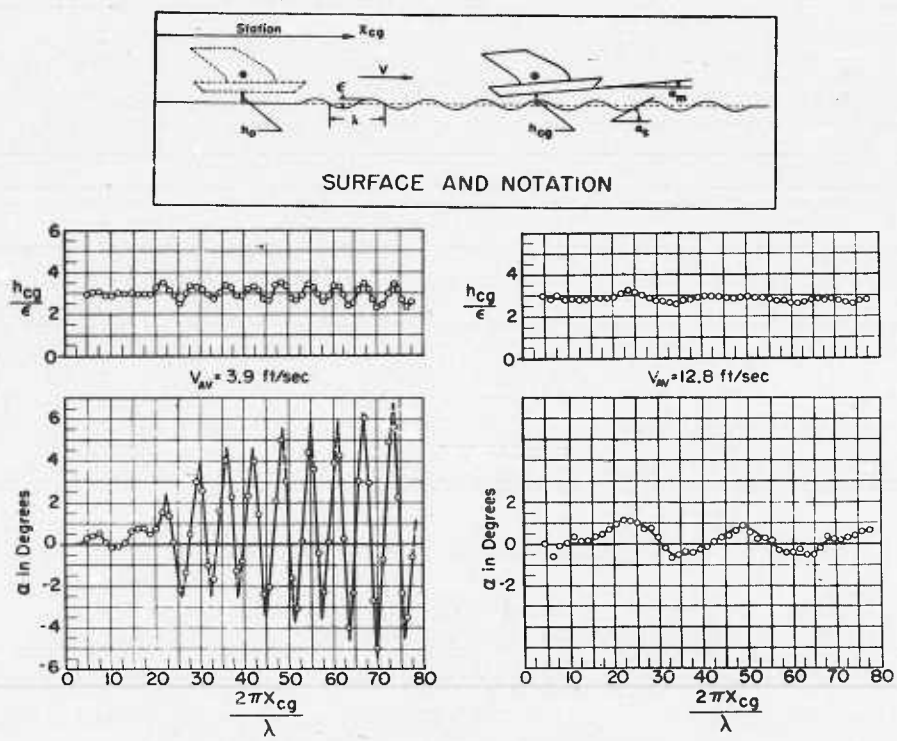

Figure 4. Typical data for 7-foot dynamic GEM model

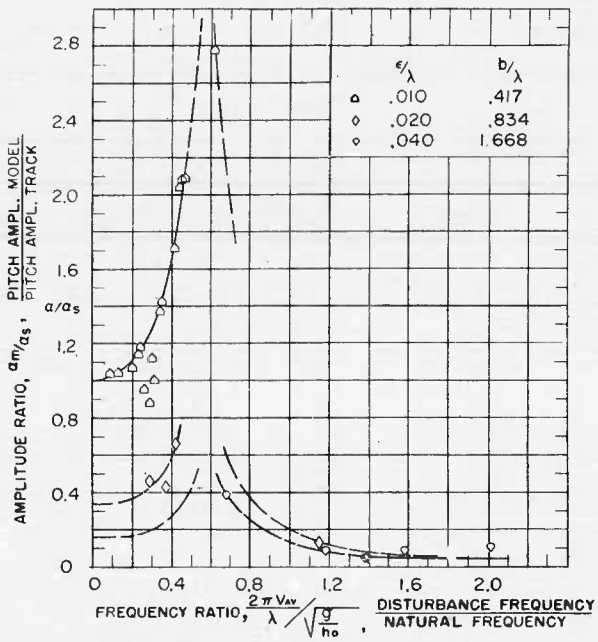

Figure 5. Effect of velocity on pitching for a 7-foot dynamic GEM model over a sine wave surface

Figure 6. 7-foot dynamic GEM model as equipped for manned flight

EFFECT OF VEHICLE PLANFORM ON AUGMENTATION

By Anibal A. Tinajero, Aerodynamics Laboratory, David Taylor Model Basin, Washington, D. C.

SUMMARY

The currently available test results pertinent to the planform effect on augmentation parameter of peripheral jet ground effect machines (GEM's) are briefly summarized. The results suggest that for planforms with circular ends and with an "integrated-system" (lift and propulsive forward thrust obtained from the same jet momentum) the percentage loss in augmentation decreases as the length to width ratio of vehicle increases.

For the hovering condition (no thrust obtained by deflection of air flow at nozzle), the augmentation obtained for a given value of ground proximity parameter is independent of model length to width ratio (augmentation is the same regardless of planform).

Symbols

S reference area in ft^2 (plan area enclosed by outer edge of nozzle exit)

S_b base area in ft^2 (plan area enclosed by center line of nozzle exit)

h altitude in ft measured from the surface to the lower edge of the nozzle exit

G nozzle width in ft

C perimeter in ft measured at the nozzle center line in the nozzle exit (the nozzle exit is taken normal to the jet discharge direction; see Figure 3)

C_{min} the perimeter that a circle having an area S_b would enclose

$$C_{min} = C\left[\frac{\sqrt{\pi^2 + 4\pi\left(\frac{b}{a} - 1\right)}}{\pi + 2\left(\frac{b}{a} - 1\right)}\right]$$

Θ normal jet discharge angle in degrees measured from vertical at the nozzle exit; negative for an inward inclined jet (see Figure 3)

β tangential jet deflection angle in degrees (see Figure 3)

J scalar total peripheral jet momentum flux in lbs

L total lift in lbs

T propulsive thrust in lbs (parallel to base line and vehicle center line)

A augmentation ratio; the ratio of total lift to total jet momentum

$$A = \frac{L}{J}$$

T/J propulsive thrust ratio

INTRODUCTION

The David Taylor Model Basin ground cushion research program was expanded to include development of practical aerodynamic information pertaining to the design of peripheral jet, ground effect machines (GEM's). With the above task in mind, a preliminary investigation of the effect of vehicle planform on augmentation parameter was undertaken.

The present paper attempts to summarize the results obtained. Detailed description of the experiments and findings are largely omitted; these will be formally presented in a DTMB report to be published soon.

MODELS AND APPARATUS

Models and apparatus used to investigate these parameters were simple and rather unconventional to allow for the many adjustments and configuration changes required.

Description of models

Planforms. Four basic planforms were tested to evaluate the relative merits of planform configuration for GEM's. A sketch of the planforms is shown in Figure 1. All the planforms had a 1-inch-diameter hole at the center, which was required for installation of the ground board and model to the test stand.

Nozzles. A sketch of a typical nozzle is shown in Figure 2. Forty-two nozzles were utilized for the hovering tests (zero propulsive thrust). The number of nozzles utilized for other configurations varied according to the propulsive thrust desired. This decrease in number of nozzles was due to spacing difficulty caused by the deflection of the nozzles, to the desired tangential jet deflection angle β (see Figure 3). Calibration of the nozzles was done by blasting the air of each nozzle over a modified chemical-type balance. The results were in close agreement with the momentum theory.

Description of test facility

Test stand. A static test stand shown in Figure 4 was used to support the models, and to obtain the lift and propulsive thrust measurements. The "thrust table" had flexible supports in the thrust direction, and an air supply pipe installed through the top. The air supply pipe had a gap that permitted the "thrust table" to deflect in the thrust direction, causing only a very small loss of pressurized air.

Instrumentation. The propulsive thrust was measured by means of a straingauge beam (cantilever type) located at the end of the "thrust table." A Thompson straingauge (counter-type) indicator was used in conjunction with the straingauge. The upstream air pressure was indicated by two pressure gauges (dial type).

Miscellaneous equipment. An aluminum ground board (shown in Figure 4), with an overall diameter of 3.5 ft, was utilized to simulate the ground and to serve as a loading platform to measure lift. The construction of the ground board was such that only insignificant surface deflections would be encountered due to loading. The friction on the center fair-lead was reduced by lubrication with graphite powder.

PROCEDURE

The test was divided in two parts, the hovering tests (zero propulsive thrust) and the propulsive thrust tests.

Hovering. The nozzles were aligned (see Figure 4b) so that the tangential jet deflection angle β would be zero, and the normal jet discharge angle Θ set at -45° for all conditions.

For the individual upstream air pressure values for which the nozzles had been calibrated, standard weights were added or subtracted (by counterbalancing the ground board with a pulley system) and the height or altitude h (see Figure 3) was recorded.

Propulsive thrust test. The propulsive tests were carried out in the same fashion as in the hovering condition, except that β was varied for the different propulsive thrusts desired. The angle β was varied along the perimeter of the planform.

After lift had been obtained as described above, the ground board was removed and thrust readings were recorded for the same upstream pressure values used for the lift part of the test.

RESULTS AND DISCUSSION

The results obtained from the hovering and propulsive thrust tests will be briefly summarized.

Hovering. The augmentation was obtained from the following equation:

$$A = \frac{L}{J} \tag{1}$$

for the different jet momentum values. These results are presented in Figure 5, where they are plotted versus the ground-proximity parameter

$$\left(\frac{4\ S_b}{hC} = \frac{D}{h} \text{ of a circular planform} \right)$$

Figure 5 shows that $\frac{4\ S_b}{hC}$ truly defines the ground proximity parameter, regardless of planform shape.

Within the design range,

$$4 \leq \frac{4\ S_b}{hC} \leq 20$$

the augmentation obtained is approximately 80 per cent of that predicted by theory (non-mixing theory). That is to say, the augmentation "efficiency" $\eta_A = 0.8$ for the design range.

Figure 6 permits a comparison of augmentation obtained between planforms. The augmentation values have been plotted versus a "comparison ground-proximity parameter",

$$\frac{4\ S_b}{h\ C_{min}} = \frac{4\ S_b}{hC} \left[\frac{\pi + 2\ \frac{b}{a} - 1}{\sqrt{\pi^2 + 4\pi\left(\frac{b}{a} - 1\right)}} \right] \tag{2}$$

The results point out that the best planform for the hovering condition is circular. The values of augmentation obtained for values of $\frac{4\,S_b}{h\,C_{min}}$ above 20 are not too reliable, since h was very small.

Propulsive thrust. Typical results obtained from the lift tests with propulsive thrust are presented in Figure 7. The propulsive thrust factor $\frac{T}{J}$ represents the percentage of total jet momentum converted to static thrust by deflecting the jet tangentially. The augmentation drops considerably as $\frac{T}{J}$ approaches unity.

A simple mathematical analysis was made to confirm the $\frac{T}{J}$ obtained for values of β used in the tests. The results obtained were in agreement with test values.

To determine the planform effect on an "integrated system" (lift and propulsive thrust from the same jet momentum), the augmentation values were plotted versus the comparison ground-proximity parameter. A typical plot of these values is shown in Figure 8. From a chosen value of $\frac{4\,S_b}{h\,C_{min}}$ (from plots as in Figure 8), the cross plots for Figure 9 were made. Figure 9 shows the merits of increasing the planform length to width ratio for an integrated system. The percentage loss in augmentation is defined by the following equation:

$$\frac{\triangle A}{A_{(T/J\,=\,O)}} = \frac{A_{(O<\,T/J\,<\,1)} - A_{(T/J\,=\,O)}}{A_{(T/J\,=\,O)}} \qquad (3)$$

CONCLUDING REMARKS

For hovering (T/J = O), at a fixed value of $\frac{4\,S_b}{hC}$, within the design range, augmentation is independent of planform. However, at a fixed value of $\frac{4\,S_b}{hC}$, with fixed S_b or fixed C, the altitude decreases with increasing $\frac{b}{a}$. The circular planform is optimum for the hovering condition.

For an "integrated system" the augmentation loss decreases as the length to width ratio increases for a given value of T/J. That is to say, longer length to width ratios will produce smaller augmentation losses for a given value of thrust.

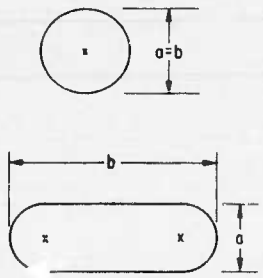

b/a	b	a
1	1.50'	1.50'

b/a	b	a
2	1.833'	0.917'
3	1.980'	0.660'
4	2.063'	0.516'

Figure 1. Sketch of planforms tested

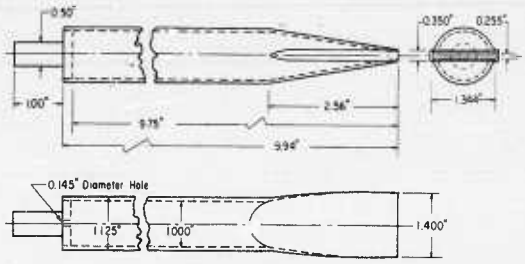

Figure 2. Sketch of typical nozzles

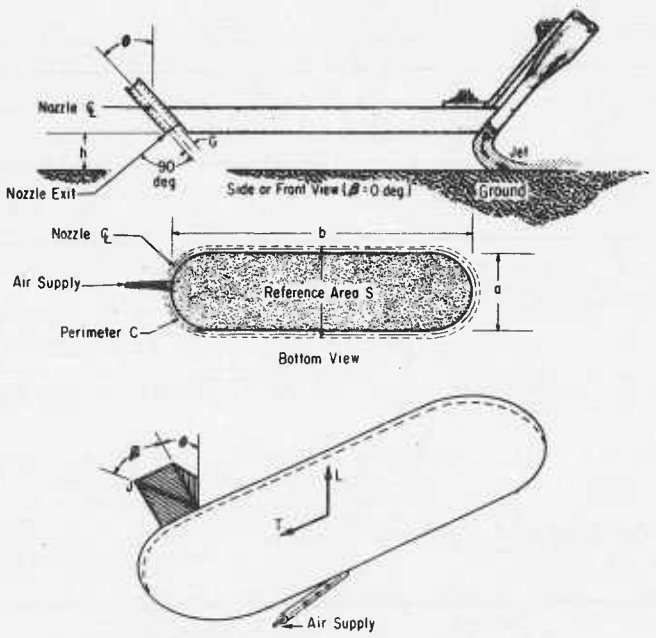

Figure 3. Sketch showing planform geometry notation

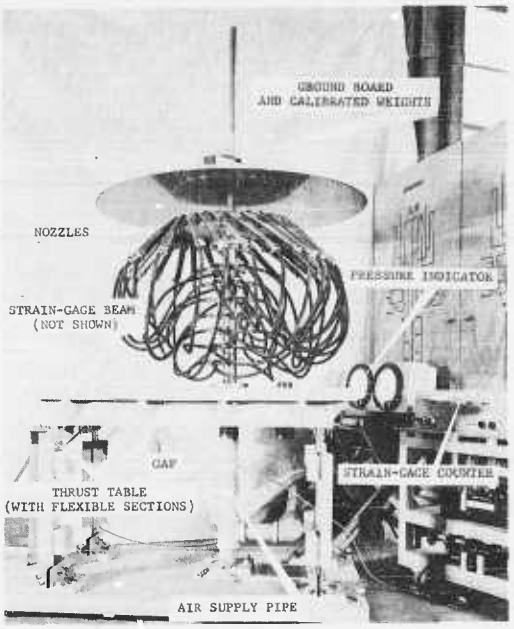

Figure 4. Test set-up

(a) Typical nozzle arrangement for lift test $\left(\frac{b}{a} = 1\right)$;

(Ground board is removed for thrust test)

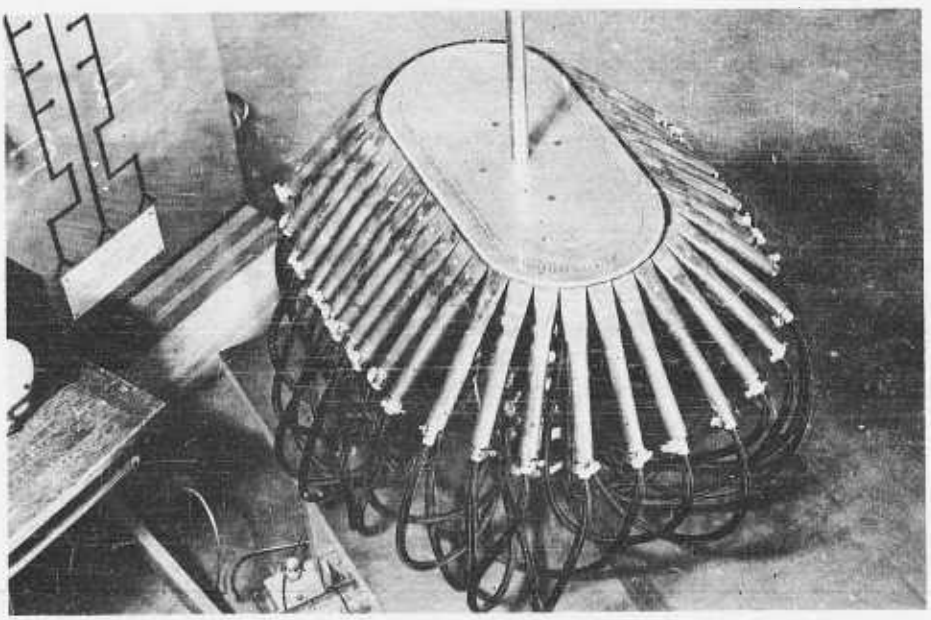

Figure 4 (Concluded)

(b) Typical nozzle arrangement for hovering tests $\left(\frac{b}{a} = 2\right)$; ground board not shown

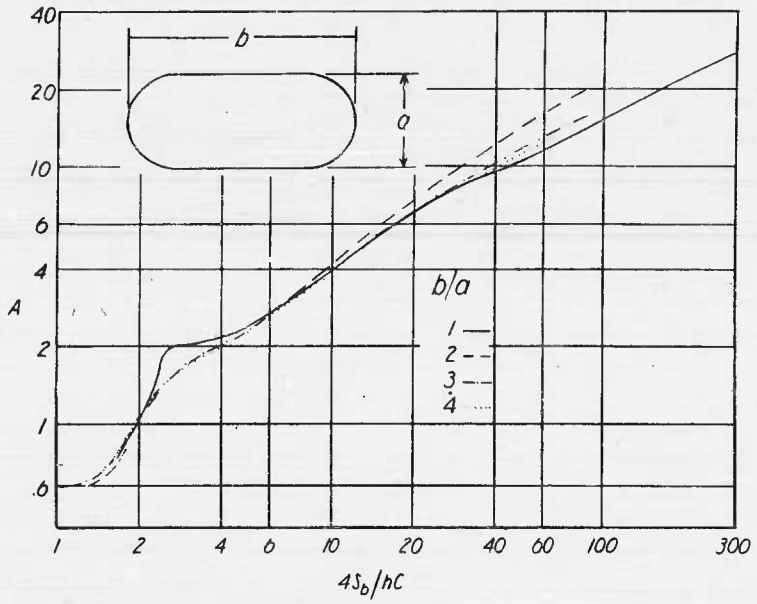

Figure 5. Augmentation variation vs ground proximity parameter (T/J = 0)

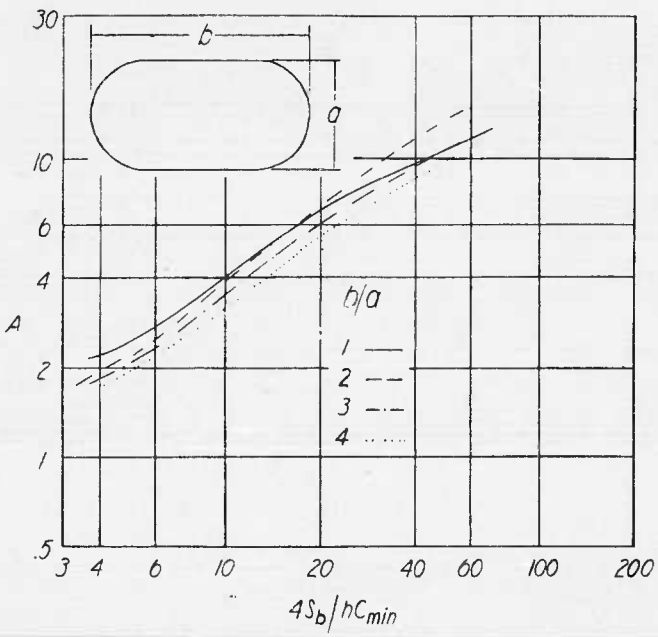

Figure 6. Comparison of augmentation variation vs equivalent ground proximity parameter (T/J = 0)

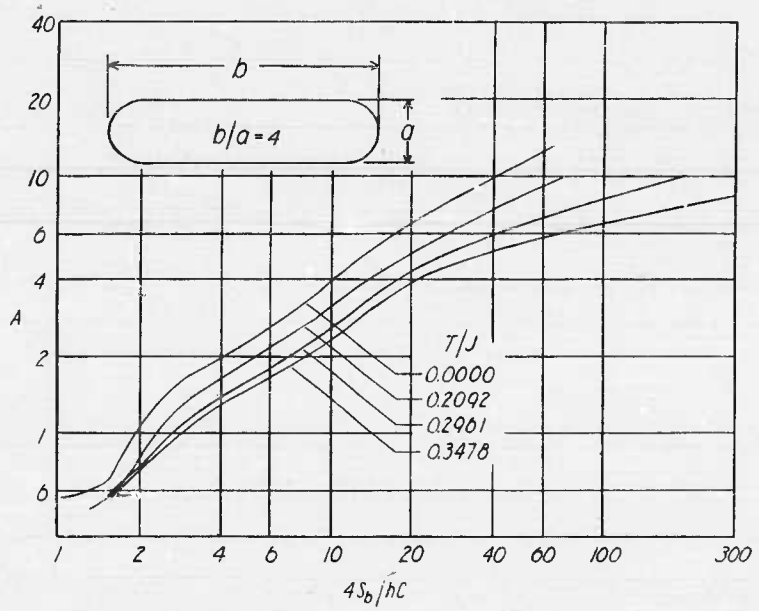

Figure 7. Augmentation variation for an increase in forward propulsion

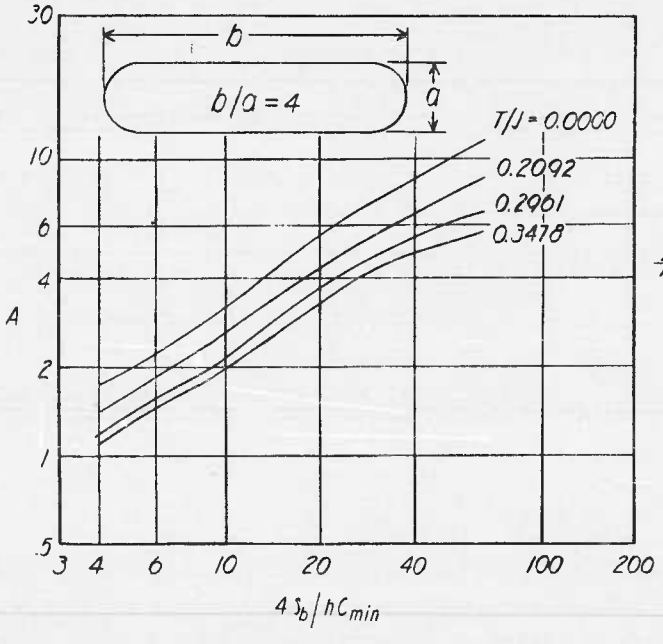

Figure 8. Augmentation variation for an increase in forward propulsion vs equivalent ground proximity parameter

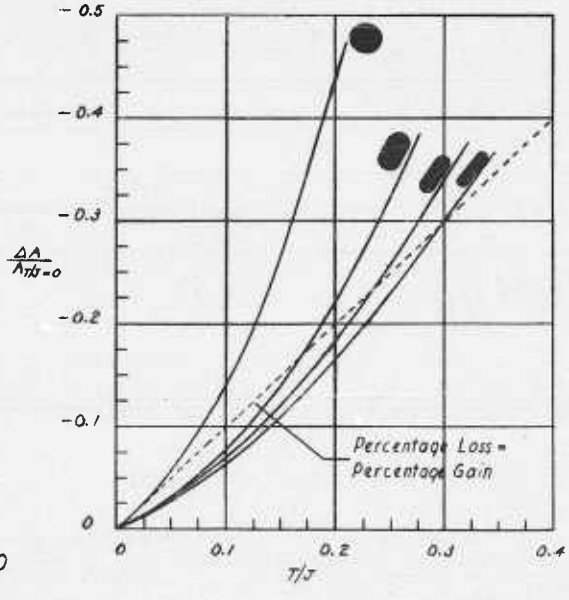

Figure 9. Percentage loss in augmentation vs percentage gain in forward propulsion ($4S_b/hC_{min} = 8$)

AERODYNAMIC CHARACTERISTICS OF A 3-FOOT DIAMETER POWERED ANNULAR JET MODEL

By Arthur E. Johnson, Aerodynamics Laboratory, David Taylor Model Basin, Washington, D. C.

INTRODUCTION

Tests of a 3-ft diameter, powered, annular jet model have been made at the David Taylor Model Basin as part of its Ground Effect Machine (GEM) research program. Not all of the planned experiments using this model have been completed but most of the test objectives have been reached. The aims of the investigation were to gather data for comparison with hovering theory, to secure information on the effects of forward motion on the lift-producing mechanism, and to determine the effectiveness of certain auxiliary jets in providing stability. This paper concerns the first two of these; that is, the performance of this model in hovering and in forward flight. Not enough stability data have been processed yet to afford a comprehensive analysis.

Symbols

S	reference area in ft^2 (plan area enclosed by outer edge of nozzle exit)
h	altitude in ft measured from the surface to the lower edge of the nozzle exit
C	perimeter in ft measured in the nozzle centerline in the nozzle exit
L	total lift in lbs
ρ	air density in slugs per ft^3
P	shaft power delivered to the compressor in ft lb/sec
M	figure of merit, $M = \frac{1}{2\sqrt{\rho S}} \cdot \frac{L^{3/2}}{P}$
η_{aoh}	apparent overall hovering efficiency, $\eta_{aoh} = \frac{M}{\frac{S}{hC}}$
G	nozzle width in ft
Θ	jet discharge angle in degrees measured from vertical at the nozzle exit; negative for an inward-inclined jet
Δp	effective base pressure in lbs/ft^2 gauge (total base pressure lift, accounting for the static pressure over the nozzle exit, divided by $S - \frac{GC}{2}$)
p_{tj}	weighted-average jet total pressure in lbs/ft^2 gauge, measured at the nozzle exit, the pressure at a point being weighted proportional to the normal velocity at that point

η_A augmentation "efficiency" factor

$$\eta_A = \frac{\Delta p}{(2p_{t_j} - \Delta p)(1 - \sin\Theta)\frac{G}{h}}$$

V_j average jet velocity in ft/sec measured at the nozzle exit

η_{int} internal efficiency factor

$$\eta_{int} = \frac{V_j \, GC \, p_{tj}}{p}$$

J scalar total jet momentum flux in lbs

V_o free stream velocity in ft/sec

C_L lift coefficient $C_L = \dfrac{L}{\frac{1}{2}\rho S V_o^2}$

$L_{g.c.}$ ground cushion lift (total power-on lift minus total lift with no internal flow and jet curtain simulated

$C_{L,\,g.c.}$ ground cushion lift coefficient

$$C_{L,\,g.c.} = \frac{L_{g.c.}}{\frac{1}{2}\rho S V_o^2}$$

A augmentation factor

$$A = \frac{L_{g.c.}}{J}$$

D total drag in lbs

ρ power-required parameter

$$\rho = \frac{2(P + 1.25\, D\, V_o)\ \sqrt{\rho S}\ \frac{S}{hC}}{L^{3/2}}$$

MODEL AND TEST DESCRIPTION

The model was designed to have a large internal cavity into which certain geometric modifications could be installed as soon as such refinements could be developed using other models and test techniques. In the meantime, tests were begun on the original configuration to establish basic ideas of the model's behavior. Figure 1 shows the model in its original configuration mounted in the hovering test rig. The model was axisymmetric and consisted essentially of a Fiberglas-plastic shell, a flat sheet-metal base, and an

electrically driven fan. Radial sheet-metal ribs divided the internal cavity into eight equal sectors. The circumferential nozzle, however, was continuous. The nozzle had a mean diameter of approximately 3 ft, with an exit area about equal to the fan area. The nozzle was inclined inward at an angle of 45°.

The framework of the hovering test rig was attached rigidly to the model at one end (Figure 1) and was free to pivot at the other end about a horizontal axis. The pivot could be raised and lowered to keep the model level and to afford the altitude measurement. A wire yoke went over pulleys to a counterweight that was varied to alter the apparent weight of the model.

A simplified model of one of the sectors of the 3-ft model was used to develop modifications to internal geometry. Various changes were tried until the best duct efficiency and augmentation efficiency were obtained. Internal modifications are shown in Figure 2. They are the inner nozzle wall extension, and inserts A and B. In addition, a stator and a new fan were installed and, for the wind tunnel tests, a large inlet fairing was supplied (Figure 3). In hovering tests the original inlet performed satisfactorily but at forward velocity substantial inlet loss was incurred. This loss proved to be materially reduced by this fairing.

In the hovering tests, lift, altitude, and electric motor output power were measured. In the tunnel, tunnel velocity, of course, and drag were also measured. In addition it was necessary to isolate the lift produced purely by the ground cushion from the ordinary aerodynamic lift a body has due to its shape. Accordingly, power-off measurements of lift and drag were made with the inlet sealed and with wooden blocks situated between the nozzle exit and the ground board to simulate the position of the annular jet.

RESULTS

Hovering performance. Hovering performance of the original configuration is presented in Figure 4. For comparison, Figure 4 also shows a theoretical curve based on Chaplin's detailed performance equation (reference 1). Comparison with the simplified limit theory $\left(M = \frac{S}{hC}\right)$ shows the model to have an apparent overall hovering efficiency, η_{aoh}, of 29 per cent.

Several improvements were made as a result of tests of the sector model. First of all, it was learned that augmentation efficiency, η_A, would be increased from about 0.6 to about 0.8 by extending the inner wall of the nozzle (Figure 2). Secondly, the inserts already mentioned were developed. Lastly, it was learned that η_A was independent of the jet deflection, Θ, at least in the range tested, from -60° to -30°.

Hovering performance of the modified configuration is presented in Figure 5. Again, the theoretical prediction is shown for comparison. Comparison with limit theory shows that η_{aoh} has increased to about 53 per cent.

Cruising performance. Consider first the influence of forward motion on augmentation as it is affected only by the forces actually involved in creating the ground cushion. The augmentation factor, then, of a cruising GEM is shown in Figure 6 as a percentage of the maximum theoretical augmentation factor of a hovering machine. It is plotted against a scale which is proportional to velocity.

Next consider the effects of speed on gross lift and drag. These effects may be described in terms of power required and cruise economy parameters. Figure 7 gives the power required, nondimensionalized by the lift and area. This gives a direct comparison

of power required between different size-height ratios for GEM's of the same wing loading. Tangents to these curves through the origin indicate points representing the most economical cruise conditions. These points are plotted in Figure 8 to show the variation of the best cruise economy with the size-height parameter. The ordinate is proportional to gross ton-miles per horsepower-hour. The predicted curve, shown for comparison, was calculated from performance relationships of reference 1.

CONCLUSION

On the basis of the results of these tests it appears that hovering performance can be predicted with a degree of accuracy adequate at least for developmental projects. The prediction of cruise performance characteristics is cruder but can be made at least in order of magnitude. Definitive data are still required. Investigations at the David Taylor Model Basin over the next year will be aimed at obtaining more realistic data both on cruise performance and on stability and control.

REFERENCE

1. Chaplin, H. R., "Ground Cushion Research at the David Taylor Model Basin - A Brief Summary of Progress to Date." Paper presented at the University of Toronto Institute of Aerophysics Decennial Symposium, October 1959.

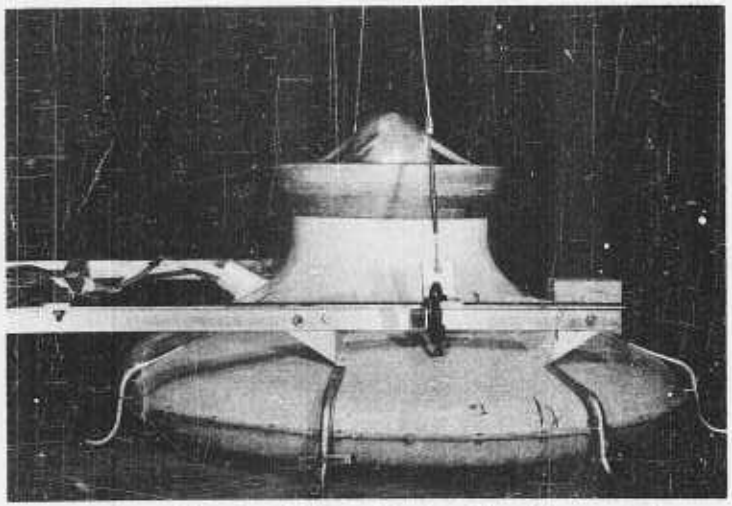

Figure 1. View of model in original configuration mounted in the hovering test rig

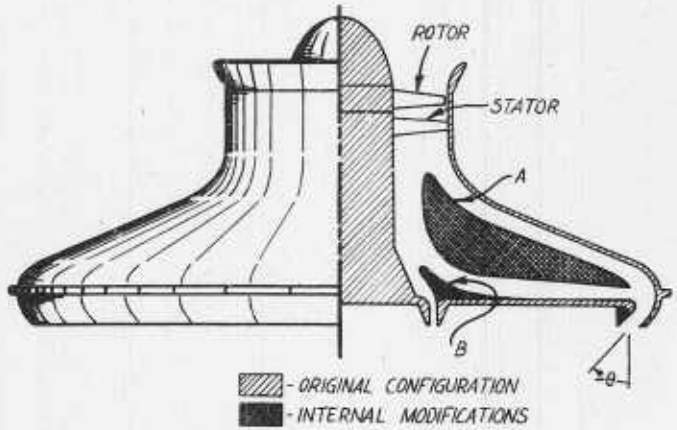

Figure 2. Half-section view of 3-foot diameter model showing internal modifications

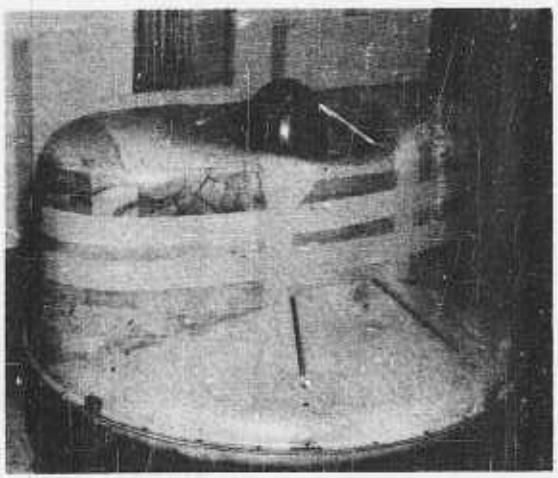

Figure 3. Three-quarter rear view of model in modified configuration

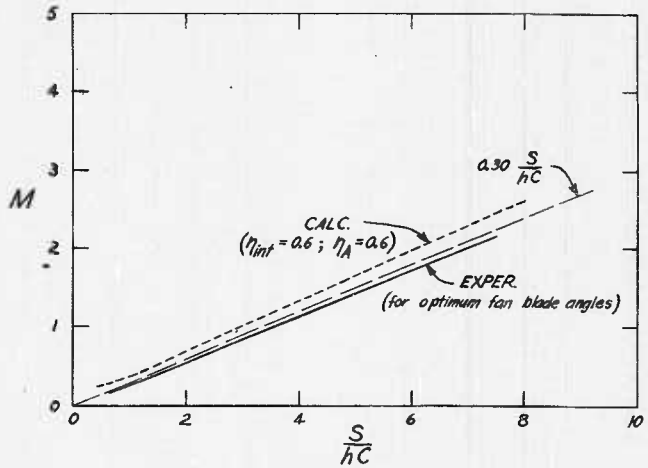

Figure 4. Hovering performance of original configuration

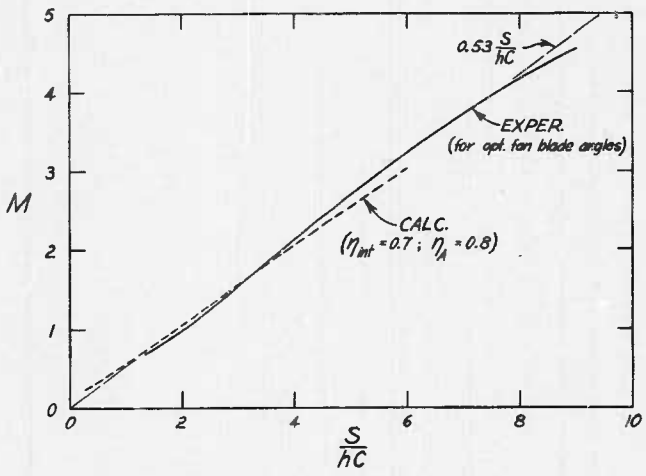

Figure 5. Hovering performance of modified configuration

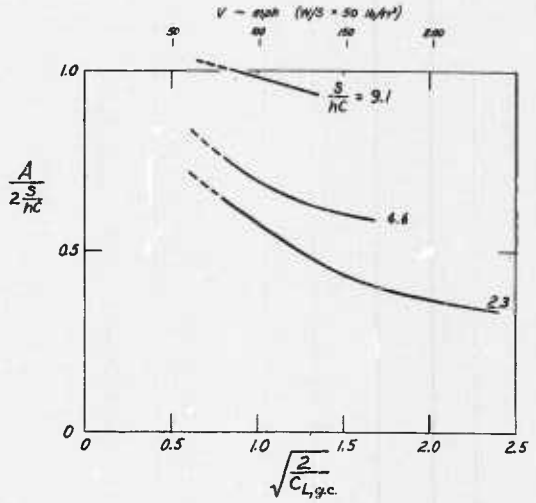

Figure 6. Effect of speed on augmentation

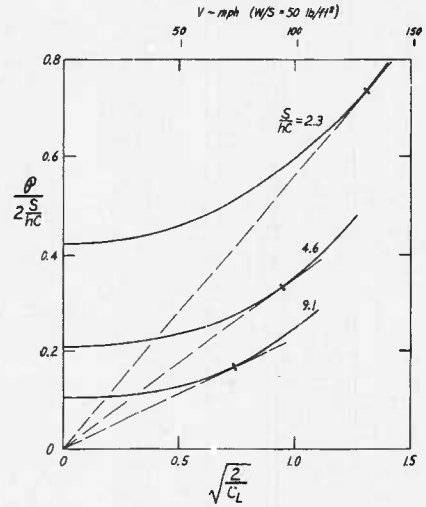

Figure 7. Effect of speed on power required

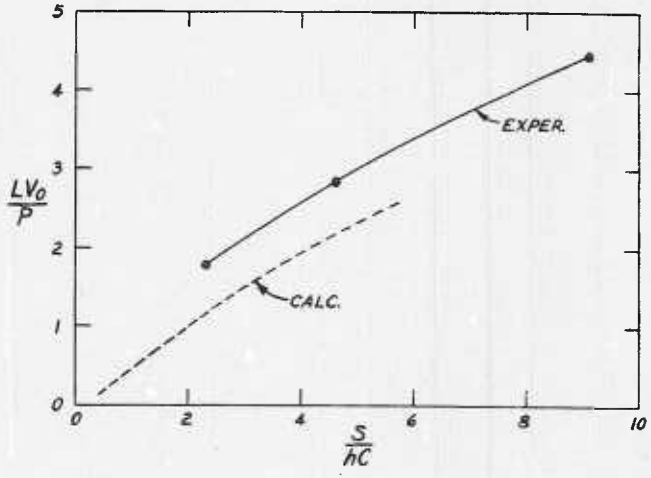

Figure 8. Optimum cruise economy

EFFECTS OF SURFACE GEOMETRY AND VEHICLE MOTION ON FORCES PRODUCED BY A GROUND PRESSURE ELEMENT

By H. C. Higgins and L. W. Martin, Boeing Airplane Company, Wichita, Kansas

INTRODUCTION

First order approximations of performance and stability of ground effect vehicles are more difficult to describe than similar characteristics of conventional aircraft. In the case of an airplane, forces and moments resulting from attitude and velocity are sufficient. In the ground pressure vehicle, attitude, velocity, nozzle pressure, and altitude have first order effects. Furthermore, the geometry of the earth's terrain must be considered in a discussion of ground vehicle performance while the motion of the atmosphere is assumed at rest for most airplane problems. Therefore, the performance description of the "simple" ground effect vehicle is more complex than that of airplanes by an order of three. A correspondingly larger amount of experimentation must be accomplished before parametric optimization can be realized.

Good information supported by adequate theory is available on static lift, and agreement is found between results of independent investigators. However, published information is meager on the effects of velocity, attitude, and terrain characteristics. The results of a few tests in these areas are offered in the hope that they will help to fill the gaps and contribute to the technology of ground reaction.

TEST DESCRIPTION

This is a report of a scale-model test program. The program included wind tunnel and static tests of a family of models having a characteristic dimension in the order of 15 inches. Most testing was done at a range of variables typifying realistic conditions for a ground pressure vehicle. Characteristic values of several variables were:

plenum pressure = 1.1 atmosphere

height = 0.1 x characteristic length

nozzle area = .02 x base area

The height was extended above useful values in order to examine the mechanism of lift and stability.

Static tests were conducted on an air rig that measured air parameters, normal force, and moment and was adjustable in height and pitch (see Figure 1).

Wind tunnel tests were conducted in the Walter H. Beech Memorial Tunnel at the University of Wichita. Secondary air was fed the model through a system minimizing air feed interaction on the balance. Since the mechanism of lift and moment caused by the nozzles and base pressure was of major interest, tare values with no secondary flow were measured and subtracted from all data shown in this report.

The principal subject of these experiments centered on stability, and most model variation was a result of attempts to improve this characteristic. A conventional circular planform, single peripheral nozzle arrangement was used as a basis for comparison. The other models were rectangular or elliptical with a variety of nozzle arrangements.

RESULTS

Lift. The usual definition of lift augmentation was used, which is the ratio between measured normal force and the theoretical nozzle thrust for expansion from plenum pressure to ambient pressure of the measured mass flow.

Figure 2 shows the static lift characteristics of a rectangular model provided with internal base nozzles intended to provide stability. As has been reported by others, the interior nozzles detract from the lift efficiency. The lift penalty of interior nozzles or slots is shown for several heights.

Figure 3 shows a typical variation in lift with inclination of the ground pressure element. The lift penalty of pitch varies with the model shape and nozzle configuration but the penalties for all models were small for small angles. The curve on the left, the zero inclination lift, is in general agreement with the published literature in the field.

Results of experiments on the effect of forward speed on lift are shown in Figure 4 for the case of zero angle of attack. Small effects on lift, generally unfavorable, were noted when accelerating from rest to about 50 knots. As speed increased to 100 knots, most configurations showed a large dynamic lift, apparently due to an increased camber effect produced by the secondary air flow. The 3:1 ellipse showed the largest dynamic lift, as would be expected from its larger aspect ratio. The dynamic lift of the ellipse was equivalent to a lift coefficient of about unity if it is assumed that the base pressure contribution was constant with speed.

The inward-directed nozzle on the circular planform was superior to the vertical nozzle and the outward-directed nozzle was the worst of the three circular annular arrangements although they all developed about the same amount of dynamic lift.

The double annular configuration failed to develop dynamic lift. The assumption is made that the general lower lift efficiency of this arrangement, caused by the mixing of adjacent jets, increased with forward speed and canceled the lift developed by circulation.

Pitch and roll stability. Figure 5 shows the moments measured during static conditions for the model of Figures 2 and 3. The moments were measured about the centroid of the base and in this case are shown for rotation about the short axis, which we will call pitch. It is difficult to generalize about stability from the information shown on the plot. Conditions of positive, neutral, and negative stability are seen with apparently unsystematic discontinuities. The plot shown on Figure 6 was prepared in an effort to make this information more amenable to analysis. This is the stability of the reference circular planform. The chart plots the parameter:

$$(2/LD_e)\ (dM/d\alpha)$$

multiplied by 1000 for numerical convenience where,

- L lift, lbs
- D_e equivalent diameter, (diameter of circle having same area as base)
- M moment, ft lbs
- α pitch deflection, degrees

This is analagous to the conventional airplane stability parameter, $dC_M dC_L$. It indicates the motion of the center of pressure caused by pitch deflections. Positive values

are unstable and a disturbance from equilibrium will cause upset; negative values are stable and the moments produced from a pitch disturbance tend to restore the initial con-tion. The arbitrary quantities in the parameter are the use of degrees instead of radians and the radius of the equivalent circle as the characteristic length. If the parameter is equal to the value 1,000 per degree, it indicates that the center of pressure will move at the rate of one radius per degree of pitch.

The plot shows lines of constant value of the stability parameter as a function of height and attitude. Certain characteristics of the mechanism of stability are readily seen. Above some critical altitude, the stability parameter is zero and there is no interaction between the ground and the element. At very low altitudes and small deflections in pitch, the element is stable, which is consistent with the first order theory that the lower side operates at a greater local lift than the higher side due to its lower local altitude. Above an altitude of about 0.3 D and at zero pitch, the stability is remarkably sensitive to pitch. At this height the jet sheet is tending to converge and is stagnating on the surface as a simple free jet. The stagnation point of such a jet is very sensitive to angular change and the position of the stagnation point effects base pressure and therefore pitching moment. The isolated "cloud" of stability at $h/D = 0.2$ is not explained.

Figure 7 shows the stability parameter as measured with the rectangular element previously discussed. The data are shown for pitching moments about the short axis. Large differences are seen between this configuration and the circular element. The critical altitude was lower; the extreme sensitivity to pitch at small angles disappeared; and the area of favorable stability at low altitudes extended through a much greater area. These effects can be explained by noting that the "x" - shaped interior nozzle divides the base into four relatively independent systems. The critical height of these smaller systems is less than the critical height of an element using a single peripheral nozzle and the critical height is further reduced by the inward slanting peripheral jet. In other words, the jet sheets tend to converge at a distance determined by nozzle angle and the equivalent diameter of the individual segments of the base. Furthermore, it is axiomatic that a peripheral jet in the shape of a polygon will converge more rapidly than a circular jet having the same area.

The disappearance of the extreme pitch sensitivity at small angles was probably caused by the four systems tending to stabilize each other's stagnation points at near critical altitudes. The increase in the area of favorable stability at low altitude was the result of the increased independence of segments of the base due to the isolating effect of the interior jets. The unexplained stable "cloud" at $h = .2\, D_e$ has now split and become two stable "clouds" at about $\pm 12°$ pitch.

Figure 8 shows the stability of the rectangular model for roll about the long axis. Three major differences are noted in comparison to pitch stability (about the short axis). There was an extremely small stable region; sensitivity at small angles reappeared; and the critical height was lowered. These effects are explained by the shorter dimensions about the axis of rotation and a probable blending of the two lateral systems producing an effect similar to three circular nozzles arranged along the roll axis.

It was seen that the addition of small interior nozzles improved pitch stability in comparison with the peripheral nozzle. Larger interior nozzles should be expected to increase the stability further, since by increasing the energy of the sheets separating the base segments, the independence of these sections from each other should increase. Figure 9 shows test results of this effect. When the interior slot width was increased to two-thirds of the peripheral slot, the model was stable in pitch up to $h = .24\, D_e$ for all the pitch angles tested. More important than this, the rolling moments became stable for a reasonable range of altitudes and angles.

The wind tunnel moment data were unsatisfactory due to interaction between the secondary air system and the pitch balance. However, a set of base pressure taps was provided on the longitudinal axis of each model's base, and certain conclusions can be drawn from these data. These pressures are shown at zero speed in Figure 10 for variation of angle of attack of a circular peripheral jet. Fairly good correlation can be made between this pressure sample and the lift force which was accurately measured. Furthermore the figure shows general agreement with pitching moments measured on the static rig. At a height of .05 D, the base pressures changed with angle of attack in a stable manner. At a height of .50 D, the opposite was true, as was shown in the static rig stability data.

The effect of forward speed on base pressures is shown on Figure 11. At the lower altitude we see an initial loss of base pressure as speed increases from zero with only minor changes in moment. As speed increases above 50 knots, a diving moment develops. The higher altitude case shows an increase of diving moment with speed throughout the test range. The conclusion is drawn that the speed stability for the circular element is unsatisfactory except at very low speeds and altitudes. It should be remembered that stability contributions of other vehicle components, such as an air inlet, are not included in these data.

Surface irregularities. Figure 12 shows the measurement of the change in lift as the element progresses over cliffs of various heights. In this test, equilibrium was not maintained. Instead, absolute altitude was kept constant and the anticipated reduction in lift as the ground falls away is readily seen. The transition in lift was relatively smooth.

Figure 13 shows the pitching moments that result from this cliff-jumping. Initially, the element tends to fall off the cliff with the leading edge pitching down, but after the center of the element has passed the edge of the cliff a restoring moment appears which looks very favorable. The initial pitch down moment is caused by the localized higher lift produced by the base portion still on the plateau. The pitch-up moment is caused by the cliff itself which turns the circulation air beneath the base to produce a stagnation point forward of the model center line. It should be mentioned that these data are static measurements and are not to be confused with the complete dynamic problem.

Figures 12 and 13 show the effects for the case of the element navigating a variety of cliff heights. Figure 14 shows the similar cliff problem for a variety of initial altitudes and a single cliff height. It is seen that the moment characteristics change considerably as altitude is increased. In fact, at an altitude of .23 D, the moments are unfavorable throughout the maneuver.

In an attempt to generalize on the effects of surface roughness, the static response of an element was measured when operating over a family of idealized geometric disturbances, as shown in Figure 15. The change in lift as a function of position over roughness was minor, although it is interesting to note that the maximum lift changed from peak to valley, below model centerline, when the distance between peaks became greater than .5 D. The average lift was approximately equal to the lift measured above a smooth surface located midway between peaks and valleys.

Figure 16 shows typical pitching moment as the element flies over a sinusodal surface. The pitching disturbance is fairly small when reduced to center of pressure shift.

Dynamic lift. Extending these static data to a realistic dynamic condition requires a knowledge of the damping terms occurring when motion is present. The special case of oscillating vertical motion was examined. As a matter of fact, the ground was oscillated instead of the element due to limitations of the test equipment, but the test was a fair approximation of the real case of the moving element and a stationary surface.

Figure 17 shows the results of this experiment. The measured lift at an average height of .05 D is shown during a five-cycle per second oscillation.

These tests were run at two mean heights of .05 D and .1 D with a .05 D peak to peak amplitude. Frequency was varied from zero to ten cycles per second. It was found that the lift and base pressure lag was negligible within this range of variables, indicating that the virtual mass of air involved in lift was quite small. It appears that the frequency range examined covers most of the significant full scale spectrum.

The complete dynamic analysis will require much more extensive information than shown here.

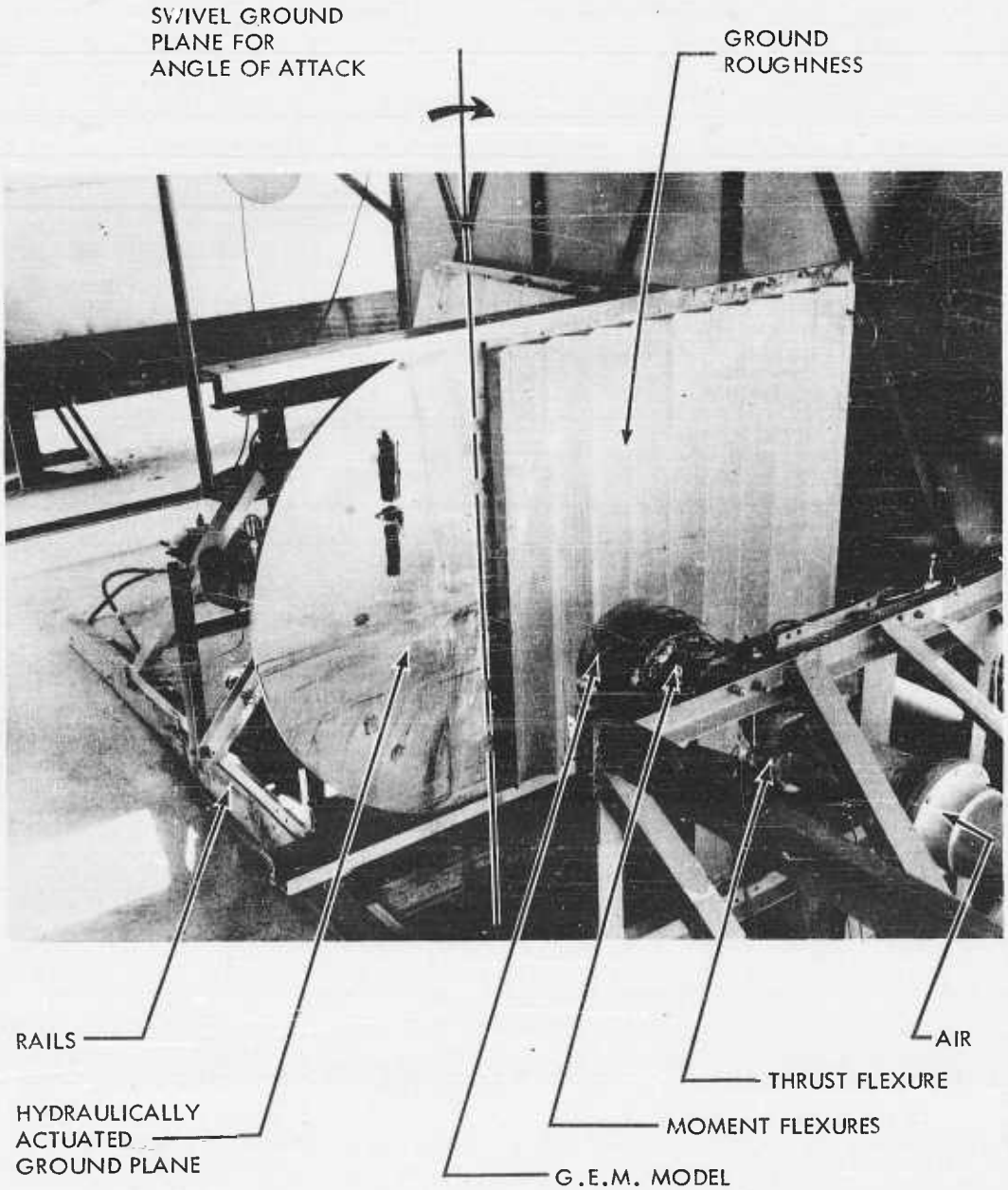

Figure 1. Static test stand

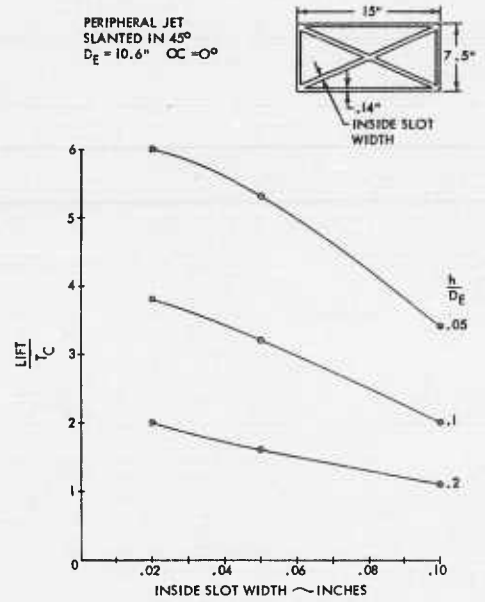

Figure 2. Effect of inside stability slots on lift

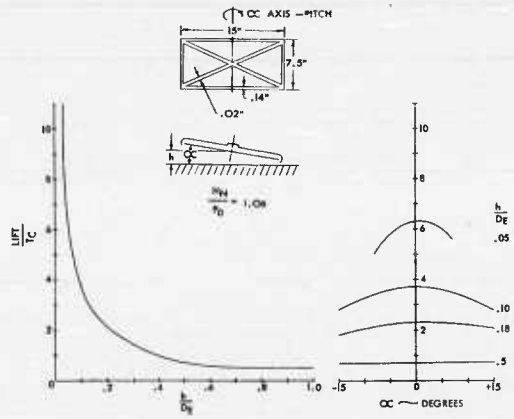

Figure 3. Typical variation in lift with angle of attack (∝)

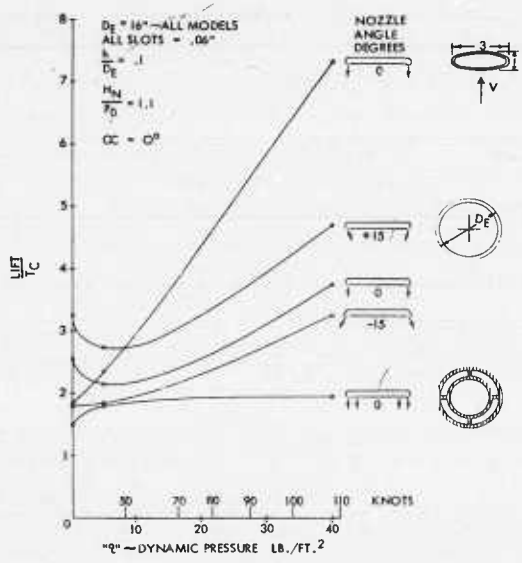

Figure 4. Effect of forward speed on lift

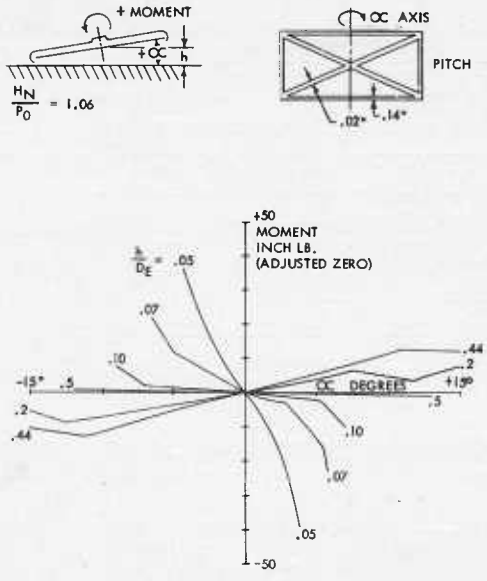

Figure 5. Moment versus angle of attack (∝) "typical data"

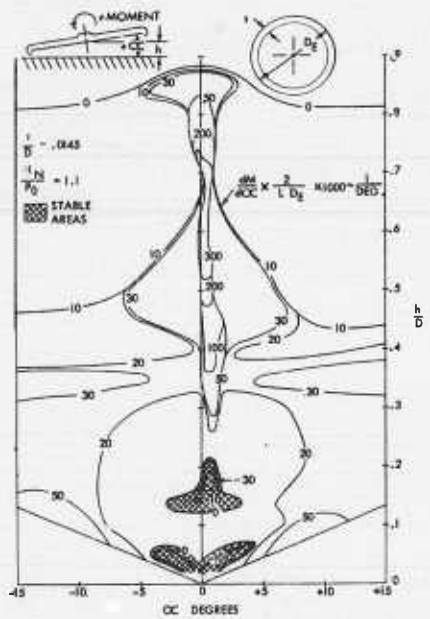

Figure 6. Static stability

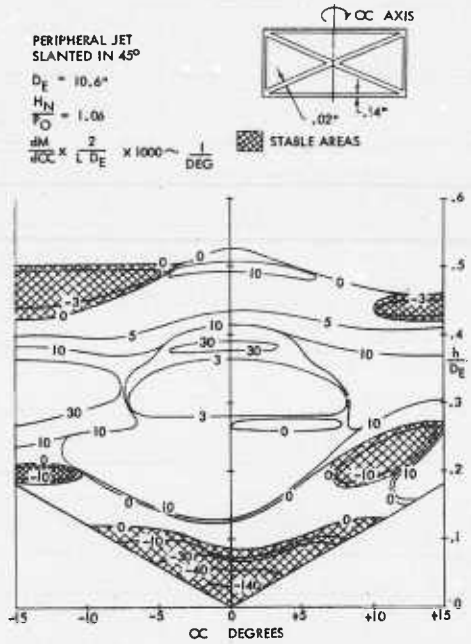

Figure 7. Static stability - pitch

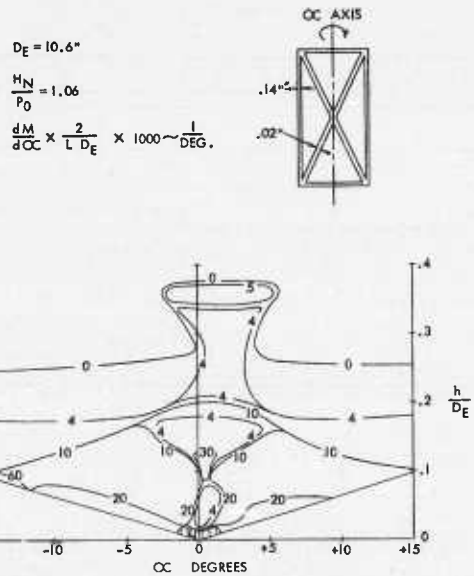

Figure 8. Static stability - roll

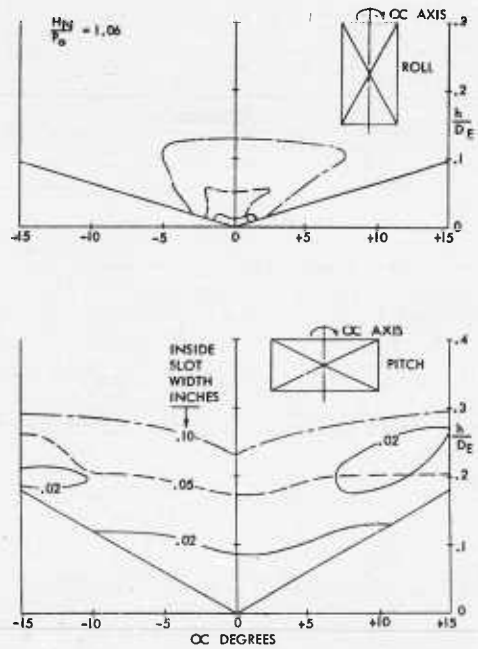

Figure 9. Growth in stable areas as inside slot width increases

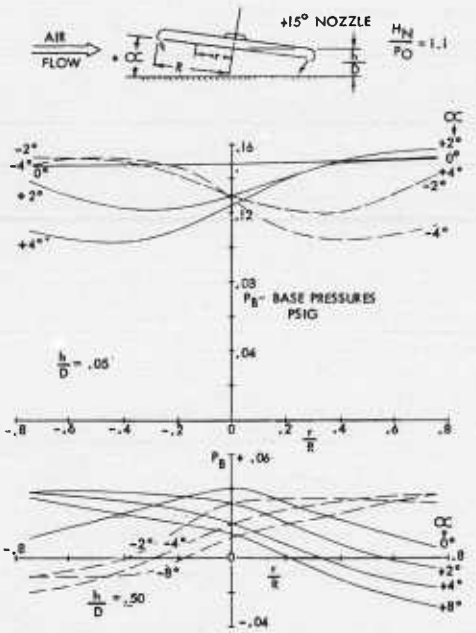

Figure 10. Effect of angle of attack (α) on base pressures (typical)

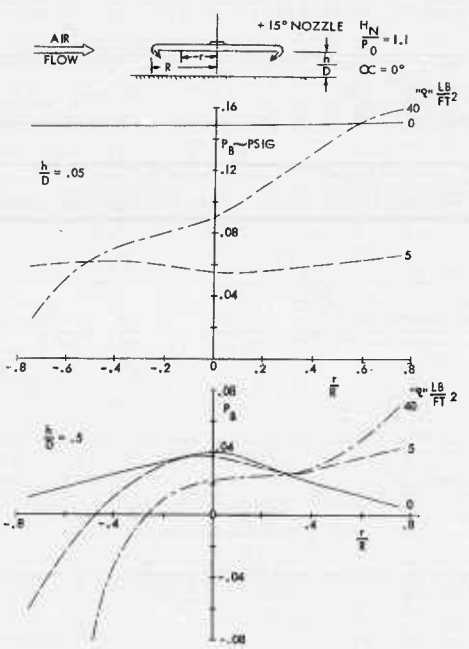

Figure 11. Effect of speed on base pressures

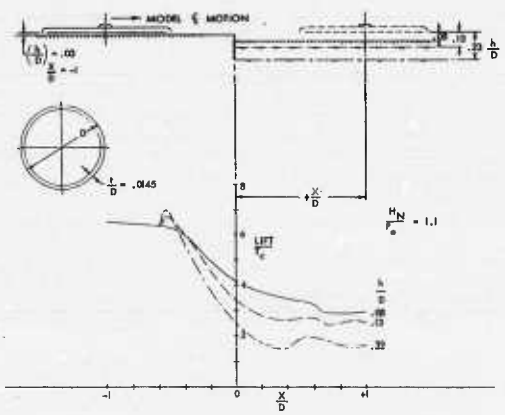

Figure 12. Effect of step height and position on lift

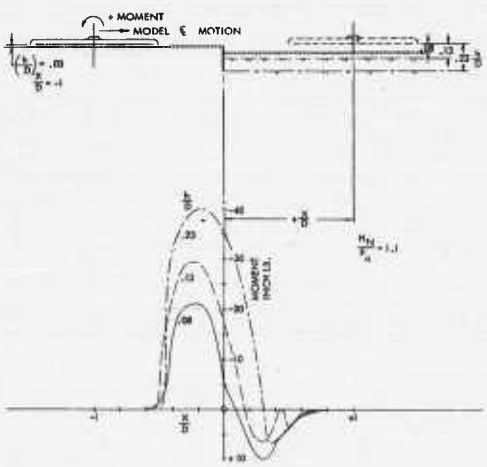

Figure 13. Effect of step height and position moment

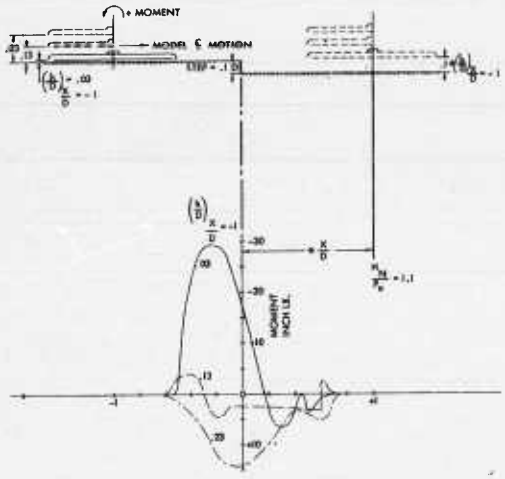

Figure 14. Effect of height above step on moment

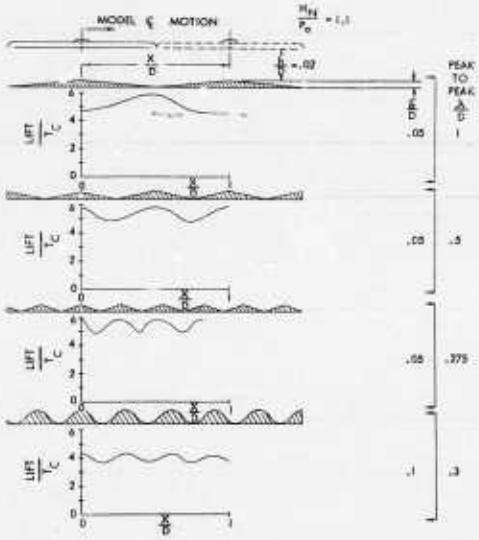

Figure 15. Effect of ground wave form on augmentation

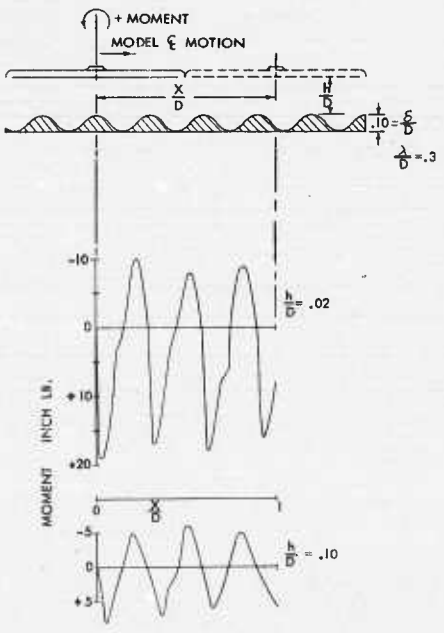

Figure 16. Moment due to typical ground wave

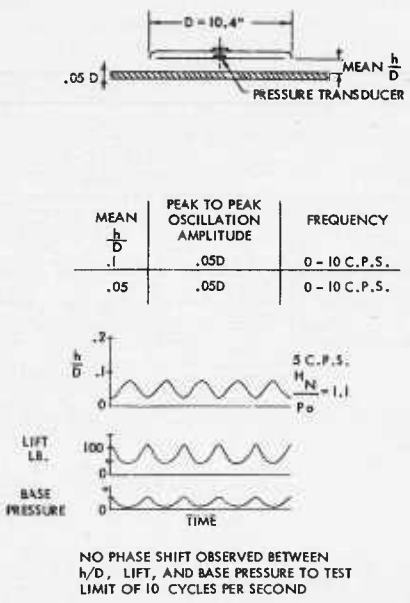

Figure 17. Lift phase shift due to vertical bouncing

THE PRINCIPLES OF GROUND EFFECT VEHICLES

By Toivo J. Kaario, Valmet Corporation, Finland

Symbols

ρ	density of air
b	span
h	average height of gap (in general, the side gap only)
h_e	effective height of gap = $c_g h$
A	area of wing
A_h	area of gap
V	velocity of flow in relation to vehicle
V_p	velocity of vehicle
V_r	critical velocity of vehicle
V_a	absolute velocity of flow related to surrounding air
α	attack angle of wing based on edges forming side gaps
L	lift of wing = weight of vehicle
D	total drag of vehicle
p	net power of power plants being disposable for blowing the side gaps or for thrust. (The losses at air intakes, in channels and exhausts, in blowers or propellers, and at rear gap are included in power plant efficiency.)
p_h	power to blow a gap
Δp	pressure differential wing underside/surrounding air - wingloading
C_L	lift coefficient from the equation $L = \frac{1}{2} C_L \rho V_p^2 A$
C_h	drag coefficient for drag caused by blow of side gaps (see C_L)
C_t	drag coefficient for drag related to square of speed (see C_L)
C_g	gap coefficient. The energy of flow at discharge point of structure (compared to the energy of surrounding air) divided by the power used to blow at correct angle a gap formed as a perfect nozzle and of same height
η_f	efficiency of propulsion (Froude eff.) = $\frac{2}{1 + \frac{V}{V_p}}$

ε speed ratio V_r/V_p

μ gap ratio $2\ h_e/b$

INTRODUCTION

The surface air craft is an aerial vehicle. Generally, when it moves, it moves wholly in air. Most of the problems involved are aerodynamic. The pressure beneath the wing can be built up by ram effect of a moving vehicle or by a blower. The proper place for the forward-facing opening of the ram wing is the gap between the wing and the surface. The ram wing is not airborne at low speeds, and therefore, especially on water, the powerloading must be of the same small category as that of an aircraft.

DISCUSSION

Remarks on stability. The necessary stability in height and the levelness of position could be achieved by feelers, scattered in proper amount on the area of a wing, sensing the distance between the wing and surface and giving impulses to power elements for correction.

One such combined and, indeed, very simple system is the bottom surface of a wing itself influenced by air flow beneath it. The presumption is that by changing position the velocities of the flow are also altered in the proper direction and magnitude in order to effect a pressure change big enough for all circumstances. That this phenomenon is dependent on the form of the wing becomes apparent in Figure 1., where the three blown wings are at a standstill. When this flow is superimposed by the flow caused by a horizontal speed, the magnitude of the forces will be altered, but practical experience has shown that within certain limits enough stability is maintained up to fairly high speeds. Theoretical knowledge of this phenomenon should be useful, but it is more important to know that it will give the service desired.

Definition of critical speed. In all of the following investigations it will be assumed for simplicity, in contradiction to the actual case where there must be different speeds and pressures even for reasons of stability, that the lift is evenly distributed over the entire area of the wing; in other words, the pressure is constant. The actual case is at a disadvantage, because for a given weight there are places of higher pressure, which increases the power consumed for lift.

It is apparent that there is a forward speed, when big changes occur in the flow character of the wing. The flow, which at low speeds has been outward, in all the gaps will change its direction in the front gap. This speed is reached when the dynamic pressure related to the forward speed reaches the value of the pressure differential between both sides of the wing. At greater speed the wing is supplied with air both by the blower and by the inward flow from the front gap instead of losing air through it. This speed may be called critical.

In one other sense it is critical also. The lift coefficient of the wing as a function of the speed is presented by a hyperbolically shaped curve, as shown in Figure 2. At speeds smaller than the critical there are no positions of the wing that in air space or at the proximity of the ground could give bigger lift than the wing has in its proper position. Therefore the air-coupled contact to the ground is maintained in all circumstances. Quite the opposite is the case at supercritical speeds. When the wing, from one cause or another, reaches a predetermined inclination, it will accelerate upward.

The limits of the critical inclination angles, which will give the same lift as the zero angle, will depend upon the form of the wing and its weight distribution.

The definition of the critical speed

$$V_r = \sqrt{\frac{2\,\Delta P}{\rho}} \tag{1}$$

is useful also in calculating the performance of a ground effect vehicle. For several reasons the supercritical speed range is far more interesting and more promising than the subcritical speed range.

Power of a blown gap at standstill. Gap coefficient. The power used to blow a gap of the form of a perfect nozzle (Figure 1) follows from the Bernoulli equation:

$$P_h = \sqrt{2}\, A_h \frac{\Delta P^{3/2}}{\sqrt{\rho}} \tag{2}$$

Two different methods of utilizing power in hovercrafts have been in use: direct blowing from the main volume beneath the wing and the air curtain method. In the former simple system, the power used and the gap coefficient are directly proportional to the flow; but, in the latter system, because the air may be blown with a higher pressure than Δp, the gap coefficient must be defined in another way. The gap coefficient is now the energy of the flow discharged from the structure divided by P. This definition also eliminates the losses encountered in the channels of the structure.

Power of a blown gap when moving. Equivalent drag. Lift/drag ratio. In all the following investigations it will be assumed that the wing has a rectangular planform. The power needed to blow the side gaps is independent of the forward speed when the angle of discharge is the right one.

Figure 3 shows the spanwise profile of a wing of infinite length or of some shorter length, which is supplied with air at the leading edge and discharged in a proper way at the trailing edge. The speed on both sides of the wing perpendicular to the paper is the same and cannot be altered when the wing is frictionless. The flow picture in the plan is independent of the motion of the wing and hence also the power.

At the leading edge at supercritical speed, the flow is inward and does not lose energy to the surrounding air. The trailing edge discharges backward and gives propulsion power. The efficiency is defined by the Froude's equation. The equivalent drag of the side-gap blow power is hence inversely proportional to the speed, the loss due to the blowing of the rear gap is at all reasonable speeds small, and the power for the front gap is zero at supercritical speed (if the loss inside the wing is neglected).

It can be shown by using the power equation (2) that the equivalent drag coefficient at the side gap blowing is

$$C_h = \mu \varepsilon^3 \tag{3}$$

The lift coefficient is

$$C_L = \varepsilon^2 \tag{4}$$

and the lift-drag ratio

$$L/D = \frac{\varepsilon^2}{\mu\varepsilon^3 + C_t} \tag{5}$$

The drag is

$$D = \left(\mu\varepsilon + \frac{C_t}{\varepsilon^2} \right) \Delta p\, A \tag{6}$$

and the total net power for lift and propulsion,

$$P = P_h + \frac{1}{2} C_t \rho V_p^3 A \tag{7}$$

The propulsion efficiency of the rear gap blowing is

$$\eta_f = \frac{2}{1 + \sqrt{1 + \varepsilon^2}} \tag{8}$$

ε	η_f
2	0.62
1	0.83
0.5	0.95

The assumption has been that the speed V_p is not retarded when air enters the wing. This should be near the truth for most practical cases concerning the rational hovercraft and for greater speeds of the ram wing also. (Figure 4.)

In an air curtain system, air should have the proper speed in the direction of the movement. When calculating the accumulated energy of flow at the discharge point in the structure and at the gap coefficient the pressure, the speed, and the angle of discharge should be taken into account. The speed may be divided into the direction of motion and another direction perpendicular to that.

Moment plane. For some purposes it may be useful to investigate the real forces, produced by the discharge through the gaps. Assuming that the pressure effect on an area of a vertical plane parallel to the direction of motion is Ap, it will easily be found, that the height of such a moment plane is 2 h for the wing of Figure 3. The smaller pressures at the nozzle give the required balance for the system. The moment plane for the wing of Figure 5, incorporating a Bordasch nozzle, should then have the height h; otherwise, the system cannot be in balance because at all vertical planes, where air is motionless, the pressure is Δp. In the air curtain method the moment plane can have the height h, but when the craft is moving, there are other moment planes in the structure (see Figure 6). In an air curtain system the power needed does not correspond to the moment plane of a plain wing.

Although a circular wing gives the least power at a standstill, at supercritical speed, however, a rectangular planform provides the minimum, for a given span and area,

because the length of the moment plane is decisive. The wing of an aircraft is also a moment plane, but because the mass handled by it is proportional to the speed, the power for the lift is inversely proportional to the speed. The flow through the side gaps of a ground effect vehicle is independent of the speed, and hence also of the power. The moment plane parallel to the span has another magnitude because the flow is nearly proportional to the speed.

Lift, gap, and drag of the ram wing. The maximum lift coefficient of a thin wing, forming at its side and rear edges a closed (but at the leading edge, open) vessel, should be about 1. The vehicle needs speed before becoming airborne.

At subcritical speeds the drag of the bottom surface is the lift multiplied by the tangent of the angle of attack of the average bottom surface element. If the geometry of the wing remains unaltered and the height of the gaps is even along the sides, which should be purposeful, the drag remains at increasing constant speed, but the gap increases because the designed front gap is supplying more air. The air must be retarded to give a pressure rise, and hence the side gap flow has a forward component. The absolute velocity of discharge is

$$V_a = \sqrt{V_r^2 + \left(V_p - \sqrt{V_p^2 - V_r^2} \right)^2} \qquad (9)$$

At critical speed the power for side gap is blowing two times and, at speed $V_p = 2V_r$ about 7 per cent greater than the ideal power of a hovercraft. Figure 7 gives an approximation of the streamlines between the wing and the surface at airborne speed. The rear gap blowing does not neet power, as shown in Figure 8. The wing functions much like a ramjet engine.

Drag caused by friction. The drag of the thin profiles is mainly composed of skin friction only and depends upon the Reynolds' number. Use may be made of the equation

$$C_t = 2 \frac{0.455}{(\log R)^{2.58}} \qquad \text{(related to A)} \qquad (10)$$

One interesting point is the skin friction of the bottom of a ground effect vehicle. In a special case, when relative velocity V of the main air mass under the wing is half of the forward speed V_p, the skin friction should be cut in half, because the bottom of the wing and the surface have a velocity Vp/2 in relation to the air mass. This could also be a practical case when side gaps and vehicle speed are small, but generally skin friction should be greater.

Calculation of a 1000-ft craft and some design points. The equations given could be used for various investigations. The seven variable parameters affect performances as L/D ratio and power. From the power equation, e.g., it will be seen that the power needed to hold a given weight at a given height is inversely proportional to the wing loading.

To make matters simpler, a craft of 1,000-ft span is considered as a design example. For lack of better knowledge, the planform is a square. 1,000 ft is easier to calculate than 10 ft or 100 ft, because the latter must have superstructures to accommodate the payload and the power plants. 1,000 ft may be also nearer the size of a truly good ground effect vehicle. It should be remembered that there have been other aerial vehicles of almost the same length and about half the volume. This size should cover two reasonably big waves.

In Figure 9 the L/D ratio is given as a function of speed and the effective gap for a craft of 30,000 tons. It has been assumed that the drag coefficient C_t is constant = 0.003, although in fact it is a function of the speed. In Figure 10 the L/D ratio is shown as a function of the weight or wing loading at speeds of 250 knots and, for one h_e value, at 125 knots.

In Figure 11 is shown the plan, profile, and nose section of such a craft. For lack of better knowledge the power is divided fifty-fifty for lift and propulsion, which is about true at 250 knots, 10 feet, and 30,000 tons. It should be noted that all the power of wing engines can be used for thrust and the thrust engines can be used for gap control by taking more air through the front gap at supercritical speeds by pushing the blown front gap forward, thereby relieving the lift engines at subcritical speeds. The efficiency of free propellers should be a little better since they are more suitable for control. The lift engines are placed in front. If they should be put on the sides, flush intakes should be used. The intakes work with a small amount of free diffusion or a small amount of forced acceleration. Some of the power tunnels may be equipped with thrust reversers for additional control. The corners of the wing are left free for stability reasons.

The power needed depends upon the wave height, the gap coefficient, and the regularity demanded on a specified route. A guess is that 1,500,000 shaft hp should do the work for 30,000 tons and 250 knots. This seems fairly high, but the powerloading is over 40 lbs/hp and more than 10 times greater than the powerloading of a modern transport aircraft when the speed payload capacity is taken into consideration. To the other inherent advantages of a ground effect vehicle may be added the fact that the power needed for starting is small and the engines always have plenty of air to breathe, a counterweight to the great density which must be mastered.

For reasons of initial cost and rationed capacity the craft should be light, but the decrease of speed and the L/D ratio will limit this tendency. A ground effect vehicle of this size should have, by the most cautious valuation, a L/D ratio 3 times greater than an aircraft and also the payload/gross weight ratio in same proportion. The power economy is thereby 10 times greater.

The structure cannot always be prevented from coming into contact with smaller or larger masses of water at full speed. To prevent endangering the stability or structural integrity, certain parts could be made elastic. It is even better to lose a part of structure than to risk too great impacts. The world speed record on water lies within these speed brackets. To spare weight, special docks could be used, where the weight of the wing is evenly distributed on pylons when the engines are not running.

In the calculations the following limitations have been neglected: the uneven lift distribution, the power loss due to the different energies of flows near the front gap, the lift of the upper side of the wing and other unforeseen effects. However, all of these limitations overwhelmed by the uncertainty of the gap coefficient, the maximum wave height to be mastered, the average wave height, the oscillations that the craft may experience, and the determination of reasonably safe clearance.

A ground effect vehicle of this size is an aircraft with an infinite lift coefficient, with one g and with a L/D ratio up to 200.

Control of average gap and inclination. The only source for control of the average gap is power. The lift engines can be used at the proper power and the wing may have a regulated front gap, so that thrust engines can also be used for this purpose. The known ground effect vehicles have inherent stability, but to get the side gaps even, to have countermeasures for variable weight distribution, and also to have the maximum inherent stability range, additional controls are desirable. The rear end of the wing may have a

divided flap (Figure 12) to give the channel formed by the wing and the surface the desired form to control separately the gap height and the moment of air forces. This control design should be most effective: the models have shown the great influence of the wing trailing edge.

Some early experiments and a new design. In January 1935, a towed man-carrying ram wing of size 6 1/2 x 8 1/2 ft was tested with good results. The gross weight was over 200 lbs, the measured drag 13 lbs, and the power 1 1/2 hp. The operator was lying prone in the profiled wing.

Although only three free starts and free flights were made from snow with a powered craft 16 hp, due to various unhappy incidents (a crash, unsuitable power plants, quite insufficient for a start from water which was also tried) the craft of the type shown in Figure 13 was frequently used in the winters of 1935 and 1936.

The hovercraft 20 hp of Figure 14 was made in the year 1949. Two controlled free flights were made from an airport, but the propulsive force and speed were small. It hovered with four men on board. Tests on water were also made.

Figure 15 gives the main points of design of a 10 ft craft powered by a Volkswagen engine, now under construction. The amount of superstructure to accommodate payload and power plant will be clearly seen.

What is demanded from a ground effect vehicle is payload, speed, and reasonable safety with a minimum of effort. It may be hoped that in certain branches this new vehicle will outclass other modes of transportation by a good margin.

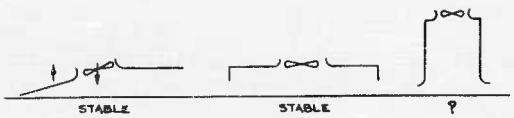

Figure 1.

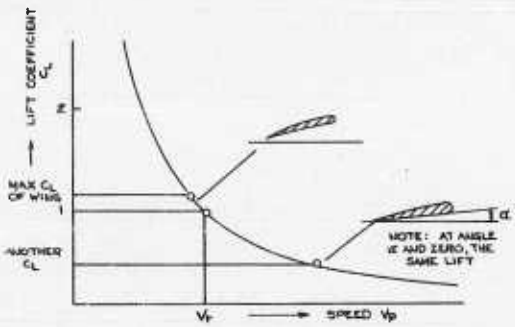

Figure 2.

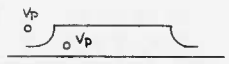

Figure 3.

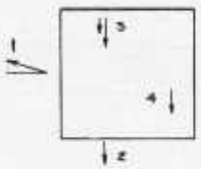

CONSIDERATIONS FOR VELOCITY AT BOTTOM

0 STABILITY
1 V_a
2 η_F
3 LOSS CAUSED BY DIFFERENT ENERGIES OF FLOW
4 C_f
5 POWER PLANT EFFICIENCIES

Figure 4.

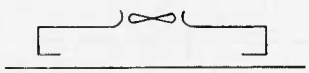

Figure 5

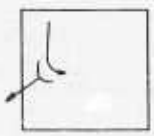

Figure 6.

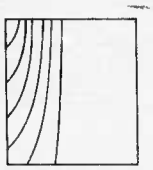

Figure 7.

Figure 8.

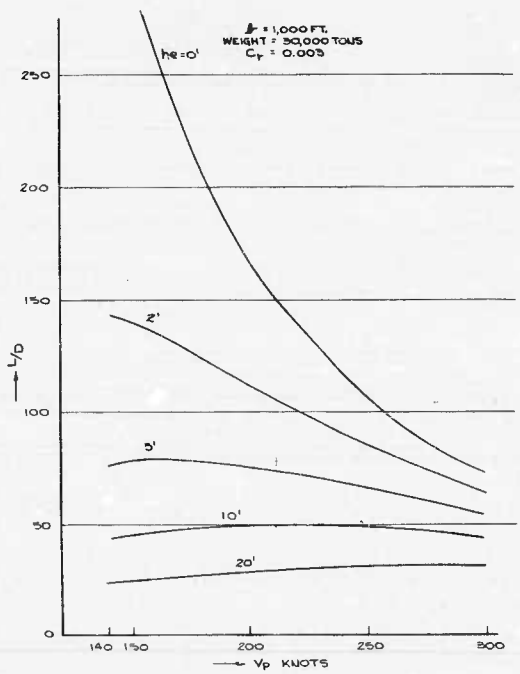

Figure 9.

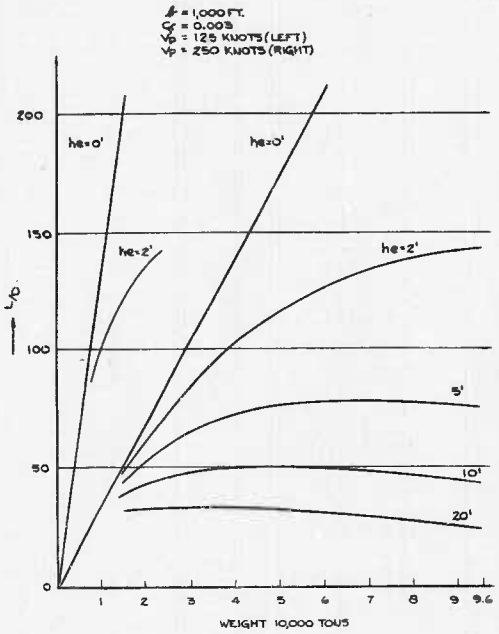

Figure 10

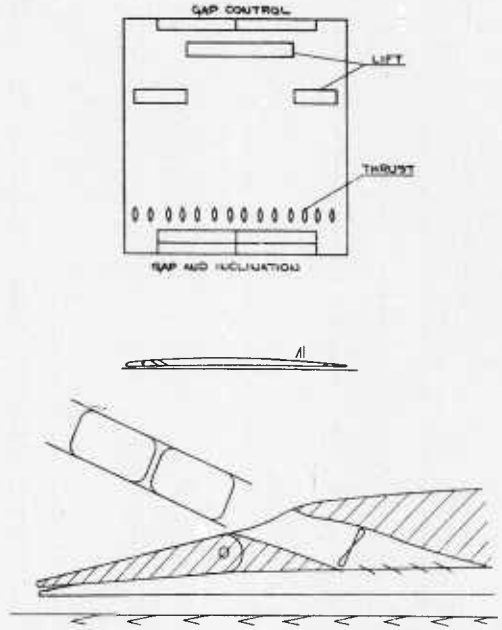

Figure 11.

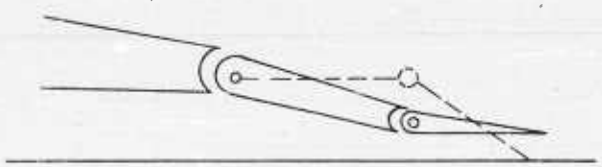

Figure 12.

Figure 13.

Figure 14.

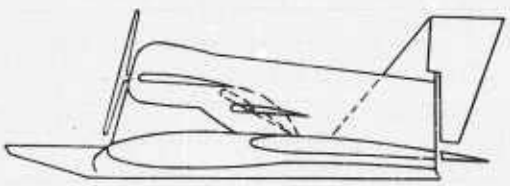

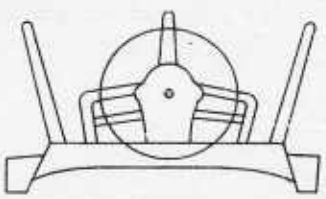

Figure 15.

THEORETICAL AND EXPERIMENTAL RESEARCH ON ANNULAR JETS OVER LAND AND WATER

By Lawrence R. Mack and Ben-Chie Yen,
Iowa Institute of Hydraulic Research, Iowa

ABSTRACT

Chaplin's theory on the effect of jet mixing on an annular jet is valid only when the jet impinges on the ground some distance after the lateral mixing has penetrated to the centerline of the jet sheet. His theory is modified to give a result applicable also to the case in which the impingement occurs before this penetration reaches the centerline. A simple theory is developed for predicting the augmentation of lift of an annular jet over land in the presence of an ambient wind. Preliminary wind tunnel experiments showed good agreement with the predicted percentage reduction of augmentation due to the ambient wind. A nonsymmetrical pressure distribution on the nozzle base giving rise to a pitching moment was observed for large wind velocities.

An analytical model for a jet over water was assumed. On the basis of this model the governing equations have been integrated (some numerically) for both the two-dimensional and axisymmetric annular jets. The optimum angle of discharge has been obtained for the two-dimensional case. The two most important results are: (1) whereas the augmentation over land is independent of the jet momentum, it does depend on it over water, and (2) the augmentation over water is always less than that over land for the same altitude ratio (with respect to the undisturbed water surface). Experimental data on the base plate pressure distribution and the water surface configuration are presented.

INTRODUCTION

The results reported in this paper are drawn from different phases of the annular jet research which is being conducted at the Iowa Institute of Hydraulic Research with the financial support of the Office of Naval Research, Contract Nonr 1509(03). That support and the help of J. K. Malsy and S. P. Garg in the preparation of this report are gratefully acknowledged by the authors.

Portions of this paper have been adapted from portions of the thesis (reference 1) of one of the authors. Another phase of study, that on an annular jet moving over water, has not yet advanced to the stage of reporting results. In all the work performed, the primary interest has been on the flow of the jet after it leaves the nozzle and on the interaction of the jet with the land or water surface against which it is directed, rather than on the design of the nozzle itself or on the design of a practical ground effect vehicle.

NOTATION

A	augmentation factor over land or water from "perfect jet" theory; ratio of total lift to total jet momentum flux
A_m	augmentation factor considering effect of mixing
A_w	augmentation factor considering effect of ambient wind
a_b	area of nozzle base

a_j	area of jet efflux section
b	horizontal distance from nozzle centerline to a point on the jet sheet (two-dimensional)
C	a constant
G	width of jet efflux section
h	vertical distance below nozzle base of a point on the jet sheet
h_a	altitude of nozzle base above ground or free water surface
J	total jet momentum flux
j	jet momentum flux per unit length
k_2	dimensionless constant in Chaplin's approximate entrainment function
m	jet mass flow per unit length
p	pressure; pressure difference across jet sheet
p_1	pressure (gauge) in base cavity (over water)
$\triangle p_w$	pressure (gauge) in base cavity (with wind)
$\triangle p'$	pressure (gauge) just outside windward side of jet
$\triangle p''$	pressure (gauge) just outside leeward side of jet
R	radius of curvature of jet sheet
R_1	radius of curvature on windward side of jet
R_2	radius of curvature on leeward side of jet
r	horizontal distance from nozzle axis to a point on the jet sheet (axisymmetric)
s	arc length along jet sheet from nozzle exit
V	velocity
γ	specific weight of water
Θ	angle of divergence of jet from downward vertical (Θ is negative when jet is directed inward)
ν	kinematic viscosity of air
ρ	mass density of air

Subscripts.

a	at ground; condition where jet leaves water surface

c	condition just before impingement
e	entrained
j	jet
o	condition at jet exit
w	wind; condition where jet first contacts water surface

EFFECT OF JET MIXING

Chaplin (reference 2) has developed a theory accounting for the effect of jet mixing on a two-dimensional "annular" jet within the ground effect. The particular choice that he makes for the entrainment function, however, limits the application of his result to altitudes above the ground sufficiently large that the mixing has become fully established before the jet reaches the ground. It is the purpose of this section to extend Chaplin's results to the case in which impingement occurs while the jet is still in the zone of flow establishment.

The assumptions made by Chaplin are given briefly below. Each jet curves outward at a constant radius of curvature R until it impinges on the ground at an angle Θ_c from the vertical. The entrainment fromthe base cavity (which for steady flow must equal the inward mass flow from the impingement) is taken as half of the total entrainment m_{ec} into the jet, upstream from the impingement. The ratio of the entrained mass flow to the total mass flow m_c of the jet just before impingement may be represented by

$$\frac{m_{ec}}{m_c} = f\left(\frac{s_c}{G}\right) \tag{1}$$

where s_c is the distance along the jet path from the nozzle to the impingement point, and G is the width of the "annular" gap.

On the basis of these assumptions of the geometry of the flow and of mass and momentum balances of the flows entering and leaving the impingement region, he obtained

$$1 - \sin\Theta_c = f\left(\frac{s_c}{G}\right) \tag{2}$$

$$\frac{s_c}{G} = \frac{2b_o}{G}\,\frac{h_a}{2b_o}\,\frac{\Theta_c - \Theta_o}{\sin\Theta_c - \sin\Theta_o} \tag{3}$$

$$A_m = \cos\Theta_o + \frac{\sin\Theta_c - \sin\Theta_o}{h_a/b_o}\,\frac{1 - \sin\Theta_2}{2} \tag{4}$$

$$\frac{A_m - \cos\Theta_o}{A - \cos\Theta_o} = \frac{\sin\Theta_c - \sin\Theta_o}{1 - \sin\Theta_o} + \frac{h_a}{2b_o}\,\frac{1 - \sin\Theta_c}{1 - \sin\Theta_o} \tag{5}$$

where $2b_o$ is the base width (note that $2b_o$ of this paper equals the b of Chaplin's report), h_a is the elevation of the nozzle above the ground, Θ_o is the angle of divergence of the jet from the vertical at the jet exit (Θ_o is negative when directed inward), A_m is the augmentation factor with the effect of mixing considered, and A is the augmentation predicted by the nonmixing "perfect jet" theory.

On the basis of the mixing length analysis of Tollmien (reference 3) Chaplin (reference 2) chose the function f in the following form:

$$\frac{m_{ec}}{m_c} = f\left(\frac{s_c}{G}\right) = \begin{cases} 1 - \sqrt{\dfrac{k_2\, G}{s_c}} & , \quad s_c > k_2\, G \\ 0 & , \quad s_c < k_2\, G \end{cases} \tag{6}$$

where k_2 is a dimensionless constant whose value depends on the pressure ratio of the jet.

The distance k_2G corresponds to the length of the zone of flow establishment of a mixing jet; that is, to the distance from the jet efflux section to the point where the penetration of lateral mixing reaches the centerline of the jet. The entrainment function f given by equation (6) completely ignores the entrainment in the zone of flow establishment and inadequately represents it for an additional distance of approximately the same length.

Albertson, Dai, Jensen, and Rouse (reference 4) determined that the air entrainment by a two-dimensional submerged jet is given by

$$\frac{m_{ec}}{m_c} = f\left(\frac{s_c}{G}\right) = \begin{cases} 1 - \dfrac{1}{0.62}\sqrt{G/s_c} & , \quad s_c/G > 5.3 \\ \dfrac{0.080\, s_c/G}{1 + 0.080\, s_c/G} & , \quad s_c/G < 5.3 \end{cases} \tag{7}$$

Inspection of Figure 13, reference 4, shows an experimental value of 2.6 for k_2 as opposed to the 5 derived by Chaplin (reference 2) from Forthmann's (reference 5) measurements. That k_2 of Albertson, et al., is 2.6 may also be seen by comparing equations (6) and (7) for large s_c/G. Since both values of k_2 were for pressure ratios giving essentially incompressible flow, this discrepancy is unexplained.

Assuming equation (7) to represent the entrainment adequately both in the zone of flow establishment and in the zone of established flow, the results of equations (2), (3), (5), and (7) are plotted in Figure 1 as $(A_m - \cos\Theta_o)/(A - \cos\Theta_o)$ versus $h_a/2b_o$, with $2b_o/G$ as parameter for the particular case $\Theta_o = 0^o$.

As was pointed out by Chaplin in reference 6, the two-dimensional solution affords a good approximation to the solution of the corresponding axisymmetric problem at very low relative altitudes if $2b_o$ is replaced by r_o. Hence Figure 1 has been labeled so that it may be used for either the two-dimensional or axisymmetric cases. The locus of $s_c/G = 5.3$ is also shown in this figure.

Both the original investigation of the effect of mixing by Chaplin (reference 2) and the present modification of his theory make use of entrainment measurements made on a jet

discharging into an infinite fluid. The accuracy of using the entrainment function for such a freely discharging jet to represent that of a jet directed against the ground is questionable and should be checked by experiments.

EFFECT OF WIND

Let us consider a circular disk of radius r_o situated a distance h_a above the ground and parallel to it. A thin jet of uniform momentum j_o per unit length and velocity V_j is being exhausted downward from the circumference of this disk at an inclination of Θ_o^j from the vertical. A wind of velocity V_w is flowing from left to right, parallel to the ground (or, conversely, the disk is moving horizontally from right to left at velocity V_w).

A single line is taken to represent adequately the path of the jet. The ratio h_a/r_o is restricted to sufficiently small values that $r/r_o \approx 1$. This means that the variation along the jet path of the momentum per unit length and of the radius of curvature of the path may be neglected. A uniform pressure Δp_w (gauge) is assumed within the cavity enclosed by the ground, the jet sheet, and the nozzle base. If the jet sheet is considered as a cylinder held in the wind flow, then its windward surface will experience an increase of pressure $\Delta p'$s and its leeward surface a reduction $-\Delta p''$ from atmospheric.

It is assumed that the most vulnerable part of the jet (that is, the leeward side where the reduction of pressure due to the wind is greatest) curves to become tangent to the ground. Then since the pressure difference across the jet will be smaller, and hence the radius of curvature greater everywhere else, all other parts of the jet will impinge upon the ground sending a portion of their flow into the base cavity and out beneath the leeward side. The radius of curvature of the jet will vary continuously from the windward "leading edge" to the leeward "trailing edge." The assumed jet configuration is illustrated in Figure 2 (Θ_o is negative as shown).

The pressure difference across the jet on the leeward side is $\Delta p_w - \Delta p''$. For h_a/r_o small enough that $r/r_o \approx 1$, momentum considerations yield

$$\Delta p_w - \Delta p'' = \frac{J}{2\pi r_o R_2} \tag{8}$$

where J is the total momentum flux of the jet, $J = 2\pi r_o j_o$.

By geometry

$$R_2 = \frac{h_a}{1 - \sin \Theta_o} \tag{9}$$

The augmentation factor incorporating the effect of wind A_w is given by the total lift divided by the jet momentum:

$$A_w = \frac{1}{J}\left[J \cos \Theta_o + \pi r_o^2 \Delta p_w\right] \tag{10}$$

Through the use of equations (8) and (9) this may be rewritten as

$$A_w = \cos \Theta_o + \frac{1 - \sin \Theta_o}{2\, h_a/r_o} + \frac{\pi r_o^2 \Delta p''}{J} \tag{11}$$

It is here assumed that $\Delta p''$ may be represented by

$$\Delta p'' = C \frac{\rho V_w^2}{2} \tag{12}$$

where C is a constant (negative) depending upon the Reynolds number of the wind flow and ρ is the mass density of air. Noting that the first two terms on the right side of equation (11) are equal to A, the augmentation factor when V_w is zero, and that the total jet momentum J is given by

$$J = \rho a_j V_j^2 \tag{13}$$

where a_j is the area of the jet exit section, we may rewrite equation (11) as

$$A_w = A + \frac{C}{2} \frac{a_b}{a_j} \left(\frac{V_w}{V_j} \right)^2 \tag{14}$$

where $a_b = \pi r_o^2$ is the area of the nozzle base.

Let us now determine C. The Reynolds numbers, computed on the basis of the wind velocity V_w and the diameter $2r_o$, ranged from 24,700 to 44,700 for the wind tunnel experiments mentioned in this section. Detailed pressure distributions around cylinders at these Reynolds numbers do not appear to be readily available. Figure 126 of "Elementary Mechanics of Fluids" (reference 7) shows that the coefficient of drag of a circular cylinder is nearly constant between Reynolds numbers of 1,000 and 200,000. Since the coefficient of drag depends upon the pressure distribution around the cylinder, it can be inferred that the pressure distribution is also nearly constant in this range. The pressure distribution around a cylinder at a Reynolds number of 186,000 shown in Figure 122 of reference 7 is thus assumed applicable at all Reynolds numbers from 1,000 to 200,000. It is seen that the pressure on the leeward side is about $-\rho V_w^2/2$; that is, $C \approx -1$.

Substituting this value for C, we obtain

$$A_w = A - \frac{1}{2} \frac{a_b}{a_j} \left(\frac{V_w}{V_j} \right)^2 \tag{15}$$

and

$$\frac{A_w}{A} = 1 - \frac{h_a/r_o}{2(h_a/r_o) \cos \Theta_o + 1 - \sin \Theta_o} \frac{a_b}{a_j} \left(\frac{V_w}{V_j} \right)^2 \tag{16}$$

for $1,000 < 2r_o V_w/\nu < 200,000$, where ν is the kinematic viscosity of air. Curves of equation (16) for $\Theta_o = 0^o$ have been plotted in Figure 3.

These equations may not be quantitatively accurate because of the use of pressure data obtained on an infinitely long cylinder in place of the unknown distribution on the jet sheet, a very short "cylinder." It is believed, however, that the dependence of A_w/A on h_a/r_o, a_b/a_j, and V_w/V_j as given is qualitatively correct.

In order to test this belief, preliminary wind tunnel experiments were performed with a crude nozzle. This nozzle had an exit angle Θ_o of 0^o and an area ratio a_b/a_j of 5.76. It was operated primarily at an altitude ratio h_a/r_o of 1/4 for velocity ratios V_w/V_j from zero to 0.59. These tests showed that A_w/A indeed varied inversely with the square of V_w/V_j. The slope of A_w/A vs. $(V/V_j)^2$, however, was only about 9/10 of that predicted by equation (16). This indicates that for this particular altitude, exit angle, and area ratio, C has the value of approximately -0.9.

For h_a/r_o of 1/4 the effect of wind on the jet base was found to be a general reduction of pressure for V_w/V_j of 0.3 or less. For higher values of the velocity ratio the reduction of pressure on the windward side of the base was considerably greater than that on the leeward side. It was also found that the V_w/V_j ratio at which a pronounced pressure imbalance first occurred was lower for $h_a/r_o = 1/2$ than for $h_a/r_o = 1/4$. If an annular jet vehicle were moving forward at a velocity sufficiently high that such a pressure imbalance were encountered on the base of the vehicle, the resulting pitching moment would cause a serious stability problem. It is probable that the weaknesses in the jet sheet of the experimental nozzle made it more susceptible to the occurrence of a strong pitching moment than would a nozzle of perfectly uniform jet strength. Nevertheless, the possibility of a pitching moment acting on a uniform jet at high forward velocity should be carefully investigated.

ANALYSIS OF AN ANNULAR JET OVER WATER. TWO-DIMENSIONAL CASE

The operation of an annular jet over water differs from that over land in one important aspect. The water surface will be deformed from the horizontal by the action of the jet. An analysis of the jet flow must then give consideration to the configuration of the water.

In order to make such an analysis, assumptions like those of Chaplin's "perfect jet" analysis (reference 6) are made. The jet is assumed to be thin and nonmixing so that a single line adequately represents its path. The pressure p_1 in the region enclosed by the jet, the nozzle base, and the water surface is assumed uniform. The total momentum flux is taken to be constant along the jet path. Further assumptions needed are that the pressure at all points in the water is hydrostatic, that the jet's initial contact with the water is at an angle Θ_w with the vertical, and that the jet leaves the water surface at an angle Θ_a. The jet is assumed not to penetrate the water, but rather to depress the surface in such a manner that the jet path during its contact with the water is tangent to the deformed water surface. From the assumptions of constant pressure in the base cavity and hydrostatic pressure in the water it follows that that portion of the water surface in contact with the base cavity must be horizontal.

That part of the jet which has the base cavity air on one side and atmospheric air on the other is called the air region. That part of the jet path which has water on one side and atmospheric air on the other is called the water region. The atmospheric pressure is taken as zero. From momentum considerations, the radius of curvature of the jet path R is equal to the momentum flux per unit length j divided by the pressure difference p across the jet path. All statements made so far in this section apply both to two-dimensional and axisymmetric annular jets over water.

Let us now consider a two-dimensional nozzle of base width $2b_o$ discharging air with momentum j_o per unit length at an exit angle Θ_o with the vertical. At any point along the jet path with arc length s from the exit, the position will be denoted as h below the base plate vertically and b from the centerline horizontally. The jet path at this point has a

radius of curvature R and makes an angle Θ with the vertical. The geometric configuration is shown in Figure 4.

The governing equations may be obtained from geometric and momentum considerations as

$$dh = ds \cos \Theta \tag{17}$$

$$db = ds \sin \Theta \tag{18}$$

$$ds = R\, d\Theta \tag{19}$$

and

$$R = j_o/p \tag{20}$$

since $j = j_o$ for a two-dimensional jet. The pressure p is given in the air region by

$$p = p_1 \tag{21}$$

and in the water region by

$$p = p_1 + \gamma(h - h_w) = \gamma(h - h_a) \tag{22}$$

where γ is the specific weight of water.

From equations (20) and (21) it is seen that the path of the jet in the air region is an arc of constant radius. It follows readily that in the air region

$$h = (j_o/p_1)\ (\sin \Theta - \sin \Theta_o) \tag{23}$$

and

$$b = b_o + (j_o/p_1)\ (\cos \Theta_o - \cos \Theta) \tag{24}$$

In the water region equations (17), (19), (20), and (22) may be combined to give

$$dh = \frac{j_o}{\gamma(h - h_a)} \cos \Theta\, d\Theta \tag{25}$$

which may be integrated to yield

$$\frac{h^2 - h_w^2}{2} - h_a(h - h_w) = \frac{j_o}{\gamma}(\sin \Theta - \sin \Theta_w) \tag{26}$$

Substitution of the hydrostatic relation

$$h_a = h_w - \frac{p_1}{\gamma} \tag{27}$$

into equation (26) and solution of the quadratic give

$$h = h_a + \sqrt{\frac{2j_o}{\gamma}}\sqrt{\frac{p_1^2}{2j_o\gamma} - \sin \Theta_w + \sin \Theta} \tag{28}$$

in the water region. Similarly equations (17), (18), (25), and (28) may be combined to yield

$$b = b_w + \sqrt{\frac{j_o}{2\gamma}} \int_{\Theta_w}^{\Theta} \frac{\sin \Theta \, d\Theta}{\sqrt{\frac{p_1^2}{2j_o\gamma} - \sin \Theta_w + \sin \Theta}} \tag{29}$$

Unfortunately, the result of this integration cannot be expressed in closed form using elementary functions. Hence numerical procedures were followed to locate the jet path in the water region.

An interesting relation can be obtained without knowing the path. Equating the net horizontal forces on the jet in the water region to its change in horizontal momentum in that region yields

$$-\frac{\gamma}{2}(h_w - h_a)^2 = j_o \sin \Theta_a - j_o \sin \Theta_w \tag{30}$$

or, upon substitution of equation (27),

$$\sin \Theta_a - \sin \Theta_w + \frac{p_1^2}{2j_o\gamma} = 0 \tag{31}$$

Thus the leaving angle Θ_a can be computed directly without knowing the position of the leaving point if j_o, p_1, and Θ_w are known. Equation (31) may also be obtained from equation (28) by setting $h = h_a$ when $\Theta = \Theta_a$.

An expression for the base pressure p_1 is now derived.

$$p_1 = j_o/R_o = j_o (\sin \Theta_w - \sin \Theta_o)/h_w \tag{32}$$

Elimination of h_w from equations (32) and (27), solution of the resultant quadratic for p_1, and rejection of the root which would give negative p_1 give

$$p_1 = \frac{1}{2}\left[-\gamma h_a + \sqrt{\gamma^2 h_a^2 + 4\gamma j_o (\sin \Theta_w - \sin \Theta_o)} \right] \tag{33}$$

It is noted that the governing equations presented are insufficient by one to determine all unknown quantities in terms of the four quantities (Θ_o, b_o, j_o, and either h_a or p_1) which could be specified or demanded. Unless some procedure such as maximizing or minimizing an energy expression might yield an additional relation, experimental results must be relied on to determine the extra unknown, which is taken to be Θ_w. Although both logic and the axisymmetric experiments reported later under "Experiments on an Annular Jet over Water" seem to indicate that Θ_w is somewhat less than 90°, the experiments appear to show that choosing $\Theta_w = 90°$ is not far in error (as well as being very convenient). It is assumed that this value can be applied to the two-dimensional jet as well; for the remainder of this section, then, Θ_w is taken as 90°.

To trace the jet paths, numerical integrations were performed after the variables had been changed to the dimensionless forms $p_1/\gamma b_o$, $j_o/\gamma b_o^2$ and length/b_o. Although for

plotting purposes it is just a dummy, the arc length s/b_o was chosen as the independent variable since it alone is always finite and increasing. Several jet paths are shown in Figure 5, all for $\Theta_o = 0^o$.

Equation (33) giving p_1 as a function of h_a and j_o has been plotted in Figure 6 for $\Theta_o = 0^o$. It is seen from this figure that, for a constant j_o, p_1 increases as h_a decreases and that this increase is more rapid at low altitudes than at high.

The augmentation factor, that is, the ratio of the total lift to the total jet momentum flux, is

$$A = \frac{1}{2 j_o} \left[2 j_o \cos \Theta_o + 2 b_o p_1 \right] = \cos \Theta_o + \frac{b_o p_1}{j_o} \tag{34}$$

After substitution of equation (33) for p_1, this becomes

$$A = \cos \Theta_o + \frac{1}{2} \frac{\gamma_{b_o}^2}{j_o} \left[-\frac{h_a}{b_o} + \sqrt{\left(\frac{h_a}{b_o} \right)^2 + 4 \frac{j_o}{\gamma_{b_o}^2} (1 - \sin \Theta_o)} \right] \tag{35}$$

This equation has been plotted in Figure 7 for $\Theta_o = 0^o$. In contrast to the augmentation against ground, which is independent of the jet momentum, it is observed that the augmentation against water depends rather strongly on the jet momentum. This qualitative difference between the two cases is a direct result of the deformability of the water surface in contrast to the immobility of a land surface.

As will be discussed in more detail in the next section, it is believed that $\Theta_a > 180°$ is physically unrealistic. Hence the locus of $\Theta_a = 180°$ has been plotted in Figures 6 and 7, and the curves of these figures shown only for conditions for which $\Theta_a < 180°$.

The optimum exit angle is defined as that for which the lift, and hence the augmentation, is a maximum. Setting $dA/d\Theta_o$ equal to zero yields

$$\tan \Theta_{o_{opt}} = -\frac{1}{\sqrt{\left(\frac{h_a}{b_o} \right)^2 + 4 \frac{j_o}{\gamma_{b_o}^2} \left(1 - \sin \Theta_{o_{opt}} \right)}} \tag{36}$$

Since the radical has a positive value, it is clear that the optimum Θ_o is always a negative angle, as was the case over land. Equation (36) has been solved by trial and error and the results plotted in Figure 8. It is seen that the magnitude of the optimum exit angle varies inversely with both the relative altitude and the jet momentum. It is also noted that, for a given jet momentum, the optimum Θ_o varies least with h_a/b_o for very low altitudes.

As has been noted by previous writers, making Θ_o too large negatively raises the possibility that the two jets might come together on the centerline and continue as a "solid" rather than annular jet. A limiting value of Θ_o in the range $\Theta_o \leq 0$ may be obtained from equation (24) by requiring b to be greater than zero.

$$\frac{b}{b_o} = 1 + \frac{j_o}{b_o p_1} (\cos \Theta_o - \cos \Theta) > 0 \tag{37}$$

Substitution of p_1 from equation (33) and setting of $\Theta = 0$ for the limiting condition of the two jet sheets becoming tangent to each other as $b \rightarrow 0$ yield

$$\cos \Theta_o \geq 1 - \frac{\gamma b_o^2}{2 j_o} \left[-\frac{h_a}{b_o} + \sqrt{\left(\frac{h_a}{b_o} \right)^2 + 4 \frac{j_o}{\gamma b_o^2} (1 - \sin \Theta_o)} \right] \tag{38}$$

for $\Theta_o \quad 0$.

ANALYSIS OF AN AXISYMMETRIC JET OVER WATER

The analysis of an axisymmetric annular jet over water proceeds from the same assumptions and the same supposed configuration as in the two-dimensional case. However, the momentum flux per unit length j is not constant along the jet path for axisymmetric flow, although the total momentum flux J is. That is

$$J = 2\pi r j = 2\pi r_o j_o = \text{constant} \tag{39}$$

As a result, the radius of curvature R varies continuously along the jet path in the air region as well as in the water region. Figure 4 shows the geometric configuration for the axisymmetric case if b, b_o are replaced by r, r_o and it is remembered that R is variable in both regions.

The governing equations are the same as for the two-dimensional case except that equation (20) is replaced by

$$R = \frac{j_o}{p} \frac{r_o}{r} \tag{40}$$

and b in equation (18) is replaced by r to read

$$dr = ds \sin \Theta \tag{41}$$

Thus equations (17), (41), (19), (40), (21), and (22) are the governing equations for an axisymmetric jet over water.

In the air region substitution of equations (19), (40), and (21) into equation (41) gives

$$dr = \frac{j_o r_o}{p_1 r} \sin \Theta \, d\Theta \tag{42}$$

which may be integrated to yield

$$\frac{1}{2}(r^2 - r_o^2) = \frac{j_o r_o}{p_1} (\cos \Theta_o - \cos \Theta) \tag{43}$$

or

$$r = \sqrt{r_o^2 + \frac{2 j_o r_o}{p_1} (\cos \Theta_o - \cos \Theta)} \tag{44}$$

Likewise, substitution of equations (41), (42), and (44) into equation (17) and integration yield

$$h = \sqrt{\frac{j_o r_o}{2 p_1}} \int_{\Theta_o}^{\Theta} \frac{\cos \Theta \; d\Theta}{\sqrt{\frac{p_1 r_o}{2 j_o} + \cos \Theta_o - \cos \Theta}} \tag{45}$$

Like equation (29), this integral cannot be evaluated by ordinary means. It is, however, the same integral that has been evaluated numerically by Chaplin, its value being plotted in Figure 3 of reference 6.

In the water region substitution of equations (19), (40), and (22) into equations (17) and (41) gives

$$dh = \frac{j_o r_o}{\gamma (h - h_a)} \frac{\cos \Theta \; d\Theta}{r} \tag{46}$$

and

$$dr = \frac{j_o r_o}{\gamma (h - h_a)} \frac{\sin \Theta \; d\Theta}{r} \tag{47}$$

If either h or r is eliminated between these equations, the resultant equation is a second-order highly nonlinear differential equation whose analytical solution appears impossible. Hence numerical integrations were performed to locate the path of the jet; in these integrations Θ_w was taken as 90°. The results are tabulated in Table 1 below. Some typical jet-path profiles among those listed in Table 1 are illustrated in Figures 9 and 10. As is seen from the upper curve of Figure 9 or from Table 1, operation of nozzle at negative h_a/r_o is not necessarily impossible.

In carrying out these integrations it was noticed that, for a given jet momentum, if too high a pressure (or too low a relative altitude) were assumed, the leaving angle Θ_a would be found to be greater than 180°; that is, the jet would have turned past a vertically upward direction and become directed up and also inward toward the nozzle axis. This is considered physically unreasonable since it would require a "cliff" of water leaning out over the depression in the water surface. Hence all conditions which led to $\Theta_a > 180°$ were rejected. It is believed that, in actual operation, conditions leading to Θ_a greater than some critical leaving angle less than 180°, possibly as low as 135°, would give rise to an instability of the water surface, such as the formation of a heavy spray.

Just as this possible instability of the water surface may restrict operation at negative or too small h_a/r_o ratios, an instability of the jet sheet itself restricts operation at certain larger altitudes. If an annular jet is held too high above a surface, either water or land, it will tend to collapse to a "solid" jet, with a considerable reduction in lifting power. That altitude, or range of altitudes, at which the jet changes from annular to "solid" is known as the critical altitude. Experimental values of the critical altitude over water are discussed in the next section.

The augmentation factor is related to the pressure and momentum by

$$A = \frac{1}{J}(J \cos \Theta_o + \pi r_o^2 p_1) = \cos \Theta_o + \frac{1}{2} \frac{p_1/\gamma r_o}{j_o/\gamma r_o^2} \tag{48}$$

TABLE 1. Axisymmetric jet over water, ($\Theta_o = 0^o$)

$\frac{J_o}{\gamma r_o^2}$	$\frac{p_1}{\gamma r_o}$	A	$\frac{h_w}{r_o}$	$\frac{r_w}{r_o}$	$\frac{h_a}{r_o}$	$\frac{r_a}{r_o}$	θ_a (degrees)
	0.50	1.125	2.772	3.000	2.272	4.121	129.19
2.00	0.80	1.20	1.890	2.449	1.090	3.524	149.30
	1.00	1.25	1.570	2.236	0.570	3.223	163.17
	0.25	1.125	2.772	3.000	2.522	3.841	116.93
1.00	0.50	1.25	1.569	2.236	1.069	3.109	138.53
	0.80	1.40	1.047	1.871	0.247	2.624	165.29
	0.15	1.15	2.399	2.769	2.249	3.408	111.49
	0.25	1.25	1.569	2.236	1.319	2.916	123.06
0.50	0.40	1.40	1.046	1.871	0.646	2.548	139.96
	0.50	1.50	0.861	1.732	0.361	2.374	151.54
	0.60	1.60	0.728	1.633	0.128	2.215	164.26
	0.70	1.70	0.635	1.558	-0.065	2.071	176.08
	0.075	1.15	2.399	2.769	2.324	3.229	104.61
0.25	0.125	1.25	1.570	2.236	1.445	2.736	112.75
	0.25	1.50	0.861	1.732	0.611	2.263	131.42
	0.50	2.00	0.459	1.414	-0.041	1.821	170.73
	0.03	1.15	2.399	2.769	2.369	3.067	99.34
	0.05	1.25	1.570	2.236	1.520	2.565	104.15
0.10	0.10	1.50	0.861	1.732	0.761	2.088	115.27
	0.20	2.00	0.459	1.414	0.259	1.771	137.21
	0.30	2.50	0.315	1.290	0.015	1.596	160.30
	0.015	1.15	2.399	2.769	2.384	2.986	96.59
	0.025	1.25	1.570	2.236	1.545	2.470	99.97
0.05	0.05	1.50	0.861	1.732	0.811	1.988	107.70
	0.10	2.00	0.459	1.414	0.359	1.685	122.14
	0.15	2.50	0.315	1.290	0.165	1.555	137.38
	0.20	3.00	0.244	1.225	0.044	1.467	152.62

The augmentation versus the relative altitude with jet momentum as the parameter is shown in Figure 11. Through the use of this figure and equation (48), it is possible to obtain the base pressure corresponding to any desired operating conditions within the scope of the figure.

As may be seen from Figure 11, the augmentation attained against ground may be obtained from the solution over water as the limiting case of zero jet momentum. Since every operating jet must have a finite positive momentum, it is clear that the augmentation over water is always less than that over land for the same altitude ratio (with respect to the undisturbed water surface). This statement is applicable both to two-dimensional and axisymmetric nozzles.

EXPERIMENTS ON AN ANNULAR JET OVER WATER

Tests were performed on an axisymmetric annular jet discharging air normal to a free water surface. The nozzle, consisting of an outer shell and a center body, was machined of lucite. The base plate diameter $2r_o$ was 7 inches and the width of the annular gap was 1/2 inch. The whole flow boundary was well streamlined. Seventeen piezometric holes were located on the base plate. Pointed upstream into the 6-inch air supply pipe was a stagnation tube opposite which, on the wall of the supply pipe, was a piezometric hole. The piezometric and stagnation tubes were led out through four streamlined instrument passages.

The nozzle was held over a five-feet-square water tank whose depth was 2-3/4 feet. The nozzle could be raised or lowered through a distance of about 4 inches. It was rigidly connected to a 6-inch brass pipe 4 feet long which in turn was welded to a 90° bend containing three vanes to minimize the effect of spiral flow. A blower with a 3 hp motor was used to supply air. At full gate it could supply a head of about 3 inches of water at the nozzle exit. A hook gauge was used for measuring the position of the water surface and pressures were read by use of a differential manometer.

The velocity of the jet along the centerline of the annulus was measured and the results are shown in Figure 12. It is seen that the minimum velocity differed from the maximum by 2.5 per cent. The position of this low velocity was beneath the inner edge of the bend, indicating that the use of vanes did not entirely eliminate spiral flows.

The pressure distributions on the nozzle base are presented in Figures 13 and 14. It is noted that the pressure is very nearly uniform for $h_a/r_o \leq 1$. At altitude ratios of 1.5 and 2.0 a slight increase in pressure is observed near the center of the base. This increase seems to be due to the jet mixing. Because of the mixing, an eddy will be present underneath the nozzle base. For axisymmetric flow the center of the jet base will be a stagnation point and hence will have a higher static pressure than nearby points. The mixing will be greater at high elevations than at low, in agreement with Figures 13 and 14. The total force on the base plate was obtained by integration of the pressure distributions.

It was attempted to measure the pressure distribution on the base at a relative altitude of 2.5. However, at this elevation the nozzle was at the lower limit of the critical-altitude range, in which there were considerable fluctuations in the jet configuration. Hence, reliable data for $h_a/r_o = 2.5$ could not be obtained.

The critical altitude was found to cover the range $2.50 \leq h_a/r_o \leq 2.75$. For these relative altitudes an initially annular jet would suddenly change to a "solid" jet, then fluctuate back and forth between annular and "solid." During these fluctuations the base pressure would be positive for the annular configuration and negative for the "solid" configuration. The fluctuations were accompanied by a very violent dancing of the water surface beneath the nozzle. Within the critical-altitude range two factors affected the fluctuations.

The higher h_a/r_o, the greater was the percentage of time that the configuration was "solid." The smaller the jet momentum, the greater was the percentage of time that the configuration was annular. For $2.70 < h_a/r_o < 2.75$, the jet might be initially annular, but once changed to "solid" it would not return to annular. For $h_a/r_o > 2.75$, no matter how low the jet momentum was made, an annular jet sheet could not be established. The critical-altitude range found here for an annular jet over water is comparable to that observed against ground by Von Glahn (reference 8) $2.4 \leq h_a/r_o \leq 3.2$.

Visually, the depression of the water surface had the shape of a half doughnut, or, better yet, a mold from a machine making automobile tires. Moderate to large-sized ripples were present on the entire water surface. For virtually all operating conditions, some splashing occurred both under the nozzle and on the upward sloping face of the water region. The splashing was more serious at low altitude ratios and with large jet momentums. The very violent waves under the nozzle at critical altitude ratios have already been mentioned.

Because of the splashing and of the ripples on the surface the measurements of the water surface profiles shown in Figure 15 are not completely reliable. They do appear, however, to give a qualitative picture of the surface profile ignoring the ripples. (Note that the horizontal and vertical scales in Figure 15 are different.) The surface directly under the base of the nozzle is at a uniform depression from the free water level. The surface rises slightly just inside the point where the jet first meets the water, then follows the jet around the curve of the water region. The water rises up a little above the free water level just outside the point where the jet leaves the surface. This stationary rise is somewhat like the bow wave of a ship.

The water level in the central portion of the depression is slightly higher than that at the bottom of the curve of the water region indicating that $\Theta_w < 90°$. It appears, however, that if the rise in water level just inside where the jet meets the water and the "bow wave" just outside where it leaves the surface are ignored, the geometric configuration used in the mathematical analysis including the use of $\Theta_w = 90°$ is an acceptable first approximation.

The experimentally obtained values of the augmentation factor were plotted against the jet momentum in Figure 16 and smooth curves were faired in for each altitude ratio tested. From these curves the experimental curves of Figure 17 were prepared showing augmentation versus altitude ratio for constant jet momentums. The theoretical curves for values of $j_o/\gamma r_o^2$ of 0.05 and 0.10 are also plotted in Figure 17. It is noticed that the experimental values of the augmentation factor lie below the theoretical prediction for low relative altitudes, but that the agreement becomes much closer as h_a/r_o increases toward 2.0. It is further observed that the agreement between theory and experiment is better for the smaller value of the jet momentum. As may be seen from both Figure 16 and Figure 17, the augmentation is greater for smaller values of the jet momentum, as was predicted by the theoretical analysis.

CONCLUSION

The qualitative agreement of the experimental results reported herein with three aspects of the theoretical analysis is believed significant. The experimental data qualitatively confirm that: (1) the augmentation of an annular jet in forward motion over land varies inversely with the square of the forward flight velocity; (2) the assumed mathematical model of the jet path and water-surface configuration for an annular jet hovering over water is an acceptable first approximation; and (3) whereas the augmentation of an annular jet hovering over land is independent of the jet momentum, that over water varies inversely with the jet momentum. To the writers' knowledge each of these analytical results is new, so that the qualitative check on them afforded by the experiments is especially important.

The present analysis of the effect of mixing, although sharing with Chaplin's work (reference 2) the drawback of basing entrainment into an annular jet near ground on that of a freely discharging jet, is an improvement because it does consider the entrainment which takes place within the zone of flow establishment.

REFERENCES

1. Yen, B. C., "An Annular Jet Directed against a Nearby Water Surface." M. S. Thesis, State University of Iowa, August 1959.

2. Chaplin, H. R., "Effect of Jet Mixing on the Annular Jet." David Taylor Model Basin Aero Rept. 953, February 1959.

3. Tollmien, W., "Calculation of Turbulent Expansion Processes" ("Berechnung turbulenter Ausbreitungsvorgänge"). NACA Tech. Mem. 1085, September 1945. (Translated from Zeitschrift für angewandte Mathematik und Mechanik, vol. 6, 1926, p. 1-12.)

4. Albertson, M. L., Dai, Y. B., Jensen, R. A., and Rouse, H., "Diffusion of Submerged Jets." Transactions American Society of Civil Engineers, Vol. 115, p. 639, 1950.

5. Forthmann, E., "Turbulent Jet Expansion" (Uber turbulente Strahlausbreitung). NACA Tech. Mem. 789, March 1936. (Translated from Ingenieur-Archiv, vol. 5, 1934, p. 42-54.)

6. Chaplin, H. R., "Theory of the Annular Nozzle in Proximity to the Ground." David Taylor Model Basin Aero Rept. 923, July 1957.

7. Rouse, H., "Elementary Mechanics of Fluids." John Wiley & Sons, 1946.

8. Von Glahn, U. H., "Exploratory Study of Ground Proximity Effects on Thrust of Annular and Circular Nozzles." NACA Tech. Note 3982, April 1957.

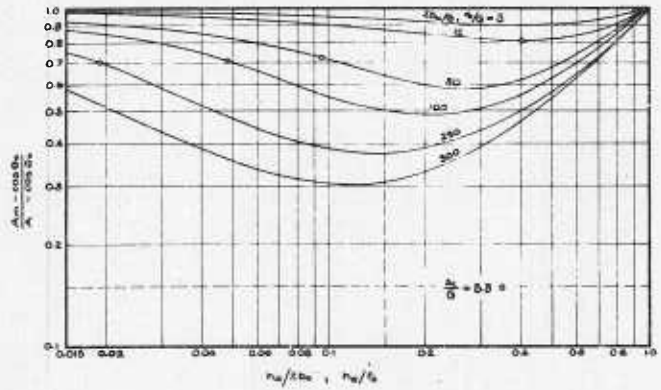

Figure 1. Effect of mixing on augmentation
$\theta_o = 0°$

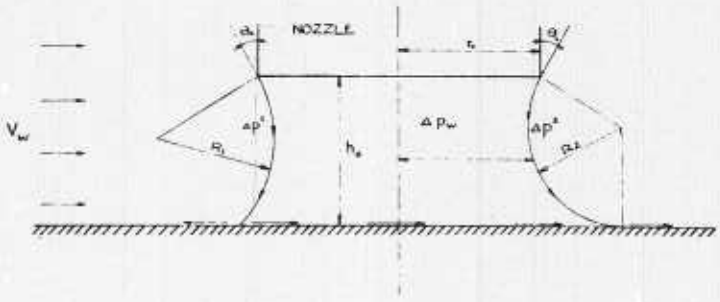

Figure 2. Configuration of axisymmetric jet in wind

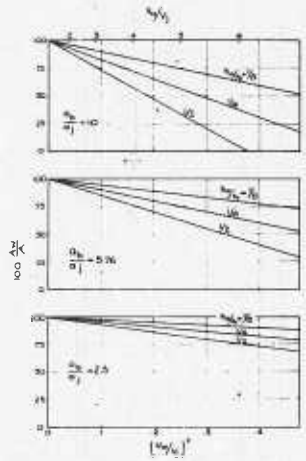

Figure 3. Effect of ambinet wing on augmentation
$\theta_o = 0°$

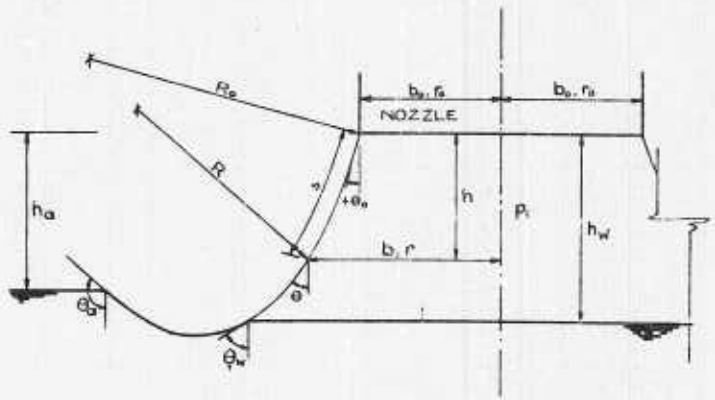

Figure 4. Jet configuration over water

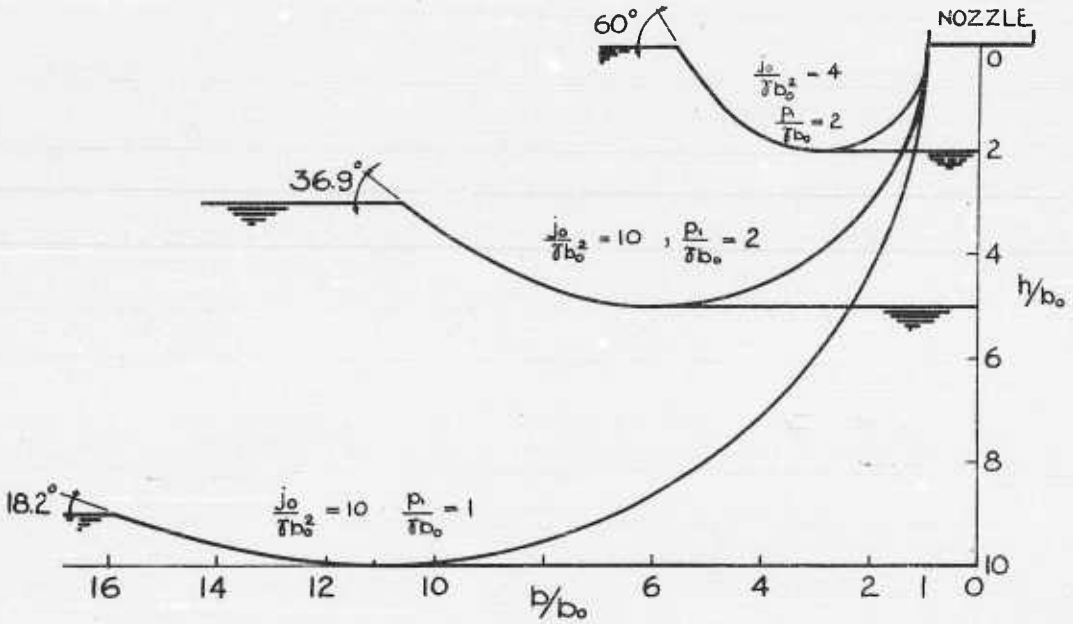

Figure 5. Two-dimensional jet paths over water

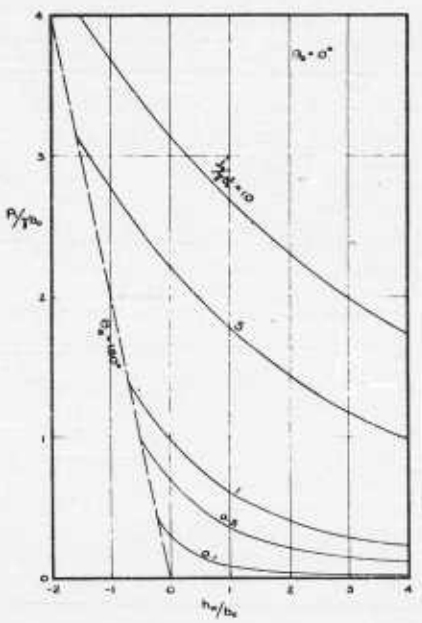

Figure 6. Relation between base pressure, relative altitude, and jet momentum over water, two-dimensional case

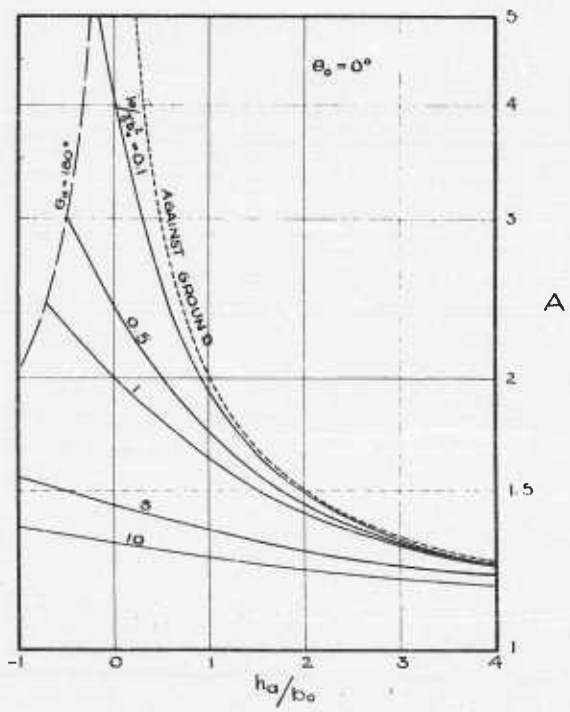

Figure 7. Augmentation over water, two-dimensional case

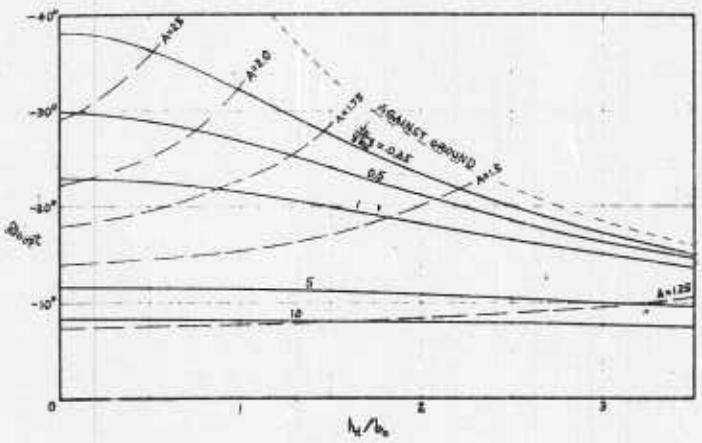

Figure 8. Optimum exit angle over water, two-dimensional case

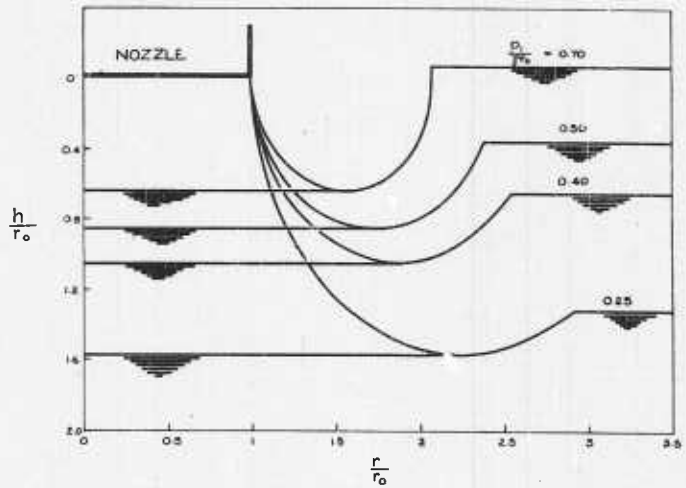

Figure 9. Axisymmetric jet paths over water, $j_o/\gamma\ r_o^2 = 0.5$

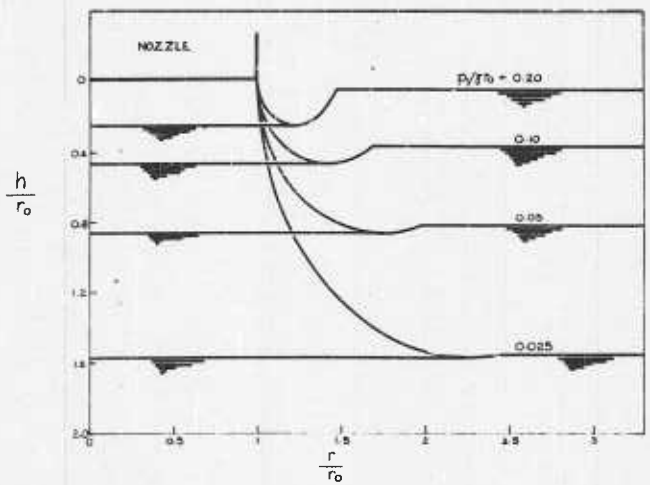

Figure 10. Axisymmetric jet paths over water, $j_o/\gamma\ r_o^2 = 0.05$

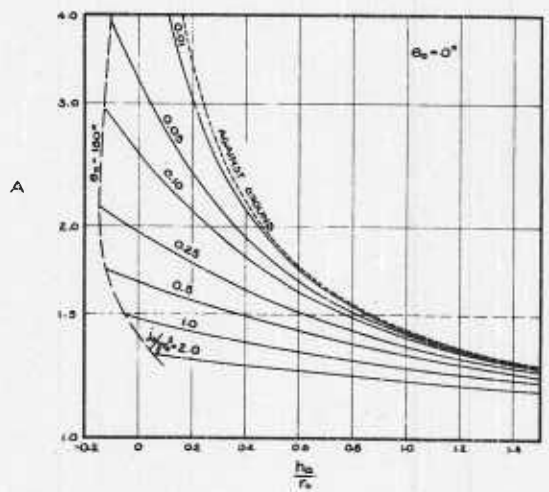

Figure 11. Augmentation over water, axisymmetric case

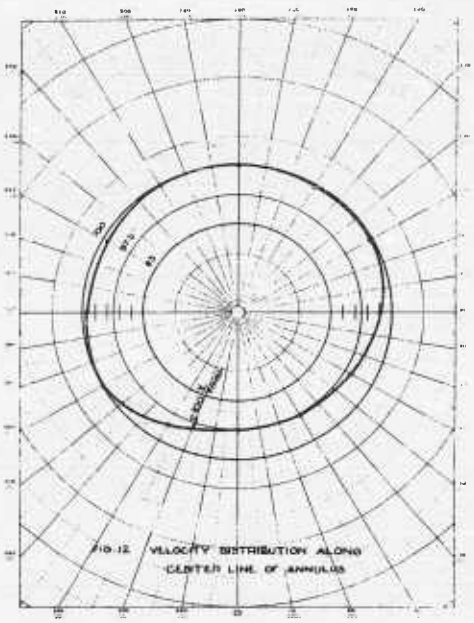

Figure 12. Velocity distribution along center line of annulus

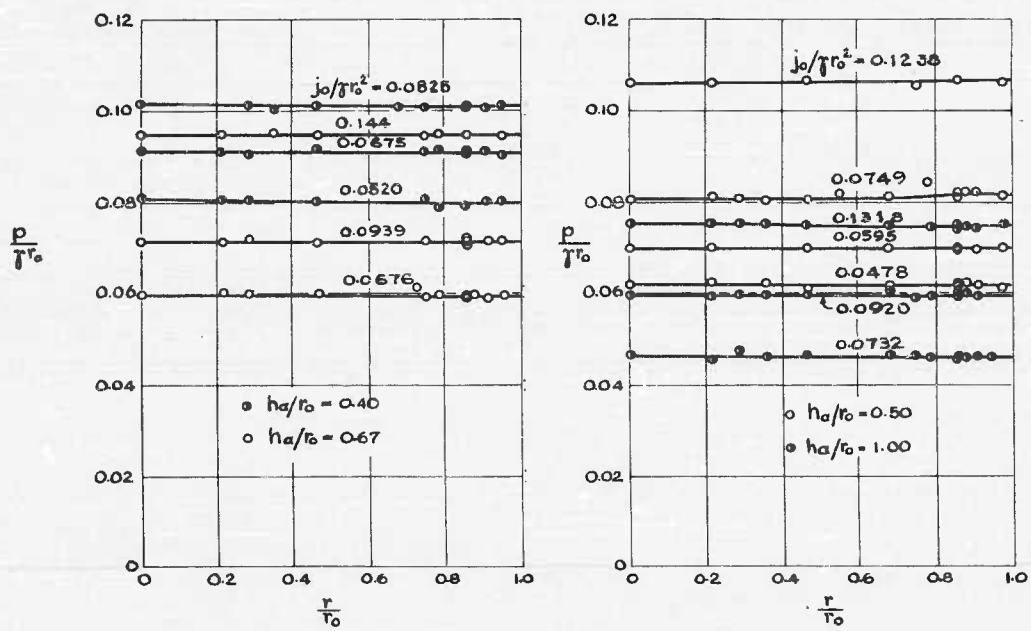

Figure 13. Pressure distribution on base of nozzle

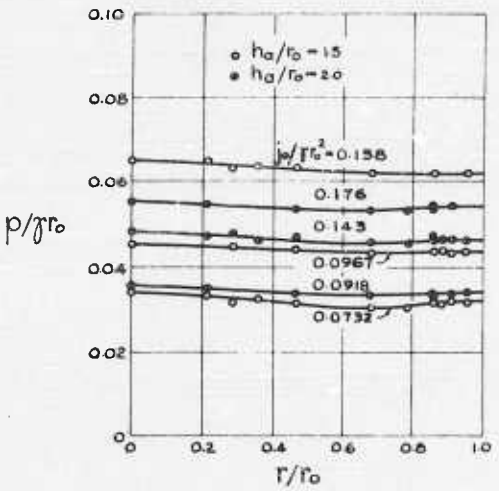

Figure 14. Pressure distribution on base of nozzle

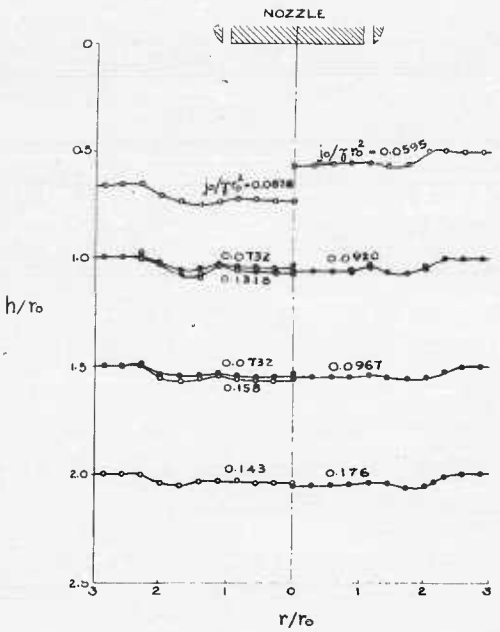

Figure 15. Water surface profiles

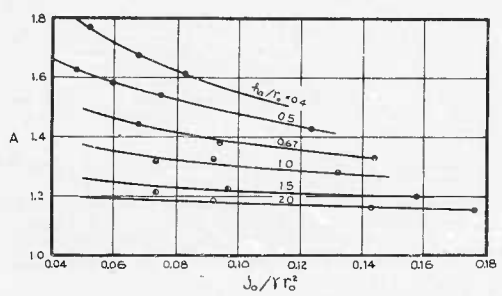

Figure 16. Augmentation (experimental) over water

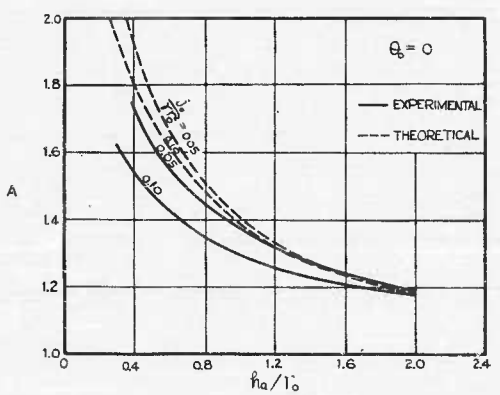

Figure 17. Theoretical and experimental augmentations over water

PERFORMANCE POSSIBILITIES OF SUBSONIC AIRPLANES TAKING-OFF AND LANDING ON THE GROUND CUSHION

By W. Z. Stepniewski, Vertol Aircraft Corporation,

INTRODUCTION

In recent years, considerable theoretical and test efforts have been directed toward various aspects of the ground proximity phenomena with the aim of applying them to vehicles that remain throughout their whole mission within the ground cushioning. (For a review of this effort, see reference 1.) Numerous experimental ground effect machines either have been or are being built.

In contrast to the above activity, little attention has been given to aircraft that would use the ground effect phenomena only as a means of support at take-off and landings. In cruise the wings would provide the aerodynamic lift.

Due to the presence of wings a new vertical dimension can be added, thus greatly increasing the relative freedom from the state of the terrain surface already exhibited by ground effect vehicles. It should be emphasized, however, that in order to make freedom from the state of the ground surface operationally practical, hovering and transition heights should be large enough (more than, say, 3 - 4 ft) to clear obstacles that may be found in an open field. Furthermore, the length of the "ground run" over the surface and the total distance required to clear a 50 ft obstacle (at take-off and landing) should be comparable to those established for STOL aircraft.

In winged aircraft, the wing appears as the most suitable principal surface for supporting the aircraft through the pressure difference created by the ground effect. Since, on one hand, presently available data on ground proximity effects refer either to circular or only slightly elongated planforms, while on the other the hovering height may depend on both the span and the chord, it will be assumed that the wing is either of a circular planform (AR = 1.27) or of an aspect ratio not higher than 2. Performance possibilities of such low aspect ratio aircraft equipped with the means of creating a ground cushion will be discussed. It is obvious, however, that as more is learned about the ground effect characteristics of elongated and more complicated planforms, the possibility of combining wings of higher aspect ratio with ground proximity phenomena, as well as using the bottoms of fuselages as ground effect surfaces, should also be investigated.

Symbols

ahp — air horsepower

AR — aspect ratio

C_L — wing lift coefficient

C_{D_o} — profile drag coefficient

$C_{D_f} = w/wf$ — aircraft parasite drag coefficient

$C_\mu = \frac{S_j}{S}\left(\frac{V_j}{V}\right)^2$ — momentum coefficient

GW	gross weight, lbs
L	lift, lbs
L/D	lift to drag ratio
S	wing area, ft^2
S_j	jet exit area, ft^2
V_{des}	design cruising speed, ft/sec or knots
V_{cl}	flying speed at best climb, ft/sec or knots
W_o	take-off gross weight, lbs
W_f	fuel weight, lbs
e	span effectiveness coefficient
f	equivalent flat plate area, ft^2
h	hovering height, ft
r_{o_e}	equivalent radius ft
w	wing loading
$W_f=GW/f$	equivalent flat plate area loading, lbs/ft^2
δ	jet flap angle, degrees
η_{pr}	propulsive efficiency
η_c	ratio of air horsepower to shaft horsepower
$\mathcal{Z}$	ratio of actual to optimum wing loading

Subscripts.

cl	climb
cr	cruising
des	design
W&E	wing and empenage

DESIGN PRINCIPLES

From the point of view of the design philosophy of ground effect aircraft, it is desirable that the following requirements be fulfilled:

1. Installed shaft, or air, horsepower is established on the basis of the design cruising speed at the prescribed cruise altitude and not by hovering.

2. Rate of climb in forward flight, ceiling, and range should be comparable with those of conventional fixed wing aircraft of the same gross weight and power class. However, some performance handicap resulting from the assumed low aspect ratio can be tolerated.

3. Flying qualities in forward flight should be similar to those of corresponding conventional aircraft.

4. In case of a complete power failure, the aircraft should be capable of landing from a glide.

5. For the sake of simplicity, the same basic flow system that creates the ground effect in hovering should be used for propulsion in other regimes of flight.

An aircraft fulfilling the above requirements can be visualized as having its ground effect propulsion system arranged in a way schematically shown in Figures 1A and 1B. For either of these schemes, the following three basic stages between vertical take-off and cruising can be distinguished.

Hovering. Here the flow is directed toward the periphery of the wing and ejected in a way required to form the air cushion. It may be added at this point that in this stage it would be desirable to have the c. g. of the aircraft at the c. g. of the projected area bordered by the air skirt.

Transition. At this stage, part of the air is directed rearward to create the necessary acceleration. As the aircraft accelerates to higher forward speeds, more and more air is directed rearward, either along the trailing edge (Scheme A) or through the louvers (Scheme B). Eventually, at the end of the ground run, it may be assumed that in Scheme A all air is ejected at some angle (δ) with reference to the wing chord. In this way, as the aircraft starts to climb, a jet flap effect, as well as forward thrust, are created at the same time.

In Scheme B, the last phase of the transition would be different in the respect that only part of the air would be directed through the trailing edge to form a jet flap, while the remaining part would be ejected directly aft. In this latter solution the jet flap air may be ejected at a larger angle δ than in Scheme A, as the necessary forward thrust can be provided by the air ejected directly aft through the louvers.

As long as at least some part of the air is ejected at an angle with reference to the chord, thus forming a jet flap, the center of pressure of the wing will remain aft and close to the center of gravity of the planform. This means that the c. g. position favored in hovering would still be beneficial in this case.

Cruise. Upon reaching a proper altitude and speed, all the air can be ejected straight aft as required to provide the necessary forward propulsion (solutions A and B in Figure 1). At this stage, when the air is ejected straight aft, the center of pressure of the wing moves forward toward locations more common to conventional air foil sections.

It can be seen from the above considerations that in practice either a compromise position for c. g. should be selected for all the flight stages, or when c. g. is located aft to satisfy hovering and transition then a large horizontal empennage should be accepted to provide a sufficient degree of static longitudinal stability. In addition the c. g. location should also be considered from the point of view of the engine-out condition.

GENERAL PERFORMANCE

Following the philosophy that the aircraft should be designed first for the cruise condition, the wing loading is optimized for the assumed operational cruising speed and operational altitude. In Figure 2 optimum wing loadings are shown for design cruising speeds up

to 350 knots and design cruise altitude of S. L. and 15,000 ft. In the above calculations it is assumed that the aircraft profile drag resulting from the wing and empennage is $C_{D_o} = .0125$.

Having optimized the wing loading, the installed power required per unit (one lb) of the aircraft gross weight will depend on the ratio of its gross weight (W) to the equivalent flat plate area (f). This ratio w_f will be called the equivalent flat plate area loading. Figure 3 gives some idea of the general trend for variation of this value vs. the gross weight of transport and cargo aircraft. Since the first aircraft using ground proximity phenomena will probably be of a rather small size, the equivalent flat plate area loadings of 1,000, 2,000, and 4,000 are considered as typical in the present study. Figure 4 gives some indication of the maximum values of the lift to drag ratio (L/D), that can be expected for the aircraft, presently being considered depending on the design cruising speed, the design cruise altitude, and probable values of the equivalent flat plate area loading.

Due to design considerations (power-off landing, etc. deviations from the optimum wing loading may be expected. A decrease in the lift to drag ratio at the design cruising speed and altitude when the wing loading differs from its optimum value is shown in Figure 5.

Installed air power loadings for aircraft of an aspect ratio of 2 are shown in the upper part of Figure 6 vs. the design cruising speed at S. L. and 15,000 ft. These power loadings refer to the military or maximum continuous rating of the jet engines. They were computed by assuming that, at the design cruising speed and altitude, 85 per cent of the available normal rated gas power was used and the propulsive efficiency (η_{pr}) equaled 80 per cent. For the turboshaft-powered aircraft the installed SHP loading based on military or maximum continuous rating) could be obtained by dividing the values given in the upper part of Figure 6 by the conversion efficiency (η_c), reflecting efficiencies of the compressor and ducting up to the jet exit.

Knowing the wing loading and the installed air power loading values, it is possible to calculate (reference 2) the height of hovering in ground effect. This height, expressed as a ratio of the actual elevation from the ground to the equivalent radius (h/r_{o_e}), is shown at the bottom of Figure 6. It can be seen that, for aircraft optimized for both S. L. and for 15,000-ft cruising, altitudes over the ground amounting to at least a few feet can be expected for aircraft of practical size. This should permit the clearance of many obstacles that may be encountered in unprepared fields. It should be noticed from Figure 6 that aircraft optimized for a 15,000-ft cruise altitude and having lower wing loadings (see Figure 2) show better height to equivalent radius ratios. Since due to a lower wing loading their linear dimensions will be larger than those of aircraft optimized for S/L operations, therefore they should be capable of hovering at higher absolute elevations from the ground.

Figure 7 suggests the possible range of aircraft that incorporate ground effect aspects. It can be seen from this figure and from Figure 4 that, for aircraft designed for 150 to 100 knot cruising speeds at which lift to drag ratios of about 8 can be expected, ranges close to 600 or 700 nautical miles can be obtained if the weight devoted to fuel were 20 per cent of the gross.

As to the rate of climb in forward flight, Figure 8 indicates that aircraft optimized for a design cruising speed of, say, about 150 and higher should have a satisfactory performance in this respect.

PROPULSIVE EFFICIENCY

It should be noticed that range values were given in assuming 80 per cent propulsive efficiency while rates of climb are indicated for propulsive efficiencies of 70 and 80

per cent. The calculations of Appendix I, which are summarized in Figure 9, show that the propulsive efficiency at a given ratio of the wing loading to the equivalent flat plate area loading or, in other words, at a given value of the parasite drag coefficient (C_{D_f}) depends on the ratio of the jet exit area to the wing area (S_j/S). It can be seen from Figure 9, for instance, that for C_{D_f} of about .02 the jet exit area should amount to about 2.4 per cent of the wing area if a propulsive efficiency of 80 per cent is to be obtained in cruise. But, in order to maintain this same value of propulsive efficiency in climb, the jet exit area should be increased to over 8 per cent of the wing area. By making the jet exit area equal to about 4 per cent of the wing area, the propulsive efficiency in climb would drop to about 70 per cent.

The above considerations clearly indicate that, in practical designs, solutions should be provided to vary the jet exit area within rather wide limits, if good efficiencies both in cruise and climb have to be achieved. Furthermore, in the configuration scheme shown in Figure 1A, a provision should be made for changing the direction of flow at the trailing edge from that required in hovering ($\delta \geq 90°$) to that required in transition and climb ($\delta \approx 30°$) and in cruise ($\delta = 0°$).

TAKE-OFF

At take-off, a horizontal thrust component should be provided in order to accelerate the aircraft to its minimum flying speed. This is achieved by giving an aft component to the internal air flow through arrangements shown either in Scheme A or B of Figure 1. In addition to the provision of a horizontal thrust component, the air is ejected in such a way that the jet flap effect is obtained. Due to this jet flap effect the wing lift coefficient is increased over that with no blowing.

Figure 10 is given as an example of what order of magnitude of (C_L) lift coefficients can be expected for low aspect ratio wings, when air is ejected at relatively small deflection angles ($\delta = 30°$) so that a propulsive thrust may be provided as well. The solid line in Figure 10 (extrapolated as a broken one) is reproduced from actual wind tunnel tests of a 60° delta wing of AR = 1.65 (reference 3) while the continuous broken line represents a relationship between C_L and the momentum coefficient (C_μ) for a wing of an aspect ratio AR = 2.0, as predicted from reference 4.

In order to obtain some idea of the order of magnitude of C_μ's and the aerodynamic lift per unit of wing area of a practical ground effect aircraft, Figure 11 is given. In this figure, C_μ corresponding to three values of the jet exit area to the wing area (S_j/S is plotted vs. the forward speed, for an aircraft designed for a 150 knot cruise at 15,000 ft. It is assumed for simplicity that all of the air horsepower installed is used to produce the jet flap flow. This assumption, although completely nonrealistic at the beginning of the take-off run, probably would approximate the actual situation quite closely at the end of this run for Scheme A of Figure 1.

Using C_μ's values from Figure 11 and the more conservative C_L values from Figure 10, the lift per unit of wing area (L/S) was computed and plotted vs. the forward speed (V) in Figure 11. It is obvious that, when L/S becomes equal to the wing loading w, free flight becomes possible. It can be seen from Figure 11 that, depending on the S_j/S ratio the minimum flying speed in the considered example would be included between 40 and 45 knots.

The "ground run" distance was computed using two assumptions. In the first case it was assumed that the horizontal thrust component increases linearly from zero to its full value achieved when the take-off velocity is reached and when the air is ejected at the

trailing edge at an angle $\delta = 30°$. In the second case the horizontal thrust component was assumed constant and equal to its maximum value corresponding to $\delta = 30°$.

The ground run distances computed under the above assumptions are shown vs. the jet exit area to wing area ratio in Figure 12 (broken line). In the same figure the total take-off distances required to clear a 50-ft obstacle are plotted vs. the S_j/S ratio.

Actual take-off distances will probably be somewhere between the two considered cases. As it can be seen from Figure 12, STOL-type take-offs can be expected from airplanes using a ground cushion to support them at take-off.

Through a proper direction of the air ejection, the aerodynamic lift and the horizontal negative thrust of the same order of magnitude as in take-offs can be obtained at landing. In addition, due to a low aspect ratio, steep glide angles can be achieved. These two factors permit one to expect that the landing distances will be similar to those at take-off shown in Figure 12.

WIND TUNNEL MODEL TESTS

In order to check the performance possibilities of the ground effect airplane, a program of wind tunnel tests was established at the Forrestal Research Center of Princeton University. A powered model (Figure 13), designed and built under the supervision of T. E. Sweeney and B. Nixon, is being tested both outside and in the tunnel.

In the present configuration the model has a peripheral slot directed at 45° inward and a spanwise slot ejecting air perpendicularly to the bottom surface. Tests were performed with all slots open, front side and spanwise slots taped when air was ejected only at the trailing edge at an angle $\delta = 135°$, and with all slots taped.

Although the results available at present are of a very preliminary nature, some of them are presented here. They should be considered to be of a qualitative rather than a quantitative nature.

In Figure 14, C_L vs. the angle of attack is shown with blowing through all slots and no blowing for the cases when the model is: (1) far from the ground, (2) at a relative distance equal to .285 of the maximum wing chord, and (3) at .1035 C_{max} from the ground. It can be seen from Figure 14 that ground proximity increases the slope of the lift curve and seems to improve the $C_{L_{max}}$ values both with and without blowing.

In Figure 15 the same aspects are shown with blowing through the trailing edge only; the results are similar to those shown in Figure 14.

In Figure 16 the influence of C_μ on C_L is shown and it should be noticed that those effects are of the same order of magnitude as those shown in Figure 10.

CONCLUSIONS

From this review of the performance possibilities of subsonic airplanes taking-off and landing in a ground cushion, it may be stated that these aircraft could have a performance comparable with that of conventional fixed wing aircraft of the same gross weight and power class. The capability of hovering a few feet from the ground and making relatively short take-off and landing runs at a height that would permit the clearance of many natural obstacles encountered on unprepared fields can make these aircraft rather attractive for some civilian and military applications. But, in order to develop these potential possibilities into actual operational hardware, much more study and testing are required.

APPENDIX

Propulsive efficiency in cruise and climb.

Froud's propulsive efficiency (η_{pr}) is defined as

$$\eta_{pr} = \frac{2}{1 + (V_j/V)} \tag{1}$$

Hence,

$$V_j/V = (2/\eta_{pr}) - 1 \tag{1a}$$

where V_j is the slipstream velocity in the fully developed wake and V is the velocity of flight.

The relative jet exit area (S_j/S) required to provide a desired propulsive efficiency at the design cruising speed (V_{des}) could be established from the following considerations:

The thrust required at design cruising speed is:

$$\frac{GW}{(L/D)_{opt}} = S_{j_{cr}} \rho V_j (V_j - V_{des}) \tag{2}$$

where $S_{j_{cr}}$ is the jet exit area in cruise.

Dividing both sides of equation (2) by the wing area (S), so selected that optimum wing loading W_{opt} is obtained, the jet exit to the wing area ratio becomes

$$(S_j/S)_{cr} = \frac{W_{opt}}{(L/D)_{opt} \rho V_{des}^2 (V_j/V_{des}) \left[(V_j/V_{des}) - 1\right]} \tag{3}$$

But optimum wing loading (W_{opt}) for the design cruising speed and altitude (i.e., air density ρ) is

$$W_{opt} = \frac{1}{2} \rho V_{des}^2 \sqrt{\pi e AR \, C_{D_{o_{W\&E}}}} \tag{4}$$

while the corresponding lift to drag ratio,

$$(L/D)_{opt} = \frac{1}{2} \sqrt{\frac{\pi e AR}{C_{D_{o_{W\&E}}} + W_{opt}/W_f}} \tag{5}$$

where e is the span effectiveness coefficient and $C_{D_{o_{W\&E}}}$ is the wing and empennage contribution to the aircraft's profile drag.

Substituting equations (1a), (4), and (5) into equation (3), the following is obtained:

$$(S_j/S)_{cr} = \sqrt{\frac{C_{D_{o_{W\&E}}}\left[C_{D_{o_{W\&E}}} + (W_{opt}/W_f)\right]}{\left[(2/\eta_{pr}) - 1\right]\left[(2/\eta_{pr}) - 2\right]}} \tag{6}$$

Equation (6) permits one to compute the relative jet exit area at the design cruising speed for any desired value of propulsive efficiency and an expected $W_{opt}/W_f = C_{D_f}$ value. Assuming $\eta_{pr_{cr}} = .8$, the S_j/S values were calculated as a function of C_{D_f} and plotted in Figure 9.

A relationship between the jet exit area to wing area ratio required at best climb, $(S_j/S)_{cl}$, in order to obtain a given propulsive efficiency ($\eta_{pr_{cl}}$) in this regime of flight, can be obtained in a similar manner. In doing this, it should be remembered that the lift coefficient for best climb is:

$$C_{L_{cl}} = \sqrt{3\pi e AR\left(C_{D_{o_{W\&E}}} + C_{D_f}\right)} \tag{7}$$

and the lift to drag ratio at best climb is

$$(L/D)_{cl} = \frac{1}{4}\sqrt{\frac{3\pi e AR}{C_{D_{o_{W\&E}}} + C_{D_f}}} \tag{8}$$

while the square of the speed of flight for the best climb, V_{cl}, (at the wing loading W_{opt}) is

$$V_{cl}^2 = V_{des}^2 \sqrt{C_{D_{o_{W\&E}}}\Big/3\left(C_{D_{o_{W\&E}}} + C_{D_f}\right)} \tag{9}$$

Substituting equations (1a), and (4), and (8) into equation (3) and remembering that climb is performed at a speed V_{cl} referred to the design flying speed V_{des} by equation (9), the following is obtained:

$$(S_j/S)_{cl} = \frac{2\left(C_{D_{o_{W\&E}}} + C_{D_f}\right)}{\left[(2/\eta_{pr}) - 1\right]\left[(2/\eta_{pr}) - 2\right]} \tag{10}$$

From equation (10) the jet exit area to wing area ratio required to provide propulsive efficiencies of 80, 70, and 60 per cent at forward speed corresponding to best climb were calculated and plotted in Figure 9 vs. $C_{D_f} = W/W_f$ values.

REFERENCES

1. Matthews, G. B., and Wosser, J. L., "Ground Proximity: a Critical Review." IAS Paper 59-121.

2. Chaplin, H., and Stephenson, B., "Preliminary Study of the Hovering Performance of Annular Jet Vehicle in Proximity to the Ground." David Taylor Model Basin Aero Rept. 947, 1958.

3. Williams, J., and Alexander, A. J., "Some Exploratory Jet-Flap Tests on a 60° Delta Wing." Aeronautical Research Council (British) Rept. 19,140, 1947.

4. Lowry, J. G., and Vogler, R. D., "Wind-Tunnel Investigation at Low Speeds to Determine the Effects of Aspect Ratio and End Plates on a Rectangular Wing and Jet Flaps Deflected 85°.

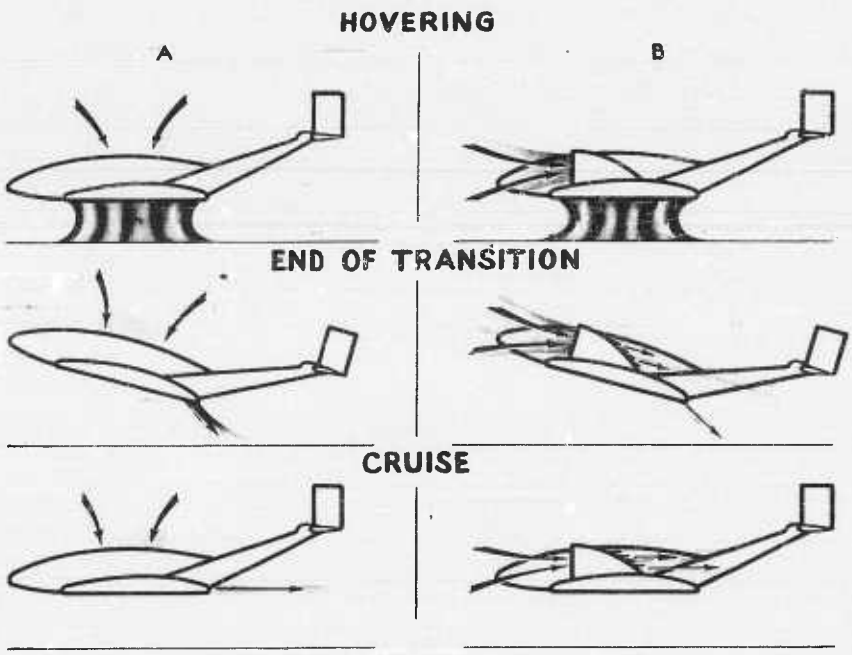

Figure 1.

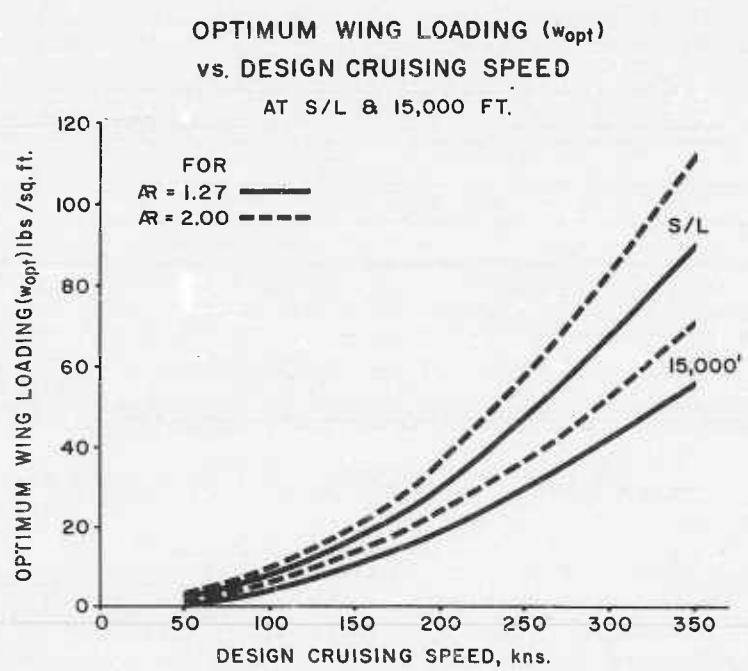

Figure 2.

AIRCRAFT STATISTICAL CHART

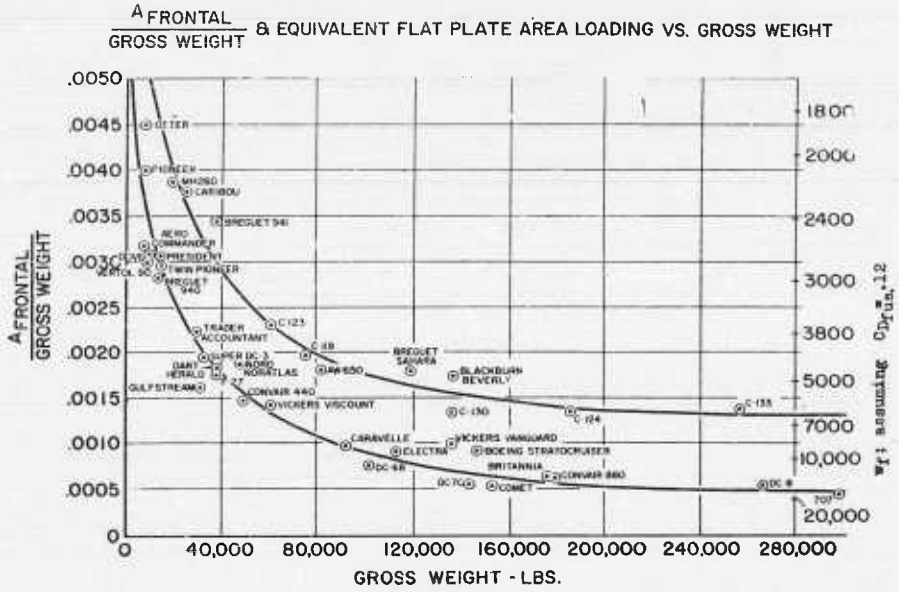

Figure 3.

(L/D)max vs. DESIGN CRUISING SPEED
FOR S/L & 15,000 FT. CRUISE ALT.

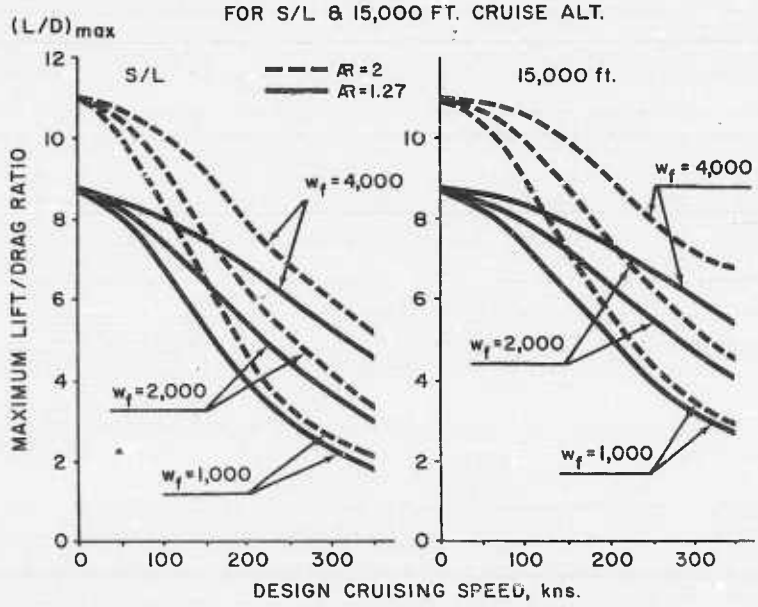

Figure 4.

DECREASE IN L/D DUE TO DEVIATION
FROM OPTIMUM WING LOADING

$(L/D)_{\zeta} / (L/D)_{opt} = f(\zeta)$

ζ = ACTUAL WING LOADING / OPTIMUM WING LOADING

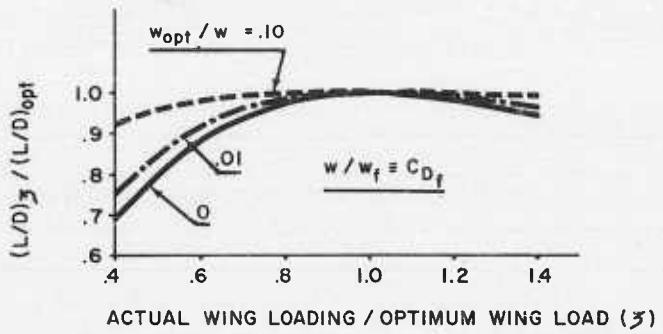

Figure 5.

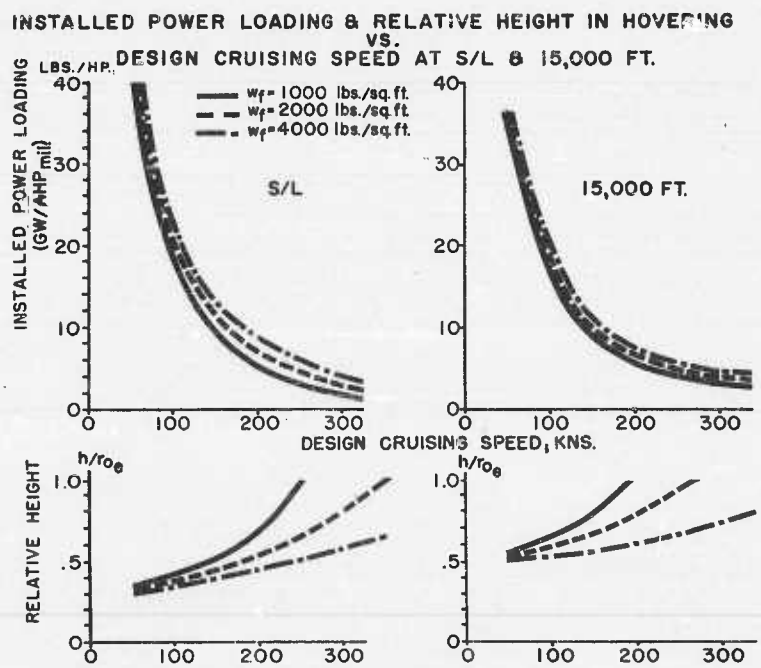

Figure 6.

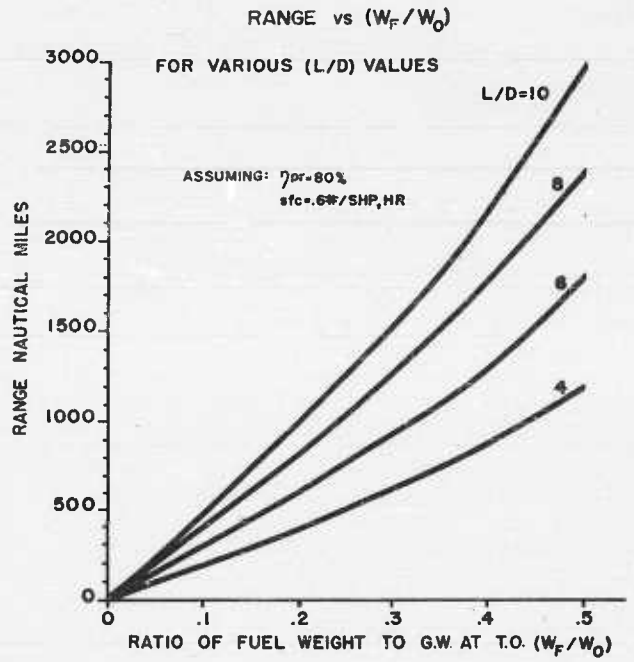

Figure 7.

BEST RATE OF CLIMB IN FWD. FLIGHT OF AIRCRAFT OPTIMIZED FOR GIVEN CRUISING SPEED AND ALTITUDE vs. DES. CRUISING SPEED

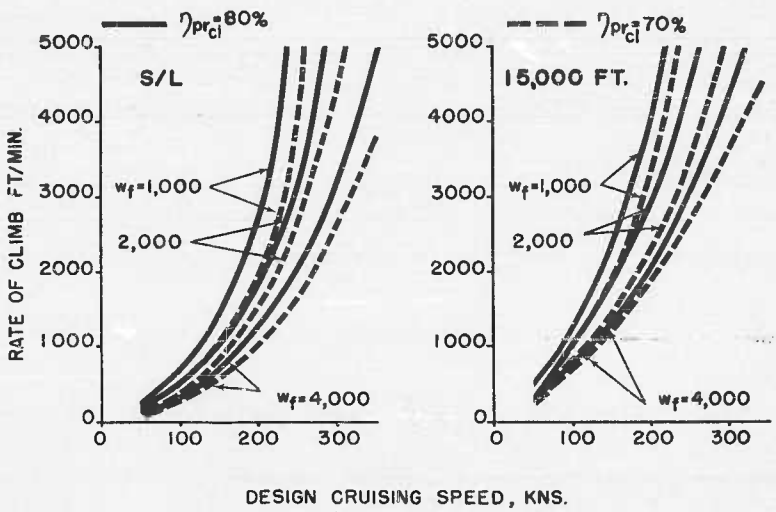

Figure 8.

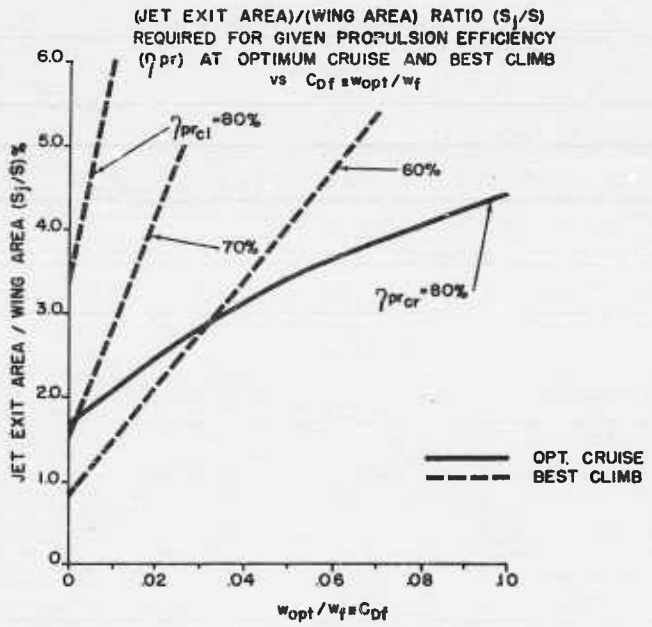

Figure 9.

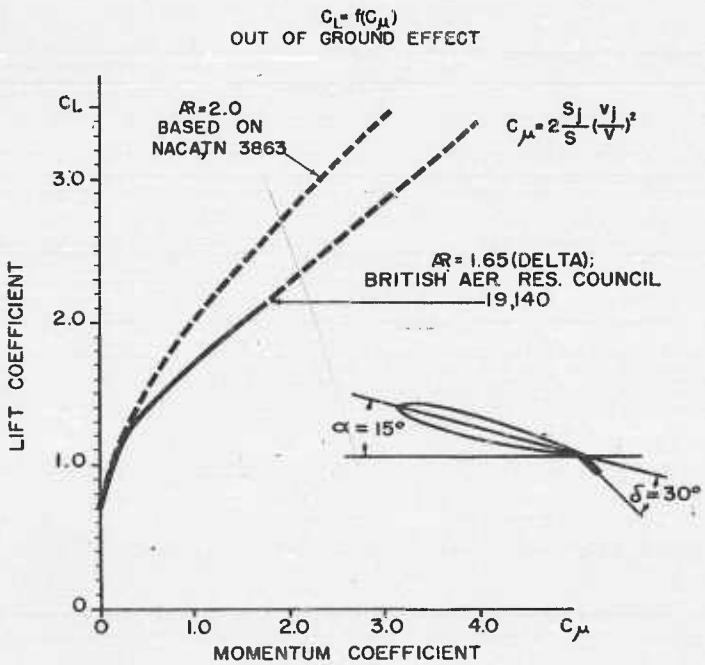

Figure 10.

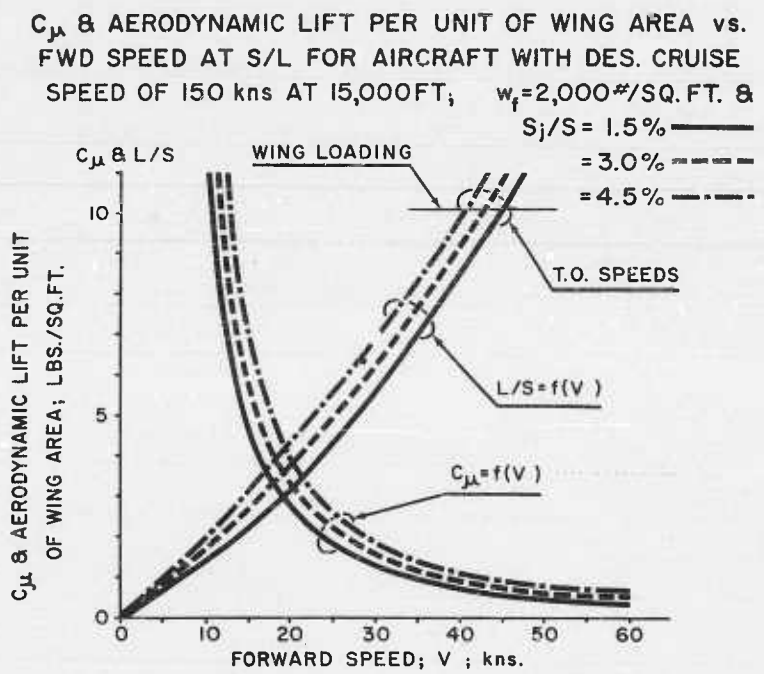

Figure 11.

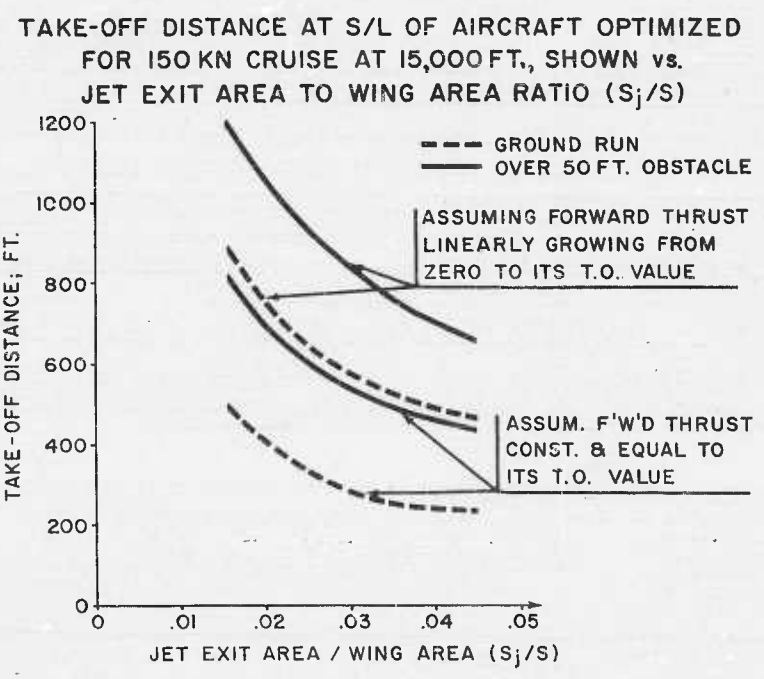

Figure 12.

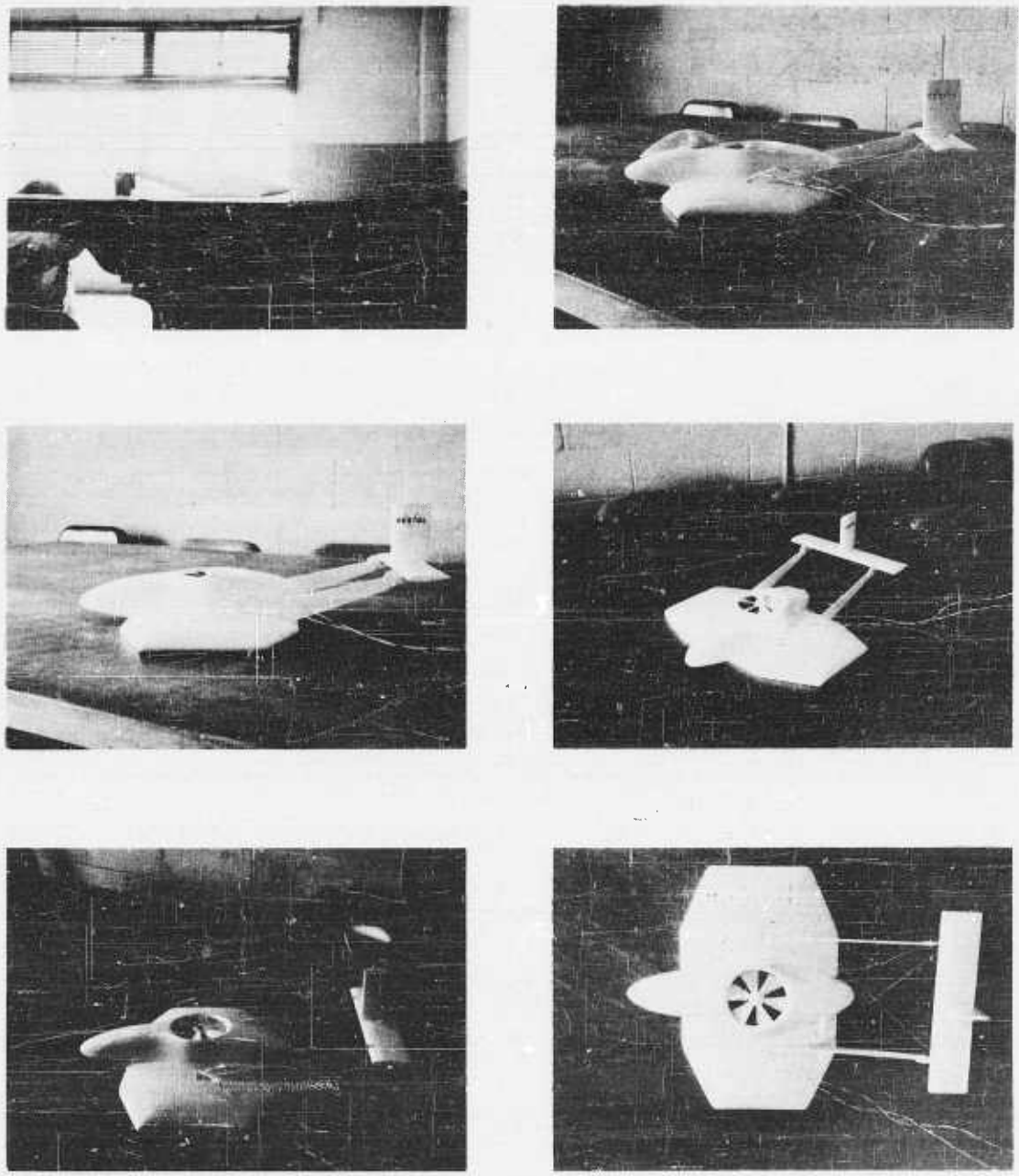

Figure 13. Model of Vertol ground proximity aircraft tested at Princeton University

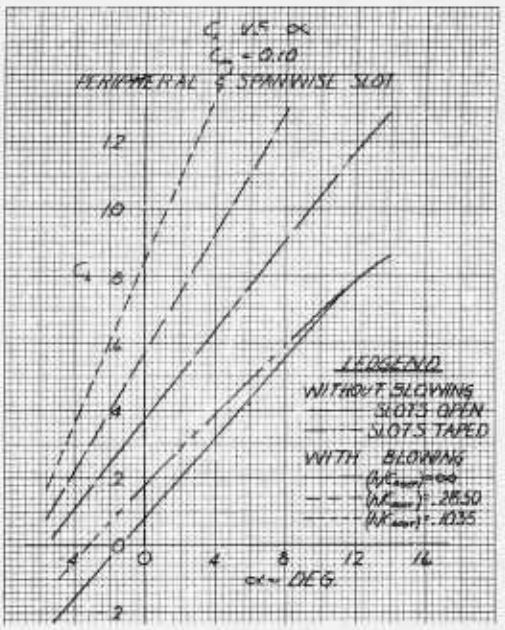

Figure 14.

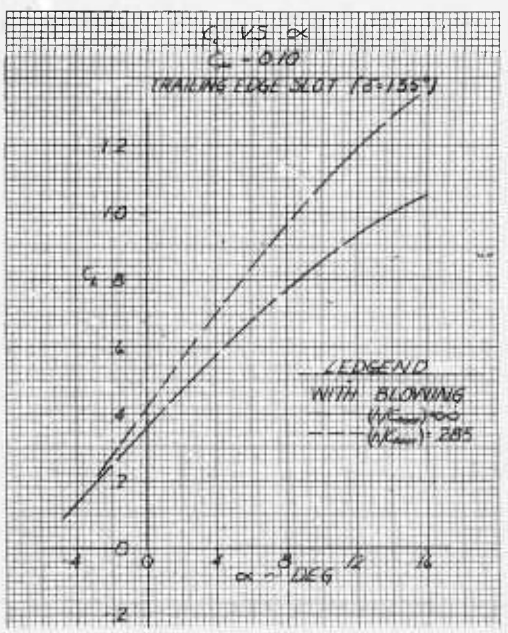

Figure 15.

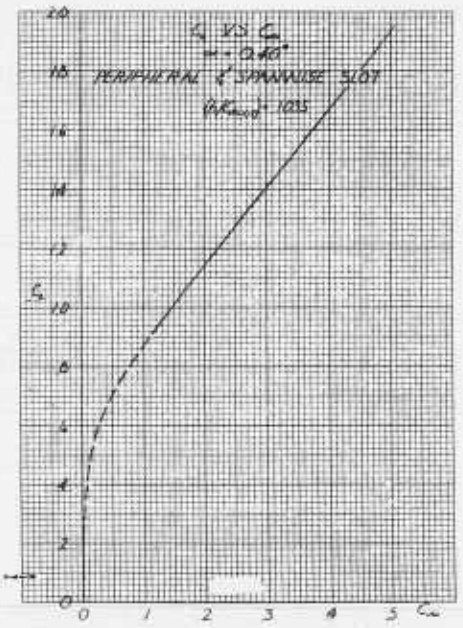

Figure 16.

FEASIBILITY OF GROUND EFFECT AIRBORNE LOGISTICS VEHICLES

By James E. Loos, Convair, A Division of General Dynamics Corporation, San Diego, California

ABSTRACT

Within the limits of the available theoretical and experimental data, a study was made of the feasibility of large airborne logistic vehicles operating within the ground effect. The vehicles considered are large vehicles with diameters of the order of 400 ft and operate at as low a height as possible. The vehicle planforms considered are circular and elongated with length to width ratios of two and three. A single annular jet at the planform circumference is used.

Generalized hovering performance showing the effects of height, vehicle configuration, jet configuration, and jet properties within the range of interest for large ground effect vehicles are presented. The possible propulsion system arrangements and structural arrangements are reviewed. The structural weight, propulsion system weight, and payload are compared to the vehicle gross weight for a range of vehicle size. Finally a very brief economic evaluation is made.

Symbols

A	lift augmentation factor $\frac{L}{m_j V_j}$
a	planform width
b	planform length
C	planform circumference
D	base diameter, measured at the inside of the jet
FPR	fan pressure ratio
g	gravity constant
h	height form the surface to the vehicle base
HP_{fan}	fan air horsepower
HP_j	jet air horsepower
j	jet momentum per unit length
L	total vehicle lift
m_j	jet mass flow
Δp_b	average base pressure above atmospheric

Δp_j	average jet pressure above atmospheric
R	radius of curvature of the jet
S_b	area of base inside jet
S_j	jet area
t	jet thickness
V_j	jet velocity
W_{aj}	jet airflow
Θ	jet angle from the vertical (negative when jet is turned in)
η_A	augmentation efficiency

INTRODUCTION

Recent development work has shown that large lifting ability can be realized when operating within the ground effect. This, together with the development of nuclear reactors and large air-breathing engines, may permit the development of airborne logistic vehicles capable of spanning the oceans at relatively high speed without the disadvantages associated with surface travel.

The purpose of the work discussed in this paper was to establish parameters for the design of large logistic Ground Effect Machines. This work has been carried out under the sponsorship and support of the Bureau of Aeronautics, (Contract NOas-6167-c). Preliminary requirements were defined to give the capability of carrying 1,000,000 lbs of cargo over the ocean at a speed of approximately 100 knots, with the further capability of rising and alighting on land or on the surface of the water.

Because of the preliminary state of the art, it was realized that many questions and problems would arise which could not be properly analyzed. However, it was felt that the feasibility of this type of vehicle could be demonstrated, and it was hoped that this study would aid in directing some of the future development work on the ground effect principle.

Initial study effort consisted of a review of the available theoretical and experimental work. The theoretical work reviewed included that done by Chaplin, Boehler, Matthews, Pinnes, and Rethorst (references 1 through 7). The applicable experimental work reviewed included that which had been done prior to July 1959 at the David Taylor Model Basin, the three NASA Research Centers, the Forrestal Research Center, and the State University of Iowa (references 8 through 14). Much of this experimental work was exploratory in nature and was done with relatively unsophisticated models. In addition, very little of these early experiments dealt with the extremely low height to diameter ratios of interest to the large vehicles under consideration.

As is well known, ground effect vehicles can be designed around one of several principles such as the plenum chamber or leakage device, single or multiple annular jets, air bearing devices, or labyrinth seal techniques. The jet arrangement chosen for the vehicles of this study consists of a single continuous annular jet at the periphery of the vehicle. Almost all of the theoretical work and most of the experimental data available at the beginning of this study were based on this type of jet arrangement.

The discussions which follow will begin with a short review of the theory on which this study is based. Equations relating the various design parameters are derived from this theory, and the effects of these parameters on the vehicle performance are shown for a selected range of the design variables. The effects of forward speed are then introduced and the total power required for the various vehicles is shown. Various propulsion system arrangements and structural arrangements are discussed and finally the effects of the various design variables on the vehicle payload are illustrated.

DEFINITIONS AND THEORY

Since limited experimental data were available at the beginning of this study, it was decided to base the study on the theory and an efficiency factor for correlation of the theory and the available experimental data. The derivations follow the theoretical work done by Chaplin, Boehler, and Matthews (references 1, 4, and 6) with some small modifications to make the resulting equations more directly applicable to the large vehicles and low operating heights of this study.

A schematic drawing of the circular annular jet ground effect machine is shown in Figure 1. It can be seen that the base diameter, D, is measured to the inside of the jet; the height, h, is the distance from the surface to the vehicle base; and the jet angle, Θ, is measured from the vertical with negative values denoting that the jet is turned inward.

The total lift of this vehicle is made up of vertical component of the jet momentum plus the pressure differential on the base area and jet area. This is expressed in equation (1):

$$L = m_j V_j \cos \Theta + \Delta p_j S_j \cos \Theta + \Delta p_b S_b \tag{1}$$

The momentum derivations of Chaplin and Boehler (references 1 and 4) show that the theoretical base pressure differential is equal to the momentum flux per unit jet length divided by radius of jet curvature. A term called augmentation efficiency can now be introduced to account for viscous and other effects, so that the actual base pressure differential can be expressed in terms of this theoretical value:

$$\Delta p_b = \frac{j}{R} \eta_A \tag{2}$$

where j is the momentum flux per unit jet length, R is the radius of jet curvature, and η_A is the augmentation efficiency.

Since the jet exit static pressure varies from the base pressure on the inside to ambient pressure on the outside, Chaplin's assumption expressed in equation (3) is also used.

$$\Delta p_j = \frac{\Delta p_b}{2} \tag{3}$$

Although there are several definitions for the lift augmentation factor, in this study it is defined as the ratio of the total lift to the jet momentum. With this definition, the lift augmentation factor is given by equations (4):

$$A = \frac{L}{m_j V_j} = \cos \Theta + \frac{(1 - \sin \Theta)\left(\frac{t}{D}\right) \eta_A \cos \Theta}{2\left(\frac{h}{D}\right)} + \frac{(1 - \sin \Theta)_A}{4\left(\frac{h}{D}\right)\left(1 + \frac{t}{D} \cos \Theta\right)} \tag{4}$$

For application to large ground effect machines only the low values of h/D are of interest. Figure 2 shows the effects of jet angle and jet thickness on the augmentation factor for these heights. Directing the annular jet inward can result in large increases in augmentation factor. Figure 2 also shows that jet thickness does not have as significant an effect as does the jet angle.

For the large vehicles under consideration the jet thickness will be on the order of 1 per cent or less of the diameter. Therefore, assuming t/D = 0 will result in very small errors which are conservative. This assumption simplifies the basic equations so that the total lift and the lift augmentation factor can be expressed by equations (5) and (6),

$$L = m_j V_j \cos \Theta + \triangle p_b \, S_b \tag{5}$$

$$A = \cos \Theta + \frac{(1-\sin \Theta)\,\eta_A}{4\,(h/D)} \tag{6}$$

For a thin jet, equation (5) applies to any arbitrary planform. Also, for a thin jet, the average jet length is equal to the circumference of the base. Therefore, the lift augmentation factor for an arbitrary planform is given by equation (7),

$$A = \cos \Theta + \frac{(1-\sin \Theta)\,\eta_A}{4} \left(\frac{4S_b}{h\,C} \right) \tag{7}$$

The height parameter, $\frac{4S_b}{hC}$, is equivalent to D/h for a circular planform so that the augmentation equations are compatible. With this simplified derivation, the lift augmentation factor depends only on the jet angle, height parameter, and augmentation efficiency.

APPLICATION OF THEORY

In the design of a ground effect vehicle it is necessary to know the relationship between the total lift, base area, base pressure, and the area, angle, velocity, airflow, and power of the annular jet. Using the above equations and definitions, these parameters can be related by equations (8) through (11):

$$\frac{L}{S_b} = \frac{A \times \triangle p_b}{A - \cos \Theta} \tag{8}$$

$$\frac{S_j}{S_b} = \frac{\left(L/S_b\right)}{A\,\rho_j\,V_j^{\,2}} \tag{9}$$

$$\frac{Wa_j}{S_b} = \frac{(L/S_b)\,g}{A\,V_j} \tag{10}$$

$$\frac{HP_j}{S_b} = \frac{1}{1100} \rho_j V_j^3 \left(\frac{S_j}{S_b}\right) \left[1 + \left(\frac{S_j}{S_b}\right) \frac{(1-\sin\Theta)}{4} \left(\frac{4 S_b}{hC}\right) \eta_A\right] \qquad (11)$$

The lift parameter, L/S_b, depends only on the augmentation factor and the base pressure, and the variation with height parameter is shown in Figure 3 for a jet angle, Θ, of -45° and an augmentation efficiency, η_A, of 80 per cent. As also shown in Figure 3 the higher values of the height parameter used here actually indicate lower operating heights. For example, with a circular planform a value of 100 for the height parameter indicates an operating height, h, which is 1 per cent of the vehicle diameter while a value of 10 indicates a height of 10 per cent of the vehicle diameter.

If the jet airflow is supplied by a fan or compressor, the fan pressure ratio together with the internal losses will determine the jet total pressure. For a given base pressure, the jet static pressure is determined from the previous assumption that the average jet pressure is the average of base pressure and the ambient pressure. These pressures, together with the jet temperature, determine the jet velocity and density.

Using the jet angle, augmentation efficiency, and base pressures of Figure 3, the variation in the jet airflow and jet air horsepower parameters are shown in Figure 4 for a fan pressure ratio of 1.10 and internal duct losses of 2 per cent of the fan exit total pressure. It can be seen that the airflow and power requirements decrease with lower operating heights. This indicates that, as would be expected, it is advantageous to operate as close to the surface as possible.

Parameter curves similar to those shown in Figures 3 and 4 can be calculated for any combination of jet angle, augmentation efficiency, base pressure, fan pressure ratio, and internal duct loss. These curves can be used directly for a design utilizing a circular planform since the height parameter, $\frac{4S_b}{hC}$, becomes simply the ratio of the base diameter to the height, D/h. For other planforms the relationship between the base area, S_b, and the vehicle circumference, C, is required.

In this study, elongated planforms consisting of rectangles with semi-circular ends were considered in addition to the circular planforms. For this type of elongated planform, the required geometric relations can be determined for any given length to width ratio. Therefore, specifying the ratio of the vehicle length to the vehicle width defines the planform.

EFFECTS OF VARIOUS PARAMETERS ON VEHICLE PERFORMANCE

After the equations defining the annular jet performance were derived, it was desired to investigate the overall effects of the various parameters. In order to do this it was necessary to define the vehicle geometry, gross weight, operating height, and jet geometry.

As just mentioned, the vehicle planforms under consideration in this study were circular planforms and elongated planforms consisting of rectangles with semi-circular ends. For the performance comparison, such elongated planforms with overall length to width ratios of two and three were compared with the circular geometry. These three planforms are illustrated in Figure 5. Also listed in Figure 5 are the values of the design variables used in the vehicle comparison.

Rough preliminary studies indicated that the vehicle payload would be somewhere between 20 per cent and 40 per cent of the gross weight. Since a payload of approximately

1,000,000 lbs was desired, a gross weight of 4,000,000 lbs was chosen for the detailed vehicle comparison.

As was pointed out previously, it is most efficient to operate ground effect machines as close to the surface as possible. Since the vehicles under consideration are required to operate over the ocean surface, the design height must be sufficient to clear the tops of the waves. Since the effects of operating over an uneven surface with an annular jet were not known at the beginning of this study, it was assumed that the performance would be the same as operating over a smooth surface with the height measured to the bottom of the wave trough. In view of these operating requirements, a design height of 12 ft was chosen. Observations of wave heights over a span of several years in both the North Atlantic and Pacific Oceans indicate that vehicles with this design height should be able to operate 90 per cent of the time.

An annular jet angle, Θ, of -45° was used even though the theory indicates that a greater angle would be more efficient for the operating heights under consideration. As experimental data were not available for annular jets turned in more than 45°, this additional gain in lift augmentation had not been confirmed.

Much of the early test data indicated augmentation efficiencies of about 50 per cent. More recent testing at DTMB of carefully designed annular jet models has shown augmentation efficiencies of approximately 80 per cent. For this study it was assumed that the annular jet could be designed to operate efficiently over the limited desired operating height and an augmentation efficiency of 80 per cent was used.

Lifting unit pressures, or base pressures, from 20 psf to 50 psf were investigated together with fan pressure ratios of 1.03 to 1.40.

With these values of jet angle, augmentation efficiency, base pressure, and fan pressure ratio, the design parameters can be determined as a function of the height parameter, $\frac{4\ S_b}{hC}$.

The desired total lift and operating height, together with a cross-plot from the curve of lift parameter, determine the required vehicle size and the value of the height parameter to be used in determining the required jet area, jet airflow, and jet air horsepower. The variation in required vehicle size for the various planforms is shown in Figure 6 as a function of the base pressure. These areas correspond to diameters from 302 ft to 492 ft for the circular planforms and similar dimensions for the other planforms. At a given base pressure a reduction in required base area indicates that more lift is being provided by the jet itself, and therefore more jet momentum is required.

The variation of the required jet airflow and jet air horsepower for the circular planforms with internal duct losses of 2 per cent is shown in Figure 7 as a function of fan pressure ratio and base pressure. Even though the vehicles with the higher base pressures are smaller in size, it can be seen that they require greater jet airflow and power. With increasing fan pressure ratio the required jet airflow decreases while the required jet power increases.

Figure 8 shows the effect of vehicle planform on the required jet airflow and power for a base pressure, Δp_b, of 30 psf and internal duct losses of 2 per cent. It can be seen that the elongated planforms require more jet airflow and power. This is to be expected since, for a given base area, the circumference and thus the annular jet is longer for these planforms than for the circular planform.

The importance of internal duct efficiency is illustrated in Figure 9 where the required jet airflow and fan power are shown for several internal duct losses. The fan horsepower shown here is that power added to the air by the fan and differs from the jet horsepower shown previously in that the fan horsepower includes the internal duct losses. The internal efficiency has a large effect on the required fan horsepower especially at the low fan pressure ratios.

EFFECTS OF FORWARD FLIGHT

Discussions to this point have been restricted to a description of the hovering performance of the ground effect machine. However, for any useful vehicle, the effects of forward speed must also be considered.

Lift augmentation in the hovering case is derived from the presence of a pressure bubble beneath the vehicle base. Forward flight must certainly influence the magnitude and shape of this pressure bubble. At the beginning of this study very little information was available to show the effects of forward flight on the lifting capabilities and on the relation between base pressure and the jet properties. Early data from DTMB tests (reference 8) of a very small model showed some loss in lift with forward speed. Other test data from the Langley and Ames Research Centers (references 10 and 11) indicated very little change. In addition, theoretical work at DTMB indicated that with forward speeds the local power requirements of the annular jet may vary because of the variation in the ambient pressure field. In the absence of consistent or conclusive data it was assumed for this study that forward flight does not change the ground effect or the relation between the various parameters.

Using this assumption, the jet velocity, airflow, and power requirements do not change with forward speed. However, the power input to the airflow used in the lifting jet does change with speed. In the hovering case the power input is determined from the required jet power plus the internal duct losses. During forward flight, part of the jet total pressure can be realized by utilizing ram effect so that the required power input to the air used in the lifting jet is less than for the hovering case.

For forward flight, the overall drag which must be overcome is made up of the vehicle aerodynamic drag plus the momentum or ram drag of the air which is used for the annular jet. This momentum drag is the product of the jet mass flow and the flight velocity and can be quite large. In fact, in most cases it is considerably greater than the aerodynamic drag.

Because of the very limited experimental drag data available for ground effect vehicles, an estimated aerodynamic drag has been used in this study. The build-up of the estimated aerodynamic drag for a vehicle with a length to width ratio of three is shown in Figure 10, together with the total drag for the other planforms. The total drag is composed of profile drag, base drag, component drag, and an allowance for interference and surface irregularities. The profile drag was estimated in the manner presented by Hoerner (reference 15) for two-dimensional airfoils modified for three-dimensional effects and adjusted for the wetted area of the ground effect machines. The base drag was estimated from the empirical data presented by Hoerner. The fins, cabin, nacelles, and pylons were treated as blunt bodies or wing profiles. The drag was increased by 15 per cent of the profile drag to allow for interference and surface irregularities.

The thrust required for forward flight may be achieved in one of several ways such as tilting of the entire vehicle, deflection vanes in the jet exits, separate forward thrust engines mounted atop the vehicle, or convertible engines that may be used primarily for lift with part of the thrust diverted for forward speed. For this study it was assumed that separate forward thrust engines mounted atop the vehicles would be used. Since the

forward speeds of interest are relatively low, large turboprop engines were used. Vehicle control could be obtained by using differential thrust of these engines. Vehicle braking could be accomplished by reversing the pitch of the propellers.

The total required vehicle power depends on the power required for lifting and the power required to overcome the aerodynamic drag and ram drag. In the hovering case the power required for lifting is a maximum. With increasing forward speed, the required fan power decreases because part of the power is supplied by ram effect. However, with increasing speed the power required to overcome the aerodynamic and ram drag increases at a greater rate than the fan power decreases so that the maximum installed power is required at the highest forward speed.

The build-up of the total required power is shown in Figure 11 for the vehicles with circular planform and a base pressure, Δp_b, of 30 psf. The solid curves are for internal losses of 2 per cent while the dashed curves are for internal losses of 5 per cent. The aerodynamic drag is the same in each case since the vehicles are the same size. It can be seen that the ram drag is always greater than the aerodynamic drag and increases with decreasing fan pressure ratio as the required jet airflow increases. The lifting horsepower is the fan horsepower and includes the ram effect and the effect of the internal duct losses. The large effect of internal duct efficiency on the power requirements can readily be seen. Another significant point which is well illustrated by these curves is that the required lifting horsepower greatly exceeds the other components of the total required horsepower.

The total required power at the design speed is shown in Figure 12 for the circular planforms over the range of base pressure and fan pressure ratio and for the elongated planforms at a base pressure of 50 psf. The required power for the elongated planforms decreases with lower base pressure in a manner similar to that shown for the circular planform. These curves are for internal duct losses of 2 per cent. For internal losses of 5 per cent the total required power would be greater, as was illustrated previously. For any value of base pressure the circular planform has the minimum power requirements. The 2:1 planform required 6 per cent to 8 per cent greater power and the 3:1 planform required 15 per cent to 18 per cent greater power than the circular planform. For each planform the minimum power requirements occur at the lowest value of base pressure. However, the low base pressures require a larger vehicle size for the 4,000,000 lb total lift. This in turn requires greater structural weight. The overall effect on payload is discussed later in this paper.

It should be pointed out that the total vehicle installed power would be greater than the values shown here since these values do not include fan efficiencies or propeller efficiencies.

PROPULSION SYSTEM ARRANGEMENT

Since the vehicles under consideration are required to span the oceans, the minimum endurance considered reasonable with a design speed of 100 knots is about 30 hours. As shown in Figure 12 the minimum total required power for any of the vehicles is about 150,000 horsepower. Thus, it can be seen that even with a fuel consumption of only 0.5 lbs of fuel per horsepower per hour the total fuel required would be greater than 50 per cent of the vehicle gross weight. This fact makes nuclear power quite attractive for this application. Also for the large power requirements the nuclear shielding per unit power can be made considerably lighter than for the smaller powers used in present aircraft work. Therefore, for this study, only nuclear power was considered.

As shown previously, the annular jet arrangement required large amounts of low pressure air. It appears that lift fan engines are the most efficient type of engine to use to supply this air. The total airflow of a typical large lift fan engine at normal power is

shown in Figure 13 as a function of the fan pressure ratio. This type of engine uses a turbojet engine as a gas generator. The jet exhaust is expanded through a turbine which drives a large low-pressure-ratio fan. Under static and low speed conditions this gives a large increase in thrust and airflow. This type of engine is particularly adaptable to the application under study since the gas generator and the fan can be widely separated if desired. Thus, it is possible to group the gas generators around the nuclear reactor and still have the fans at any desired location.

Two possible fan locations are illustrated in Figure 14. In the lower arrangement, the fans are located adjacent to the gas generators near the center of the vehicle. In the upper arrangement the fans are located directly over the annular jet at the rim of the vehicle. The arrangement with the fans in the center requires large ducts to handle the fan airflow, which is at 1 to 3 psig and essentially ambient temperature. The arrangement with the fans at the rim uses much smaller ducting but the jet exhaust is at about 20 psig and 1,000°F. An analysis of the duct weights for these two arrangements indicated that the fan-in-center arrangement has a duct weight about 67 per cent greater than the duct weight of the fan-at-the-rim arrangement.

An analysis of the internal duct losses for the fans in the center showed that the minimum loss between the fans and the annular jet would be about 5 per cent of the fan discharge total pressure. In the previous discussions of vehicle performance it was shown that this much internal duct loss can have a large effect on the power requirements. The arrangement with the fans at the rim of the vehicles does not have these large duct losses but may have an air distribution problem, in that one fan supplies air to a considerable length of the annular jet. If this distribution problem becomes serious it can be relieved by using a greater number of small fans. Thus, one gas generator could drive two, three, or even four fans.

The possible performance gains, together with the favorable weight comparison, indicate that the arrangement with the fans at the rim of the vehicle is optimum. This arrangement results in some losses between the gas generators and the fans. However, these losses can be kept relatively small, and they do not affect the annular jet properties as directly as pressure losses after the fan discharge.

STRUCTURAL ARRANGEMENTS

In order to begin the structural design part of the study it was necessary to establish the type, size, and weight of the cargo to be transported, and the various cargo-handling requirements. One of the biggest advantages of this type of vehicle over conventional cargo ships is that it can be landed on the beach or other flat areas for direct loading or unloading.

With this in mind, it was decided to design the floor to support any truck which is allowed on the highway. The loads for this condition were taken as those used by the California Highway Department for bridge design and are shown in Figure 15. The floor was also to support a typical aircraft cargo loading of 300 lbs per ft^2. Heavier or more concentrated loads than either of these conditions would require temporary flooring to distribute the load. The requirement of being able to handle highway trucks also established the minimum cargo-hold clearances of 15 ft height and 15 ft width as shown in Figure 15. For turning and maneuvering of the trucks, however, these clearances should be increased if structurally feasible without excessive weight penalty.

Since the vehicles under consideration have a large base area in order to attain the required total lift, the total available floor area could never be loaded with cargo without at the same time exceeding the maximum payload weight. Therefore, only some sections of the floor have to be designed to the maximum loads shown in Figure 15. Other sections

of the floor would be designed to lower loads criteria and could be used if a low density cargo was to be handled.

The various conditions which were investigated for possible vehicle structural design loads are illustrated in Figure 16. A limit design load factor of 1.5 g was selected. This together with the normal aircraft factor of safety of 1.5 results in an ultimate design load factor of 2.25 g.

The vehicle loads for the flight conditions are illustrated schematically as Condition I in Figure 16. In this condition the uniform lifting pressure supports the vehicle gross weight which is composed of an approximately uniform structural weight, a concentrated reactor shield assembly weight, and various cargo loadings. For some of the vehicles with elongated planforms two reactor shield assemblies were used instead of one, as illustrated here.

For alighting on land it was felt that some type of landing gear was needed which would adjust to a slightly uneven terrain. One possibility is a ring of pneumatically or hydraulically balanced support pads. The loads for this arrangement are illustrated as Condition II, A. If some type of water flotation gear is needed it might also be used for alighting on land. In this case the loading would be as shown in Condition II, B.

For alighting on smooth water without flotation gear, the loads would be the same as in flight since the water would provide a uniform support. This is illustrated as Condition III, A, 1. Because of the large planform area of these vehicles the water displacement would be less than one foot.

For alighting in waves without flotation gear, the result could be as illustrated in Condition III, A, 2. The buoyancy effects are such that relatively small waves can lift sections of the vehicle clear of the water. Since the ratio of wave length to wave height varies over a wide range, it is possible to encounter a condition where the vehicle is supported only at the ends as illustrated. This produces very large loads in the vehicle structure, especially for the elongated vehicles. One such condition which was investigated in some detail produced a maximum bending moment of about six times the maximum bending moment resulting from any of the other conditions. Designing to this condition would result in a weight penalty of at least 30 per cent to 40 per cent of the structural weight. In view of this it is felt that, if there is a requirement of alighting in waves, some type of flotation gear would be required to change the structural loading.

One type of flotation gear considered consisted of two large inflatable rubberized canvas bags also suitable for alighting on land. These bags require a pressure of only 100 to 200 psf to support the vehicle. They would be compartmentized for vehicle stability and would be deep enough to suspend the vehicle free of the water. The amount of air in the bags would be varied to provide the desired clearance for land operation. The landing loads with this type of gear are illustrated in Condition III, B, and would be identical whether alighting on land or on smooth or rough water.

This flotation gear provides an additional advantage in that the underside of the vehicle floor would not have to be designed to withstand hydrostatic pressure. Also, the annular plenum chamber and associated fairing could be of lighter construction since they are always clear of the water and not subject to wave loads. Each of these features results in some structural weight savings.

One possible structural arrangement for the circular vehicles consists of radial and circumferential trusses as illustrated in Figure 17. This structural arrangement fits well with the propulsion system arrangement which has the lifting fans near the center of the vehicle, as shown in this drawing. The large ducts from the fans to the annular jet run

between the radial trusses. Also shown in this drawing are the large turboprop engines used for forward propulsion. Section C shows how part of the annular jet plenum chamber swings upward to provide access to the interior of the vehicle. Several of these doors would be located around the periphery for loading and unloading.

With the lifting fans at the rim of the vehicle the grid-type structure shown in Figure 18 is possible. This structural arrangement consists of a series of longitudinal and transverse trusses. Sufficient space is available through these trusses for the relatively small ducting required between the gas generators near the center of the vehicles and the lifting fans at the rim of the vehicle. As with the other structural arrangement, several loading and unloading doors are provided.

Also illustrated in this drawing is the idea of designing only part of the floor to support the maximum cargo loads. One lane of cargo bays between each of the access doors provides ample space for the maximum amount of heavy cargo that could be handled. Some of the area inside of these bays would be designed to support lighter loads. The area outside of the heavy cargo bays would be constructed of lightweight structure and would not be capable of supporting any cargo loads.

The grid arrangement of trusses shown in this drawing would be better for manufacturing and internal cargo handling than the radial and circumferential truss arrangement of Figure 17. The structural weights of the two arrangements would be very nearly the same. In view of this, together with the previous conclusion that the propulsion system arrangement with the fans at the rim was superior to that with the fans in the center, the grid structural arrangement was used for the vehicle weight comparison.

A drawing of an elongated vehicle with a length to width ratio of 3 is shown in Figure 19. The grid structural arrangement with the lifting fans at the rim of the vehicle also appears best for this vehicle. Two reactor shield assemblies are used in this arrangement because of the extreme vehicle length. A row of cargo bays designed for heavy cargo would be provided along each side of the vehicle between the access doors.

These vehicles would be constructed almost entirely of aluminum alloy. In order to prevent or minimize corrosion, the simultaneous use of different materials would be avoided wherever possible and corrosion-preventing methods would be applied. For hot air or exhaust ducts and other hot sections near the engines and the reactors, steel or titanium would be required.

The main structural grid would be built-up of truss-like longitudinal and transverse beams. Aluminum alloy tubing or open beam structure would be used. A judicious selection between bolting, riveting, or welding would be made in each case for the most advantageous type of joints.

For the roof and floor of the vehicles two types of structures were investigated for their advantages. These basic structural types are an open beam and skin-type construction or a closed honeycomb sandwich construction. The honeycomb sandwich floor could provide some weight-saving, but the durability of the lightweight honeycomb core under repeated heavy cargo loading is questionable.

Due to the large sizes being considered, the assembly of the vehicles would probably have to be done outside of most hangars or shops. However, the simple structural arrangement permits the separate construction of large sub-assemblies so that only the final assembly of the vehicle would be done in the open. A special problem would be imposed by the installation of the reactor shield assembly into the vehicle because of the large vehicle dimensions and the great weight of the reactor shield assembly. However, the overall

vehicle arrangement is such that the construction costs per pound would be considerably less than for conventional airplane construction.

VEHICLE COMPARISON

After the foregoing investigations of the vehicle performance, propulsion system arrangements and requirements, and structural arrangements and requirements were completed, a weight breakdown of the various vehicles was made.

Such a weight breakdown is shown in Figure 20. It can be seen that the total gross weight of 4,000,000 lbs is made up of the structural weight, propulsion system weight, weight of miscellaneous items, and payload. The structural weight includes the weight of the trusses, roof, floor, bulkheads, fairings, cargo doors with mechanism, landing gear, reactor compartments and supports, annular plenum chamber and nozzle, crew compartment, and vertical fin. The propulsion system includes the reactor shield assembly with associated plumbing and radiators; the lift fans, gas generators and associated ducting; the turboprop engines, propellers, nacelles, pylons and associated ducting; engine controls; starting and lubricating systems; oil required for 30 hours of flight time; and an auxiliary power plant. The miscellaneous items include instruments, navigation aids, hydraulic system, pneumatic system, electrical system, electronics, furnishings, air conditioning and anti-icing system, and a 20 man crew. The payload is then that portion of the gross weight remaining after accounting for all of the above items.

Since it was shown previously that vehicles with very low or very high fan pressure ratios have excessive power requirements, the detail weight estimates were done only for fan pressure ratios of 1.08 to 1.20. Figure 20 shows that for the circular vehicle with a base pressure, Δp_b, of 30 psf the payload varies from about 40 per cent to 42 per cent of the gross weight with the maximum payload of 1,700,000 lbs available at a fan pressure ratio of 1.08.

The variation of payload for the range of design variables of this study is shown in Figure 21. The payload varies from about 25 per cent of the gross weight for the 3:1 planform with a base pressure of 20 psf to as high as 50 per cent at the gross weight for the circular and 2:1 planforms with a base pressure of 50 psf.

The weights shown for the elongated planforms assume the use of a pair of twin reactor shield assemblies, except for the smallest vehicle with the 2:1 planform. The use of a single reactor assembly for these vehicles would result in lighter shielding, but the structure weight would increase because of increased bending moments and the installed power would increase slightly because of the longer ducts. The net effect would be an increase in payload of about 3 per cent to 4 per cent of the gross weight for the 2:1 planform and no change in the payload for the 3:1 planform.

For each planform the maximum payload occurs at a fan pressure ratio of 1.08 to 1.10 with the highest base pressure. This is a result of the lower structural weight of these smaller vehicles. However, these vehicles require greater power than those with lower values of base pressure.

The selection of the optimum design variables would depend on an economic evaluation which includes the effect of the change in payload and power requirements. A very rough check of the economics of transporting cargo by this type of vehicle indicated costs in the

area of 5 cents per ton-mile. However, the detailed cost analysis required for the selection of the optimum values of the design variables was beyond the scope of this study.

CONCLUDING REMARKS

During all of this study, certain parameters have been neglected because of the lack of necessary information. These include the following:

1. Effects of operation over waves or other uneven terrain on the performance, stability and control, and motion of the ground effect vehicle.
2. Necessity of and means for pitch and roll control.
3. Jet impingement effects on waves and spray, and the effects of the spray on the vehicle loads and the intake system.
4. Combined aerodynamic effects and ground effects during forward flight.
5. Dynamic stability and control of the vehicle.
6. Distribution of airloads.

Any of these neglected parameters could have a large effect on the design and performance of ground effect vehicles.

In this study it was assumed that the ground effects of a vehicle with an annular jet were not changed with forward speed. It is realized that this assumption may not be strictly valid. The jet power may have to be varied around the vehicle periphery to maintain the desired base pressure or there may be some other changes in the lift augmentation factor with forward speed.

The breakdown of the required power indicated that even at the design speed of 100 knots the power required for lifting was 50 per cent to 80 per cent of the total power. This appears to be a possible area for improvement. Possibly other jet arrangements could maintain the desired base pressure with less jet airflow and jet power.

From all of these question areas it is clear that continued theoretical studies and experimental research are required before the optimum design of a ground effect vehicle can be completed.

In conclusion, it can be stated that the feasibility of large ground effect airborne logistic vehicles has been shown although it is dependent on several assumptions. The use of chemical fuel for ground effect vehicles requiring extended range or endurance does not appear possible. With improvement in the state of the art, especially in lifting power requirements, the vehicle performance and payload could be greatly increased.

REFERENCES

1. Chaplin, H. R., "Theory of the Annular Nozzle in Proximity to the Ground." Aero Rept. 923, Aerodynamics Lab., DTMB, July 1957.

2. Chaplin, H. and Stephenson, B., "Preliminary Study of the Hovering Performance of Annular Jet Cehicles in Proximity to the Ground." Aero Rept. 947, Aerodynamics Lab., DTMB, August 1958.

3. Chaplin, H. R., "Effect of Jet Mixing on the Annular Jet." Aero Rept. 953, Aerodynamics Lab., DTMB, February 1959.

4. Boehler, G. D. and Spindler, R. J., "Aerodynamic Theory of the Annular Jet, Part." Rept. AR 581-R, Aerophysics Co., December 1958.

5. Pinnes, R. W., "A Power Plant Man's Look at the Ground Effect Machine." Rept. DR-1958, Research Division, Bureau of Aeronautics, April 1959.

6. Matthews, G. B. and Wosser, J. L., "Ground Proximity - A Critical Review." Presented at the IAS National Summer Meeting, Los Angles, California, June 16-19, 1959. IAS Paper 59-121.

7. Rethorst, S. and Royce, W. W., "Lifting Systems for VTOL Vehicles." Presented at the IAS National Summer Meeting, Los Angeles, California. June 16-19, 1959. IAS Paper 59-123.

8. Tinajero, A. A., "Comparison of Experimental to Theoretical Design Parameters of a 6 Inch Annular Jet Model with a Jet Angle of 45 Degrees Hovering in Proximity to the Ground and Experimental Results for Forward Flight." Aero Rept. 954, Aerodynamics Lab., DTMB, May 1959.

9. Von Glahn, U. H., "Exploratory Study of Ground Proximity Effects on Thrust of Annular and Circular Nozzles." NACA TN 3982, April 1957.

10. Unpublished Research, NASA Ames Research Center.

11. Unpublished Research, NASA Langley Research Center.

12. Unpublished Research, David Taylor Model Basin.

13. Unpublished Research. Princeton University, Aeronautical Engineering Department.

14. Unpublished Research, Insitute of Hydraulic Research, State University of Iowa.

15. Hoerner, S. F., "Aerodynamic Drag." Published by the author. Copyright 1951.

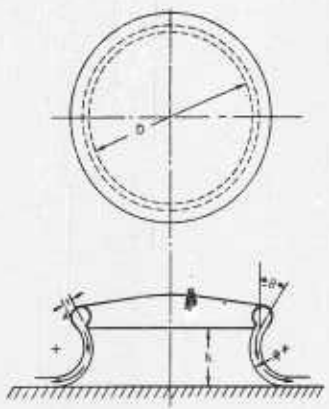

TOTAL LIFT:

$$L = m_j V_j \cos\theta + \Delta p_j S_j + \Delta p_b S_b \quad (1)$$

Figure 1. Schematic drawing of circular annular jet ground effect machine

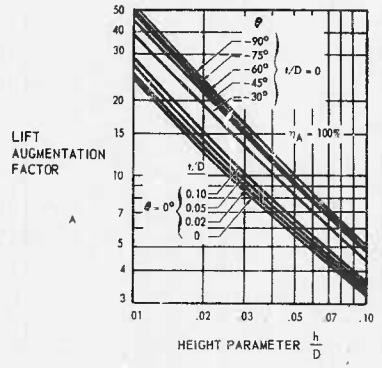

$$A = \frac{L}{m_j V_j} = \cos\theta + \frac{(1-\sin\theta)(\frac{t}{D})\eta A \cos\theta}{2\frac{h}{D}} + \frac{(1-\sin\theta)\eta A}{4\left(\frac{h}{D}\right)\left(1+\frac{t}{D}\cos\theta\right)} \quad (4)$$

FOR $\frac{t}{D} = 0$

$$L = m_j V_j \cos\theta + \Delta p_b S_b \quad (5)$$

WITH CIRCULAR PLANFORM:

$$A = \cos\theta + \frac{(1-\sin\theta)\eta A}{4(h/D)} \quad (6)$$

WITH ARBITRARY PLAN FORM

$$A = \cos\theta + \frac{(1-\sin\theta)\eta A}{4}\left(\frac{4S_b}{hC}\right) \quad (7)$$

Figure 2. Effect of jet angle, θ, and jet thickness, t, on lift augmentation

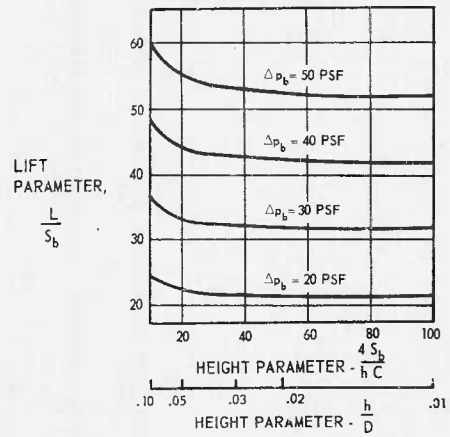

THIN ANNULAR JET
$\theta = -45°$
$\eta_A = 80\%$

$$\frac{L}{S_b} = \frac{A \times \Delta p_b}{A - \cos\theta}$$

Figure 3. Lift parameters for arbitrary planform

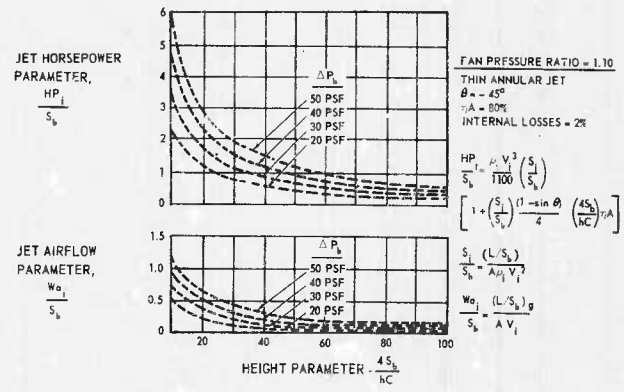

$$\frac{HP_j}{S_b} = \frac{\rho V_j^3}{1100}\left(\frac{S_j}{S_b}\right)\left[1+\left(\frac{S_j}{S_b}\right)\frac{(1-\sin\theta}{4}\left(\frac{4S_b}{hC}\right)\eta A\right]$$

$$\frac{S_j}{S_b} = \frac{(L/S_b)}{\lambda \mu_j V_j^2}$$

$$\frac{Wa_j}{S_b} = \frac{(L/S_b)g}{A V_j}$$

Figure 4. Jet parameters for arbitrary planform

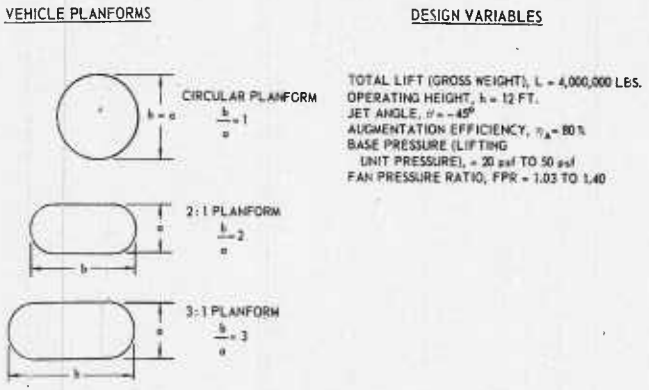

Figure 5. Planforms and design variables used in vehicle comparison

PLANFORM LENGTH TO WIDTH RATIO b/a	BASE AREA, S_b, SQUARE FEET			
	Δp_b = 20 PSF	Δp_b = 30 PSF	Δp_b = 40 PSF	Δp_b = 50 PSF
1	190,300 (a = 492')	121,700 (394')	90,500 (340')	71,800 (302')
2	189,600 (a = 326')	121,100 (260')	89,900 (224')	71,300 (200')
3	188,300 (a = 260')	120,100 (208')	89,200 (179')	70,700 (159')

Figure 6. Variation of required size of ground effect machine

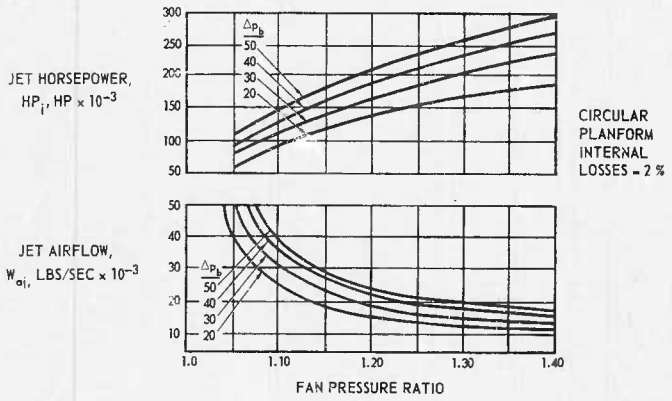

Figure 7. Required jet airflow and jet horsepower for various base pressures

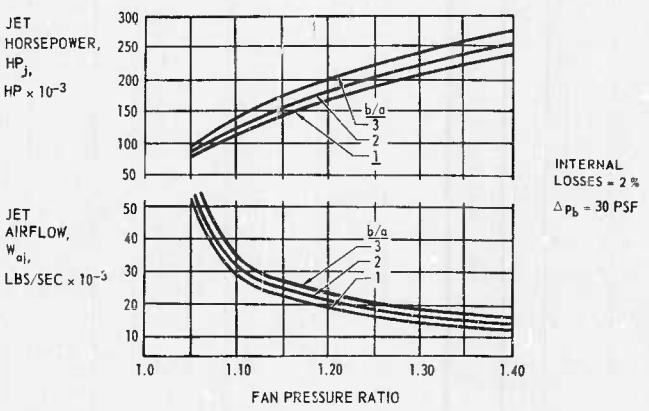

Figure 8. Required jet airflow and jet horsepower for different vehicle planforms

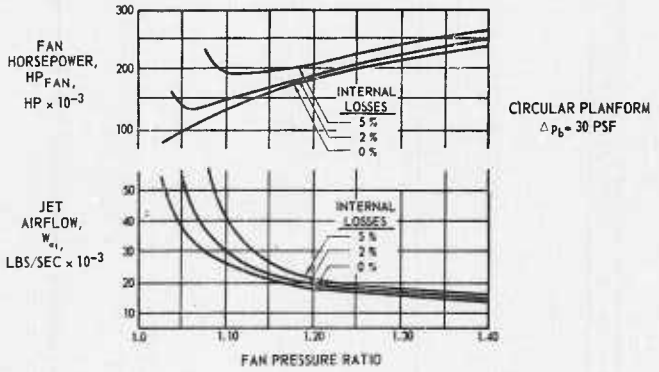

Figure 9. Required jet airflow and jet horsepower with various internal duct losses

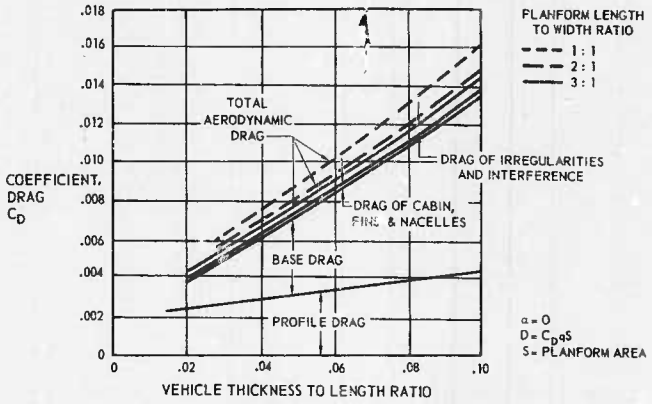

Figure 10. Estimated aerodynamics drag of the ground effect machine

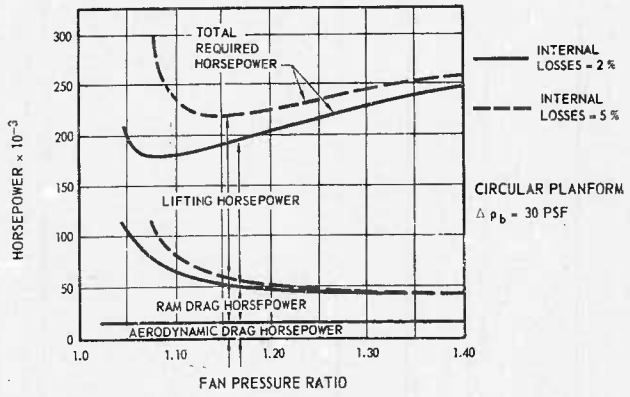

Figure 11. Build-up of total required power at flight speed, V_o = 100 knots

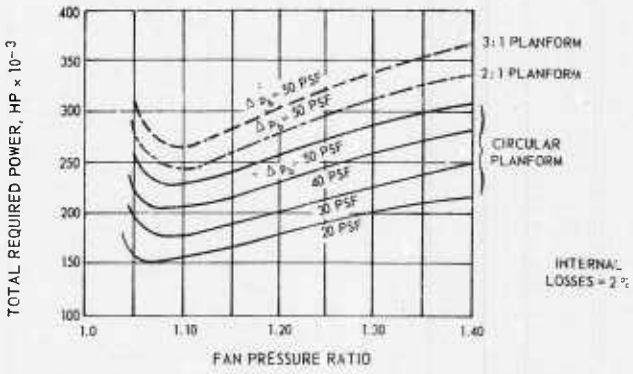

Figure 12. Total required power at flight speed, V_o = 100 knots

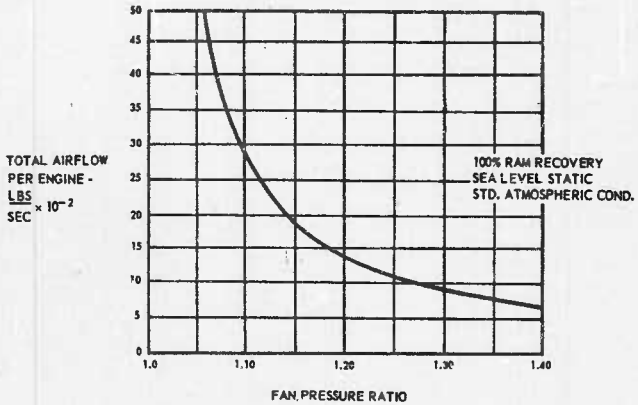

Figure 13. Total airflow of a typical large lift fan engine

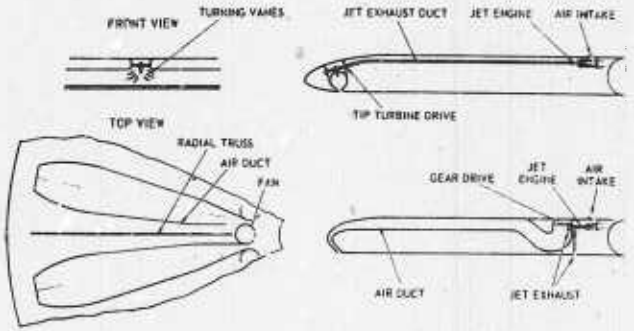

Figure 14. Possible fan locations

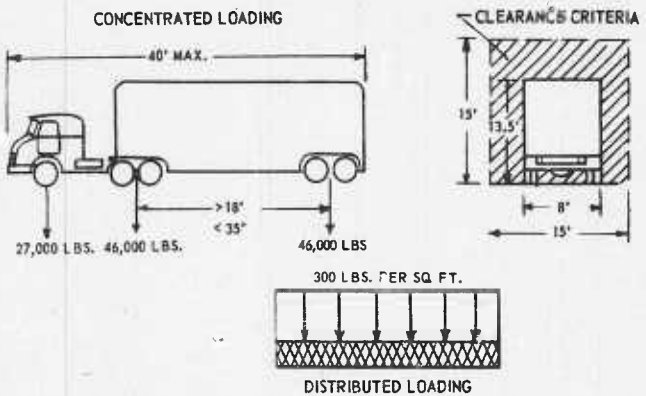

Figure 15. Local floor design criteria

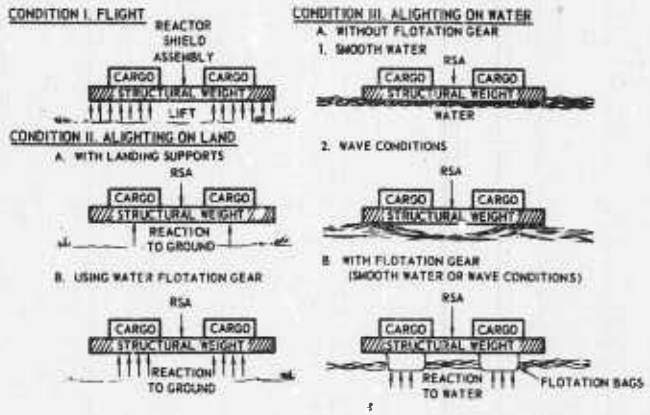

Figure 16. Structural design conditions

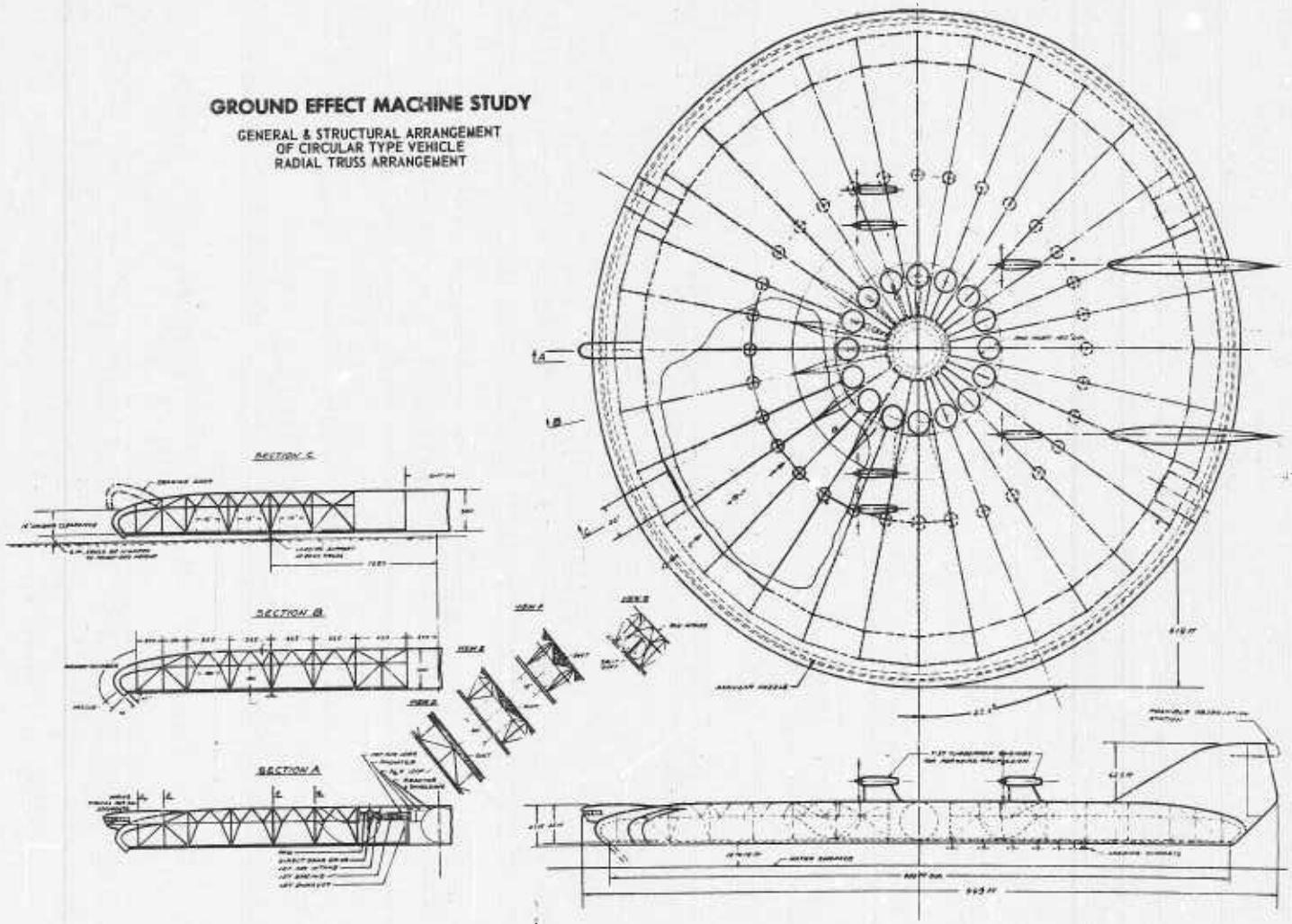
GROUND EFFECT MACHINE STUDY
GENERAL & STRUCTURAL ARRANGEMENT
OF CIRCULAR TYPE VEHICLE
RADIAL TRUSS ARRANGEMENT
SECTION C
SECTION B
SECTION A

Figure 17.

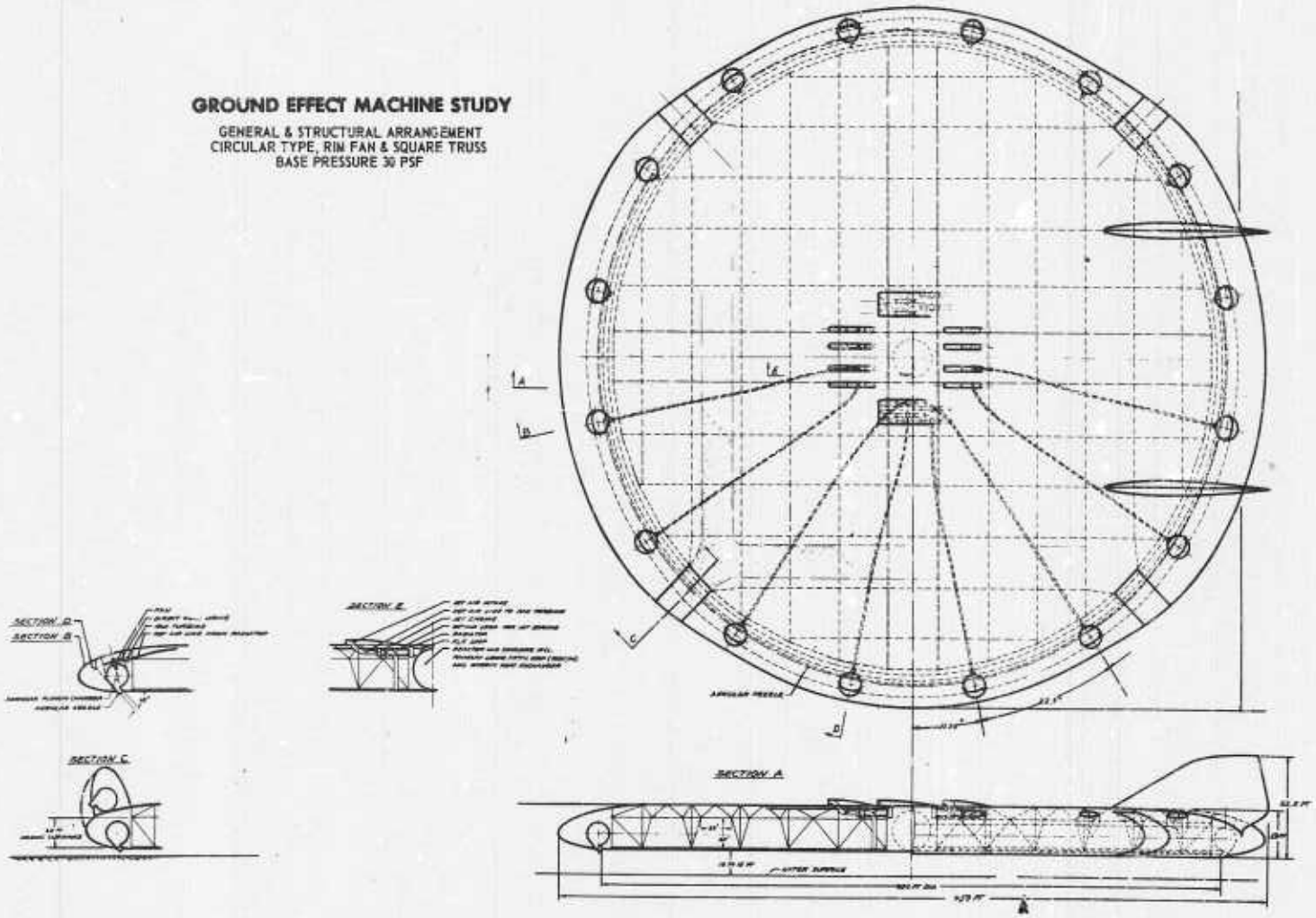
GROUND EFFECT MACHINE STUDY
GENERAL & STRUCTURAL ARRANGEMENT
CIRCULAR TYPE, RIN FAN & SQUARE TRUSS
BASE PRESSURE 30 PSF
SECTION A
SECTION B
SECTION C
SECTION D
SECTION E

Figure 18.

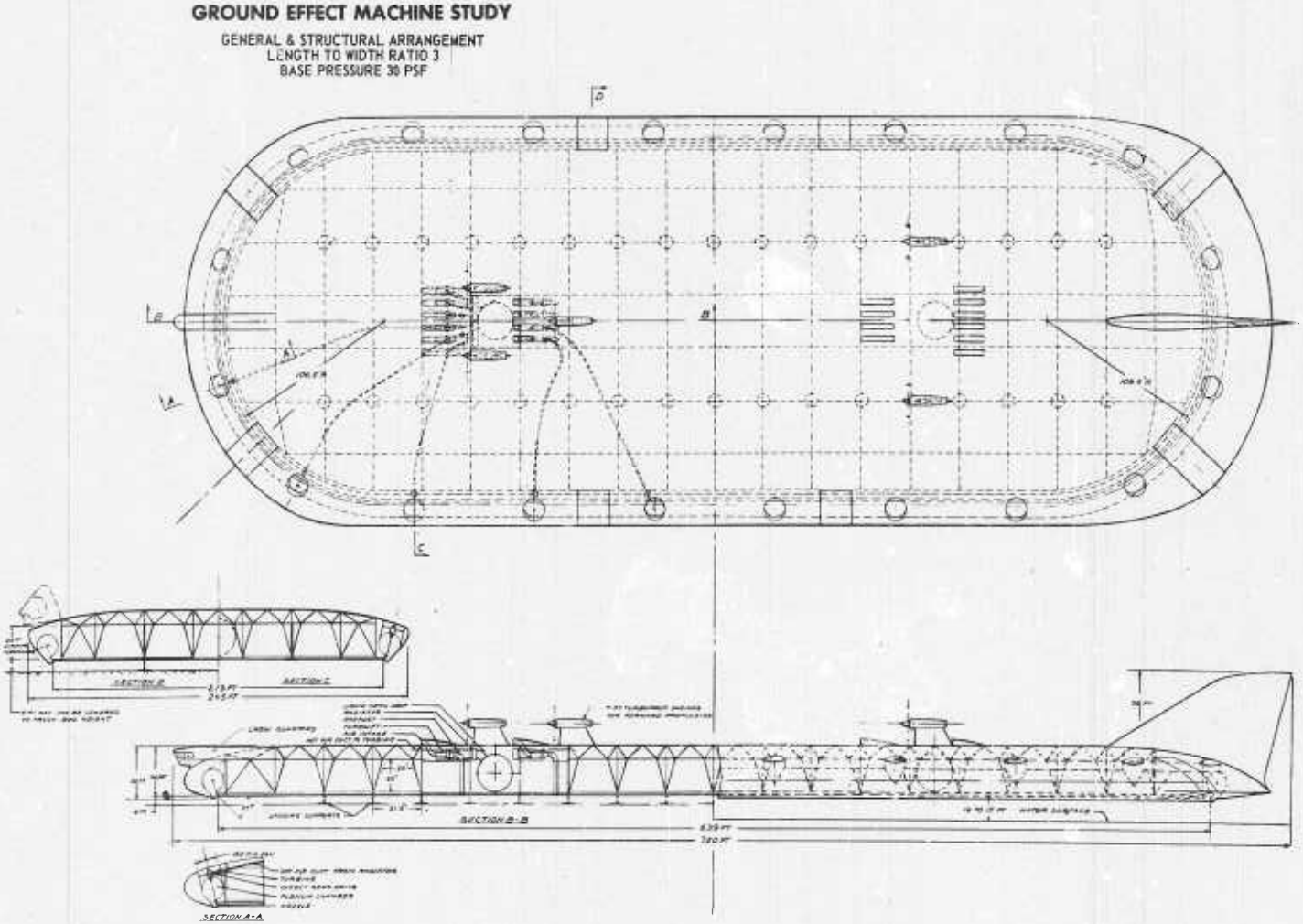
GROUND EFFECT MACHINE STUDY
GENERAL & STRUCTURAL ARRANGEMENT
LENGTH TO WIDTH RATIO 3
BASE PRESSURE 30 PSF
SECTION B-B
SECTION A-A

Figure 19.

WEIGHT BREAKDOWN OF GROUND EFFECT MACHINE

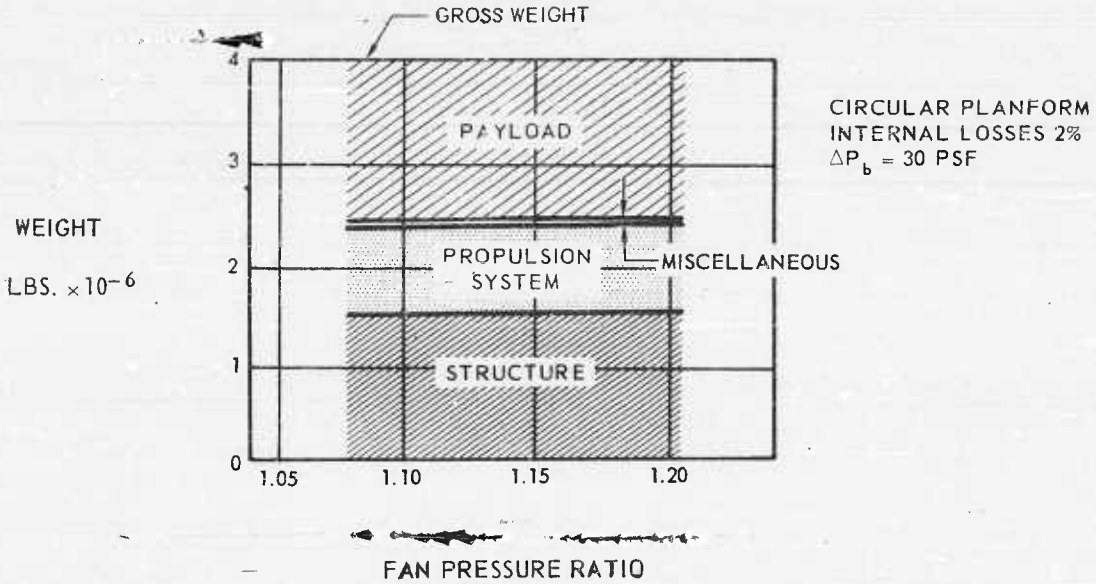

Figure 20.

VARIATION IN PAYLOAD OF GROUND EFFECT MACHINE

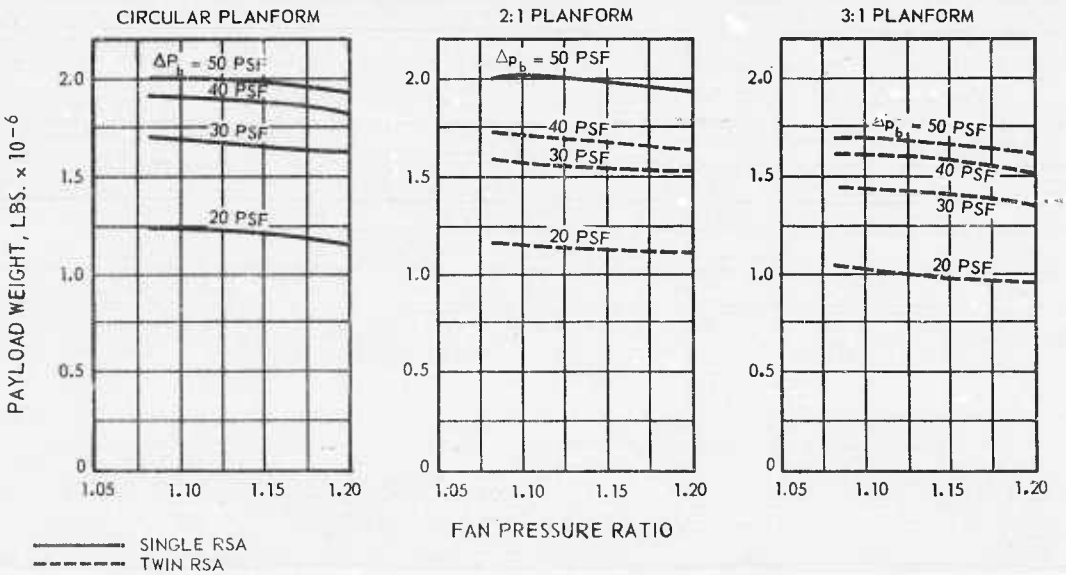

Figure 21.

THE HOVERING PERFORMANCE OF A TWO-DIMENSIONAL GROUND EFFECT MACHINE OVER WATER

By Arthur E. Hirsch, Hydrodynamics Laboratory, David Taylor Model Basin, Washington, D. C.

INTRODUCTION By Lt(JG) Lincoln D. Cathers, Preliminary Design Branch, The Bureau of Ships, Washington, D. C.

The bureau of ships is actively interested in ground effect machines, as we forsee a useful application of this phenomenon over water. There are many missions in which higher speeds would provide increased tactical advantages. However, even though we have seen many working models perform over water, the fact remains that we must direct our efforts to further understand why and how ground effect machines work. Our aim is to obtain the information necessary to design these craft and to accurately predict their performance. The most reliable way to pursue this end is to conduct a thorough model testing program complemented by theoretical work where desirable.

In the fall of 1958 a partnership was organized between the ship designers in the bureau of ships and the physicists and hydrodynamicists at the David Taylor Model Basin with the objective to further pursue this concept for possible marine applications. The program presently underway is directed toward the development of a craft designed to operate mostly, if not entirely, over water.

The design of a craft for over-water use poses many difficult problems such as the presence of waves and a highly corrosive atmosphere. Conversely, the over-water application affords us some distinct advantages in that we have no trees, ditches, or hills with which to contend. Even though this craft operates over water, it is not a ship in the usual sense of the word. Rather, it is a marriage between an airplane and a ship.

To aid the work at the David Taylor Model Basin, we in the bureau of ships have endeavored to furnish guidance as to (1) possible missions, (2) reasonable values of sea conditions to consider during testing, (3) meaningful values of speeds to investigate and (4) other pertinent design information. The bureau of ships will prepare feasibility studies when sufficient data becomes available.

The body of this report will deal with hovering performance of our two-dimensional model over water. Subsequent work will be directed toward obtaining forward motion data in both calm water and waves. Stability and control at forward speeds will also be given a through study.

The selection of a wall-sided model for extensive testing has caused considerable comment. We believe that there is a net gain in having these longitudinal SKEGS in the water. At 50 to 70 knot speeds, the amount of increased drag at forward speed is more than offset by the drastic reduction in power to hover at a given altitude. Also, at these speeds there appears to be merit in using marine propulsion and ship-type rudders.

In summary, we are interested in obtaining design data. It is this design data that is missing but absolutely necessary for a rational design of a craft utilizing the ground effect principle.

Viewing the ground proximity vehicle as a seaworthy vessel rather than as a novel aircraft presents numerous problems, which are centered around the seaworthiness of

the craft. Present estimates indicate that a seaworthy craft with marine propulsion would have a weight of at least 20-30 lb/ft^2. This is too heavy for a reasonably powered annular craft flying at a practical altitude. However, the augmentations predicted for a two-dimensional craft are very attractive and, if they prove realizable, it is likely that a practical Hydro-skimmer boat can be designed.

With this in mind, a highly simplified small boat was constructed in such a fashion that useful information would be yielded as quickly as possible (Figures 1, 2, and 3). Any resemblance to future prototypes will be fortuitous. In order to check the crafts performance and to make a reliable comparison with theory, three types of performance measurements were made. Base pressures were measured at 8 stations along the bottom. Figure 4 shows the distribution of these gauges. The velocity of the air in the ducts leading to the nozzles was measured by a pressure gauge located in each duct. Pitot tube surveys of the duct and a system of adjustable air deflection fins assured us that the pressure reading at the installed position could be interpreted to yield a reliable value of air velocity at the nozzles. Lastly, the total lift on the craft was measured by a spring balance scale.

Testing is still in progress at the present. Since the end of July, when the model was completed, we have made two series of tests: one where the jets were perpendicular to the surface or at an angle with the perpendicular of 0°, and another where the jets were inclined inward toward the midship's region at an angle of -40° with the perpendicular. In each of these conditions the craft was operated at a number of fixed heights from the surface with different power inputs, and measurements of lift, jet velocity, and base pressures were made.

A preliminary analysis of the data has been made and several curves have been obtained (Figure 5). Augmentations have been computed from the data and are plotted against the ratio of the height to the length of base between jets. The augmentation here is defined as in Chaplin's report, "The Theory of the Annular Nozzle in Proximity to the Ground," the ratio of the total lift to the lift due to the jet alone. As can be seen, there is considerable scatter in the data; however, there is a clear indication that there is good agreement with the theoretical curve until the point where (h/t) height to jet thickness is equal to 1. Below this point the theory no longer holds. An estimated curve based on an increasing jet velocity, as the effective jet width is reduced, has been plotted as dashed lines. No claims are made for the validity of this curve; it simply indicates that the data are proceeding in a reasonable direction. As can be seen, augmentations up to about 20 can be obtained for useful configurations.

Figure 6 is a plot of the augmentations obtained where the jet angle was -40°. This plot indicates that the data do not agree as well with the simple theory as do the 0° jet data. This is not particularly surprising. What is important is that there is a tendency for greater augmentation with the angle change, and advantage can be taken of this feature.

A further set of plots was made (Figure 7) where air horsepower, i.e., the horsepower delivered at the jets, is plotted against the height to base length ratio for various lift per ft^2. With our present model, lifts as great as 20 lb/ft^2 can be obtained. Obviously a more efficient blower system could generate greater lifts with the same motor power. Figure 8 shows a similar plot for the -40° jet angle. Lifts obtained are somewhat better than those for the 0°, which are indicated by the dashed lines superimposed on the plot.

Our work with the two-dimensional model shows much promise. We are planning to continue the use of this model to determine augmentation in hovering and underway, with other nozzle widths and angles, in addition to making lift and drag measurements underway both in still water and in waves. In addition, plans are being developed for the construction of a model of a prototype to be used for further testing.

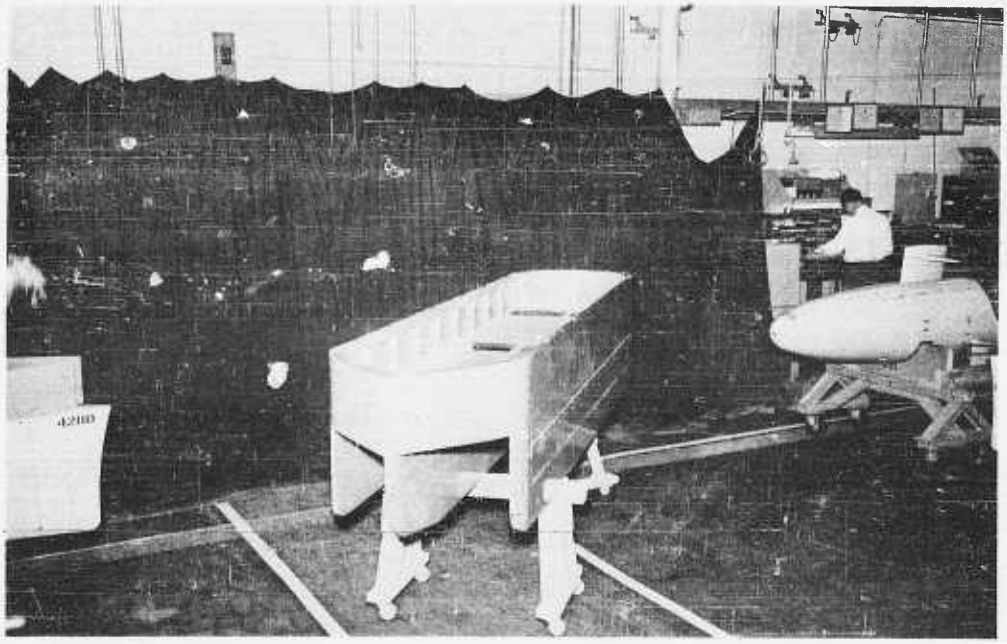

Figure 1.

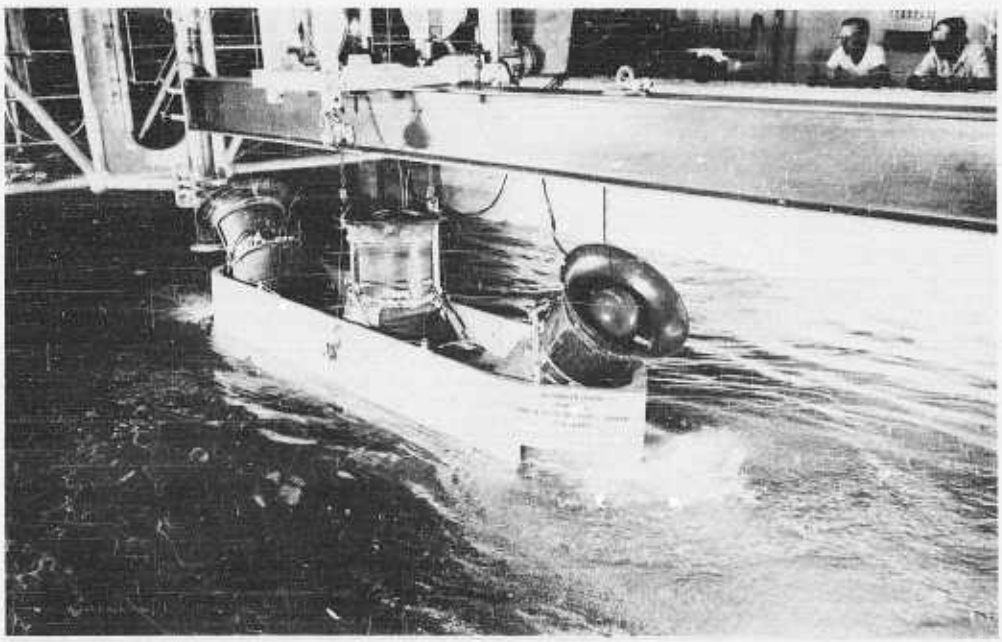

Figure 2.

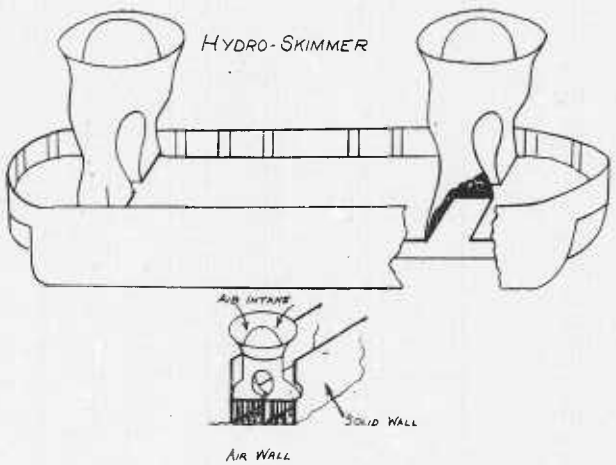

Figure 3.

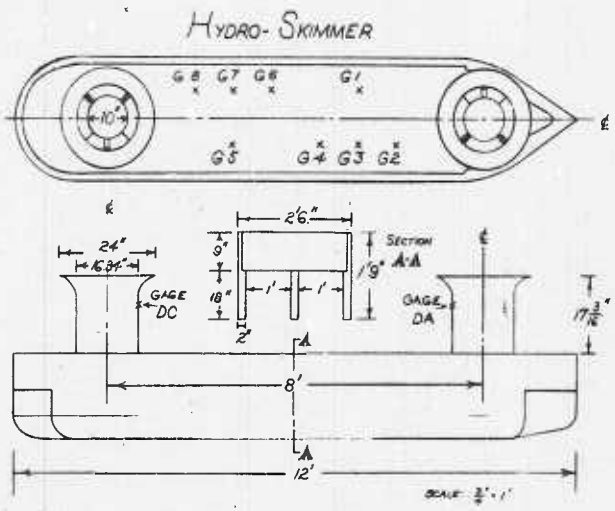

Figure 4.

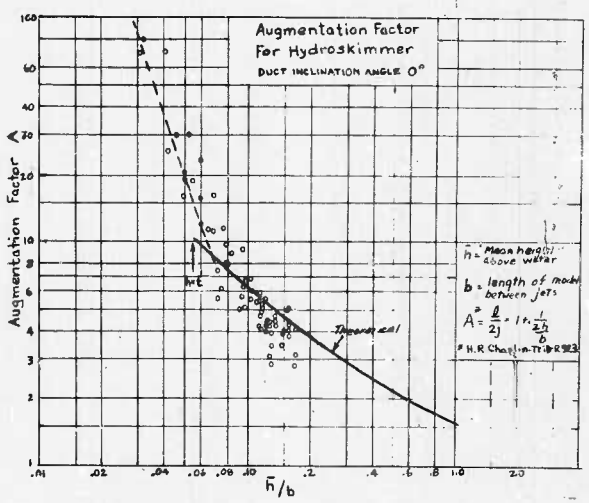

Figure 5.

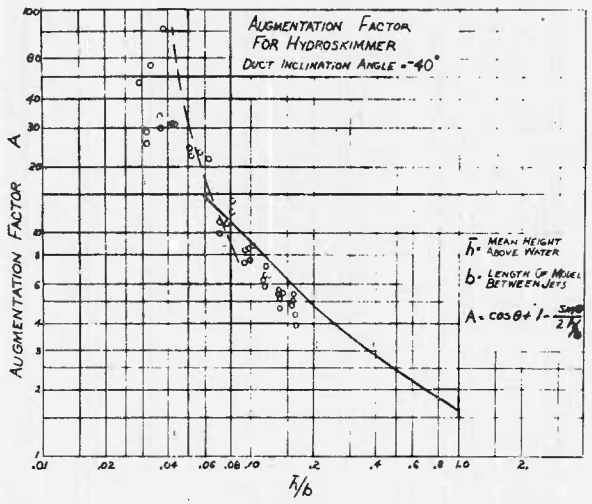

Figure 6.

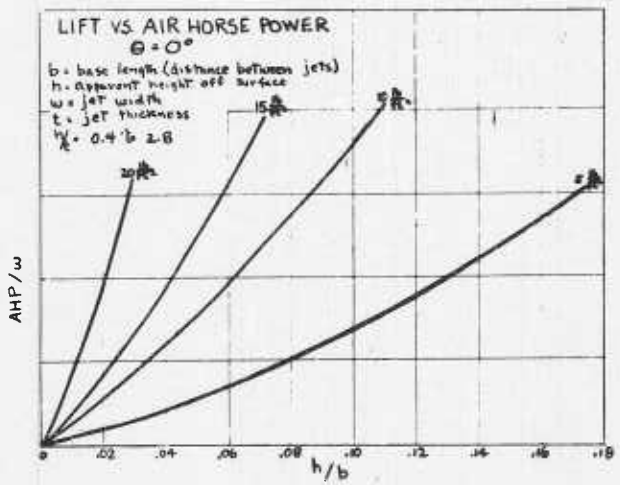

Figure 7.

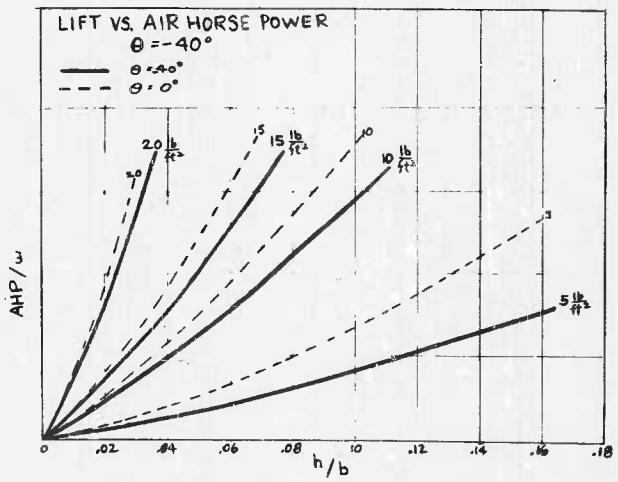

Figure 8.

TEST EXPERIENCE AND COMMENTS ON AIR CUSHION VEHICLES

By National Research Associates, Inc., College Park, Maryland

INTRODUCTION

In light of the interest and activity demonstrated by this symposium it is hard to realize that a scant five years ago the air cushion vehicle, in this country at least, was just an idea. As a matter of fact, it was an idea viewed with considerable skepticism by most of those to whom it was proposed. It was this skepticism - and our curiosity - which motivated our initial tests on the peripheral jet concept.

Our basic hypothesis was that the horizontal change of momentum of a jet sheet should be equal to the integration of the horizontal pressure across the jet sheet as indicated in Figure 1. In equation form this was:

$$MV_j \ (1 + \mathrm{Sin}\beta) = h \cdot \Delta p$$

or

$$\frac{\Delta p}{q_j} = 2\frac{t}{h} \ (1 + \mathrm{Sin}\beta) \text{ for a unit width}$$

This fundamental relationship has since been derived more elegantly by others but it included the major variables, the effects of which we wished to examine.

EARLY TESTS

The first tests were performed with a most homespun apparatus fabricated out of cardboard with the jet sheet air being supplied by a shrieking Eureka vacuum cleaner. Since this apparatus was small scale and two-dimensional, the static pressure developed was less than indicated by the hypothesis, but it proved to us that, qualitatively at least, the anticipated effect could be obtained.

These test results led us to construct another two-dimensional model, shown in Figure 2, which could be used for demonstration purposes. This model was more nearly representative of the cross section of a vehicle and, through the Plexiglass face, tufts showing the internal air flow pattern were visible. The air supply was again provided by a vacuum cleaner blower.

Some of the test results obtained from this simple apparatus are shown in Figures 3 and 4. Figure 3 shows the typical variation of lift pressure with the jet angle for a constant height. Figure 4 illustrates an interesting phenomenon which has received little attention but will be worthy of further study if operation at comparatively large h/D ratios or transition to flight out of ground effect is anticipated.

It will be noted that the height at which the drop in pressure occurs varies with the angle of the jet discharge. Although not shown by the curves, the drop in pressure occurs very suddenly as height is increased to the critical value and an unstable, vibrating, or bouncing condition is initiated. As the height is increased further this unstable condition is terminated and the pressure rises to the value with no ground effect. It is interesting

to note that, as a rough observation, the onset of this condition occurs when the intersection of the extension of the jet discharge velocity vectors occurs at the ground plane.

OTAC PROGRAM

The first government contract to study the feasibility of peripheral jet air cushion vehicles was given to National Research Associates, Inc., by the Army Ordnance Tank-Automotive Command. Time does not permit a comprehensive review of the testing conducted under this program; hence this discussion will necessarily be limited to a general description of the work done and a brief analysis of some of the more important results.

The program was initiated with the construction and testing of a small free-floating stability model. This model, which was approximately 15 inches square, was designed to provide basic information on stability characteristics and hovering performance of peripheral jet configurations with a view toward application to Army Ordnance vehicle requirements. Initial tests of this model verified earlier indications of a tendency toward static instability at low heights for this type of configuration, unless some means was provided for effectively blocking cross flows under the base. Stabilizing jet sheets, which isolated the corners of the vehicle base, accomplished this on the small model, and subsequent tests indicated stable operation over a wide range of terrain conditions and over water. Figure 5 shows a photograph of this model operating over water. The operating height was of the order of one inch, with an estimated lifting force of 37 lbs/hp being generated.

In order to establish possible scale effects and to verify extension of the configuration feasibility to large scale as well as small scale models, a 5-ft square operating mockup was constructed and tested as the next step in the Army program. This mockup, shown in Figure 6, was powered with a 5 hp gasoline engine driving 4 axial flow fans. The basic weight of this vehicle was approximately 76 lbs.

Tests performed with this operating mockup included free-floating qualitative performance tests, captive performance tests, and pressure survey and flow pattern studies. The first of these series of tests provided visual observation and photographic data concerning basic hovering ability and inherent stability characteristics over a variety of surface conditions, including smooth concrete, irregular terrain, and water. Stable operating qualities were exhibited under all operating conditions. Heights of the order of 6 inches were observed during these tests.

Captive performance tests, in which the vehicle was effectively suspended in an offload rig, provided more detailed information concerning height vs. weight relationships. Some results of these tests are presented in Figure 7. At the low heights, the general hyperbolic form of height vs. weight for this type of configuration is illustrated in this figure. At larger heights, a constant lifting force independent of height was approached.

Further controlled tests to obtain detailed flow and pressure data were performed with this operating mockup held rigidly in a scaffold. Vehicle base pressures, exit nozzle pressures, and internal and external flow patterns were observed during these tests at several heights above the ground plane.

On the basis of an equivalent diameter determined from the total base area, augmentation ratios obtained agree reasonably well with theoretical values for circular annular jets at low heights. Significant departures from theory were observed at the greater heights, with negative base pressures being obtained at h/D ratios greater than about 0.70.

To add a touch of realism to the feasibility demonstrations, an operating mockup of approximately 5 ft by 10 ft with a body simulating an armored vehicle was fabricated. The resulting configuration, one version of which is illustrated in Figure 8, was successfully

demonstrated as a free-floating, essentially uncontrolled vehicle over various terrains and over water.

TWO-DIMENSIONAL TESTS

Other phases of the overall test efforts at National Research Associates concerned with the peripheral jet configuration include some two-dimensional investigations using a specially developed two-dimensional test stand. Parameters of interest in these tests include jet nozzle width, angle, and height above the ground plane. Although somewhat limited in application, the results of these tests are being used to provide a basis for the development of improved vehicle design.

STATIC TEST STAND

An additional, and what is felt to be an extremely important phase of the Army program at National Research Associates consists of the development of a full scale static test stand for ground effect vehicles. Recently initiated, this program will culminate shortly in a test stand capable of providing full scale three-dimensional data for direct application to design and evaluation of a wide range of large size ground effect vehicle configurations. Data concerning vehicle height, the angle of inclination with ground plane, exit nozzle design, and flow and pressure variations will be readily obtainable with this facility. An artist's drawing of this test stand is shown in Figure 9 and a small desk-top model of this test stand is on display as part of the symposium exhibit.

MAN-CARRYING VEHICLE

The actual construction and delivery of full-scale, man-carrying vehicles for Army Ordnance and the Marine Corps has occupied the largest part of the balance of the GEM activities at National Research Associates during the past few months. These vehicles, which are on exhibition at this symposium, are prototype research configurations. The Marine Corps vehicle is illustrated in Figure 10. Weighing about 1100 lbs and measuring approximately 8 by 14 ft, they are designed to operate at heights from 9 to 15 inches. Power is supplied by two air-cooled engines rated at 40 horsepower at 6,500 rpm, each of which drives two 42-inch, 6-bladed propeller fans located at each end of the vehicle. The supporting air cushion is developed by a 10-inch peripheral jet fed by a specially designed internal ducting system. Stabilizing jets are included on each corner of the vehicle base. Fore and aft and turning controls are accomplished by deflection of the peripheral jet sheet.

In operation, these vehicles exhibit generally stable hovering characteristics. Control capability has been demonstrated to be somewhat limited, and appears to be one of the most important areas of development in this type of vehicle. Representative preliminary hovering performance data obtained with these vehicles is illustrated in Figure 11. As shown in this figure, a height of one foot has been achieved at a total fan horsepower of 52 hp with a 175-lb operator on board. As an example, increasing the payload to 400 lbs, including the operator and one passenger, reduced the height by about 2 inches from an initial height of 8 inches at 43 fan hp.

Further tests on these vehicles should fill a very important gap in existing information on ground effect vehicles from both a performance and an operational standpoint.

HIGH SPEED AIR CUSHION BOAT

Another type of air cushion vehicle, upon which we have done development testing, is a high speed boat. The air cushion is employed in this case to reduce drag rather than to provide high mobility.

Test results indicate that this type of boat has favorable resistance characteristics when compared with hydrofoils or planing hulls at high speeds. Most of our tests have been conducted with a man-carrying boat of 5-ft beam by 11-ft length, propelled by a 5-hp outboard motor. The air cushion is provided by blowers driven by a separate 2-1/2 hp engine.

During tests without the air cushion this boat indicated a top speed of 5 knots. When the air cushion was established the speed increased to 17 knots. Experience also indicates that this type of boat gives a smoother ride over choppy water than a conventional hull.

This boat has been modified to accommodate a larger engine, and further tests are presently being conducted at higher speed ranges.

PLENUM CHAMBER VEHICLES

Plenum chamber vehicles are endowed with the outstanding virtue of structural simplicity. It is a mistake, however, to assume that their internal flow and performance characteristics are also simple. The literature contains little information concerning plenum chamber analysis or performance, and the information available does not appear to be adequate or accurate.

Lack of time precludes a full discussion, but some of the unique characteristics of plenum chambers will be mentioned. Perhaps the outstanding feature is great height stability, the lifting pressure varying inversely with a function of the square of the height as compared with the inverse linear variation of the peripheral jet. This pressure variation is so rapid that substantial negative "lifting" pressures may be established at a comparatively low value of h/D.

A careful analysis and also experiments reveal that, except for certain special conditions, the lifting pressure within the plenum is not uniform and may even be negative in some regions, even though the net effective pressure is positive. The assumption that the lifting pressure is equal to the total pressure of the flow is not justified and leads to overly optimistic performance estimates.

Another interesting feature of the plenum chamber is that the lifting pressure is a function of the fourth power of the ratio of the fan diameter to the overall plenum diameter. Thus the lift capability is very sensitive to the size of the blowing fan employed.

Analysis and tests performed at National Research Associates indicate that plenum chamber vehicles of practicable configuration will be restricted to operation at h/D values of less than about 0.04. This is probably too low for high mobility vehicles; but for some applications where fairly smooth surfaces are available the plenum chamber vehicle may be attractive because of its virtue of simplicity.

As a result of our studies at National Research Associates, we have developed a new concept of plenum chamber incorporating "controlled flow." Compared with a simple plenum chamber, a vehicle employing "controlled flow" can carry several times the gross weight at the same height or the same load up to several times as high. Time does not permit a discussion of this new concept, but a small operating model will be exhibited during the demonstration period.

COMMENTS

As a general outgrowth of our experience in this field, we have developed a philosophy that the type of air cushion technique employed should be determined to best fit the intended application. As examples of this philosophy, we believe that the peripheral jet

technique is best suited for high mobility vehicles where terrain clearance is important; whereas, for a boat or land vehicle to operate over a smooth surface, a plenum air cushion may be preferred.

We also feel that, in regard to applications, air cushion vehicles should be viewed without bias introduced by current types of transportation such as aircraft or ships. We feel that through uninhibited concepts the use of these vehicles will lead to a whole new era of transportation.

In looking to the future it is clear that much research is required to provide a thorough understanding of the basic phenomena involved in air cushion vehicles. The vehicle designer also needs more data for his use in designing efficient vehicles-particularly in regard to blowing and ducting problems. More study is also needed to determine optimum propulsion and control systems and to determine the influence of these systems on the overall vehicle design.

Looking further into the future, we anticipate that there is much more to come in this field. With time and increased activity new configurations and concepts will be originated, with the result that economical high speed transport and military vehicles will be developed. We fully expect that before the passage of another decade we will see air cushion vehicles being employed for many purposes with a lower cost per ton mile than can be achieved by any other form of transportation.

And we might add, in closing, that this stimulating symposium will be viewed in retrospect as a major factor in accelerating this anticipated progress.

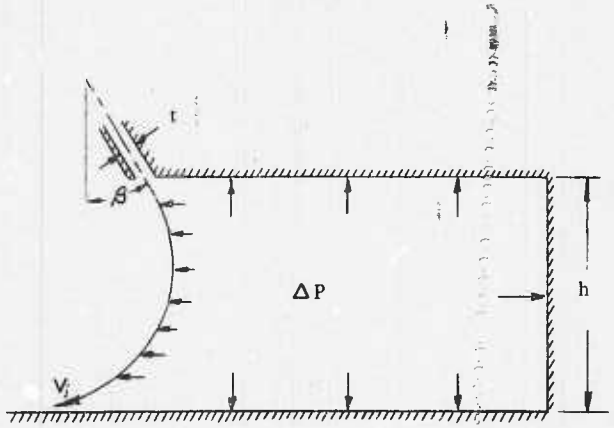

Figure 1. Two-dimensional annular jet flow diagram

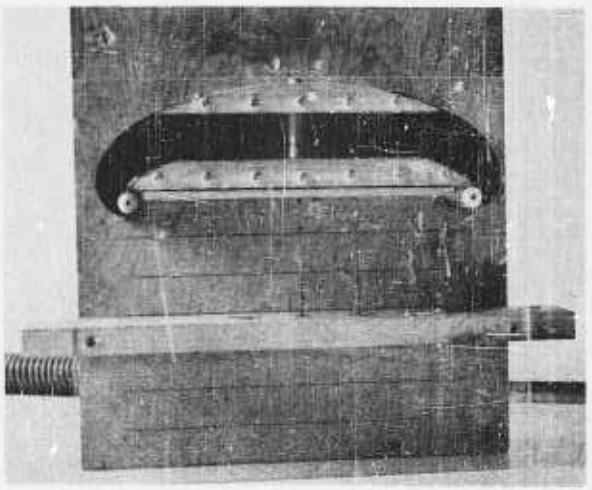

Figure 2. Two-dimensional test fixture

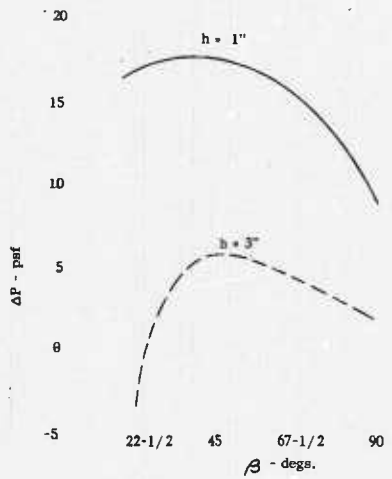

Figure 3. Δ P vs. β. Original tests

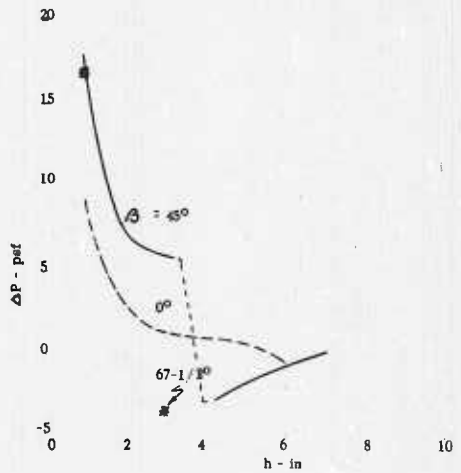

Figure 4. Δ p vs. h. Original tests

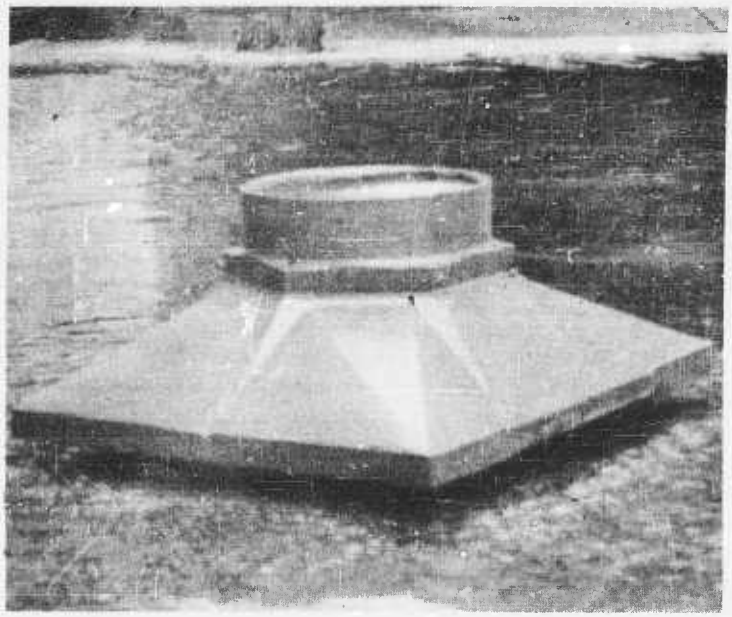

Figure 5. 15 Inch stability model

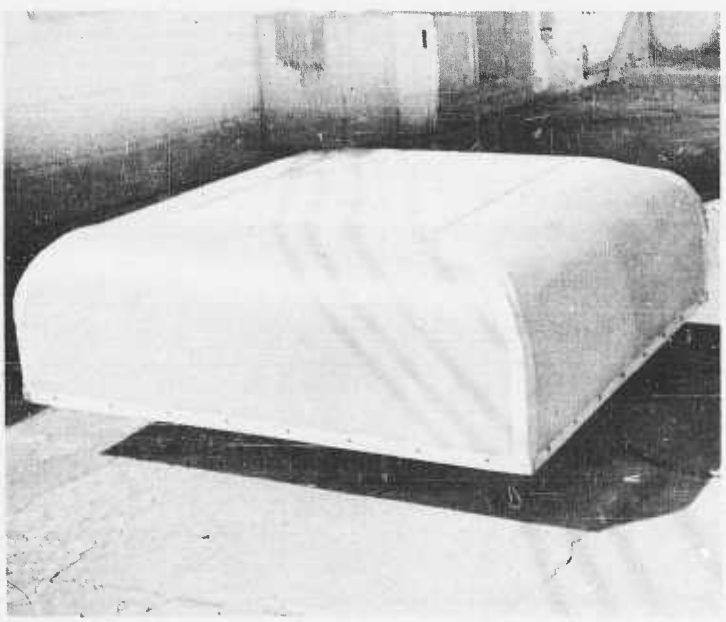

Figure 6. Operating mockup. Box configuration

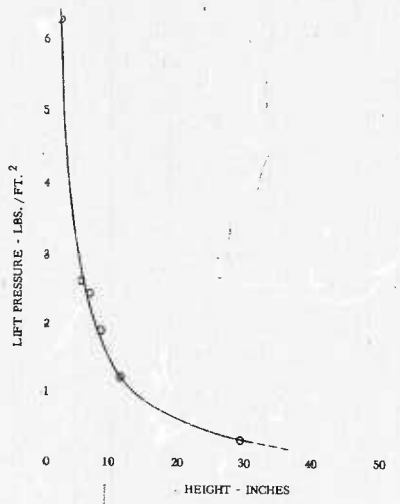

Figure 7. Lift vs. height. Operating mockup

Figure 8. Operating mockup. Armored configuration

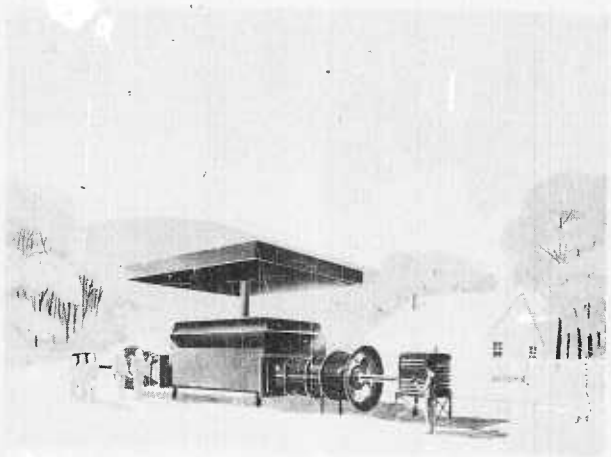

Figure 9. Full scale static test stand

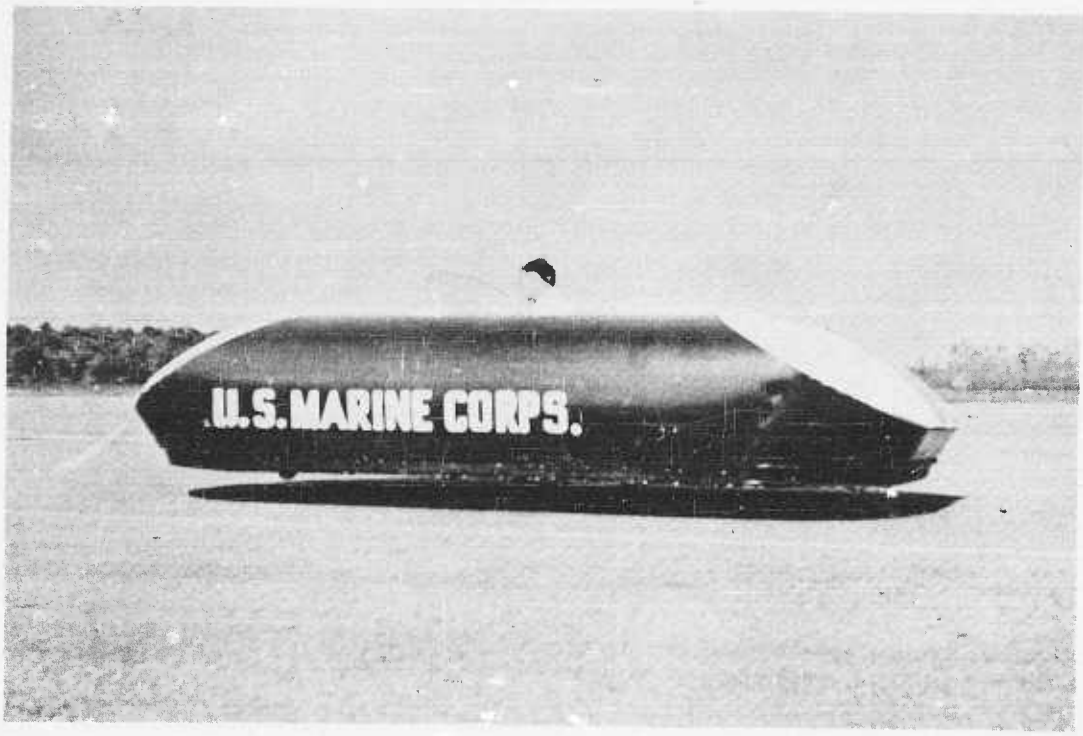

Figure 10. Pegasus I vehicle

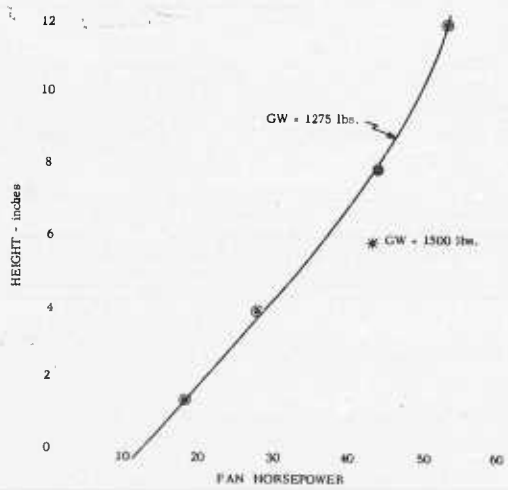

Figure 11. Height vs. fan horsepower - Pegasus I

PROPULSION SYSTEM EXPERIMENTS

By James F. Sutton, Georgia Division, Lockheed Aircraft Corporation,
Marietta, Georgia

Lockheed Aircraft Corporation has studied the problems of take-off and landing distance reduction for aircraft for a number of years. The design objective for an efficient vehicle is to move a payload from one point to another in the most economical fashion in the proper time. For cruise between take-off and landing, no system more efficient than that using a fixed wing has been found. The weight expended for a wing pays for itself by permitting the attainment of high lift to drag ratios at forward speed. This results in fuel-saving far exceeding the weight of the wing. Other benefits such as improved stability also accrue due to the wing.

The portions of the mission other than cruise are the take-off and landing. Most aircraft optimized for the cruise portion of the mission result in thrust to weight ratios of 0.25 to 0.4 at take-off. This is obviously too low to permit vertical take-off as the wing is ineffective. Hence the propulsion system must be overpowered if vertical take-off is to be obtained. The magnitude of the penalty of excess weight and drag for providing this capability must be minimized.

One concept we have studied used ejectors to augment vertical lift to reduce the size and weight of the propulsion system. Early in the study of this concept, literature search revealed little applicable data; consequently, an extensive test program was initiated. This program included static tests of a number of configurations, various wind tunnel investigations, and hovering operation of a test vehicle. The purpose of this paper is to present some of the ways that ground proximity affects the performance of ejectors as observed during these experimental programs.

Figure 1 shows a schematic of an ejector. It consists of a primary nozzle discharging gases having kinetic energy into a mixing section. Secondary air is entrained by the primary jet in the mixing section. Use of a diffuser may permit higher secondary flow and higher augmentation for certain configurations. The amount of augmentation obtained is dependent upon proper optimization of a number of geometric parameters.

Operation of an ejector with the discharge against a ground plane results in decreased augmentation. Figure 2 shows the reduction of force relative to that obtained out of ground effect as the distance to the ground plane is reduced. This is for a two-dimensional ejector; that is, an ejector with end plates. The height above the ground plane is expressed in terms of the outlet width, w. The thrust reduction is extreme for the location of the outlet close to the ground plane. In fact, a vehicle using such a system would need unreasonably long landing gear.

The parallel outlets, located so as to provide a base area between the outlets, permit positive base pressure forces to offset the momentum thrust loss. Typical values are shown in Figure 3 for a two-dimensional system. The thrust has been referenced to that obtained in free air with a single ejector having the same geometric and dynamic parameters. One observes that, at heights below nine times the outlet width, significant augmentation due to the positive base pressure forces is obtained. The base pressure is positive and not only compensates for the loss of momentum, but provides additional force.

For the particular geometry shown, the two jets impinge at a height of nine times the width. This causes pumping of the base area so that the base pressure force becomes

negative. A constant base pressure force equal to 13 per cent less thrust than would occur for the two outlets without a base between them is realized beyond this height. Removal of the end plates and an outward tilt of the jets reduce this loss out of ground effect and will be discussed later.

Ground plane pressures were investigated as possibly shedding some light on the problem of ground blast. In Figure 4 a plot of the static pressure on the ground plane normal to the plane of the two-dimensional jets is shown for a height of 2.2 times the outlet width, i.e., in ground effect. The ordinate is the ratio of the local static pressure to the dynamic pressure of the primary jet in the ejector.

In ground effect, three distinct pressure peaks may be observed. The impingement of the jets on the ground plane results in a static pressure equal to the dynamic pressure of the jet as it is turned through 90 degrees. Impingement of the two jets turned towards the center results in a third peak approximately equal in magnitude to the dynamic pressure of the jet.

Also shown in this figure is the pressure on the base between the outlets. In ground effect, the base pressure is positive and uniform across the base for the two-dimensional case.

Figure 5 shows the static pressure distribution on the ground plane at a height of 15.5 times the outlet width. The two jets coalesce into a single jet at a height of 4 w, so that from that point the flow is a single jet with a pressure peak on the centerline. Diffusion and mixing of the jet with ambient air reduces the magnitude of the pressure at the centerline.

Entrainment of the air in the base region reduces the static pressures below ambient as shown by the lower curve. The pressure distribution is uniform across the base. All of the data presented in the foregoing figures are two-dimensional. For two adjacent outlets, the three-dimensional effects are beneficial in that air may flow into the base area between the jets when the vehicle is out of ground effect, reducing the negative base pressure. At the same time, little loss of ground effect augmentation is realized. Figure 5 shows the vertical forces as a function of height. The forces have been referenced relative to the thrust produced by a single ejector out of ground effect. As the height increases, the base pressure forces are reduced with a corresponding reduction in the vertical force. In ground effect, air flows out of the base area between the jets.

At a height equal to 7.6 times the outlet width, the base pressure force is negative enough to reduce the augmentation below that obtained in free air with a single ejector. Air flows into the base, relieving the negative pressure. The pressures are not uniform along the base so that no sharp peak in the augmentation occurs, as it did in the two-dimensional case. For the particular configuration shown, the centerlines of the jets were normal to the plane of the outlets. Slight canting of the jets outwards increases the area available for the inflow of air, so that the loss out of ground effect may be decreased even further than that shown. Since the flow parallel to the ejector centerlines is a very low velocity flow, ground blast effects in this direction are minimized.

All of the data presented to this point are static. The ability to hover, while useful, is not very productive in transporting payload. In fact, no airborne vehicle hovers as well as it moves in forward flight, other than a balloon.

Forward speed can result in significant increases in lift, that is, augmentation. Ground effect on a wing is beneficial in that induced drag is reduced by an apparent increase in aspect ratio. The propulsion system can contribute large increases in lift, as for jet flap or blowing boundary layer control systems. Figure 6 shows the relative increase of lift

versus air speed for a particular aircraft configuration utilizing ejectors at an angle of attack of 6 degrees. The solid line shows the increase in lift due to aerodynamic forces on the wing out of ground effect. As the speed increases, the aerodynamic lift is additive to the vertical force generated by the propulsion system. In ground effect, with the outlets at a height of 2.3 times the outlet width, the augmentation is significant. This is due to the effect on the wing and on the base between the propulsion system outlets. At 80 knots, the increase is 24 per cent. Also shown is the total drag of the system including momentum of the secondary air into the ejector, parasitic and induced drag as well as the thrust component of the jets. In other words, this is the total force on the model in the flight direction. Reynolds number corrections have not been applied. These result in higher lift and reduced parasitic drag.

The preceding figure showed the effects on lift and drag at a constant angle of attack. For an aircraft, however, it is of interest to know the thrust available by tilting the aircraft for acceleration and forward flight at a constant lift equal to the aircraft weight. For the configuration presented in Figure 6, this is shown in Figure 7 as the acceleration thrust available relative to the lift required to support the aircraft. The free air curve shows an acceleration thrust varying from 31 per cent to zero at 94 knots. The dotted line shows that the thrust is increased as the induced drag is decreased so that faster acceleration to flight speed will occur if the transition is made in ground effect.

In summary, judicious compromises of the propulsion system and the aerodynamic configuration appear to offer advantages in ground effect vehicles. However, the final evaluation of any vehicle will depend on how well it transports a payload a given distance in a given time.

Fig. 1 EJECTOR SCHEMATIC

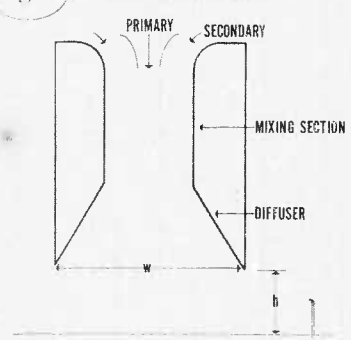

Figure 1.

Fig. 2 GROUND EFFECT ON A SINGLE EJECTOR

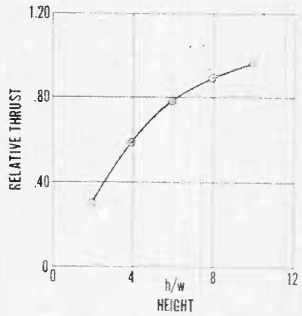

Figure 2.

Fig. 3 GROUND EFFECT ON PARALLEL EJECTORS

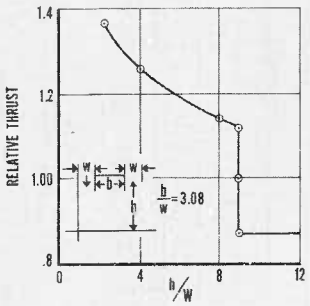

Figure 3.

Fig. 4 GROUND PLANE PRESSURE DISTRIBUTION

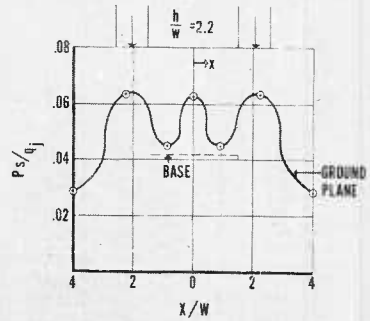

Figure 4.

Fig. 5 GROUND PLANE PRESSURE DISTRIBUTION

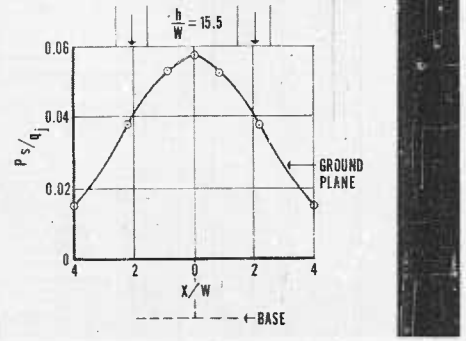

Figure 5.

Fig. 6 3-DIMENSIONAL GROUND EFFECT AUGMENTATION

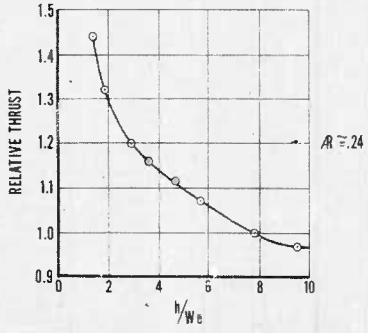

Figure 6.

Fig. 7 EFFECT OF FORWARD SPEED

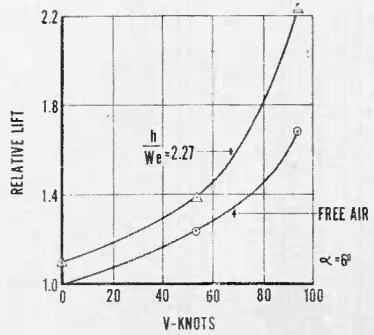

Figure 7.

Fig. 8 ACCELERATION THRUST

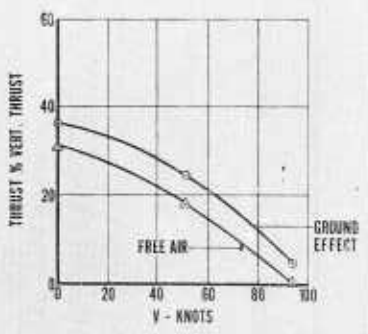

Figure 8.

THE ROLE OF THE GROUND EFFECT VEHICLE IN TRANSPORTATION

By Aeronutronic, A Division of Ford Motor Company,
Los Angeles, California

SUMMARY

The basic objective of this study is to provide a means for evaluating the role of the ground effect vehicle in transportation. There are two basic transportation regimes in which the ground effect vehicle may play a role. The first of these is in operation over all forms of unprepared terrain. The annular jet and plenum chamber typify the ground effect vehicle in this role.

Another basic category to consider is the use of ground effect vehicles over prepared surfaces, such as roads or rails. The Levapad or air-bearing concept exemplifies this approach. Time does not permit a thorough discussion of both of these applications and since the operation over all types of unprepared terrain appears to offer the greatest potential, particularly to the military, this paper will consider this aspect.

The basic power requirements of off-the-road ground effect vehicles are summarized and compared with the power-speed relationship of other modes of transportation. This provides the opportunity to assess the relative merits of the various systems in context with the power requirements. This approach, although useful, cannot provide the comprehensive foundation from which the future of these machines can be conclusively established; however, it does provide the first step in the evaluation of the role that the ground effect vehicle could conceivably play in transportation.

In summary, the data presented herein, although somewhat qualitative in nature, do provide the opportunity to examine the performance potential in its proper perspective. It is apparent that the ground effect vehicle can provide a flexibility of operation over all types of terrain to an extent unmatched by other forms of ground and water transportation. The power requirements to achieve this flexibility appear to be consistent with the potential.

In the final analysis, this flexibility of operation must be reviewed with respect to the economic and operational characteristics of these machines. The answer to this problem is extremely complex. Only after considering the initial costs, maintenance costs, crew costs, etc., can a position be established. In order to do this, detailed estimates of the structure, propulsion, and control aspects of the vehicle must be considered.

This work has been conducted under contract for the Transportation Research and Engineering Command (TRECOM) of the U. S. Army Transportation Corps, Fort Eustis, Virginia.

POWER REQUIREMENTS FOR GROUND EFFECT VEHICLES

Hovering power. In any discussion of the hovering power requirements for ground effect vehicles, there are two broad and distinctly different areas of application to be considered:

2. Ground effect vehicles that are capable of operating over rough and unimproved terrain. Examples of such terrain are water, sand, snow, natural fields with ditches, holes, rocks, and debris, and all the various types of natural terrain normally encountered in off-the-road transportation. Ground effect vehicles utilizing

the principle of the plenum chamber or the annular jet typify the class of ground effect vehicles which offer the potential of operating over such terrain.

2. A second broad area to be considered is the operation over improved terrain. This is typified by the use of prepared highways, rail systems, etc. The Levapad or air-bearing concept offers potential application to such operation.

It is impossible, due to the limited time available, to present a discourse of both these operations. Since the operation over unprepared surfaces appears, at this time, to represent the broadest area of application and the one of greatest potential for the military, this paper will be confined to a discussion of the annular jet and plenum chamber and how these vehicles compare to other means of transportation that currently exist.

In any quantitative discussion, it is necessary to first settle on a frame of reference. There are, in the case of ground effect vehicles, many logical definitions that can be utilized in defining a frame of reference. After examining the alternatives, it is our opinion that the frame of reference suggested by H. Chaplin, of the David Taylor Model Basin, appears to be the most useful. Chaplin, in reference 1, suggests the use of a reference aerodynamic lifting system operating out of the ground effect. By means of simple momentum considerations the lift and power required can be defined. Such a system is illustrated in Figure 1. The basic consideration is: given a planform area S and a lift requirement, what is the power required? By simple momentum considerations, the lift that can be generated is equal to the mass flow through the planform area S times the increase in velocity imparted to this mass flow. The power required is given by the rate of change of kinetic energy. This can be expressed as one-half the mass flow times the square of the velocity imparted to the air. Solving these two expressions for the velocity results in the expression for the power required. Since the power required is proportional to the cube of the velocity, the power for any given lift will be a minimum when the entire planform area S is utilized and the velocity imparted to the air is uniformly distributed throughout this planform area. Since the velocity increment that must be applied is directly related to the planform loading $\frac{W}{S}$, the fundamental necessity of maintaining low planform loading in order to minimize the power required is evident. This ideal lifting system is representative of what may be achieved by the use of a ducted fan (shrouded propeller) system.

The concept, then, is to define the power required for the annular jet and the plenum chamber in terms of this reference power, and to further show how the power required varies as a function of the height of the vehicle above the ground.

Annular jet. The basic theoretical considerations relative to the power required for the annular jet has been very adequately defined by the work of Chaplin in reference 1. The power required for annular jets of circular planform may be expressed as a function of the height to diameter ratio:

$$P_T = \left[\frac{\sqrt{1 + \frac{S_J}{S_b}} \left(\frac{1}{\sqrt{\frac{S_J}{S_b}}} + \sqrt{\frac{S_J}{S_b}} \, \frac{1 - \sin \Theta_o}{\frac{4h}{d}\sqrt{1 + \frac{S_J}{S_b}}} \right)}{\left(\cos \Theta_o + \frac{1 - \sin \Theta_o}{\frac{4h}{d}\sqrt{1 + \frac{S_J}{S_b}}} \right)^{3/2}} \right] \frac{W}{2\sqrt{\rho}} \sqrt{\frac{W}{S}}$$

$$P_T = G_T P_{i_\infty}$$

The pertinent variables are illustrated in Figure 2. In order to express G_T as a function of the external diameter d, rather than the base diameter d_b, the approximation $S = S_J + S_b$ is introduced.

As written, it is apparent that the required power is given by the function in the brackets, times the power required of the reference lifting system operating out of ground effect. We have defined the term in the brackets "G_T," which we refer to as the "theoretical hovering ground effect power factor." The basic concept behind the use of this ground effect power factor is that this is the term that illustrates the reduction in the power required, due to the presence of the ground.

Figure 3 illustrates the variation in the theoretical hovering ground effect power factor G_T, as a function of the height to the diameter ratio, $\frac{h}{d}$, for optimum annular jets. The terminology optimum means that at each $\frac{h}{d}$ the values of S_J and Θ_o are the values that minimize the power requirements. This optimization process is described in reference 1.

Plenum chamber. The basic concept of the plenum chamber is to design an inlet and actuator system in which the total head Δp supplied by the fan or actuator is supplied to the plenum chamber in the form of static pressure. In order to accomplish this, the inlet area must be large with respect to the outlet or leakage area around the periphery of the vehicle.

The effective exit area will be smaller than the area defined by the perimeter times the height, due to the fact that the air in the process of accelerating will produce the so called vena-contracta, thus reducing the exit area. The exit area may be expressed as

$$S_J = (\pi d\ h)\ C$$

where C is the discharge coefficient. The theoretical, two-dimensional value of C is 0.6. The pertinent geometry is illustrated in Figure 4.

The lift, or gross weight that may be supported with a circular planform is given by

$$W = \Delta p S = \Delta p \frac{\pi d^2}{4}$$

The velocity at the exit is given by

$$V_J = \sqrt{\frac{2\ \Delta p}{\rho}} = \sqrt{\frac{2}{\rho}\ \frac{W}{S}}$$

The theoretical power required is given by the volume flow times the pressure rise, or

$$P_T = \Delta p\ S_J\ V_J$$

By substituting for Δp, S_J and V_J, the power may be expressed as

$$P_T = 11.3\ C \frac{h}{d} \left[\frac{W}{2\sqrt{\rho}} \sqrt{\frac{W}{S}} \right]$$

Thus, in a manner similar to the annular jet, the power required for the plenum chamber may be expressed as a theoretical havering ground effect power factor, G_T, times the power required of the reference lifting system. The variation of G_T with $\frac{h}{d}$ is shown in in Figure 3.

As noted in Figure 3, the plenum chamber is shown for various values of the discharge coefficient C. Although two-dimensional theory indicates that C = 0.6, it may be possible to reduce this coefficient. The introduction of some type of aerodynamic spoiler arrangement may efficiently reduce the effective exit area considerably. To the best of our knowledge, the plenum chamber concept has not received, to date, the same attention as the annular jet; and, therefore, it is too early to conclude that the annular jet inherently enjoys a performance advantage over the plenum chamber.

Inherent in this theory is the assumption that the flow velocity in the plenum chamber is low. This will only be true for low values of $\frac{h}{d}$. This theory is not applicable for $\frac{h}{d}$ greater than approximately .2.

In summary, the theoretical hovering power requirements may be summarized as

$$P_T = G_T \left[\frac{W}{2\sqrt{\rho}} \sqrt{\frac{W}{S}} \right]$$

To be noted in Figure 3, the region of primary interest for ground effect vehicles is the low $\frac{h}{d}$ region of from near 0 to say .2, for it is here that the large reduction in power required may be achieved. In this region, G_T varies approximately linearly with $\frac{h}{d}$. The line represented by the optimum annular jet (which corresponds to a plenum chamber with a discharge coefficient equal to .38), will be used to present some generalizer performance information. With this approximation, the theoretical hovering power is given by

$$P_T = 4.3 \frac{h}{d} \frac{W}{2\sqrt{\rho}} \sqrt{\frac{W}{S}}$$

The above theoretical hovering power requirement is only part of the story, in that in the design of any system such as this in which an inlet, fan, or actuator system and ducting are necessary parts, the relative efficiency of these components must be given very careful consideration. In order to illustrate this, the definition of the installed shaft power (G_S) is presented in Figure 5 as a function of the previously described theoretical power requirements.

Let us consider two typical ground effect systems that have equal theoretical power requirements. The first consideration is: does the theoretical power required truly represent the air conditions necessary at the exit of the vehicle? The limited test data available, to date, indicate that these simple momentum theories are really very good and such factors as viscous effects represents only minor additional power requirements. A typical result is that these simple momentum theories will predict the power required within 10 to 20 per cent. For illustration we have added an additional 10 per cent over and above the theoretical power requirements.

The next factor to be considered is the losses involved in ducting the air from the actuator down to the exit conditions. This is a serious problem, and, unless careful consideration is given, the overall ducting efficiency may be so poor that the vehicle may not be feasible. Figure 5 is schematic in nature in that it simply illustrates what these losses become and that the losses will be of the order of 10 per cent even when extreme care is exercised.

Another serious consideration is the conversion of shaft power into aerodynamic power at the actuator or fan. Consider, for example, the common propeller or rotor system. Even with careful attention to the design details, it is difficult to achieve an efficiency like 86 per cent.

In summary then, Figure 5 illustrates the wide variation between the power required as predicted by simple momentum theory and the necessary installed shaft power. In order to present some pertinent design information in subsequent sections, we have utilized a factor of 70 per cent between theory and installed shaft power. It is believed that this is an efficiency factor that can be achieved in a well-designed system.

Utilizing the approximation for G_T as a function of $\frac{h}{d}$ and incorporating the 70 per cent efficiency factor just described, the following expression for the horsepower required per foot of altitude can be derived for circular planforms.

$$P_S = \frac{4.3}{.7} \frac{h}{d} \left[\frac{W}{2\sqrt{\rho}} \sqrt{\frac{W}{S}} \right]$$

$$\frac{HP}{Foot} = \frac{.13\,(W)^{3/2}}{\sqrt{\sigma}\ d^2}, \text{ where } \sigma = \frac{\rho}{\rho_o}, \text{ air density ratio.}$$

These data are summarized in the design chart presented in Figure 6. This chart illustrates the horsepower required to hover for each foot of altitude, as a function of the diameter of the circular planform, and the gross weight of the vehicle. To assist in interpretation of these results, lines of constant planform loading are superimposed. This chart graphically illustrates the large reductions in the horsepower required as the size of the vehicle increases.

Although this chart is quite useful in quickly estimating the hovering power requirements, it is misleading in that the advantages of low planform loading are being confused with the fundamental reduction in power required with increases in the size. To illustrate, Figure 7 is presented to show this fundamental beneficial effect of size. As illustrated, the hp per ft per ton of gross weight is presented as a function of the planform area, for constant values of planform loading. The large reductions in power required as the size increases are evident. The reason is quite apparent from a consideration of the simple momentum theory. The lift that is generated depends on the area which increases with the square of the diameter. The perimeter, which determines the power required, varies directly with the diameter. For example, if the diameter is doubled, the area and therefore the lift increases by a factor of 4, whereas the perimeter and therefore the power required increases by only a factor of 2. As a result, the horsepower per unit lift is reduced by a factor of 2. This basic and simple relationship is what is illustrated in Figure 7. To be noted is the inherent increase in efficiency in ground effect vehicles as the size increases (assuming that the altitude remains constant).

To date we have been limited to a discussion of circular planforms. There are many practical problems associated with the circular planform that necessitate serious consideration of other geometric planforms. Again, if we go back to the simple theory and recognize that the fundamental factor to be considered is the ratio of planform area to perimeter, then it is fairly easy to generalize the ground effect power factor for all kinds of planforms. Figure 8 illustrates how G_S, the shaft hovering ground effect power factor, will vary with a parameter analogous to $\frac{h}{d}$. By simply replacing d with S, the planform area divided by $\frac{\ell}{4}$, the planform perimeter, the first order approximation of the effect of planform is considered. G_S can then be expressed as

$$G_S = 1.55 \frac{h}{S/\ell}$$

Figure 9 illustrates the shaft horsepower required per ft of altitude and is shown as a function of the planform loading and the perimeter. This curve, although general in nature and useful for rapid design estimations, is difficult to use to point out the effects of planform.

To illustrate the effects of the variation of planform consider Figure 10. These data show the power required relative to that for a circular planform with constant area, weight, and height. Elliptical, rectangular, and triangular planforms are illustrated.

An interesting and practical consideration that is worthy of mention is the effect of a width limitation. This is a fundamental limitation which is encountered in the use of ground effect vehicles operating on the highway with other forms of transportation where the width is limited to eight ft. Figure 11 shows the horsepower required as a function of the length-to-width ratio of the vehicle for the three geometric planforms previously considered. These results are for constant width, gross weight, and altitude. As noted, the beneficial effects of increasing the planform area S far outweigh the detrimental effects of the higher fineness ratio planforms.

Before leaving this discussion of hovering power requirements, it is worthwhile to note that the reduction in power afforded by operation within the ground effect is really nothing new. For example, the helicopter industry has been well aware of this phenomenon for a number of years and utilizes it for operation in the overloaded condition. To illustrate the comparable reductions in power required when operating within the ground effect with helicopters, Figure 12 is presented. As shown, the general trend is very similar to that of ground effect vehicles. In fact, when it is realized that with both types of machines the principle of operation is fundamentally the same, that is to say, both utilize the same basic aerodynamic concept of accelerating a mass of air in the vertical direction, it would be surprising if the ground effect were materially different.

Since helicopters are designed primarily to operate outside the ground environment, the design considerations are different, and as a consequence the vehicles do not look as if they belonged to the family of ground effect vehicles. However, if one were to start with the helicopter and design it to work exclusively within the ground effect, the design conditions would lead to a configuration markedly different from the current family of helicopters; in fact it would undoubtedly bear a striking resemblance to what we presently conceive ground effect vehicles to be.

Power required for hill climbing. The power requirements previously considered deal only with those necessary to sustain the vehicle above the ground. There are fundamentally two other requirements which must be considered in defining the power requirements for ground effect vehicles. One of these is the power required to maintain the vehicle on a slope and to further propel the vehicle up a hill at a given velocity. The maintenance of the vehicle in the hovering condition on a slope is quite easily handled by considering the geometry of the situation and by considering the average height of the vehicle as the input to the hovering power requirements. The power required to drive the vehicle up a slope can be determined quite easily by considering simply the weight, angle of incline, and the velocity. Figure 13 is presented to illustrate these power requirements.

Power required in forward motion. In the previous considerations of the power required in hovering, there is available a firm theoretical basis for the estimations. In addition, there are available some experimental data which prove the validity of the theory.

However, in considering the power required to overcome the drag of the vehicle in forward motion, the problem is not only considerably more complex but there is very little directly applicable experimental data available as of this writing. In spite of this, it is believed that the drag estimates presented herein are representative of what can be achieved by a thorough understanding of the physical principles involved, and by careful attention paid to the design parameters which influence the drag of the vehicle. The basis for this position is the wealth of data, both theoretical and experimental, defining the drag characteristics of both aircraft and automobiles.

Ground effect vehicles are analogous to modern jet aircraft in that a determination of the thrust and drag of the vehicle involves consideration of the air that is ingested by the vehicle and the air that flows around the external surface of the vehicle. Further, the analogy may be extended to include the system of "keeping the books." In normal aircraft practice, the air taken on board the vehicle is considered in the analysis of the propulsion system. The analysis considers the change in the momentum of the air as it flows through the system, and reflects in the determination of the net thrust of the propulsion system; whereas in the determination of the drag of the aircraft, the air that flows over the external surface of the vehicle is considered.

In any consideration of the thrust and drag characteristics of ground effect vehicles, one is immediately faced with the problem of what is considered thrust and what is considered drag. In the case of ground effect vehicles, the problem is more difficult than usual because the air, which in forward motion has a momentum parallel to the path of motion, is brought on board the vehicle and is then exhausted out the bottom of the vehicle in a vertical or nearly vertical direction. Whether this change in the horizontal momentum of this air should be charged to the drag or should be charged as part of the lifting system of the vehicle is a moot point. In the final analysis, the end result should be the same if the books are kept properly; however, there are advantages and disadvantages to the different schemes and it is extremely difficult to prove that one system is better than another. It very often depends on the past experience and personal preference of the individual analyst.

However, in order to define the drag of the vehicle, a system must be chosen and adhered to in the course of the analysis. The horizontal momentum of the air brought on board the vehicle, due to its motion with respect to the vehicle, is often considered as momentum drag. In defining the drag of ground effect vehicles, we have chosen a system that does not consider this as drag but as a component of power required in connection with the lifting system. The reason for this is really quite fundamental. The kinetic energy of this air can be converted into potential energy in the form of an increase in static pressure if it is handled properly. Assuming that the conversion takes place in an efficient manner, this increase in static pressure can relieve the actuator or fan of its duty to compress the air. To illustrate, at a forward speed such that the dynamic pressure is equal to the pressure required beneath the vehicle, and if this dynamic pressure is converted at 100 per cent efficiency into static pressure, the fan or actuator normally used for this purpose can be eliminated. This is the principle of the so-called "q-sled" which some people refer to. The point is that there can be a trade-off between the power required to drive the fan of the lift system and the power necessary to maintain this conversion of kinetic energy to pressure energy.

Throughout this analysis, the power required to maintain this conversion of kinetic energy that the on-board air possesses into pressure energy is charged to the lift system and therefore should not be considered in the definition of the drag. It is recognized that

this can be confusing. However, when it is remembered that this air is brought on board in order to provide lift, it is logical that any power required to sustain the process should be considered as lift power and not drag power requirements.

The limited amount of test data available indicates that the air power at the exit of the vehicle necessary to maintain the lift is independent of the forward velocity (reference 2). This is in marked contrast to the variation of the induced horsepower for a helicopter operating out of ground effect. However, the helicopter data that has been reviewed to date indicates that if the helicopter is operating close to the ground, its induced horsepower required also appears to be independent of forward speed, or nearly so. Therefore, in estimating the power requirements in forward motion, it has been assumed that the power required for the maintenance of lift is the same as that developed in the hovering power discussions presented previously.

It should be noted that, although the power required to maintain the lift is constant, the manner in which this power is expended depends on the speed. As the speed is increased, the power input to the fan will reduce by an amount that must be used to produce a horizontal thrust. This horizontal thrust must be applied to cancel out the loss in horizontal momentum possessed by the air brought on board the vehicle, or the system will not be in equilibrium.

In order to proceed, an assumption as to the efficiency of this conversion must be made. For simplicity, it has been assumed that the conversion can be accomplished with 100 per cent efficiency. Admittedly this is optimistic, but it is well established that this conversion can be made with an efficiency of 90 per cent or better at the design point.

Now consider the so-called profile drag of such vehicles. We know that if the vehicle is made extremely streamlined (that is to say, of high fineness ratio) the profile drag coefficient can be reduced to the point where it is composed primarily of the skin friction drag which is of the order of .005, based on the planform area S. However, it must be realized that in order to achieve such a low drag the planform shape will be very poor from the lifting aspects and the power requirements for lift will be extremely high.

At the other end of the spectrum we can minimize the power required for lift by utilizing a circular planform and, as a consequence, the profile drag will be high. This profile drag will be composed primarily of pressure drag rather than friction drag and can get extremely high depending upon both the frontal area and the base area of the vehicle.

Undoubtedly the proper balance between these two extremes can be achieved, although it depends on a great many factors. For example, to arrive at a good compromise, one must consider the structural aspects (which play such an important role in determining the empty weight), practical considerations such as how the vehicle will be loaded and unloaded, and many, many more complex considerations. In the final analysis, in order to achieve the proper external dimensions of the vehicle, it is a difficult job, depending to a great extent on the intended use of the vehicle.

However, in order to provide some "ball park" estimates of the power required to overcome the drag, we have attempted to estimate what we believe can be obtained if sufficient emphasis is placed on reducing the drag of such vehicles. Figure 14 illustrates the results of this preliminary analysis. The horsepower per ton of vehicle is shown as a function of the vehicle's forward velocity. A spread in drag coefficient from .05 to .1, based on the planform area, is considered to represent a typical range. In order to provide these data in the form of power requirements, a propulsive efficiency of 70 per cent was assumed.

In summary, data are presented which give the design data necessary to estimate the power required to sustain lift both in hover and forward flight, the power required to maintain the vehicle on slopes, and the power required to maintain the vehicle in a stabilized condition in forward motion. Admittedly, some of the data are based strictly on estimates, in particular, the power required to overcome the drag. However, it is believed that these data are of the right order of magnitude, and are of sufficient accuracy to proceed with a comparison of the power requirements for ground effect vehicles as compared to other modes of transportation.

SUMMARY OF POWER REQUIREMENTS

The overall objective of this brief study is to define the power requirements for ground effect vehicles in order to compare these requirements with those of more conventional means of transportation.

This summary is presented in Figure 15. In this chart the horsepower required per ton of gross weight is shown as a function of velocity. The data for the ground effect vehicles were established from the design charts presented herein. The data for the other modes of transportation were taken from reference 3.

Undoubtedly, a much more meaningful plot would show the horsepower required per ton of useful load. However, this would be an extremely complicated plot and very difficult to formulate. It is believed that comparing the horsepower required per ton of gross weight does provide a meaningful foundation from which a preliminary evaluation of the role of the ground effect vehicle in transportation may be established.

Consider the position of the ground effect vehicle in this power-speed spectrum. As stated earlier, this study would be confined to considerations of vehicles capable of off-the-road operation. Therefore, this must be interpreted in terms of a representative altitude range. For purposes of illustration, it was considered that altitudes in the range of one foot to ten feet would provide a significant and realistic off-the-road capability.

The upper boundary illustrated in Figure 15 is typical of small vehicles (approximately 5 tons) operating 3 ft off the ground. By way of contrast, this is also representative of 50-ton vehicles operating at 9 ft. The lower boundary represents a 50-ton vehicle operating one foot off the ground. It must be emphasized that we do not claim that all ground effect vehicles will fall within the bounds illustrated. On the contrary, it would be very easy to conceive conditions that would lead to power requirements both greater than and less than those illustrated. We are simply attempting to illustrate a representative set of power conditions in order to compare these vehicles with other means of transportation.

Consider first the comparison of the ground effect vehicles with automobiles and trucks. At first glance the ground effect vehicle does not appear to fare too well. However, if the automobile or truck is to achieve this kind of performance, a paved highway in good condition will be required. In addition, in practice the practical range of speed conditions is limited to 60 to 70 miles per hour. It is important to realize that this initial impression involves the comparison of an off-the-road ground effect vehicle with an on-the-road wheeled vehicle.

Further, the wheeled vehicles are soon restricted to the 30 to 40 miles per hour speed range with only minor degradations in the pavement. In fact, the wheeled vehicle very rapidly runs into serious problems with further degradations in the road. Once it is required to surmount even relatively small obstacles, the speed capability rapidly diminishes to very low values of the order of a few miles per hour.

When the broad spectrum of terrain features that are encountered in off-the-road travel is considered, the wheeled vehicle is soon abandoned in favor of tracked vehicles.

There is no question that the tracked vehicle offers a significant increase in off-the-road capability. However, in the totality of terrain considerations, the tracked vehicle soon reaches a point of zero or near zero mobility.

In view of the tremendous flexibility of operation afforded by the ground effect vehicle over nearly all types of off-the-road terrain, the power requirements appear to be consistent with the performance advantages. This statement presumes a need for such an off-the-road mobility. There appears to be no question about the military value of such a capability. In fact, there are many commercial applications which could capitalize on such utility.

Before we leave this discussion of flexibility of operation, consider the train with its convoy of cars with the automobile and trucks. The train certainly offers considerable reductions in the power required. In spite of this the automobile and truck enjoy a prominent place in the transportation picture. Undoubtedly; the rail system with its attendant inflexibility of operation, in terms of terminal points relative to the road system, is at a serious disadvantage.

One obvious solution to this off-the-road terrain problem is to cast off all the terrain restraints completely and to fly. However, in so doing we solve one problem at the expense of introducing many more. The airplane requires the use of landing fields, which under many circumstances is an acceptable solution. As noted, the aircraft enjoys a preeminent position in the realm of high speed transportation and, in fact, this part of the transportation picture is dominated by this machine. However, there is a tremendous portion of the transportation market that cannot accept this restriction. We all own automobiles instead of airplanes because we can't afford to maintain an airfield in our backyard.

When helicopters were first introduced, it was thought: now here is the answer to all of our transportation problems. We have the flexibility of landing and taking off pretty much at will; we have reasonably good speed characteristics; and with the tremendous reduction in the relative cost of horsepower within the last fifty years it is apparent that the high power requirements, although a disadvantage, could be considered acceptable. In the low speed spectrum of travel the helicopter enjoys a position because of its unique capabilities. The very fact that it can take off, hover, and land in a vertical attitude is sometimes a priceless commodity.

In spite of this bright picture these machines have not been universally acceptable on the scale that was originally envisioned. This is not the time and place to present a full discourse on the reasons why. There are many factors to be considered. It is believed sufficient for the purpose of this study to state that such factors as the high skill requirements of the operator, the relatively high cost of maintenance due to the mechanical complexity are but a few of the considerations. Before leaving the helicopter, it is worthwhile to remember that in order to achieve one of its most attractive features, namely, vertical take-off landings, installation of the power required at zero speed is a necessity. The large reductions in power required in the speed range of 40 to 80 miles per hour can be useful in reducing the low speed cruise fuel consumption, or perhaps using the vehicle in an STOL configuration.

Now the question is: where do the ground effect vehicles fit into things? It is believed that the potential of these vehicles for overland operation is best illustrated when it is recognized that they possess inherently a flexibility of operation much more akin to that of the helicopter, although admittently not as good, but vastly superior to that of the wheel or tracked vehicles in off-the-road type operation. As far as the power required is concerned it seems to be quite compatible with this tremendous flexibility of operation.

Therefore, it is believed that the acceptance of this mode of transportation will, in the final analysis, depend on other aspects of the problem.

One of the fundamental considerations that immediately arises is that of control. If these vehicles are to move at high speeds close to the ground, a safe and powerful control system which can demonstrate characteristics along the lines we presently consider necessary for automobiles and trucks will be necessary. This is a serious and fundamental consideration and appears to be quite a formidable one. For example, consider foa a moment the ability of our present day automobile to come to a stop. This is a characteristic we all, far too often, take for granted, but in retrospect we must realize that the automotive engineer has worked long and hard to produce the remarkably efficient and reliable system that he has put at our disposal. Figure 16 illustrates the stopping distance as a function of forward velocity typical of our modern automobile.

On first glance it would appear that this ground effect vehicle sliding along the surface of the ground on its cushion of air will never be able to approach this degree of effectiveness; however, let us consider one aspect of this situation. If a horizontal propeller is used to provide the thrust necessary to maintain the vehicle in forward motion, this device can be used to provide a brake by simply reversing the propeller pitch. This technique is employed in modern propeller-driven aircraft. Figure 16 illustrates very approximately the resulting braking distance if this technique is employed.

Although it can be argued that this does not provide a braking capability nearly as good as the automobile, nevertheless it does represent a considerable braking action. By further exercising our ingenuity and perhaps incorporating such devices as aerodynamic speed brakes or other techniques, it should be possible to provide a satisfactory braking system. In conclusion, it would appear that if we can provide a vehicle that is competitive costwise, reliable, safe, and easy to maintain and operate there are undoubtedly many areas of applications both in the commercial and military field which offer tremendous potentialities.

Before concluding we should consider the potential of these vehicles in the role of an over-water device. As illustrated in Figure 15, the ship represents a very efficient means of transportation in the water at low speeds. The power requirements for speeds over approximately 30 to 40 miles per hour get completely out of hand. The existing alternative of either the helicopter and/or the airplane again is available.

Since the ground effect vehicle can operate with the same facility over the water as it can over the land, it again may also play a role. In fact, it can be argued that it is in this over-water application that the ground effect vehicle offers its greatest potential. There is no question that for the large machines which we have noted as being inherently efficient, the ocean does not present the same restrictions as to size as does the land. On sober reflection, the idea of extremely large vehicles designed to carry a large number of passengers or a great tonnage of cargo across the ocean at relatively high speeds, is not as far fetched as it appears at first thought. Suffice it to say, as long as speed is a consideration (and it always has been in the past) the ground effect vehicle may very well carve out a significant niche in the over-water transportation field. Again, such factors as cost, reliability, safety, etc., will play a tremendous role in the determination of the acceptance of this means of travel.

REFERENCES

1. Chaplin, H. and Stephenson, B., "Preliminary Study of the Hovering Performance of Annular Jet Vehicles in Proximity to the Ground." David Taylor Model Basin Aero Rept. 947, August 1958.

2. Carter, A. W., and Kuhn, R. Unpublished data. NASA, Langley, September 1959.

3. Gabrielli, G., and von Karman, Th., "What Price Speed?" Mechanical Engineering, Vol. 72, No. 10, October 1950.

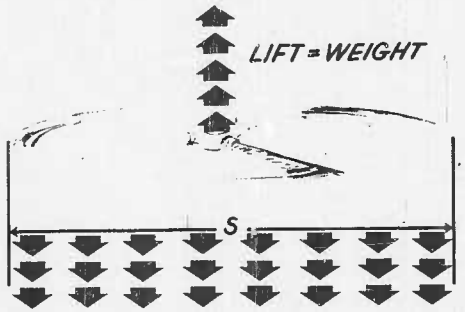

LIFT = MASS FLOW (VELOCITY INCREMENT) = $(\rho SV)V$ = WEIGHT

POWER = RATE OF KINETIC ENERGY = $\frac{1}{2}(\rho SV)V^2$

IDEAL HOVERING POWER (OUT OF GROUND EFFECT) = $P_i = \frac{W}{2\sqrt{\rho}}\sqrt{\frac{W}{S}}$

Figure 1. Reference hovering power out of ground effect

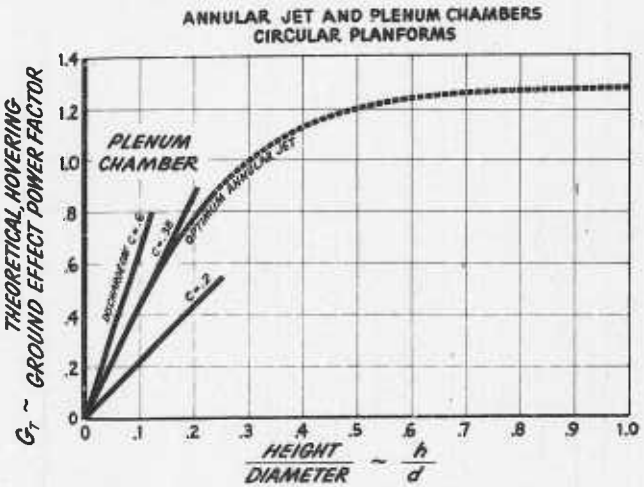

Figure 3. Theoretical hovering ground effect power factor

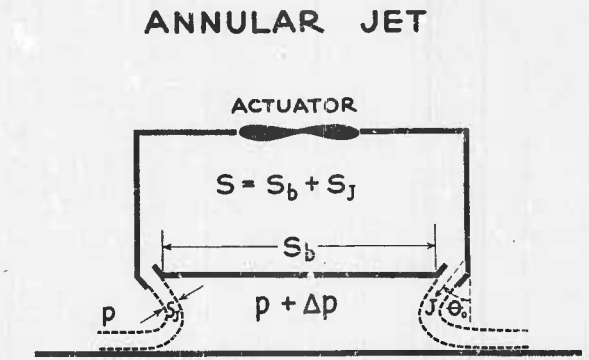

THEORETICAL HOVERING POWER REQUIRED = $G_T\left[\frac{W}{2\sqrt{\rho}}\sqrt{\frac{W}{S}}\right]$

G_T DEPENDS UPON: HEIGHT - h
PLANFORM AREA - S
PERIMETER - ℓ
JET AREA - S_J
JET ANGLE - θ_J
JET MOMENTUM - J

Figure 2. Principles of hovering

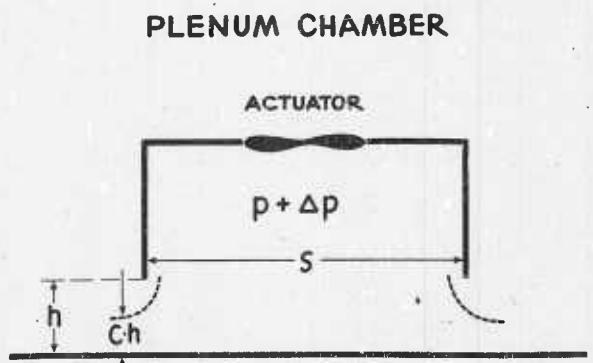

THEORETICAL HOVERING POWER REQUIRED = $G_T\left[\frac{W}{2\sqrt{\rho}}\sqrt{\frac{W}{S}}\right]$

G_T DEPENDS UPON: HEIGHT - h
PLANFORM AREA - S
PERIMETER - ℓ
DISCHARGE COEFFICIENT - C

Figure 4. Principles of hovering

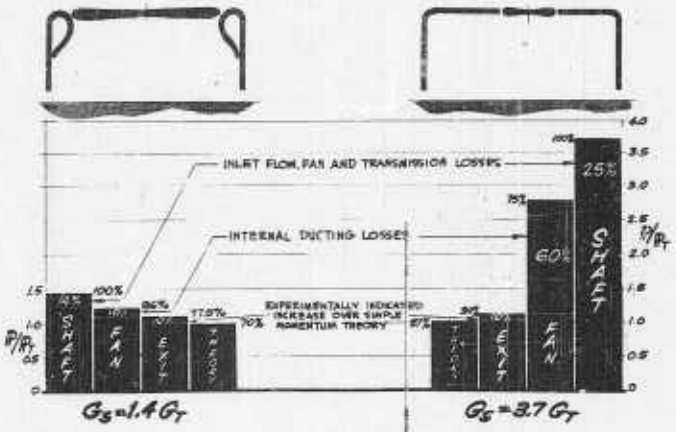

Figure 5. Shaft power requirements

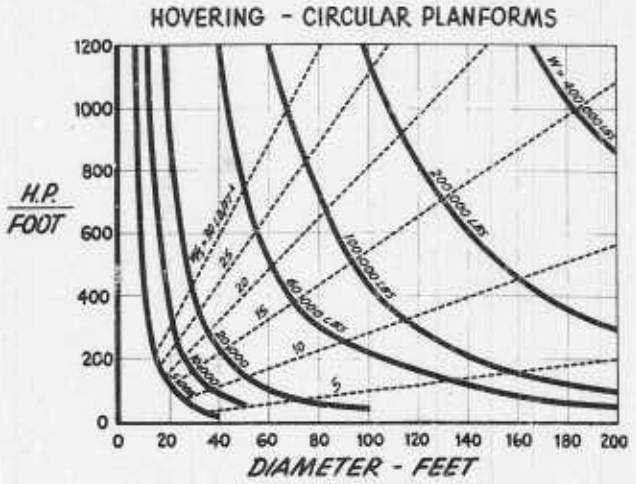

Figure 6. Shaft horsepower required

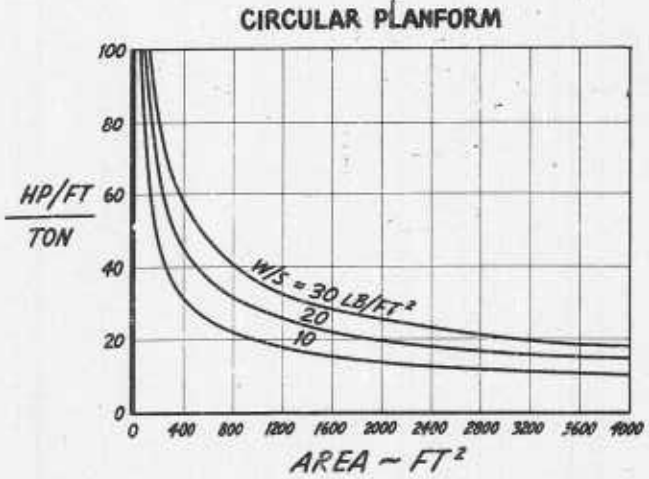

Figure 7. Effect of size

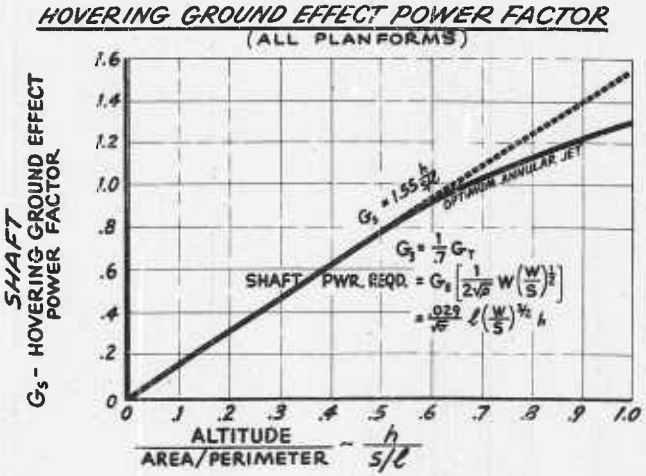

Figure 8. Shaft

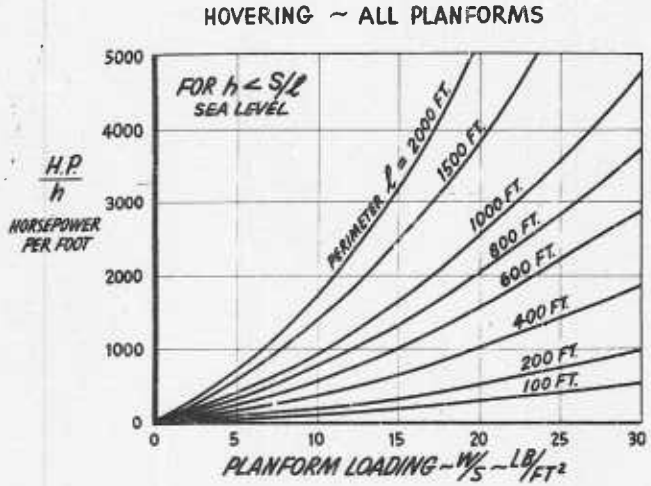

Figure 9. Shaft horsepower required

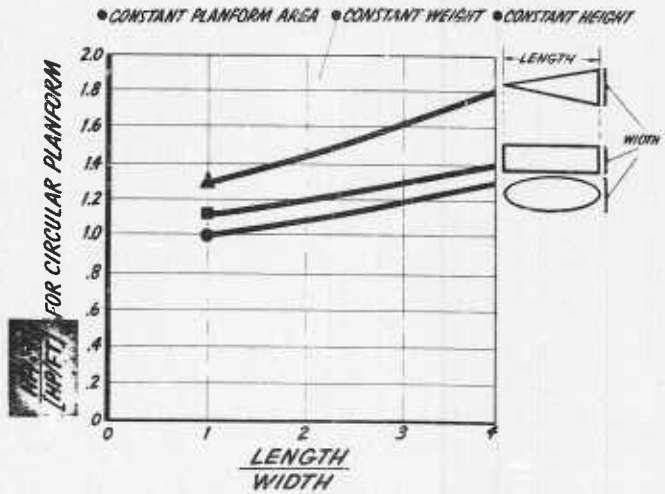

Figure 10. Effect of non-circular planform

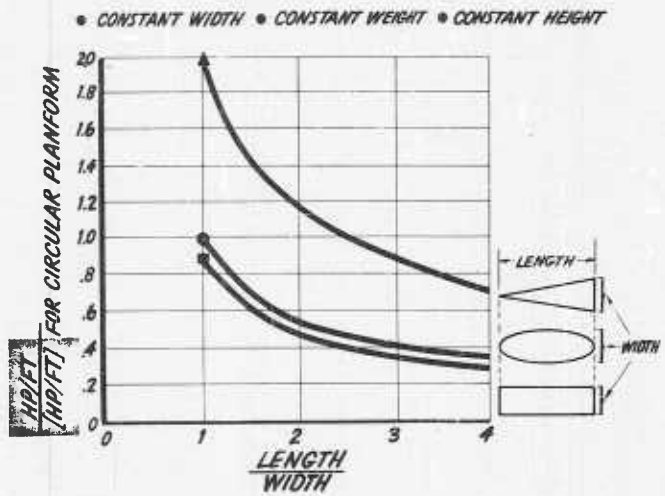

Figure 11. Effect of width limitation

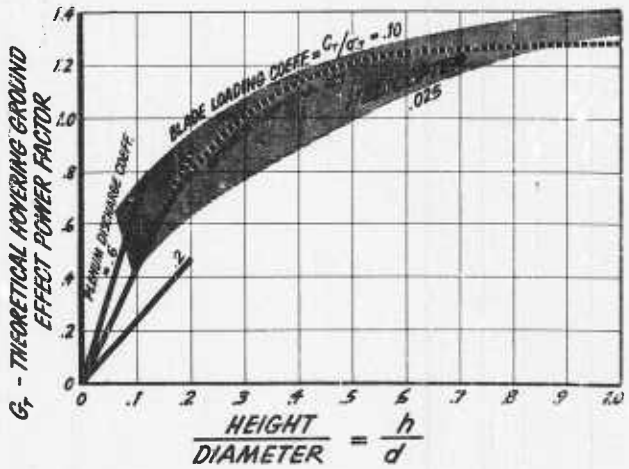

Figure 12. Ground effect on helicopter hovering power

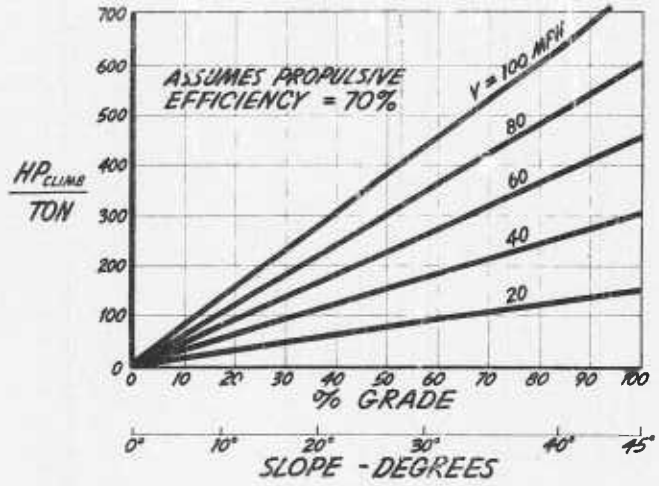

Figure 13. Power required for hill climbing

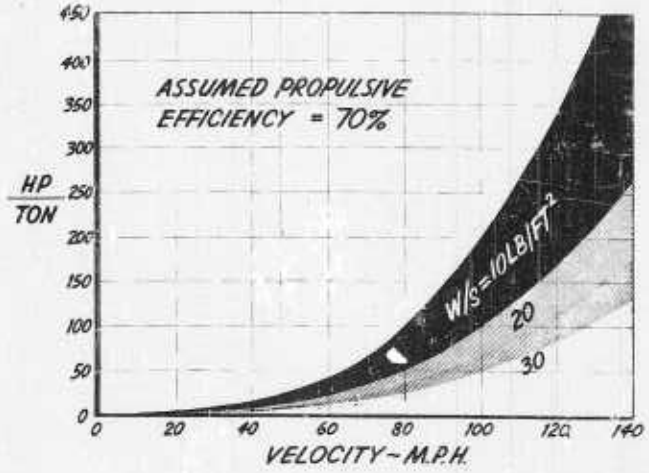

Figure 14. Power required to overcome drag

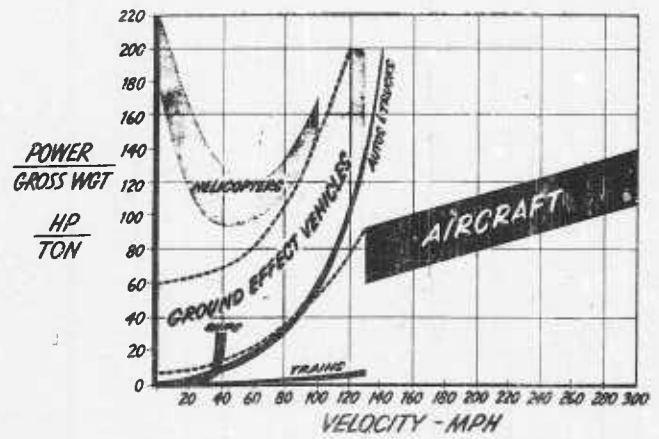

Figure 15. Power requirements

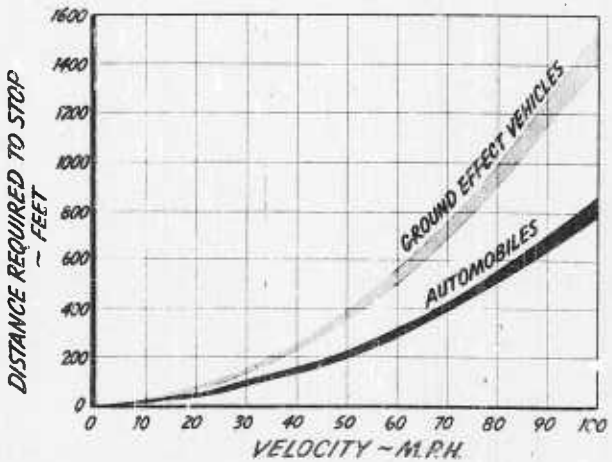

Figure 16. Stopping distance

PERFORMANCE TESTING OF A FIVE-FOOT AIR CUSHION MODEL

By K. G. Wernicke, Bell Helicopter Corporation, Fort Worth, Texas

SUMMARY

Hovering tests of a five-ft circular air cushion model have been conducted for a range of h/D's from .012 to 1.2. Configurations tested include the plenum chamber with various types of internal flow and vertical annular jets with three jet thicknesses. The overall efficiency (ratio of ideal air horsepower to brake horsepower) was found to be in the vicinity of 50 per cent for most of the configurations tested. The critical height, the height where augmentation due to ground effect is suddenly lost, occurred at an h/D = .5 for the annular jets.

INTRODUCTION

Numerous theoretical analyses have been made of the various air cushion phenomena. For certain ranges of h/D they have been found to be inadequate. In the case of the annular jet at heights less than the jet thickness, most of the theoretical analyses are obviously incorrect. Equations derived for the plenum chamber which assume static conditions inside the plenum will be inaccurate at the h/D's above .1.

This model program was originated to resolve the above problems and to answer such questions as: Can efficient diffusion be obtained inside the plenum chamber when in ground effect and also when out of ground effect? Why wasn't a vena-contracta present at the discharge of previous plenum chamber models? It was felt that the test results would be useful in vehicle design since the fan losses and internal losses would be included in the data.

SYMBOLS

A	total area, $\frac{\pi}{4}D^2$, ft^2
A_b	base plate area, ft^2
A_j	jet area, $tC_{j\ av}$, ft^2
$C_{j\ av}$	average circumference of the jet, ft
D	skirt diameter, ft
h	height of edge of skirt above ground, ft
hp	horsepower
K_r	contraction ratio of discharge of plenum chamber, i.e., ratio of thickness of discharge to height
p	ideal power, ft lbs/sec
T	total thrust or lift, lbs

t	jet thickness, ft
η	overall efficiency, ratio of ideal hp to brake hp
ρ	air density, slug/ft^3
σ	air density ratio, ratio of actual density to standard density

The 2:1 diffuser section is removable. Three skirts of different diameters can be used with the base plate to provide annular jets of 1.02-, 2.10-, and 4.00-inch thickness. These jets provide jet area to fan area ratios of 1/2:1, 1:1, and 2:1. An internal cone is used to provide a duct of approximately constant area ratio for the 2.10-inch annular jet. The model is supported by a beam balance arrangements, as shown in Figure 2.

Thrust is recorded to the nearest ounce. Propeller speed is read and held at 3000 ± 10 rpm by an electronic counter. A microammeter is used to read torque from a strain-gauged element that restrains rotation of the electric motor frame within the nacelle. The system is calibrated so that the horsepower can be read directly from the microammeter, The power measurement is accurate to within .02 bhp. Height was recorded to the nearest 1/8 inch. Each configuration was tested at four propeller pitch settings.

The model was suspended in such a fashion that it was free to roll and pitch about its center of gravity. After numerous static and dynamic instabilities were encountered, this freedom was locked out for the remainder of the performance testing.

DISCUSSION OF PLENUM CHAMBER TEST RESULTS

Four different plenum chamber configurations were tested. The internal flow differed in each configuration. The air flow followed the wall of the cone from the fan down to the skirt with the diffuser section in, and also with it removed. This type of flow is shown in Figures 3 and 4. Spoiler skirts were attached to the inside of the cone to force the flow to leave the wall. With a spoiler skirt attached to the propeller shroud, a jet of air was produced inside the plenum chamber.

Flow attached to wall. Performance with the diffuser section in and out is compared in Figure 5. The curves in this figure and the following figures are envelope curves of the test points. The lower pitch settings were more efficient at low h/D's while the higher pitch settings were more efficient at high h/D's.

The diffuser section showed an unexpected performance advantage at low heights. The diffuser section improved the efficiency by [illegible] per cent below h/D = .04. At h/D = .25, the diffuser-out configuration was better by 10 per cent. The reason for the flow attaching to the wall with the diffuser section out may have been due to the uneven velocity distribution across the fan. The untwisted propeller produces a high velocity at the shroud and a progressively lower velocity toward the center.

Theoretical lines assuming 40 to 60 per cent efficiency are shown in Figure 5. The following equation is derived assuming stagnant air inside the plenum chamber:

$$T = .315 \left(\frac{D}{h} \right)^{2/3} \left(\frac{1}{K_r} \right)^{2/3} \left(\rho A\, p^2 \right)^{1/3}$$

This equation appears as a straight line on the log-log scale in Figure 5. It is seen that the test data correlate with this equation below h/D = .10 when K_r = .62 is used.

A second equation is obtained by including the momentum thrust due to the vertical velocity across the base of the plenum chamber. This equation breaks down when the discharge area exceeds the base area, which occurs at $h/D = .25/K_r$:

$$T = .315 \left(\frac{D}{h} \right)^{2/3} \left(\frac{1}{K_r} \right)^{2/3} \left[1 + \left(\frac{4h}{D} \right)^2 K_r^2 \right] \left(\rho A p^2 \right)^{1/3}$$

It is seen in Figure 5 that, with the diffuser in, the test results follow this equation up to an $h/D = .25$ when an efficiency of $\eta = .50$ is used. With the diffuser out, the efficiency rises from 45 to 60 per cent at $h/D = .25$.

Static stability. The formal static stability tests with this model have not begun yet. However, free hover flights of the model indicated static attitude instability in pitch and roll above a height of two inches. With the flow attached to the wall, a hover height of 5-1/2 inches ($h/D = .09$) was possible. The reason for the static instability can be explained as follows: since the air follows the wall, the flow at the skirt is vertical. This vertical velocity produces momentum thrust at the periphery. When the model is tilted, the vertical velocity decreases at the side closest to the ground. This decrease in momentum thrust is more effective than the increase in static pressure, so that the net result is an unstable rolling moment.

Static stability could be obtained by placing a spoiler skirt on the inside above the main skirt. (See Figure 6.) This spoiler forces the flow to leave the wall of the cone. A pocket of stagnant air is trapped between the skirt and spoiler; the variation of static pressure inside this pocket is stabilizing. Performance is decreased by the spoiler. The static stability could be increased by moving the spoiler skirt in or it could be decreased by moving it out toward the main skirt. At 5-3/4 inches above the main skirt, the stability was considered satisfactory up to the maximum free hover height of four inches ($h/D = .067$).

Jet flow. Jet flow was obtained by attaching a spoiler skirt to the propeller shroud. The performance of this configuration is compared in Figure 7 with the standard configuration and with the spoiler skirt 5-3/4 inches above the main skirt. It is seen that this configuration has the poorest performance and dips very low at $h/D = .07$. However, this configuration exhibited the strongest stability in free hover tests. There is no contraction at the discharge which accounts for the poorer performance at low h/D's. The test data correlate with the theoretical curve ($K_r = 1.0$) up to an h/D where the discharge area equals the fan area.

When an area ratio of 1:1 is exceeded, the discharge is not thick enough to maintain a seal and the plenum chamber is vented to the atmosphere. Figure 8 shows the flow pattern. It is believed that the dip in the curve is a result of the recirculating air. When the plenum chamber is vented to the atmosphere, the total pressure of the recirculating air will approach atmospheric. Due to the high velocity of the recirculating air, the static pressure on the walls of the plenum chamber falls below atmospheric and produces negative lift. As height is increased further, the strength of the recirculating air decreases, until finally at $h/D = 1.0$ there is pure jet flow with minimum recirculation. The performance at $h/D = 1.0$ is identical to the ducted fan when tested by itself. Out of ground effect, this configuration would be superior to other air cushion configurations.

Free hover could be obtained for heights slightly above 2 inches (the height for discharge area = fan area) but strong vertical pulsing or bobbing took place. This was caused by the seal breaking down and then re-establishing.

It is evident that plenum chamber vehicles with internal jet flow will be limited to a height where the discharge area equals the fan area. In free hover tests it was noticed that a 3-inch height could be obtained before the seal broke down with the 2:1 diffuser section installed. However, performance data were not obtained for this configuration.

DISCUSSION OF ANNULAR JET TEST RESULTS

The annular jet configurations tested included vertical jets with three different thicknesses of t = 1.02, 2.10, and 4.00 inches. The performance of the annular jets is compared in Figure 9. There is no internal duct, but the flow follows the wall of the cone as it did with the plenum chamber. The critical height occurs at h/D = .5. The thrust of the one-inch annular jet decreases rapidly as height is increased above h/D = .5.

Notice that the four-inch annular jet shows the best performance at low h/D's. This is because it is actually functioning as an efficient plenum chamber for heights less than 4 inches. At higher heights, it shows poorer performance than the two-inch jet. It should be better but, due to poor diffusing, its efficiency drops to 30 per cent. To supply air to the 4-inch jet, an expansion of 2:1 is required. The efficiency of the two-inch and one-inch annular jets is approximately 50 per cent with the two-inch jet showing slightly higher efficiency.

Correlation. The theoretical equation which fits the test data best is based on thin jet theory with the addition of a back pressure in the jet equal to one half of the base pressure.

$$T = 1.59 \left(1 + \frac{A_{j/2} + A_b}{hC_{j\ av}} \right) \left[\rho A_j \left(\frac{p}{1 + \frac{A_j}{hC_{j\ av}}} \right)^2 \right]^{1/3}$$

This equation, along with the plenum chamber equation, is shown in Figure 10 with the test results for the 2.10-inch annular jet. The correlation indicates that the equation is adequate for heights greater than the jet thickness. For heights less than the jet thickness, the plenum chamber equation with a contraction ratio of $K_r = .62$ gives good agreement with the test data.

Internal losses. The efficiency of the annular jet is seen to be approximately 50 per cent, the same as for the plenum chamber configuration. Since previous tests indicated a maximum efficiency of 62 per cent for the ducted fan by itself, the internal system is about 80 per cent efficient, i.e., $.80 \times 62 \approx .50$. The annular jets did not have the internal ducting but the flow was attached to the wall of the cone, and the internal losses were low as a result of this. In this model, the flow had to make two bends of 45 degrees. In a design where the flow bends through a greater angle, higher losses would be encountered unless turning vanes were employed.

To evaluate internal losses a little further, a two-inch annular jet was tested with an internal cone which provided a duct system of approximately constant 1:1 area ratio for the full length of the duct. It is seen in Figure 11 that this configuration has slightly higher performance than the unducted configuration. The internal cone was removed and a spoiler skirt was attached to the shroud. This produced jet flow inside. It is seen that for this configuration efficiency drops below $\eta = .30$ at high h/D's. The internal losses of this configuration are greater than should be encountered in a practical vehicle design.

As in the case of the plenum chamber with the flow attached to the wall, it is suspected that the efficiency of the annular jet will decrease when means for stabilization are included.

CONCLUSIONS

Performance of the plenum chamber can be predicted if the proper contraction ratio is used. The contraction ratio depends on the type of internal flow. The plenum chamber configuration with internal jet flow will be limited in obtainable h/D by the size of the fan. An efficient diffuser could be employed to raise this limitation.

The performance of the vertical annular jet can be predicted. For heights greater than the jet thickness, thin jet theory including a back pressure in the jet equal to one half the base pressure is adequate. For heights less than the jet thickness, the plenum chamber equation with a contraction ratio of .62 is found to give good correlation.

The annular jet showed only the slightest performance advantage over the plenum chamber configuration with flow following the wall. The plenum chamber with flow following the wall was superior to the annular jets at h/D = .20.

An overall efficiently of 50 per cent was typical of the configuration tested. It should be easy to exceed 50 per cent overall efficiency in a practical vehicle design. The flow did not have to bend through large angles in the model. However, turning vanes of simple design could be used to minimize the turning losses when large turning angles are required. A carefully designed air supply system or ducted fan section, as used here, is very important if the overall efficiency is to be high.

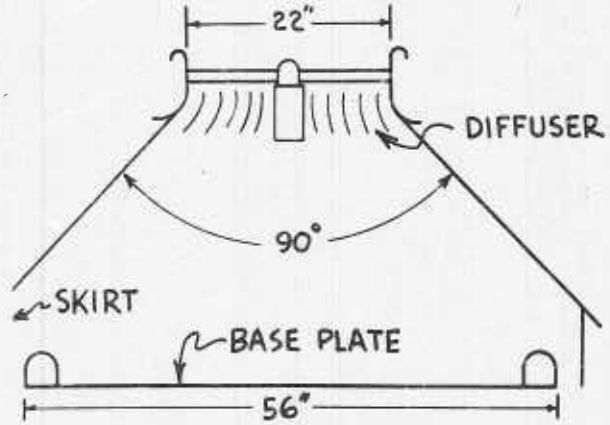

Figure 1. Model cross section

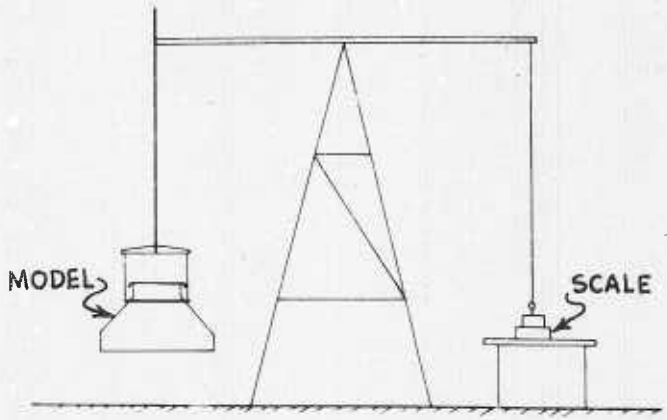

Figure 2. Balance stand

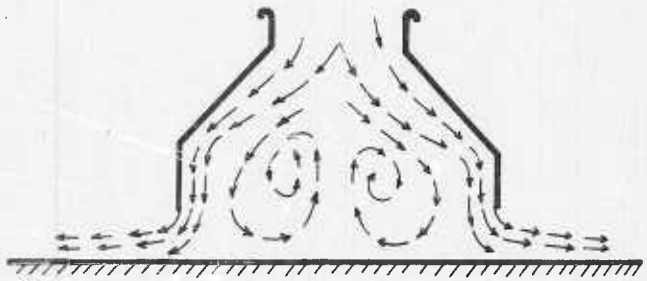

Figure 3. Plenum chamber with flow following wall

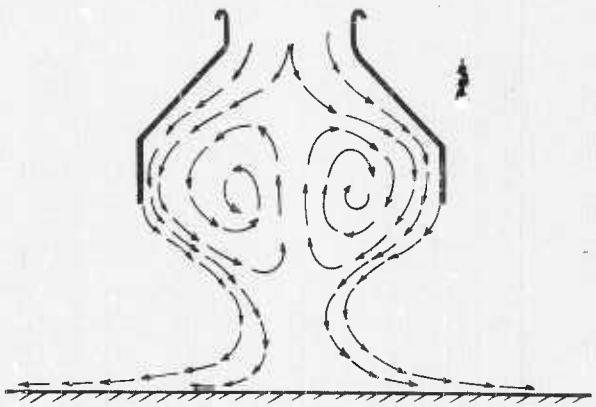

Figure 4. Plenum chamber above $h/d = .5$ flow following wall

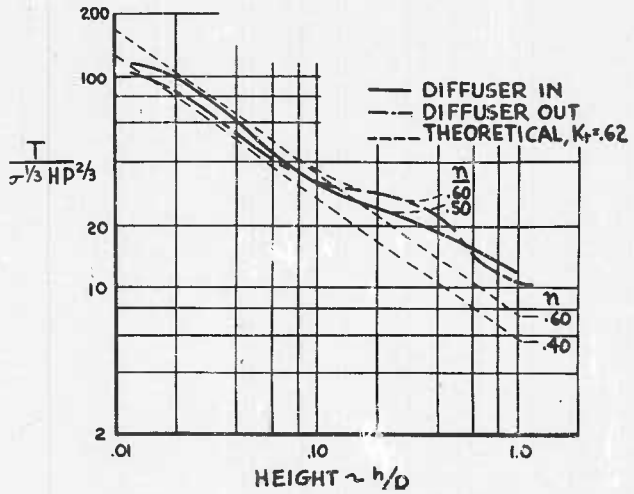

Figure 5. Plenum chamber flow following wall

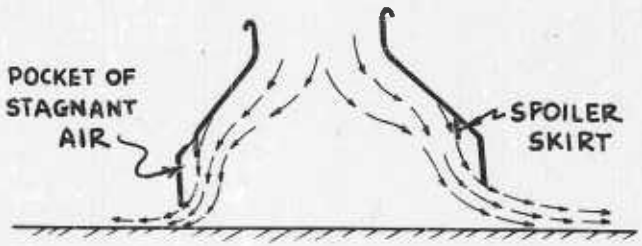

Figure 6. Static stability of plenum chamber

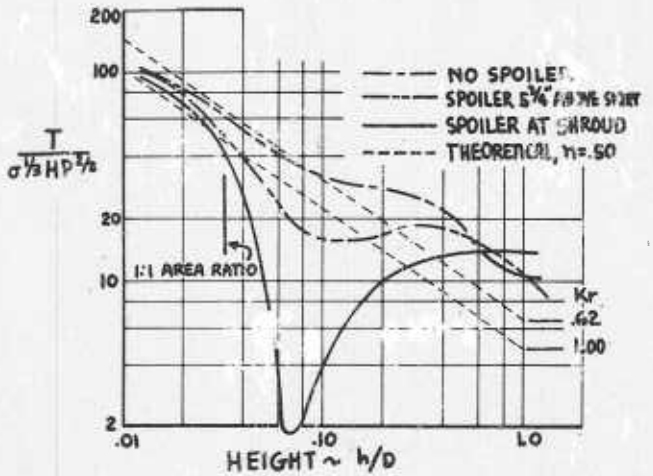

Figure 7. Plenum chamber diffuser removed

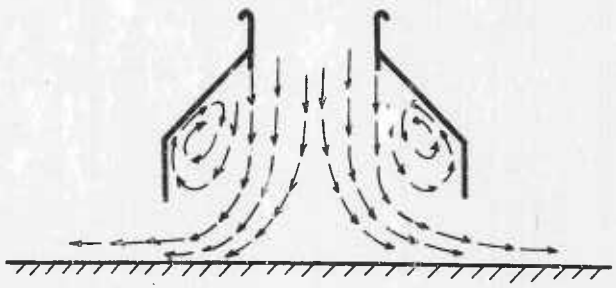

Figure 8. Plenum chamber - jet flow

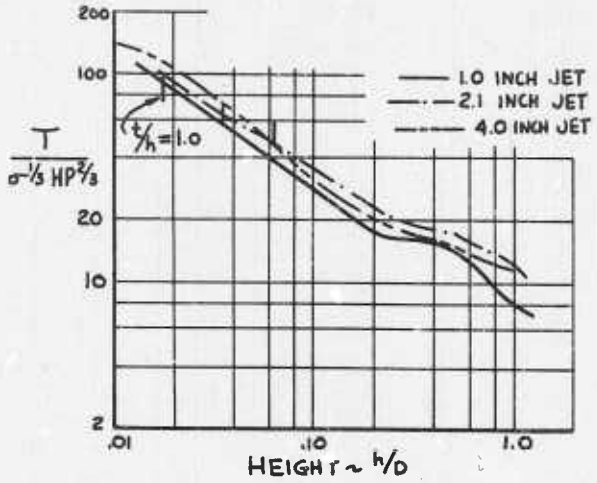

Figure 9. Annular jets diffuser out

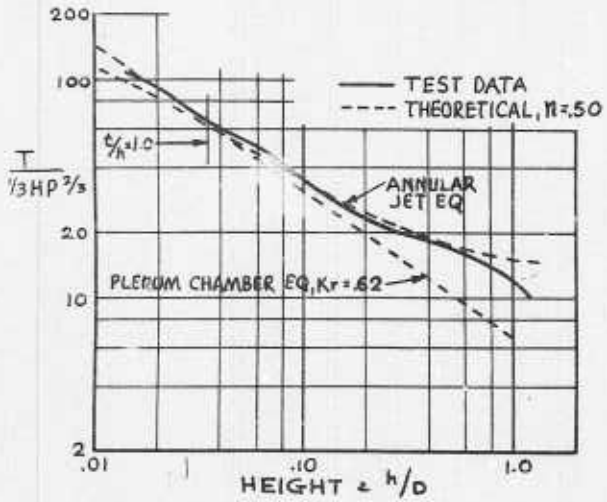

Figure 10. Correlation with theory
2 inch annular jet, diffuser out

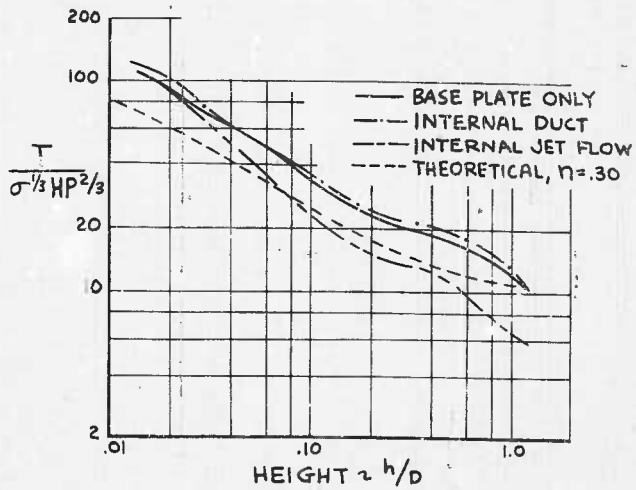

Figure 11. Internal losses
2 inch annular jet, diffuser out

SIMPLIFIED MOMENTUM THEORY SOLUTIONS FOR THE AUGMENTATION FACTOR OF HOVERING ANNULAR JET VEHICLES

By Thomas M. Clancy, Erco Division, ACF Industries, Incorporated

INTRODUCTION

This paper outlines simplified methods by which the augmentation factor may be determined for annular jet ground effect vehicles. Approximate and exact solutions are given for thin jet circular planform vehicles. It is shown herein that the same methods are applicable to vehicles of any planform shape.

SYMBOLS

A	augmentation factor ($= W/F_j$)
A_b	base area
A_j	jet area at exit station
A_s	vertical projection of jet sheet area
AR	nozzle aspect ratio ($=\ell_j/t$)
b	vehicle side length
d	width of two-dimensional platform
F_b	base force
F_j	jet thrust
f_j	two-dimensional jet thrust (i.e., jet thrust for unit depth)
h	reference height of vehicle above ground plane
ℓ_b	base perimeter
ℓ_j	mean length of jet
p_c	cavity pressure, absolute
p_o	ambient pressure, absolute
Δp_c	cavity pressure, gauge
R	radius of curvature of jet
r_b	base radius of platform
t	jet thickness
W	vehicle gross weight

r_i radius of circle inscribed in base outline of regular polygon planforms

Θ_o inclination of jet from vertical (positive when jet is inclined inward toward center of cavity.

TWO-DIMENSIONAL CASE

Shown in Figure 1 is a two-dimensional view of an annular jet exhausting vertically downward through a distance h to a ground plane. Two jets of equal strength, f_j, are shown, separated by a base of width d. The reference length normal to the plane of the figure is taken as unity.

In the process of starting, the flow from each jet impacts on the ground directly below each nozzle and splits into two parts: one half of the flow moving outward tangent to the ground, the other half moving inward. Since jets on either side are supplying air to an enclosed cavity, the cavity attempts to attain a pressure equal to the total pressure in the jet. However, as the cavity pressure rises above the ambient pressure existing outside of the jet sheets, the horizontal pressure difference causes the sheets to move outward. The final equilbrium position of the jet sheets is approximately as shown in the figure. The jets become tangent to the ground in the ideal case but, for the case of a viscous fluid, they impact on the ground at a shallow angle. The significance of this is that a stagnation point appears on the ground which causes a small inflow of air to the cavity replacing air that is entrained from the cavity by viscous induced mixing along the inner wall of the jet.

The exact shape of the jet is not known, and in fact does not have to be known in order to determine the cavity pressure in two-dimensions.

The theory of reference 1 arrives at an expression for cavity pressure by writing an equation for the forces acting on an elemental fluid particle of the jet. Thus the pressure difference acting across the jet sheet is considered as balanced by the centrifugal force of the fluid element in curvilinear translation. This method encounters several difficulties:

(1) an integration must be performed in order to determine cavity pressure,

(2) the jet sheet must be assumed as thin ($t/h \ll 1$), and (3) the shape of the jet must be approximated.

The method presented herein solves for the cavity pressure without any of these difficulties. This approach was first suggested by the author in August 1958, and is reviewed here rather briefly in two-dimensions. As will be shown later in this paper, the same approach leads to simplified exact and semi-exact solutions for arbitrary planform shapes.

Confining attention to the left-hand side of Figure 1, the total momentum flux of the jet for unit depth is equated to the forces acting horizontally across the sheet as follows:

$$f_j \times 1 = (p_c - p_o) \times h \times 1 = \Delta p_c \cdot h$$

and the well-known solution for Δp_c is given immediately as $\Delta p_c = f_j/h$. A differential expression is not required in the above equation since the component of force due to pressure acting horizontally along the curved jet sheet is identical to the force that would exist on a vertical wall of height h and unit depth.

The pressure difference is assumed to be hydrostatic throughout the cavity. Thus the vertical force available from the cavity pressure is $\Delta p_c \cdot d \cdot 1$, which assists the vertical jet thrust reactions in supporting the platform.

It is noteworthy that, other than the assumption of a cavity maintained at constant pressure, the above approach requires only that the jets become tangent to the ground. Jet tangency at the ground, in turn, follows from the assumption of an inviscid flow.

APPROXIMATE THREE DIMENSIONAL SOLUTIONS

A circular planform annular jet vehicle with a jet exhausting vertically downward is shown in Figure 2. The downwardly moving jet turns through 90° and flows radially outward along the ground. Considering a horizontal equilibrium around 2π, the jet is seen to have a radially inward reaction that is balanced by a radially outward pressure force required to hold the sheet in equilibrium. Thus

$$F_j = \Delta p_c \cdot 2\pi r_b h$$

where: $2\pi r_b h$ is the area of the vertical projection of the jet sheet.

Hence $$\Delta p_c = F_j / 2\pi r_b h$$

The vertical equilibrium condition gives

$$W = F_j + F_b = F_j + \Delta p_c \cdot \pi r_b^2$$

Dividing through by F_j and substituting the above expression for Δp_c yields the augmentation factor as:

$$A = \frac{W}{F_j} = 1 + \frac{1}{2h/r_b}$$

Figure 3 shows a fragmentary section of a circular planform vehicle with the jet exhausting inwardly at an angle Θ_o to the vertical. The inwardly flowing portion of the jet has a diminishing horizontal component of momentum and is thus associated with a "drag" force acting on the cavity. Thus the cavity pressure must be higher than for the case of the vertically issuing jet. Viewed differently, the cavity pressure must be higher to force additional curvature in the jet sheet. Using the convention that Θ_o is positive when the jet is inclined inward, and writing horizontal equilibrium (around a circular planform), there results:

$$F_j + F_j \sin \Theta_o = \Delta p_c \cdot 2\pi r_b h$$

The vertical equilibrium condition is

$$W = F_j \cos \Theta_o + F_b$$

Following the steps as above for the case of $\Theta_o = 0$, the augmentation factor becomes

$$A = \cos \Theta_o + \frac{(1 + \sin \Theta_o)}{2h/r_b}$$

The above approach, which might be referred to as a type of "horizontal equilibrium around 2π," gives an exact solution in the two-dimensional case. The solution in three dimensions, however, is only approximate. The reason for this may be explained as

follows: in the former case, the pressure integral was projected back to a plane surface (of unit depth) whereas, in the latter case, the pressure integral is projected to a curved wall. This difficulty is resolved in a later portion of this paper by using a different approach, and an exact solution is obtained.

The augmentation factors derived thus far are seen to be identical to those given in reference 1, although quite different methods were employed for determining the cavity pressure.

A first attempt at determining the augmentation factor for planform shapes other than circular ones is suggested as a generalization of the formula derived for the circle as follows:

$$A = \frac{W}{F_j} = 1 + \frac{F_b}{F_j} = 1 + \frac{\Delta p_c}{F_j} \times A_b$$

and, as derived above,

$$\frac{\Delta p_c}{F_j} = \frac{1}{A_s} = \frac{1}{\ell_b \cdot h}$$

Thus, A is generally given as

$$A = 1 + \frac{A_b}{\ell_b \cdot h} \quad (\Theta_o = 0)$$

Inserting the general expression for the area and perimeter of a regular polygon of n sides, we then have

$$A = 1 + \frac{nr_i^2 \tan(\pi/n)}{2nr_i \, r\tan(\pi/n) \cdot h} = 1 + \frac{1}{2h/r_i}$$

In the above expression, the augmentation factor is independent of the number of sides and is simply based on the vehicle height and the inscribed radius.

It is to be noted that the radius of a circle inscribed on the planform base is deemed a better reference for A than the "equivalent diameter" referred to elsewhere in the literature, at least for the case of regular planforms. In a manner of speaking, the portions of the planform that overhang the inscribed circle are lost for purposes of augmentation, since the same augmentation would be available by designing directly to the inscribed circle.

Figure 4 shows the approximate solutions derived for circular planforms, with the h/r_b replaced by h/r_i. Data from Aerophysics Company and National Research Associates flying models are superimposed. The rectangular shapes, being 15-1/2 inches long by 13-1/2 inches wide, were considered close enough to "square" to warrant inclusion. All of the models represented, with the exception of the hexagons, were fitted with stabilizing jet slots. These slots do not permit maximum augmentation because they handle air that would otherwise be more efficiently ducted through the perimeter.

The data points shown should be used with some caution for the following reasons: (1) most of the models were of small scale, and (2) they were constructed and tested over a year ago at a time when, one may recall, it seemed more important to convince the skeptics that a ground cushion existed, by demonstrating operating models, than to make precise measurements. The real significance of this data, then, is that planform shapes with discontinuities do not leak all or most of the cavity pressure at the corners as was once feared, at least for low aspect ratio nozzles. The spreading of the jet at the corners is undeniably a weakening effect, however, which should be taken into account by designers of noncircular planform vehicles. Thus, we see that planforms with sharp corners, in addition to having a lower augmentation, are further hampered by the augmentation drop caused by the necessity of designing to relatively low aspect ratios.

EXACT THREE-DIMENSIONAL SOLUTION

Consider a circular planform vehicle with an infinitely thin jet issuing vertically downward and curving outward on a radius of curvature equal to the height of the vehicle, thereby becoming tangent to the ground. A vertical cutting plane is passed through the center of the vehicle as shown in Figure 5. The cutting plane is arbitrarily limited to the area beneath the base of the vehicle. An exact expression for cavity pressure (and therefore augmentation factor) may be determined from the well-known principle that the integral of the pressure over a fixed boundary is equal to the load supported by the system. In the present case, the boundary is artificial but may be considered as a fixed boundary since it represents a plane of symmetry.

Horizontal equilibrium taken along the x axis yields the following equation:

$$F_j/\pi = F_1 + 2F_2$$

where F_1 represents the pressure integral over the surface of the cutting plane on the rectangular area between the vehicle base and the ground. F_2 represents the pressure integral over the surface of the cutting plane on the area segment between the jet sheet and the ground. F_j/π is the x component of the vehicle jet thrust.

A constant pressure p_c is assumed in the cavity. Since the jet does not stagnate on the ground, the area segment between the jet sheet and the ground is also at the pressure p_c. The jet is assumed thin and, therefore, its pressure integral in the cutting plane is zero.

The horizontal equilibrium expression may be expanded as follows:

$$F_j/\pi = (p_c - p_o)\, 2r_b h + (p_c - p_o) \cdot 2 \cdot \left[h^2 - \frac{\pi h^2}{4} \right]$$

and

$$F_j = \Delta p_c \cdot 2\pi r_b h + \Delta p_c \cdot \pi h^2 \left[\frac{4-\pi}{2} \right]$$

In the above expression, the first term on the right-hand side is seen to be the same as that given previously for the approximate case. The second term then represents a superimposed "pressure integral" required to yield an exact solution.

Since as shown previously, $A = 1 + \dfrac{\Delta p_c \pi r_b^2}{F_j}$, after making the substitution for

Δp_c, the exact solution for the circular planform case becomes

$$A = 1 + \frac{1}{\frac{2h}{r_b} + \left(\frac{4-\pi}{2}\right)\left(\frac{h}{r_b}\right)^2}$$

The exact thin jet solution for $\Theta_o = O$ is derived in a similar manner to that shown above, and will be merely outlined briefly here. The sheet position is shown in the vehicle fragmentary section of Figure 6. The cutting plane lies in the plane of the paper. The horizontal thrust force is now equated to the "pressure integral" over the area $2r_b h$, plus the integral over the area designated as A' in the figure, minus the integral over the area designated as B':

$$(1 + \sin \Theta_o)\, F_j/\pi = \Delta p_c \cdot 2r_b h + \int_s A' \Delta p_c - \int_s B' \Delta p_c$$

Once again, an integration is not required since cavity pressure is assumed to be hydrostatic throughout.

Therefore

$$(1 + \sin \Theta_o)\, F_j/\pi = \Delta p_c \cdot 2r_b h + \Delta p_c \left[\frac{h^2}{(1+\sin \Theta_o)^2}\left(\cos \Theta_o (2 - \sin \Theta_o) - \frac{\pi}{2} + \Theta_o\right)\right]$$

$$- \Delta p_c \frac{h^2}{(1+\sin \Theta_o)^2}\left[2\Theta_o - \sin 2\Theta_o\right]$$

But

$$A = \cos \Theta_o + \frac{(1 + \sin \Theta_o)\, \Delta p_c\, \pi r_b^2}{F_j}$$

Substituting the expression for Δp_c into the augmentation factor expression yields

$$A = \cos \Theta_o + \frac{1 + \sin \Theta_o}{\frac{2h}{r_b} + \frac{h^2}{r_b^2 (1 + \sin \Theta_o)^2}\left[2 \cos \Theta_o + \cos \Theta_o \sin \Theta_o - \frac{\pi}{2} - \Theta_o\right]}$$

The above expression is plotted in Figure 7. The optimum values for Θ_o are indicated in the figure by the dotted line. It is worthy of note that the exact thin jet solution derived above gives indentical results to those determined in reference 1. The values of $\Theta_{o\ OPT}$ lie within a few degrees of the values given in reference 1. The significant point is, of course, that the above solution is arrived at rather easily by the expedient of applying the horizontal equilibrium condition.

EXTENSION TO ARBITRARY PLANFORM

It may be said in general that any annular jet configuration possessing a plane of symmetry is susceptible to solution by the method of this paper. The so-called "pressure integrals" taken over the cutting plane can, of course, be used in the form shown above for any planform shape by replacing the $2r_b$ by the vehicle span. The horizontal component of thrust normal to the cutting plane, however, must be separately derived for each case (i. e., the F_j/π component is only true for the circular planform case). This thrust component is most readily determined by writing an expression for the average pressure of the jet along the ground and integrating over the proper length of the jet. To illustrate, for the case of a square planform (see Figure 8):

$$\text{average jet pressure along ground perimeter} = \frac{F_j}{(4b + 2\pi h)t}; \quad (\Theta_o = 0)$$

where: b is vehicle side length, R is assumed equal to h, and t is an arbitrary thickness assigned to the jet on the ground.

Then the x component of thrust is

$$F_{j_x} = \frac{F_j}{(4b + 2\pi h)\ t} \cdot (bt) + \int_{-\pi/2}^{\pi/2} \frac{F_j}{(4b + 2\pi h)\ t} \cdot (dA \cos \phi)$$

where ϕ is the angular position of the element dA with respect to the x axis, but

$$\int_{-\pi/2}^{\pi/2} (dA \cos \phi) = 2ht$$

Therefore

$$F_{j_x} = \frac{F_j \cdot b}{4b + 2\pi h} + \frac{F_j \cdot 2h}{4b + 2\pi h} = \frac{F_j(b + 2h)}{4b + 2\pi h}$$

Examination of the above expression reveals that the x component of thrust is generally given as total thrust times the ground length of the cutting plane divided by the ground perimetal length of the jet. For the case of h small, the x component is simply $F_j/4$.

Writing the complete equation, then,

$$F_{j_x} = \frac{F_j(b + 2h)}{4b + 2\pi h} = \Delta p_c \left[bh + 2\left(h^2 - \frac{\pi h^2}{4} \right) \right]$$

The augmentation factor for the square planform becomes

$$A = 1 + \frac{1}{\left(\frac{4 + 2\pi h/b}{1 + 2h/b} \right) \left(\frac{h}{b} + \frac{h^2}{b^2} \left(\frac{4-\pi}{2} \right) \right)}$$

The derivation above, for the square planform, has been conducted in terms of the side length b, rather than the radius of the inscribed circle, because the latter reference dimension is recommended for use only in cases where approximate solutions are satisfactory. In addition, it should be noted that the above solution represents the case of a vertically issuing jet ($\Theta_o = O$); however, it is a relatively simple matter to superimpose the effect of variable Θ_o as was shown separately in the circular planform case. This refinement, together with solutions for other planform shapes, are omitted in the interest of highlighting the method. The author is convinced that the "cutting plane" method represents a powerful, yet simple, tool for use in vehicle design. One important feature is that the solution goes from approximate to exact form by simple superposition of "pressure integrals." Thus the designer has the choice of obtaining desired degrees of exactitude in direct proportion to the effort employed.

CONCLUSION

The augmentation factor solutions in this paper are submitted with a minimum of experimental substantiation, for purposes of brevity only. The circular planform solutions, both approximate and exact, yield identical results to those of reference 1 despite the fact that the methods used herein are quite different. Therefore, in lieu of experimental verifications in this paper, the reader is referred to reference 1 wherein the solutions are shown to agree well with the data available at that time. The experiments referred to are, of course, those of von Glahn (reference 2). The author is aware that contradictory data have subsequently appeared, as for example in reference 3. This latter data shows momentum theory in a poor light; however, the model used in this case had an undercut base giving thereby a larger than normal cavity. If the data in reference 3 is evaluated in terms of base height above ground rather than nozzle height, a large shift can be made with the result that momentum theory still appears valid at low h/r_b. The exceptionally high aspect ratio of the test ($AR \geq 1500$) may also have influenced the data, since the model is quite small and the jet is extremely thin, possibly too thin for continuity in the sheet.

The second method employed in this paper (equilibrium taken across a cutting plane) can be extended to show the trend of nozzle aspect ratio effects first discovered in reference 2. This extension has been partly completed by the author. The results show that about 50 per cent of the aspect ratio effect can be accounted for. Unfortunately, proper treatment of this extension of present methods is too lengthy for inclusion here. The effect of the aspect ratio on augmentation factors, using momentum theory, is the subject of a paper now in preparation.

REFERENCES

1. Chaplin, H. R., "Theory of the Annular Nozzle in Proximity to the Ground." David Taylor Model Basin Aero Rept. 923, Navy Department, Washington, D. C., July 1957.

2. Von Glahn, U. H., "Exploratory Study of Ground Proximity Effects on Thrust of Annular and Circular Nozzles." NACA Tech. Note 3982, April 1957.

3. Tinajero, A. A., "Comparison of Experimental and Theoretical Design Parameters of a 6-inch-diameter Annular Jet Model with a Jet Angle of -45° Hovering in Proximity to the Ground; and Experimental Results for Forward Flight at Zero Angle of Attack." David Taylor Model Basin Aero Rept 954, Navy Department, Washington, D. C., May 1959.

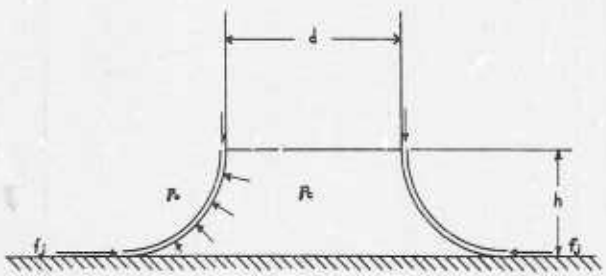

Figure 1. Two-dimensional annular jet platform

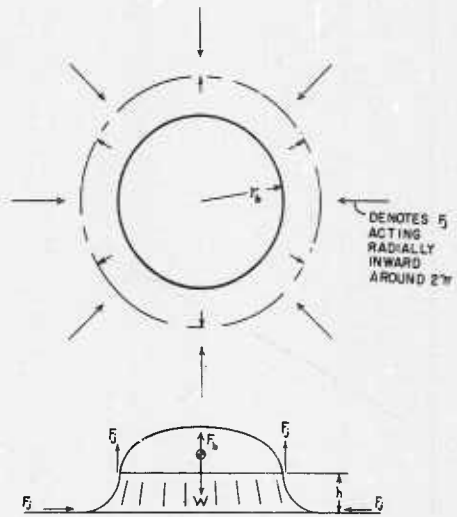

Figure 2. Circular planform vehicle in hovering

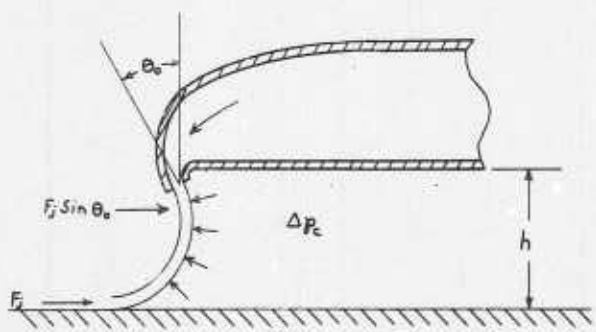

Figure 3. Fragmentary section of vehicle with inwardly inclined jet

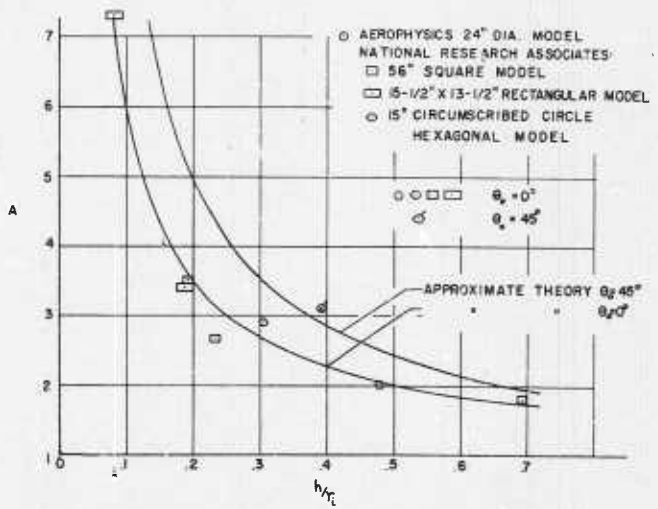

Figure 4. Comparison of theoretical and experimental augmentation factors

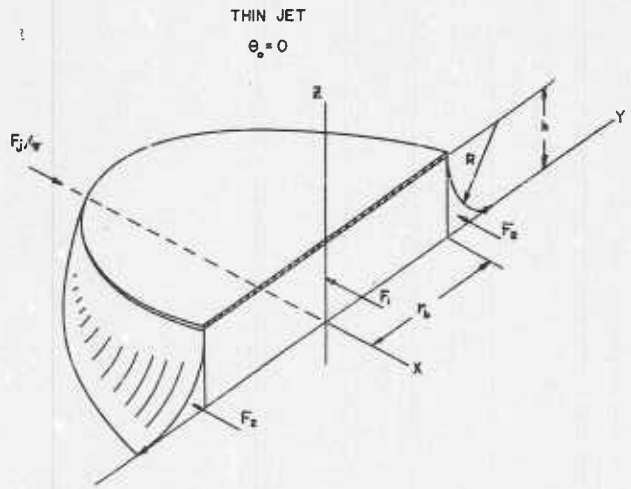

Figure 5. Equilibrium across the vertical cutting plane of a circular planform vehicle

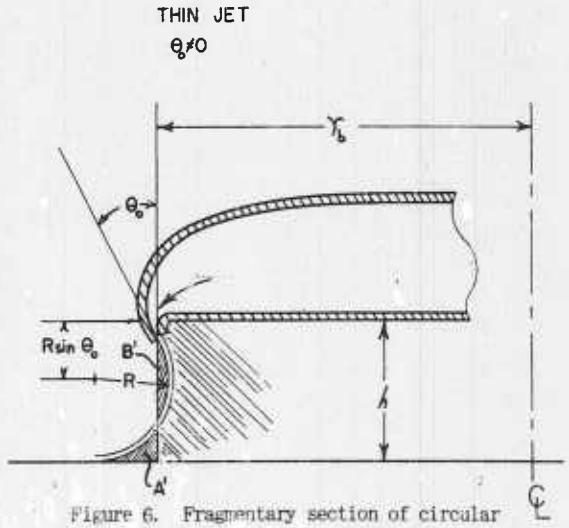

Figure 6. Fragmentary section of circular planform vehicle

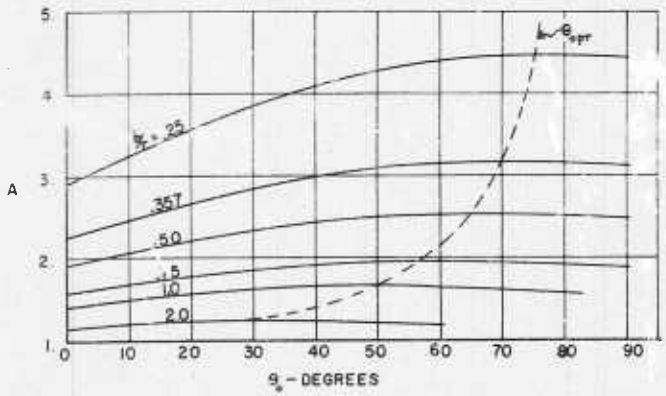

Figure 7. Augmentation factor for the circular planform by exact momentum theory

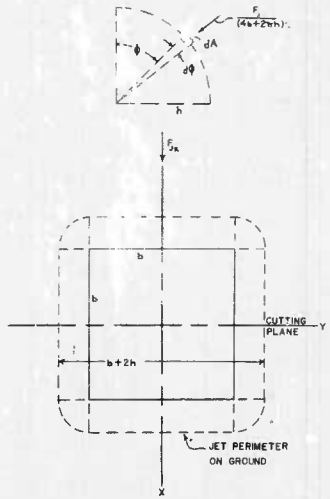

Figure 8. Equilibrium across the vertical cutting plane of a square planform vehicle

GROUND CUSHION FLOW VISUALIZATION STUDIES

By Donald G. Sachs, Boeing Airplane Company,

The widespread interest in ground cushion vehicles stimulated the Aero-Space Division of the Boeing Airplane Company to conduct some simple experimental work to help evaluate the concept.

It was felt that much of the basic knowledge required could be gained by a visual study of the flow beneath typical base configurations. The test set-up for the study is shown in Figure A. The model was a cylinder (18-inch I. D.) which could be fitted with a series of 3/4-inch thick plywood bases. Air was supplied to the model from a pressurized plenum. Base pressure data on the model and the glass ground plane were measured by a hand-held static probe. Additional data recorded were the ground plane load and the tuft movement.

Figures 1 through 7 show typical model base pressure profiles obtained during the test. In all cases, the nozzle pressure ratio was maintained at approximately 1.04. All testing was done statically (zero translational velocity).

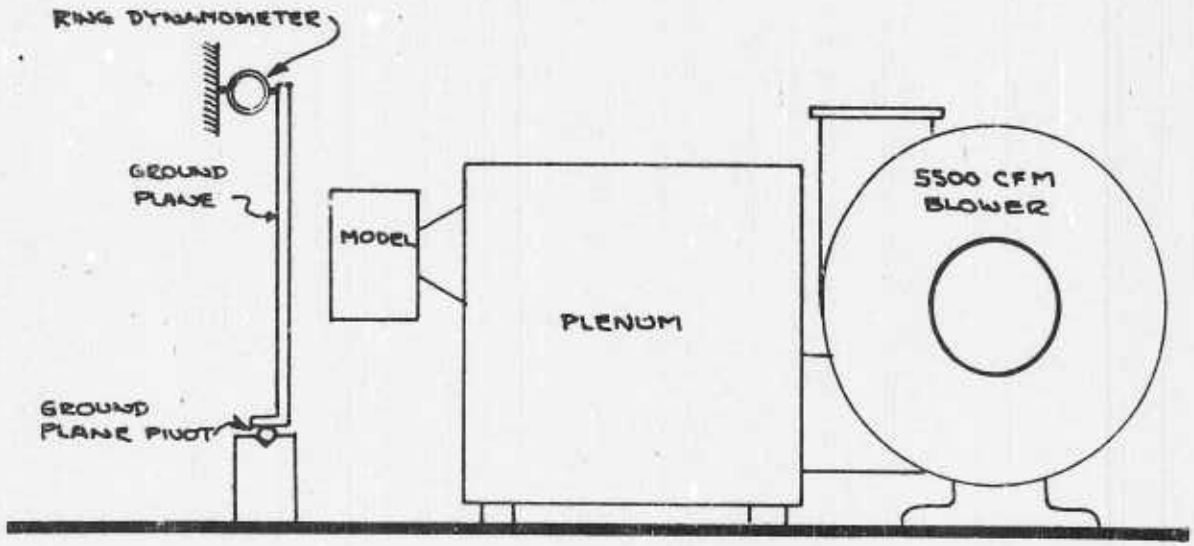

Figure A. Test installation

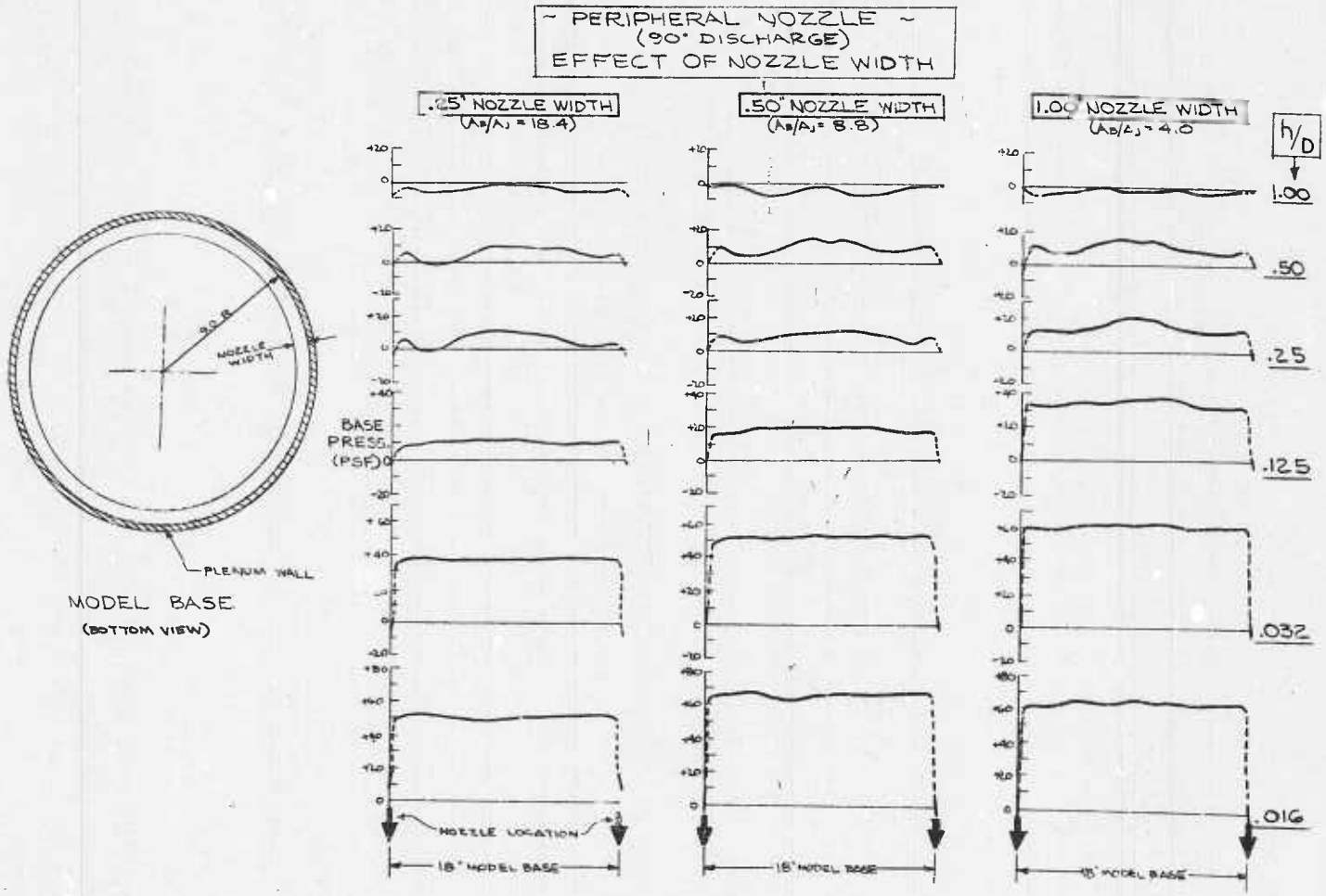
~ PERIPHERAL NOZZLE ~
(90° DISCHARGE)
EFFECT OF NOZZLE WIDTH
.25" NOZZLE WIDTH
(AB/AJ = 18.4)
.50" NOZZLE WIDTH
(AB/AJ = 8.8)
1.00" NOZZLE WIDTH
(AB/AJ = 4.0
h/D
1.00
.50
.25
.125
.032
.016
BASE PRESS. (PSF)
NOZZLE LOCATION
18" MODEL BASE
90°
NOZZLE WIDTH
PLENUM WALL
MODEL BASE
(BOTTOM VIEW)

Figure 1.

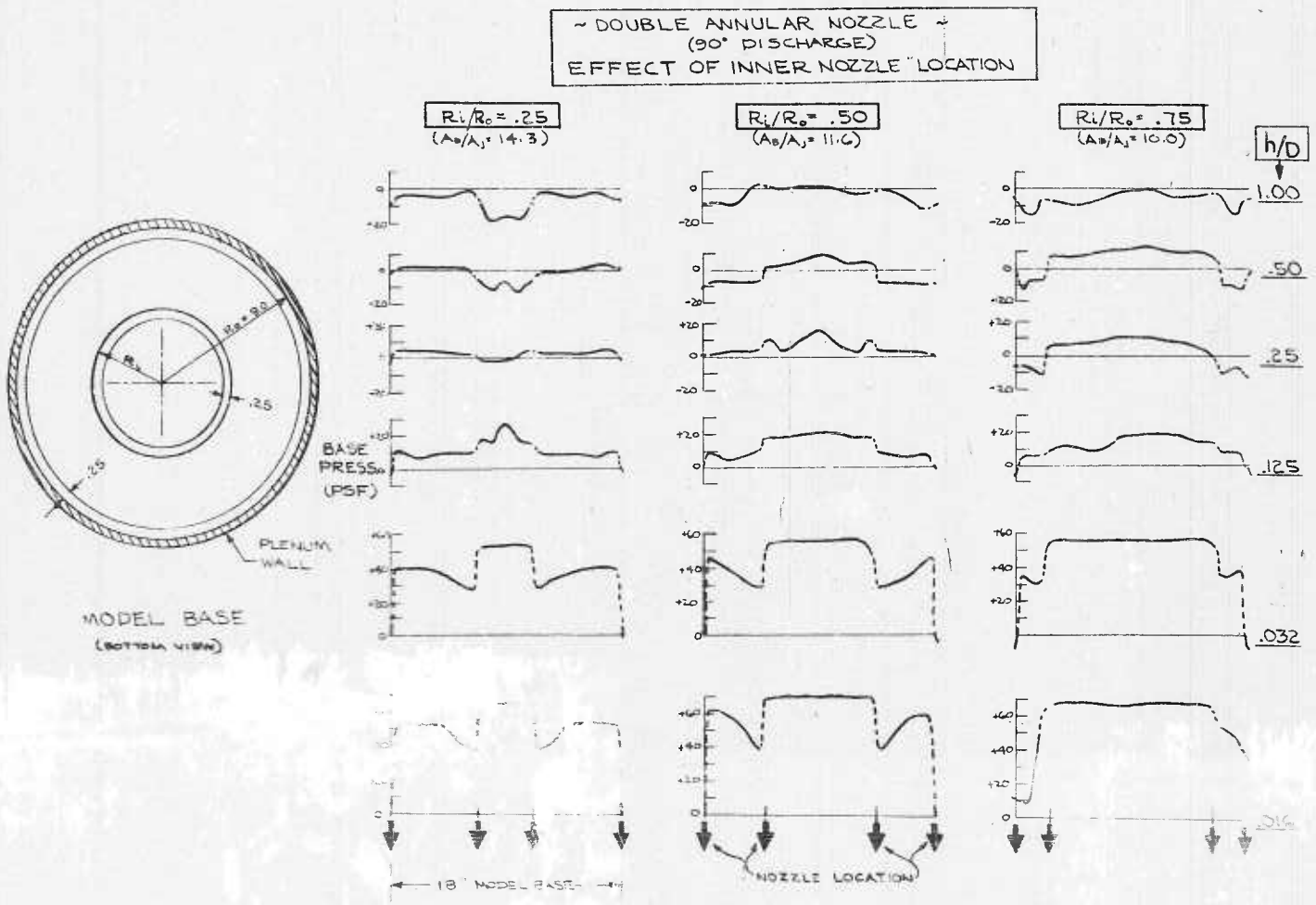
~ DOUBLE ANNULAR NOZZLE ~
(90° DISCHARGE)
EFFECT OF INNER NOZZLE LOCATION
Ri/Ro = .25
(Ab/Aj = 14.3)
Ri/Ro = .50
(Ab/Aj = 11.6)
Ri/Ro = .75
(Ab/Aj = 10.0)
h/D
1.00
.50
.25
.125
.032
.016
BASE PRESS. (PSF)
MODEL BASE
(BOTTOM VIEW)
PLENUM WALL
.25
.25
18" MODEL BASE
NOZZLE LOCATION

Figure 2.

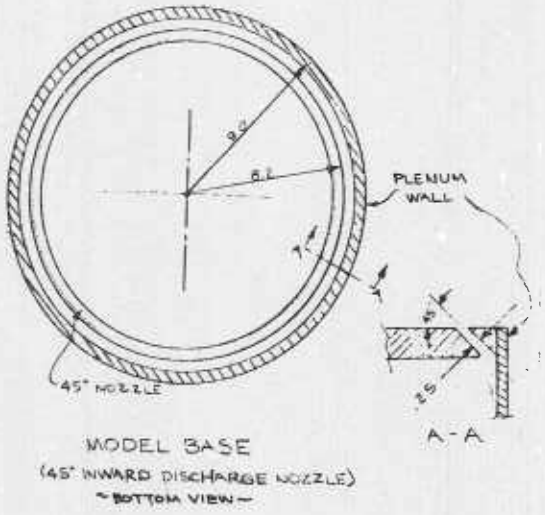
PLENUM WALL
45° NOZZLE
A-A
MODEL BASE
(45° INWARD DISCHARGE NOZZLE)
~BOTTOM VIEW~

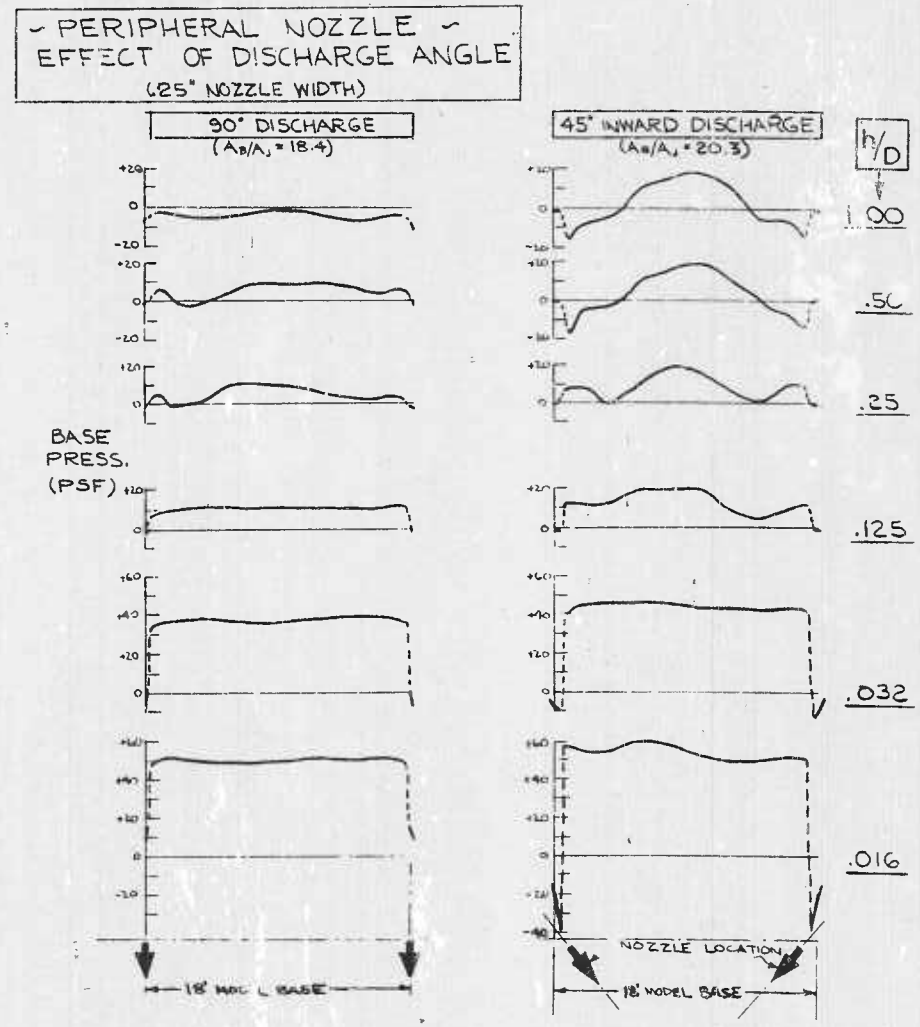
~ PERIPHERAL NOZZLE ~
EFFECT OF DISCHARGE ANGLE
(.25" NOZZLE WIDTH)
90° DISCHARGE
(AB/A, = 18.4)
45° INWARD DISCHARGE
(AB/A, = 20.3)
h/D
1.00
.50
.25
.125
.032
.016
BASE PRESS. (PSF)
NOZZLE LOCATION
18" MODEL BASE

Figure 3.

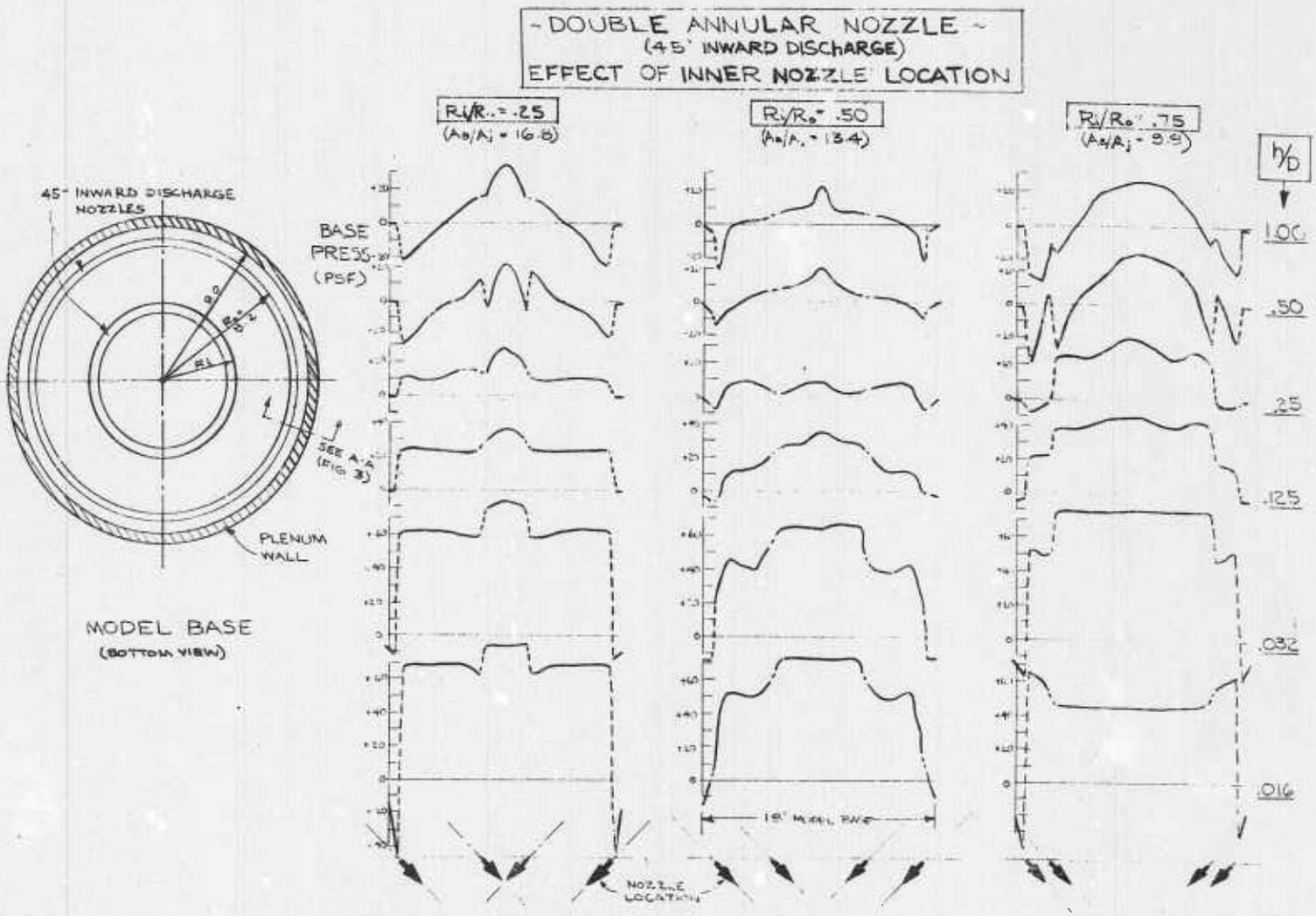
- DOUBLE ANNULAR NOZZLE -
(45° INWARD DISCHARGE)
EFFECT OF INNER NOZZLE LOCATION
Ri/Ro = .25
(Ao/Ai = 16.8)
Ri/Ro = .50
(Ao/Ai = 13.4)
Ri/Ro = .75
(Ao/Ai = 9.9)
h/D
1.00
.50
.25
.125
.032
.016
BASE PRESS. (PSF)
45° INWARD DISCHARGE NOZZLES
PLENUM WALL
MODEL BASE
(BOTTOM VIEW)
SEE A-A (FIG 3)
NOZZLE LOCATION
18" MODEL DIA

Figure 4.

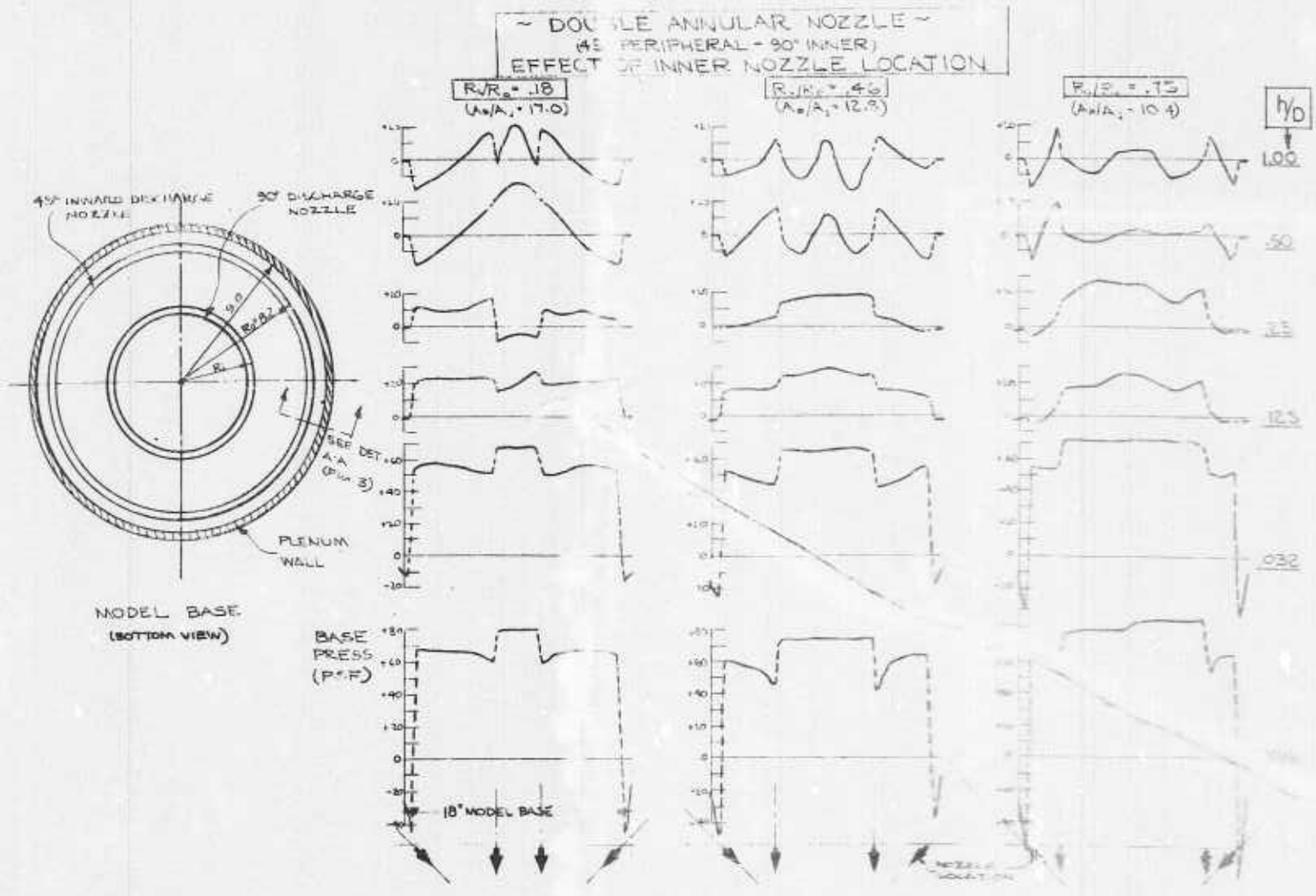
~ DOUBLE ANNULAR NOZZLE ~
(45° PERIPHERAL - 90° INNER)
EFFECT OF INNER NOZZLE LOCATION
R_J/R_o = .18
(A_o/A_j = 17.0)
R_J/R_o = .46
(A_o/A_j = 12.8)
R_J/R_o = .75
(A_o/A_j = 10.4)
h/D
1.00
.50
.25
.125
.032
45° INWARD DISCHARGE NOZZLE
90° DISCHARGE NOZZLE
PLENUM WALL
REF DET A-A (PLAN B)
MODEL BASE
(BOTTOM VIEW)
BASE PRESS (P*F)
18" MODEL BASE

Figure 5.

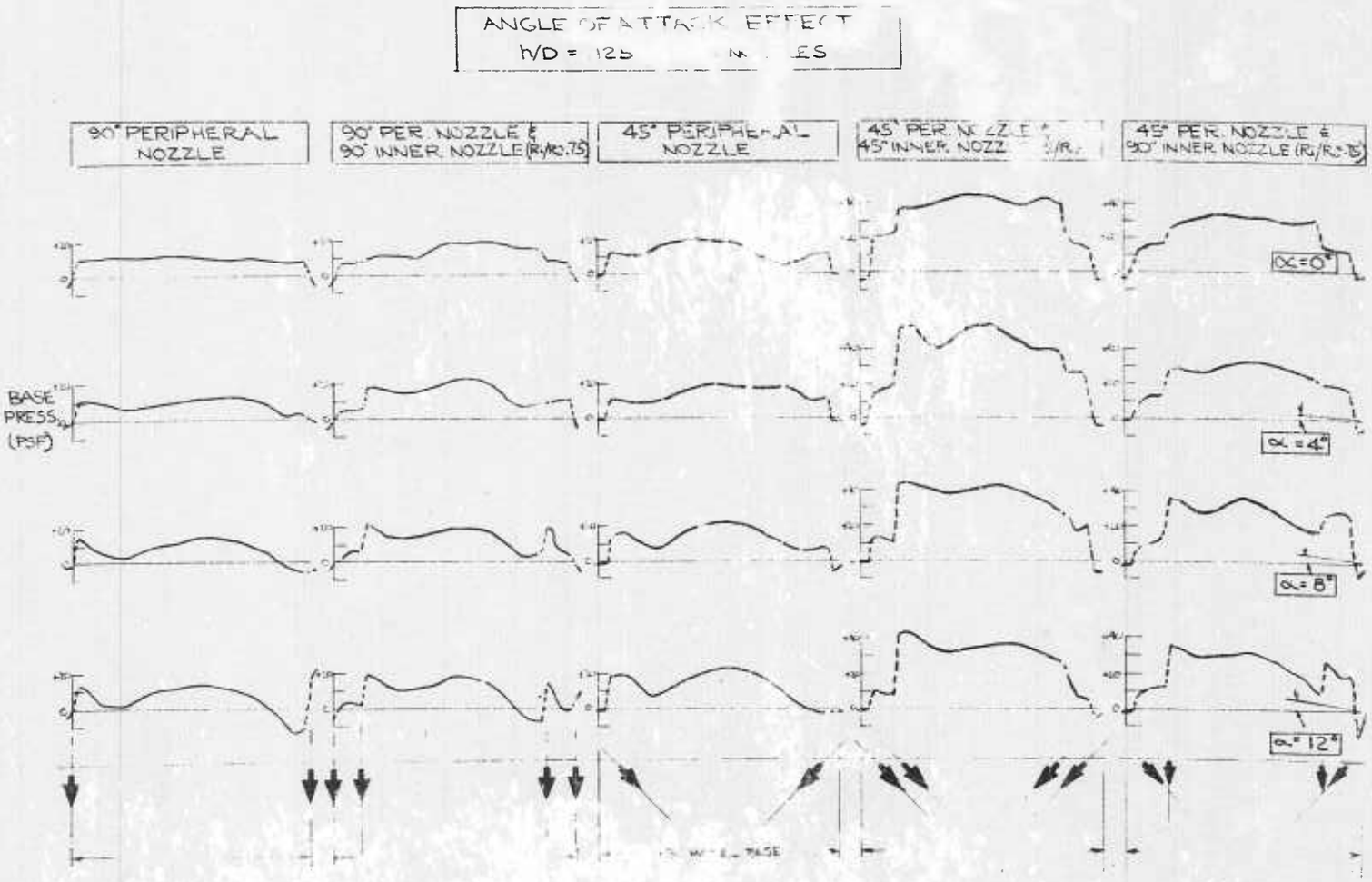
ANGLE OF ATTACK EFFECT
h/D = 125
90° PERIPHERAL NOZZLE
90° PER. NOZZLE & 90° INNER NOZZLE (R/R=.75)
45° PERIPHERAL NOZZLE
45° PER. NOZZLE & 45° INNER NOZZ
45° PER. NOZZLE & 90° INNER NOZZLE (R/R=.75)
BASE PRESS. (PSF)
α=0°
α=4°
α=8°
α=12°

Figure 6.

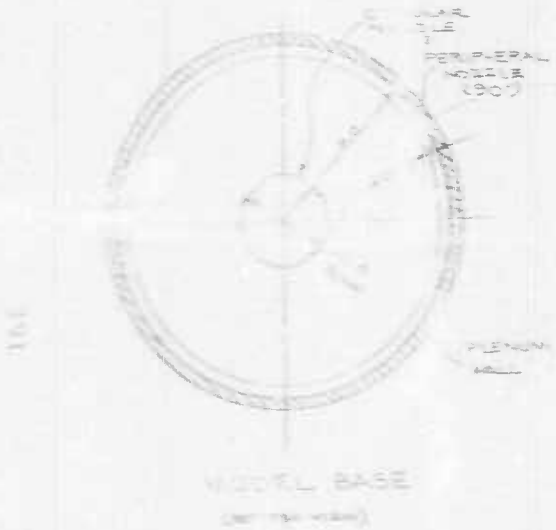

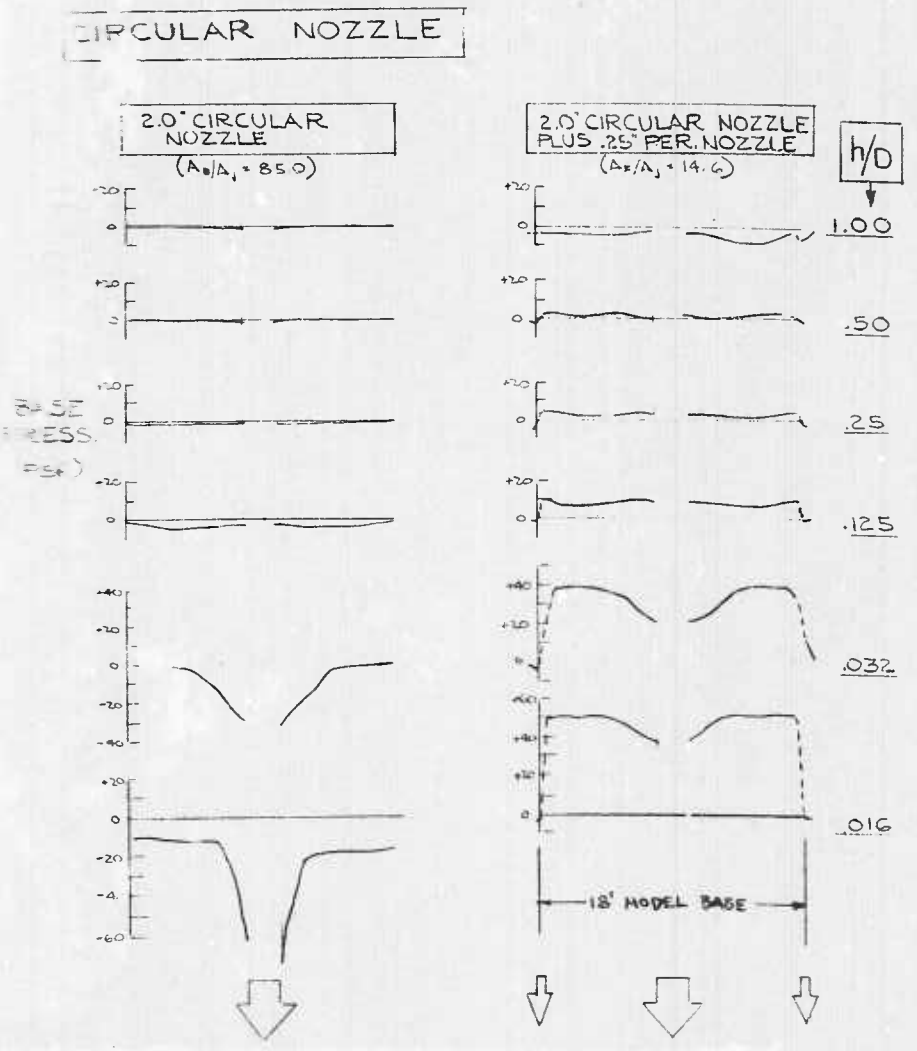
CIRCULAR NOZZLE
2.0" CIRCULAR NOZZLE
(A₀/Aⱼ = 8.50)
2.0" CIRCULAR NOZZLE PLUS .25" PER. NOZZLE
(A₀/Aⱼ = 14.6)
h/D
1.00
.50
.25
.125
.032
.016
18" MODEL BASE

Figure 7.

UNCLASSIFIED